DOT/FAA/AR-04/44

Office of Aviation Research
Washington, D.C. 20591

Statistical Data for the Boeing-747-400 Aircraft in Commercial Operations

January 2005

Final Report

U.S. Department of Transportation
Federal Aviation Administration

NOTICE

Technical Report Documentation Page

1. Report No.	2. Government Accession No.	3. Recipient's Catalog No.
DOT/FAA/AR-04/44		

4. Title and Subtitle	5. Report Date
STATISTICAL DATA FOR THE BOEING-747-400 AIRCRAFT IN COMMERCIAL OPERATIONS	January 2005
	6. Performing Organization Code

7. Author(s)	8. Performing Organization Report No.
Todd Jones, John W. Rustenburg, Donald A. Skinn, Daniel O. Tipps, and Thomas DeFiore	UDR-TR-2003-00159

9. Performing Organization Name and Address	10. Work Unit No. (TRAIS)
University of Dayton Research Institute Structural Integrity Division 300 College Park Dayton, OH 45469-0120	11. Contract or Grant No. Grant No. 2001-G-005

12. Sponsoring Agency Name and Address	13. Type of Report and Period Covered
U.S. Department of Transportation Federal Aviation Administration Office of Aviation Research Washington, DC 20591	Final Report
	14. Sponsoring Agency Code ANM-100

15. Supplementary Notes

The Federal Aviation Administration William J. Hughes Technical Center COTR was Thomas DeFiore.

16. Abstract

The Federal Aviation Administration (FAA), supported by the University of Dayton, conducts research on the structural integrity requirements for the U.S. commercial transport airplane fleet. The primary objective of this research is to support the FAA airborne data monitoring systems research program by developing new and improved methods and criteria for processing and presenting large commercial transport airplane flight and ground loads usage data. The scope of activities performed involved (1) defining the service-related factors that affect the operational life of commercial aircraft; (2) designing an efficient software system to reduce, store, and process large quantities of optical quick-access recorder data; and (3) providing processed data in formats that will enable the FAA to reassess existing certification criteria. Equally important, these new data will also enable the FAA, the aircraft manufacturers, and the airlines to better understand and control those factors that influence the structural integrity of commercial transport aircraft.

Presented herein are analyses and statistical summaries of the data collected from 11,066 flights representing 95,883 flight hours from Boeing 747-400 aircraft during operational usage recorded by a single airline. The flight loads data include statistical information on accelerations, speeds, altitudes, flight duration and distance, gross weights, speed brake cycles, thrust reverser usage, and gust velocities encountered. In addition, specialized aircraft usage data that the FAA can use to support development of ground loads certification criteria are included. These new data formats show aircraft usage as it relates to aircraft speed, attitude, and rate data at touchdown by airport. Statistical data were also developed to provide the FAA with information that it can use to establish the initial design requirements for an onboard nitrogen-generating system to be used for fuel tank inerting. These statistical formats were developed from 1984 flights to show how the B-747-400 descent rates vary during the descent phase of the flight as a function of altitude, gross weight, engine rotor speed, and computed airspeed for operations into capacity-limited and non-capacity-limited airports.

17. Key Words	18. Distribution Statement
Optical quick access recorder, Flight profiles, Flight loads, Ground loads, Systems operational data, Statistical loads data, Descent profiles, Descent rate	This document is available to the public through the National Technical Information Service (NTIS) Springfield, Virginia 22161.

19. Security Classif. (of this report)	20. Security Classif. (of this page)	21. No. of Pages	22. Price
Unclassified	Unclassified	241	

PREFACE

The Flight Systems Integrity Group of the Structural Integrity Division at the University of Dayton Research Institute performed this work under Federal Aviation Administration (FAA) Grant No. 2001-G-005 entitled "Assessment of Actual Operational Usage on Large Wide-Body Transport Aircraft." The program manager for the FAA was Mr. Thomas DeFiore of the FAA William J. Hughes Technical Center at Atlantic City International Airport, New Jersey, and the program technical advisor was Mr. John Howford, FAA Chief Scientific and Technical Advisor for Loads/Aeroelasticity. Mr. Daniel Tipps was the principal investigator for the University of Dayton and provided overall technical direction for this effort. Mr. Donald Skinn developed the data reduction algorithms, programmed the data reduction criteria, and performed the data reduction. Mr. John Rustenburg and Mr. Todd Jones performed the data analysis, created the graphical presentations, and prepared the final report.

TABLE OF CONTENTS

APPENDICES

LIST OF FIGURES

LIST OF TABLES

LIST OF ACRONYMS

c.g.	Center of gravity
DFDAU	Digital Flight Data Acquisition Unit
DFDR	Digital Flight Data Recorder
FAA	Federal Aviation Administration
GAG	Ground-air-ground
MO	Magneto-optical
OQAR	Optical Quick-Access Recorder
PSD	Power spectral density
rms	Root mean square
UDRI	University of Dayton Research Institute

EXECUTIVE SUMMARY

The University of Dayton supports the Federal Aviation Administration (FAA) by conducting research on the structural integrity requirements for the U.S. commercial transport airplane fleet. The primary objective of this research is to support the FAA Airborne Data Monitoring Systems Research Program by developing new and improved methods and criteria for processing and presenting large commercial transport airplane flight and ground loads usage data. The scope of activities performed involved (1) defining the service-related factors that affect the operational life of commercial aircraft; (2) designing an efficient software system to reduce, store, and process large quantities of optical quick-access recorder data; and (3) reducing, analyzing, and providing processed data in statistical formats that will enable the FAA to reassess existing certification criteria. Equally important, these new data will also enable the FAA, the aircraft manufacturers, and the airlines to better understand and control those factors that influence the structural integrity of commercial transport aircraft.

Presented herein are analyses and statistical summaries of data collected from 11,066 flights representing 95,883 flight hours of Boeing 747-400 aircraft during operational usage recorded by a single airline. The flight loads data include statistical information on accelerations, speeds, altitudes, flight duration and distance, gross weights, speed brake cycles, thrust reverser usage, and gust velocities encountered. In addition, specialized aircraft usage data that the FAA can use to support development of ground loads certification criteria are included. These new data formats show aircraft usage as it relates to aircraft speed, attitude, and rate data at touchdown by airport. Statistical data were also developed to provide the FAA with information that it can use to establish the initial design requirements for an onboard nitrogen-generating system to be used for fuel tank inerting. These statistical formats were developed from 1984 flights to show how the B-747-400 descent rates vary during the descent phase of the flight as a function of altitude, gross weight, engine rotor speed, and computed airspeed for operations into capacity-limited and non-capacity-limited airports.

1. INTRODUCTION.

The Federal Aviation Administration (FAA) has an ongoing airborne data monitoring systems research program to collect, process, and evaluate statistical flight and ground loads data from transport aircraft used in normal commercial airline operations. The objectives of this program are (1) to acquire, evaluate, and use typical operational in-service data for comparison with the prior data used in the design and qualification testing of civil transport aircraft and (2) to provide a basis to improve the structural criteria and methods of design, evaluation, and substantiation of future airplanes. The University of Dayton Research Institute (UDRI) supports the FAA's efforts by developing the technology for reducing, processing, analyzing, and reporting on the operational flight and ground loads data received from the airlines participating in the FAA program and by conducting research studies.

Since the inception of the FAA's Airborne Data Monitoring Systems Research Program, the scope of the Flight Loads Program has steadily expanded to include research on data collected from several aircraft operators and on aircraft models such as the Boeing 737, B-767, MD-82/83, A320, CRJ100, and BE-1900D. While current program research efforts are tailored primarily to support the FAA and the aircraft structural design community in evaluating design criteria related to the strength, durability, and damage tolerance of the basic airframe structure, much of the data that are available, when provided in meaningful statistical formats, can provide the aircraft operator with some valuable insight into how its aircraft and aircraft systems are being used during normal flight and ground operations. In an effort to improve the data content and to disseminate meaningful data to the larger community of designers, regulators, and aircraft operators, UDRI has made changes, deletions, and additions to the statistical data formats as presented in past reports. These changes occur throughout the data presentation section of this report.

This report contains statistical flight and ground loads data developed for the B-747-400 aircraft and is based on 11,066 flights and 95,883 hours of aircraft operations by a single airline carrier. It also includes specialized data formats involving aircraft usage that can be used for harmonization of international criteria for ground loads certification. In addition, statistical descent rate information has been developed from 1984 flights that can be used by the FAA to establish initial design requirements for an onboard nitrogen-generating system.

2. AIRCRAFT DESCRIPTION.

The B-747-400 is an advanced long-range airliner that incorporates major aerodynamic improvements over earlier B-747 models, including the addition of winglets to reduce drag, new avionics, and a new flight deck. The B-747-400 has a range of approximately 7,260 nautical miles (13,450 km). It delivers better fuel economy, lower noise, and lower operating costs than the previous B-747 models and continues to be the world's fastest subsonic jetliner, cruising at Mach 0.85.

Table 1 presents certain operational characteristics and major physical dimensions of the B-747-400 aircraft, and figure 1 presents a three-view drawing showing front, top, and side views of the aircraft.

TABLE 1. B-747-400 AIRCRAFT CHARACTERISTICS

Maximum Taxi Weight Maximum Takeoff Weight Maximum Landing Weight Maximum Zero-Fuel Weight	877,000 lb 875,000 lb 652,000 lb 555,000 lb
Fuel Capacity	53,985 U.S. gallons
Four Rolls-Royce RB211-52H	at 59,500 lb maximum thrust each
Wing Span Reference Wing Reference Area Wing MAC Wing Sweep	195.67 ft 5650 ft^2 327.78 in 37.5 degrees
Length Height Tread Wheel Base, Nose to Wing Gear Nose to Body Gear	231 ft 10 in 63 ft 8 in 36 ft 1 in 78 ft 11.5 in 89 ft 0.5 in

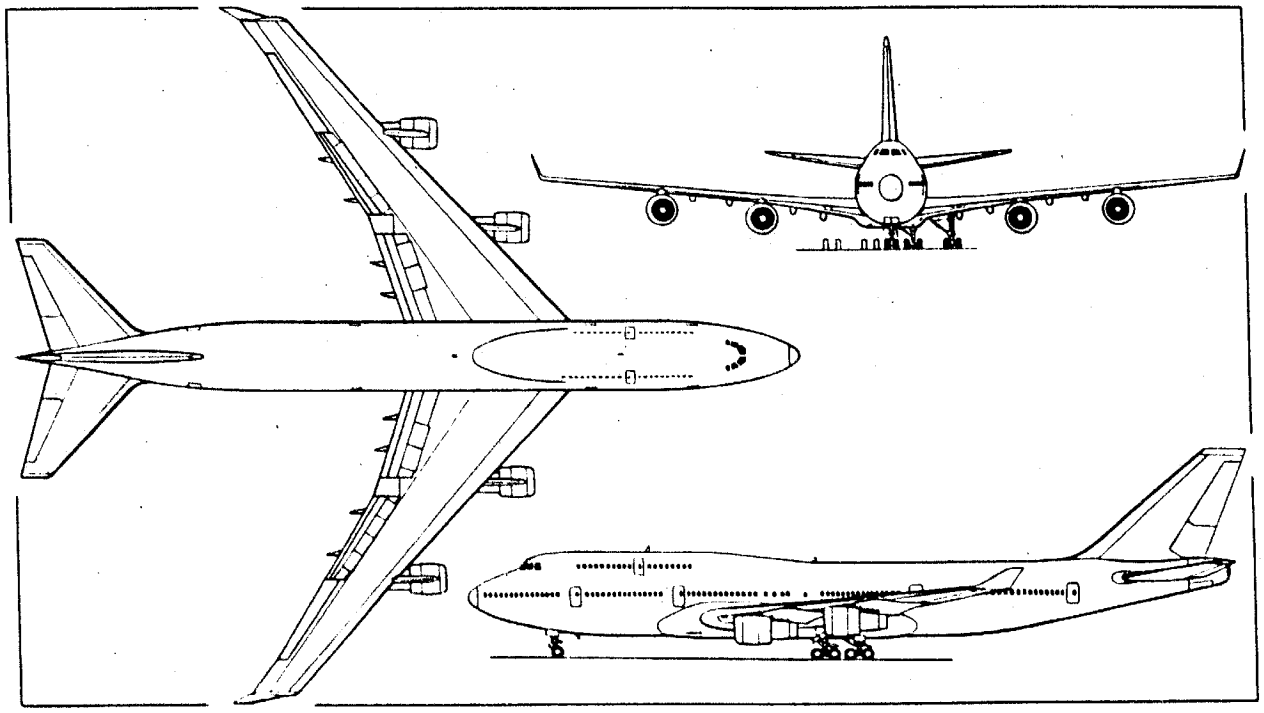

FIGURE 1. B-747-400 THREE-VIEW DRAWING

3. AIRLINE DATA COLLECTION AND EDITING SYSTEMS.

The airline data collection and editing system consists of two major components: (1) the data collection system installed onboard the aircraft and (2) the ground data editing station. A schematic overview of the system is shown in figure 2. The data collection and editing systems are discussed in more detail below.

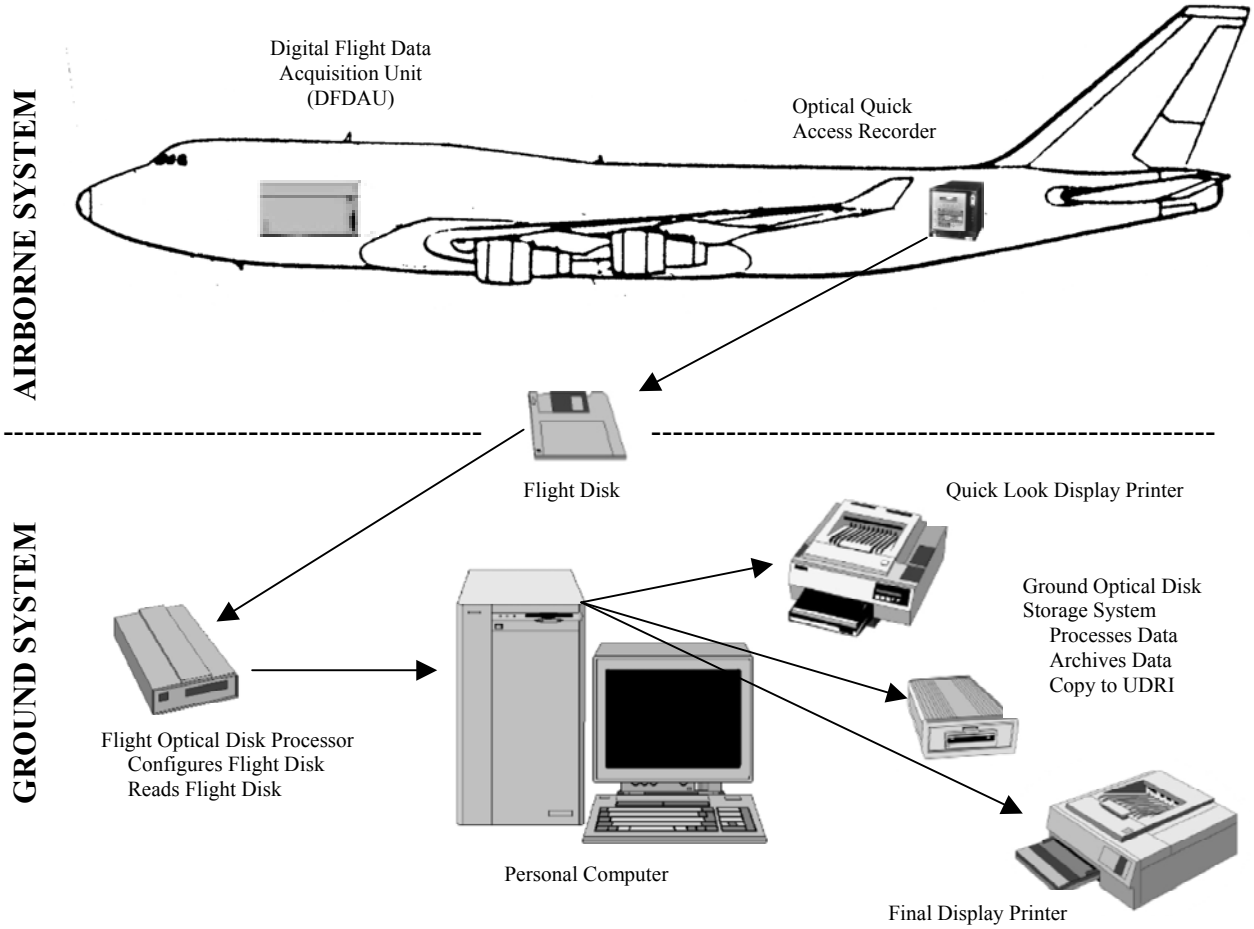

FIGURE 2. AIRLINE RECORDING AND EDITING SYSTEM

3.1 AIRLINE DATA COLLECTION SYSTEM.

The onboard data collection system for the B-747-400 consists of a Digital Flight Data Acquisition Unit (DFDAU), a Digital Flight Data Recorder (DFDR), and an Optical Quick-Access Recorder (OQAR). The DFDAU collects sensor signals and sends parallel data signals to both the DFDR and the OQAR. The OQAR is equipped with an optical disk, which can store up to 300 hours of flight data, whereas the DFDR uses a 25-hour looptape. The optical disk is periodically removed from the OQAR and forwarded to the ground-processing station.

3.2 AIRLINE DATA EDITING SYSTEM.

The airline ground data editing station consists of a computer, a magneto-optical (MO) disk drive, and flight data editing software. The software performs a number of functions during the process of transferring the raw flight data into a DOS file format onto the hard disk. The most important of these functions includes a data integrity check and removal of flight sensitive information. Data considered sensitive are those that can be used to readily identify a specific flight. The desensitized data are forwarded to UDRI for flight loads processing and analysis.

4. UNIVERSITY OF DAYTON RESEARCH INSTITUTE DATA PROCESSING.

The recorded flight and ground loads parameter data were provided by the airline to UDRI on MO disks containing binary files for multiple flights for different airplanes. This section discusses the recorded parameters received from the airline, identifies those parameters processed by UDRI, describes the methods used to extract or compute parameters that are not recorded, and describes how these data are then processed by UDRI through a series of computer software programs to extract the final data required to develop the statistical data formats.

4.1 RECORDED DATA PARAMETERS.

Table 2 lists the recorded data parameters provided by the airline to UDRI for each recorded flight.

TABLE 2. RECORDED PARAMETERS PROVIDED TO UDRI

Parameter	Sampling Rate	Parameter	Sampling Rate
Vertical Acceleration	16 per second	Mach Number	1 per second
Lateral Acceleration	4 per second	Pressure Altitude	1 per second
Longitudinal Acceleration	4 per second	Gross Weight	1 per 64 seconds
Aileron Position - 2 Right and 2 Left	2 per second each	Fuel Quantity	64 per second
Elevator Position - 2 Right and 2 Left	4 per second each	Bank Angle	4 per second
Rudder Position - Upper and Lower	2 per second	Pitch Angle	4 per second
Horizontal Stabilizer Position	1 per second	Magnetic Heading	4 per second
Flap Position - 2 Right and 2 Left	1 per second	True Heading	1 per second
Spoiler/Speed Brake Position - 4 and 12	1 per second each	Latitude	1 per second
N1 Engine - Right and Left	1 per second each	Longitude	1 per second
N2 Engine - Right and Left	1 per second each	Total Air Temperature	1 per second
Thrust Reverser Status - Engine 1 and 2	1 per second each	Radio Altitude	1 per second
Throttle Resolver Angle - 2 Right and 2 Left	1 per second each	Autopilot - Left, Center, Right	1 per second each
Exhaust Gas Temperature - 2 Right and 2 Left	1 per second each	Anti-Ice, 2 Wing, 4 Nacelle, 4 Cowling	1 per second each

TABLE 2. RECORDED PARAMETERS PROVIDED TO UDRI (Continued)

Parameter	Sampling Rate	Parameter	Sampling Rate
Squat Switch - Main, Right/Left and Nose	16 per second each 2 per second	Inertial Vertical Velocity	4 per second
Landing Gear Down and Locked - 4 Main Gear, Nose Gear	1 per second each	Glide Slope - Left, Center, Right	1 per second
Brake Pedal Angle - Right and Left	2 per second each	Wind Speed	1 per second
Calibrated Airspeed	4 per second	Wind Direction	1 per second
True Airspeed	1 per second		
Ground Speed	4 per second		

However, not all the parameters listed in table 2 are used for statistical analysis and data presentation. The highlighted parameters were used by UDRI to create time history files, compress onto MO disks, and process through the data reduction software for statistical analysis and data presentation.

4.2 COMPUTED PARAMETERS.

Certain information and parameters needed in subsequent data reduction were not recorded and needed to be extracted or derived from available time history data. Derived gust velocity, $U_{de,}$ and continuous gust intensity, U_{σ}, are important statistical load parameters that are derived from measured vertical accelerations. This derivation of U_{de} and U_{σ} requires knowledge of atmospheric density, equivalent airspeed, and dynamic pressure. These values were calculated using equations that express the rate of change of density as a function of altitude based on the International Standard Atmosphere.

4.2.1 Atmospheric Density.

For altitudes below 36,089 feet, the density ρ is expressed as a function of altitude by

$$\rho = \rho_o (1-6.876\times10^{-6}\times H_p)^{4.256} \tag{1}$$

where ρ_0 is air density at sea level (0.0023769 slugs/ft^3) and H_p is pressure altitude (ft). Pressure altitude is a recorded parameter.

4.2.2 Equivalent Airspeed.

Equivalent air speed (V_e) is a function of true airspeed (V_T) and the square root of the ratio of air density at altitude (ρ) to air density at sea level (ρ_0) and is expressed as

$$V_e = V_T\sqrt{\frac{\rho}{\rho_0}} \tag{2}$$

True airspeed (V_T) is derived from Mach number (M) and speed of sound (a):

$$V_T = Ma \tag{3}$$

Mach number is dimensionless and is a recorded parameter. The speed of sound (a) is a function of pressure altitude (H_p) and the speed of sound at sea level and is expressed as

$$a = a_0 \sqrt{(1 - 6.876 \times 10^{-6} \times H_p)} \tag{4}$$

Substituting equations 1 and 4 into equation 2 gives

$$V_e = M \times a_0 \times (1 - 6.876 \times 10^{-6} \times H_p)^{0.5} \times (1 - 6.876 \times 10^{-6} \times H_p)^{2.128} \tag{5}$$

which simplifies to

$$V_e = M \times a_0 \times (1 - 6.876 \times 10^{-6} \times H_p)^{2.626} \tag{6}$$

where the speed of sound at sea level a_0 is 1116.4 fps or 661.5 knots.

4.2.3 Dynamic Pressure.

The dynamic pressure (q) is calculated from the air density and velocity as

$$q = \frac{1}{2} \rho V^2 \tag{7}$$

where

ρ = air density at altitude (slugs/ft^3)
V = true air speed (ft/sec)

4.2.4 Derived Gust Velocity.

The derived gust velocity (U_{de}) is computed from the peak values of gust incremental vertical acceleration as

$$U_{de} = \frac{\Delta n_z}{\overline{C}} \tag{8}$$

where Δn_z is the gust peak incremental vertical acceleration and $\overline{C}$ is the aircraft discrete gust response factor considering the plunge-only degree of freedom and is calculated from

$$\overline{C} = \frac{\rho_0 V_e C_{L_\alpha} S}{2W} K_g \tag{9}$$

where

ρ_0 = 0.002377 slugs/ft^3, standard sea level air density
V_e = equivalent airspeed (ft/sec)
C_{L_α} = aircraft lift-curve slope per radian
S = wing reference area (ft^2)
W = gross weight (lb)
K_g = $\dfrac{0.88\mu}{5.3+\mu}$ = gust alleviation factor
μ = $\dfrac{2W}{\rho g \bar{c} C_{L_\alpha} S}$
ρ = air density, slug/ft^3, at pressure altitude (Hp), from equation 1
g = 32.17 ft/sec^2
$\bar{c}$ = wing mean geometric chord (ft)

In this program, the lift-curve slope, C_{L_α}, is the lift-curve slope for the entire airplane.

4.2.5 Continuous Gust Intensity.

Power spectral density (PSD) functions provide a turbulence description in terms of the probability distribution of the root mean square (rms) gust velocities. The rms gust velocities or continuous gust intensities, U_σ, are computed from the peak gust value of vertical acceleration using the PSD technique, as described in reference 1 as

$$U_\sigma = \frac{\Delta n_z}{\overline{A}} \tag{10}$$

where

Δn_z = gust peak incremental vertical acceleration

$\overline{A}$ = aircraft PSD gust response factor = $\dfrac{\rho_0 V_e C_{L\alpha} S}{2W} F(PSD)\ in\ \dfrac{1}{ft/sec}$ (11)

ρ_0 = 0.002377 slugs/ft^3, standard sea level air density
V_e = equivalent airspeed (ft/sec)
C_{L_α} = aircraft lift-curve slope per radian
S = wing reference area (ft^2)
W = gross weight (lb)

$$F(PSD) = \frac{11.8}{\sqrt{\pi}}\left[\frac{\bar{c}}{2L}\right]^{\frac{1}{3}} \sqrt{\frac{\mu}{110+\mu}},\ dimensionless \tag{12}$$

$\bar{c}$ = wing mean geometric chord (ft)
L = turbulence scale length, 2500 ft

$$\mu = \frac{2W}{\rho g \bar{c} C_{L_\alpha} S}, \; dimensionless \tag{13}$$

ρ = air density (slugs/ft^3)
g = 32.17 ft/sec^2

To determine the number of occurrences (N) for U_σ, calculate

$$N = \frac{N_0(o)_{ref}}{N_0(o)} = \frac{\pi \bar{c}}{203} \left[\frac{\rho}{\rho_0} \mu \right]^{0.46}, \; dimensionless \tag{14}$$

where $\bar{c}$, ρ, ρ_0, and μ are defined above. Then each U_σ peak is counted as N counts at that U_σ value. This number of counts is used to determine the number of counts per nautical mile (*nm*),or

$$\frac{counts}{nm} = \left(\frac{N}{distance\ flown\ in\ counting\ interval} \right) \tag{15}$$

Finally, the number of such counts is summed from the largest plus or minus value toward the smallest to produce the cumulative counts per nautical mile.

4.2.6 Flight Distance.

The flight distance was obtained either by determining the stage length of the flight or by integrating the range with respect to changes in aircraft velocity as a function of time.

The stage length was defined as the distance from departure airport to destination airport and was determined as the great circle distance in nautical miles between the point of liftoff (departure) and the point of touchdown (destination). Appendix B describes the calculation of great circle distance. The time histories of longitude and latitude are matched against the UDRI-generated phase of flight file to determine the geographical location of the aircraft at the point of liftoff and the point of touchdown.

The integrated flight distance, D, is obtained by the numerical integration from the time at liftoff (t_0) to the time of touchdown (t_n), and V_T is the average true velocity during Δt.

$$D = \sum_{t_0}^{t_n} \Delta t \cdot V_T \tag{16}$$

4.2.7 Rate of Climb.

Although the rate of climb was a recorded value on the B-747-400, it was not always a recorded value on other aircraft; therefore, UDRI continued its previous practice of calculating these

values. The rate of climb was obtained by numerical differentiation of the change in pressure altitude with time.

$$RC = \sum_{t_1}^{t_2} \frac{\Delta H_p}{\Delta t} \tag{17}$$

4.3 DATA REDUCTION OPERATIONS.

The data reduction phase retrieved the data from the MO disks provided by the airline, processed it through a series of computer programs that convert the data to UDRI-compatible formats, and provided statistical information on aircraft usage, ground loads, flight loads, and systems operation. The data processing flow chart is shown in figure 3, and the flow of the processed data is discussed in subsequent paragraphs.

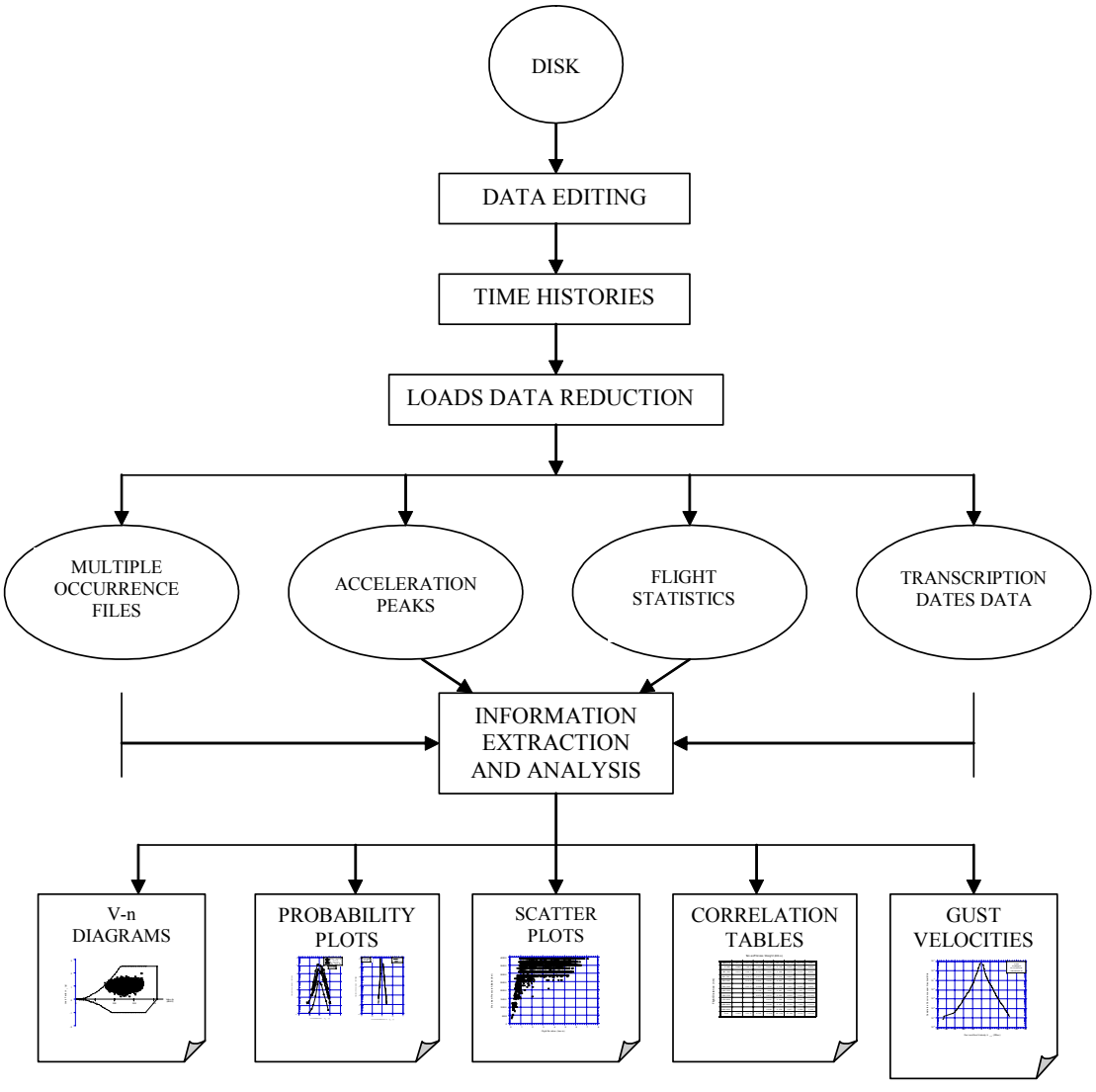

FIGURE 3. DATA PROCESSING FLOW CHART

4.3.1 Initial Quality Screening.

All incoming data files were screened for acceptability. Individual flights were edited to remove erroneous or meaningless data such as discontinuous elapsed time data, evidence of nonfunctional channels or sensors, incomplete flight phases, and duplicate data sets. Files with missing, incomplete, or duplicate data were identified.

4.3.2 Time History Files.

Each MO disk provided by the airline contains multiple flights for each airplane. The files on the MO disks were separated into individual parameter time history files for each flight. Then the time history files were compressed and stored on the same 230-MB MO disks for later recall by the flight loads processing software. Data editing and verification were performed on the data as the time histories were being prepared. Message alerts indicate that obviously erroneous data have been removed and/or that questionable data have been retained but need to be manually reviewed prior to their acceptance. Table 3 lists the limits against which the data were compared. Some of the parameters from table 1 are edited and retained even though they are not currently being used.

TABLE 3. PARAMETER EDITING VALUES

Item	Minimum	Maximum
Gross Weight	400,000 lb	875,000 lb
Pressure Altitude (*Hp*)	-2,000 ft	45,000 ft
Calibrated Airspeed	0 kts	450 kts
Vertical Acceleration	-2.0 g	+4.0 g
Lateral Acceleration	-1.0 g	+1.0 g
Longitudinal Acceleration	-1.0 g	+1.0 g
Flap Handle Position	0°	40°
Elevator Position	-31°	+20°
Aileron Position	-26°	+26°
Rudder Position	-60°	+60°
Trim Position	-13.5°	+4°
Speed Brake Position	0°	51°
Throttles 1 and 2	-25°	45°
Engine N_1 and N_2	0%	120%
Thrust Reverser Status	0	1
Squat Switch (main gear)	0	1
Pitch Attitude	-10°	+30°
Bank Attitude	-40°	+40°
Mach Number	0	0.95

TABLE 3. PARAMETER EDITING VALUES (Continued)

Item	Minimum	Maximum
Ground Speed	0 kts	600 kts
Fuel Quantity	0	390,000 lb
Latitude	-90°	+90°
Longitude	-180°	+180°
Magnetic Heading	0°	360°
Radio Altitude	-20 ft	< 2,500 ft
Anti-Ice	0	1
Autopilot	0	1
Landing Gear	0	1
Glide Slope	-10	10
Inertial Vertical Velocity	-9,000 fpm	9,000 fpm
Total Air Temperature	All	All
Wind Direction	0°	360°
Wind Speed	0 kts	500 kts

4.3.3 Relational Database.

Important characteristics about each set of flights received from the airline were recorded in a relational database. The airline identifier, aircraft tail number, and the MO disk identifier received from the airline are in the data. Each flight was assigned a unique flight sequence number. The flight sequence number assigned to the first flight of the set and the number of flights in the set were also entered. The MO disk identifier, which contained the compressed time history files of all flights in the set, was also recorded.

4.3.4 Permanent Data Files.

In addition to the time history files, two other files were created and permanently stored with the time history files. The first file contained the chronologically sorted list of the phases of flight and their corresponding starting times. This file provided the means to separate flight by flight phases in subsequent data analysis processing. The second file contained the accumulated time and distance for various combinations of phase of flight and altitude band. This file provided the capability to present the data results in terms of normalized unit time and distance.

4.3.5 Loads Data Reduction.

The loads data reduction program used the compressed time history files to derive statistical information on aircraft usage, ground loads, flight loads, and systems operations. The data were then reduced in accordance with specific data reduction criteria.

4.4 DATA REDUCTION CRITERIA.

To process the measured data into statistical loads formats, specific data reduction criteria were developed for separating the phases of ground and flight operations, identifying specific events associated with the operation of the aircraft and its onboard systems, assigning sign conventions, determining maximum and minimum values and load cycles, and distinguishing between gust and maneuver load factors. These criteria are discussed in the following paragraphs.

4.4.1 Phases of Flight Profile.

The ground and flight phases were determined by UDRI from the recorded data. Each time history profile was divided into nine phases: four ground phases (taxi-out, takeoff roll, landing roll with and without thrust reverser deployed, and taxi-in) and five airborne phases (departure, climb, cruise, descent, and approach). Figure 4 shows these nine phases of a typical flight profile.

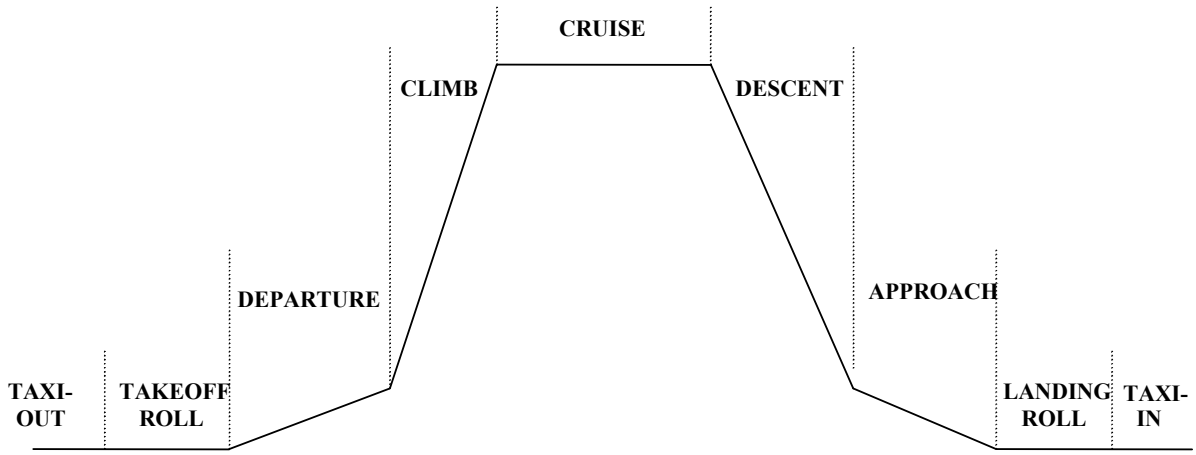

FIGURE 4. DESCRIPTION OF FLIGHT PROFILE PHASES

The criteria used to define each of these phases are summarized in table 4 and discussed in more detail in the following paragraphs.

4.4.1.1 Ground Phases.

Specific data reduction criteria were developed and used to identify the beginning and end of each ground phase of operation (taxi-out, takeoff roll, landing roll with and without thrust reverser deployed, and taxi-in).

The taxi-out phase begins when the ground speed exceeds 1 knot. All aircraft movement until the aircraft begins its takeoff roll is defined as being taxi-out.

The beginning of the takeoff roll was found by searching for ground speeds that accelerated at rates greater than 2 kts/sec for a minimum duration of 20 seconds. Then, when these values were found, the beginning of the takeoff roll was assigned as being the time slice where the first

ground speed rate change greater than 2 kts/sec for that sequence occurred. The takeoff roll ends at liftoff with the squat switch off signal.

TABLE 4. FLIGHT PHASE CRITERIA

Phase of Flight	Defining Condition at Start of Phase
Taxi-Out	From initial aircraft movement
Takeoff Roll	Ground acceleration > 2 kts/sec for at least 20 seconds beginning with the time slice where the first ground speed rate change greater than 2 kts/sec for that sequence occurred
Departure	Liftoff, squat switch off
Climb	Rate of climb ≥ 250 ft/min maintained for at least 1 minute with flaps retracted
Cruise	Rate of climb is between ±250 ft/min and flaps retracted
Descent	Rate of descent ≥ 250 ft/min occurs for at least 1 minute and flaps retracted
Approach	Rate of descent ≤ 250 ft/min occurs for at least 1 minute with flaps extended
Landing Roll	Touchdown, squat switch on
Taxi-In	End of runway turnoff to parked at the gate or recorder shutdown

The landing roll phase was defined as beginning 1 second after the squat switch signaled that the landing touchdown had occurred and ending when the aircraft begins its turnoff from the active runway. The criterion for the turnoff was based on a change in the magnetic heading following landing.

Taxi-in is defined from the point where the aircraft completed its turnoff from the active runway after its landing roll to the point when the aircraft was either parked at the gate or the recorder had shutdown. The criterion for completion of the turnoff used the magnetic heading to identify when the aircraft had either returned to taxiing in a straight line or had turned in the opposite direction.

4.4.1.2 Airborne Phases.

The airborne portion of each flight profile was separated into phases called departure, climb, cruise, descent, and approach. These phases occur between the time that the squat switch turns off at liftoff until it turns on again at landing touchdown. The beginning of each flight phase was defined based on the combinations of the squat switch position, flap settings, and the calculated rate of climb or descent over a period of at least 1 minute, as shown in table 4. Also, by definition, the departure phase cannot be less than 1 minute in length.

It should be noted that an airborne phase could occur several times per flight because it was determined by the rate of climb and the position of the flaps. When this occurs, the flight loads

data are combined and presented as a single flight phase. The UDRI software then creates a file that chronologically lists the phases of flight and their corresponding starting times.

4.4.2 Specific Events.

In addition to the ground and airborne phases, a unique set of criteria was also required to identify certain specific events such as liftoff, landing touchdown, thrust reverser deployment and stowage, and start and completion of turnoff from the active runway after landing. Figure 5 shows these phases and events.

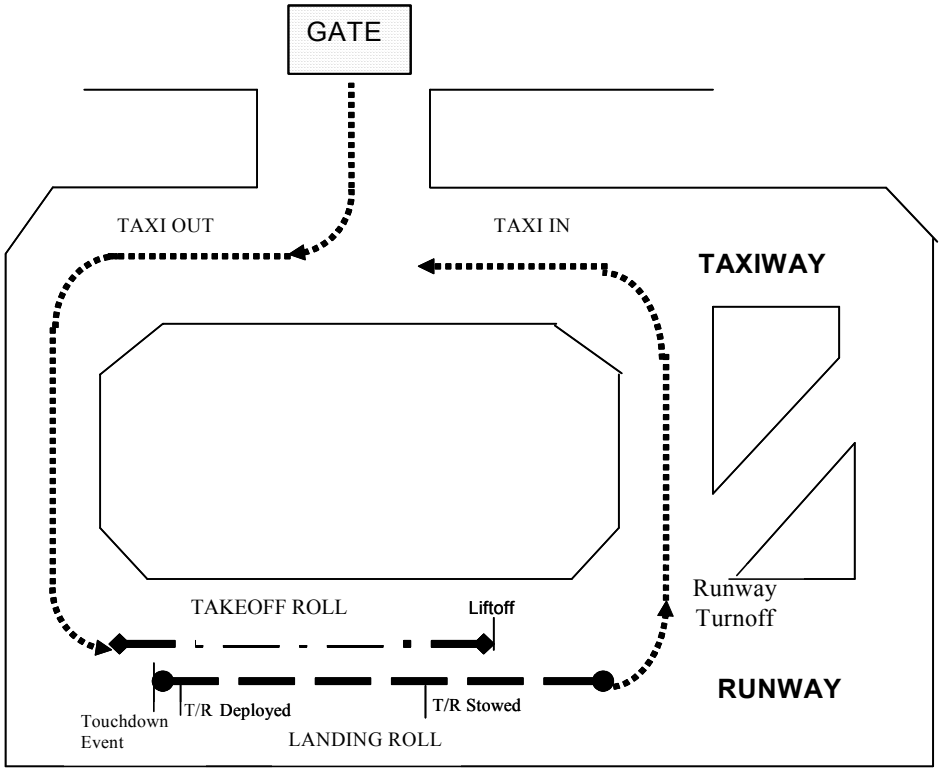

FIGURE 5. GROUND PHASES AND SPECIFIC EVENTS

The criteria used to define each of the specific events are summarized in table 5 and discussed in more detail in reference 2 and in the following paragraphs.

4.4.2.1 Liftoff.

During development of the statistical formats of pitch angle at liftoff and touchdown, UDRI concluded that the squat switch on the B-747-400 was not providing a reliable indication of when liftoff (or touchdown) was actually occurring. Therefore, to determine when liftoff actually occurred, a new algorithm was developed that identifies the liftoff point as the first reading in the series of increasing radio altitude values that were greater than 7 feet higher than the average radio altitude value that it calculated during the takeoff roll.

TABLE 5. SUMMARY OF SPECIFIC EVENTS CRITERIA

Phase/Event	Defining Conditions
Liftoff	Point of first reading in series of increasing radio altitude values greater than 7 feet higher than the average radio altitude value calculated during the takeoff roll
Landing Touchdown	From 5 seconds prior to squat switch on to 1 second afterwards
Thrust Reverser Deployment/Stowage	Thrust reverser switch on for deployment and off for stowage
Runway Turnoff	From first sequential magnetic heading change in the same direction from runway centerline and heading sequence changes >13.5° to a straight line heading or turn in the opposite direction

4.4.2.2 Landing Touchdown.

Previously, for the determination of general landing statistics, the landing touchdown was defined as the time when the landing gear touches down and the squat switch closes. However, as stated above, UDRI discovered that the squat switch on the B-747-400 was not an accurate indicator of when touchdown actually occurred. To ensure that the maximum vertical and side load factors associated with touchdown were identified, the actual touchdown event was deemed to occur within a time frame from 5 seconds prior to, until 1 second following squat switch closure. UDRI decided that it was more important to ensure capturing the touchdown event even if the 5-second time prior to squat switch closure resulted in some minor loss of flight data. The 1-second time after squat switch closure was chosen somewhat arbitrarily, but was intended to ensure that sufficient time was allowed for the aircraft to respond to the touchdown and for the vertical and side load accelerations to build to their maximum values.

4.4.2.3 Thrust Reverser Deployment or Stowage.

An on/off switch identifies when deployment or stowage of the thrust reverser occurs. Thus, by identifying when this occurs as a special event, load factor acceleration data can be obtained at the instant of thrust reverser deployment and during the time of thrust reverser usage and stowage.

4.4.2.4 Runway Turnoff.

Changes in the aircraft's magnetic heading were used to identify the beginning and end of the aircraft's turnoff from the active runway after the landing roll. After the aircraft touched down, subsequent magnetic heading readings were averaged and this average heading was defined as the runway centerline. Subsequent magnetic heading changes were then tested to identify continuous movement in the same direction away from this centerline. When the aircraft's sequential magnetic heading change exceeded 13.5° from the direction of the landing centerline, the time slice associated with the first sequential heading change from the landing centerline in the direction of the turn was defined as the beginning of the turnoff from the runway.

An alternate method was used to identify flights involving shallow turns from the runway that did not exceed the 13.5° turn criteria. This method used aircraft ground speed and magnetic heading to calculate the aircraft's position relative to the runway centerline by identifying when the aircraft's position perpendicular to the runway centerline exceeded 100 feet. The time slice associated with the first aircraft movement away from the landing centerline in the direction of the turn was defined as the beginning of the aircraft's turnoff from the runway.

The end point of the first turnoff from the active runway was also identified using magnetic heading readings. An algorithm was developed that used the changes in magnetic heading, while the aircraft was in its turn, to identify when the aircraft had either returned to taxiing in a straight line or was turning in the opposite direction. The first point that provided this indication was then defined as the end point of the turnoff from the runway. This point was also the beginning of the taxi-in phase.

4.4.3 Sign Conventions.

Acceleration data are recorded in three directions: vertical (z), lateral (y), and longitudinal (x). As shown in figure 6, the positive z direction is up; the positive y direction is starboard; and the positive x direction is forward.

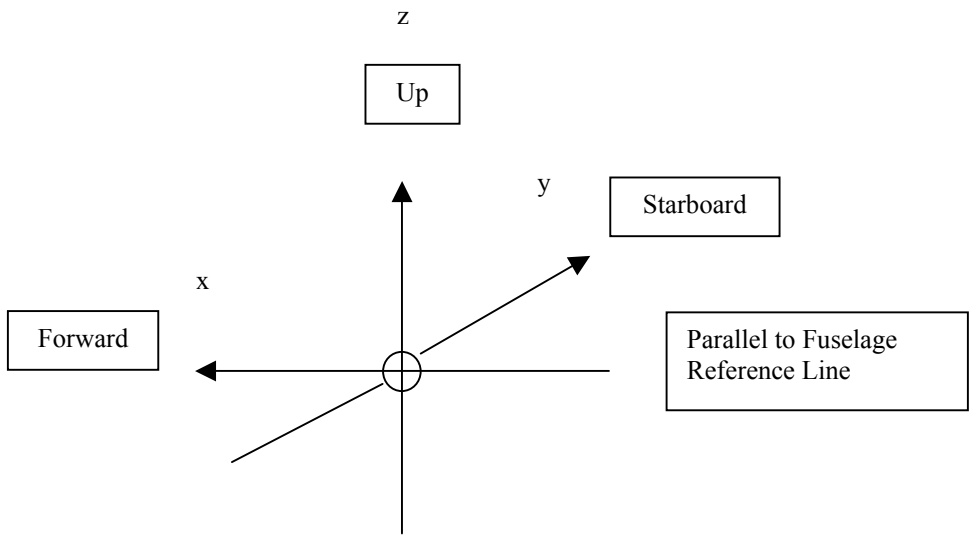

FIGURE 6. SIGN CONVENTION FOR AIRPLANE ACCELERATIONS

4.4.4 Peak Selection Technique.

The peak-between-means method presented in reference 1 was used to identify positive and negative peaks in the acceleration data. This method was consistent with past practices and pertains to all accelerations (n_x, n_y, Δn_z, $\Delta n_{z_{gust}}$, and $\Delta n_{z_{man}}$).

One peak is identified between each two successive crossings of the mean acceleration, which is the 0-g condition for lateral, longitudinal, and incremental vertical accelerations. Peaks greater than the mean were considered positive, and those less than the mean negative. A threshold zone

is defined around the mean, within which acceleration peaks were ignored because they have been shown to be irrelevant. The threshold zone is ±0.05 g for the vertical accelerations Δn_z, $\Delta n_{z_{gust}}$, and $\Delta n_{z_{man}}$, ±0.005 g for lateral acceleration n_y, and ±0.0025 g for longitudinal acceleration n_x.

Figure 7 demonstrates the acceleration peak selection technique. The sample acceleration trace contains eight zero crossings, which are circled, set off by vertical dashed lines, and labeled as C_i, i = 0 to 7. For each of seven intervals between successive mean crossings, C_{i-1} to C_i, i = 1 to 7, one peak, which is located at P_i, is identified. Those peaks lying outside the threshold zone (P_1, P_2, P_5, P_6, and P_7) are accepted and retained; whereas, those peaks lying inside the threshold zone (P_3 and P_4) are ignored.

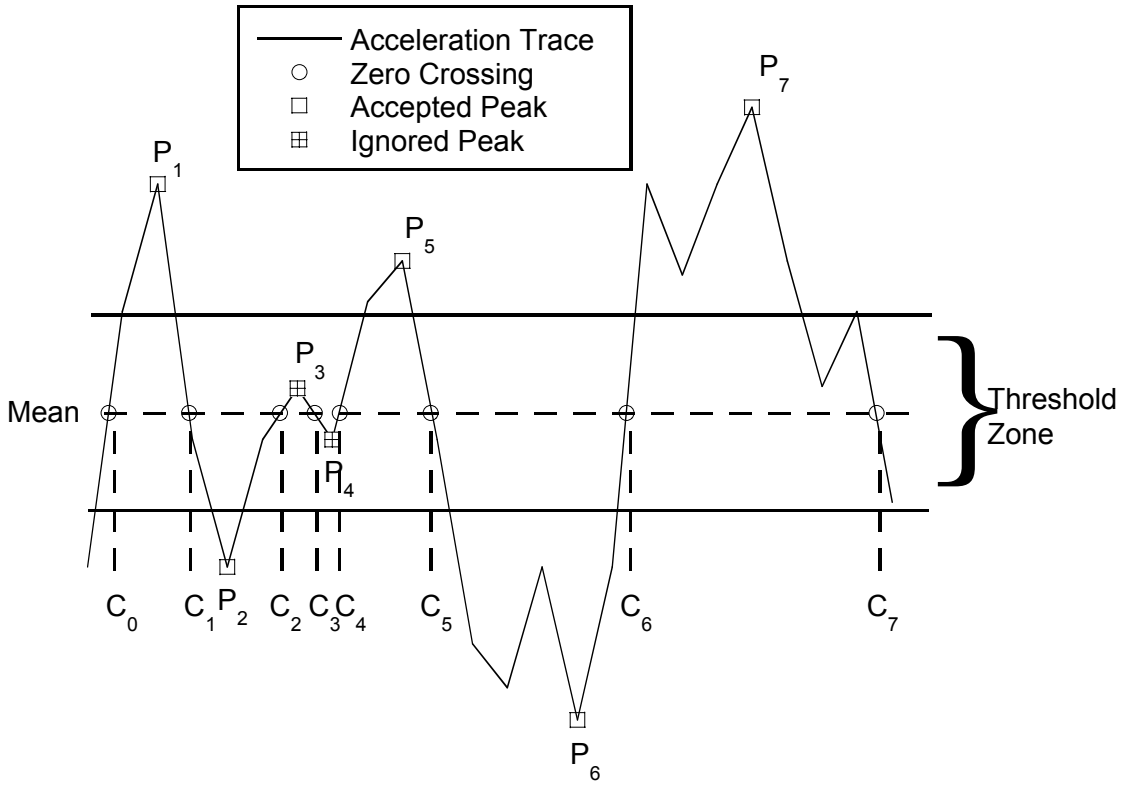

FIGURE 7. THE PEAK-BETWEEN-MEANS CLASSIFICATION CRITERIA

4.4.5 Separation of Maneuver and Gust Load Factors.

Vertical acceleration, n_z, is measured at the center of gravity (c.g.) of the aircraft and incremental vertical acceleration, Δn_z, results from removing the 1-g condition from n_z. The incremental acceleration measured at the c.g. of the aircraft in flight may be the result of either maneuvers or gusts. To derive gust and maneuver statistics, the maneuver-induced acceleration ($\Delta n_{z_{man}}$) and the gust response acceleration ($\Delta n_{z_{gust}}$) must be separated from the total acceleration history. Reference 3 reported the results of a UDRI study to evaluate methods of separating maneuver

and gust load factors from measured acceleration time histories. As a result of this study, UDRI used a cycle duration rule to differentiate maneuver-induced acceleration peaks from those peaks caused by gust loading. A review of the B-747-400 response characteristics has shown that a cycle duration of 2.0 seconds was appropriate for the B-747-400 aircraft and, thus, was used.

4.4.6 Flap Detents.

When flaps are extended, the effective deflection was considered to be that of the applicable detent, as indicated in table 6. The flap deflection ranges and placard speeds reflect the flap operational limits as provided by The Boeing Company.

TABLE 6. FLAP DETENTS (B-747-400)

Flap/Slat Detent	Minimum Flap Setting	Maximum Flap Setting	Operational Airspeed Limit (KCAS)	Design Airspeed Limit (KCAS)
1	> 0°	≤1°	280	280
5	> 1°	≤ 4.6°	260	260
10	> 4.6°	≤ 9.6°	240	252
20	> 9.6°	≤19.6°	230	242
25	> 19.6°	≤24.6°	205	205
30	> 24.6°	≤ 32.6°	180	180

KCAS = Knots calibrated airspeed

5. FLIGHT LOADS DATA PRESENTATION.

The statistical data presented in this section provide the FAA, aircraft manufacturers, and the operating airline with the information that was needed to assess how the B-747-400 aircraft was actually being used in operational service versus its original design or intended usage. The statistical data presented herein can be used by the FAA as a basis to evaluate existing structural certification criteria; to improve requirements for the design, evaluation, and substantiation of existing aircraft; and to establish design criteria for future generations of new aircraft. The aircraft manufacturer can use the data to assess the aircraft's structural integrity by comparing the actual in-service usage of the B-747-400 aircraft versus its originally intended design usage. It can also use the data to derive typical flight profiles and to update structural strength, durability, and damage tolerance analyses to establish or revise maintenance and inspection requirements for critical airframe and structural components. The airline/aircraft operator can use the data to evaluate the aircraft's current usage with respect to established operational procedures and placard limitations. It can also use the data to identify where changes in current operational procedures could provide additional safety margins, increase the service life of structural components, and improve on the economics of its operations.

Table 7 lists all the statistical formats for which the data were processed. The various data formats have been grouped together within the table in an attempt to categorize the B-747-400 data being presented on the basis of whether it pertains to aircraft usage, ground or flight loads data, or systems operational data. The aircraft usage data section describes the aircraft's operational usage in terms of distributions of flight lengths, flight duration, flight phase, flight altitudes, flight speeds, takeoff and landing gross weights, etc. The loads and system data section describe the flight and ground environment and the induced system cyclic loadings experienced by the aircraft while the aircraft performs its intended usage.

TABLE 7. STATISTICAL DATA FORMATS

Data Description	Figure
AIRCRAFT USAGE DATA	
WEIGHT AND FLIGHT DISTANCE DATA	
Cumulative Probability Distributions of Takeoff Gross Weight	A-1
Cumulative Probability Distributions of Landing Gross Weight	A-2
Cumulative Probability Distributions of Great Circle Flight Length	A-3
Correlation of Great Circle Flight Length and Integrated Flight Distance	A-4
Correlation of Takeoff Gross Weight and Great Circle Flight Length	A-5
Correlation of Takeoff Gross Weight and Great Circle Flight Length, Percent of Flights	A-6
Correlation of Takeoff and Landing Gross Weight, Percent of Flights	A-7
Percent of Integrated Flight Distance in Altitude Bands	A-8
ALTITUDE, SPEED, AND TEMPERATURE DATA	
Correlation of Maximum Altitude and Flight Duration	A-9
Cumulative Probability of Maximum Ground Speed During Taxi	A-10
Maximum Mach Number and Coincident Altitude, All Flight Phases	A-11
Maximum Calibrated Airspeed and Coincident Altitude, All Flight Phases	A-12
Cumulative Probability of Airspeed at Liftoff and Touchdown	A-13
Total Air Temperature vs True Airspeed, Altitude < 500 Feet	A-14
Total Air Temperature vs True Airspeed, Altitude 500-1500 Feet	A-15
Total Air Temperature vs True Airspeed, Altitude 1500-4500 Feet	A-16
Total Air Temperature vs True Airspeed, Altitude 4500-9500 Feet	A-17
Total Air Temperature vs True Airspeed, Altitude 9,500-19,500 Feet	A-18
Total Air Temperature vs True Airspeed, Altitude 19,500-29,500 Feet	A-19
Total Air Temperature vs True Airspeed, Altitude 29,500-39,500 Feet	A-20
Total Air Temperature vs True Airspeed, Altitude 39,500+ Feet	A-21
ATTITUDE DATA	
Cumulative Probability of Pitch Angle at Liftoff	A-22
Cumulative Probability of Pitch Angle at Touchdown	A-23
Cumulative Probability of Maximum Pitch Angle During Departure and Approach	A-24

TABLE 7. STATISTICAL DATA FORMATS (Continued)

Data Description	Figure
GROUND LOADS DATA	
LATERAL LOAD FACTOR, n_y	
Cumulative Frequency of Maximum Lateral Load Factor During Ground Turns	A-25
Cumulative Frequency of Maximum Lateral Load Factor at Touchdown	A-26
Cumulative Frequency of Maximum Lateral Load Factor During Runway Turnoff	A-27
Maximum Lateral Load Factor and Coincident Incremental Vertical Load Factor at Touchdown	A-28
Probability Distributions of Turning Angle During Runway Turnoff	A-29
Maximum Lateral Load Factor and Coincident Ground Speed During Runway Turnoff, 0-60 Degree Turns	A-30
Maximum Lateral Load Factor and Coincident Ground Speed During Runway Turnoff, 60-120 Degree Turns	A-31
Maximum Lateral Load Factor and Coincident Ground Speed During Runway Turnoff, 120-240 Degree Turns	A-32
Maximum Lateral Load Factor at Touchdown vs Maximum Yaw Angle Before Touchdown	A-33
Maximum Lateral Load Factor at Touchdown vs Mean Yaw Angle Before Touchdown	A-34
Maximum Lateral Load Factor at Touchdown vs Maximum Bank Angle Before Touchdown	A-35
LONGITUDINAL LOAD FACTOR, n_x	
Cumulative Frequency of Longitudinal Load Factor During Taxi Operations	A-36
Cumulative Frequency of Longitudinal Load Factor at Touchdown and During Landing Roll	A-37
VERTICAL LOAD FACTOR, n_z	
Cumulative Frequency of Incremental Vertical Load Factor During Taxi Operations	A-38
Cumulative Frequency of Incremental Vertical Load Factor During Takeoff Roll	A-39
Cumulative Frequency of Incremental Vertical Load Factor at Spoiler Deployment and at Touchdown	A-40
Cumulative Frequency of Incremental Vertical Load Factor During Landing Roll	A-41
Maximum Incremental Vertical Load Factor at Touchdown vs Maximum Yaw Angle Before Touchdown	A-42
Maximum Incremental Vertical Load Factor at Touchdown vs Mean Yaw Angle Before Touchdown	A-43
Maximum Incremental Vertical Load Factor at Touchdown vs Maximum Bank Angle Before Touchdown	A-44
Maximum Incremental Vertical Load Factor at Touchdown vs Coincident Airspeed	A-45
Aircraft Runway Acceleration Response	A-46
FLIGHT LOADS DATA	
GUST VERTICAL LOAD FACTOR DATA	
Cumulative Occurrences of Incremental Vertical Gust Load Factor per 1000 Hours by Flight Phase	A-47
Cumulative Occurrences of Incremental Vertical Gust Load Factor per 1000 Hours, Combined Flight Phases	A-48
Cumulative Occurrences of Incremental Vertical Gust Load Factor per Nautical Mile by Flight Phase	A-49
Cumulative Occurrences of Incremental Vertical Gust Load Factor per Nautical Mile, Combined Flight Phases	A-50
DERIVED GUST VELOCITY DATA	
Cumulative Occurrences of Derived Gust Velocity per Nautical Mile, < 500 Feet	A-51
Cumulative Occurrences of Derived Gust Velocity per Nautical Mile, 500-1,500 Feet	A-52
Cumulative Occurrences of Derived Gust Velocity per Nautical Mile, 1,500-4,500 Feet	A-53
Cumulative Occurrences of Derived Gust Velocity per Nautical Mile, 4,500-9,500 Feet	A-54
Cumulative Occurrences of Derived Gust Velocity per Nautical Mile, 9,500-19,500 Feet	A-55
Cumulative Occurrences of Derived Gust Velocity per Nautical Mile, 19,500-29,500 Feet	A-56
Cumulative Occurrences of Derived Gust Velocity per Nautical Mile, 29,500-39,500 Feet	A-57
Cumulative Occurrences of Derived Gust Velocity per Nautical Mile, 39,500-44,500 Feet	A-58
Cumulative Occurrences of Derived Gust Velocity per Nautical Mile, Flaps Extended	A-59

TABLE 7. STATISTICAL DATA FORMATS (Continued)

Data Description	Figure
DERIVED GUST VELOCITY DATA	
Cumulative Occurrences of Derived Gust Velocity per Nautical Mile, Flaps Retracted	A-60
CONTINUOUS GUST INTENSITY DATA	
Cumulative Occurrences of Continuous Gust Intensity per Nautical Mile, Flaps Extended	A-61
Cumulative Occurrences of Continuous Gust Intensity per Nautical Mile, Flaps Retracted	A-62
GUST V-n DIAGRAM DATA	
Gust Load Factor and Coincident Speed vs V-n Diagram for Flaps Retracted	A-63
Gust Load Factor and Coincident Speed vs V-n Diagram for Flaps Extended, Detents 1, 5, 10, 20, 25, and 30	A-64
MANEUVER VERTICAL LOAD FACTOR DATA	
Cumulative Occurrences of Incremental Vertical Maneuver Load Factor per 1000 Hours During Departure by Altitude	A-65
Cumulative Occurrences of Incremental Vertical Maneuver Load Factor per 1000 Hours During Climb by Altitude	A-66
Cumulative Occurrences of Incremental Vertical Maneuver Load Factor per 1000 Hours During Cruise by Altitude	A-67
Cumulative Occurrences of Incremental Vertical Maneuver Load Factor per 1000 Hours During Descent by Altitude	A-68
Cumulative Occurrences of Incremental Vertical Maneuver Load Factor per 1000 Hours During Approach by Altitude	A-69
Cumulative Occurrences of Incremental Vertical Maneuver Load Factor per Nautical Mile During Departure by Altitude	A-70
Cumulative Occurrences of Incremental Vertical Maneuver Load Factor per Nautical Mile During Climb by Altitude	A-71
Cumulative Occurrences of Incremental Vertical Maneuver Load Factor per Nautical Mile During Cruise by Altitude	A-72
Cumulative Occurrences of Incremental Vertical Maneuver Load Factor per Nautical Mile During Descent by Altitude	A-73
Cumulative Occurrences of Incremental Vertical Maneuver Load Factor per Nautical Mile During Approach by Altitude	A-74
Cumulative Occurrences of Incremental Vertical Maneuver Load Factor per 1000 Hours by Flight Phase	A-75
Cumulative Occurrences of Incremental Vertical Maneuver Load Factor per 1000 Hours, Combined Flight Phases	A-76
Cumulative Occurrences of Incremental Vertical Maneuver Load Factor per Nautical Mile by Flight Phase	A-77
Cumulative Occurrences of Incremental Vertical Maneuver Load Factor per Nautical Mile, Combined Flight Phases	A-78
MANEUVER V-n DIAGRAM DATA	
Maneuver Load Factor and Coincident Speed vs V-n Diagram for Flaps Retracted	A-79
Maneuver Load Factor and Coincident Speed vs V-n Diagram for Flaps Extended, Detents 1, 5, 10, 20, 25, 30	A-80
COMBINED MANEUVER AND GUST VERTICAL LOAD FACTOR DATA	
Cumulative Occurrences of Incremental Vertical Load Factor per 1000 Hours by Flight Phase	A-81
Cumulative Occurrences of Incremental Vertical Load Factor per 1000 Hours, Combined Flight Phases	A-82
Cumulative Occurrences of Incremental Vertical Load Factor per Nautical Mile by Flight Phase	A-83
Cumulative Occurrences of Incremental Vertical Load Factor per Nautical Mile, Combined Flight Phases	A-84
COMBINED MANEUVER AND GUST LATERAL LOAD FACTOR DATA	
Cumulative Occurrences of Lateral Load Factor per 1000 Hours by Flight Phase	A-85
Maximum Lateral Load Factor vs Coincident Gross Weight During Departure	A-86
Maximum Lateral Load Factor vs Coincident Gross Weight During Climb	A-87
Maximum Lateral Load Factor vs Coincident Gross Weight During Cruise	A-88
Maximum Lateral Load Factor vs Coincident Gross Weight During Descent	A-89
Maximum Lateral Load Factor vs Coincident Gross Weight During Approach	A-90

TABLE 7. STATISTICAL DATA FORMATS (Continued)

Data Description	Figure
GROUND-AIR-GROUND CYCLE DATA	
Ground-Air-Ground Cycle Occurrences of Maximum and Minimum Incremental Vertical Load Factor	A-91
Three-Dimensional Plot of Ground-Air-Ground Cycles	A-92
SYSTEMS OPERATIONAL DATA	
FLAP USAGE DATA	
Cumulative Probability of Maximum Airspeed in Flap Detent During Departure	A-93
Relative Probability of Maximum Airspeed in Flap Detent During Departure	A-94
Cumulative Probability of Maximum Airspeed in Flap Detent During Approach	A-95
Relative Probability of Maximum Airspeed in Flap Detent During Approach	A-96
Percent of Time in Flap Detent During Departure	A-97
Percent of Time in Flap Detent During Approach	A-98
SPEED BRAKE USAGE DATA	
Probability Distributions of Speed at Speed Brake Deployment	A-99
Probability Distributions of Maximum Speed During Speed Brake Deployment	A-100
Probability Distributions of Altitude at Speed Brake Deployment	A-101
Probability Distributions of Maximum Deployment Angle During Speed Brake Deployment	A-102
Total Hours of Coincident Speed Brake Deflection and Flap Detent	A-103
THRUST REVERSER DATA	
Cumulative Probability of Time with Thrust Reversers Deployed	A-104
Cumulative Probability of Speed at Thrust Reverser Deployment and Stowage	A-105
PROPULSION DATA	
Cumulative Probability of Percent of N_1 During Takeoff, at Thrust Reverser Deployment, and During Thrust Reverser Deployment	A-106

Figures A-1 through A-106 are presented in appendix A. For ease of understanding, most of the figures in appendix A are presented in graphical form with a minimum of numerical summaries. In an effort to make the data presentation of a more comprehensive nature, some figures include both cumulative and relative probability or frequency distribution histograms as well as line plots. Scatter plots are also included where appropriate to show the relationship between coincident parameters that are considered to be of interest and to show visible evidence of relationships, outliers, or suspicious data. The scatter plots presented in this report show that many of the plotted parameters are not related but occur in an independent random nature.

It should also be noted that the data presented in these figures are not always based on an identical number of flights or flight hours. During data reduction it was discovered that some data frames and parameters exhibited random errors and were, thus, judged to be unacceptable for use. When this occurred, those questionable data were eliminated from the statistical database for any application, either directly or indirectly, that could influence the presentation of the other data measurements. As a result, not all figures are based on data from an identical number of flights, hours, or nautical miles.

5.1 AIRCRAFT USAGE DATA.

Figures A-1 through A-16 provide statistical data on the aircraft's operational usage. Information on takeoff and landing gross weights, operational flight speeds and altitudes, aircraft attitude, and flight lengths based on normal everyday flight operations are presented. These data are primarily useful in defining typical flight profiles, including gross weight, speed, altitude, and the number of flights associated with each type profile.

5.1.1 Weight and Flight Distance Data.

This section presents statistical data on operational takeoff and landing gross weights, flight distances, and plots showing the correlation between weight and flight distance. The flight distances in figures A-1 through A-16 are based on the great circle distance (sometimes referred to as stage length) between departure and arrival points, except for figure A-4, which compares two methods of determining flight distance.

The cumulative probability distributions of gross weight during takeoff and landing are presented in figures A-1 and A-2. The occurrences of takeoff gross weight show a wide variation as one would expect due to differing fuel weights for different length flights and variable passenger and baggage loading. The landing weight distribution shows some tendency to group within a narrower range that could indicate attempts to land at a planned landing weight. It is noteworthy that some landing gross weights observed were close to the maximum design landing gross weight of 652,000 lb, listed in table 1. These were possibly associated with a flight of short duration at high takeoff weights where the airplane is fueled through, i.e., the aircraft is not refueled between flights. Figure A-6 shows the occurrence of such flights.

Figure A-3 shows the cumulative probability distribution of the great circle flight length for all B-747-400 flights. The distribution shows that 95% of all flights exceed 2500-nautical miles in length.

Figure A-4 presents a scatter plot comparison of the differences in the great circle flight length and the integrated flight distance. The great circle flight length reflects the calculated straight-line flight distance between two points in still air. The integrated flight distances represent the airborne distance flown relative to the ambient air and accounts for the impact of winds, deviations from straight-line flight, and loiter on the total distance flown by the aircraft. These distances will always be different because of deviations that occur during the flight, resulting from directional flight changes directed by the air traffic control center, increased distance flown due to holding patterns, wind direction, and to a much lesser extent, the climb and descent distances that are slightly larger than the level flight distance. For operation of the B-747-400, figure A-4 indicates that the integrated flight distance tends to be slightly longer than the great circle flight length. Hence, the aircraft is subjected to the loading environment for a longer period of time than if only the great circle flight length was considered. The flights shown with no change in great circle flight length were probably test flights or flights that turned back because they returned to the same takeoff location.

Figures A-5 and A-6 compare aircraft gross weight at takeoff with distance flown to determine whether there is any correlation between the two parameters. Figure A-5 compares the takeoff gross

weight versus the great circle flight distance flown for each individual flight as a scatter plot, whereas figure A-6 contains a tabular listing of the percent of flights that took off within the interval of gross weight shown and those that landed within the specified flight distance. While both figures indicate there is a wide variation in takeoff gross weights and flight lengths, the data does show some correlation between gross weight and great circle flight length, although considerable scatter is evident. The data also indicate that the aircraft is mostly used for flight distances exceeding 2500 nautical miles.

Figure A-7 provides a tabular listing of the percent of flights that takeoff and land within the gross weight ranges indicated. The data indicate that about 83% of the flights takeoff in a gross weight range between 650,000-900,000 lb. and about 89% of the flights land at weights between 500,000-650,000 lb.

Figure A-8 shows the distribution, expressed in percent, of the integrated flight distance by pressure altitude bands. Each column represents 100% of the flights that fall within the specified distance range. The table shows that the aircraft consistently (>80% of the time) flies at the 29,500-39,500-foot altitude band for flights greater then 1,000 nautical miles.

5.1.2 Altitude, Speed, and Temperature Data.

This section and figures A-9 through A-21 present information about the altitudes, speeds, and temperatures at which the aircraft operate. Figure A-9 shows the maximum altitude attained during each flight plotted versus the duration of the flight. The data indicate that as the flight length increases, the aircraft consistently fly at the higher altitudes. The scatter plot also indicates that as the flight duration decreases to under an hour in length, these flights, which may include some training and test flights, tend to occur at altitudes below 30,000 ft. These trends indicate a probable correlation between flight duration and the maximum altitude attained.

The cumulative probabilities of ground speed for taxi-in and taxi-out operations are presented in figure A-10. The taxi-in speed is somewhat higher than the taxi-out speed, which agrees with what has been observed with other aircraft models. This probably occurs because ground movement of inbound traffic to the terminal after landing is generally accomplished faster due to less traffic than when moving from the terminal to the takeoff position. It should be noted for this report that the taxi-in phase of operation begins after the first turnoff from the active runway compared to previous UDRI reports that included the runway turnoff speeds as part of the taxi-in phase of operation. The higher taxi-in speeds, as observed in earlier reports, probably occurred as the aircraft was exiting the runway during the turnoff.

Figures A-11 and A-12 show measured speeds plotted versus Mach number and airspeed limits, M_{MO} or V_{MO}, as defined in the aircraft flight manual. Each plotted point represents the airspeed or Mach number that yielded the greatest difference between the observed airspeed and Mach number and the speed or Mach number limit at its coincident altitude, regardless of flight phase. For example, in one flight, the maximum speed, with respect to the limit, might have been attained in the climb phase, while in another flight, the maximum speed may have occurred in a different phase. Also, it should be noted that the Mach number and airspeed points as plotted do not necessarily occur simultaneously.

Both plots indicate that there are many flights that operate at speeds or Mach number values approaching or, in a few cases, slightly exceeding the airspeed limits. The B-747-400 aircraft's onboard computers should only allow these speed limits to be exceeded for a few seconds before automatically responding to reduce the aircraft's speed to acceptable levels. Also, there is an obvious shift in the location of points away from the Mach or airspeed limit for flights starting at about 15,000 feet and below. At 5000 feet, there were no points in these flights near the airspeed limits. This is probably because other speed restrictions, such as those imposed for flap and landing gear operations, further restrict the aircraft's airspeed at these altitudes and flight distances.

Figure A-13 shows the cumulative probabilities of ground airspeed at liftoff and touchdown. It shows that the majority of takeoffs occur at speeds between 155 and 180 knots. A majority of the speeds at touchdown are between 140 and 155 knots. Comparison of the two flight phases also shows that the liftoff speeds for the B-747-400 are approximately 20 knots higher than the touchdown speeds.

Figures A-14 through A-21 contain scatter plots of the total air temperature versus the true airspeed by pressure altitude. Since these formats have three variables, they have been plotted in eight different altitude ranges to account for the altitude variable. The altitude ranges are the same ones used for the derived gust plots: < 500, 500-1,500, 1,500-4,500, 4,500-9,500, 9,500-19,500, 19,500-29,500, 29,500-39,500, and > 39,500 feet. The flights were analyzed by using a system of bins placed on the temperature and airspeed. The bin size for the temperature was 4°C and the bin size for airspeed was 10 knots. Figures A-14 through A-21 show the results of running a program that used the above criteria to bin the airspeed and temperature data for all flights accordingly. The marks on these scatter plots, therefore, do not identify individual flights, rather, they simply acknowledge that for some duration of time an airplane was in that bin of airspeed and air temperature. These plots also contain statistical data about the airspeed and temperature for the altitude range.

5.1.3 Attitude Data.

This section and figures A-22 through A-24 present statistical pitch angle data for selected phases of flight.

Figure A-22 provides the cumulative probability of maximum pitch angle at liftoff. The algorithm developed that identified the pitch angle at liftoff used the value of the maximum pitch angle that occurred within an interval of 5 seconds after the squat switch indicated liftoff. The curve shown in figure A-14 reflects the pitch angle at liftoff using the 5-second criteria.

Figure A-23 shows the cumulative probability distribution of pitch angle at touchdown/landing. The pitch angle during landing varied between 2° and 7°, with the most landings occurring at pitch angles between 4° and 6°. Although the squat switch was not a reliable indicator of the instant of touchdown, it was considered to be adequate for determining the pitch angle during landing because the pitch angle during the flare maneuver is usually held fairly constant at touchdown. Thus, the airplane rotation, which may significantly affect the pitch angle during liftoff, has a far lesser effect on the reported pitch angle at touchdown.

Figure A-24 presents the cumulative probability of maximum pitch angle during the departure and approach phases of flight. The data show that the pitch angle of the aircraft during departure varies between 12° and 22°, while during its approach, the pitch angle varies between 2° and 11°. Chai and Mason [4] attributed this difference to the fact that "with the flaps in the fully deflected position, the critical angle of attack of the wing during landing [and approach] is smaller than during takeoff [and departure]. Consequently, the pitch angle during landing is smaller than that during takeoff."

5.2 GROUND LOADS DATA.

Figures A-25 through A-46 provide statistical loads data based on the B-747-400's ground operations. The ground loads data include frequency and probability information on vertical, lateral, and longitudinal accelerations during takeoff, landing, taxi, and turning operations. These loads primarily affect the landing gear and landing gear backup structure and, to a lesser extent, the wing, fuselage, and empennage. (Statistical ground loads data for other aircraft models can be found in references 2, 5, 6, 7, 8, and 9.)

5.2.1 Lateral Load Factor Data.

This section presents lateral load factor statistical data during ground turning operations and at touchdown.

Figure A-25 shows the cumulative occurrences of the maximum lateral load factor that occurred during each ground turn (excludes the runway turnoff). The information is presented per 1000 flights for both pre- and postflight taxi and contains data for both left and right turns. The magnitudes of lateral load factor during taxi-in are slightly higher than during taxi-out. The data reported in references 5 through 9 for the B-737-400, MD-82/83, B-767-200, A320, and CRJ100 aircraft showed that during taxi-in, the lateral load factors are probably a little higher because of the higher speeds associated with taxi-in. Also, figure A-25 shows no significant difference between the number of left and right turns or their magnitudes.

Figure A-26 presents the cumulative occurrences of the maximum lateral load factor that occurred per 1000 flights at touchdown. Because of the delay in the squat switch indication of touchdown and to ensure that the maximum n_y load factor peak associated with touchdown was identified, UDRI scanned an interval of 5 seconds prior to squat switch closure to identify the maximum n_y load factor peak during touchdown. The data show that n_y peaks during the landing touchdown fall between approximately -0.25 to +0.29 g. The relative frequency distribution does not exhibit a distinguishable mode frequency, but increases as the lateral load factor approaches zero from either direction.

Figure A-27 presents the cumulative frequency of the maximum lateral load factor that occurred per 1000 flights during the first turnoff from the active runway after landing. The magnitude of lateral load factor between ±0.2 g for right and left turns is very similar, as one would expect. These side load factor occurrences are not included in the taxi-in data presented in figure A-25.

Figure A-28 presents the coincident incremental vertical load factor that occurs in conjunction with the maximum lateral load factor measured at touchdown (the same 5-second interval as defined above was used to identify touchdown).

Figure A-29 shows the probability of the turn angle (total angular measurement) experienced during 11,066 turnoffs from the active runway. The plot indicates that a significant number of turns are grouped in the 30, 90, and 180 degree range. The scatter plots, figures A-30 through A-32, show the maximum lateral load factor experienced during each turnoff versus its corresponding ground speed. The range of turn angles in each of these figures was selected to span the three turn angles that occurred most often. The data show there is considerable variation in ground speeds during the runway turnoff; there also appears to be a correlation between speed during the turn and magnitude of the lateral load factor.

Figures A-33 through A-35 contain scatter plots showing the maximum lateral load factor at touchdown versus the yaw angle and bank angle before touchdown. Since yaw angle was not a recorded parameter, it had to be derived for each landing. This was accomplished by assuming that the calculated average magnetic heading of the aircraft on the runway after landing represented the direction of the runway. Then, the calculated difference in the aircraft heading prior to touchdown with the magnetic heading of the aircraft on the runway after landing resulted in the estimated yaw angle. The maximum yaw angle reflects the highest value that was calculated during an interval from -10 seconds to -3 seconds prior to the squat switch indication of touchdown. (The interval was terminated at -3 seconds prior to touchdown to ensure that the data from touchdown were not included.) The mean yaw angle was determined by averaging the maximum yaw angles that occurred during the -10 to -3-second interval just prior to touchdown. At most, a minimal correlation exists between yaw angle and lateral acceleration at touchdown. The maximum bank angle reflects the maximum value recorded during the 50-second interval prior to touchdown.

5.2.2 Longitudinal Load Factor Data.

Longitudinal load factor statistics are presented for the pre- and postflight taxi, at touchdown, and during the landing roll phases of ground operations.

Figure A-36 presents the cumulative occurrences of longitudinal load factor during pre- and postflight taxi operations per 1000 flights. The occurrences of longitudinal load factor during taxi occurred primarily due to braking and throttle changes. The magnitude of longitudinal load factors observed during taxi varied between -0.36 and +0.28 g.

Figure A-37 shows the cumulative frequency of the maximum and minimum longitudinal load factor measured at touchdown and during the landing rollout with and without thrust reverser deployment. It appears that additional braking, which results from deployment of the thrust reversers, increases the negative longitudinal load factor spectra by approximately 0.1 g over the values seen when the thrust reversers are not in use. The maximum longitudinal load factor observed was -0.52 g, which occurred during operation of the thrust reversers. The occurrence of positive longitudinal load factors, even though very small, probably occurs due to the variations in retardation forces caused by the thrust reversers, hydraulic brakes, and rolling friction.

5.2.3 Vertical Load Factor Data.

This section presents vertical load factor statistics during ground operations involving touchdown, taxi, takeoff and landing roll (with and without thrust reverser), and at spoiler deployment; also included are the aircraft's acceleration response due to operations within this operator's system.

Figure A-38 presents cumulative occurrences of incremental vertical load factor per 1000 flights for the taxi-in and taxi-out phases of ground operations. The data show that the magnitude of the incremental vertical load factor during taxi-in is lower than for taxi-out. In previous reports, it was observed that taxi-in incremental vertical loads were slightly higher then taxi-out. This slight difference was observed on the B-737-400, MD-82/83, B-767, A320, and CRJ100 aircraft [5 through 9]. Also, the range of values for the incremental vertical load factor in figure A-30 is ±0.1 g, whereas in previous reports, this range was at least ±0.2 g and was often greater.

Figure A-39 presents the cumulative occurrences of positive and negative incremental vertical load factors per 1000 flights that occurred during the takeoff roll. While the magnitudes of load factor appear to be consistent with what one would expect during the takeoff roll, these values are primarily a function of the condition or roughness of the runway.

Figure A-40 presents the cumulative occurrences of the minimum and maximum incremental vertical load factor per 1000 flights associated with touchdown and deployment of the ground spoilers. This figure shows that approximately the same minimum incremental vertical load factor, -0.35 g, was attributable to each event. However, at touchdown, the maximum incremental vertical load factor was about 0.9 g, while at spoiler deployment, the value was around 0.4 g.

Figure A-41 presents the cumulative occurrences of incremental vertical load factor per 1000 flights during the landing roll for operations with and without thrust reversers. These curves may also include the effects of ground spoiler usage on vertical load factor because the spoilers are normally used during the landing rollout concurrently with the thrust reversers.

Figures A-42 through A-44 contain scatter plots that show the maximum incremental vertical load factor at touchdown versus the yaw angle and bank angle. The values of the yaw angle and bank angle used here are the same as those derived and used previously in figures A-33 through A-35.

Figure A-45 contains a scatter plot that shows the maximum incremental vertical load factor versus the coincident-computed airspeed at touchdown. The negative values shown indicate that the vertical load factor response during some of the landing touchdowns were higher than the positive load factor due to landing.

Figure A-46 compares the rms acceleration response to various runways used by the airline involved with this program. An rms value was calculated using the takeoff and landing roll vertical acceleration data from each airport. However, because of the close proximity of parallel runways at some airports and the questionable accuracy involved with presenting the data by runway, the rms data presented reflect the average of all runways used at each airport. The

acceleration response provides a filtered representation of the runway roughness as determined by the landing gear characteristics. The data show that in terms of B-747-400 acceleration response, the roughest runway location (Ninoy Aquino International Airport, Philippines) is over twice as rough as the smoothest runway location (Tampa International Airport, Tampa, FL).

5.3 FLIGHT LOADS DATA.

The statistical flight loads data in this section and figures A-47 through A-92 describe the aircraft's operating gust, maneuver, and combined maneuver and gust load environment.

The gust loads data are presented in the form of incremental vertical load factors, derived gust velocity, $U_{de,}$ and continuous gust intensity, U_{σ}. The derived gust velocity and continuous gust intensity are computed values, as described in section 4.2. Gust and maneuver incremental vertical acceleration data are plotted as either cumulative occurrences per 1000 hours or as cumulative occurrences per nautical mile and also may be plotted by phase of flight, altitude, flap position, etc.

This section also presents the combined total vertical and lateral load factor occurrences, due to the maneuver and gust environment, presented per 1000 hours or per nautical mile by phase of flight, and for vertical load factor for all flight phases combined. V-n diagrams showing the coincident gust and maneuver vertical load factor versus speed for the flaps retracted and extended conditions are presented. Cumulative occurrences of maximum lateral load factor versus gross weight are presented by phase of flight. Also, the excursion, between the largest negative and highest positive load factor that occurs once per flight, are paired together and presented herein as the ground-air-ground or (GAG) cycle data.

5.3.1 Gust Vertical Load Factor Data.

Cumulative occurrences of incremental vertical gust load factor are plotted as either cumulative occurrence per 1000 hours or per nautical mile by phase of flight.

Figure A-47 shows the cumulative occurrences of incremental vertical gust load factor per 1000 hours by phase of flight, and figure A-48 shows the cumulative occurrences of incremental vertical gust load factor for all the airborne phases combined per 1000 hours. The maximum incremental vertical gust load factor encountered by the B-747-400 was about 0.9 g and occurred, as shown in figure A-47, during the descent phase of flight.

Figure A-49 presents the cumulative occurrences of incremental vertical gust load factor per nautical mile by phase of flight, and figure A-50 shows the cumulative occurrences of incremental vertical gust load factor for all the airborne phases combined per nautical mile.

5.3.2 Derived Gust Velocity Data.

The magnitudes for the derived gust velocities were calculated from the measured accelerations in accordance with the procedures presented in section 4.2.4. In figures A-51 through A-58, the derived gust velocity, $U_{de,}$ is plotted as cumulative occurrences per nautical mile for altitudes from sea level to 44,500 feet. In each figure, the derived gust velocities are compared to the gust

velocity distributions presented in reference 10, which is a recognized standard that has been used in the past in establishing structural design criteria for repeated gust loads.

Figures A-59 and A-60 present derived gust velocity, U_{de}, per nautical mile for the flaps extended and retracted conditions, respectively.

5.3.3 Continuous Gust Intensity Data.

The magnitudes of the continuous gust intensities, U_{σ}, were derived from the measured accelerations in accordance with the procedures presented in section 4.2.5. The cumulative occurrences of continuous gust intensity per nautical mile for the flaps extended and retracted conditions are presented in figures A-61 and A-62, respectively.

5.3.4 Gust V-n Diagram Data.

To display the coincident speed and gust accelerations, representative V-n diagrams were developed for the flaps retracted and extended configurations for illustration purposes only. Since V-n diagrams are a function of altitude and gross weight, a gross weight of 530,000 lb was selected, based on figures A-1 and A-2, and a sea level altitude was selected.

Figures A-63 and A-64 show the coincident gust acceleration and airspeed measurements plotted on the V-n diagrams for the flaps retracted and extended configurations, respectively. All flap detent positions for which data were available (1, 5, 10, 20, 25, and 30) are shown to provide a range of flap extension conditions. Figure A-64 shows, for the flaps extended case, that a few gust acceleration points fall outside the gust V-n diagram. These results are similar to those observed on other aircraft [5, 6, and 7] with the flaps extended. One must keep in mind that the V-n diagram shown here is for only one gross weight and altitude condition. If the measured gust acceleration data were plotted against the V-n diagram for the actual gross weight and altitude conditions that existed at the time the acceleration was measured, the data might fall within the V-n diagram. Furthermore, the V-n diagram reflects only one static strength design requirement. The actual structure is designed to many different strength and rigidity design requirements, including static strength, durability, and damage tolerance. While the exceedance of a single design requirement may indicate a shortcoming in the design requirement, it does not necessarily translate into a deficiency in the overall design strength of the aircraft.

The relatively large number of points that appear outside the V-n diagram in figure A-64, for detent 25, required further analysis. Time histories for several flights were viewed to see what the exact airspeed and flap angles of the individual flights were. It was discovered that during the departure phase, while the aircraft is accelerating, there is a period of time where the flaps are at an angle above 20° and the aircraft is at an airspeed greater than the flap placard speed for detent 25. Table 6 shows how the flap detents are divided, when the flap angle is $> 20°$, $\leq 25°$, it is binned as flap detent 25 and plotted with the subsequent V-n diagram and placard speed. Therefore, a majority of the points in figure A-64 that appear outside the V-n diagram are the result of how the flap data are binned and also the acceleration of the aircraft during departure.

5.3.5 Maneuver Vertical Load Factor Data.

The maneuver loads data are presented in the form of incremental vertical load factors, either per 1000 hours or per nautical mile by phase of flight and altitude, or as combined phases.

Figures A-65 through A-69 provide the cumulative occurrences of incremental maneuver load factor per 1000 hours by altitude for each of the airborne flight phases, i.e., departure, climb, cruise, descent, and approach.

Figures A-70 through A-74 display the cumulative occurrences of incremental maneuver load factor by altitude per nautical mile (instead of per 1000 hours) in the airborne phases of flight.

Figure A-75 shows the total cumulative occurrences of incremental maneuver load factor per 1000 hours for each phase of flight, regardless of altitude. Figure A-76 contains the total cumulative occurrences of incremental maneuver load factor per 1000 hours for all flight phases combined.

Figure A-77 shows the total cumulative occurrences of incremental maneuver load factor per nautical mile for each phase of flight, regardless of altitude. Figure A-78 contains the total cumulative occurrences of incremental maneuver load factor per nautical mile for all flight phases combined.

The maximum incremental vertical maneuver load factor encountered by the B-747-400 was -0.7 g, which occurred during the descent and also during the approach phases of flight.

5.3.6 Maneuver V-n Diagram Data.

Maneuver strength is required for three different aircraft design speeds: flaps down speed (V_F), cruising speed (V_C), and dive speed (V_D). For the maneuver V-n diagram, the required limit load factors are specified in Title 14 Code of Federal Regulations (CFR) 25.337. The positive limit maneuvering load factor (n) may not be less than 2.5, and the negative limit maneuvering load factor may not be less than -1.0 at speeds up to V_C, varying linearly with speed to zero at V_D. 14 CFR 25.345 specifies that the positive limit maneuver load factor is 2.0 g's when the flaps are extended. As with the V-n diagram for gust loads, the gross weight of 530,000 lb for the flaps retracted and extended configurations and sea level density were selected to develop representative maneuver V-n diagrams.

Figures A-79 and A-80 show the maneuver V-n diagrams with flaps retracted and extended with the coincident acceleration and speed measurements. As with the gust loads, all flap detent positions for which data were available (1, 5, 10, 20, 25, and 30) are shown in figure A-80 to provide a range of flap extension conditions. Figure A-72 shows, for the flaps extended cases, that a few maneuver acceleration points occur at speeds outside the maneuver V-n diagram. This figure also shows the high number of points that occur outside the maneuver V-n diagram for flap detent 25. The reason for this is again the way the flap settings are binned and the acceleration during the departure phase of some flights.

5.3.7 Combined Maneuver and Gust Vertical Load Factor Data.

Figure A-81 shows the cumulative occurrences of the combined maneuver and gust incremental vertical load factor per 1000 hours by phases of flight, and figure A-82 shows the incremental vertical load factor occurrences for all flight phases combined.

Figures A-83 and A-84 contain the same vertical load factor data as figures A-81 and A-82, but are plotted as occurrences per nautical mile by phases of flight and for all flight phases combined. The 0.9-g incremental gust load factor encountered during the descent phase of flight is still the highest load factor recorded for the B-747-400's operation.

5.3.8 Combined Maneuver and Gust Lateral Load Factor Data.

Figure A-85 presents the cumulative occurrences of lateral load factor per 1000 hours by phase of flight. Maximum lateral load factor values between approximately -0.26 and +0.21 g were observed during flight operations of the B-747-400.

Figures A-86 through A-90 contain scatter plots that show the maximum lateral load factor versus the coincident gross weight of the aircraft during airborne phases of flight.

5.3.9 Ground-Air-Ground Cycle Data.

Figures A-91 and A-92 display occurrences of the maximum and minimum incremental vertical load factor that occurs once per flight. The load excursion between the largest negative and highest positive load factor is often referred to by aircraft design engineers as the GAG cycle. Figure A-91 presents the number of GAG cycle occurrences in tabular form, and figure A-92 shows the number of GAG cycle occurrences plotted as a three-dimensional bar chart. The GAG cycle usually contributes the most damaging fatigue cycle experienced by the aircraft wing and carry through structural assemblies. The GAG cycle that contained the widest range between negative and positive values occurred was between -0.75 and +0.55 g.

5.4 SYSTEMS OPERATIONAL DATA.

This section contains operational usage data for the flaps, speed brakes, thrust reversers, and the propulsion system. Although control surface position information was available for the aileron, rudder, and elevator systems, it was not processed because the sampling rates were deemed to be too slow to provide reliable statistical usage information for these components.

5.4.1 Flap Usage Data.

Flap usage data showing airspeed and percent of time spent by flap detent and phase of flight are presented. These data can be used to characterize the sources of repeated loads on the flaps and backup structure and other flap components. The B-747-400 flap operational speed limits for each detent setting were listed in table 6.

Figures A-93 and A-94 present the probability of the maximum airspeed encountered in various flap detents during the departure phase of flight, and figures A-95 and A-96 present similar

probability data for the approach phase of flight. Figure A-96 shows that the most probable speed at which the flaps are first deployed during the approach phase of flight for detent 5 occurs at about 220 knots, detent 10 about 212 knots, detent 20 about 202 knots, detent 25 about 180 knots, and detent 30 about 162 knots.

Figures A-97 and A-98 present the percent of time spent in each flap detent setting during the departure and approach phases of flight, respectively. Flap detents 20 and 25 are the most frequently used settings during the departure phase (35.69% and 33.82% of the time respectively), while flap detents 20 (35.4%) and 30 (23.1%) are the most often used settings during the approach phase. The low amount of time shown in detent 5 during the approach phase may explain why the speeds discussed above for detents 5 and 10 occur so closely together.

5.4.2 Speed Brake Usage Data.

Statistics on speed brake usage as a function of speed, altitude, deployment angle, and time spent at coincident flap detent and speed brake settings are of major interest to both aircraft manufacturers and airline operators. These data are presented in figures A-99 through A-102.

Figure A-99 illustrates the probability distribution of the speed at the instant of speed brake deployment, and figure A-100 gives the probability distribution of the maximum speed encountered while the speed brakes were deployed in flight. Figure A-101 presents the probability distribution of the altitude when the speed brakes were deployed, and figure A-102 presents the probability distributions of the maximum deployment angle reached while the speed brakes were deployed.

The table in figure A-103 shows the number of flight hours the aircraft was flown at coincident flap detent and speed brake settings. Almost all of the speed brake usage occurred in the flaps retracted configuration.

5.4.3 Thrust Reverser Data.

The times and speeds associated with thrust reverser operations were derived from the measured data. Figure A-104 presents the cumulative probability of time during which the thrust reversers are deployed. The data show that for 90% of the flights, the thrust reversers are deployed for less than 50 seconds. Figure A-105 presents the cumulative probability of the speed at the time the thrust reversers were deployed and stowed. Most thrust reverser deployment cycles begin at speeds between 130 and 150 knots and are stowed at speeds between 30 and 70 knots.

5.4.4 Propulsion Data.

Figure A-106 presents the cumulative probability of the maximum engine fan speed, N_1, during takeoff, at the instant of thrust reverser deployment during the landing roll, and during the time that the thrust reverser is deployed. Most takeoffs occur at fan speed values ranging greater than 85%. The fan speed at thrust reverser deployment ranges between 30% and approximately 40% and then increases up to a maximum value of over 80% during the time the thrust reverser is deployed.

6. SPECIALIZED DATA USED FOR HARMONIZATION OF INTERNATIONAL CRITERIA FOR GROUND LOAD CERTIFICATION.

The statistical data presented in this section provide additional formats that have not previously been applied to aircraft in other flight loads reports. These new formats have been specifically requested for the B-747-400 aircraft to support development of ground loads certification criteria. As the title states, this data is specialized and therefore is being presented separate from the conventional data plots in appendix A. Another reason for keeping these plots separate from the figures in appendix A is because many of the new formats required that the data be plotted by the airport, something that had never been done before.

Table 8 lists all the new statistical formats for which the data were processed. The various data formats all pertain to aircraft usage. More specifically, the new formats analyze speed, attitude, and rate data at touchdown and other phases of flight.

TABLE 8. NEW STATISTICAL DATA FORMATS

Data Description	Figure
SPEED DATA	
Cumulative Probability of Airspeed at Touchdown by Pitch Angle	C-1
Calibrated Airspeed vs Pitch Angle at Touchdown, Airport 103 Elevation < 500 Feet	C-2
Calibrated Airspeed vs Pitch Angle at Touchdown, Airport 104 Elevation < 500 Feet	C-3
Calibrated Airspeed vs Pitch Angle at Touchdown, Airport 107 Elevation < 500 Feet	C-4
Calibrated Airspeed vs Pitch Angle at Touchdown, Airport 118 Elevation < 500 Feet	C-5
Calibrated Airspeed vs Pitch Angle at Touchdown, Airport 135 Elevation < 500 Feet	C-6
Calibrated Airspeed vs Pitch Angle at Touchdown, Airport 153 Elevation < 500 Feet	C-7
Calibrated Airspeed vs Pitch Angle at Touchdown, Airport 175 Elevation < 500 Feet	C-8
Calibrated Airspeed vs Pitch Angle at Touchdown, Airport 197 Elevation < 500 Feet	C-9
Calibrated Airspeed vs Pitch Angle at Touchdown, Airport 235 Elevation < 500 Feet	C-10
Calibrated Airspeed vs Pitch Angle at Touchdown, Airport 362 Elevation < 500 Feet	C-11
Calibrated Airspeed vs Pitch Angle at Touchdown, Airport 364 Elevation < 500 Feet	C-12
Calibrated Airspeed vs Pitch Angle at Touchdown, Airport 365 Elevation < 500 Feet	C-13
Calibrated Airspeed vs Pitch Angle at Touchdown, Airport 366 Elevation < 500 Feet	C-14
Calibrated Airspeed vs Pitch Angle at Touchdown, Airport 367 Elevation < 500 Feet	C-15
Calibrated Airspeed vs Pitch Angle at Touchdown, Airport 368 Elevation < 500 Feet	C-16
Calibrated Airspeed vs Pitch Angle at Touchdown, Airport 373 Elevation < 500 Feet	C-17
Calibrated Airspeed vs Pitch Angle at Touchdown, Airport 380 Elevation < 500 Feet	C-18
Calibrated Airspeed vs Pitch Angle at Touchdown, Airport 389 Elevation < 500 Feet	C-19
Calibrated Airspeed vs Pitch Angle at Touchdown, Airport 394 Elevation < 500 Feet	C-20
Calibrated Airspeed vs Pitch Angle at Touchdown, Airports Elevation < 500 Feet	C-21
Calibrated Airspeed vs Pitch Angle at Touchdown, Airport 33 Elevation 500-1000 Feet	C-22
Calibrated Airspeed vs Pitch Angle at Touchdown, Airport 192 Elevation 500-1000 Feet	C-23
Calibrated Airspeed vs Pitch Angle at Touchdown, Airport 384 Elevation 500-1000 Feet	C-24
Calibrated Airspeed vs Pitch Angle at Touchdown, Airports Elevation 1000-4000 Feet	C-25
Calibrated Airspeed vs Pitch Angle at Touchdown, Airports Elevation 4000-5000 Feet	C-26
Calibrated Airspeed vs Pitch Angle at Touchdown, Airport 45 Elevation > 5000 Feet	C-27
Calibrated Airspeed vs Pitch Angle at Touchdown, Airport 371 Elevation > 5000 Feet	C-28
Calibrated Airspeed vs Pitch Angle at Touchdown, Airport 374 Elevation > 5000 Feet	C-29
Calibrated Airspeed vs Pitch Angle at Touchdown, Airport 275 Elevation > 5000 Feet	C-30

TABLE 8. NEW STATISTICAL DATA FORMATS (Continued)

Data Description	Figure
SPEED DATA (Continued)	
Ground Speed vs True Airspeed at Touchdown, Airport 103 Elevation < 500 Feet	C-31
Ground Speed vs True Airspeed at Touchdown, Airport 104 Elevation < 500 Feet	C-32
Ground Speed vs True Airspeed at Touchdown, Airport 107 Elevation < 500 Feet	C-33
Ground Speed vs True Airspeed at Touchdown, Airport 118 Elevation < 500 Feet	C-34
Ground Speed vs True Airspeed at Touchdown, Airport 135 Elevation < 500 Feet	C-35
Ground Speed vs True Airspeed at Touchdown, Airport 153 Elevation < 500 Feet	C-36
Ground Speed vs True Airspeed at Touchdown, Airport 175 Elevation < 500 Feet	C-37
Ground Speed vs True Airspeed at Touchdown, Airport 197 Elevation < 500 Feet	C-38
Ground Speed vs True Airspeed at Touchdown, Airport 235 Elevation < 500 Feet	C-39
Ground Speed vs True Airspeed at Touchdown, Airport 362 Elevation < 500 Feet	C-40
Ground Speed vs True Airspeed at Touchdown, Airport 364 Elevation < 500 Feet	C-41
Ground Speed vs True Airspeed at Touchdown, Airport 365 Elevation < 500 Feet	C-42
Ground Speed vs True Airspeed at Touchdown, Airport 366 Elevation < 500 Feet	C-43
Ground Speed vs True Airspeed at Touchdown, Airport 367 Elevation < 500 Feet	C-44
Ground Speed vs True Airspeed at Touchdown, Airport 368 Elevation < 500 Feet	C-45
Ground Speed vs True Airspeed at Touchdown, Airport 373 Elevation < 500 Feet	C-46
Ground Speed vs True Airspeed at Touchdown, Airport 380 Elevation < 500 Feet	C-47
Ground Speed vs True Airspeed at Touchdown, Airport 389 Elevation < 500 Feet	C-48
Ground Speed vs True Airspeed at Touchdown, Airport 394 Elevation < 500 Feet	C-49
Ground Speed vs True Airspeed at Touchdown, Airports Elevation < 500 Feet	C-50
Ground Speed vs True Airspeed at Touchdown, Airport 33 Elevation 500-1000 Feet	C-51
Ground Speed vs True Airspeed at Touchdown, Airport 192 Elevation 500-1000 Feet	C-52
Ground Speed vs True Airspeed at Touchdown, Airport 384 Elevation 500-1000 Feet	C-53
Ground Speed vs True Airspeed at Touchdown, Airports Elevation 1000-4000 Feet	C-54
Ground Speed vs True Airspeed at Touchdown, Airports Elevation 4000-5000 Feet	C-55
Ground Speed vs True Airspeed at Touchdown, Airport 45 Elevation > 5000 Feet	C-56
Ground Speed vs True Airspeed at Touchdown, Airport 371 Elevation > 5000 Feet	C-57
Ground Speed vs True Airspeed at Touchdown, Airport 374 Elevation > 5000 Feet	C-58
Ground Speed vs True Airspeed at Touchdown, Airport 275 Elevation > 5000 Feet	C-59
Delta V (Ground Speed-True Airspeed) at Touchdown, Airport 103 Elevation < 500 Feet	C-60
Delta V (Ground Speed-True Airspeed) at Touchdown, Airport 104 Elevation < 500 Feet	C-61
Delta V (Ground Speed-True Airspeed) at Touchdown, Airport 107 Elevation < 500 Feet	C-62
Delta V (Ground Speed-True Airspeed) at Touchdown, Airport 118 Elevation < 500 Feet	C-63
Delta V (Ground Speed-True Airspeed) at Touchdown, Airport 135 Elevation < 500 Feet	C-64
Delta V (Ground Speed-True Airspeed) at Touchdown, Airport 153 Elevation < 500 Feet	C-65
Delta V (Ground Speed-True Airspeed) at Touchdown, Airport 175 Elevation < 500 Feet	C-66
Delta V (Ground Speed-True Airspeed) at Touchdown, Airport 197 Elevation < 500 Feet	C-67
Delta V (Ground Speed-True Airspeed) at Touchdown, Airport 235 Elevation < 500 Feet	C-68
Delta V (Ground Speed-True Airspeed) at Touchdown, Airport 362 Elevation < 500 Feet	C-69
Delta V (Ground Speed-True Airspeed) at Touchdown, Airport 364 Elevation < 500 Feet	C-70
Delta V (Ground Speed-True Airspeed) at Touchdown, Airport 365 Elevation < 500 Feet	C-71
Delta V (Ground Speed-True Airspeed) at Touchdown, Airport 366 Elevation < 500 Feet	C-72
Delta V (Ground Speed-True Airspeed) at Touchdown, Airport 367 Elevation < 500 Feet	C-73
Delta V (Ground Speed-True Airspeed) at Touchdown, Airport 368 Elevation < 500 Feet	C-74
Delta V (Ground Speed-True Airspeed) at Touchdown, Airport 373 Elevation < 500 Feet	C-75
Delta V (Ground Speed-True Airspeed) at Touchdown, Airport 380 Elevation < 500 Feet	C-76

TABLE 8. NEW STATISTICAL DATA FORMATS (Continued)

Data Description	Figure
SPEED DATA (Continued)	
Delta V (Ground Speed-True Airspeed) at Touchdown, Airport 389 Elevation < 500 Feet	C-77
Delta V (Ground Speed-True Airspeed) at Touchdown, Airport 394 Elevation < 500 Feet	C-78
Delta V (Ground Speed-True Airspeed) at Touchdown, Airports Elevation < 500 Feet	C-79
Delta V (Ground Speed-True Airspeed) at Touchdown, Airport 33 Elevation 500-1000 Feet	C-80
Delta V (Ground Speed-True Airspeed) at Touchdown, Airport 192 Elevation 500-1000 Feet	C-81
Delta V (Ground Speed-True Airspeed) at Touchdown, Airport 384 Elevation 500-1000 Feet	C-82
Delta V (Ground Speed-True Airspeed) at Touchdown, Airports Elevation 1000-4000 Feet	C-83
Delta V (Ground Speed-True Airspeed) at Touchdown, Airports Elevation 4000-5000 Feet	C-84
Delta V (Ground Speed-True Airspeed) at Touchdown, Airport 45 Elevation > 5000 Feet	C-85
Delta V (Ground Speed-True Airspeed) at Touchdown, Airport 371 Elevation > 5000 Feet	C-86
Delta V (Ground Speed-True Airspeed) at Touchdown, Airport 374 Elevation > 5000 Feet	C-87
Delta V (Ground Speed-True Airspeed) at Touchdown, Airport 275 Elevation > 5000 Feet	C-88
Airport Elevation vs Average Delta V at Touchdown	C-89
Airport Elevation vs Absolute Value of Average Delta V at Touchdown	C-90
ATTITUDE AND RATE DATA	
Cumulative Probability of Pitch Rate at Gear Touchdown	C-91
Probability Distributions of Maximum Yaw Angle at Touchdown	C-92
Cumulative Probability of Yaw Angle at Touchdown	C-93
Probability Distributions of Maximum Bank Angle at Touchdown	C-94
Cumulative Probability of Maximum Bank Angle at Touchdown	C-95

Figures C-1 through C-95 are presented in appendix C. For ease of understanding, the figures in appendix C are presented in graphical form. In an effort to make the data presentation of a more comprehensive nature, some figures include both cumulative and relative probability. Scatter plots are also included, where appropriate, to show the relationship between coincident parameters that are considered to be of interest and to show visible evidence of relationships, outliers, or suspicious data.

As with appendix A, it should be noted that the data presented in these figures are not always based on an identical number of flights or flight hours.

6.1 SPEED DATA.

This section presents information about the speeds at which the aircraft operate.

Figure C-1 shows the cumulative probability of airspeed at touchdown based on the pitch angle of the aircraft. The pitch angles at touchdown varied between 2° and 7°. To see how the touchdown speed varied with pitch angle, the angles were binned by increments of 2 degrees. The data has been plotted in the following ranges: 0-4, 4.1-6, and 6.1-8+ degrees, bins 0-2 and 2.1-4 degrees were combined because of the low number of occurrences in the 0-2 degree range. The cumulative probability of the airspeed at touchdown was determined for each range of pitch angles and plotted on the same axis. Below a cumulative probability of 70%, the effect that pitch angle has on touchdown speed is more distinguishable. The trend in this range is as follows: the

lower the pitch angle, the higher the touchdown speed. Above the 70% probability level, the range of pitch angles 0°-4° and the range 4.1°-6° begin to cross paths.

The next series of formats plot calibrated airspeed versus pitch angle at touchdown by individual airport. Figures C-2 through C-20 contain scatter plots of calibrated airspeed versus pitch angle at touchdown by airport. The airports in these plots all have elevations of less than 500 feet. These airports also have greater than 100 flights. In order to make these plots by airport and not give away the specific location, a random number has been assigned to each airport used by the carrier. Instead of identifying the name of the airport on each plot, the assigned number was used. Figure C-21 contains all the remaining data from airports with an elevation of less than 500 feet but with fewer than 100 flights.

Figures C-22 through C-24 show the same data as the above figures but for airports with elevations between 500-1000 feet and greater than 100 flights. Figure C-25 shows a plot for airports with elevations between 1000 and 4000 feet, all had less than 100 flights. Figure C-26 shows calibrated airspeed versus pitch angle at touchdown for airports with elevations between 4000-5000 feet and less than 100 flights. Figures C-27 through C-30 show plots for all airports greater than 5000 feet in elevation.

Figures C-31 through C-59 show scatter plots of ground speed versus true airspeed at touchdown in the same manner as figures C-2 through C-30—by airport, elevation, and number of flights.

Figures C-60 through C-88 show probability of occurrence charts of the delta V (ground speed-true airspeed) at touchdown in the same manner as figures C-2 through C-30—by airport, elevation, and number of flights.

Figures C-89 and C-90 show scatter plots of the delta V at touchdown, and the absolute value of delta V at touchdown versus the airport elevation.

6.2 ATTITUDE AND RATE DATA.

This section presents statistical attitude data and pitch rate information for aircraft touchdown.

Figure C-91 shows a cumulative probability plot of the pitch rate of the aircraft when the main landing gear touches down, between main gear and nose gear touchdown, and when the nose gear touches down. The pitch rate values for main gear touchdown were calculated starting 2 seconds prior to the close of the main gear squat switch. The pitch rates during this event varied between 1.3 and -6.7 degrees/sec. However, less than 1 percent of the flights exceeded a pitch rate of -2 degrees/sec. Pitch rate values between main and nose gear touchdown were calculated 2 seconds prior to close of main gear squat switch until the close of the nose gear squat switch. The pitch rates during this time varied between -0.3 and -10.7 degrees/sec. About 1 percent of the flights exceeded a pitch rate of -2.7 degrees/sec. Pitch rate values for nose gear touchdown were calculated beginning 2 seconds prior to the nose gear squat switch close. The pitch rates during this event varied between 0.3 and -4.7 degrees/sec. About 1 percent of the flights exceeded a pitch rate of -2.5 degrees/sec.

Figures C-92 through C-95 investigate the airplanes attitude at touchdown. Figure C-92 shows a probability distribution plot of the maximum yaw angle at touchdown. Yaw angle is not a recorded parameter and needs to be calculated. This was accomplished by assuming that the calculated average magnetic heading of the aircraft on the runway after landing represented the direction of the runway. Then, the calculated difference between the aircraft heading prior to touchdown and the magnetic heading of the aircraft on the runway after landing yielded the estimated yaw angle. The yaw angle at touchdown was considered to be the value of the yaw angle calculated when the main gear squat switch closed. Figure C-92 shows a cumulative and relative probability plot of the absolute value of the yaw angle at touchdown for every flight. The touchdown yaw angles varied from 0°-12°. Most landings, however, were more likely to have yaw angles of less than 2°; only 15% of the flights exceeded touchdown yaw angles of 2°. The most probable yaw value at touchdown was 0°. Figure C-93 shows a cumulative probability plot of yaw angle at touchdown for all flights, this time showing both negative and positive yaw values.

Figure C-94 shows a probability distribution plot of the maximum bank angle at touchdown. The bank angle at touchdown was taken to be the value of the bank angle when the squat switch closed. Figure C-94 shows both the cumulative and the relative probability plot of the absolute value of the bank angle at touchdown. Bank angles at touchdown varied from 0°-4.75°. Only about 10% of the flights had bank angles at touchdown that exceeded 1.25°. The most probable value of bank angle at touchdown was around 0.25°. Figure C-95 shows a cumulative probability plot of bank angle at touchdown, showing both positive and negative values.

7. STATISTICAL DESCENT RATE DATA.

This section presents statistical descent rate data that can be used by the FAA to establish initial design requirements for an onboard nitrogen-generating system to be used for fuel tank inerting. The information, obtained from the descent phase from 1984 fights, shows how the descent rate for the B-747-400 aircraft can vary as a function of altitude, gross weight, engine rotor speed, and computed airspeed. Statistical data formats were developed to show descent rates by altitude, hold times, and actual descent profiles for flights operating into capacity-limited and non-capacity-limited airports.

Table 9 lists all the statistical data formats for which descent rate statistics were processed. The statistical data formats are graphically presented in figures D-1 through D-133 of appendix D.

TABLE 9. STATISTICAL DESCENT DATA FORMATS

Data Description	Figure
Descent Rate at Pressure Altitude for Capacity-Limited Airports With Hold Times	D-1
Descent Rate at Pressure Altitude for Capacity-Unlimited Airports With Hold Times	D-2
Mean Descent Rate at Pressure Altitude for Capacity-Limited Airports With Hold Times	D-3
Mean Descent Rate at Pressure Altitude for Capacity-Unlimited Airports With Hold Times	D-4
Descent Rate at Pressure Altitude for Capacity-Limited Airports With Hold Times Removed	D-5
Descent Rate at Pressure Altitude for Capacity-Unlimited Airports With Hold Times Removed	D-6
Mean Descent Rate at Pressure Altitude for Capacity-Limited Airports With Hold Times Removed	D-7
Mean Descent Rate at Pressure Altitude for Capacity-Unlimited Airports With Hold Times Removed	D-8
Maximum Descent Rates for Capacity-Limited Flights	D-9
Actual Descent Profiles Beginning Before Descent Phase for Capacity-Limited Flight (Flt Seq Num 2838)	D-10
Actual Descent Profiles Below 15K Feet for Capacity-Limited Flight (Flt Seq Num 2838)	D-11
Actual Descent Profiles Beginning Before Descent Phase for Capacity-Limited Flight (Flt Seq Num 3212)	D-12
Actual Descent Profiles Below 15K Feet for Capacity-Limited Flight (Flt Seq Num 3212)	D-13
Actual Descent Profiles Beginning Before Descent Phase for Capacity-Limited Flight (Flt Seq Num 1030)	D-14
Actual Descent Profiles Below 15K Feet for Capacity-Limited Flight (Flt Seq Num 1030)	D-15
Actual Descent Profiles Beginning Before Descent Phase for Capacity-Limited Flight (Flt Seq Num 2971)	D-16
Actual Descent Profiles Below 15K Feet for Capacity-Limited Flight (Flt Seq Num 2971)	D-17
Actual Descent Profiles Beginning Before Descent Phase for Capacity-Limited Flight (Flt Seq Num 2793)	D-18
Actual Descent Profiles Below 15K Feet for Capacity-Limited Flight (Flt Seq Num 2793)	D-19
Actual Descent Profiles Beginning Before Descent Phase for Capacity-Limited Flight (Flt Seq Num 3033)	D-20
Actual Descent Profiles Below 15K Feet for Capacity-Limited Flight (Flt Seq Num 3033)	D-21
Maximum Descent Rates for Non-Capacity-Limited Flights	D-22
Actual Descent Profiles Beginning Before Descent Phase for Non-Capacity-Limited Flight (Flt Seq Num 1038)	D-23
Actual Descent Profiles Below 15K Feet for Non-Capacity-Limited Flight (Flt Seq Num 1038)	D-24
Actual Descent Profiles Beginning Before Descent Phase for Non-Capacity-Limited Flight (Flt Seq Num 3574)	D-25
Actual Descent Profiles Below 15K Feet for Non-Capacity-Limited Flight (Flt Seq Num 3574)	D-26
Actual Descent Profiles Beginning Before Descent Phase for Non-Capacity-Limited Flight (Flt Seq Num 2267)	D-27
Actual Descent Profiles Below 15K Feet for Non-Capacity-Limited Flight (Flt Seq Num 2267)	D-28
Actual Descent Profiles Beginning Before Descent Phase for Non-Capacity-Limited Flight (Flt Seq Num 3034)	D-29
Actual Descent Profiles Below 15K Feet for Non-Capacity-Limited Flight (Flt Seq Num 3034)	D-30
Actual Descent Profiles Beginning Before Descent Phase for Non-Capacity-Limited Flight (Flt Seq Num 2360)	D-31
Actual Descent Profiles Below 15K Feet for Non-Capacity-Limited Flight (Flt Seq Num 2360)	D-32
Actual Descent Profiles Beginning Before Descent Phase for Non-Capacity-Limited Flight (Flt Seq Num 2021)	D-33
Actual Descent Profiles Below 15K Feet for Non-Capacity-Limited Flight (Flt Seq Num 2021)	D-34
Probability of Descent Rate for Descents Between 0-1000 Feet, Non-Capacity-Limited Airports	D-35
Probability of Descent Rate for Descents Between 1000-2000 Feet, Non-Capacity-Limited Airports	D-36
Probability of Descent Rate for Descents Between 2000-3000 Feet, Non-Capacity-Limited Airports	D-37
Probability of Descent Rate for Descents Between 3000-4000 Feet, Non-Capacity-Limited Airports	D-38
Probability of Descent Rate for Descents Between 4000-5000 Feet, Non-Capacity-Limited Airports	D-39
Probability of Descent Rate for Descents Between 5000-6000 Feet, Non-Capacity-Limited Airports	D-40
Probability of Descent Rate for Descents Between 6000-7000 Feet, Non-Capacity-Limited Airports	D-41
Probability of Descent Rate for Descents Between 7000-8000 Feet, Non-Capacity-Limited Airports	D-42
Probability of Descent Rate for Descents Between 8000-9000 Feet, Non-Capacity-Limited Airports	D-43
Probability of Descent Rate for Descents Between 9,000-10,000 Feet, Non-Capacity-Limited Airports	D-44
Probability of Descent Rate for Descents Between 10,000-11,000 Feet, Non-Capacity-Limited Airports	D-45
Probability of Descent Rate for Descents Between 11,000-12,000 Feet, Non-Capacity-Limited Airports	D-46
Probability of Descent Rate for Descents Between 12,000-13,000 Feet, Non-Capacity-Limited Airports	D-47

TABLE 9. STATISTICAL DESCENT DATA FORMATS (Continued)

Data Description	Figure
Probability of Descent Rate for Descents Between 13,000-14,000 Feet, Non-Capacity-Limited Airports	D-48
Probability of Descent Rate for Descents Between 14,000-15,000 Feet, Non-Capacity-Limited Airports	D-49
Probability of Descent Rate for Descents Between 15,000-16,000 Feet, Non-Capacity-Limited Airports	D-50
Probability of Descent Rate for Descents Between 16,000-17,000 Feet, Non-Capacity-Limited Airports	D-51
Probability of Descent Rate for Descents Between 17,000-18,000 Feet, Non-Capacity-Limited Airports	D-52
Probability of Descent Rate for Descents Between 18,000-19,000 Feet, Non-Capacity-Limited Airports	D-53
Probability of Descent Rate for Descents Between 19,000-20,000 Feet, Non-Capacity-Limited Airports	D-54
Probability of Descent Rate for Descents Between 20,000-21,000 Feet, Non-Capacity-Limited Airports	D-55
Probability of Descent Rate for Descents Between 21,000-22,000 Feet, Non-Capacity-Limited Airports	D-56
Probability of Descent Rate for Descents Between 22,000-23,000 Feet, Non-Capacity-Limited Airports	D-57
Probability of Descent Rate for Descents Between 23,000-24,000 Feet, Non-Capacity-Limited Airports	D-58
Probability of Descent Rate for Descents Between 24,000-25,000 Feet, Non-Capacity-Limited Airports	D-59
Probability of Descent Rate for Descents Between 25,000-26,000 Feet, Non-Capacity-Limited Airports	D-60
Probability of Descent Rate for Descents Between 26,000-27,000 Feet, Non-Capacity-Limited Airports	D-61
Probability of Descent Rate for Descents Between 27,000-28,000 Feet, Non-Capacity-Limited Airports	D-62
Probability of Descent Rate for Descents Between 28,000-29,000 Feet, Non-Capacity-Limited Airports	D-63
Probability of Descent Rate for Descents Between 29,000-30,000 Feet, Non-Capacity-Limited Airports	D-64
Probability of Descent Rate for Descents Between 30,000-31,000 Feet, Non-Capacity-Limited Airports	D-65
Probability of Descent Rate for Descents Between 31,000-32,000 Feet, Non-Capacity-Limited Airports	D-66
Probability of Descent Rate for Descents Between 32,000-33,000 Feet, Non-Capacity-Limited Airports	D-67
Probability of Descent Rate for Descents Between 33,000-34,000 Feet, Non-Capacity-Limited Airports	D-68
Probability of Descent Rate for Descents Between 34,000-35,000 Feet, Non-Capacity-Limited Airports	D-69
Probability of Descent Rate for Descents Between 35,000-36,000 Feet, Non-Capacity-Limited Airports	D-70
Probability of Descent Rate for Descents Between 36,000-37,000 Feet, Non-Capacity-Limited Airports	D-71
Probability of Descent Rate for Descents Between 37,000-38,000 Feet, Non-Capacity-Limited Airports	D-72
Probability of Descent Rate for Descents Between 38,000-39,000 Feet, Non-Capacity-Limited Airports	D-73
Probability of Descent Rate for Descents Between 39,000-40,000 Feet, Non-Capacity-Limited Airports	D-74
Probability of Descent Rate for Descents Between 40,000-41,000 Feet, Non-Capacity-Limited Airports	D-75
Probability of Descent Rate for Descents Between 41,000-42,000 Feet, Non-Capacity-Limited Airports	D-76
Probability of Descent Rate for Descents Between 42,000-43,000 Feet, Non-Capacity-Limited Airports	D-77
Probability of Descent Rate for Descents Between 0-1000 Feet, Capacity-Limited Airports	D-78
Probability of Descent Rate for Descents Between 1000-2000 Feet, Capacity-Limited Airports	D-79
Probability of Descent Rate for Descents Between 2000-3000 Feet, Capacity-Limited Airports	D-80
Probability of Descent Rate for Descents Between 3000-4000 Feet, Capacity-Limited Airports	D-81
Probability of Descent Rate for Descents Between 4000-5000 Feet, Capacity-Limited Airports	D-82
Probability of Descent Rate for Descents Between 5000-6000 Feet, Capacity-Limited Airports	D-83
Probability of Descent Rate for Descents Between 6000-7000 Feet, Capacity-Limited Airports	D-84
Probability of Descent Rate for Descents Between 7000-8000 Feet, Capacity-Limited Airports	D-85
Probability of Descent Rate for Descents Between 8000-9000 Feet, Capacity-Limited Airports	D-86
Probability of Descent Rate for Descents Between 9,000-10,000 Feet, Capacity-Limited Airports	D-87
Probability of Descent Rate for Descents Between 10,000-11,000 Feet, Capacity-Limited Airports	D-88
Probability of Descent Rate for Descents Between 11,000-12,000 Feet, Capacity-Limited Airports	D-89
Probability of Descent Rate for Descents Between 12,000-13,000 Feet, Capacity-Limited Airports	D-90
Probability of Descent Rate for Descents Between 13,000-14,000 Feet, Capacity-Limited Airports	D-91
Probability of Descent Rate for Descents Between 14,000-15,000 Feet, Capacity-Limited Airports	D-92
Probability of Descent Rate for Descents Between 15,000-16,000 Feet, Capacity-Limited Airports	D-93
Probability of Descent Rate for Descents Between 16,000-17,000 Feet, Capacity-Limited Airports	D-94

TABLE 9. STATISTICAL DESCENT DATA FORMATS (Continued)

Data Description	Figure
Probability of Descent Rate for Descents Between 17,000-18,000 Feet, Capacity-Limited Airports	D-95
Probability of Descent Rate for Descents Between 18,000-19,000 Feet, Capacity-Limited Airports	D-96
Probability of Descent Rate for Descents Between 19,000-20,000 Feet, Capacity-Limited Airports	D-97
Probability of Descent Rate for Descents Between 20,000-21,000 Feet, Capacity-Limited Airports	D-98
Probability of Descent Rate for Descents Between 21,000-22,000 Feet, Capacity-Limited Airports	D-99
Probability of Descent Rate for Descents Between 22,000-23,000 Feet, Capacity-Limited Airports	D-100
Probability of Descent Rate for Descents Between 23,000-24,000 Feet, Capacity-Limited Airports	D-101
Probability of Descent Rate for Descents Between 24,000-25,000 Feet, Capacity-Limited Airports	D-102
Probability of Descent Rate for Descents Between 25,000-26,000 Feet, Capacity-Limited Airports	D-103
Probability of Descent Rate for Descents Between 26,000-27,000 Feet, Capacity-Limited Airports	D-104
Probability of Descent Rate for Descents Between 27,000-28,000 Feet, Capacity-Limited Airports	D-105
Probability of Descent Rate for Descents Between 28,000-29,000 Feet, Capacity-Limited Airports	D-106
Probability of Descent Rate for Descents Between 29,000-30,000 Feet, Capacity-Limited Airports	D-107
Probability of Descent Rate for Descents Between 30,000-31,000 Feet, Capacity-Limited Airports	D-108
Probability of Descent Rate for Descents Between 31,000-32,000 Feet, Capacity-Limited Airports	D-109
Probability of Descent Rate for Descents Between 32,000-33,000 Feet, Capacity-Limited Airports	D-110
Probability of Descent Rate for Descents Between 33,000-34,000 Feet, Capacity-Limited Airports	D-111
Probability of Descent Rate for Descents Between 34,000-35,000 Feet, Capacity-Limited Airports	D-112
Probability of Descent Rate for Descents Between 35,000-36,000 Feet, Capacity-Limited Airports	D-113
Probability of Descent Rate for Descents Between 36,000-37,000 Feet, Capacity-Limited Airports	D-114
Probability of Descent Rate for Descents Between 37,000-38,000 Feet, Capacity-Limited Airports	D-115
Probability of Descent Rate for Descents Between 38,000-39,000 Feet, Capacity-Limited Airports	D-116
Probability of Descent Rate for Descents Between 39,000-40,000 Feet, Capacity-Limited Airports	D-117
Probability of Descent Rate for Descents Between 40,000-41,000 Feet, Capacity-Limited Airports	D-118
Probability of Descent Rate for Descents Between 41,000-42,000 Feet, Capacity-Limited Airports	D-119
Probability of Descent Rate for Descents Between 42,000-43,000 Feet, Capacity-Limited Airports	D-120
Probability of Occurrence of Initial Cruise Altitude for Flights Less Than 300 Nautical Miles	D-121
Mean Descent Rates at Pressure Altitude by Gross Weight Bands, 400-500K	D-122
Mean Descent Rates at Pressure Altitude by Gross Weight Bands, 500-600K	D-123
Mean Descent Rates at Pressure Altitude by Gross Weight Bands, 600-700K	D-124
Mean Descent Rate into Capacity-Unlimited Airports at Pressure Altitude by N1 Range (20%-70%)	D-125
Mean Descent Rate into Capacity-Unlimited Airports at Pressure Altitude by N1 Range (60%-110%)	D-126
Mean Descent Rate into Capacity-Limited Airports at Pressure Altitude by N1 Range (20%-70%)	D-127
Mean Descent Rate into Capacity-Limited Airports at Pressure Altitude by N1 Range (60%-110%)	D-128
Mean Descent Rate at Pressure Altitude by CAS Range (120-200 kts)	D-129
Mean Descent Rate at Pressure Altitude by CAS Range (200-260 kts)	D-130
Mean Descent Rate at Pressure Altitude by CAS Range (260-310 kts)	D-131
Mean Descent Rate at Pressure Altitude by CAS Range (310-370 kts)	D-132
Gross Weight and Pressure Altitude at Start of First Cruise	D-133

Figures D-1 and D-2 present scatter plots of the descent rates within 1000-foot altitude bands for capacity-limited and non-capacity-limited airports. These data include any hold times that occur during the descent phase and account for the occurrences of the lowest decent rates shown.

Figures D-3 and D-4 show the mean descent rates for each altitude band for the data contained in figures D-1 and D-2. Thus, these means are based on data that include hold times during the descent phase.

Figures D-5 and D-6 present scatter plots of the descent rates within 1000-foot bands for capacity-limited and non-capacity-limited airports respectively. However, in contrast to figures D-1 and D-2, these data do not include the hold times that occur during the descent phase. Thus, they show few occurrences at the lower descent rates than in figures D-1 and D-2.

Figures D-7 and D-8 show the mean descent rates for each altitude band for the data contained in figures D-5 and D-6. Thus, these means are based on data that do not include hold times during the descent phase.

Figure D-9 lists the maximum descent rates and associated altitude for nine descents into capacity-limited airports. Figures D-10 through D-21 present the descent profiles for these flights. Each flight is shown as two profiles, one presents the profile starting at a time before the start of the descent phase and the other presents the profile starting at an altitude of 15,000 feet.

Figure D-22 lists the maximum descent rates and associated altitude for nine descents into non-capacity-limited airports. Figures D-23 through D-34 present the descent profiles for these flights. Again, each flight is shown as two profiles, one presenting the profile starting at a time before the start of the descent phase and the other presenting the profile starting at an altitude of 15,000 feet.

Figures D-35 through D-77 present probabilities of descent rates for each 1000-foot altitude band for descents into non-capacity-limited airports. Figures D-78 through D-120 present identical data for descents into capacity-limited airports. The plots include a table presenting statistical information such as means and standard deviation.

Figure D-121 presents the probability of the initial cruise altitude for flights less than 300 nautical miles.

Figures D-122 through D-124 present the mean descent rates at pressure altitude as a function of gross weight intervals.

Figures D-125 through D-128 present the mean descent rates at pressure altitudes by N1 range for descents into non-capacity-limited and capacity-limited airports.

Figures D-129 through D-132 present the mean descent rates at pressure altitude by airspeed.

8. CONCLUSIONS.

This report provides valuable information about how the B-747-400 aircraft are being used during normal flight and ground operations by the airline.

The participating airline fully supported this program and provided UDRI with 11,066 flights representing 95,883 flight hours of useable B-747-400 data from typical revenue flights. Except

for some gaps and repeated frames, the recorded data were acceptable and compatible with UDRI's data processing software. The 11,066 flights were judged as sufficient to provide a representative statistical baseline of the aircraft's ground, airborne, and systems operational usage. It should be noted, however, that the above number of flights were not used in the plotting of all formats within this report.

The statistical data formats presented in this report will provide the FAA, the airlines, and aircraft manufacturers with beneficial information about the B-747-400's actual operational service usage.

The flight length data shows that the B-747-400 is used primarily in long-haul operations. A flight length of 3800 nautical miles is exceeded by 50% of the flights. In contrast, the data in reference 7 shows that the B-767-200ER, an extended range aircraft, exceeds the 3800 nautical mile flight length by only 10% of the flights.

Lateral load factors during ground turning are lower than observed on previous smaller aircraft such as the B-767-200ER, A320, B-737-400, and the MD-82. Comparing the lateral load factors frequency distributions seen on the B-747-400 with those previously seen on the above mentioned aircraft, it is clear that there is an inverse relationship between the lateral load factor during ground turning and airplane size.

Longitudinal load factors during taxi operations are generally higher for the B-747-400 than were measured on either the B-767-200ER or the A320. Interestingly, the longitudinal load factors during touchdown and landing roll do not show major differences when compared to the other aircraft.

Vertical load factors during taxi operations, takeoff roll, and landing roll are significantly lower for the B-747-400 than for the B-767-200ER or the A320.

Vertical gust load factors and maneuver load factors extracted from the vertical load factor measurements for the B-747-400 are not significantly different from the B-767-200ER and the A320.

The derived gust velocities for the B-747-400 compared favorably with the A320-derived gust velocities for all altitudes. Comparison of the B-747-400-derived gust velocities with the B-767-200ER shows reasonable comparisons for altitudes above 9500 feet. For altitudes below 9500 feet, the B-767-200ER shows higher gust velocities than the B-747-400 or the A320.

The data in appendices C and D provide data requested for special consideration. Appendix C displays formats relating aircraft speed and attitude with airport elevation. The descent rate statistics in appendix D provide individual profiles along with a range of additional formats concerning altitude, airspeed, N1, and gross weight.

9. REFERENCES.

1. de Jonge, B., "Reduction of Incremental Load Factor Acceleration Data to Gust Statistics," FAA report DOT/FAA/CT-94/57, August 1994.

2. Tipps, Daniel O., John W. Rustenburg, and Donald A. Skinn, "Study of Side Load Factor Statistics From Commercial Aircraft Ground Operations," University of Dayton Research Institute Report UDR-TR-2001-00005, January 2001.

3. Rustenburg, John W., Donald A. Skinn, and Daniel O. Tipps, "An Evaluation of Methods to Separate Maneuver and Gust Load Factors From Measured Acceleration Time Histories," FAA report DOT/FAA/AR-99/14, April 1999.

4. Chai, Sonny T. and William H. Mason, "Landing Gear Integration in Aircraft Conceptual Design," Virginia Polytechnic Institute and State University Report MAD 96-09-01, September 1996, rev. March 1997.

5. Tipps, Daniel O., John W. Rustenburg, and Donald A. Skinn, "Statistical Loads Data for Boeing 737-400 in Commercial Operations," FAA report DOT/FAA/AR-98/28, August 1998.

6. Tipps, Daniel O., John W. Rustenburg, and Donald A. Skinn, "Statistical Loads Data for a MD-82/83 Aircraft in Commercial Operations," FAA report DOT/FAA/AR-98/65, February 1999.

7. Tipps, Daniel O., John W. Rustenburg, and Donald A. Skinn, "Statistical Loads Data for B-767-200ER Aircraft in Commercial Operation," FAA report DOT/FAA/AR-00/10, March 2000.

8. Tipps, Daniel O., John W. Rustenburg, and Donald A. Skinn, "Statistical Loads Data for the Airbus A-320 Aircraft in Commercial Operations," FAA report DOT/FAA/AR-02/35, April 2002.

9. Tipps, Daniel O., John W. Rustenburg, and Donald A. Skinn, "Statistical Loads Data for Bombardier CRJ100 Aircraft in Commercial Operations," FAA report DOT/FAA/AR-03/44, July 2003.

10. Press, Harry and Roy Steiner, "An Approach to the Problem of Estimating Severe and Repeated Gust Loads for Missile Operations," National Advisory Committee for Aeronautics Technical Note 4332, Langley Aeronautical Laboratory, Langley Field, VA, September 1958.

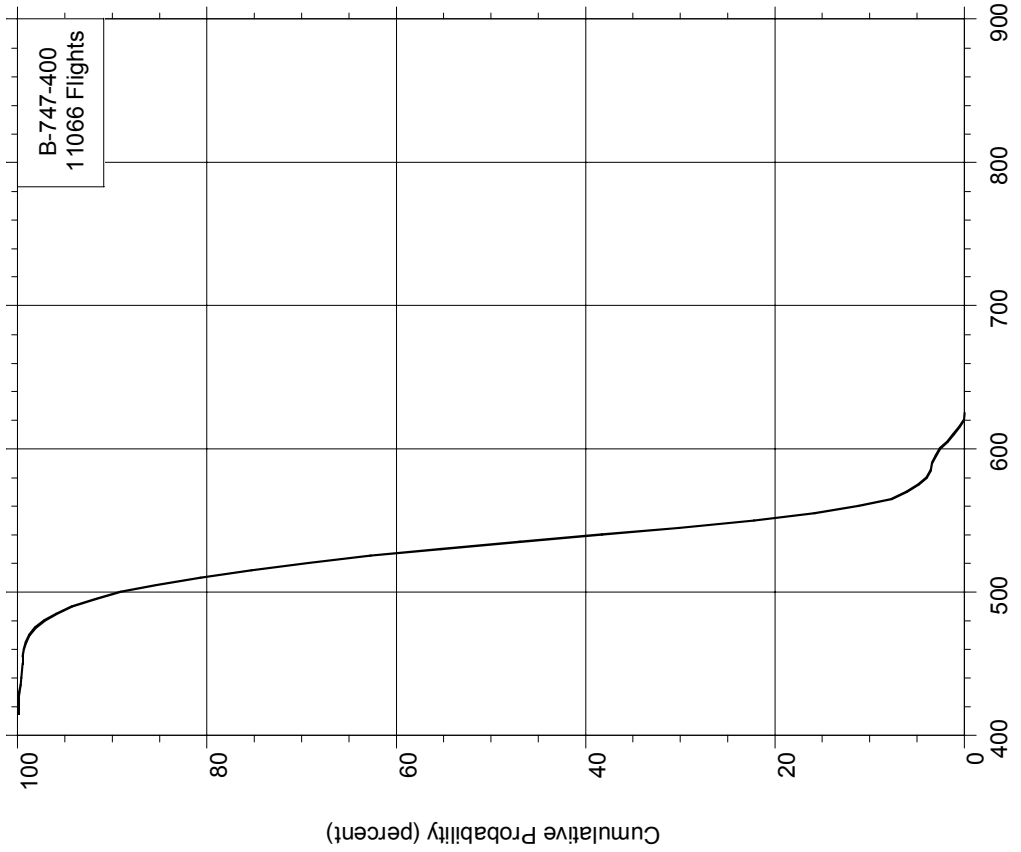

FIGURE A-1. CUMULATIVE PROBABILITY OF TAKEOFF GROSS WEIGHT

FIGURE A-2. CUMULATIVE PROBABILITY OF LANDING GROSS WEIGHT

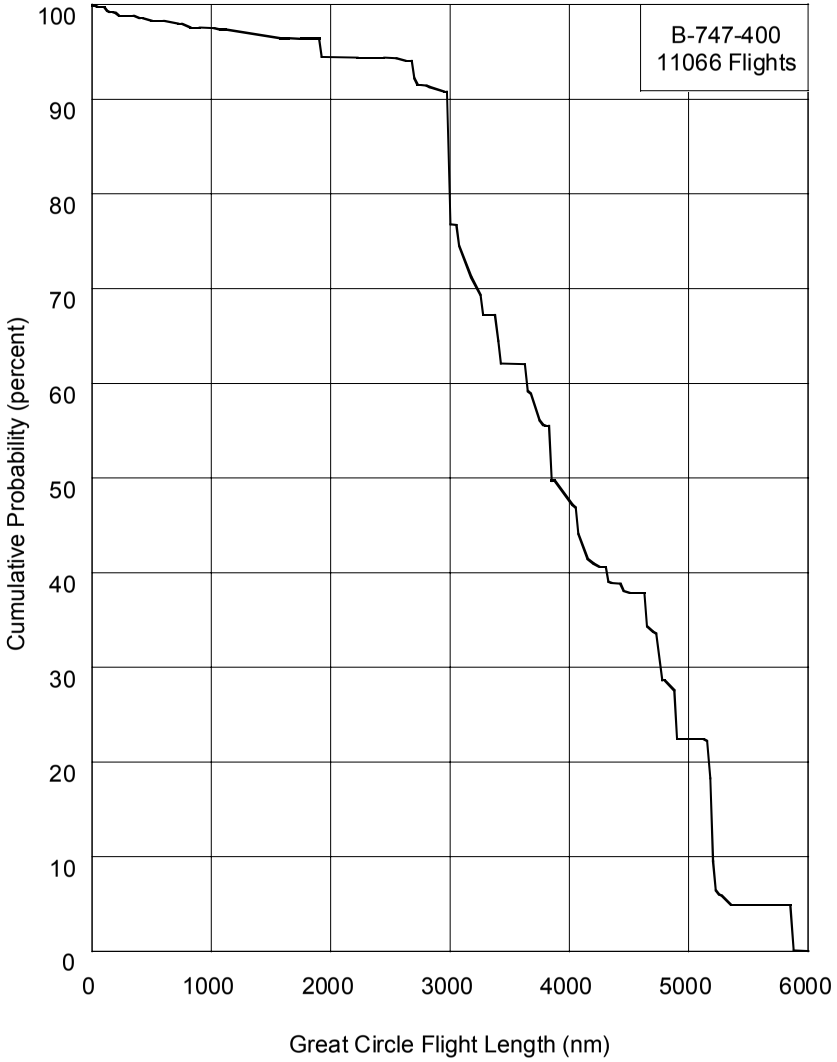

FIGURE A-3. CUMULATIVE PROBABILITY OF GREAT CIRCLE FLIGHT LENGTH

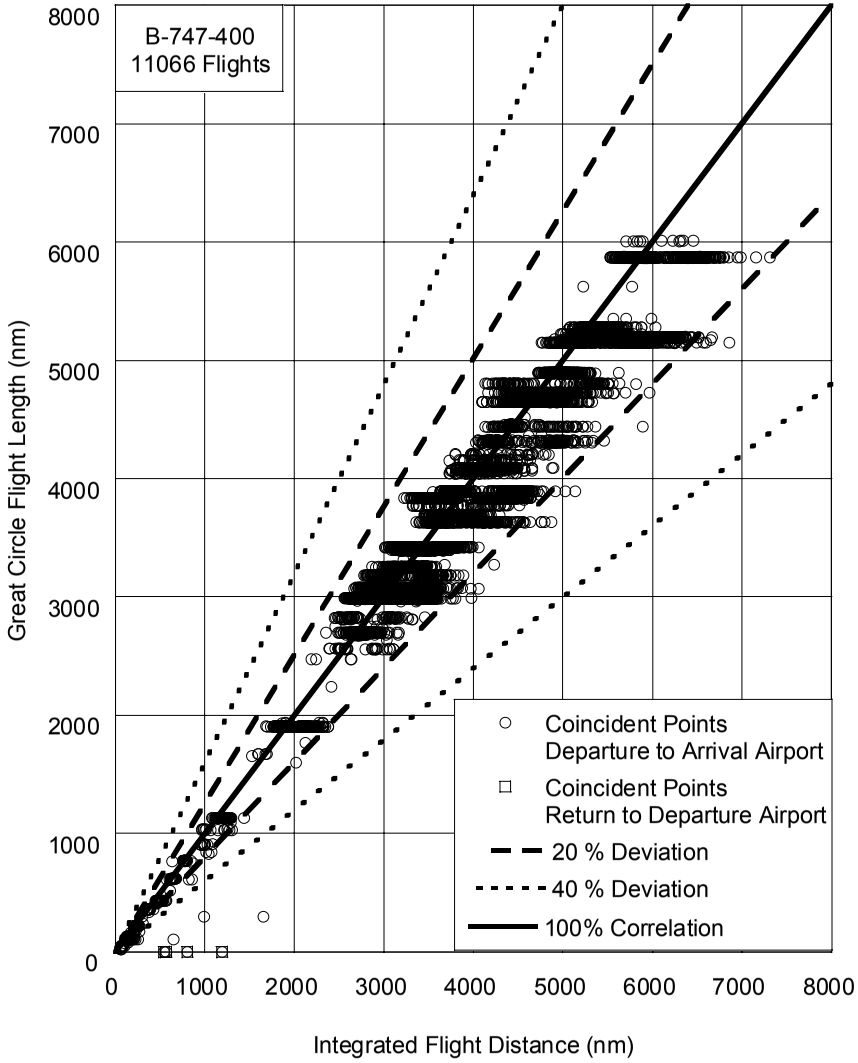

FIGURE A-4. CORRELATION OF GREAT CIRCLE FLIGHT LENGTH AND INTEGRATED FLIGHT DISTANCE

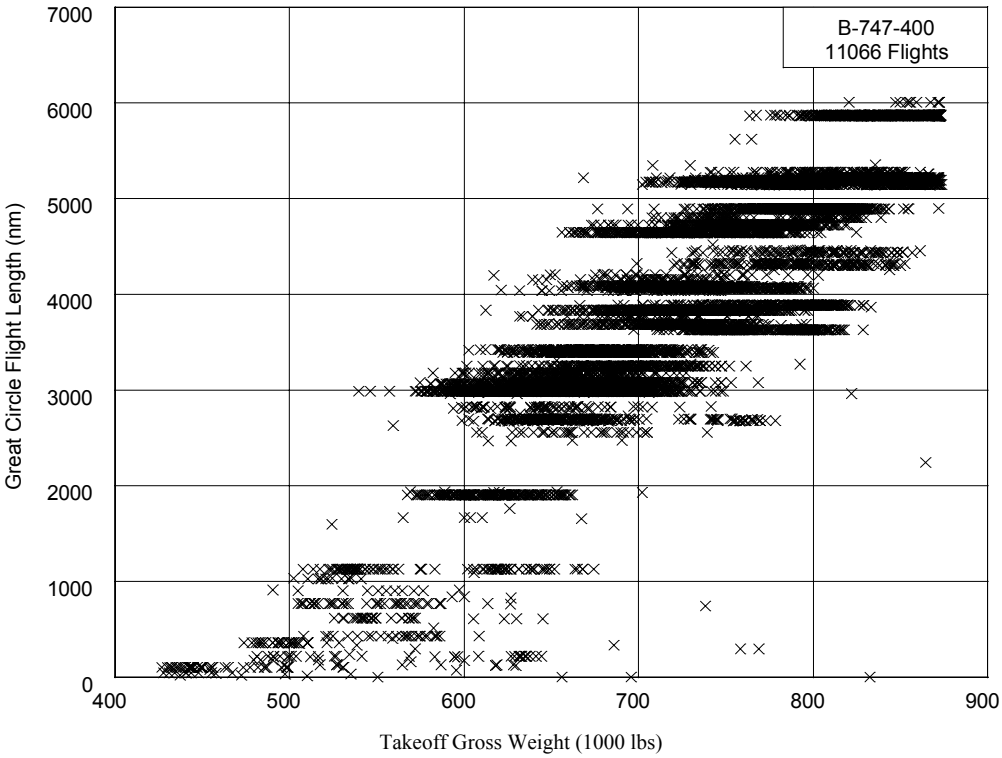

FIGURE A-5. CORRELATION OF TAKEOFF GROSS WEIGHT AND GREAT CIRCLE FLIGHT LENGTH

Takeoff Gross Weight (1000 lbs)

Great Circle Flight Length (nm)

11066Flts	400-450	450-500	500-550	550-600	600-650	650-700	700-750	750-800	800-850	850-900	Total
0- 500	0.325	0.470	0.334	0.262	0.181	0.027		0.018	0.009		1.627
500-1000		0.009	0.407	0.325	0.072		0.009				0.822
1000-1500			0.488	0.108	0.380	0.054					1.030
1500-2000			0.009	0.497	1.356	0.172	0.009				2.042
2000-2500					0.018	0.018				0.009	0.045
2500-3000			0.018	0.624	7.437	8.196	1.102	0.208	0.009		17.594
3000-3500				0.334	2.874	8.657	2.838	0.045			14.748
3500-4000					0.127	1.825	7.265	4.554	1.093		14.865
4000-4500					0.090	1.220	4.067	2.738	1.175	0.054	9.344
4500-5000						0.786	3.687	8.106	2.801	0.036	15.417
5000-5500						0.009	1.184	6.362	7.103	2.883	17.540
5500-6000								0.244	2.684	1.898	4.826
6000-6500									0.027	0.072	0.099
Total	0.325	0.479	1.256	2.151	12.534	20.965	20.161	22.275	14.902	4.952	100.000

FIGURE A-6. CORRELATION OF TAKEOFF GROSS WEIGHT AND GREAT CIRCLE FLIGHT LENGTH, PERCENT OF FLIGHTS

Takeoff Gross Weight (1000 lbs)

Landing Gross Weight (K-lbs)

11066Flts	400-450	450-500	500-550	550-600	600-650	650-700	700-750	750-800	800-850	850-900	Total
400-450	0.325	0.054	0.027	0.027		0.009					0.443
450-500		0.425	0.877	1.184	4.789	1.853	0.958	0.226	0.027		10.338
500-550			0.352	0.795	7.148	18.607	15.742	15.164	6.886	2.286	66.980
550-600				0.145	0.434	0.461	3.371	5.910	6.705	2.594	19.619
600-650					0.163	0.036	0.090	0.976	1.283	0.072	2.621
Total	0.325	0.479	1.256	2.151	12.534	20.965	20.161	22.275	14.902	4.952	100.000

FIGURE A-7. CORRELATION OF TAKEOFF AND LANDING GROSS WEIGHT, PERCENT OF FLIGHTS

Integrated Flight Distance (nm)

Altitude Band (feet)

8286 Flts	0-1000	1000-2000	2000-3000	3000-4000	4000-5000	5000-6000	6000-7000	7000-8000
39500-44500	5.72	1.68	1.49	0.53	0.17	0.52	0.45	
29500-39500	50.26	84.96	89.11	91.48	92.83	90.90	88.31	94.74
19500-29500	15.76	5.37	3.61	3.56	3.63	5.55	8.42	2.45
9500-19500	16.07	4.09	3.13	2.42	1.88	1.64	1.53	1.56
4500-9500	7.71	2.29	1.68	1.18	0.93	0.86	0.79	0.75
1500-4500	3.40	1.26	0.72	0.63	0.40	0.38	0.37	0.36
500-1500	0.76	0.27	0.18	0.14	0.11	0.10	0.09	0.08
0-500	0.32	0.09	0.08	0.06	0.05	0.04	0.04	0.05
Total	100	100	100	100	100	100	100	100

FIGURE A-8. PERCENT OF INTEGRATED FLIGHT DISTANCE IN ALTITUDE BANDS

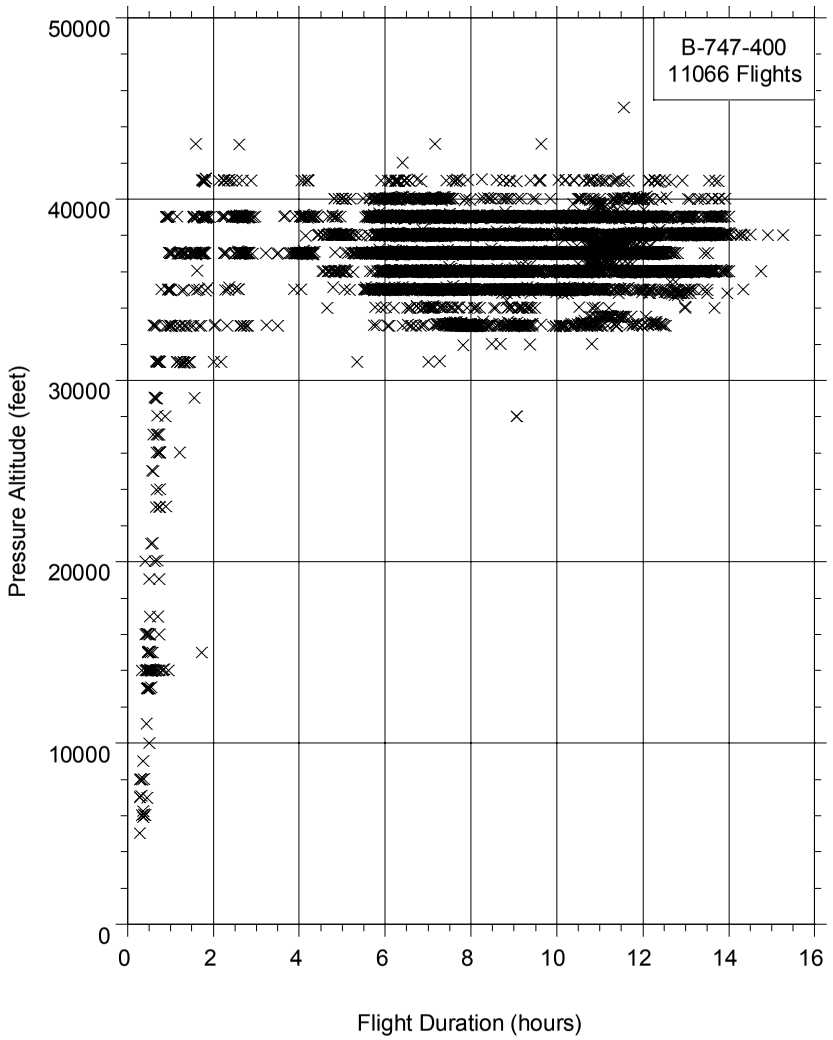

FIGURE A-9. CORRELATION OF MAXIMUM ALTITUDE AND FLIGHT DURATION

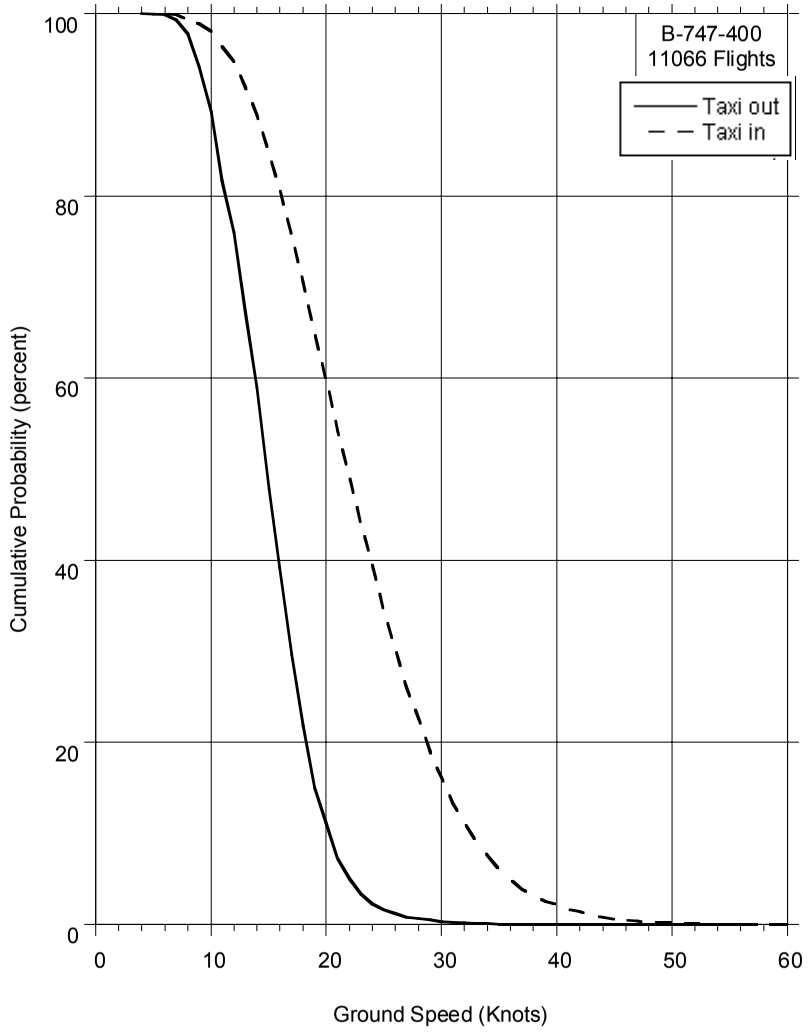

FIGURE A-10. CUMULATIVE PROBABILITY OF MAXIMUM GROUND SPEED DURING TAXI

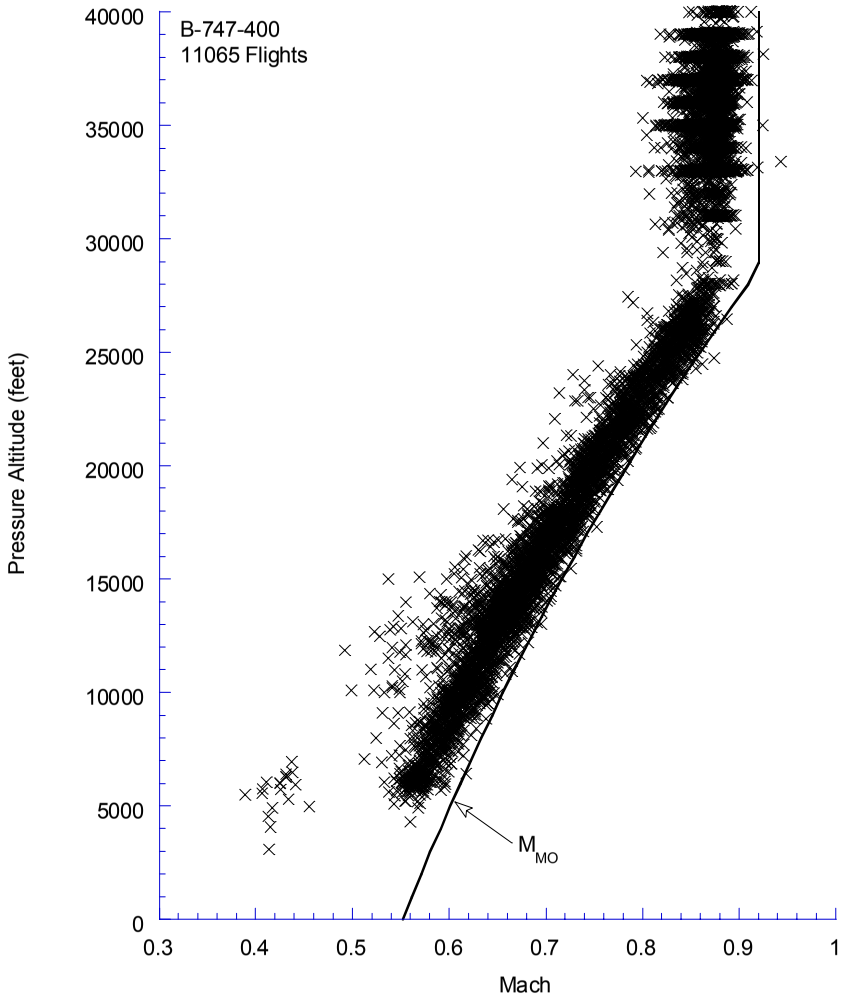

FIGURE A-11. MAXIMUM MACH NUMBER AND COINCIDENT ALTITUDE, ALL FLIGHT PHASES

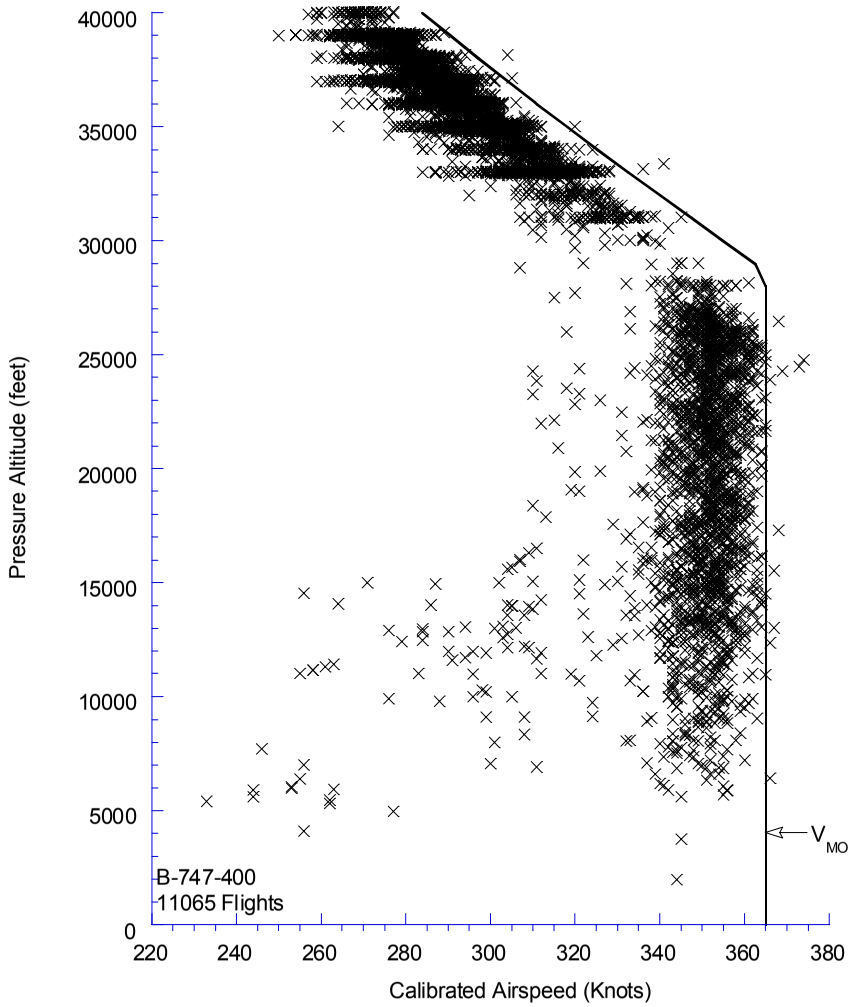

FIGURE A-12. MAXIMUM CALIBRATED AIRSPEED AND COINCIDENT ALTITUDE, ALL FLIGHT PHASES

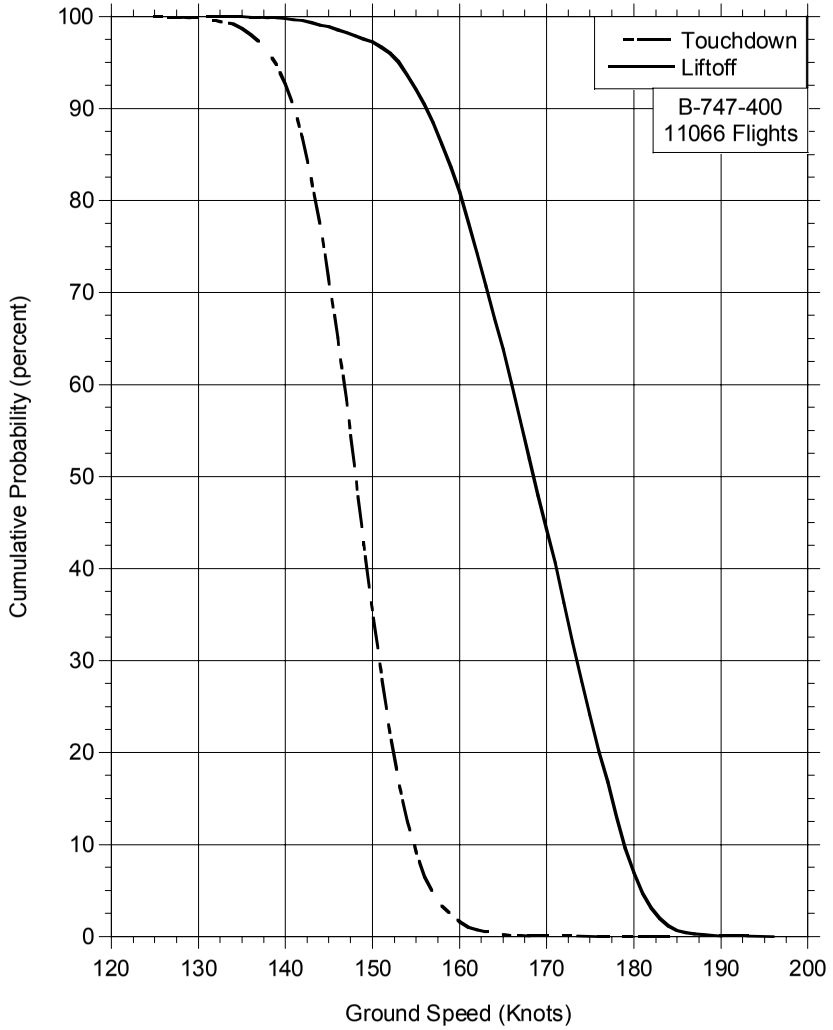

FIGURE A-13. CUMULATIVE PROBABILITY OF GROUND SPEED AT LIFTOFF AND TOUCHDOWN

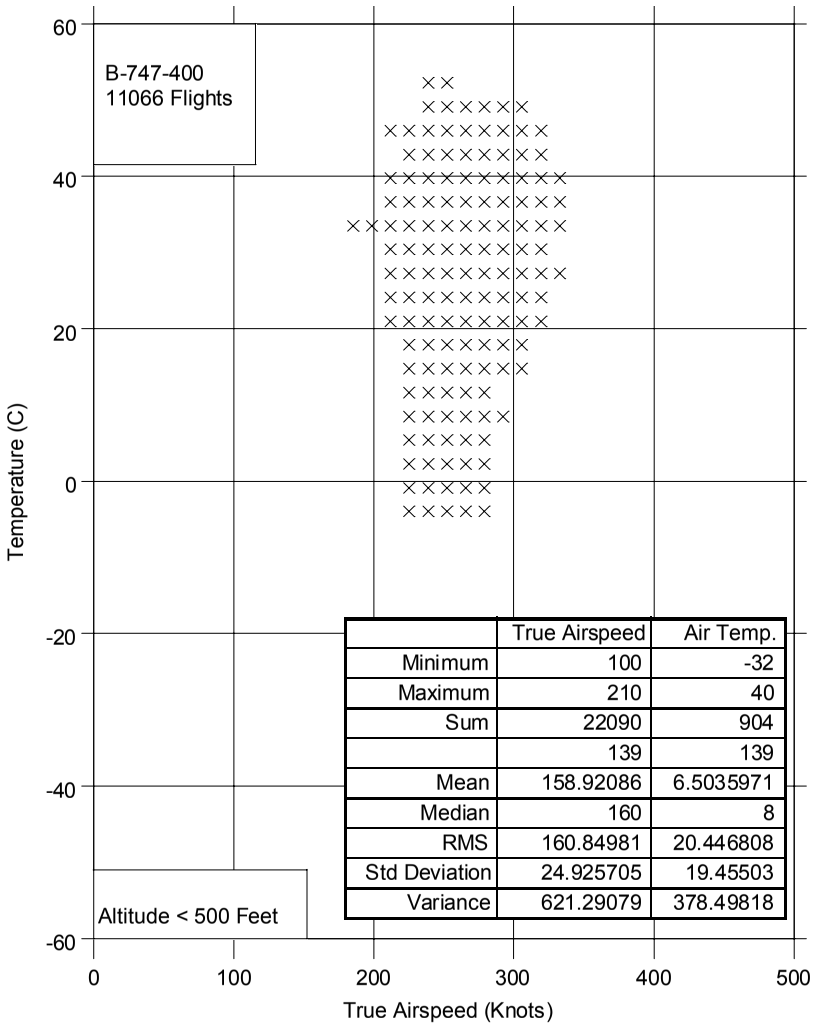

	True Airspeed	Air Temp.
Minimum	100	-32
Maximum	210	40
Sum	22090	904
	139	139
Mean	158.92086	6.5035971
Median	160	8
RMS	160.84981	20.446808
Std Deviation	24.925705	19.45503
Variance	621.29079	378.49818

FIGURE A-14. TOTAL AIR TEMPERATURE VS TRUE AIRSPEED, ALTITUDE < 500 FEET

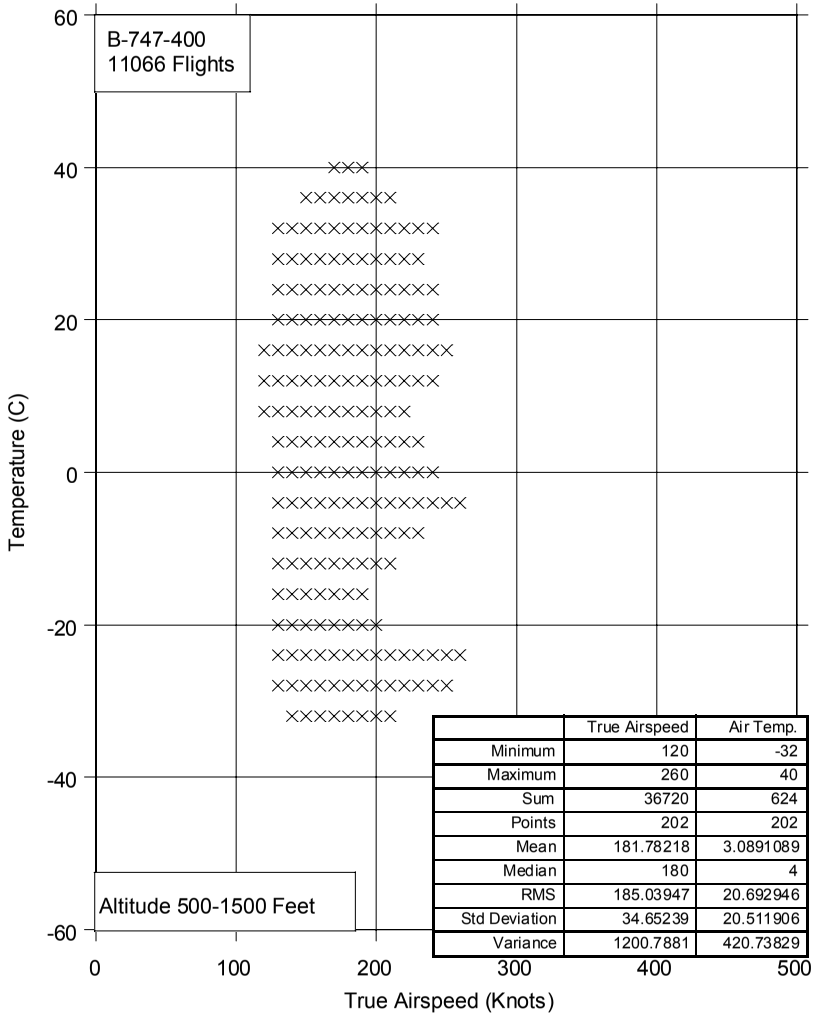

	True Airspeed	Air Temp.
Minimum	120	-32
Maximum	260	40
Sum	36720	624
Points	202	202
Mean	181.78218	3.0891089
Median	180	4
RMS	185.03947	20.692946
Std Deviation	34.65239	20.511906
Variance	1200.7881	420.73829

FIGURE A-15. TOTAL AIR TEMPERATURE VS TRUE AIRSPEED, ALTITUDE 500-1500 FEET

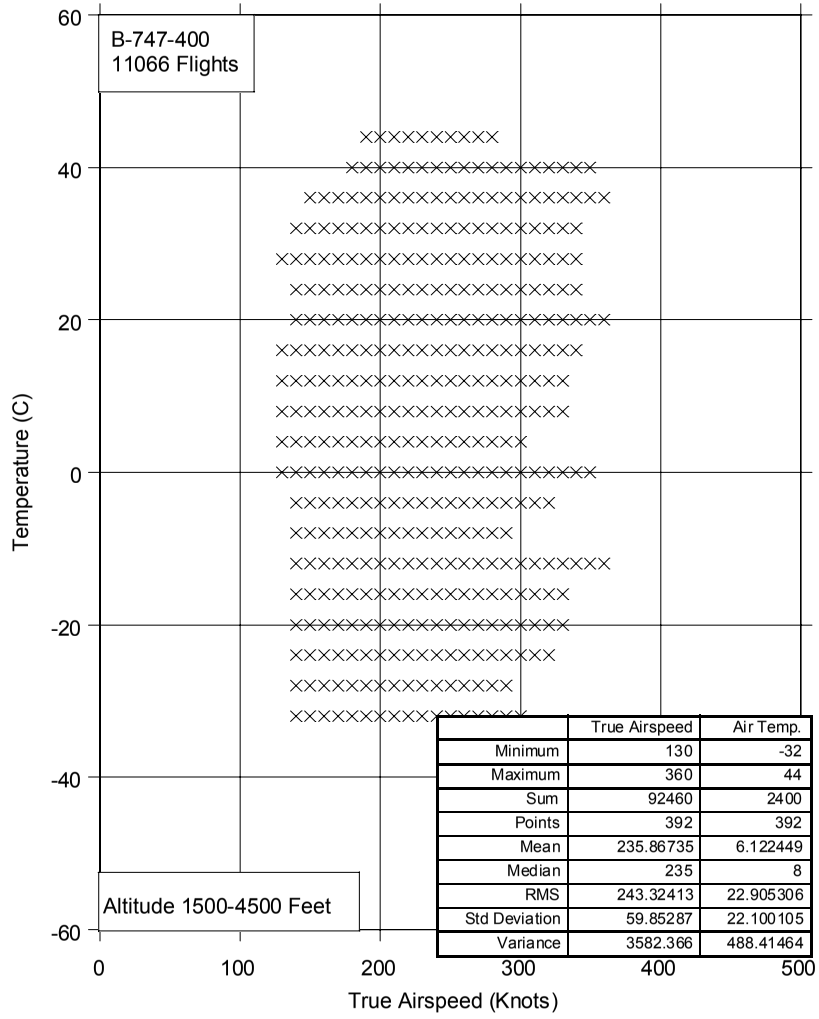

	True Airspeed	Air Temp.
Minimum	130	-32
Maximum	360	44
Sum	92460	2400
Points	392	392
Mean	235.86735	6.122449
Median	235	8
RMS	243.32413	22.905306
Std Deviation	59.85287	22.100105
Variance	3582.366	488.41464

FIGURE A-16. TOTAL AIR TEMPERATURE VS TRUE AIRSPEED, ALTITUDE 1500-4500 FEET

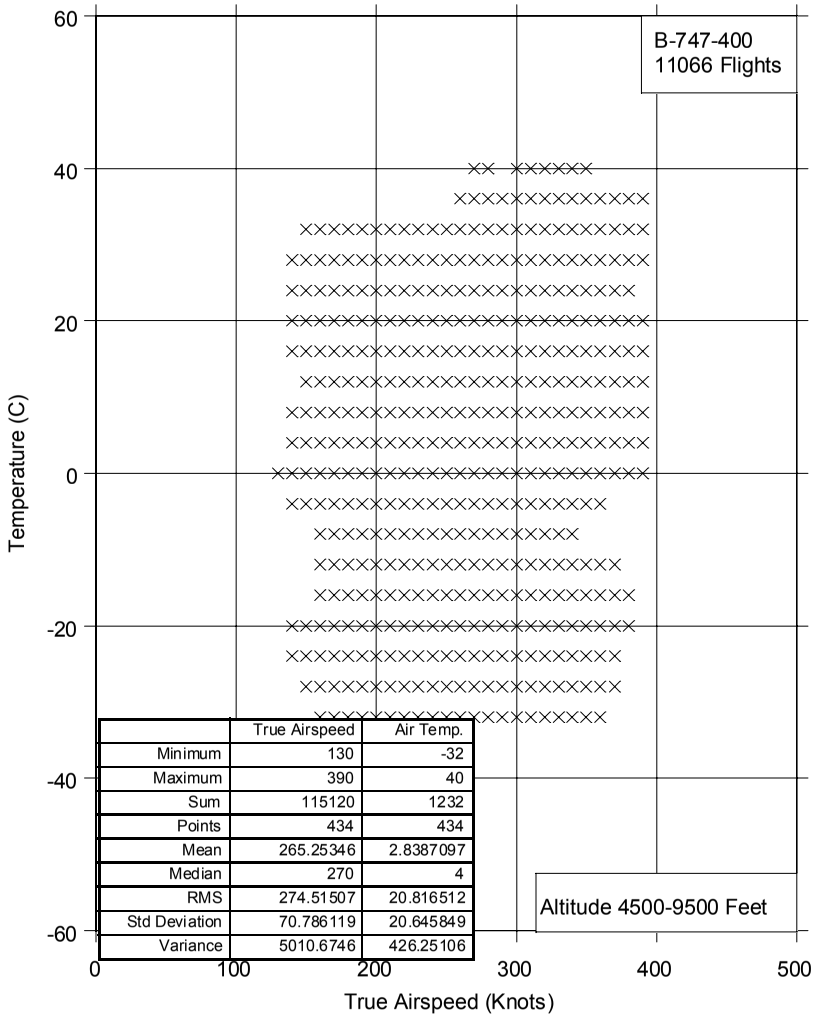

	True Airspeed	Air Temp.
Minimum	130	-32
Maximum	390	40
Sum	115120	1232
Points	434	434
Mean	265.25346	2.8387097
Median	270	4
RMS	274.51507	20.816512
Std Deviation	70.786119	20.645849
Variance	5010.6746	426.25106

FIGURE A-17. TOTAL AIR TEMPERATURE VS TRUE AIRSPEED, ALTITUDE 4500-9500 FEET

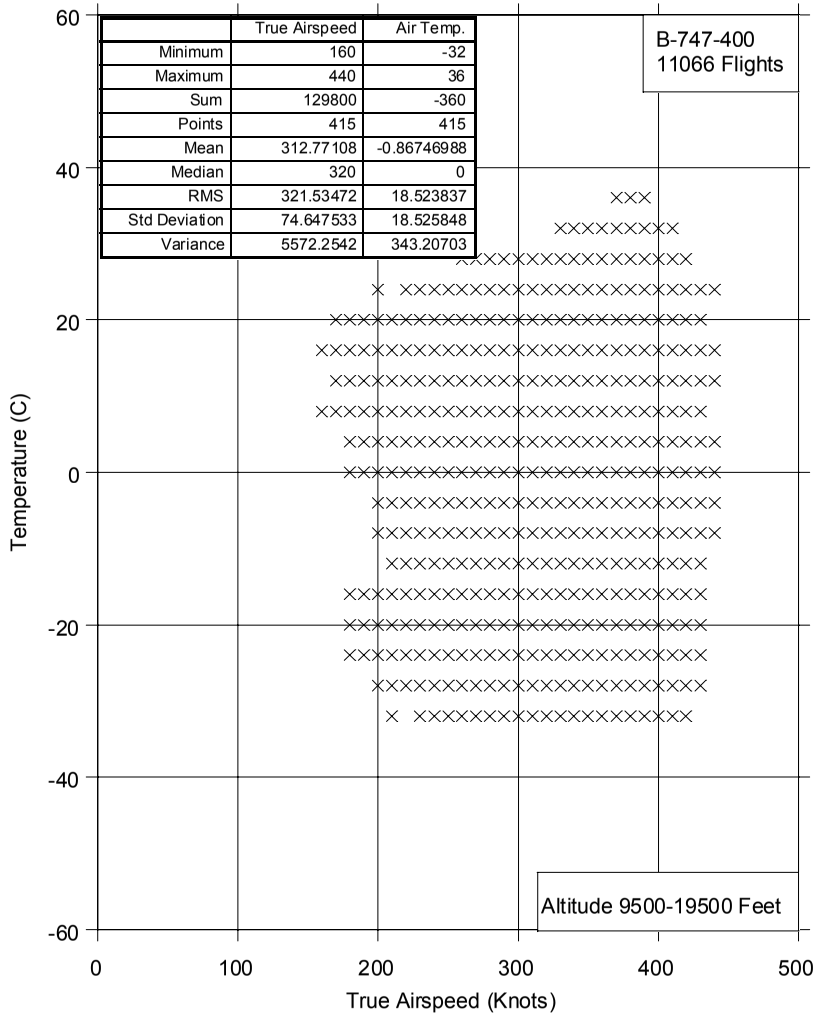

	True Airspeed	Air Temp.
Minimum	160	-32
Maximum	440	36
Sum	129800	-360
Points	415	415
Mean	312.77108	-0.86746988
Median	320	0
RMS	321.53472	18.523837
Std Deviation	74.647533	18.525848
Variance	5572.2542	343.20703

FIGURE A-18. TOTAL AIR TEMPERATURE VS TRUE AIRSPEED, ALTITUDE 9,500-19,500 FEET

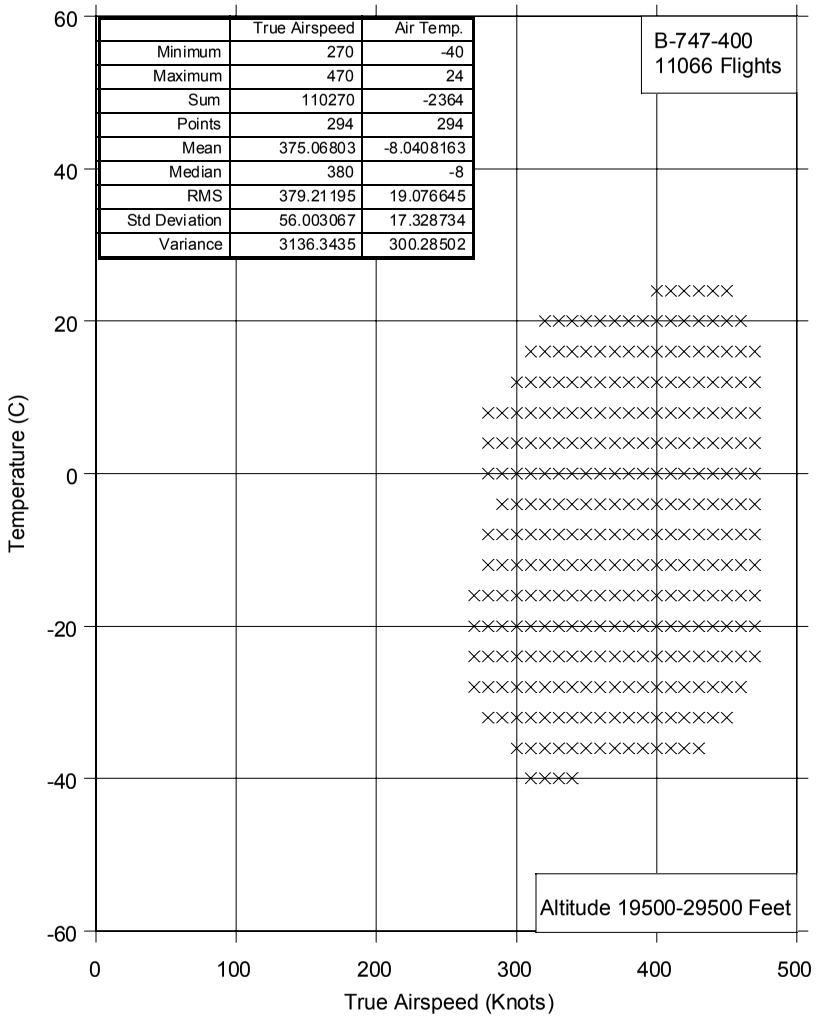

	True Airspeed	Air Temp.
Minimum	270	-40
Maximum	470	24
Sum	110270	-2364
Points	294	294
Mean	375.06803	-8.0408163
Median	380	-8
RMS	379.21195	19.076645
Std Deviation	56.003067	17.328734
Variance	3136.3435	300.28502

FIGURE A-19. TOTAL AIR TEMPERATURE VS TRUE AIRSPEED, ALTITUDE 19,500-29,500 FEET

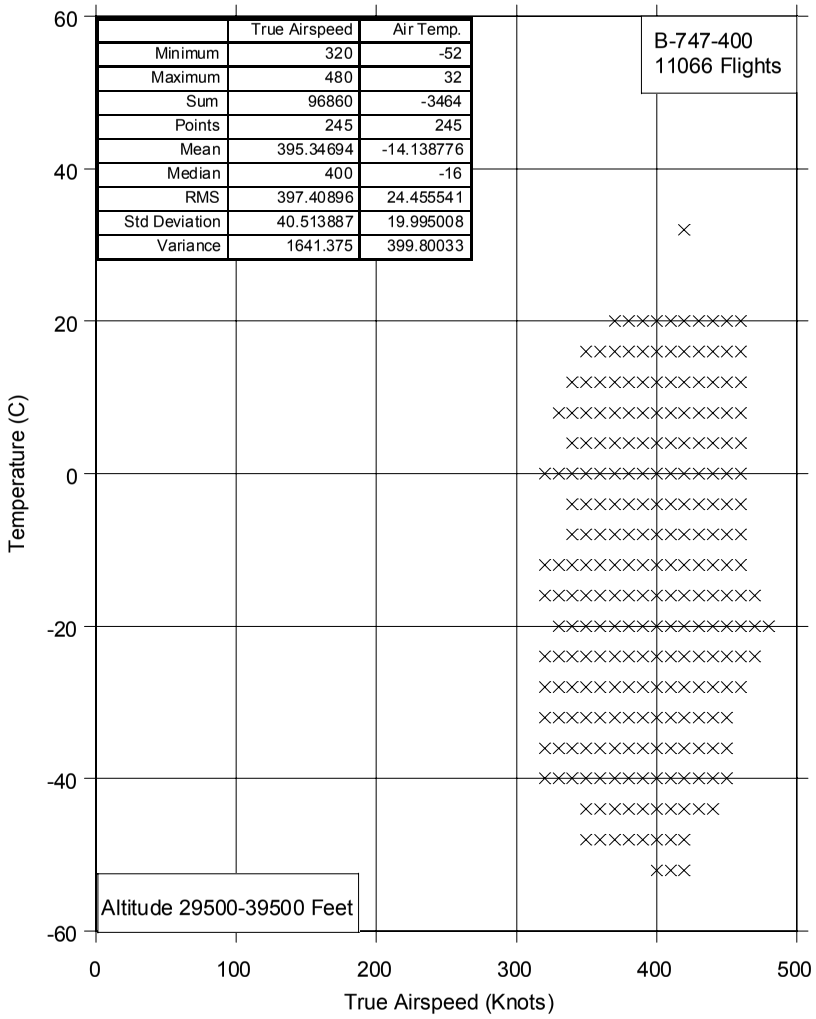

	True Airspeed	Air Temp.
Minimum	320	-52
Maximum	480	32
Sum	96860	-3464
Points	245	245
Mean	395.34694	-14.138776
Median	400	-16
RMS	397.40896	24.455541
Std Deviation	40.513887	19.995008
Variance	1641.375	399.80033

FIGURE A-20. TOTAL AIR TEMPERATURE VS TRUE AIRSPEED, ALTITUDE 29,500-39,500 FEET

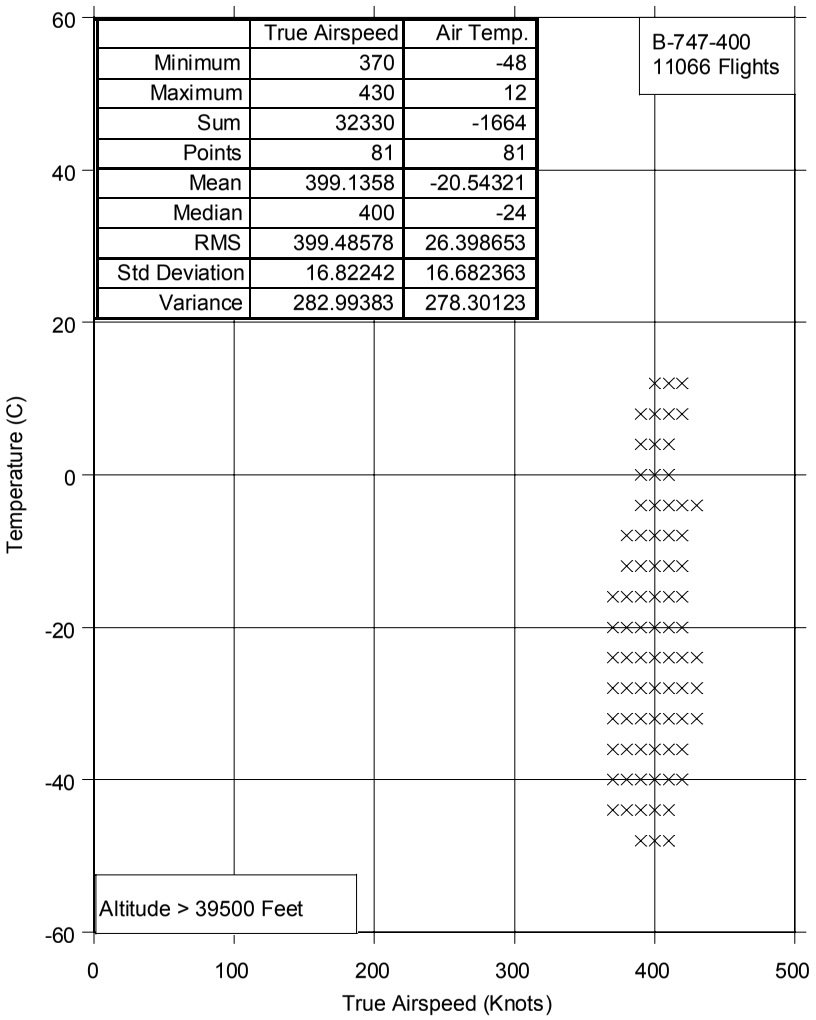

	True Airspeed	Air Temp.
Minimum	370	-48
Maximum	430	12
Sum	32330	-1664
Points	81	81
Mean	399.1358	-20.54321
Median	400	-24
RMS	399.48578	26.398653
Std Deviation	16.82242	16.682363
Variance	282.99383	278.30123

FIGURE A-21. TOTAL AIR TEMPERATURE VS TRUE AIRSPEED, ALTITUDE > 39,500 FEET

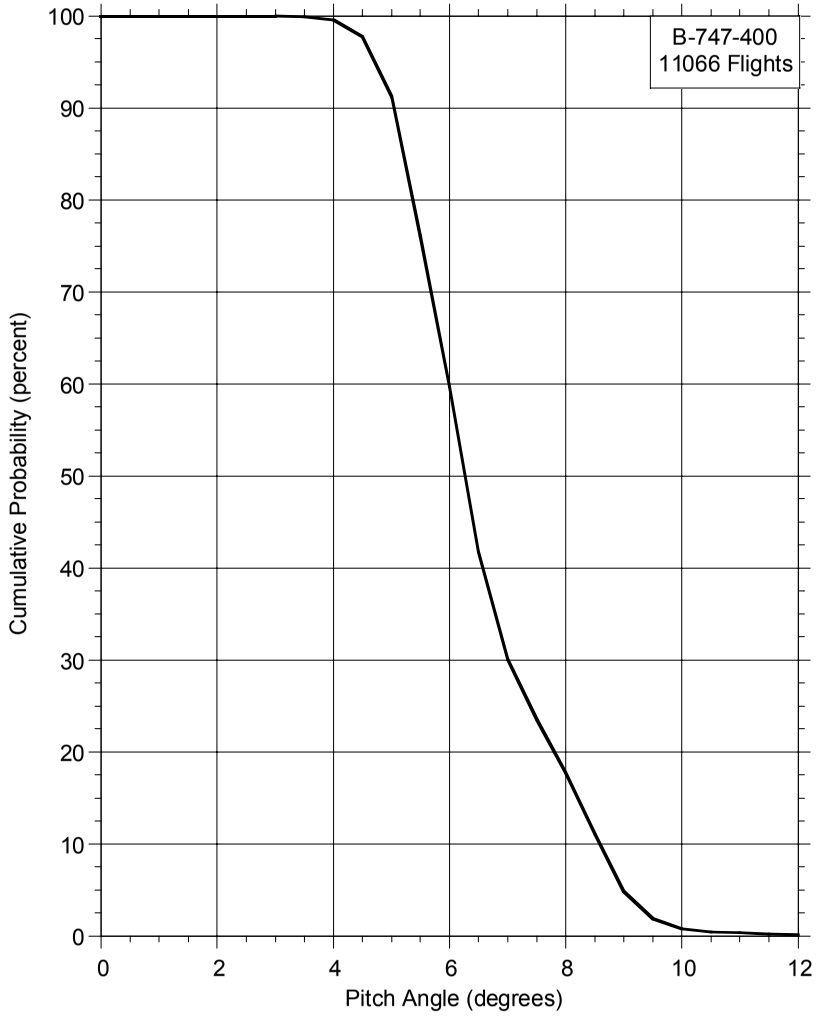

FIGURE A-22. CUMULATIVE PROBABILITY OF PITCH ANGLE AT LIFTOFF

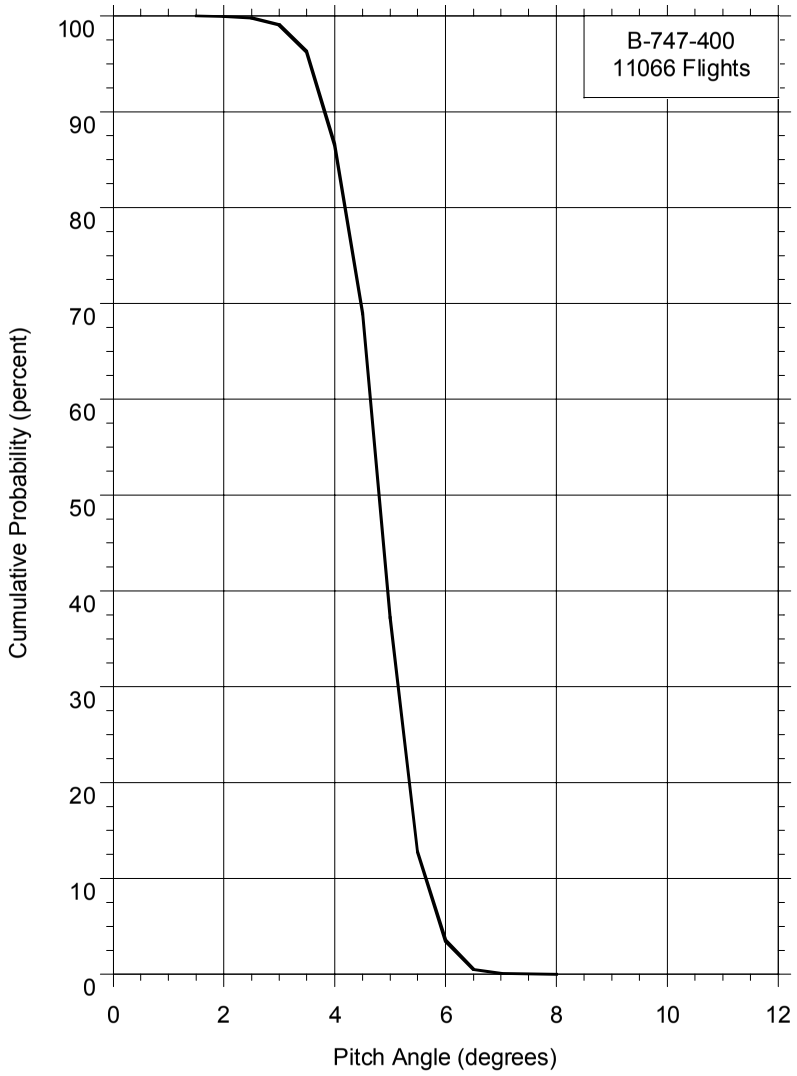

FIGURE A-23. CUMULATIVE PROBABILITY OF PITCH ANGLE AT TOUCHDOWN

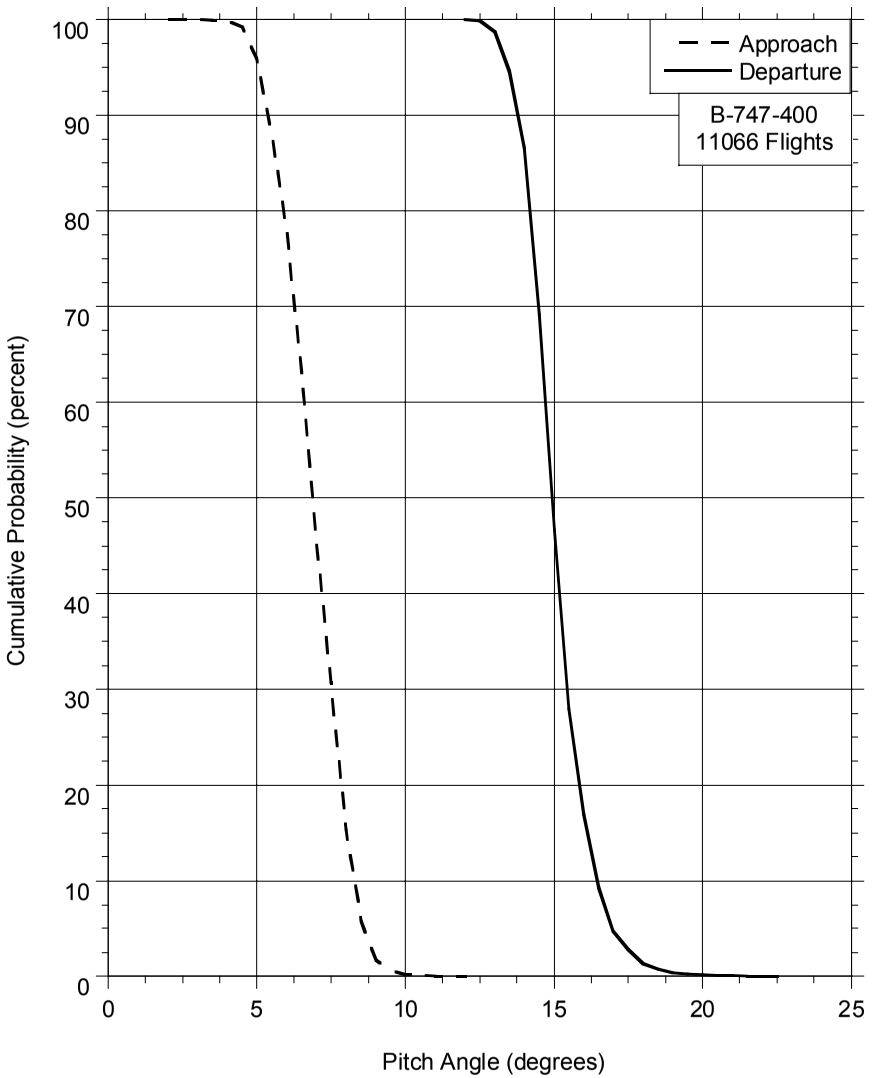

FIGURE A-24. CUMULATIVE PROBABILITY OF MAXIMUM PITCH ANGLE DURING DEPARTURE AND APPROACH

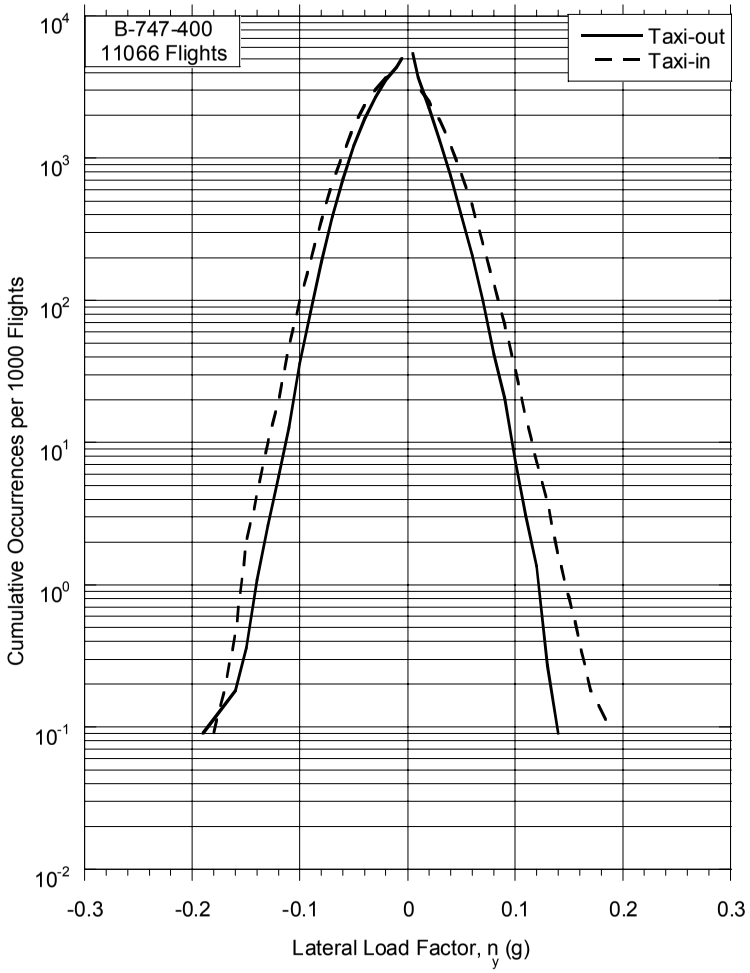

FIGURE A-25. CUMULATIVE FREQUENCY OF MAXIMUM LATERAL LOAD FACTOR DURING GROUND TURNS

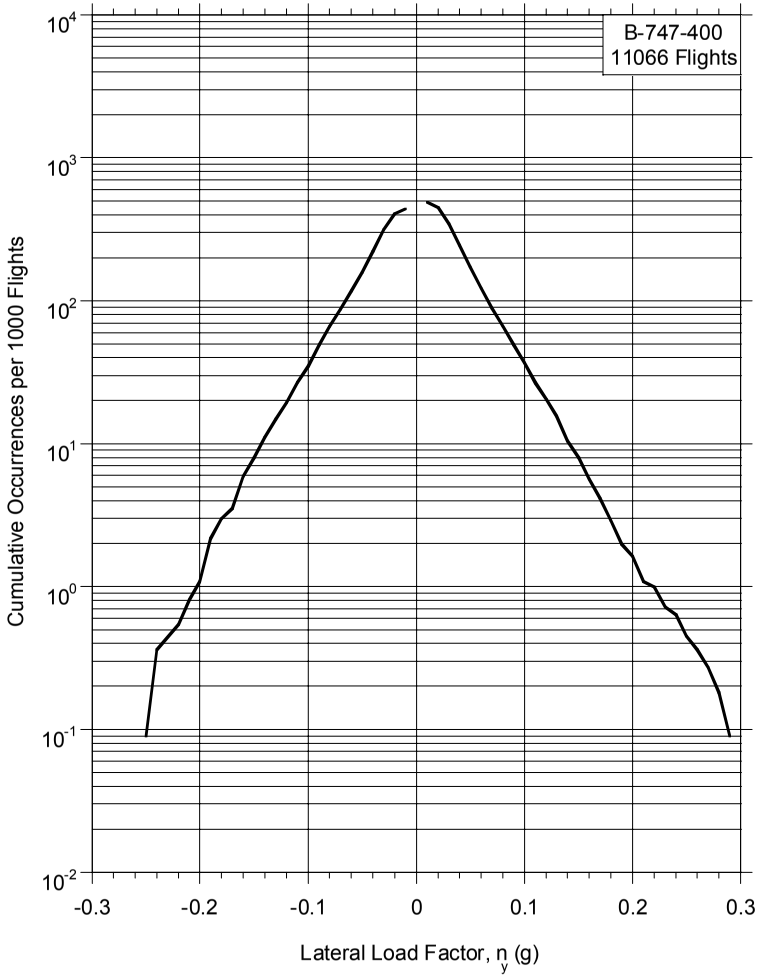

FIGURE A-26. CUMULATIVE FREQUENCY OF MAXIMUM LATERAL LOAD FACTOR AT TOUCHDOWN

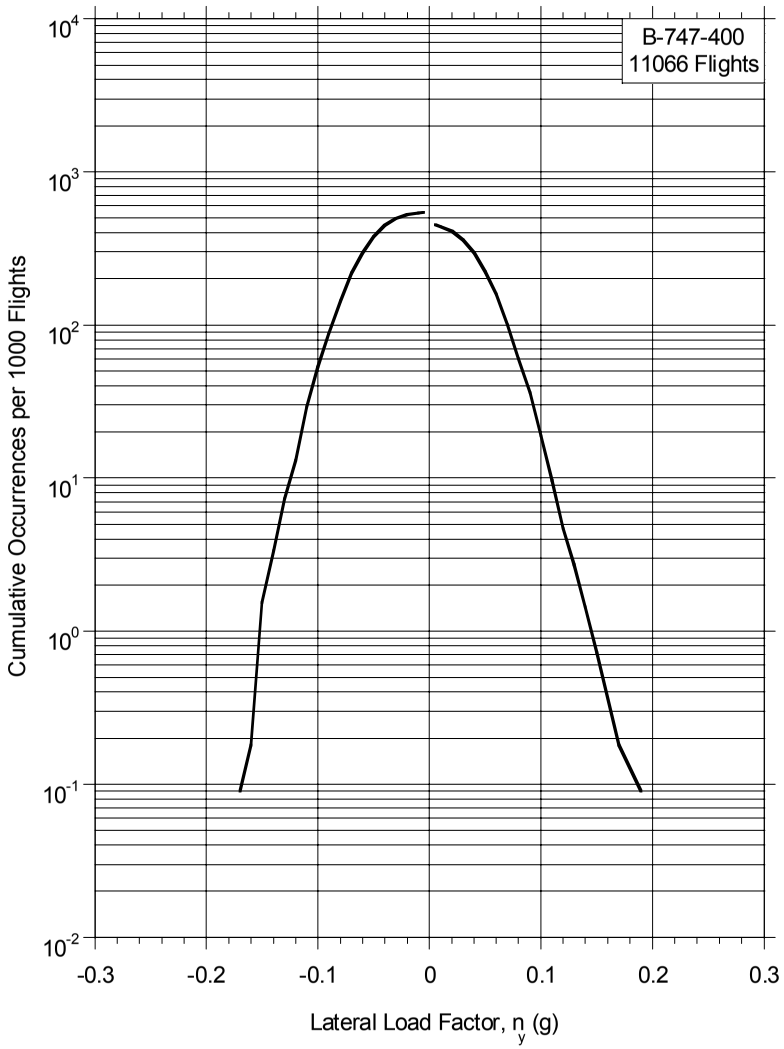

FIGURE A-27. CUMULATIVE FREQUENCY OF MAXIMUM LATERAL LOAD FACTOR DURING RUNWAY TURNOFF

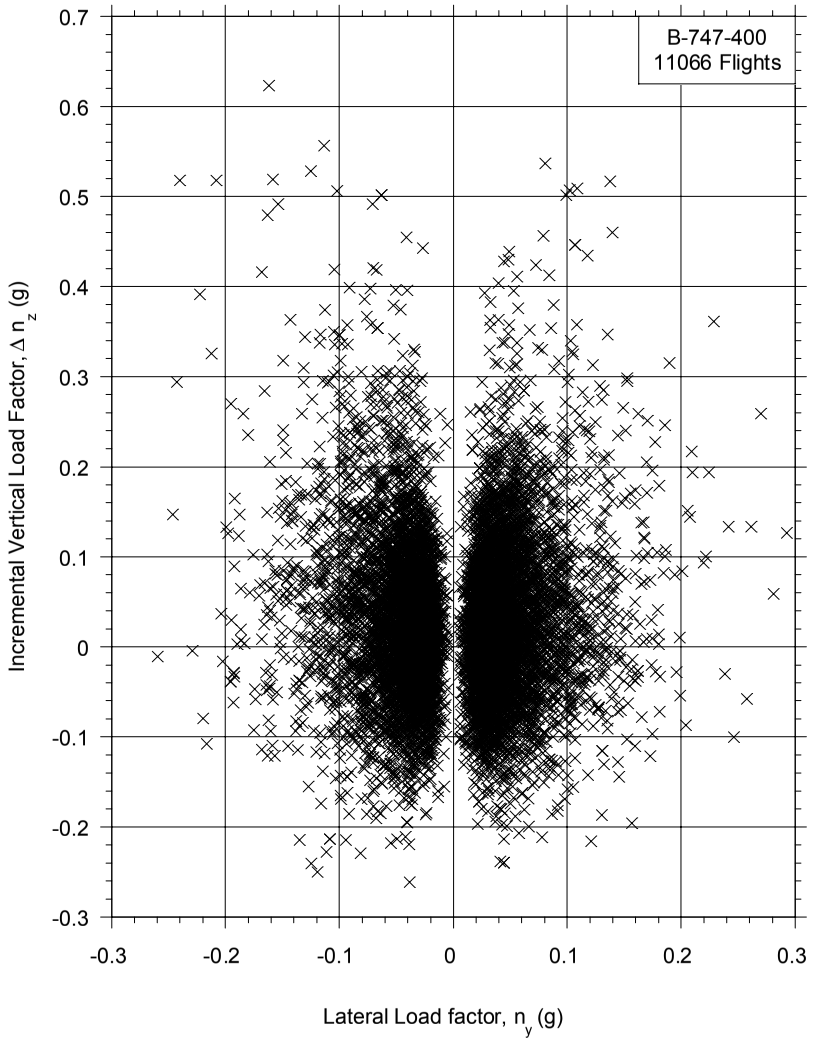

FIGURE A-28. MAXIMUM LATERAL LOAD FACTOR AND COINCIDENT INCREMENTAL VERTICAL LOAD FACTOR AT TOUCHDOWN

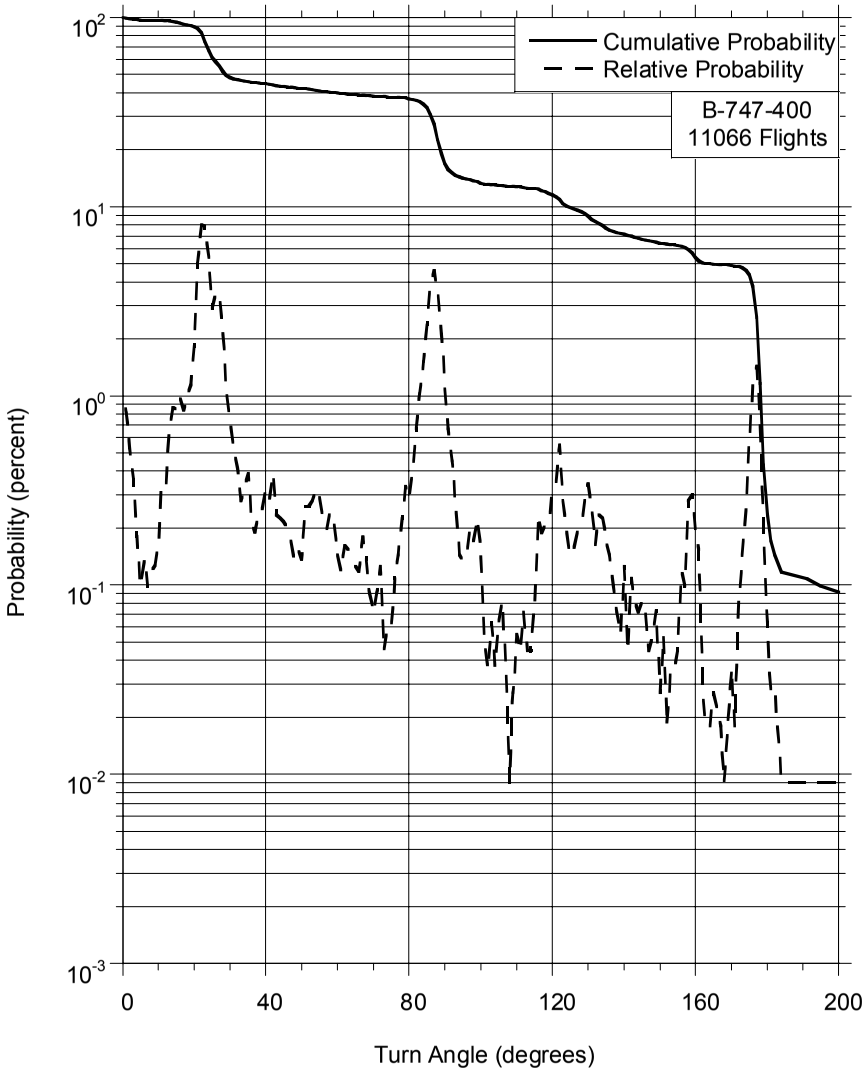

FIGURE A-29. PROBABILITY DISTRIBUTIONS OF TURNING ANGLE DURING RUNWAY TURNOFF

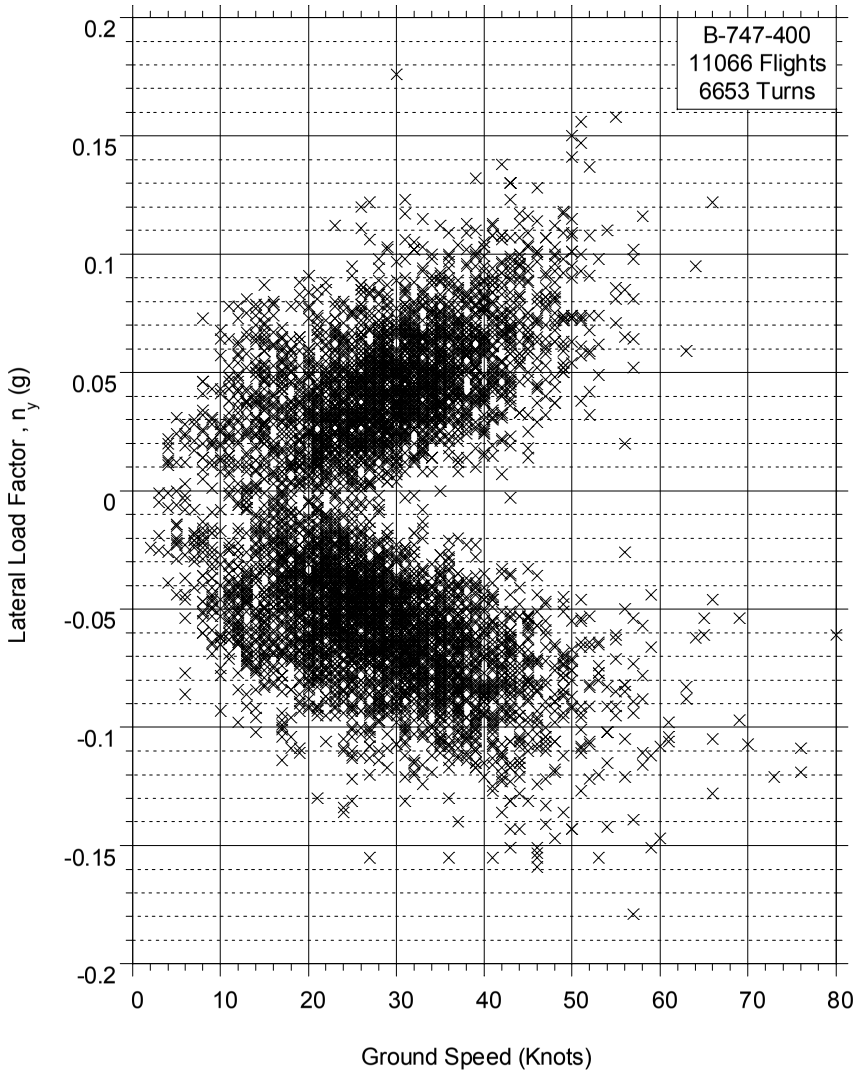

FIGURE A-30. MAXIMUM LATERAL LOAD FACTOR AND COINCIDENT GROUND SPEED DURING RUNWAY TURNOFF, 0-60 DEGREE TURNS

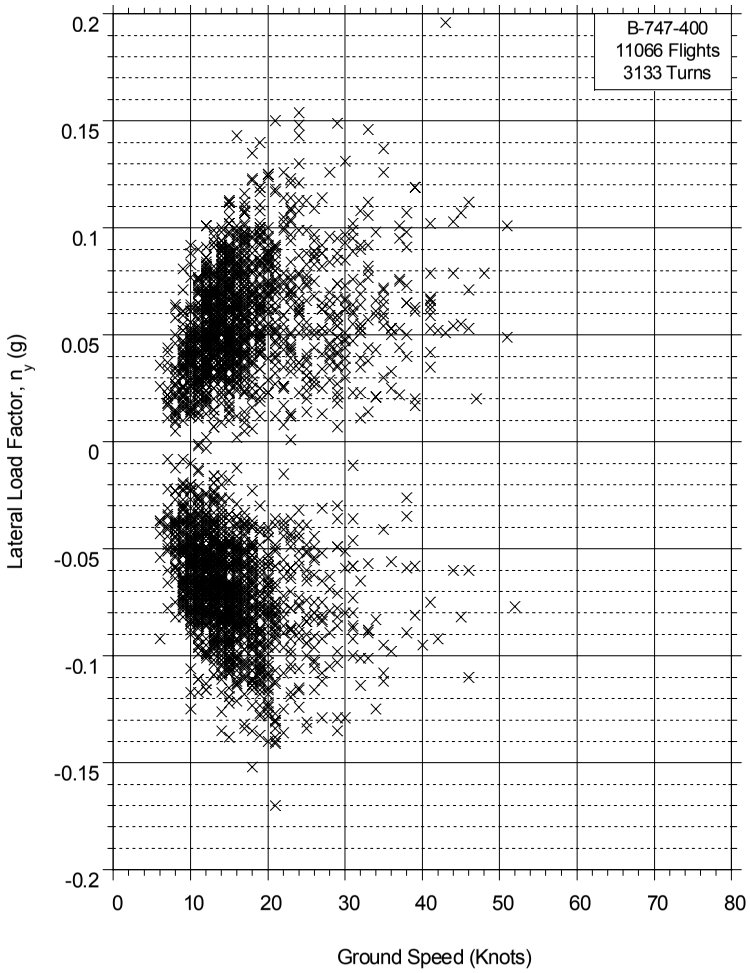

FIGURE A-31. MAXIMUM LATERAL LOAD FACTOR AND COINCIDENT GROUND SPEED DURING RUNWAY TURNOFF, 60-120 DEGREE TURNS

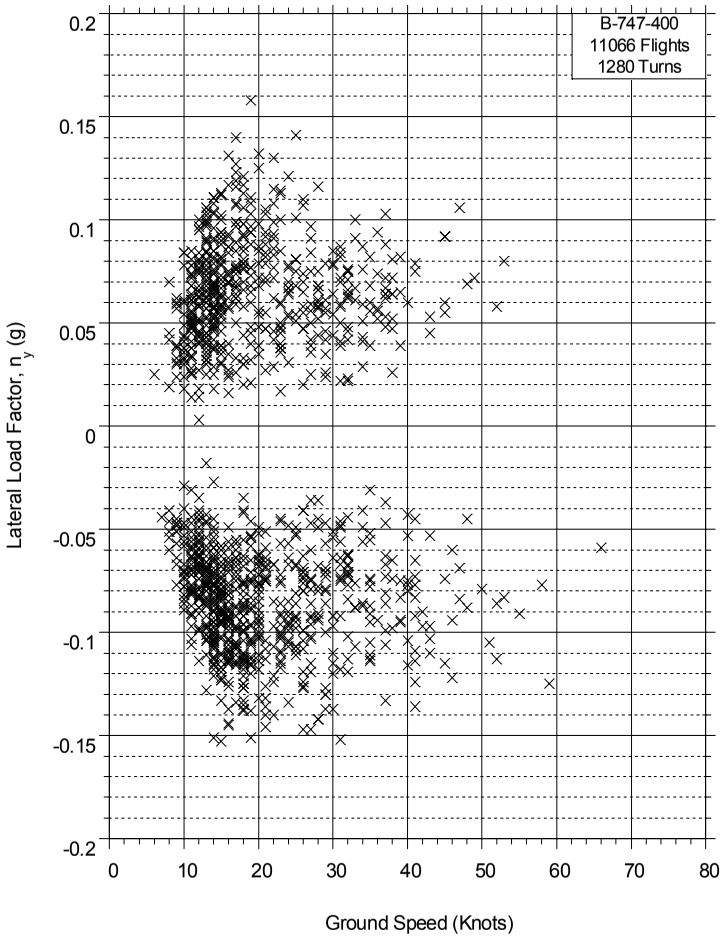

FIGURE A-32. MAXIMUM LATERAL LOAD FACTOR AND COINCIDENT GROUND SPEED DURING RUNWAY TURNOFF, 120-240 DEGREE TURNS

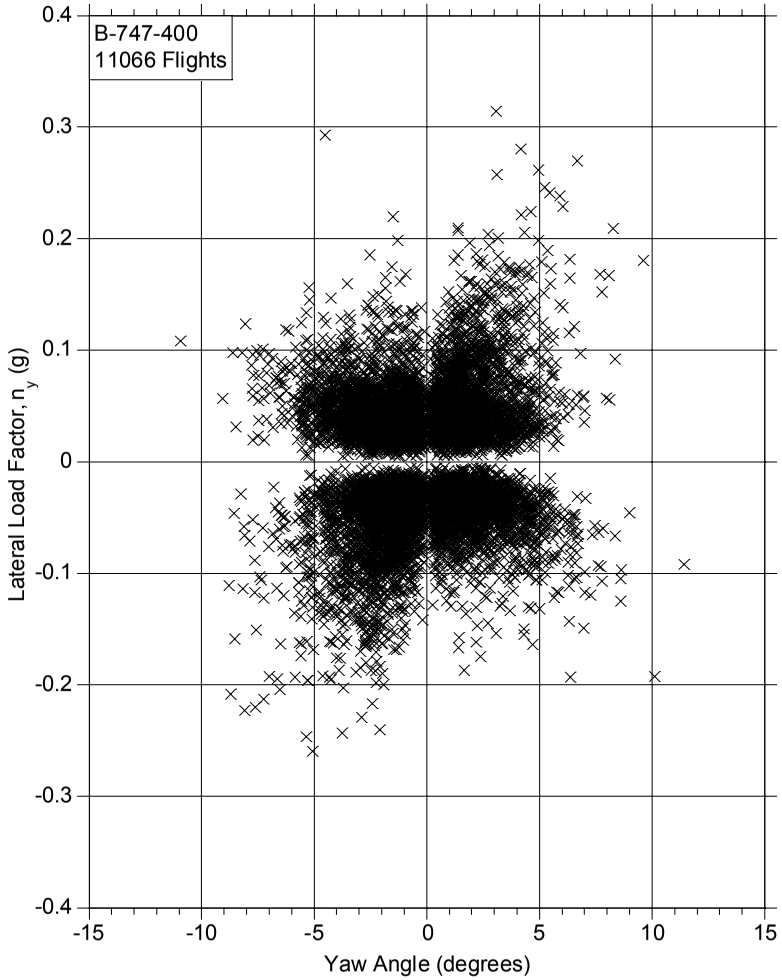

FIGURE A-33. MAXIMUM LATERAL LOAD FACTOR AT TOUCHDOWN VS MAXIMUM YAW ANGLE BEFORE TOUCHDOWN

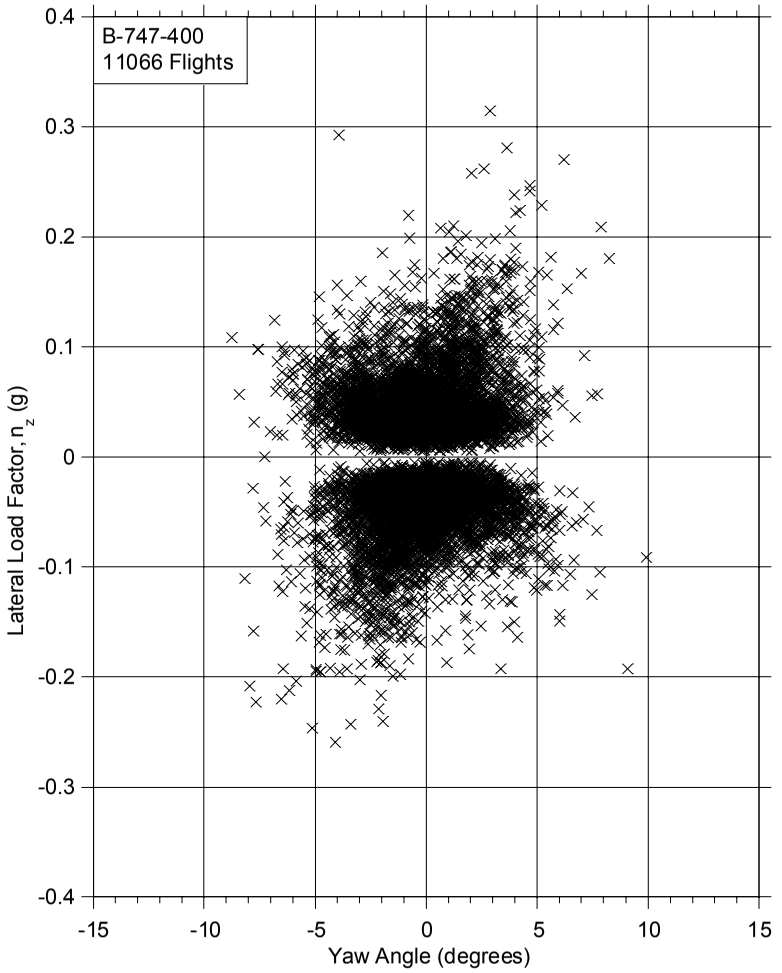

FIGURE A-34. MAXIMUM LATERAL LOAD FACTOR AT TOUCHDOWN VS MEAN YAW ANGLE BEFORE TOUCHDOWN

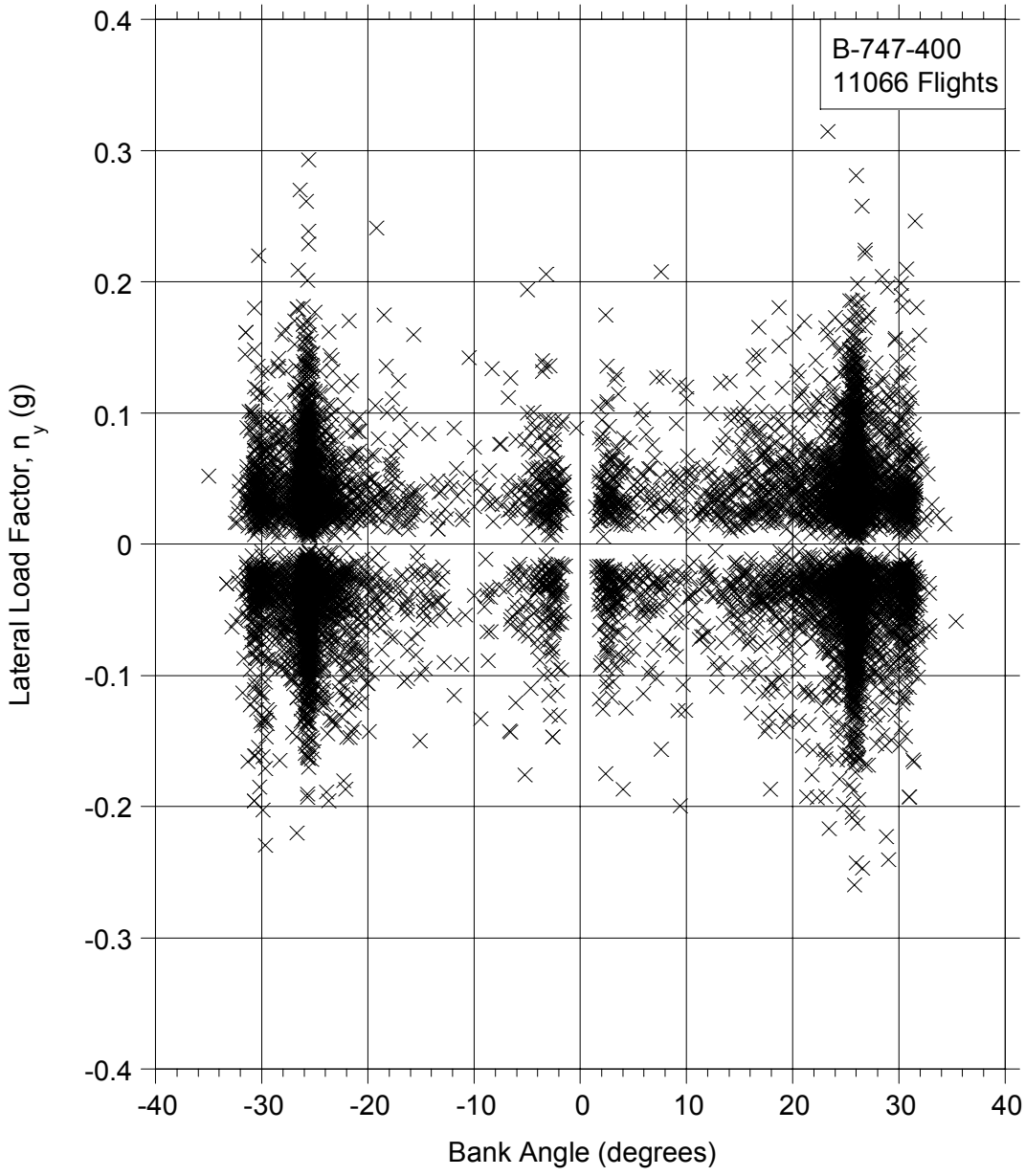

FIGURE A-35. MAXIMUM LATERAL LOAD FACTOR AT TOUCHDOWN VS MAXIMUM BANK ANGLE BEFORE TOUCHDOWN

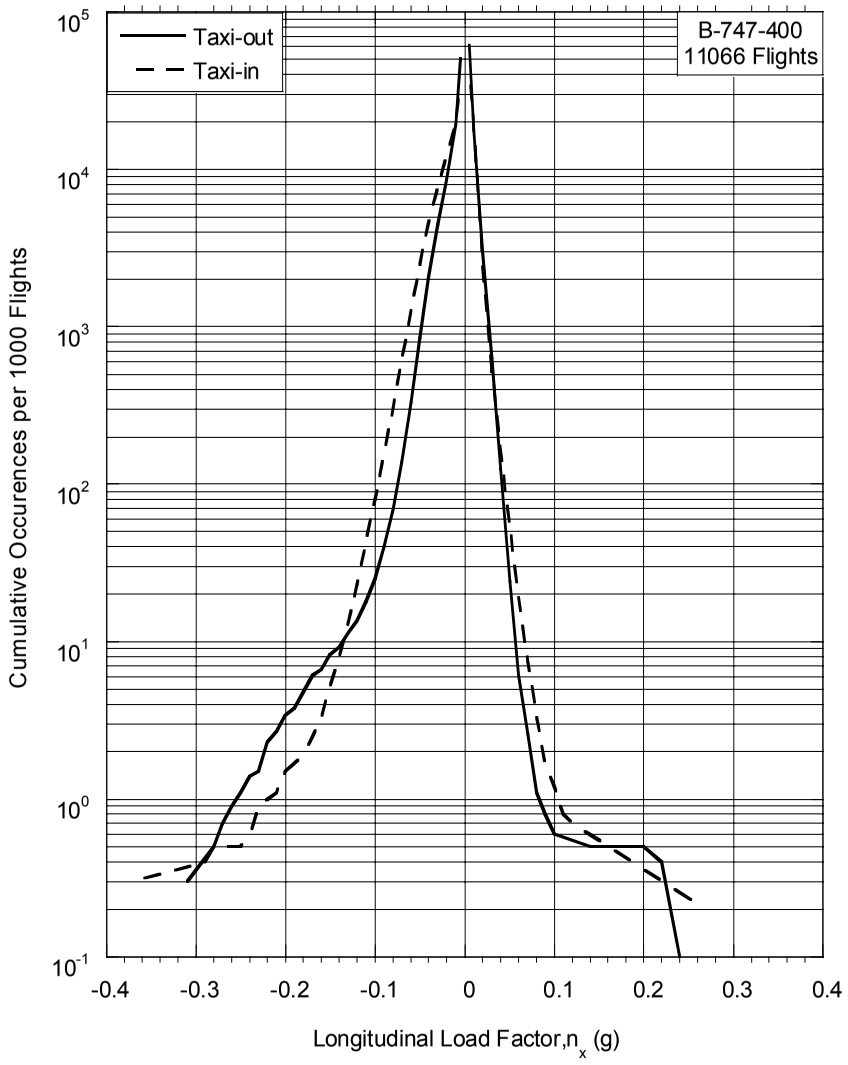

FIGURE A-36. CUMULATIVE FREQUENCY OF LONGITUDINAL LOAD FACTOR DURING TAXI OPERATIONS

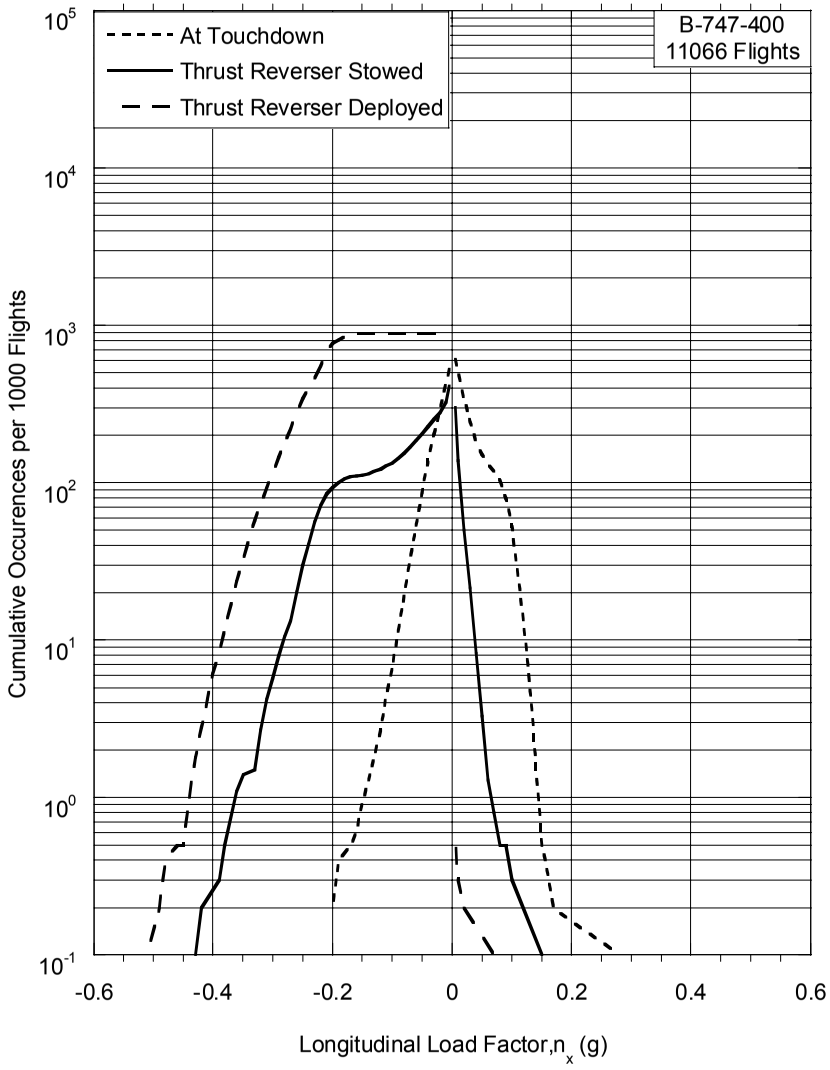

FIGURE A-37. CUMULATIVE FREQUENCY OF LONGITUDINAL LOAD FACTOR AT TOUCHDOWN AND DURING LANDING ROLL

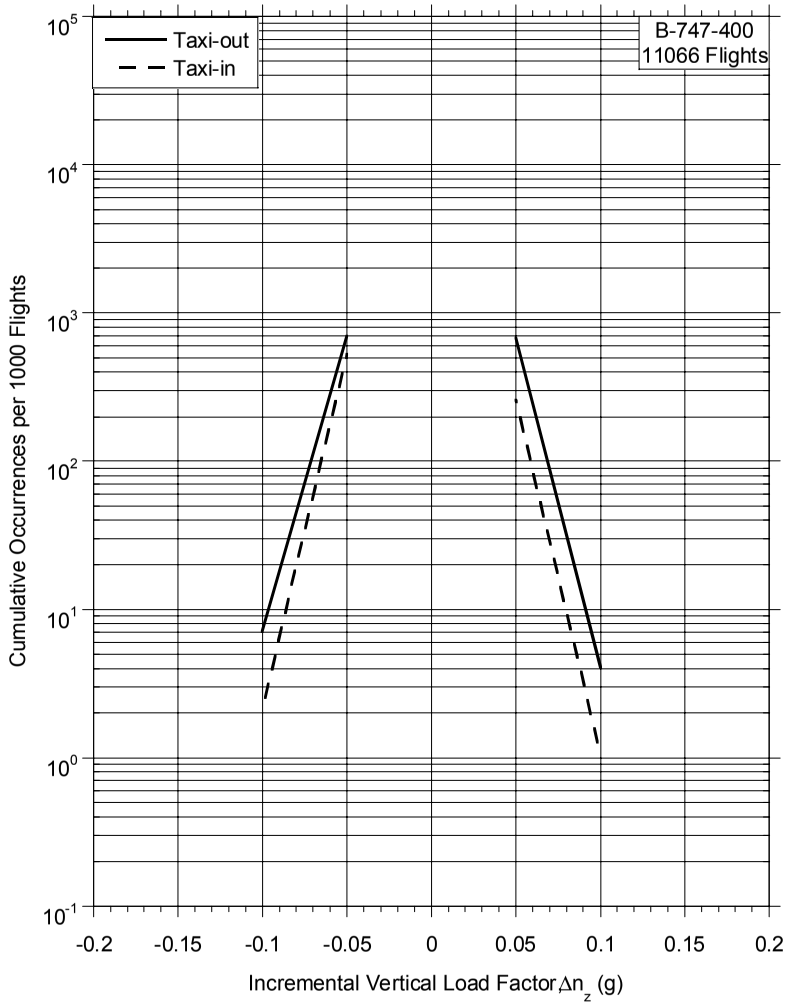

FIGURE A-38. CUMULATIVE FREQUENCY OF INCREMENTAL VERTICAL LOAD FACTOR DURING TAXI OPERATIONS

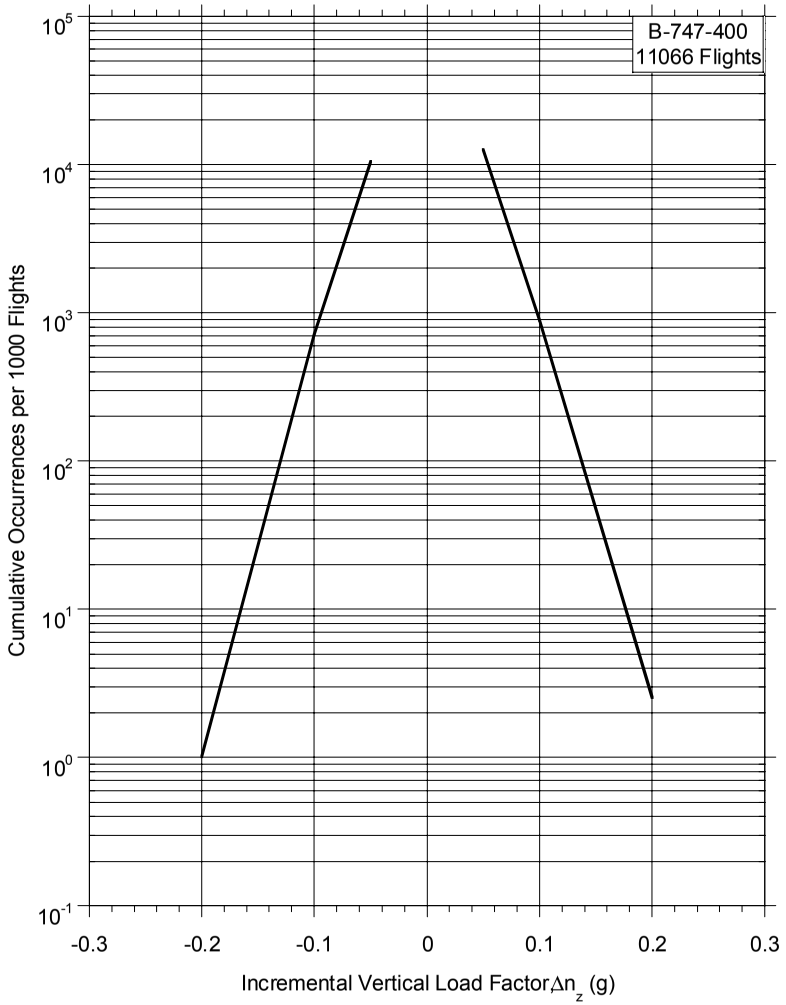

FIGURE A-39. CUMULATIVE FREQUENCY OF INCREMENTAL VERTICAL LOAD FACTOR DURING TAKEOFF ROLL

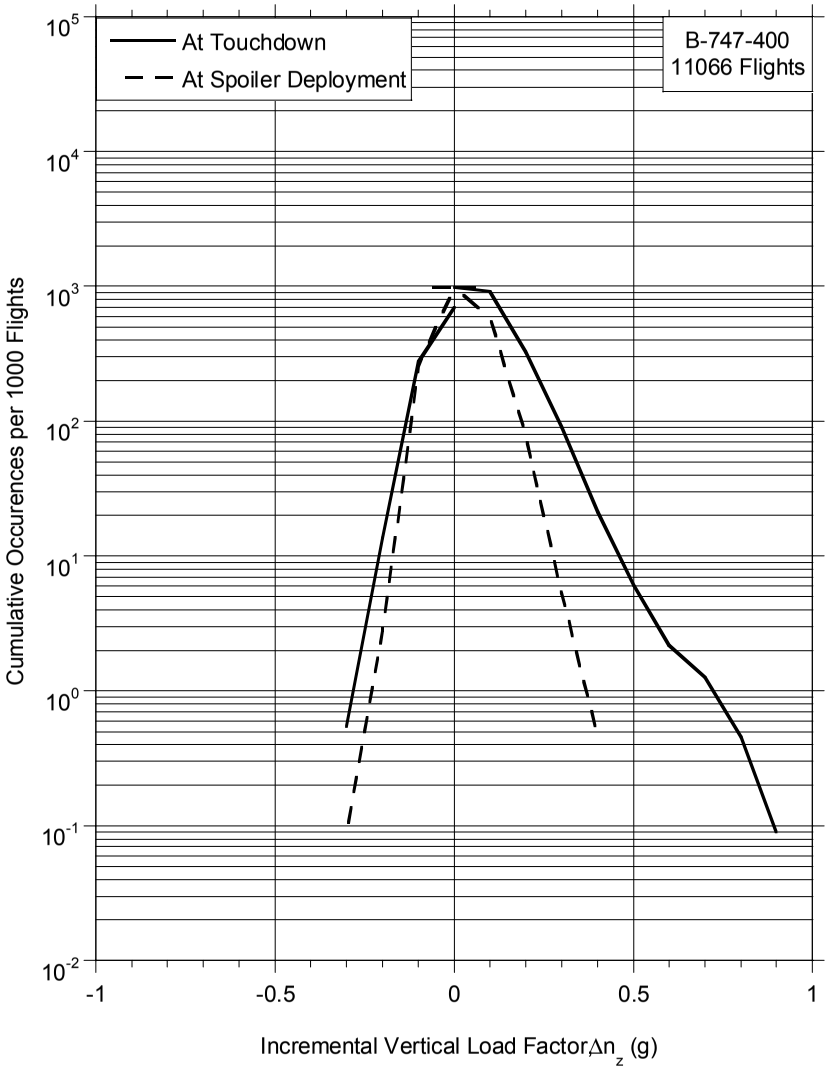

FIGURE A-40. CUMULATIVE FREQUENCY OF INCREMENTAL VERTICAL LOAD FACTOR AT SPOILER DEPLOYMENT AND AT TOUCHDOWN

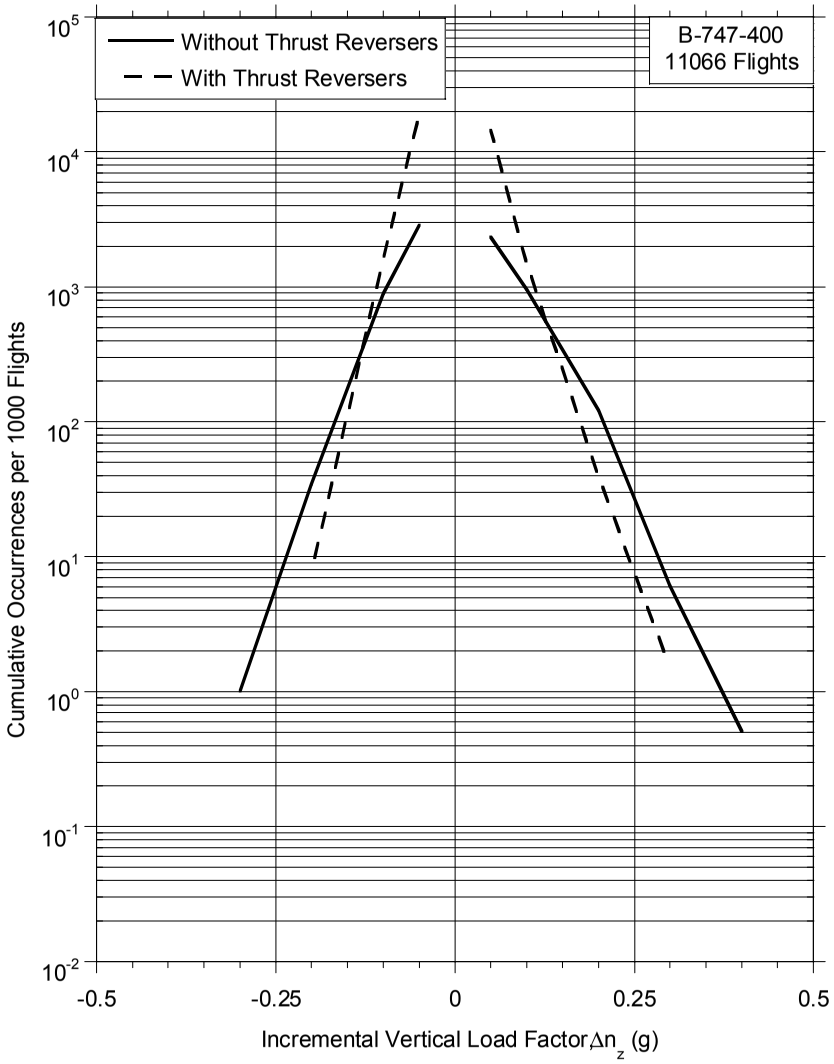

FIGURE A-41. CUMULATIVE FREQUENCY OF INCREMENTAL VERTICAL LOAD FACTOR DURING LANDING ROLL

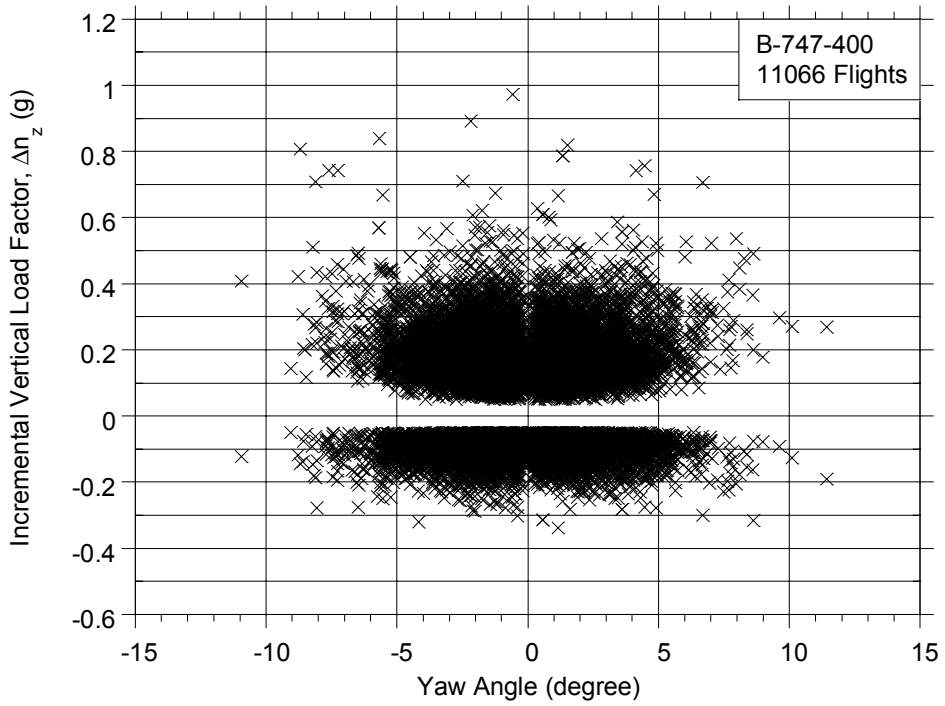

FIGURE A-42. MAXIMUM INCREMENTAL VERTICAL LOAD FACTOR AT TOUCHDOWN VS MAXIMUM YAW ANGLE BEFORE TOUCHDOWN

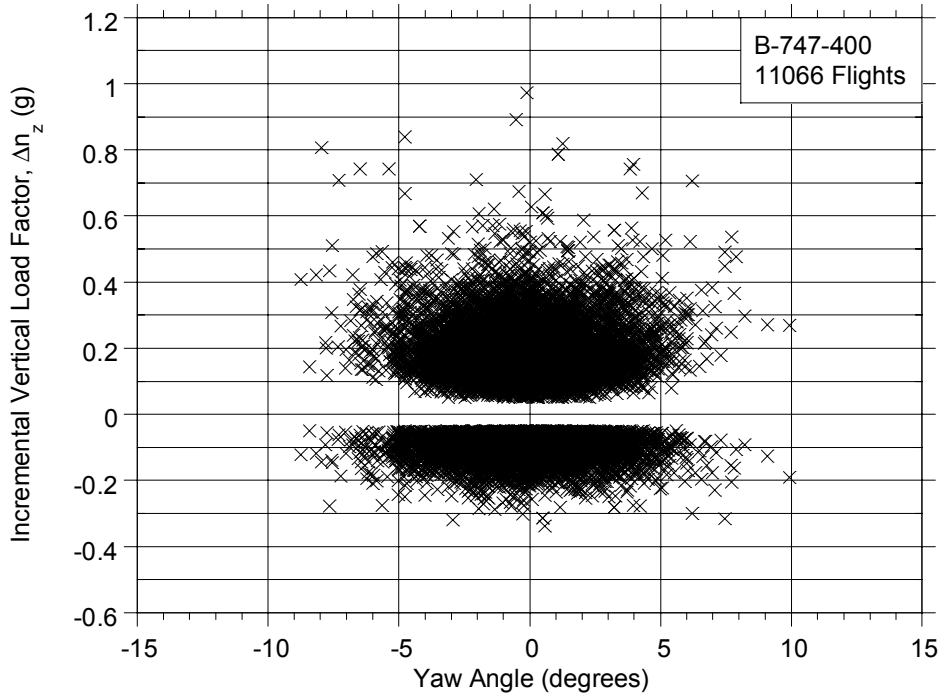

FIGURE A-43. MAXIMUM INCREMENTAL VERTICAL LOAD FACTOR AT TOUCHDOWN VS MEAN YAW ANGLE BEFORE TOUCHDOWN

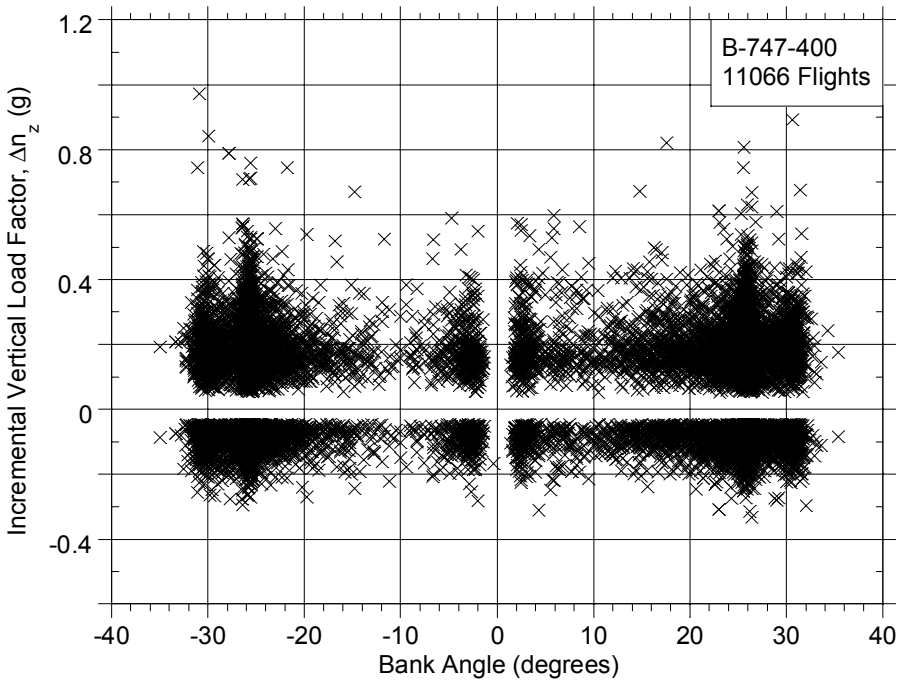

FIGURE A-44. MAXIMUM INCREMENTAL VERTICAL LOAD FACTOR AT TOUCHDOWN VS MAXIMUM BANK ANGLE BEFORE TOUCHDOWN

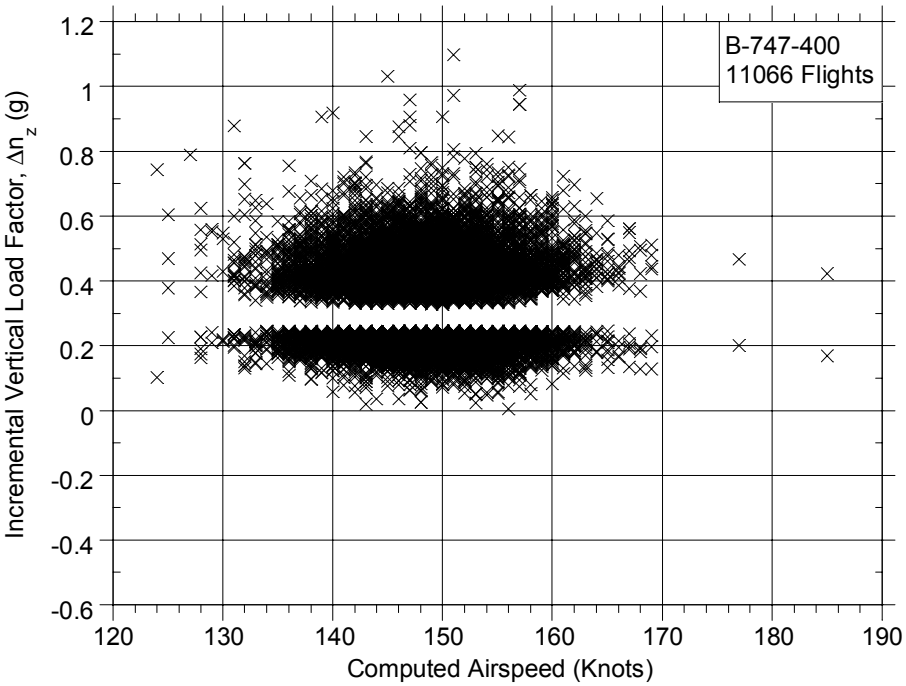

FIGURE A-45. MAXIMUM INCREMENTAL VERTICAL LOAD FACTOR AT TOUCHDOWN VS COINCIDENT AIRSPEED

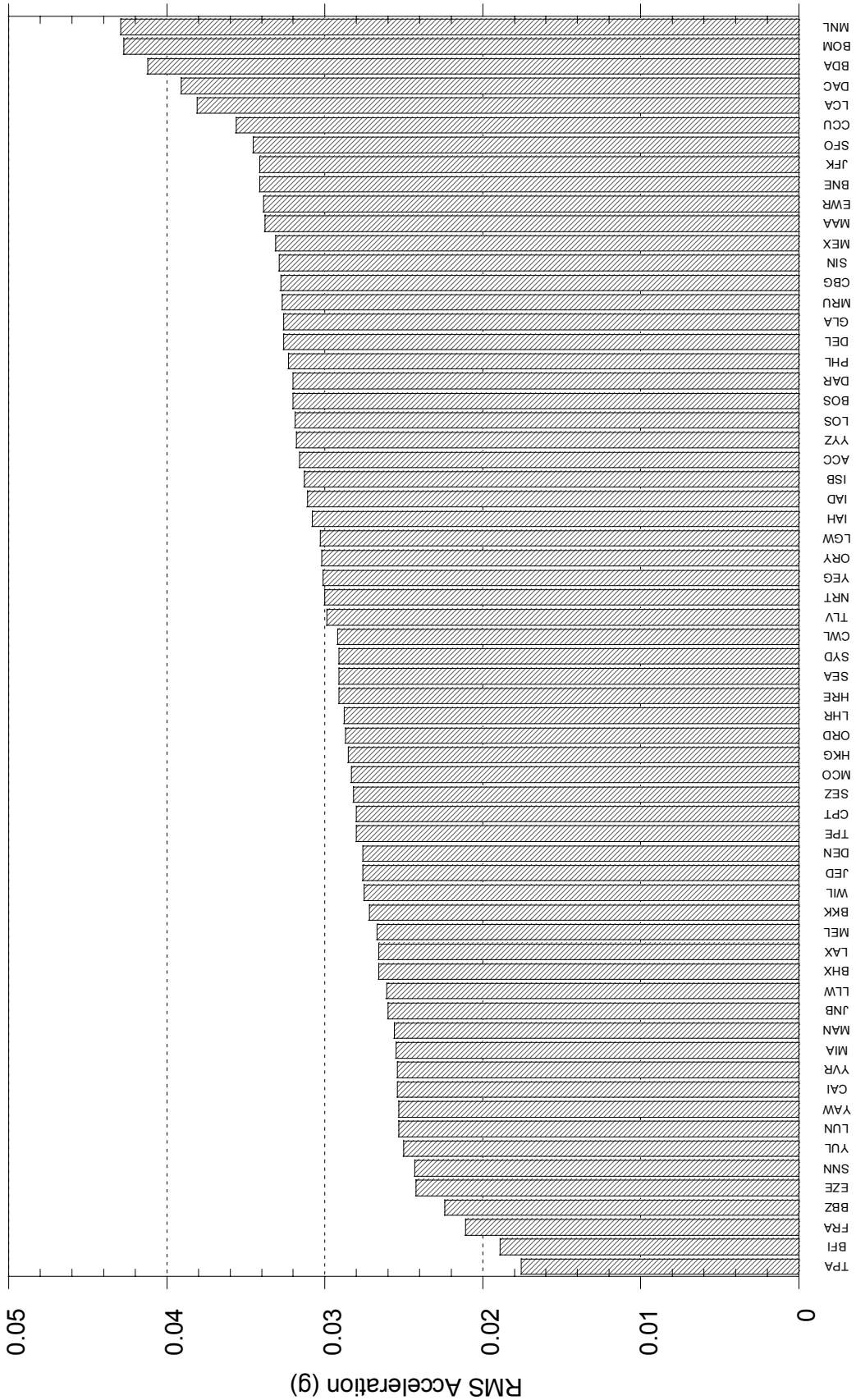

FIGURE A-46. AIRCRAFT RUNWAY ACCELERATION RESPONSE

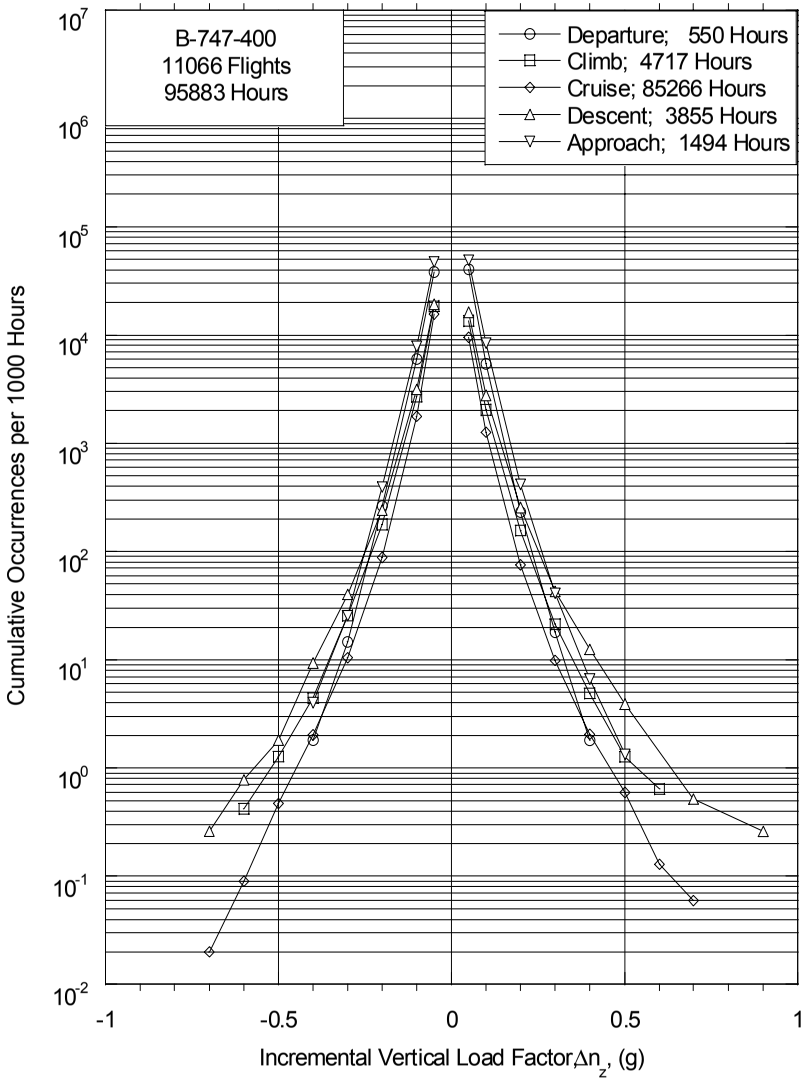

FIGURE A-47. CUMULATIVE OCCURRENCES OF INCREMENTAL VERTICAL GUST LOAD FACTOR PER 1000 HOURS BY FLIGHT PHASE

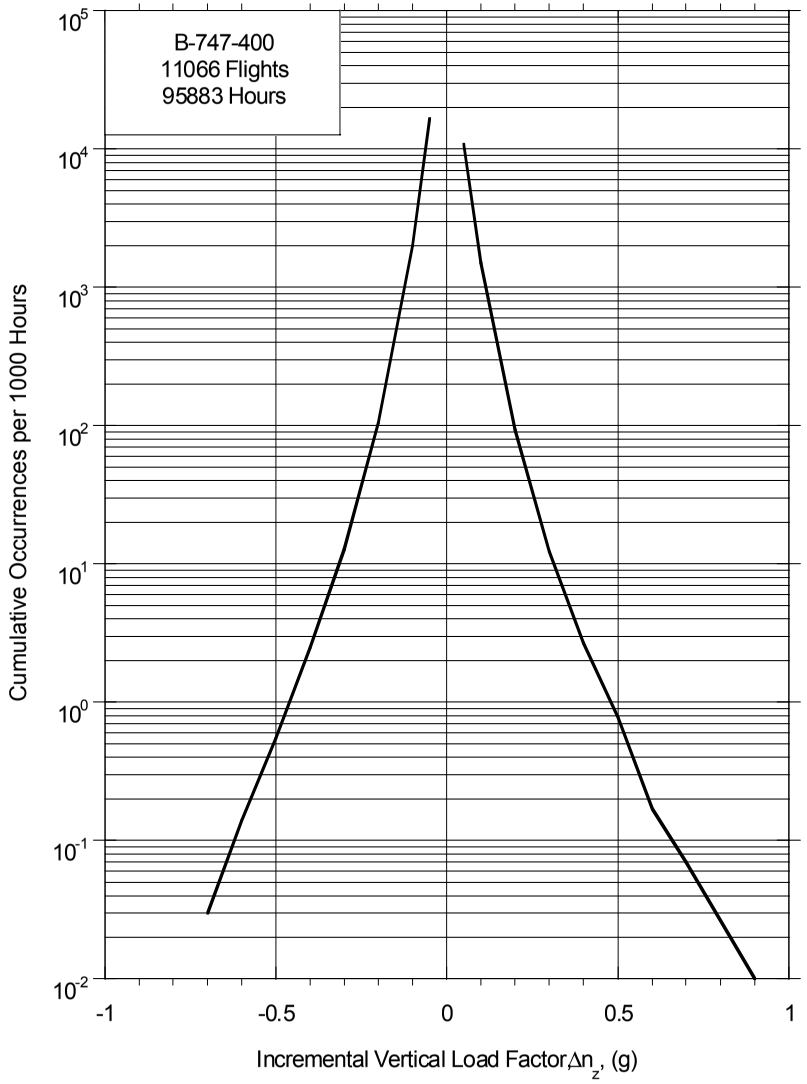

FIGURE A-48. CUMULATIVE OCCURRENCES OF INCREMENTAL VERTICAL GUST LOAD FACTOR PER 1000 HOURS, COMBINED FLIGHT PHASES

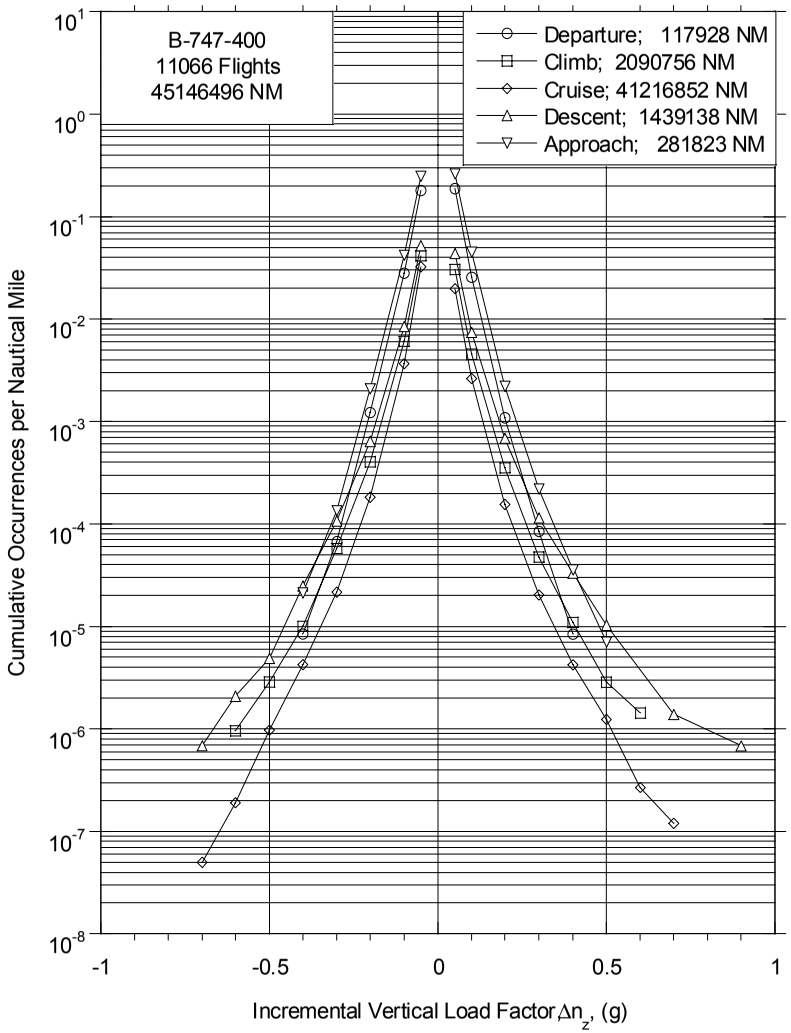

FIGURE A-49. CUMULATIVE OCCURRENCES OF INCREMENTAL VERTICAL GUST LOAD FACTOR PER NAUTICAL MILE BY FLIGHT PHASE

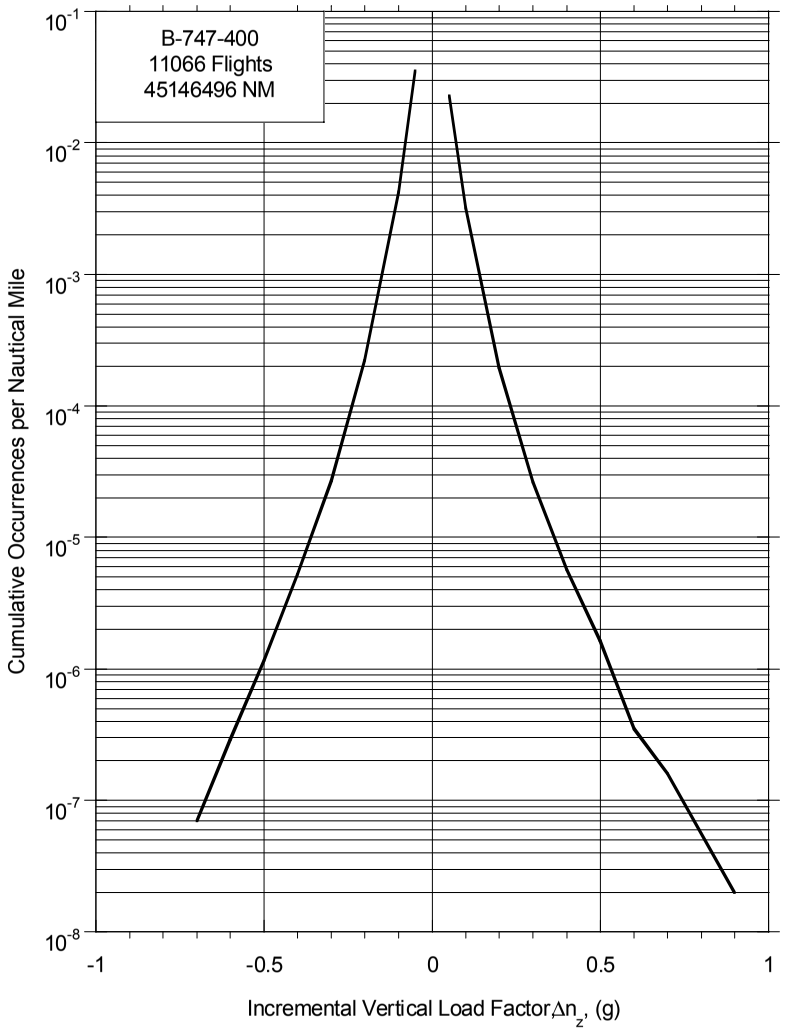

FIGURE A-50. CUMULATIVE OCCURRENCES OF INCREMENTAL VERTICAL GUST LOAD FACTOR PER NAUTICAL MILE, COMBINED FLIGHT PHASES

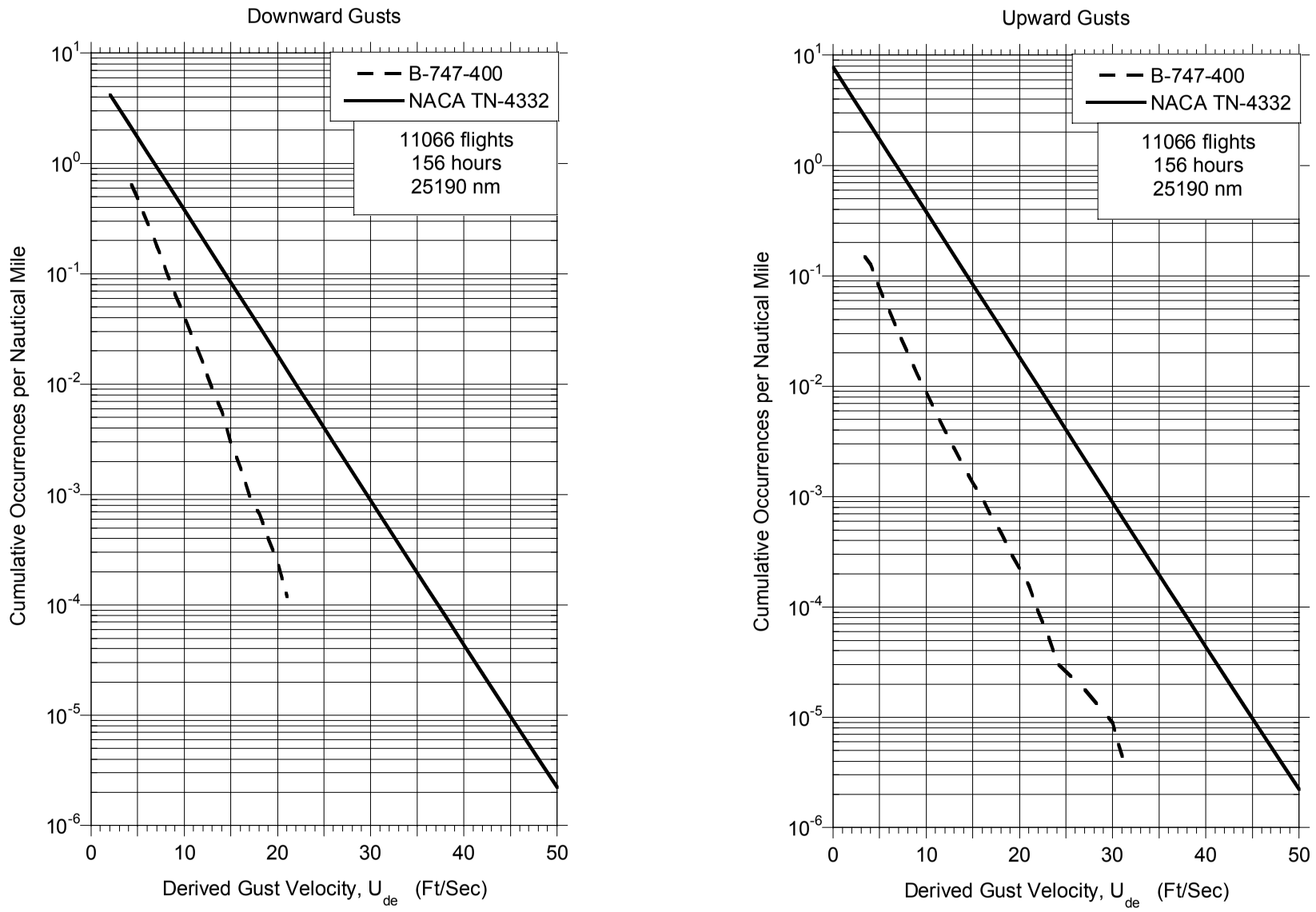

FIGURE A-51. CUMULATIVE OCCURRENCES OF DERIVED GUST VELOCITY PER NAUTICAL MILE, < 500 FEET

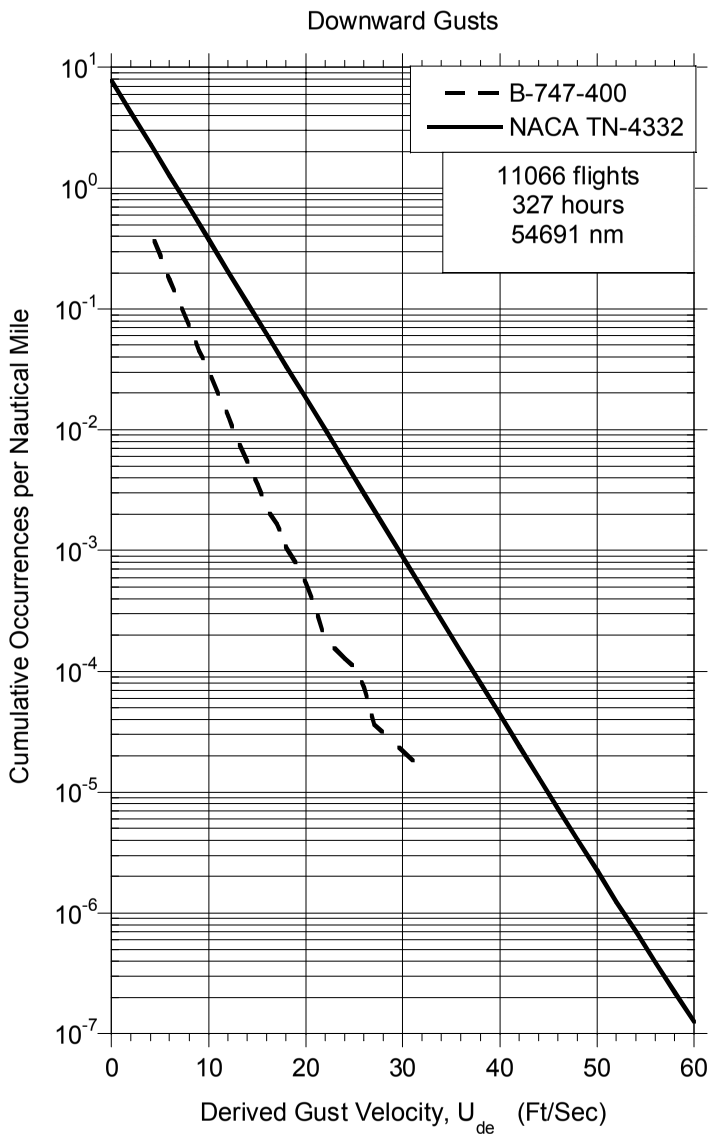

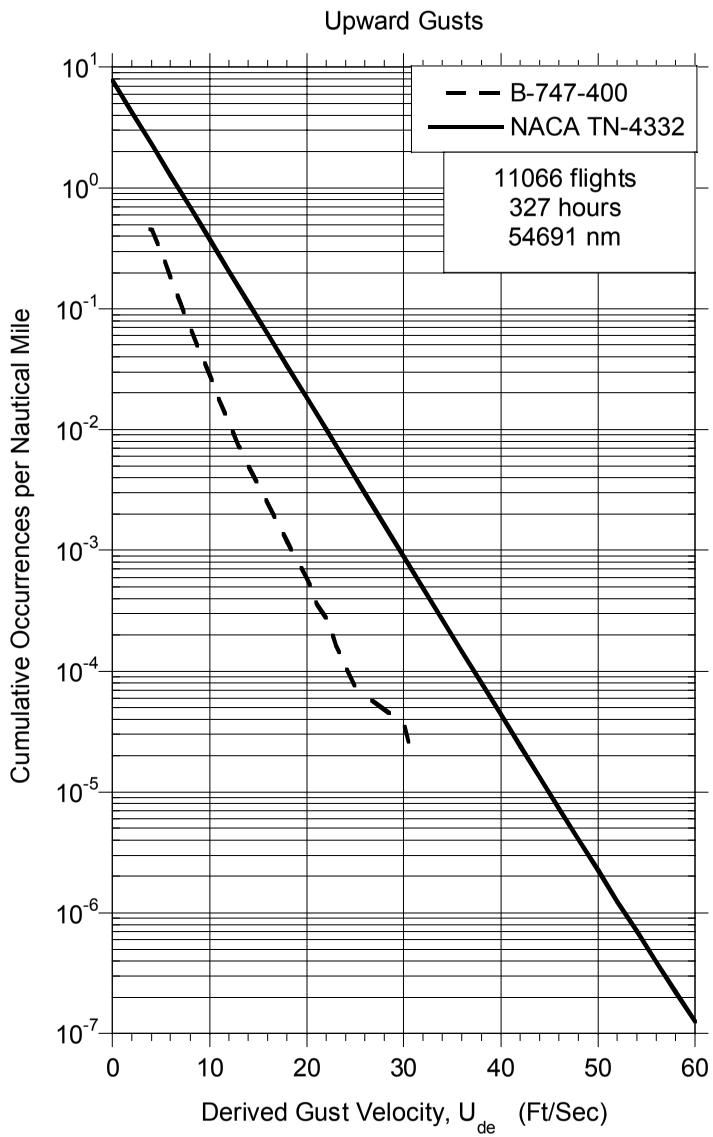

FIGURE A-52. CUMULATIVE OCCURRENCES OF DERIVED GUST VELOCITY PER NAUTICAL MILE, 500-1500 FEET

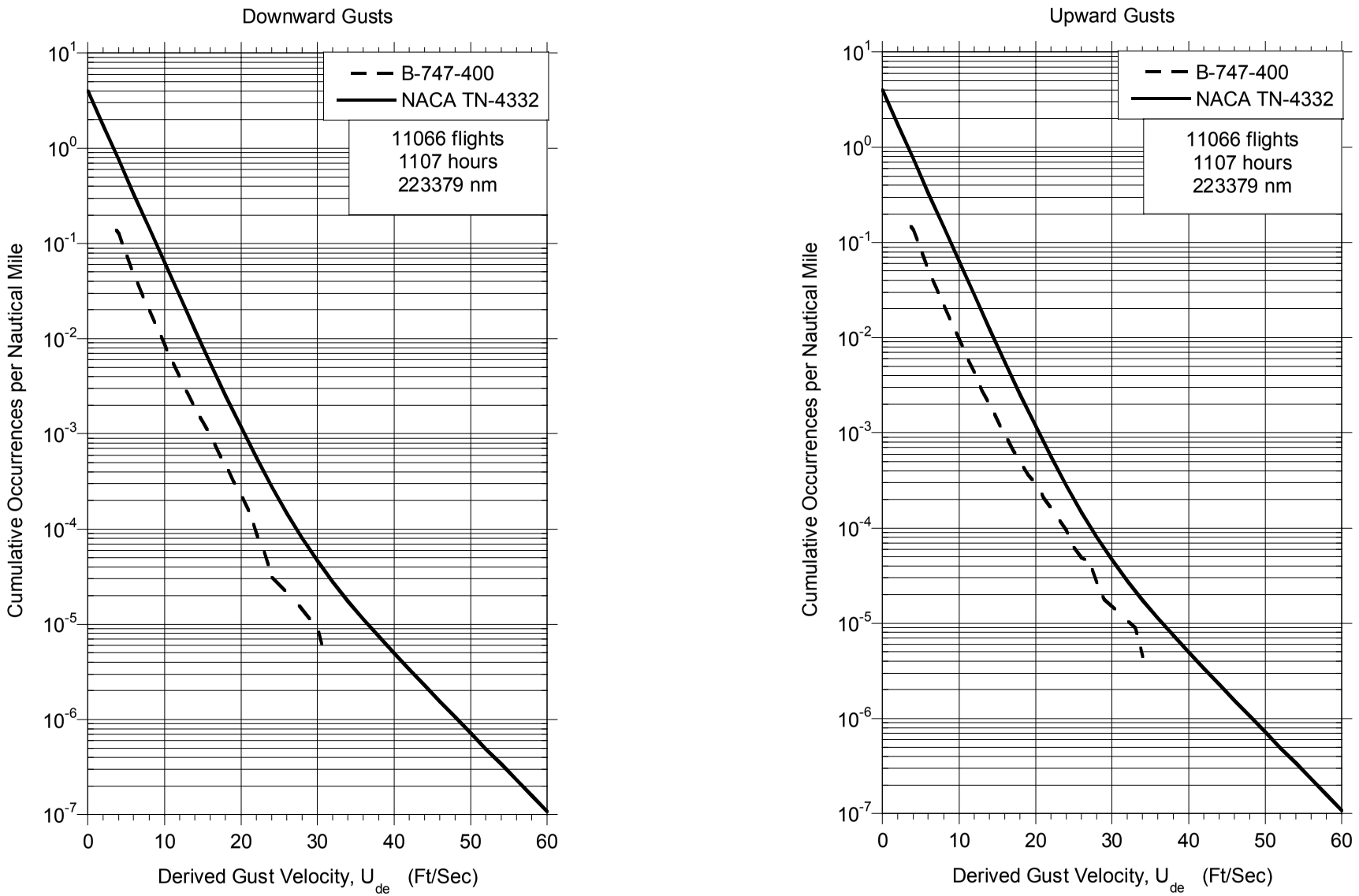

FIGURE A-53. CUMULATIVE OCCURRENCES OF DERIVED GUST VELOCITY PER NAUTICAL MILE, 1500-4500 FEET

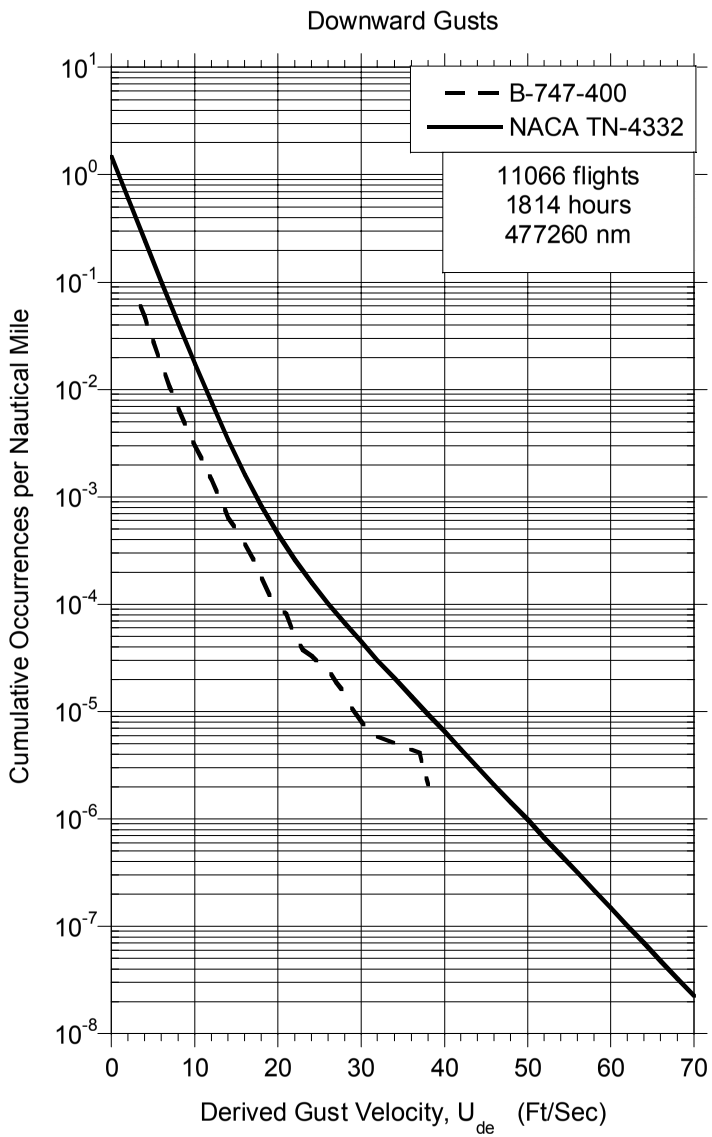

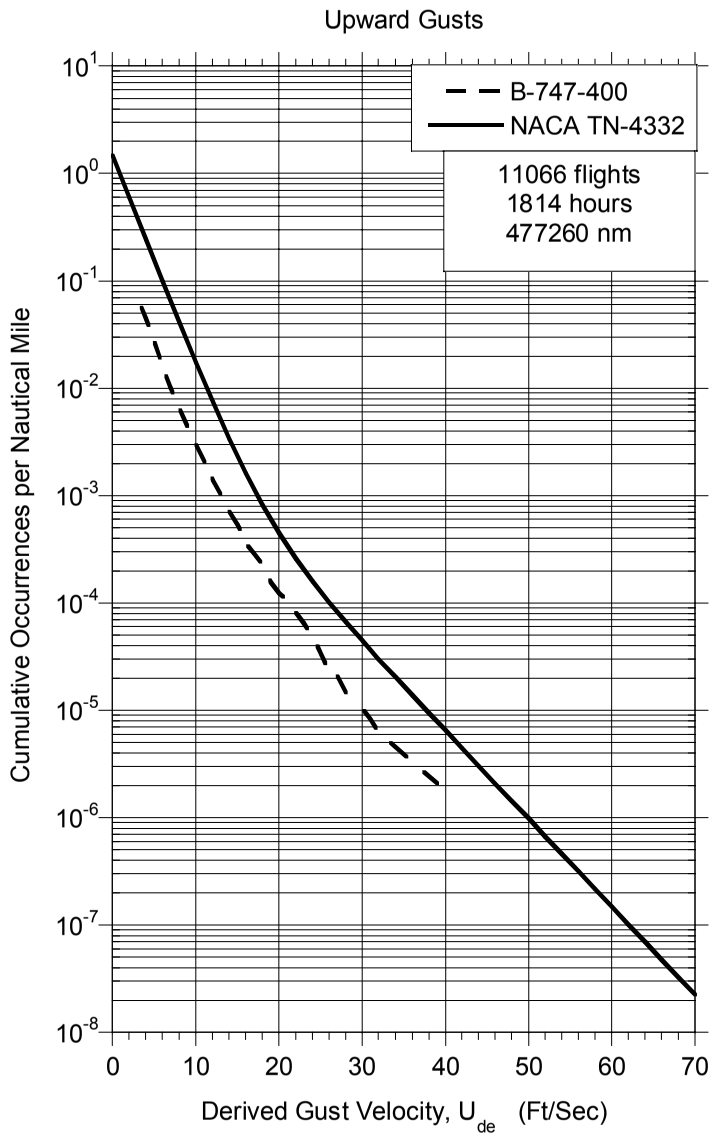

FIGURE A-54. CUMULATIVE OCCURRENCES OF DERIVED GUST VELOCITY PER NAUTICAL MILE, 4500-9500 FEET

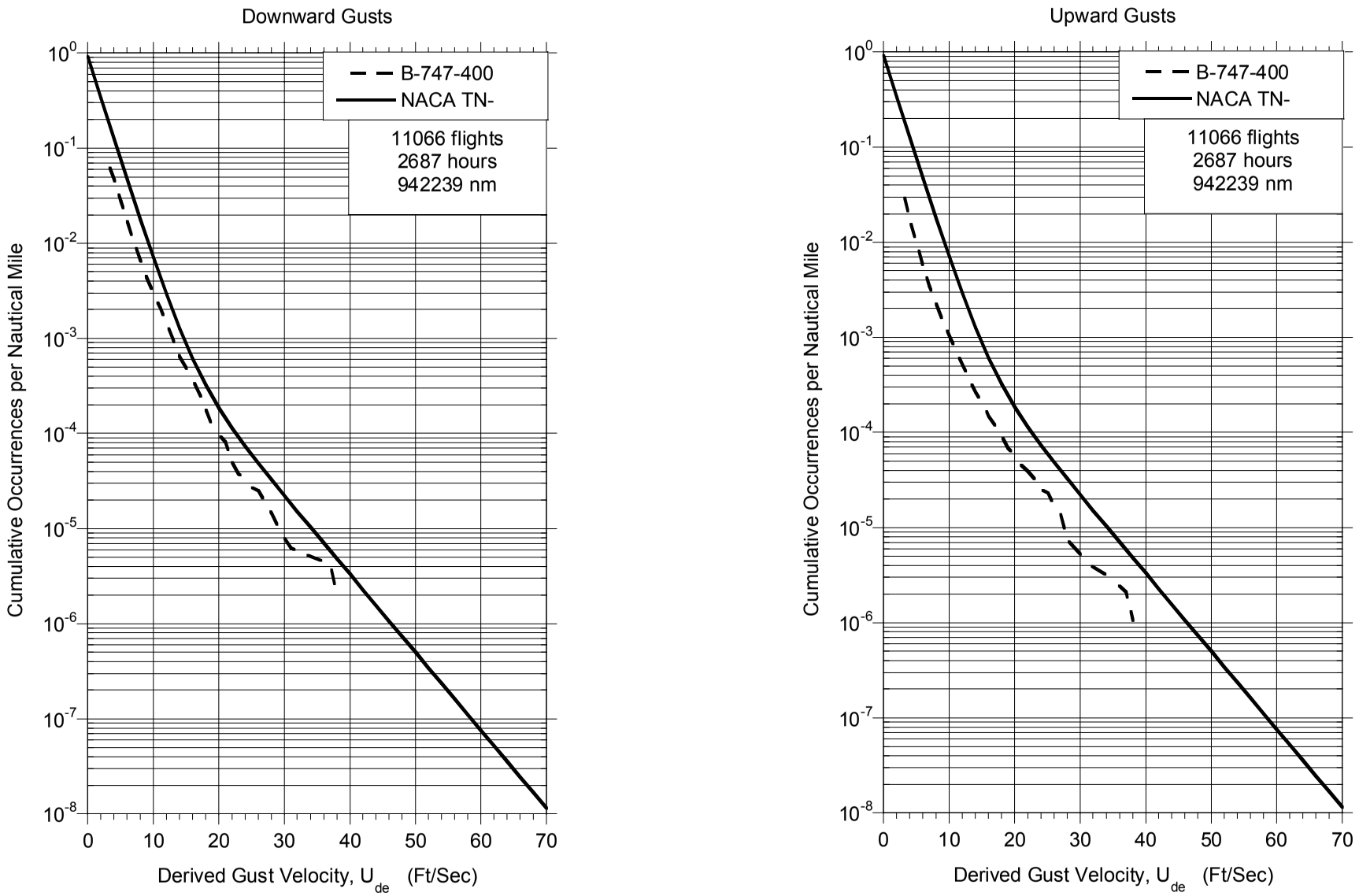

FIGURE A-55. CUMULATIVE OCCURRENCES OF DERIVED GUST VELOCITY PER NAUTICAL MILE, 9,500-19,500 FEET

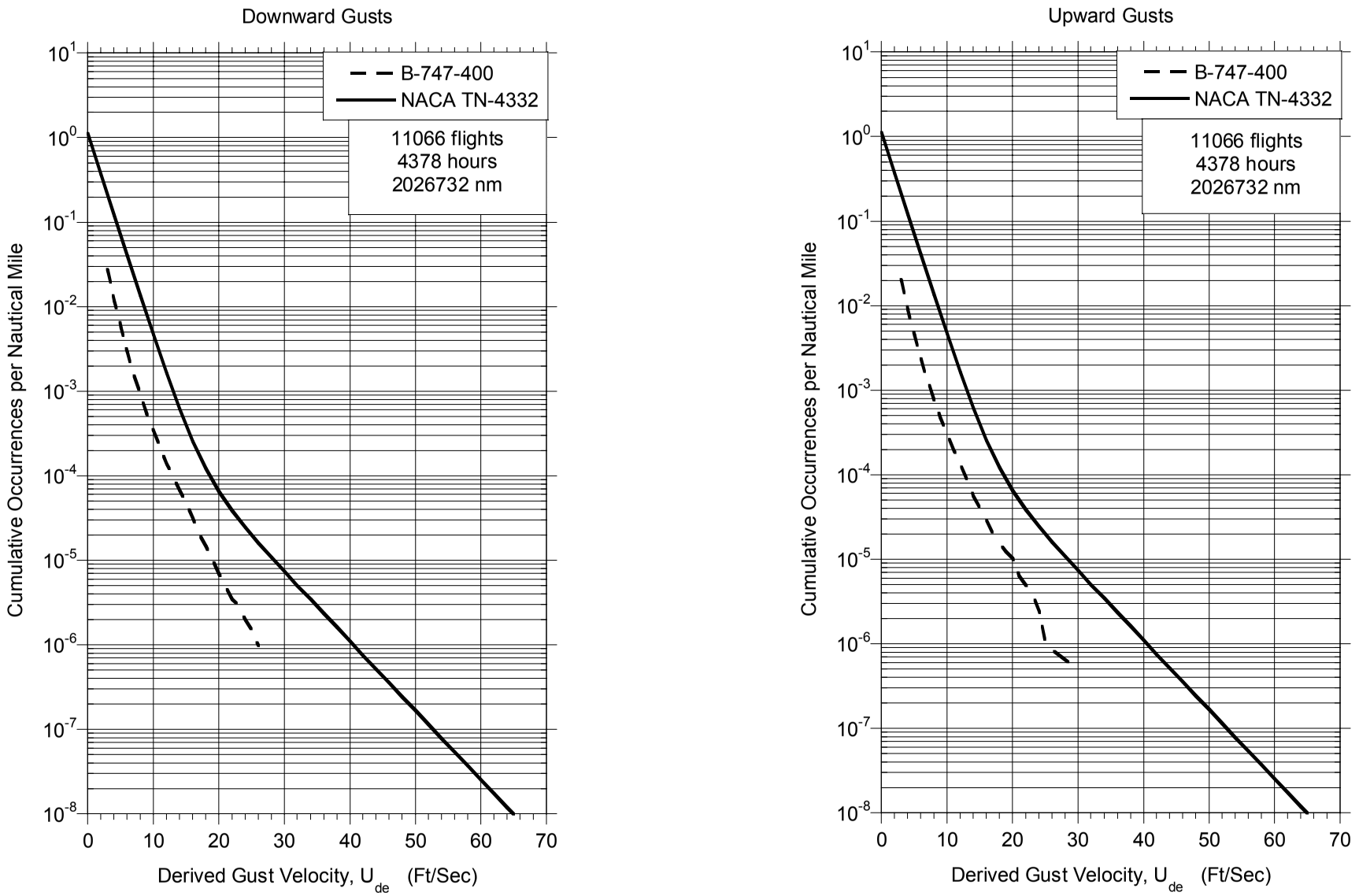

FIGURE A-56. CUMULATIVE OCCURRENCES OF DERIVED GUST VELOCITY PER NAUTICAL MILE, 19,500-29,500 FEET

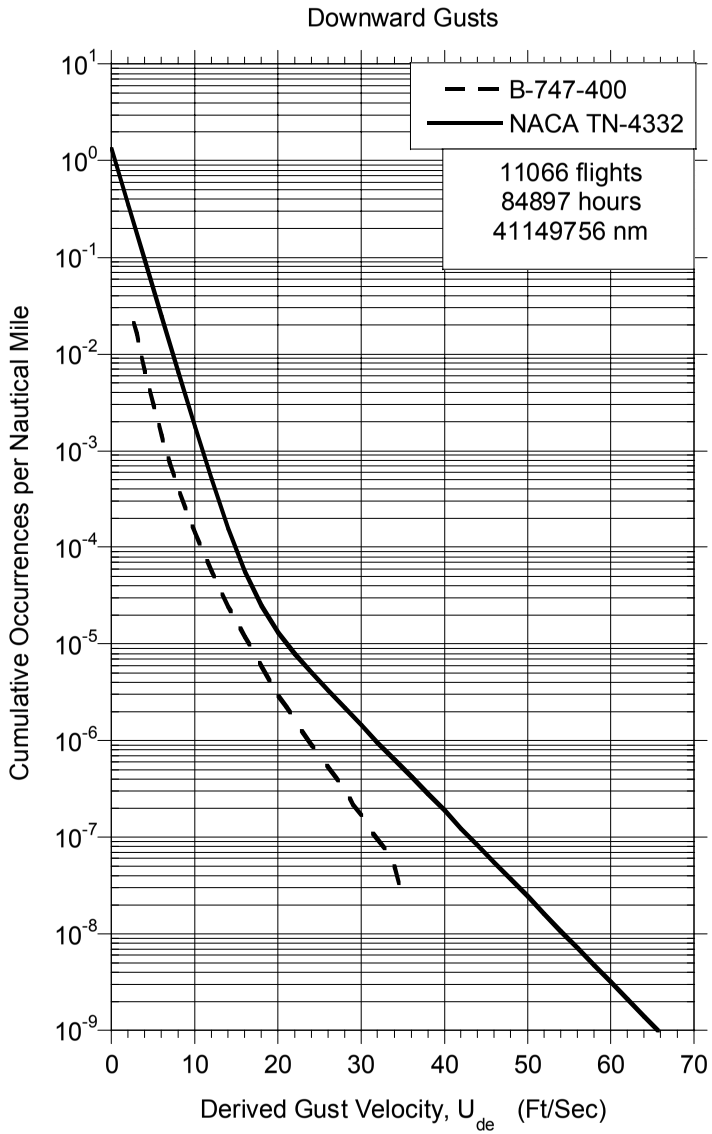

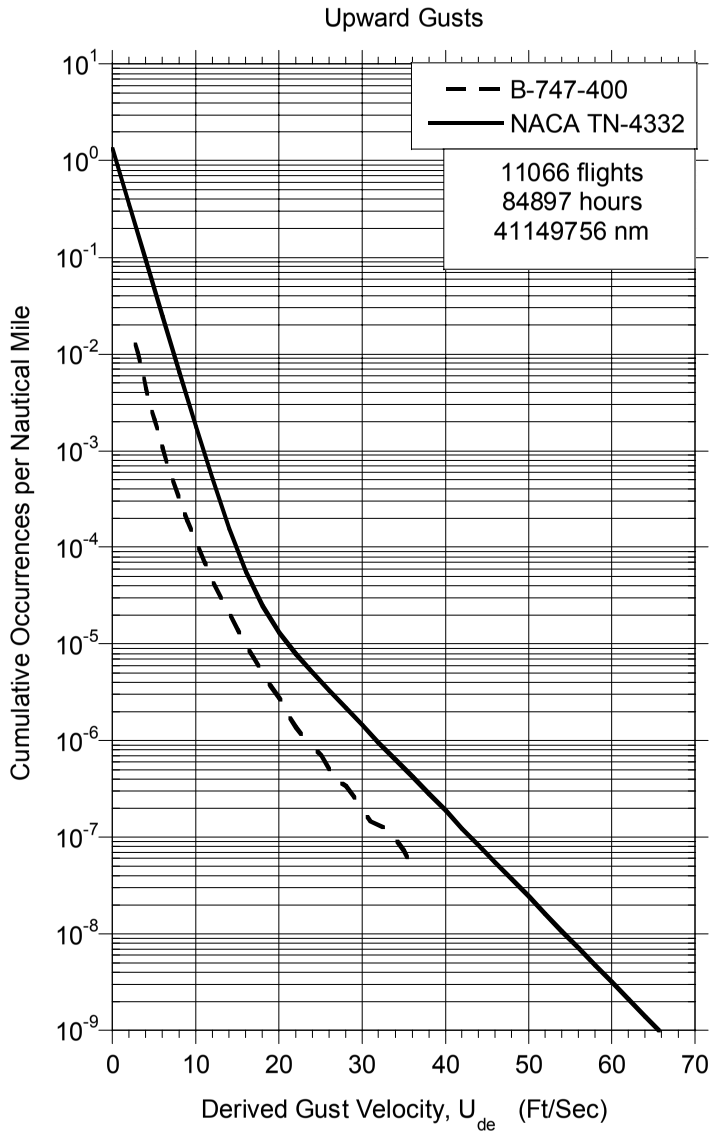

FIGURE A-57. CUMULATIVE OCCURRENCES OF DERIVED GUST VELOCITY PER NAUTICAL MILE, 29,500-39,500 FEET

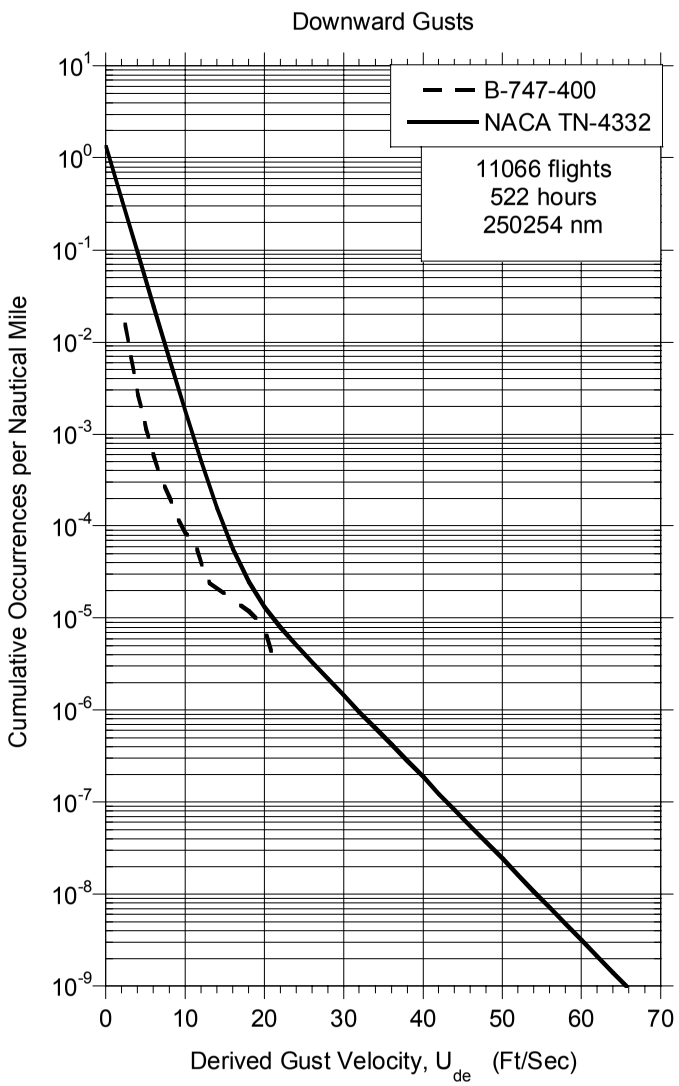

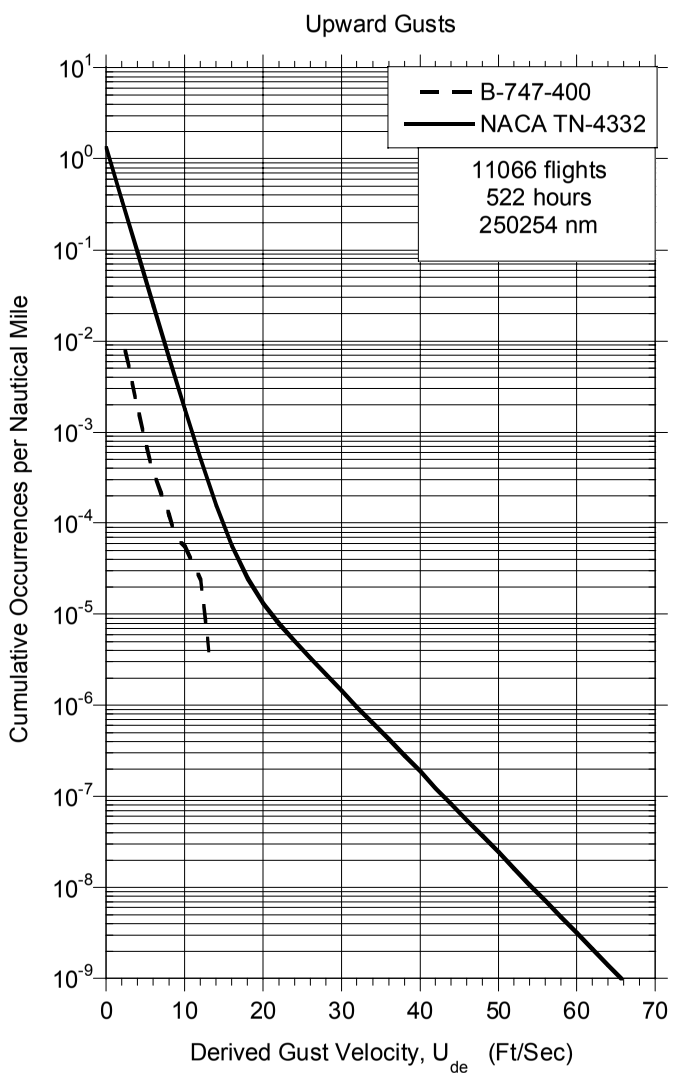

FIGURE A-58. CUMULATIVE OCCURRENCES OF DERIVED GUST VELOCITY PER NAUTICAL MILE, 39,500-44,500 FEET

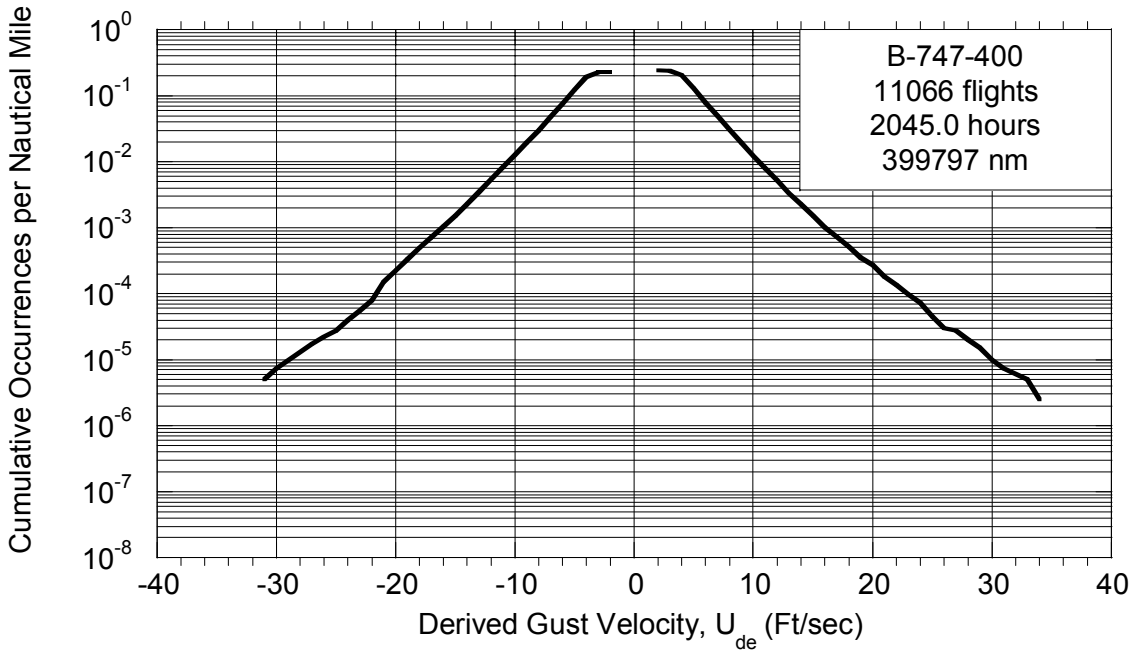

FIGURE A-59. CUMULATIVE OCCURRENCES OF DERIVED GUST VELOCITY PER NAUTICAL MILE, FLAPS EXTENDED

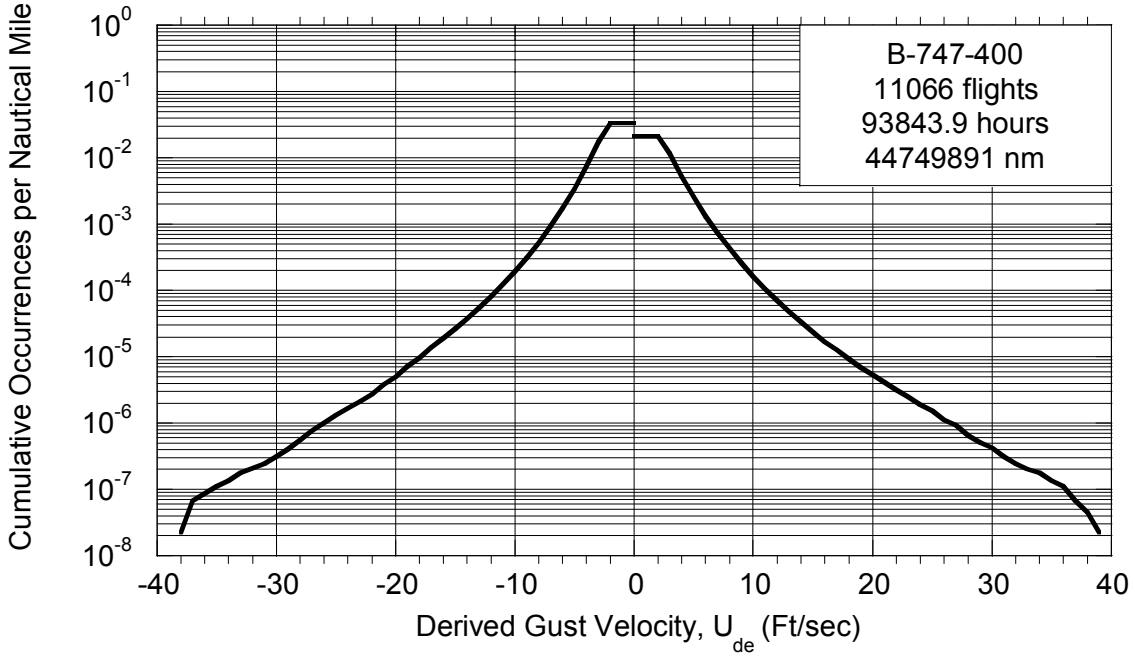

FIGURE A-60. CUMULATIVE OCCURRENCES OF DERIVED GUST VELOCITY PER NAUTICAL MILE, FLAPS RETRACTED

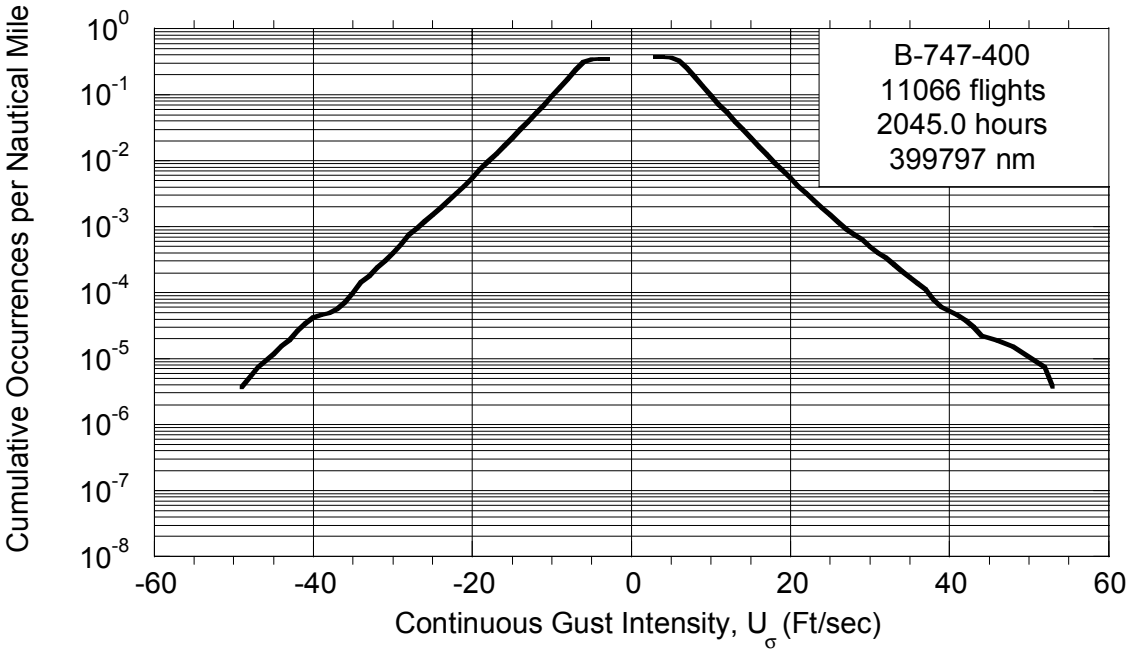

FIGURE A-61. CUMULATIVE OCCURRENCES OF CONTINUOUS GUST INTENSITY PER NAUTICAL MILE, FLAPS EXTENDED

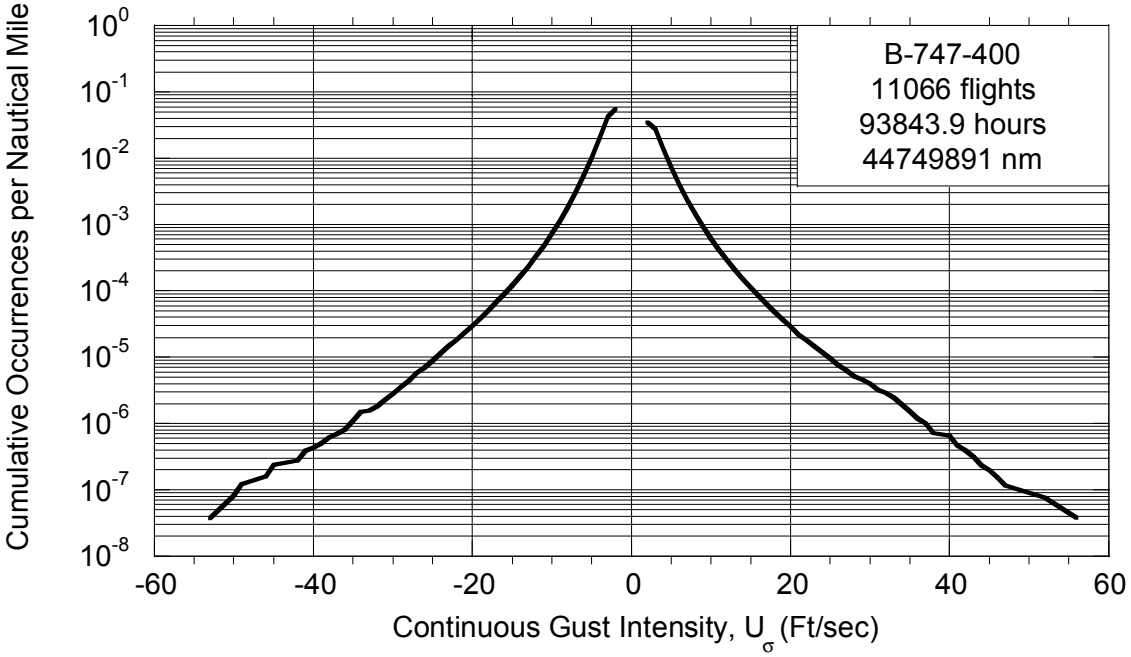

FIGURE A-62. CUMULATIVE OCCURRENCES OF CONTINUOUS GUST INTENSITY PER NAUTICAL MILE, FLAPS RETRACTED

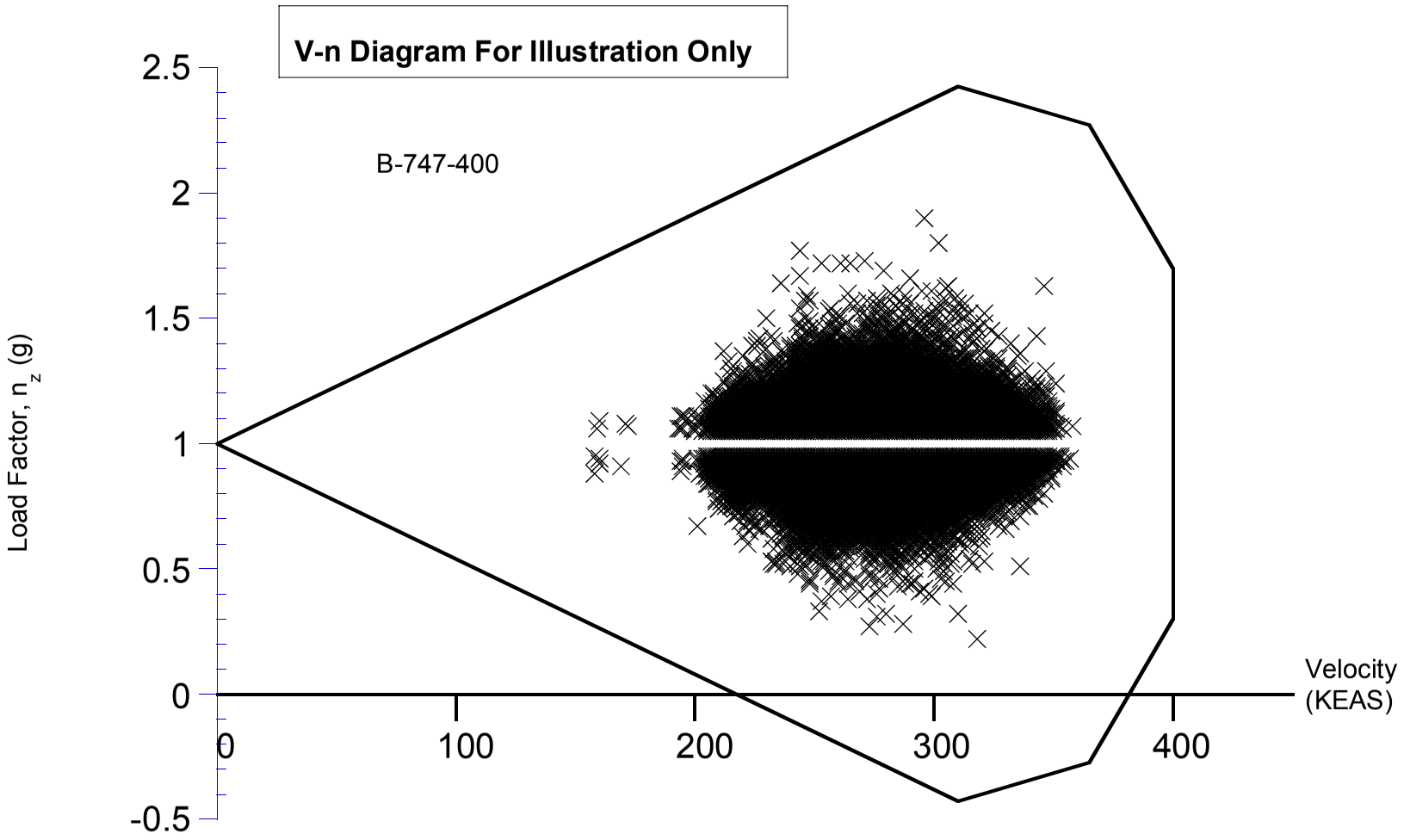

FIGURE A-63. GUST LOAD FACTOR AND COINCIDENT SPEED VS V-N DIAGRAM FOR FLAPS RETRACTED

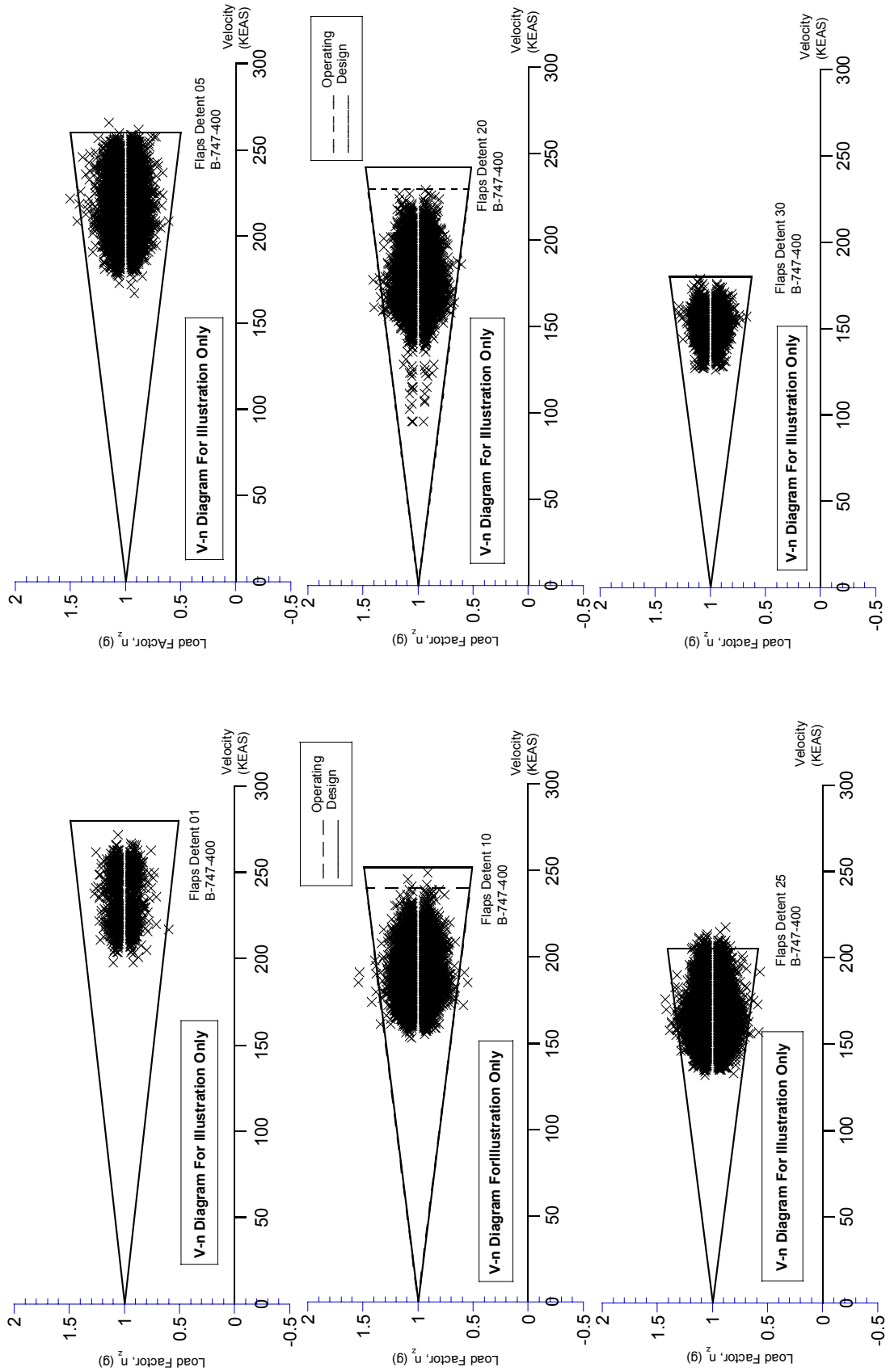

FIGURE A-64. GUST LOAD FACTOR AND COINCIDENT SPEED VS V-n DIAGRAM FOR FLAPS EXTENDED, DETENT 1, 5, 10, 20, 25, AND 30

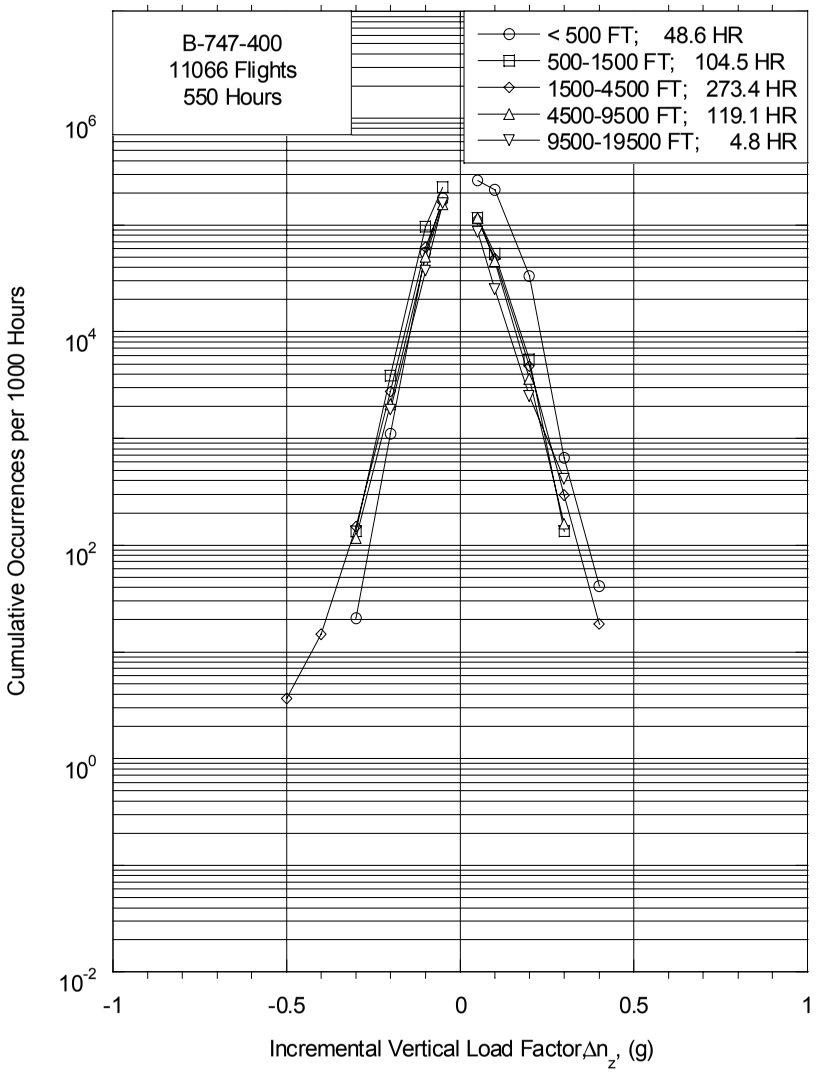

FIGURE A-65. CUMULATIVE OCCURRENCES OF INCREMENTAL VERTICAL MANEUVER LOAD FACTOR PER 1000 HOURS DURING DEPARTURE BY ALTITUDE

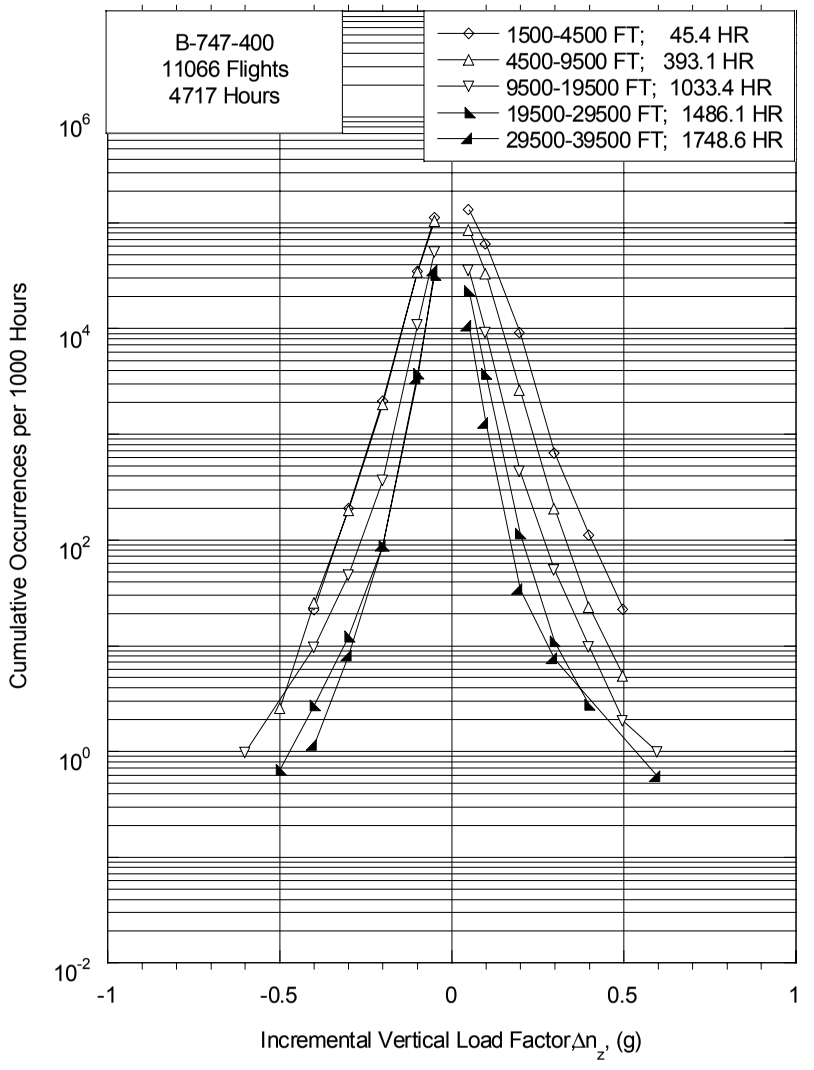

FIGURE A-66. CUMULATIVE OCCURRENCES OF INCREMENTAL VERTICAL MANEUVER LOAD FACTOR PER 1000 HOURS DURING CLIMB BY ALTITUDE

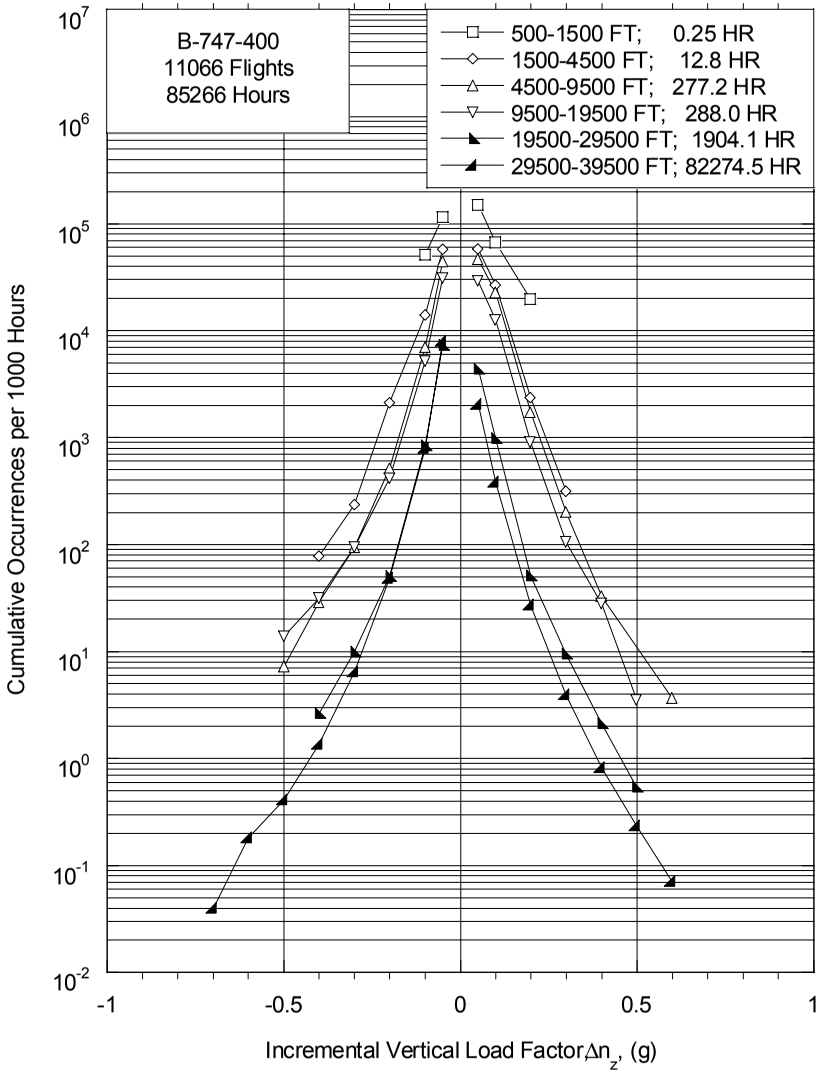

FIGURE A-67. CUMULATIVE OCCURRENCES OF INCREMENTAL VERTICAL MANEUVER LOAD FACTOR PER 1000 HOURS DURING CRUISE BY ALTITUDE

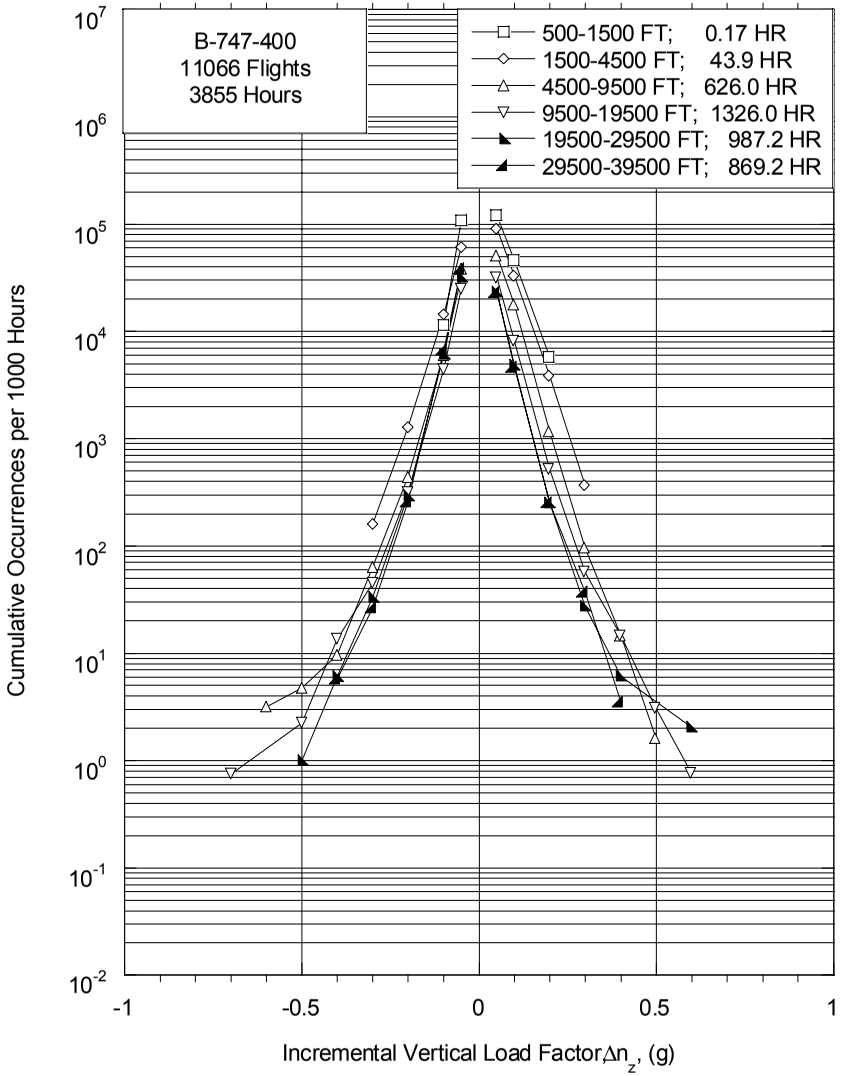

FIGURE A-68. CUMULATIVE OCCURRENCES OF INCREMENTAL VERTICAL MANEUVER LOAD FACTOR PER 1000 HOURS DURING DESCENT BY ALTITUDE

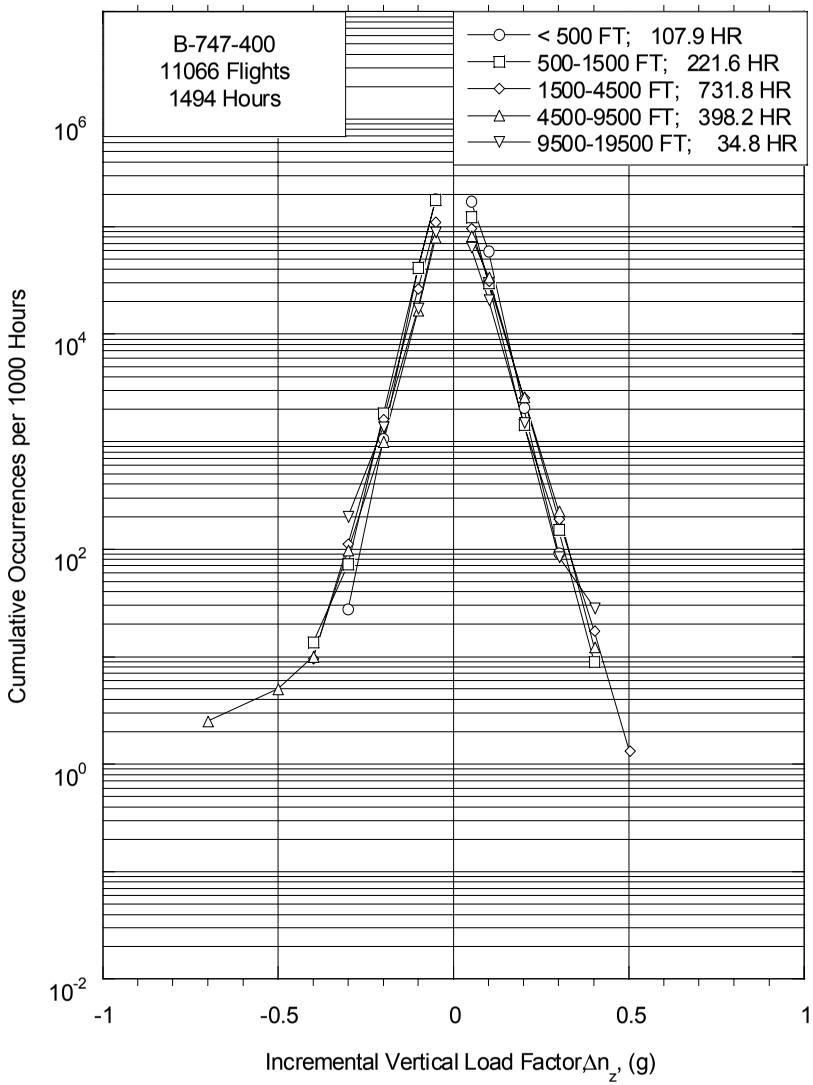

FIGURE A-69. CUMULATIVE OCCURRENCES OF INCREMENTAL VERTICAL MANEUVER LOAD FACTOR PER 1000 HOURS DURING APPROACH BY ALTITUDE

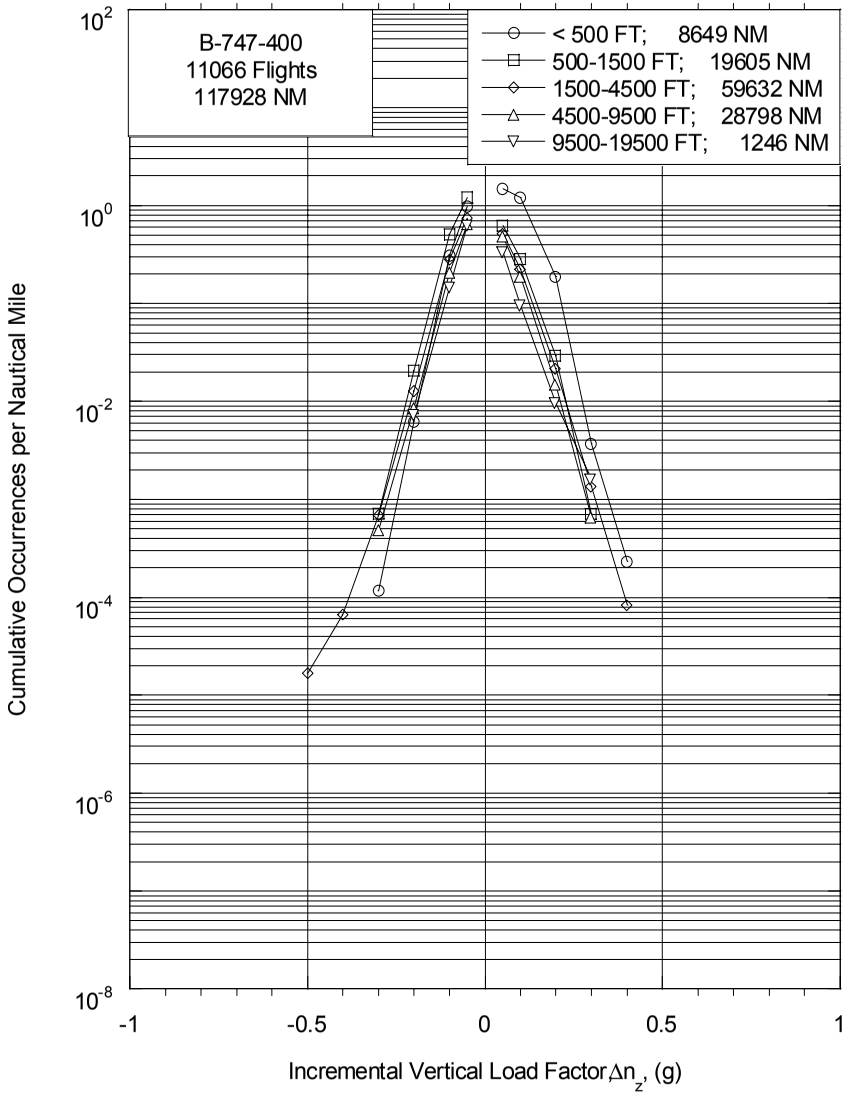

FIGURE A-70. CUMULATIVE OCCURRENCES OF INCREMENTAL VERTICAL MANEUVER LOAD FACTOR PER NAUTICAL MILE DURING DEPARTURE BY ALTITUDE

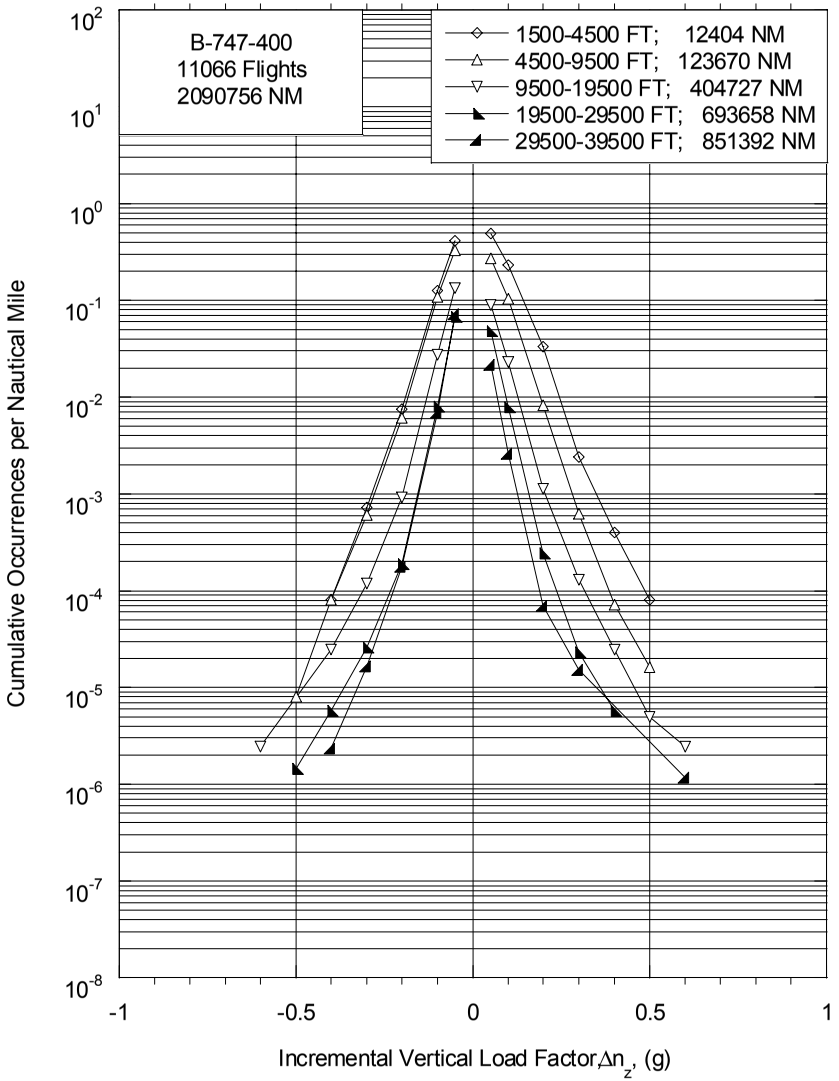

FIGURE A-71. CUMULATIVE OCCURRENCES OF INCREMENTAL VERTICAL MANEUVER LOAD FACTOR PER NAUTICAL MILE DURING CLIMB BY ALTITUDE

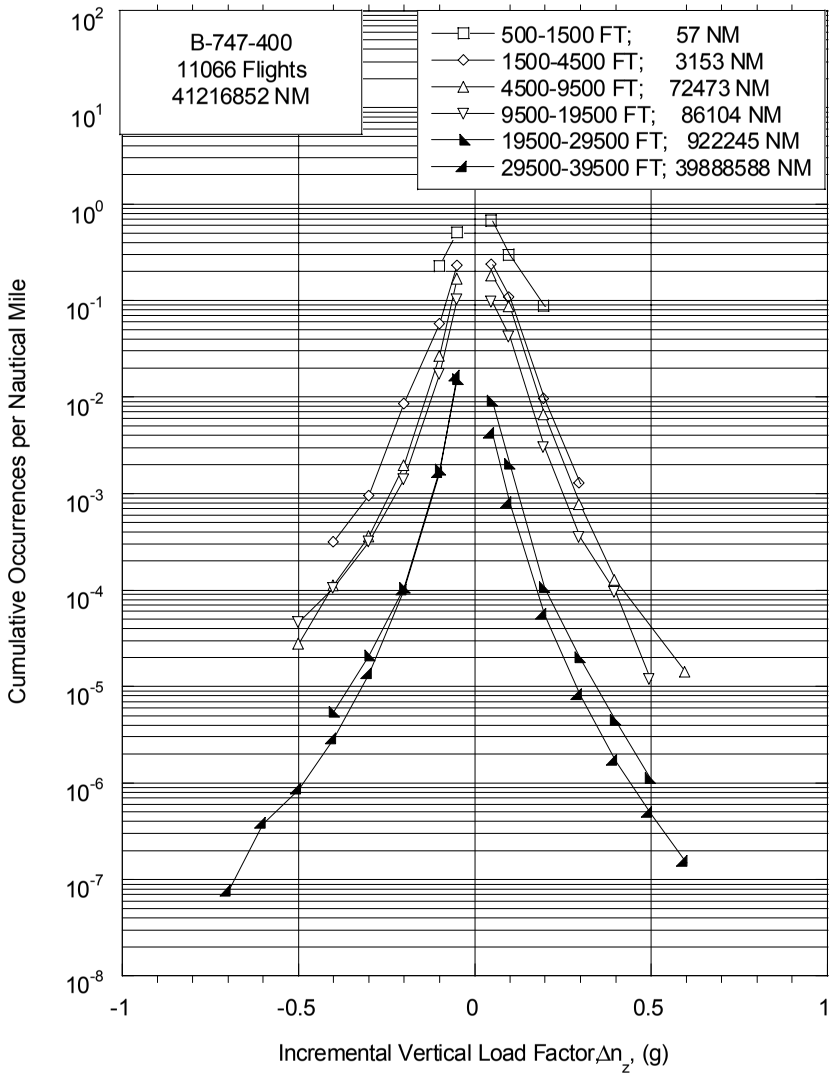

FIGURE A-72. CUMULATIVE OCCURRENCES OF INCREMENTAL VERTICAL MANEUVER LOAD FACTOR PER NAUTICAL MILE DURING CRUISE BY ALTITUDE

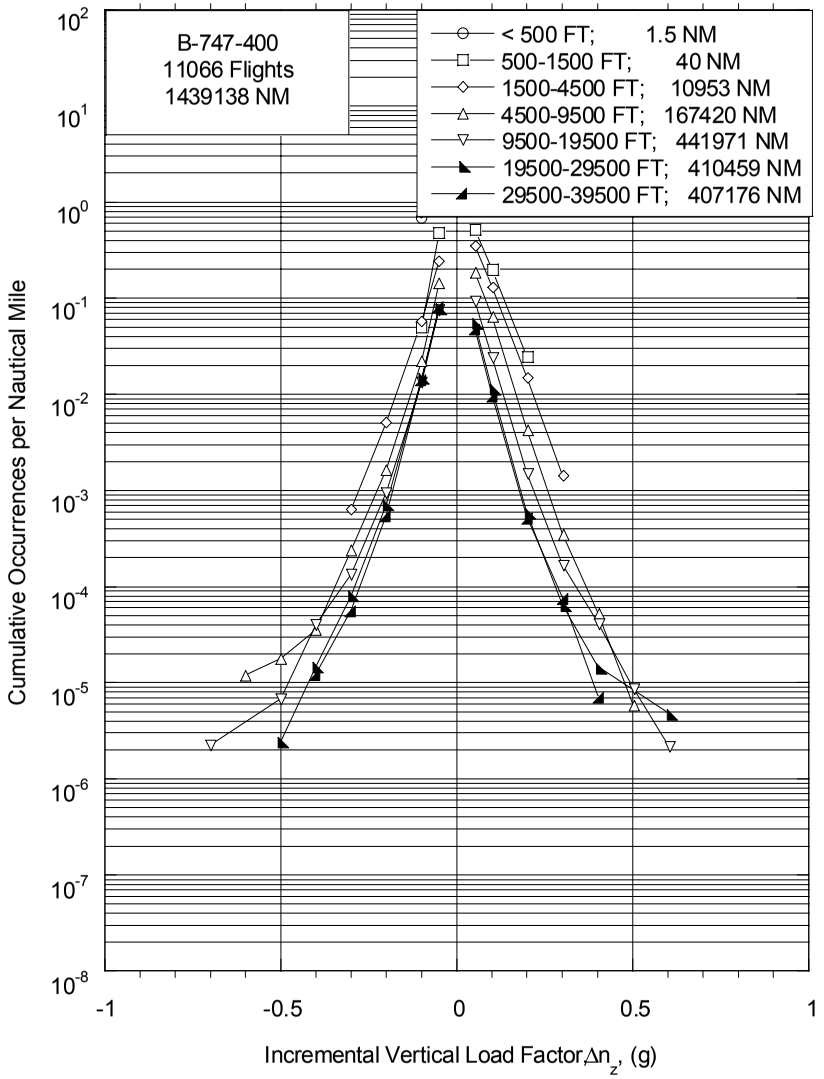

FIGURE A-73. CUMULATIVE OCCURRENCES OF INCREMENTAL VERTICAL MANEUVER LOAD FACTOR PER NAUTICAL MILE DURING DESCENT BY ALTITUDE

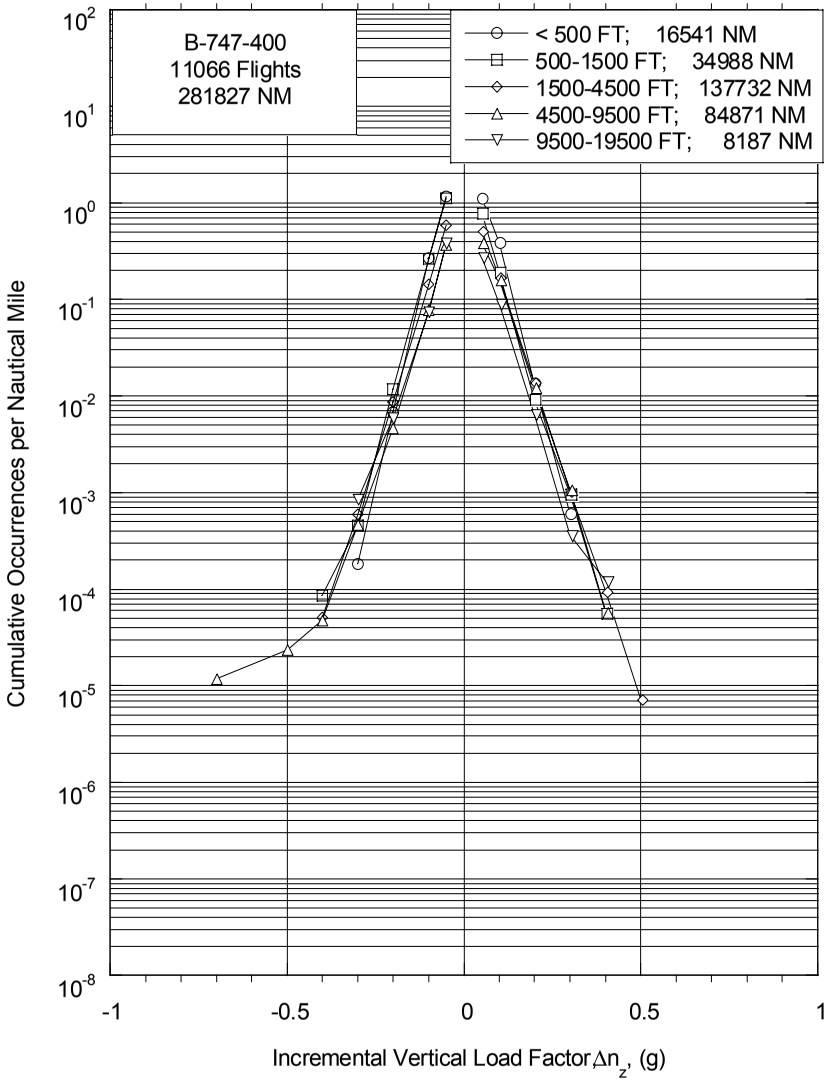

FIGURE A-74. CUMULATIVE OCCURRENCES OF INCREMENTAL VERTICAL MANEUVER LOAD FACTOR PER NAUTICAL MILE DURING APPROACH BY ALTITUDE

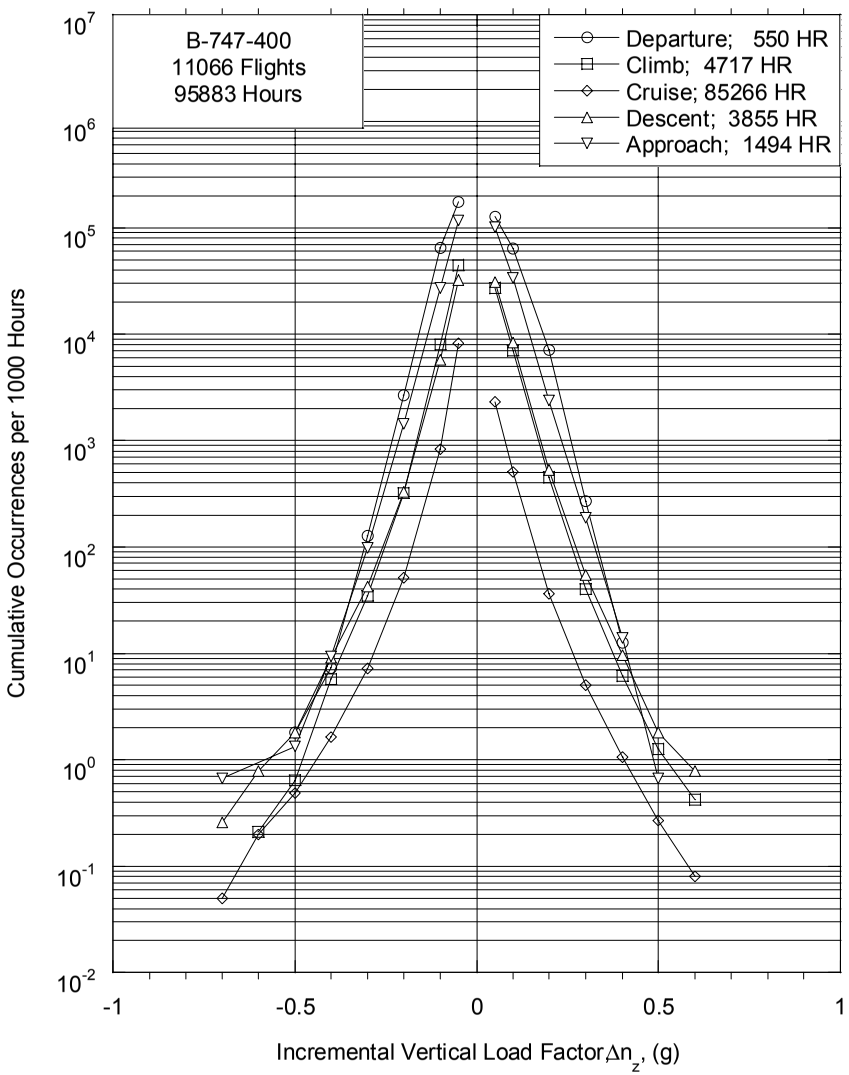

FIGURE A-75. CUMULATIVE OCCURRENCES OF INCREMENTAL VERTICAL MANEUVER LOAD FACTOR PER 1000 HOURS BY FLIGHT PHASE

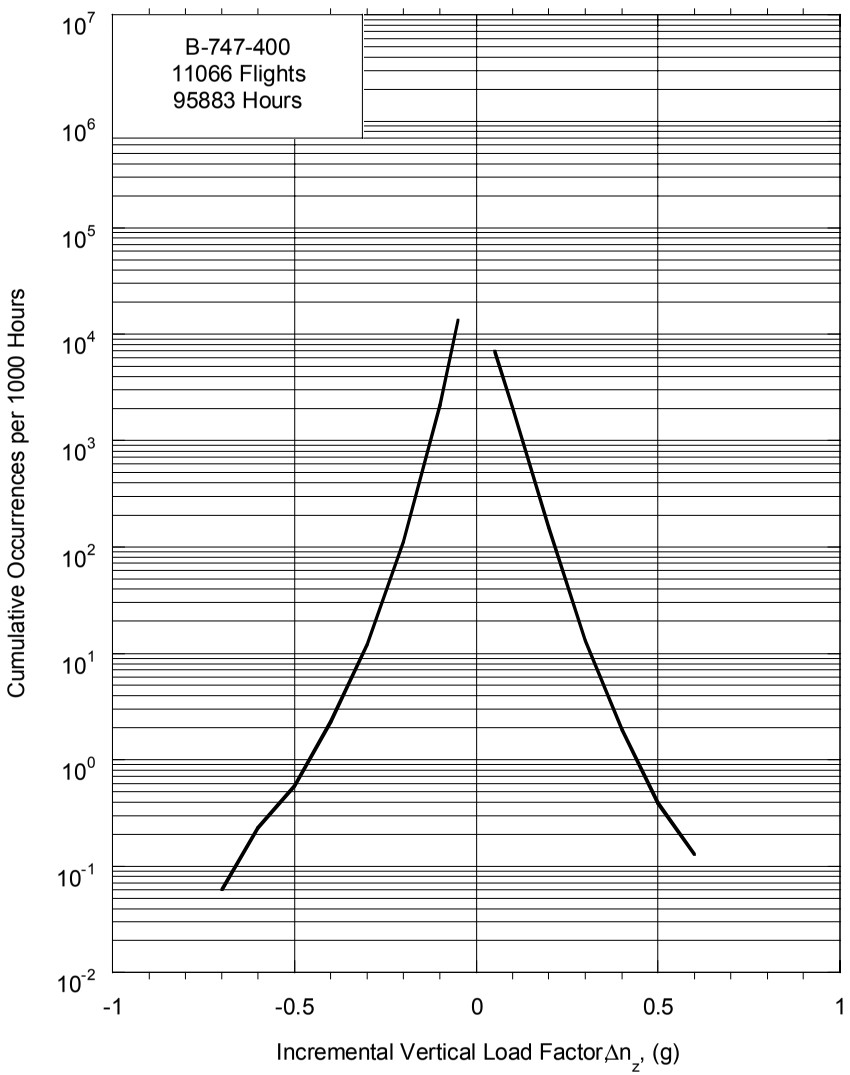

FIGURE A-76. CUMULATIVE OCCURRENCES OF INCREMENTAL VERTICAL MANEUVER LOAD FACTOR PER 1000 HOURS, COMBINED FLIGHT PHASES

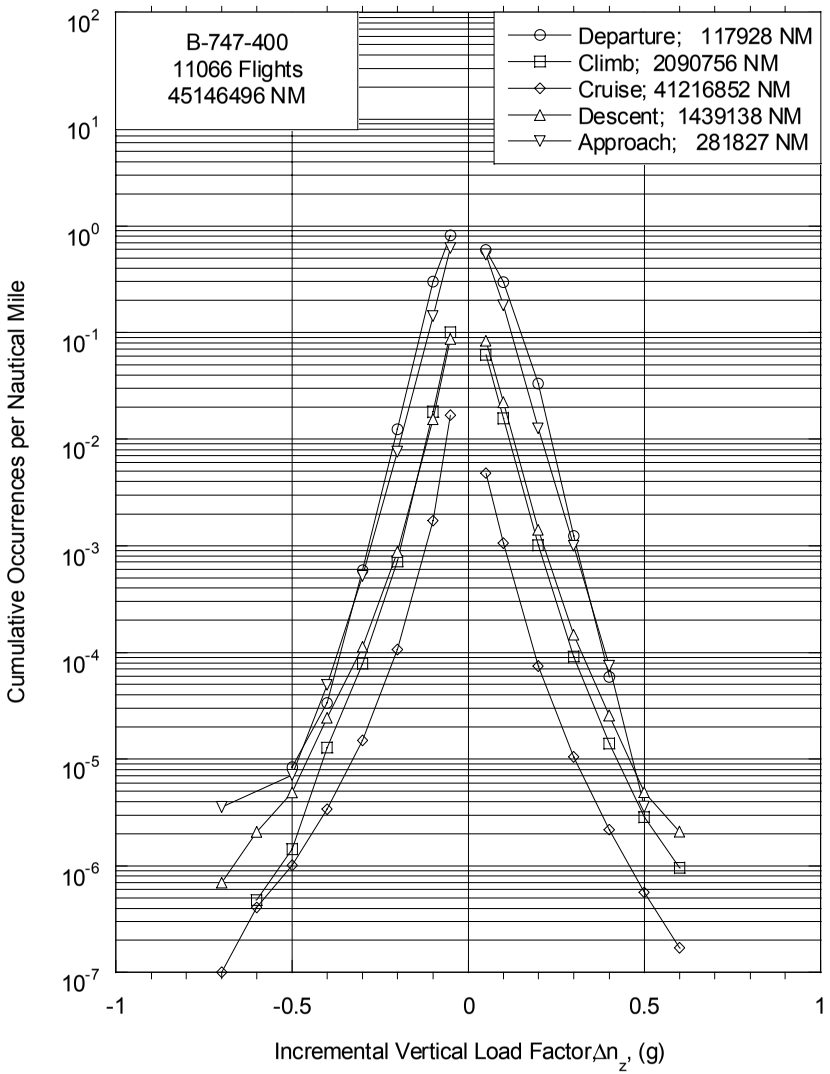

FIGURE A-77. CUMULATIVE OCCURRENCES OF INCREMENTAL VERTICAL MANEUVER LOAD FACTOR PER NAUTICAL MILE BY FLIGHT PHASE

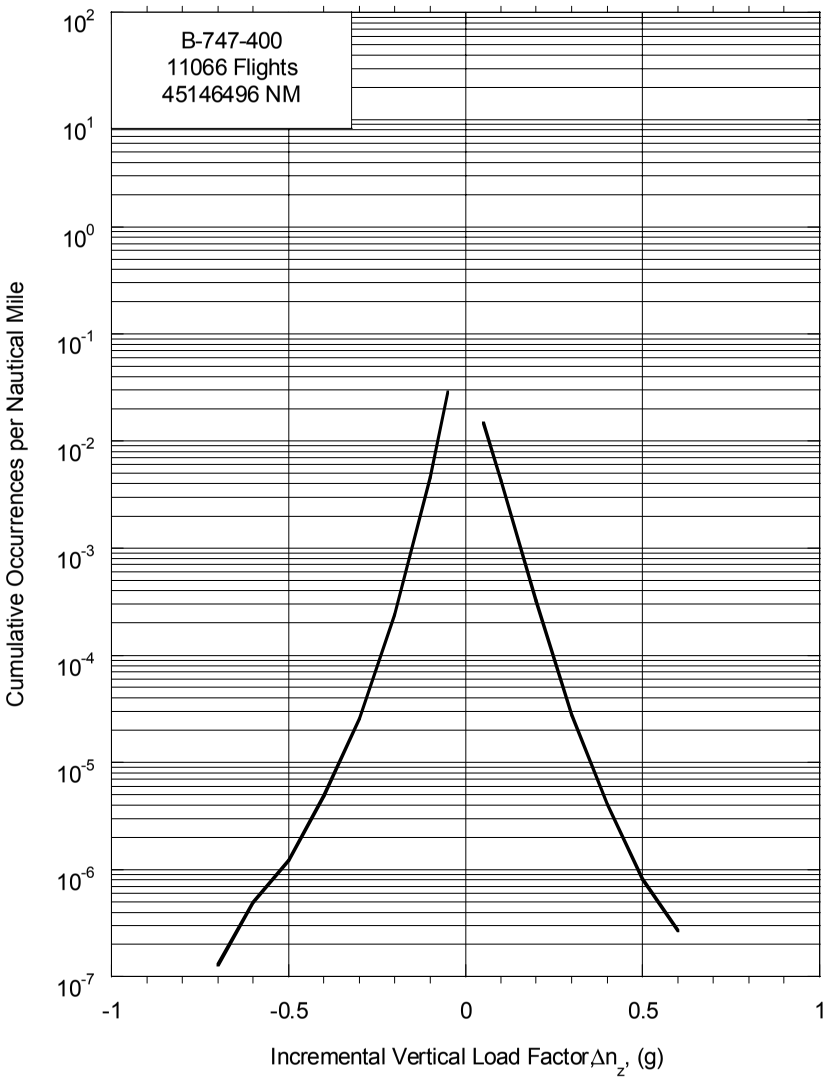

FIGURE A-78. CUMULATIVE OCCURRENCES OF INCREMENTAL VERTICAL MANEUVER LOAD FACTOR PER NAUTICAL MILE, COMBINED FLIGHT PHASES

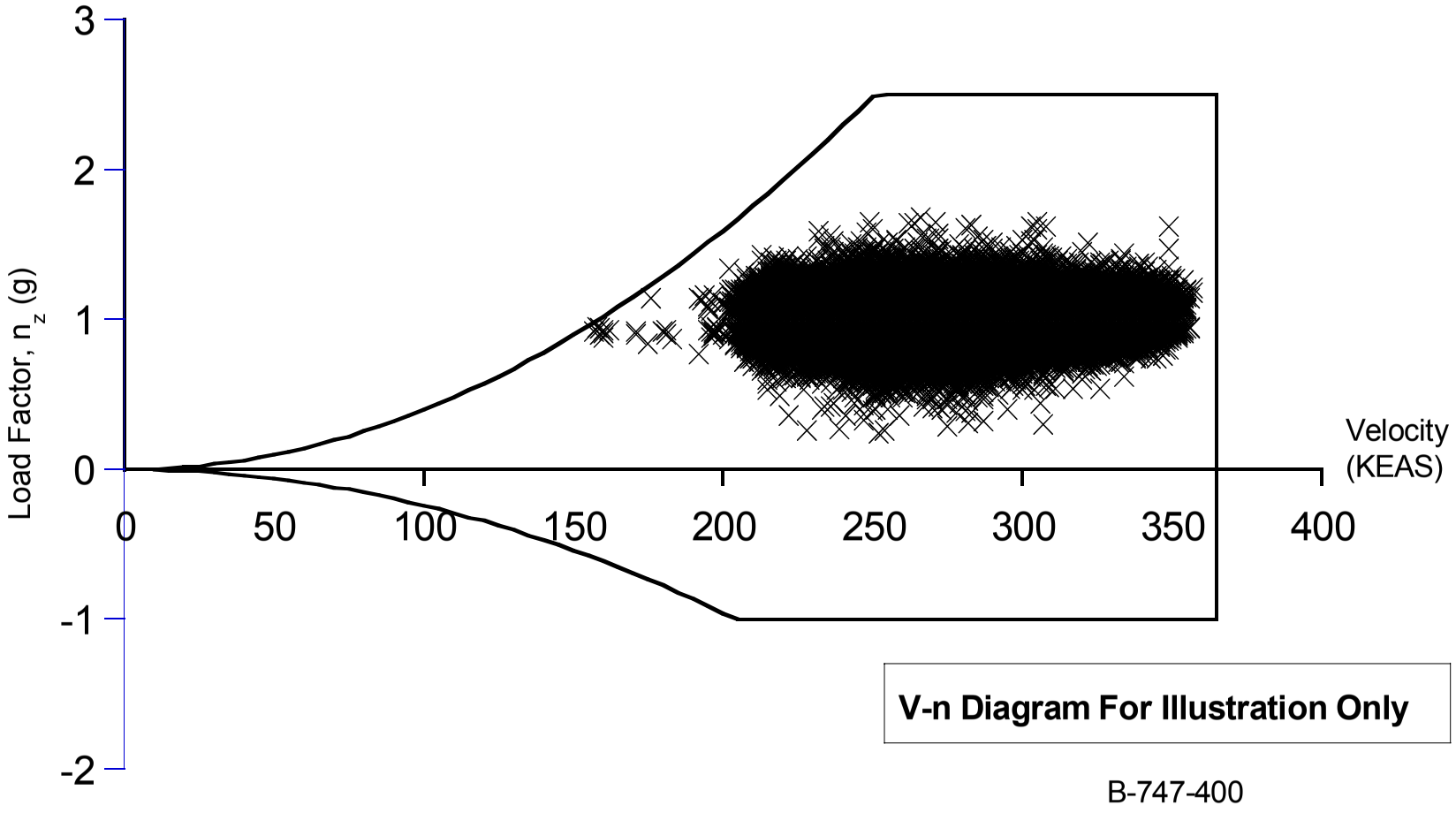

FIGURE A-79. MANEUVER LOAD FACTOR AND COINCIDENT SPEED VS V-n DIAGRAM FOR FLAPS RETRACTED

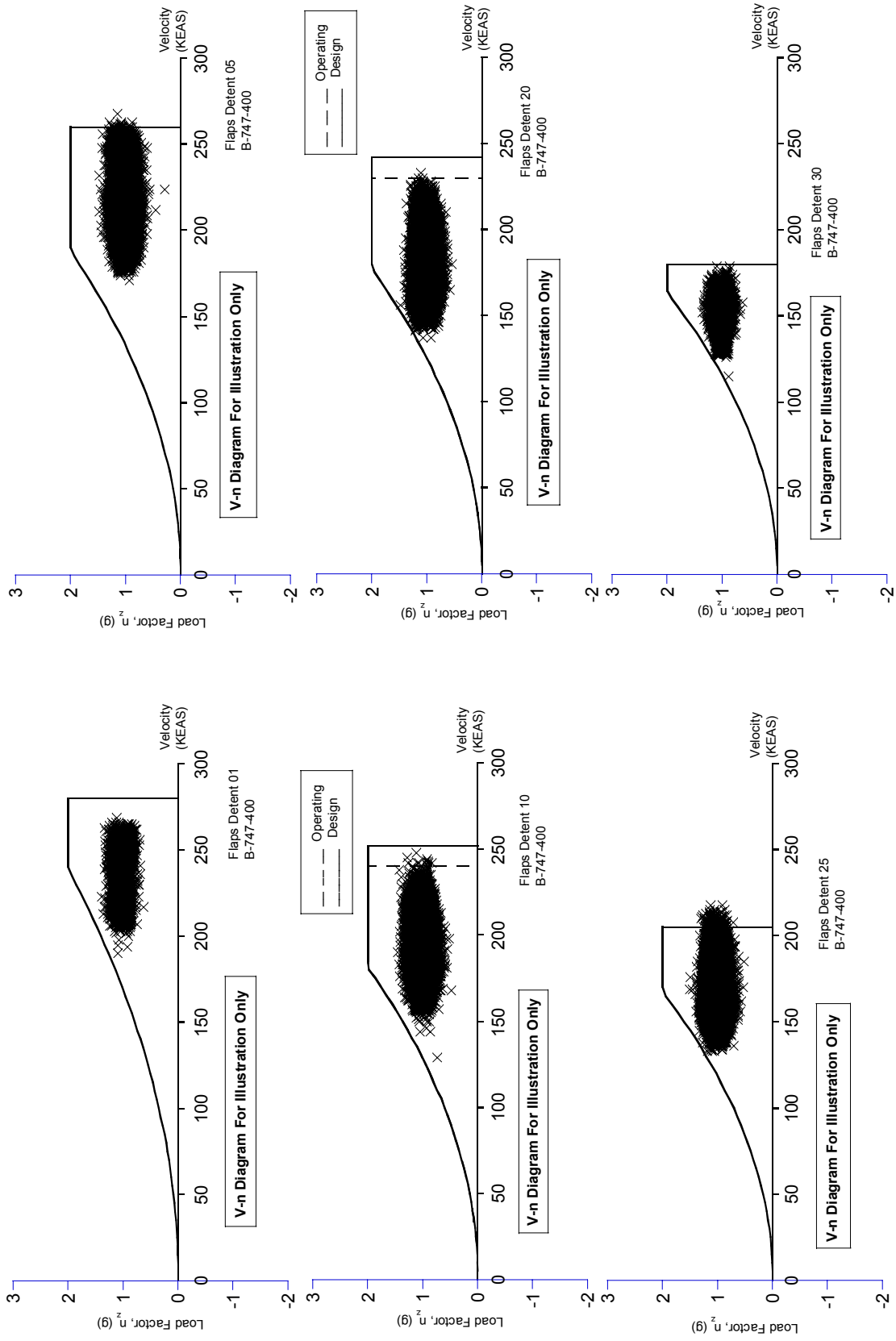

FIGURE A-80. MANEUVER LOAD FACTOR AND COINCIDENT SPEED VS V-N DIAGRAM FOR FLAPS EXTENDED, DETENT 1, 5, 10, 20, 25, AND 30

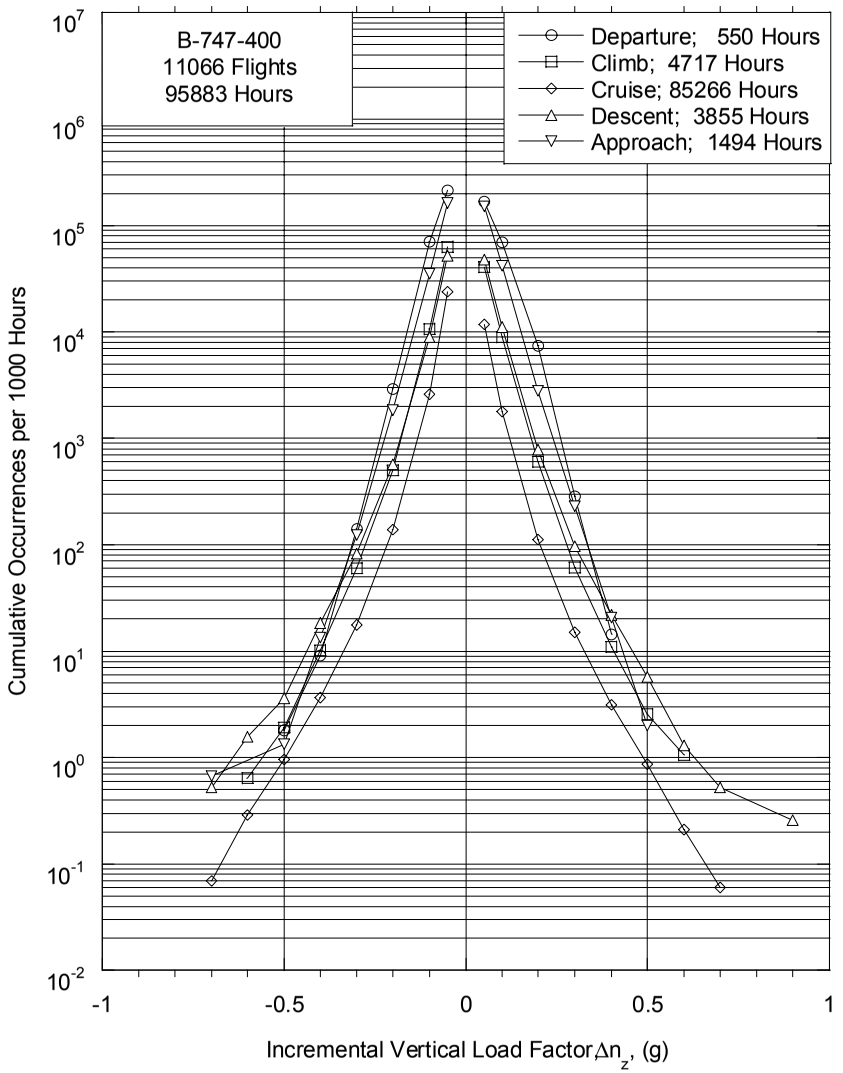

FIGURE A-81. CUMULATIVE OCCURRENCES OF INCREMENTAL VERTICAL LOAD FACTOR PER 1000 HOURS BY FLIGHT PHASE

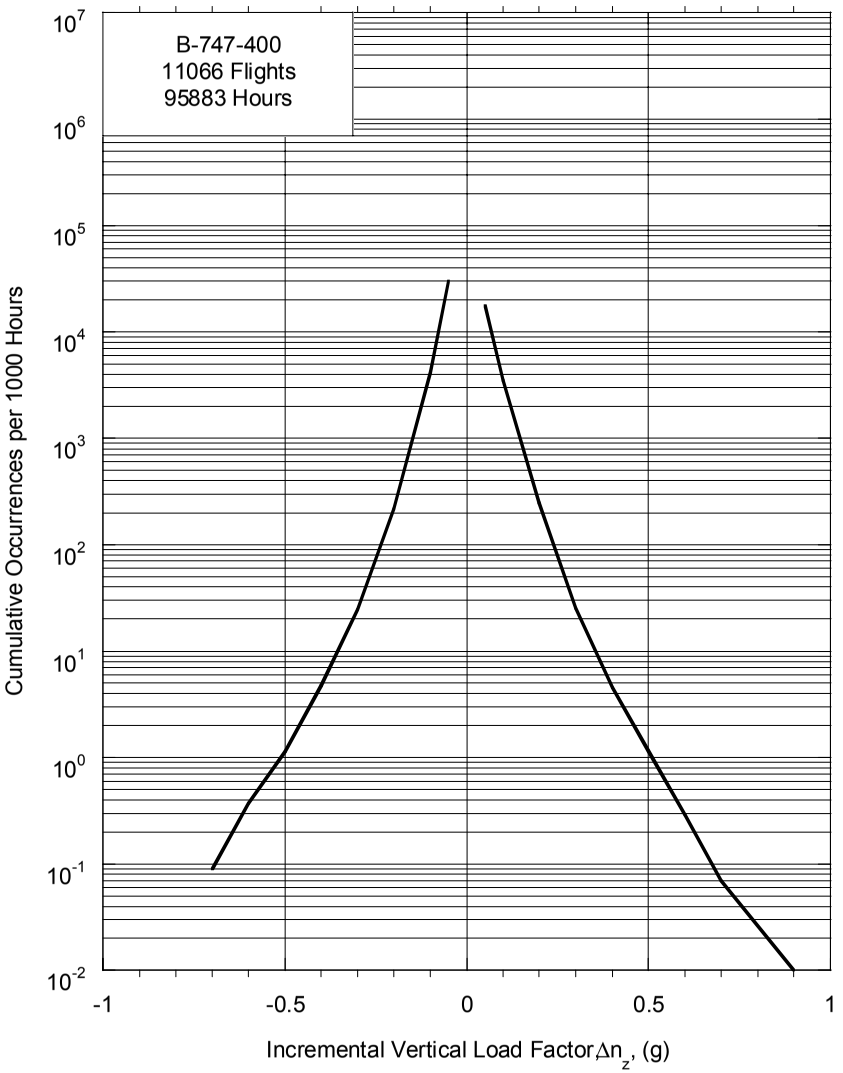

FIGURE A-82. CUMULATIVE OCCURRENCES OF INCREMENTAL VERTICAL LOAD FACTOR PER 1000 HOURS, COMBINED FLIGHT PHASES

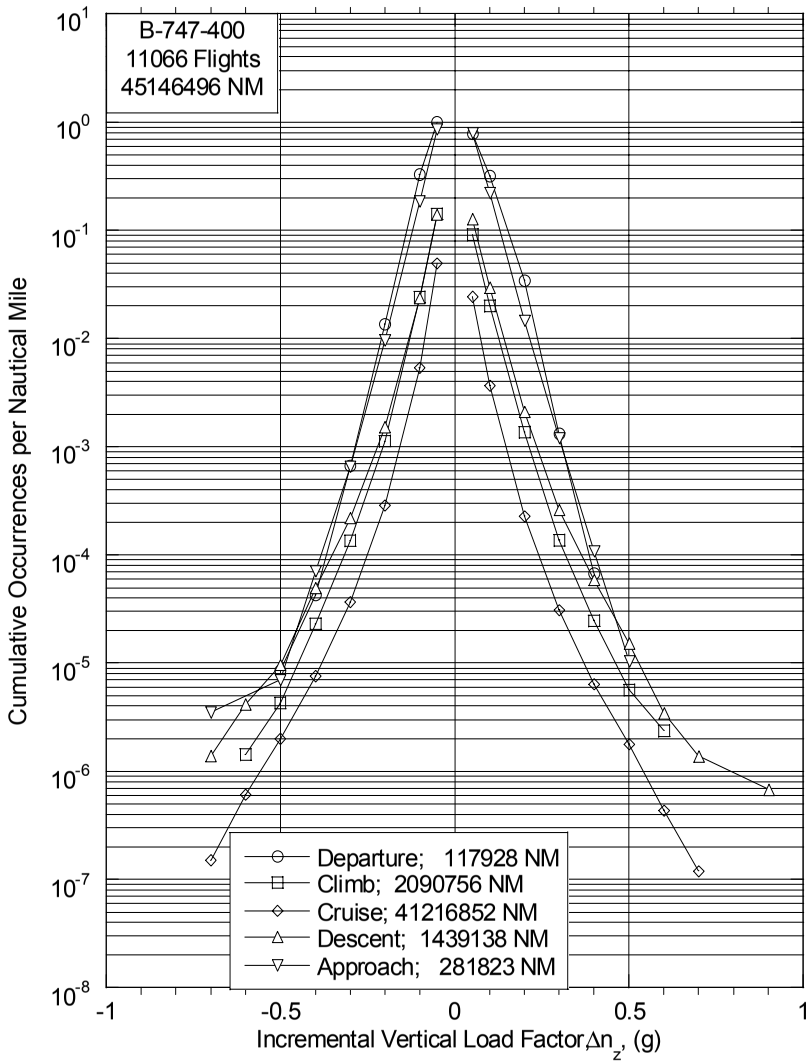

FIGURE A-83. CUMULATIVE OCCURRENCES OF INCREMENTAL VERTICAL LOAD FACTOR PER NAUTICAL MILE BY FLIGHT PHASE

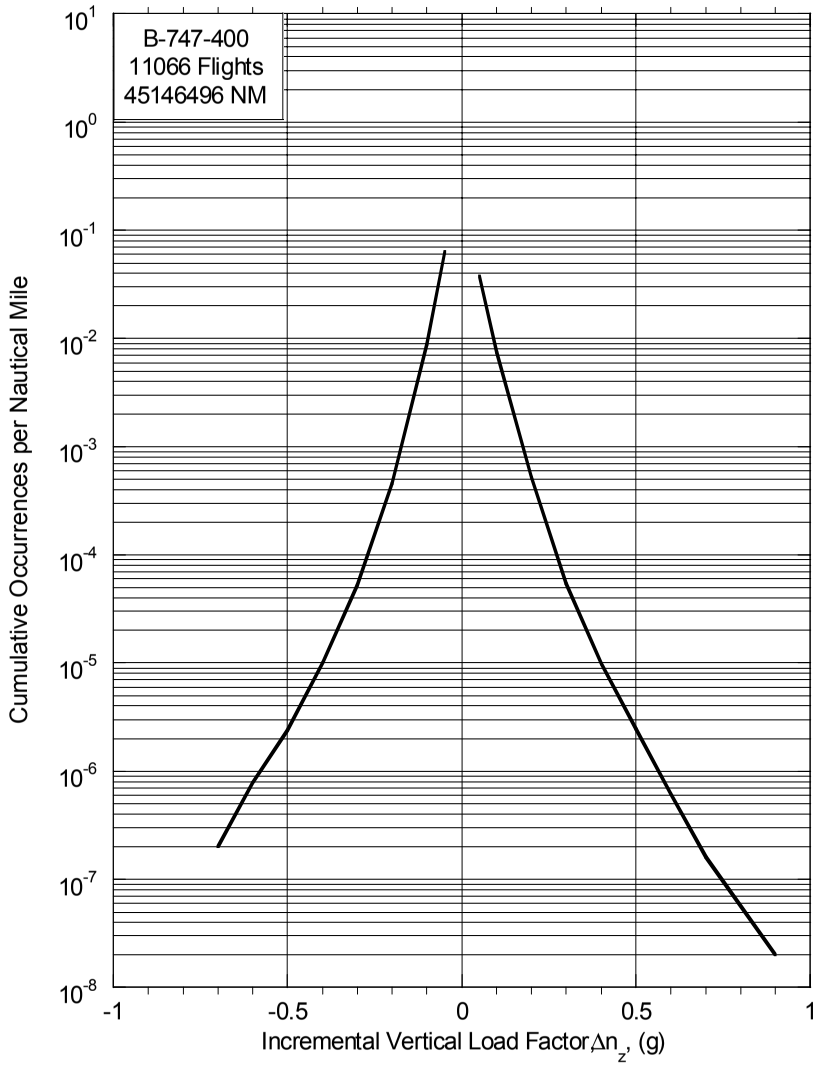

FIGURE A-84. CUMULATIVE OCCURRENCES OF INCREMENTAL VERTICAL LOAD FACTOR PER NAUTICAL MILE, COMBINED FLIGHT PHASES

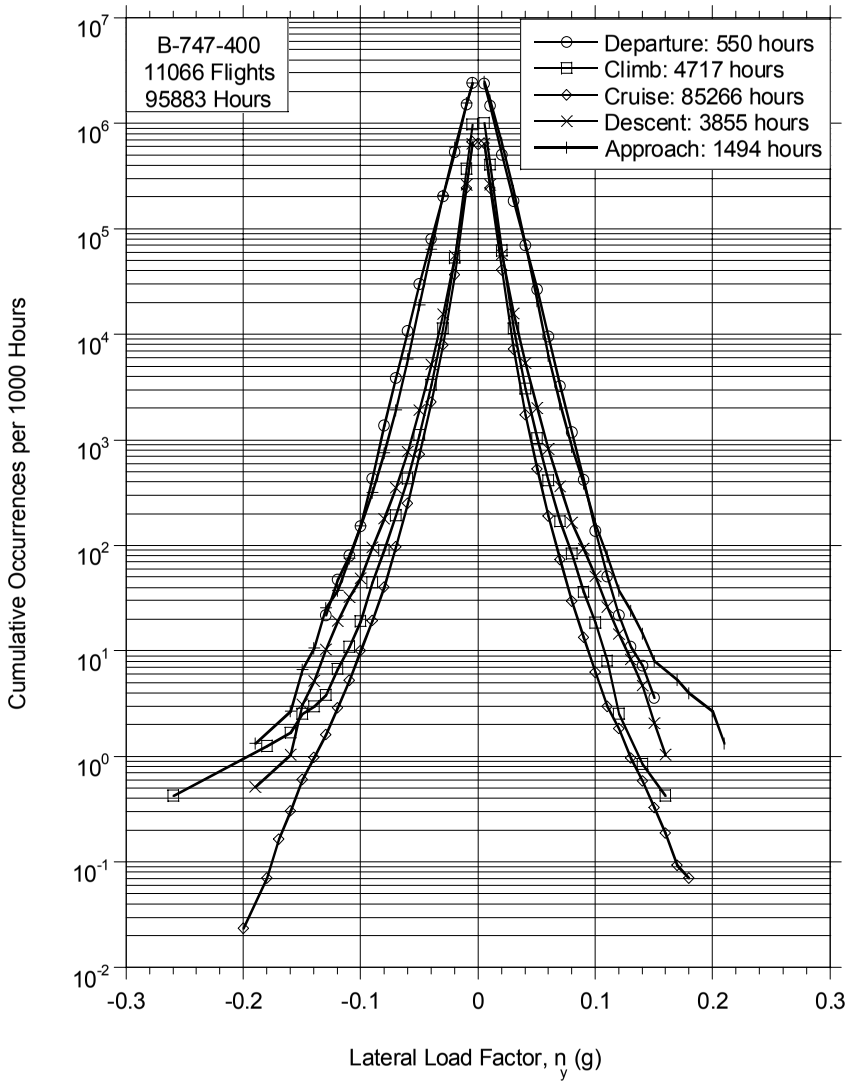

FIGURE A-85. CUMULATIVE OCCURRENCES OF LATERAL LOAD FACTOR PER 1000 HOURS BY FLIGHT PHASE

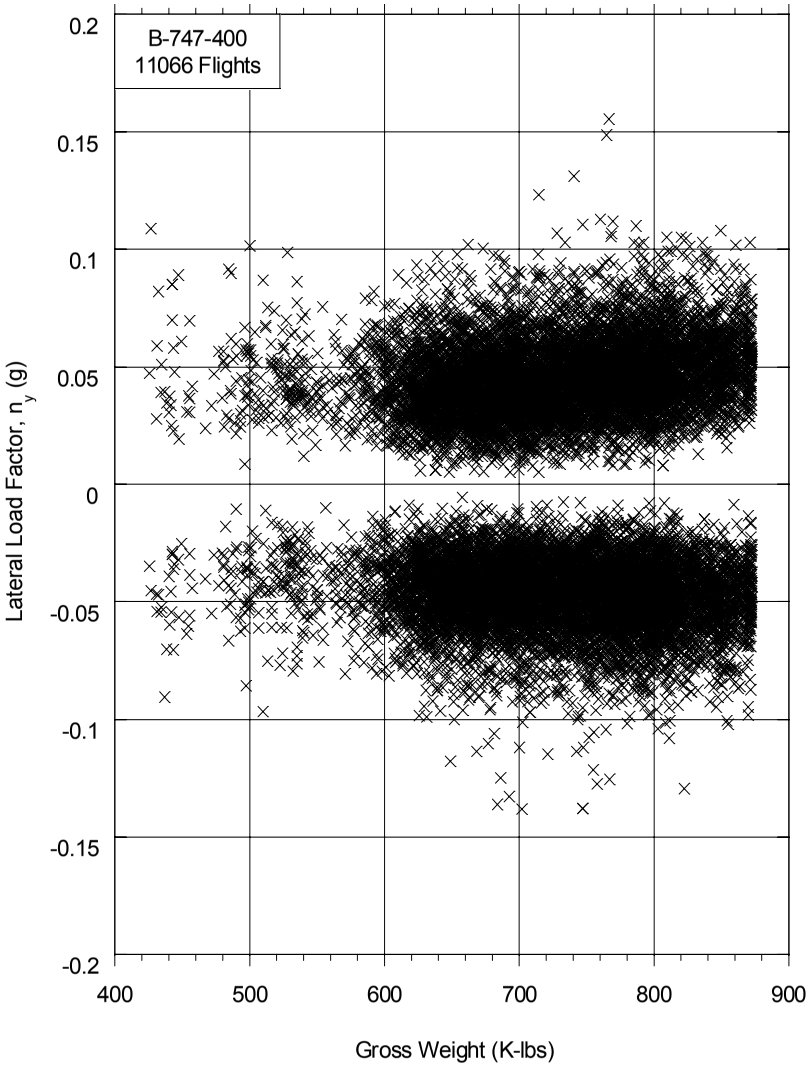

FIGURE A-86. MAXIMUM LATERAL LOAD FACTOR VS COINCIDENT GROSS WEIGHT DURING DEPARTURE

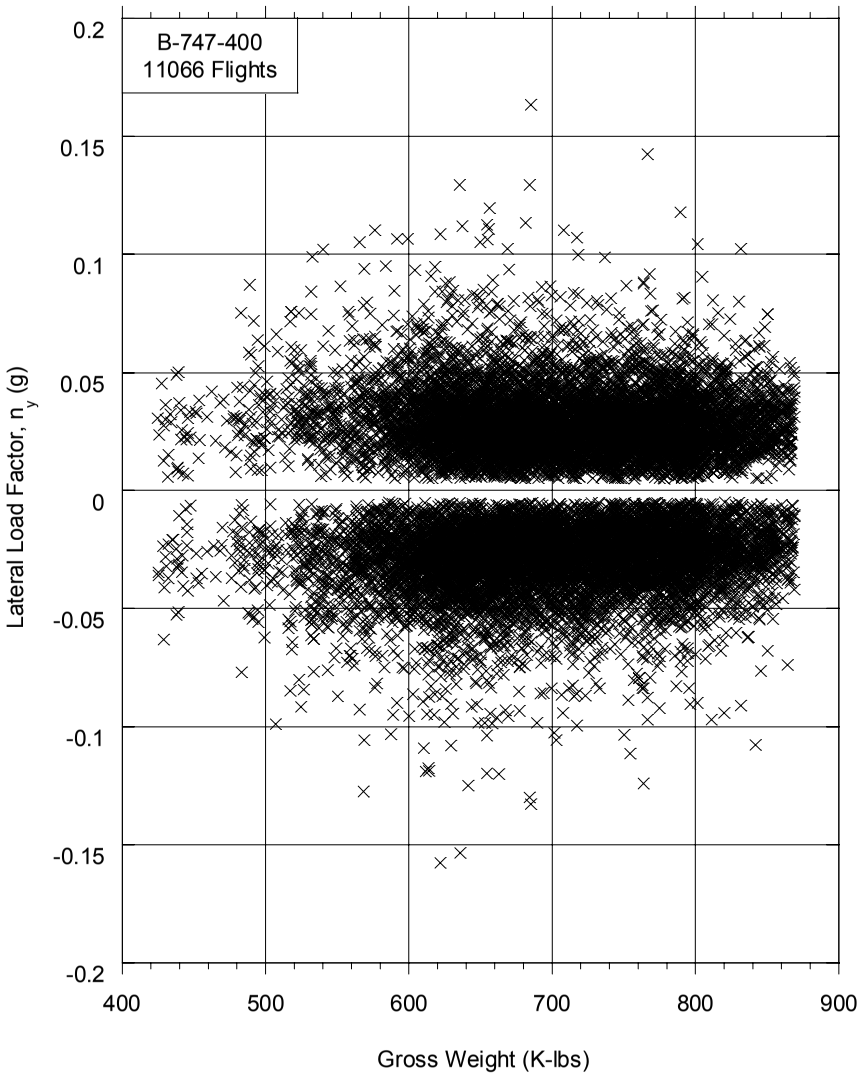

FIGURE A-87. MAXIMUM LATERAL LOAD FACTOR VS COINCIDENT GROSS WEIGHT DURING CLIMB

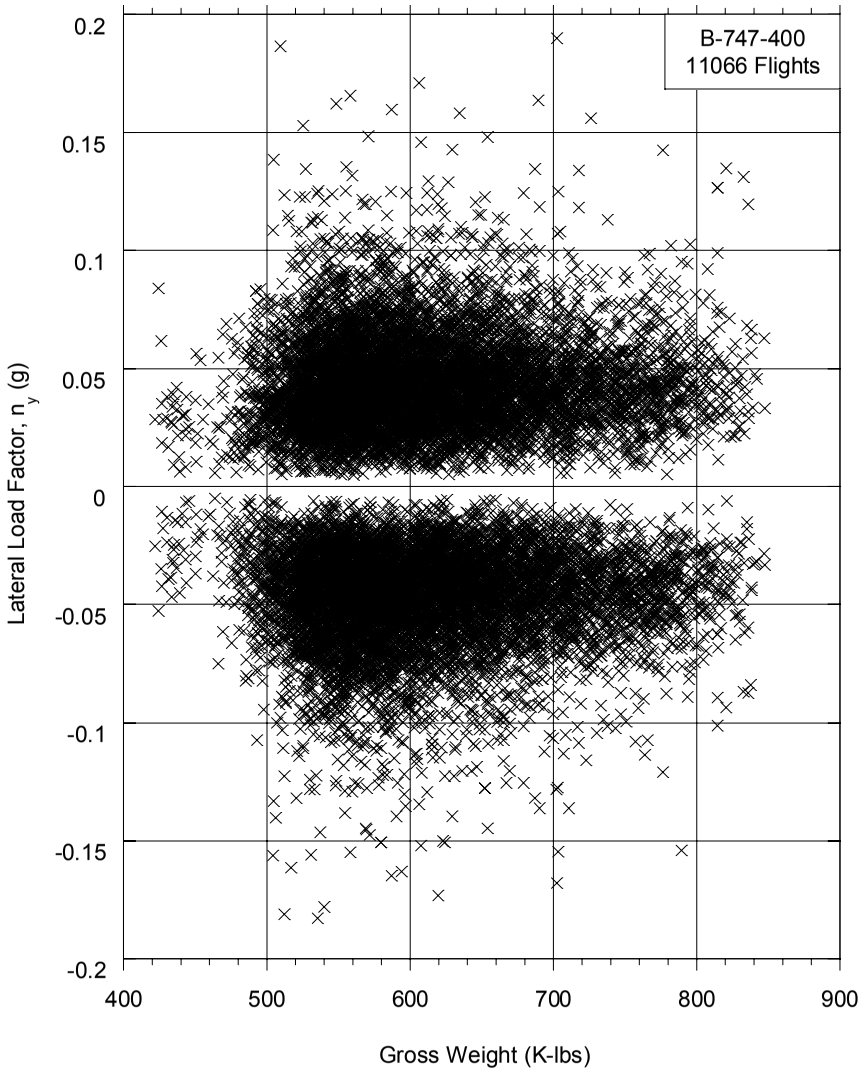

FIGURE A-88. MAXIMUM LATERAL LOAD FACTOR VS COINCIDENT GROSS WEIGHT DURING CRUISE

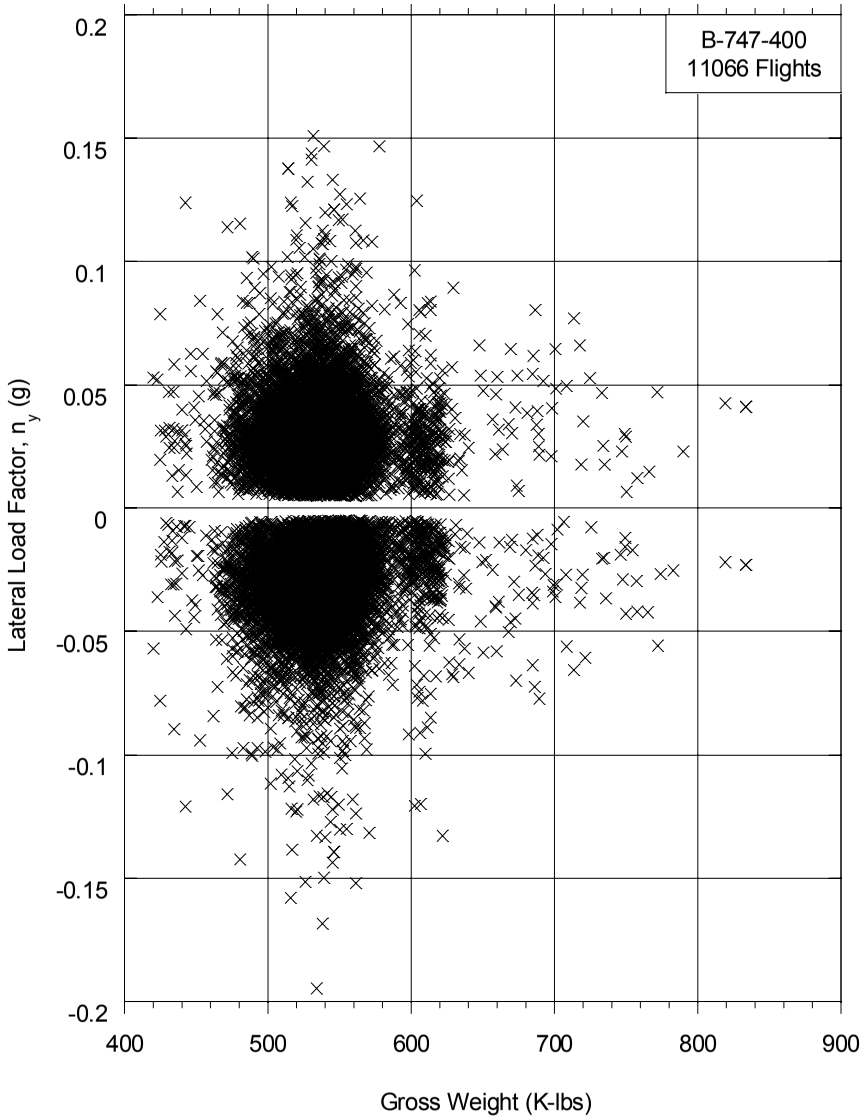

FIGURE A-89. MAXIMUM LATERAL LOAD FACTOR VS COINCIDENT GROSS WEIGHT DURING DESCENT

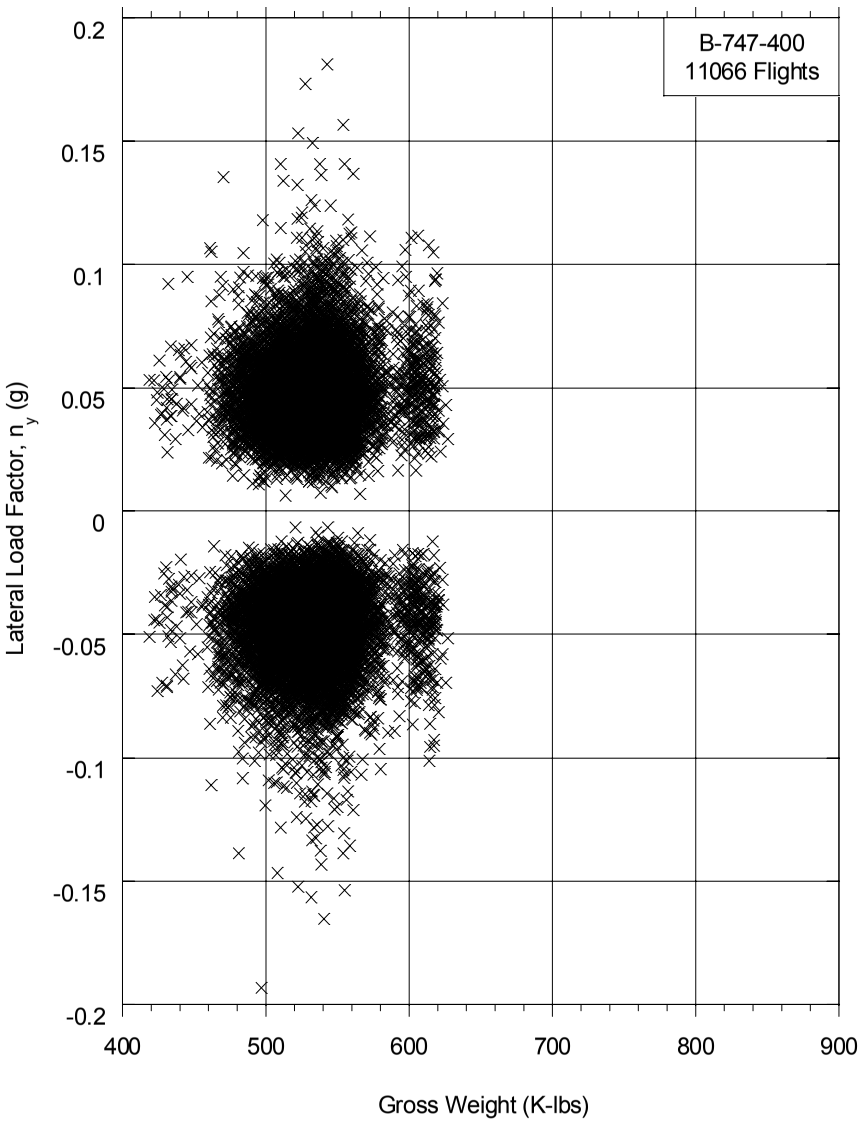

FIGURE A-90. MAXIMUM LATERAL LOAD FACTOR VS COINCIDENT GROSS WEIGHT DURING APPROACH

Minimum Incremental Vertical Load Factor, Δn_z (g)

11066 Flights	0.05	0.10	0.15	0.20	0.25	0.30	0.35	0.40	0.45	0.50	0.55	0.60	0.65	0.70	0.75	0.80	0.85	0.90
-.05																		
-.10		25	547	276	29	7	1											
-.15	1	55	1869	1623	409	104	21	3	1									
-.20		25	859	1461	642	176	52	10	7	2								
-.25		6	232	590	421	202	74	35	11	3		3						
-.30		1	47	188	176	118	64	28	14	6	2	4		1				
-.35		1	10	61	80	76	39	20	10	7	5			1				1
-.40			1	20	33	29	25	23	14	6	2	1		1				
-.45				8	16	13	13	13	4	10	4	1	2	1	1			
-.50				4	3	2	4	4	10	1	2	1						
-.55					1	4	4	4	4	2	2		1					
-.60						2	1	1	2	3	2	1	1		1			
-.65							1	1	1	3		1						
-.70							1	2		2	1	1						
-.75						1					1							

FIGURE A-91. GROUND-AIR-GROUND CYCLE OCCURRENCES OF MAXIMUM AND MINIMUM INCREMENTAL VERTICAL LOAD FACTOR

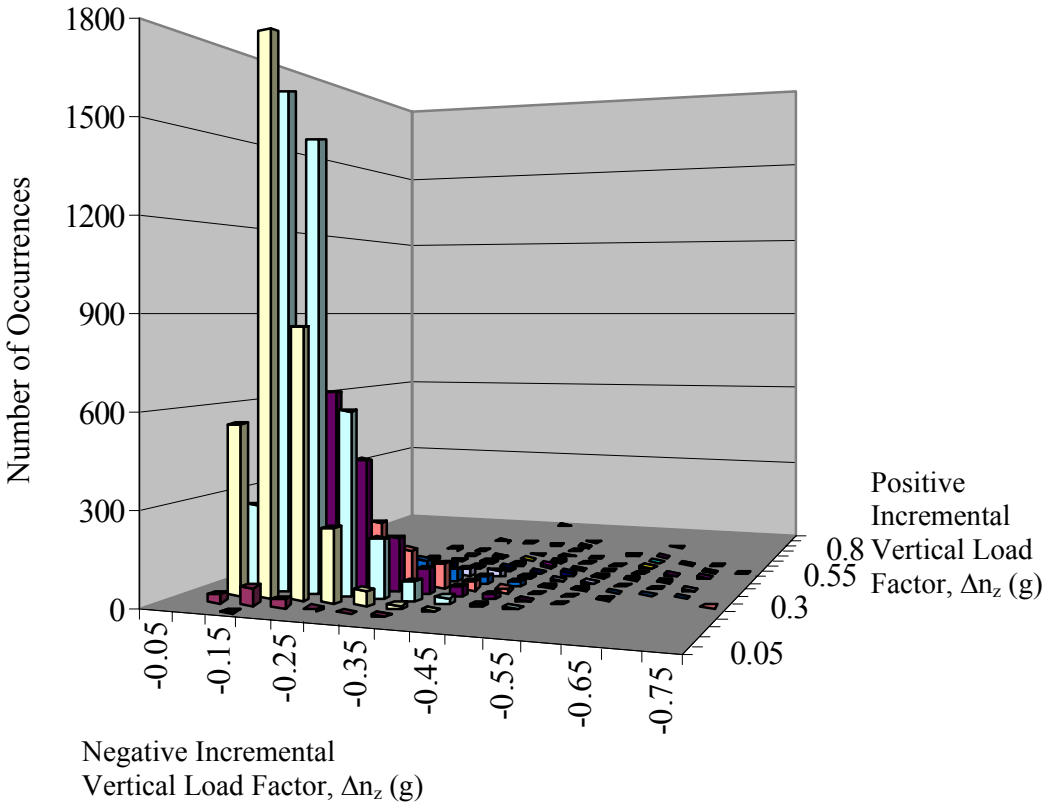

FIGURE A-92. 3-D PLOT OF GROUND-AIR-GROUND CYCLES

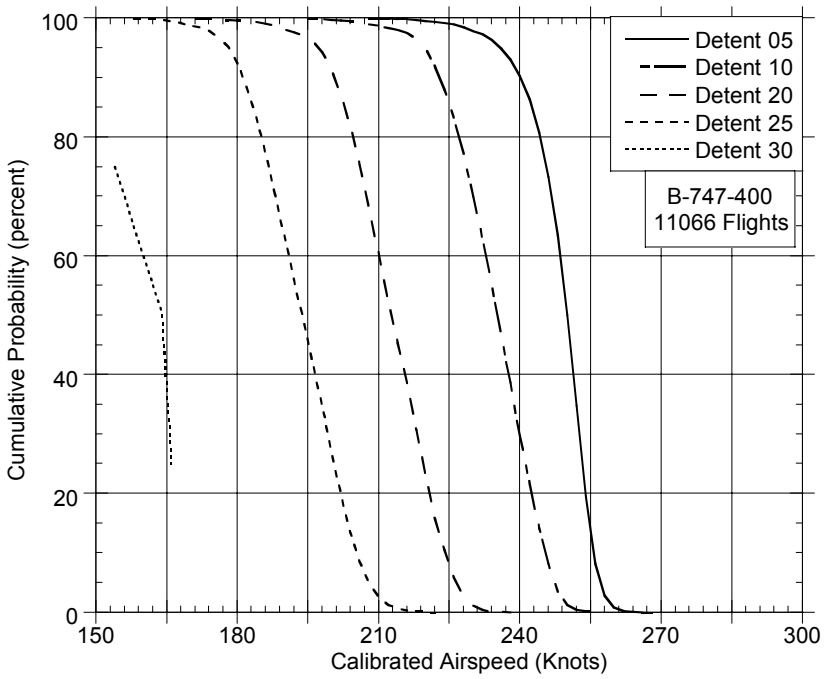

FIGURE A-93. CUMULATIVE PROBABILITY OF MAXIMUM AIRSPEED IN FLAP DETENT DURING DEPARTURE

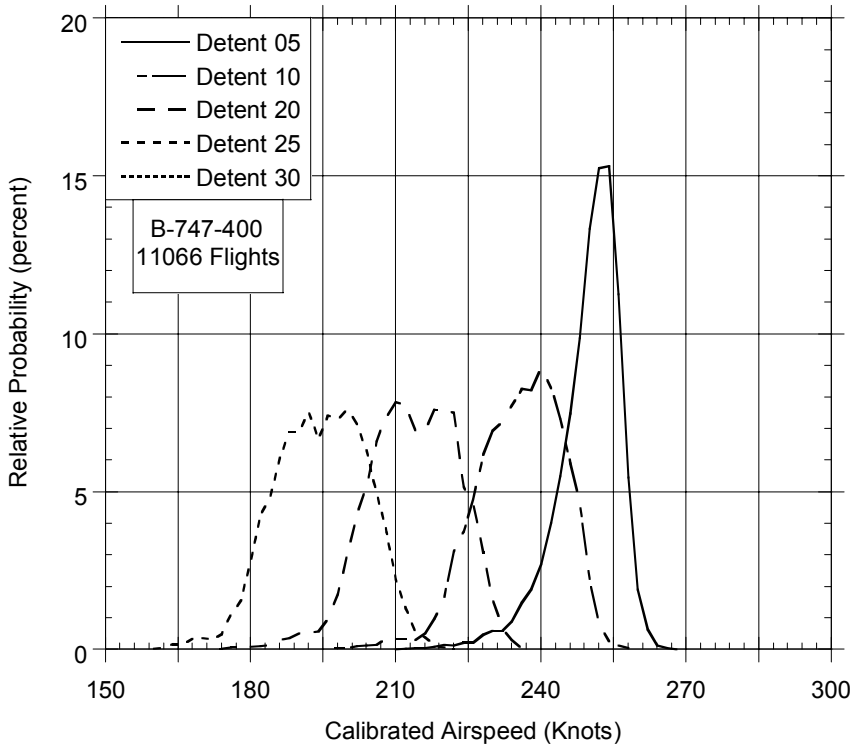

FIGURE A-94. RELATIVE PROBABILITY OF MAXIMUM AIRSPEED IN FLAP DETENT DURING DEPARTURE

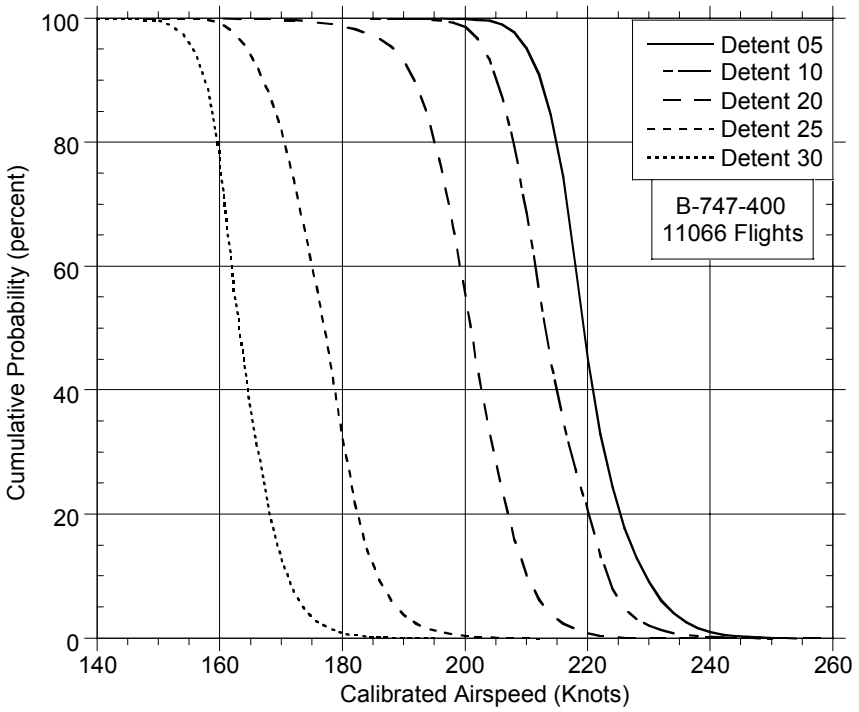

FIGURE A-95. CUMULATIVE PROBABILITY OF MAXIMUM AIRSPEED IN FLAP DETENT DURING APPROACH

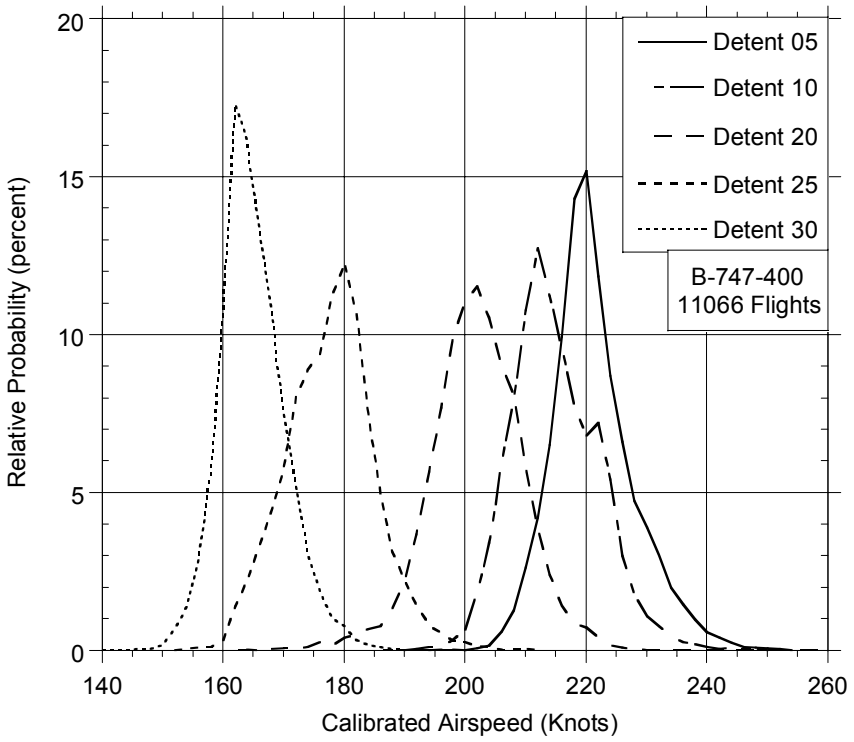

FIGURE A-96. RELATIVE PROBABILITY OF MAXIMUM AIRSPEED IN FLAP DETENT DURING APPROACH

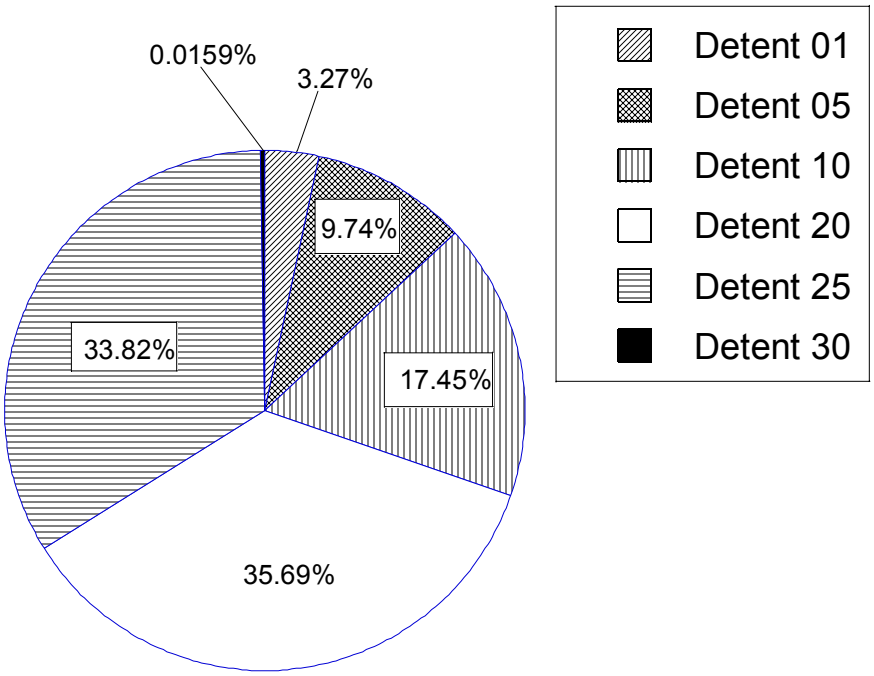

FIGURE A-97. PERCENT OF TIME IN FLAP DETENT DURING DEPARTURE

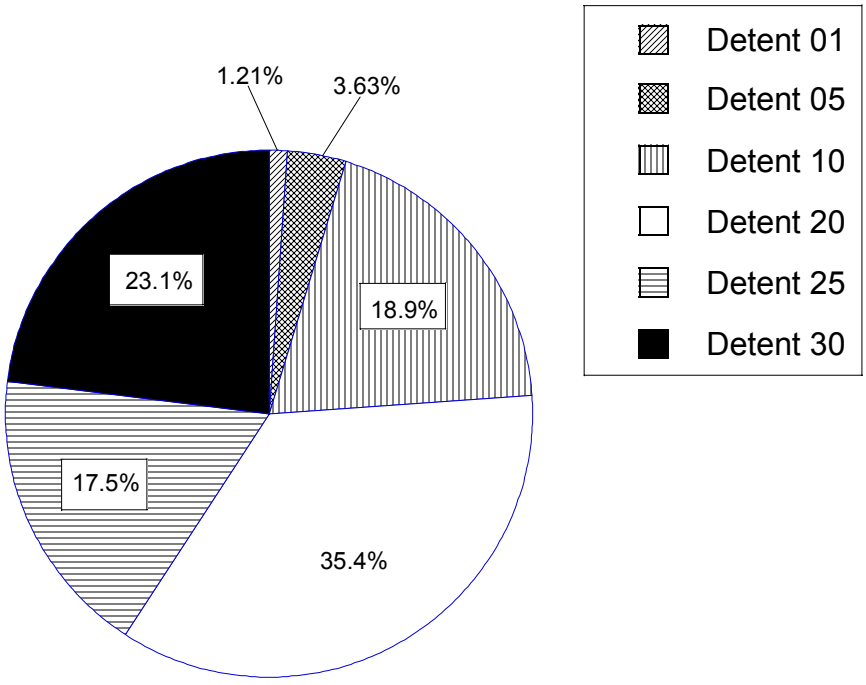

FIGURE A-98. PERCENT OF TIME IN FLAP DETENT DURING APPROACH

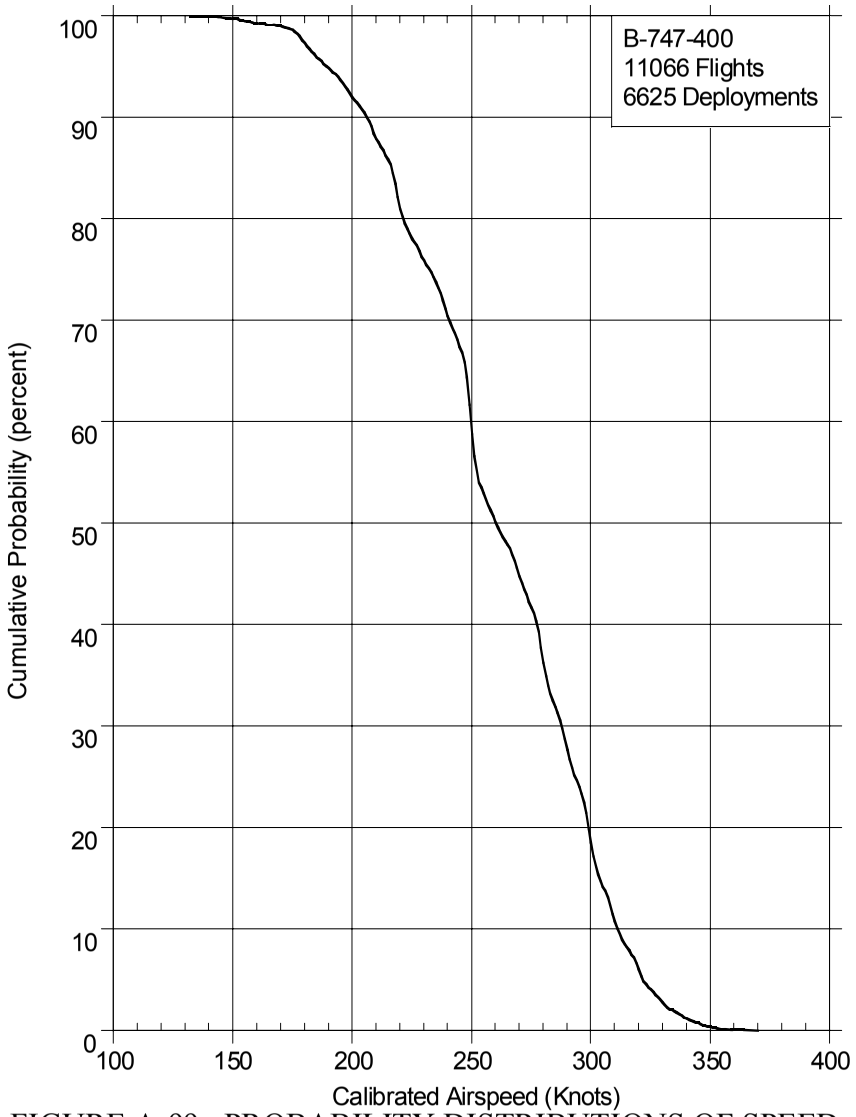

FIGURE A-99. PROBABILITY DISTRIBUTIONS OF SPEED AT SPEED BRAKE DEPLOYMENT

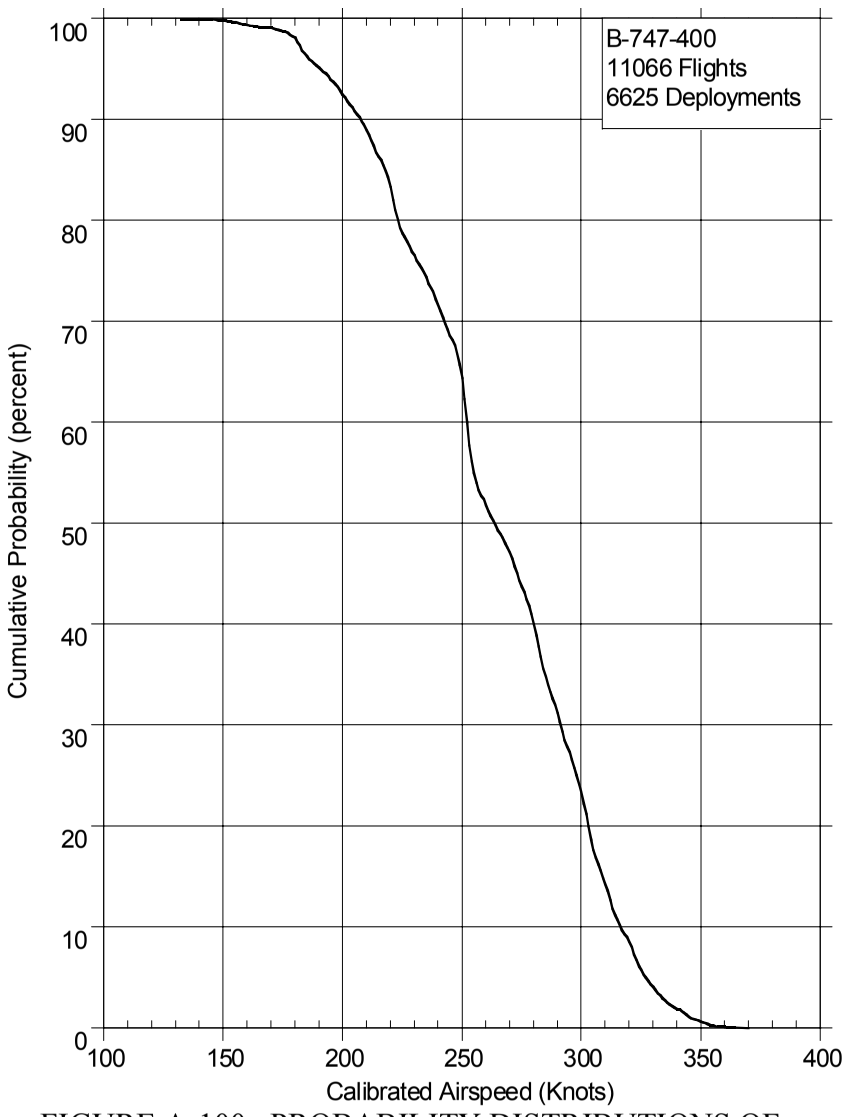

FIGURE A-100. PROBABILITY DISTRIBUTIONS OF MAXIMUM SPEED DURING SPEED BRAKE DEPLOYMENT

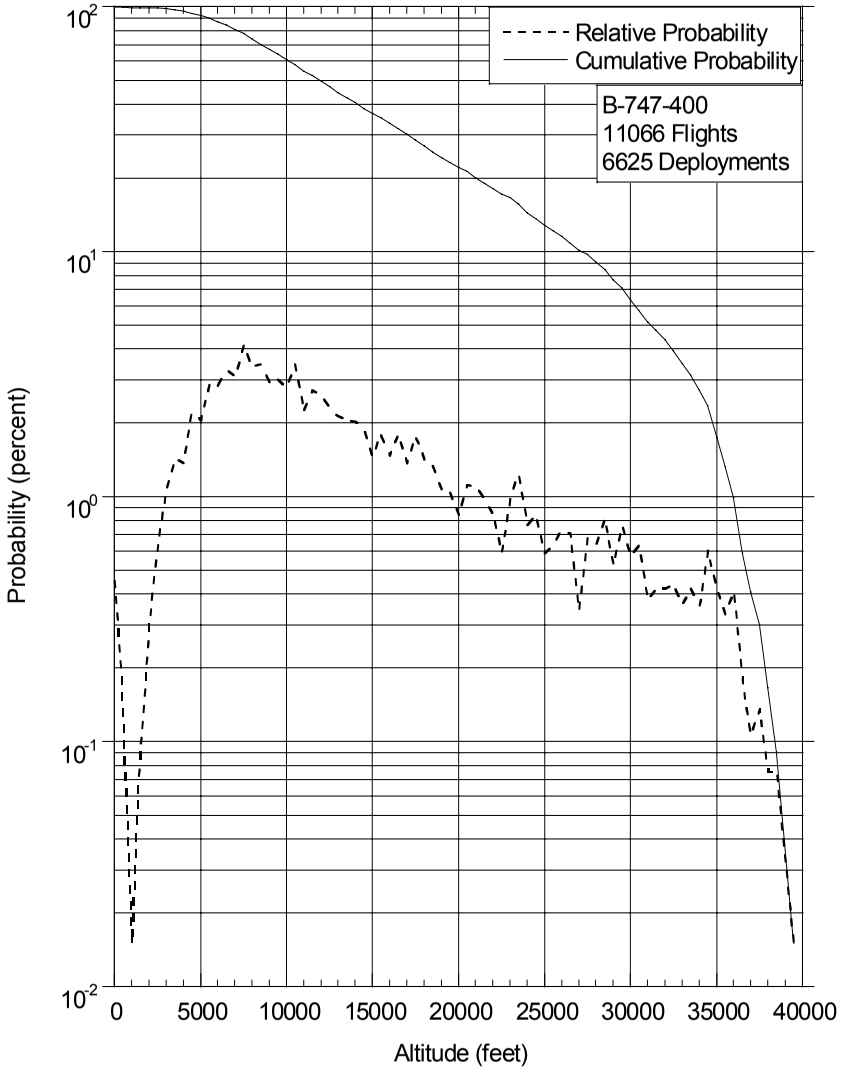

FIGURE A-101. PROBABILITY DISTRIBUTIONS OF ALTITUDE AT SPEED BRAKE DEPLOYMENT

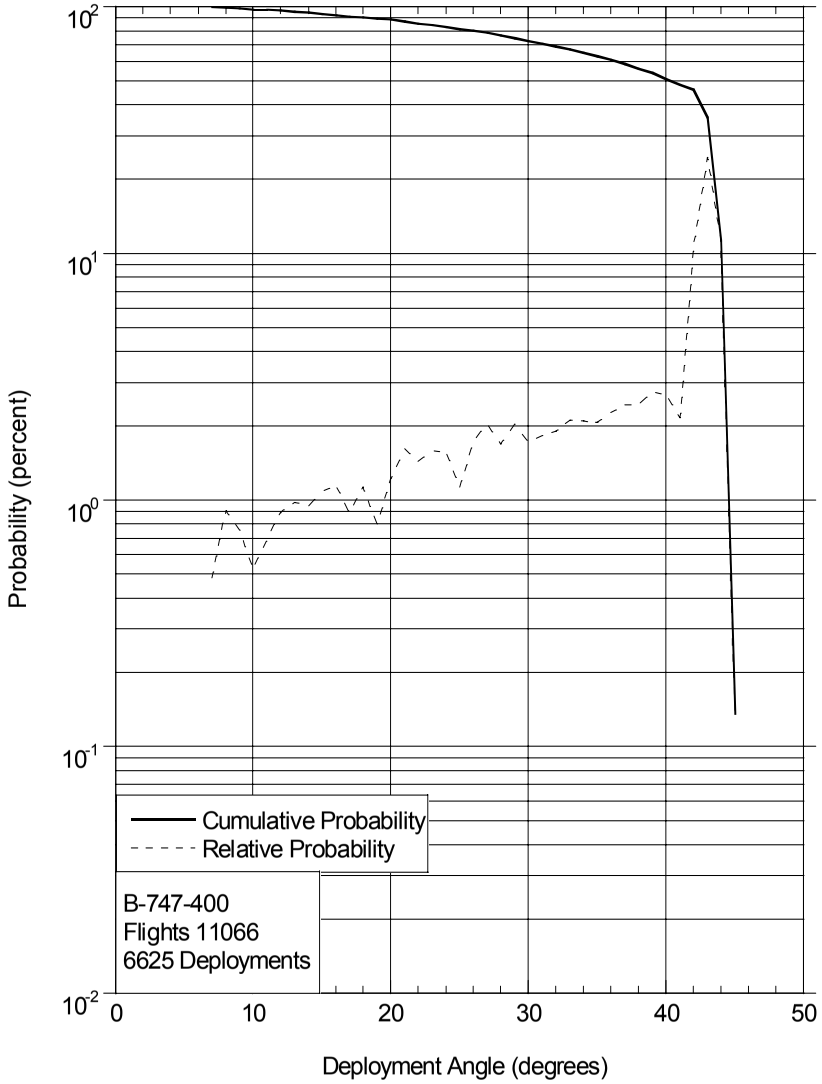

FIGURE A-102. PROBABILITY DISTRIBUTIONS OF MAXIMUM DEPLOYMENT ANGLE DURING SPEED BRAKE DEPLOYMENT

Flap Detent

Speed Brake Deflection (degrees)

11066 Flights	Detent 0	Detent 5	Detent 10	Detent 20	Detent 25	Detent 30
0	14601.0	31.6	60.5	17.8	10.9	1.1
0-1	78840.0	375.5	576.3	363.0	424.6	38.6
1-2	164.9	4.3	9.6	6.3	11.5	1.0
2-3	8.8	1.1	3.1	2.7	5.1	0.4
3-4	3.7	0.7	1.5	1.5	3.2	0.2
4-5	3.2	0.6	1.2	1.2	2.1	0.1
5-10	13.9	1.3	1.7	1.2	2.1	0.2
10-15	18.8	1.3	0.9	0.2	0.3	0.0
15-20	22.7	1.3	1.0	0.1	0.1	0.0
20-25	23.0	1.6	0.9	0.1	0.0	0.0
25-30	24.0	2.2	1.3	0.1	0.0	0.0
30-35	26.2	2.1	1.6	0.2	0.0	
35-40	26.3	2.4	1.6	0.1	0.0	0.0
40-45	61.9	15.4	9.0	0.9	0.0	0.0
45-50	0.0	0.0	0.0	0.0		

FIGURE A-103. TOTAL HOURS OF COINCIDENT SPEED BRAKE DEFLECTION AND FLAP DETENT

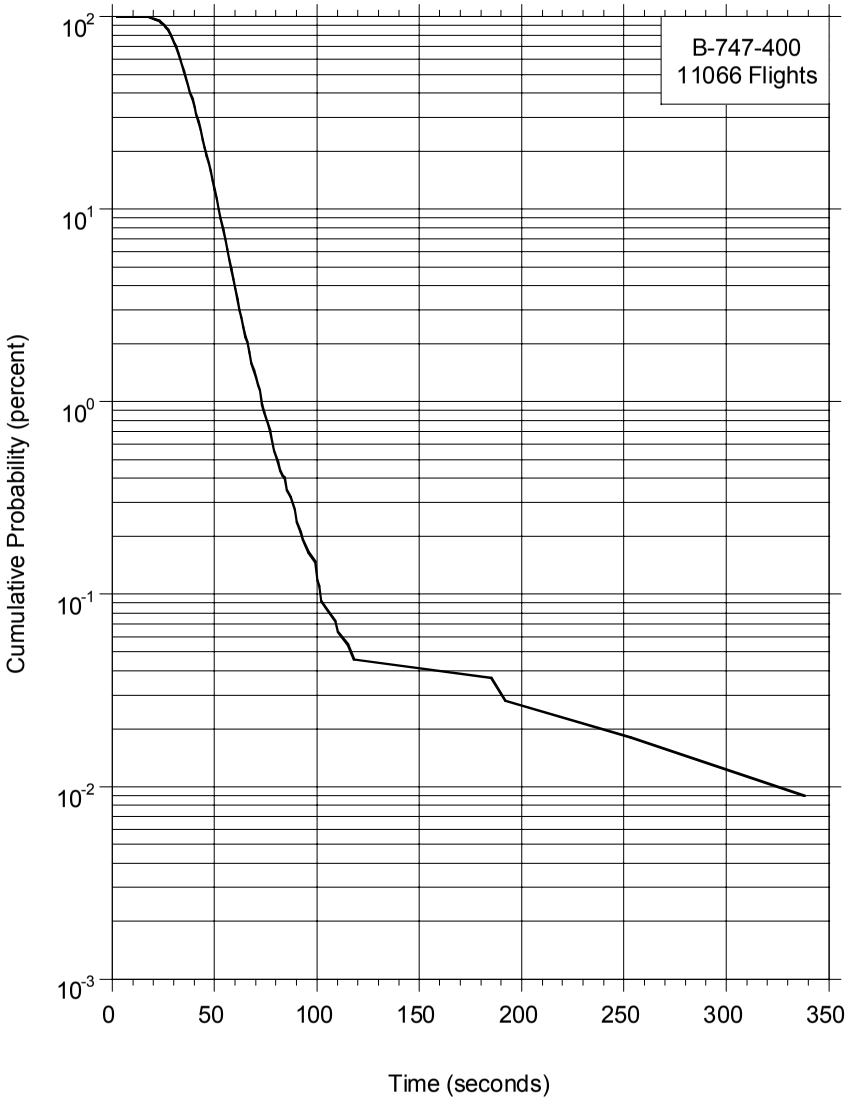

FIGURE A-104. CUMULATIVE PROBABILITY OF TIME WITH THRUST REVERSERS DEPLOYED

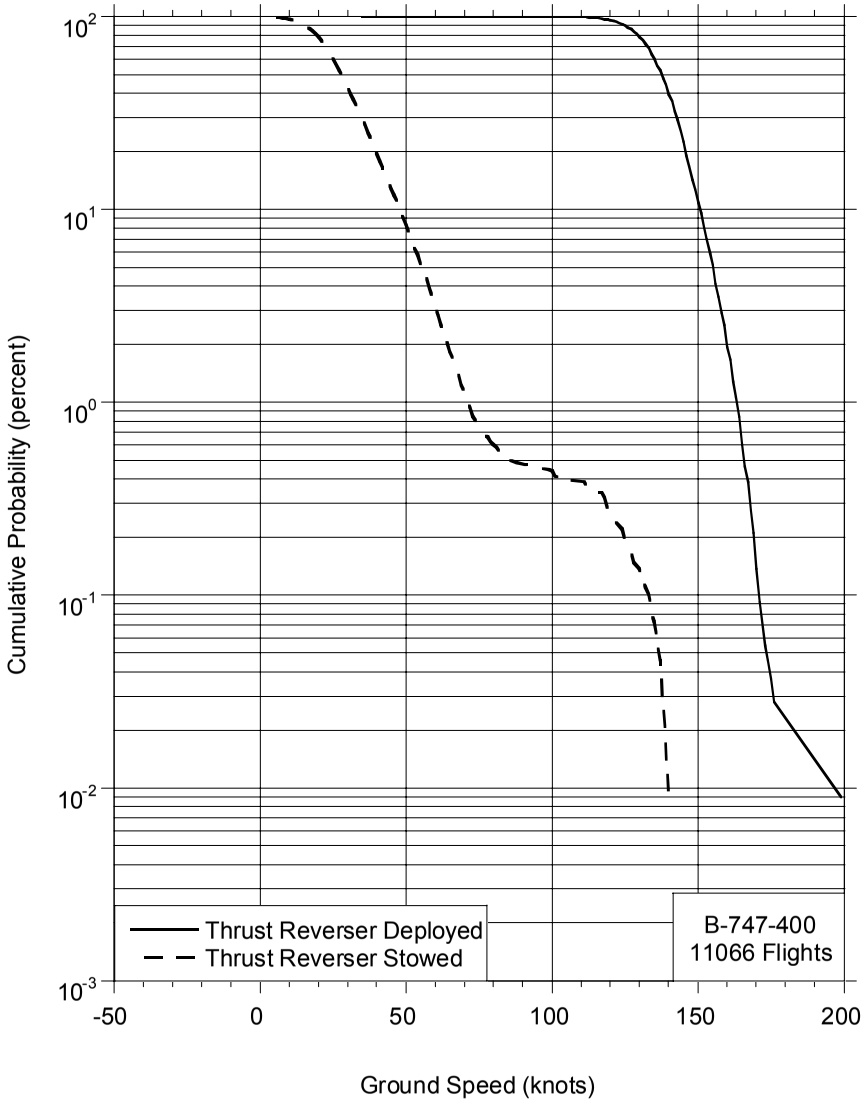

FIGURE A-105. CUMULATIVE PROBABILITY OF SPEED AT THRUST REVERSER DEPLOYMENT AND STOWAGE

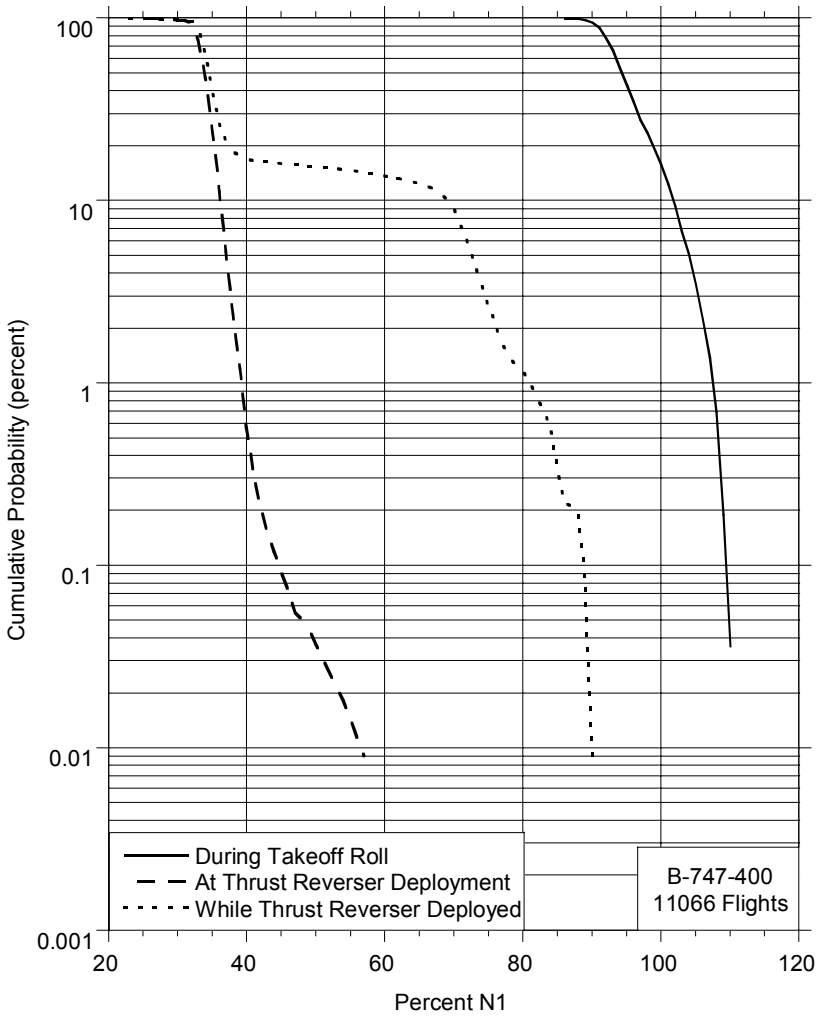

FIGURE A-106. CUMULATIVE PROBABILITY OF PERCENT N_1 DURING TAKEOFF, AT THRUST REVERSER DEPLOYMENT, AND DURING THRUST REVERSER DEPLOYMENT

APPENDIX B—GREAT CIRCLE DISTANCE CALCULATION

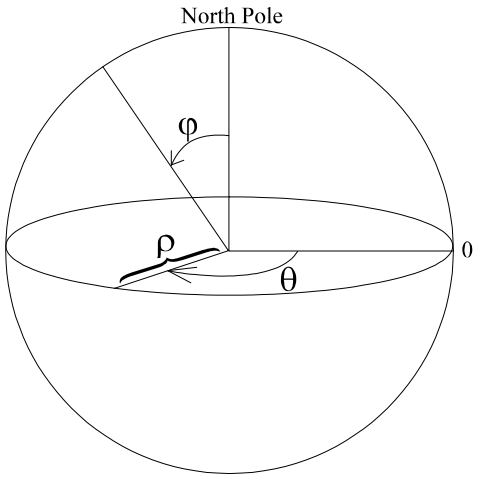

Given:

Latitude and Longitude of Departure and Destination Airports	ρ = distance from center φ = angle from North Pole θ = angle E/W of prime meridian

Procedure: (see sketch)

The standard mathematical system for spherical coordinates is shown, where three variables specify location: ρ, φ, and θ.

Let a = Great Circle Distance in angular measure.

Latitude is measured away from the Equator (0°) to the North Pole (+90°) and the South Pole (-90°); whereas in the standard spherical coordinate system, the North Pole, Equator, and South Pole lie at 0°, 90°, and 180°, respectively. Therefore,

$$\varphi = 90° - \text{latitude}$$

transforms latitude readings into equivalent angles (φ) in the standard spherical coordinate system.

Then

$$b = 90° - Latitude_{Dep}$$
$$c = 90° - Latitude_{Des}$$

where b and c are values of φ for the departure and destination locations, respectively.

Longitude is measured away from the prime meridian (0°). Longitudes to the east are positive and to the west negative. However, the standard spherical coordinate system measures its angles in the opposite direction. Therefore,

$$\theta = - \ longitude$$

transforms longitude readings into equivalent angles (θ) in the standard spherical coordinate system.

Then

$$\begin{aligned} A = & \quad (- Longitude_{Des}) - (- Longitude_{Dep}) \\ = & \quad Longitude_{Dep} - Longitude_{Des} \end{aligned}$$

where A is the value of θ between the departure and destination locations.

The following equation, based on the spherical coordinate system, allows the computation of the Great Circle Distance, a. (Law of cosines for oblique spherical triangles)

$$\cos a = \cos b \cos c + \sin b \sin c \cos A$$

Substituting for b, c, and A from the above equalities

$$\begin{aligned} \cos a = & \cos (90° - Lat_{Dep}) \cos (90° - Lat_{Des}) \\ & + \sin (90° - Lat_{Dep}) \sin (90° - Lat_{Des}) \cos (Lon_{Dep} - Lon_{Des}) \end{aligned}$$

Since

$$\begin{aligned} &\cos (90° - Lat_{Dep}) = \sin Lat_{Dep} \\ &\cos (90° - Lat_{Des}) = \sin Lat_{Des} \\ &\sin (90° - Lat_{Dep}) = \cos Lat_{Dep} \\ &\sin (90° - Lat_{Des}) = \cos Lat_{Des} \end{aligned}$$

by replacement one obtains

$$\cos a = \sin (Lat_{Dep}) \sin (Lat_{Des}) + \cos (Lat_{Dep}) \cos (Lat_{Des}) \cos (Lon_{Des} - Lon_{Dep})$$

Thus a, the angular measure of the great circle arc connecting the departure and destination locations, is obtained as

$$a = \cos^{-1} [\sin (Lat_{Dep}) \sin (Lat_{Des}) + \cos (Lat_{Dep}) \cos (Lat_{Des}) \cos (Lon_{Des} - Lon_{Dep})]$$

So, for a expressed in radians

$$GCD = a \ radians \left(\frac{180 deg.}{\pi \ radians} \right) \left(\frac{60 \ min.}{1 \ deg.} \right) \left(\frac{1 nm}{1 \ min.} \right) = \left(\frac{10800 a}{\pi} \right) nm$$

and for a expressed in degrees,

$$GCD = a \ degrees \left(\frac{60 \ min.}{1 \ deg.} \right) \left(\frac{1 \ nm}{1 \ min.} \right) = 60 a \ nm$$

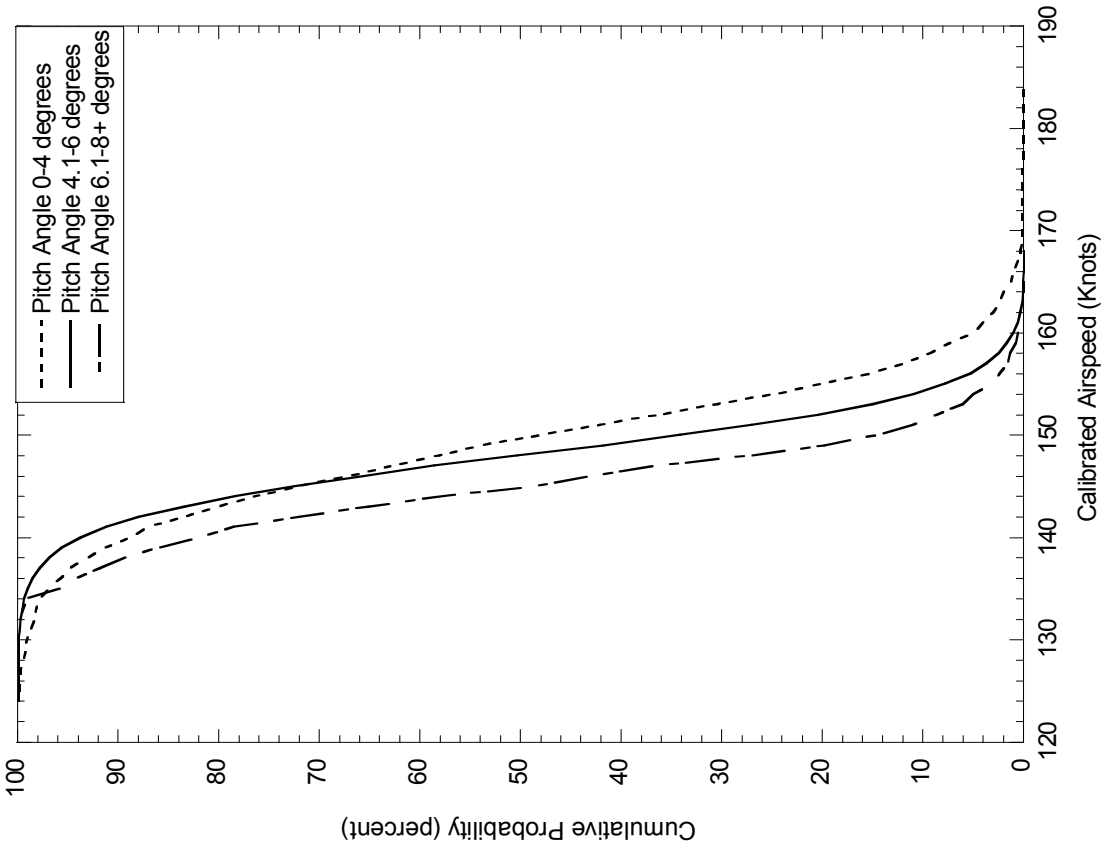

FIGURE C-1. CUMULATIVE PROBABILITY OF AIRSPEED AT TOUCHDOWN BY PITCH ANGLE

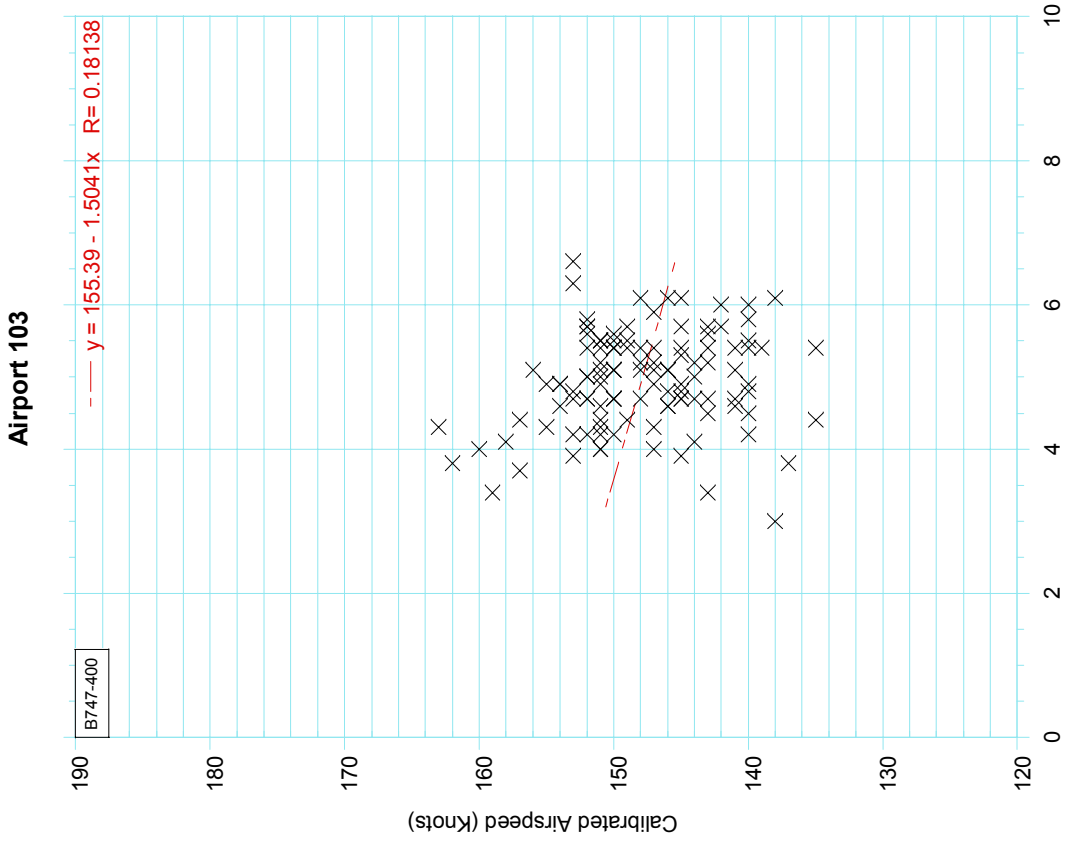

FIGURE C-2. CALIBRATED AIRSPEED VS PITCH ANGLE AT TOUCHDOWN AIRPORT 103 ELEVATION < 500 FEET

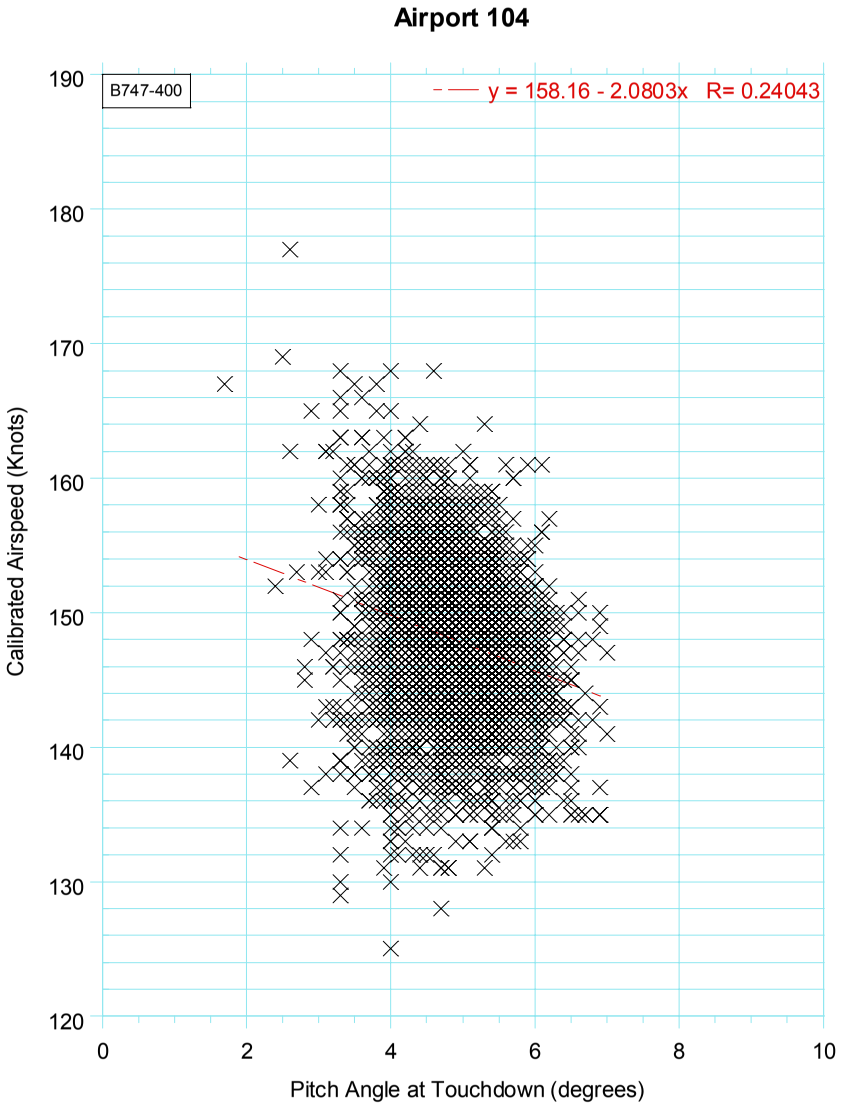

FIGURE C-3. CALIBRATED AIRSPEED VS PITCH ANGLE AT TOUCHDOWN, AIRPORT 104 ELEVATION < 500 FEET

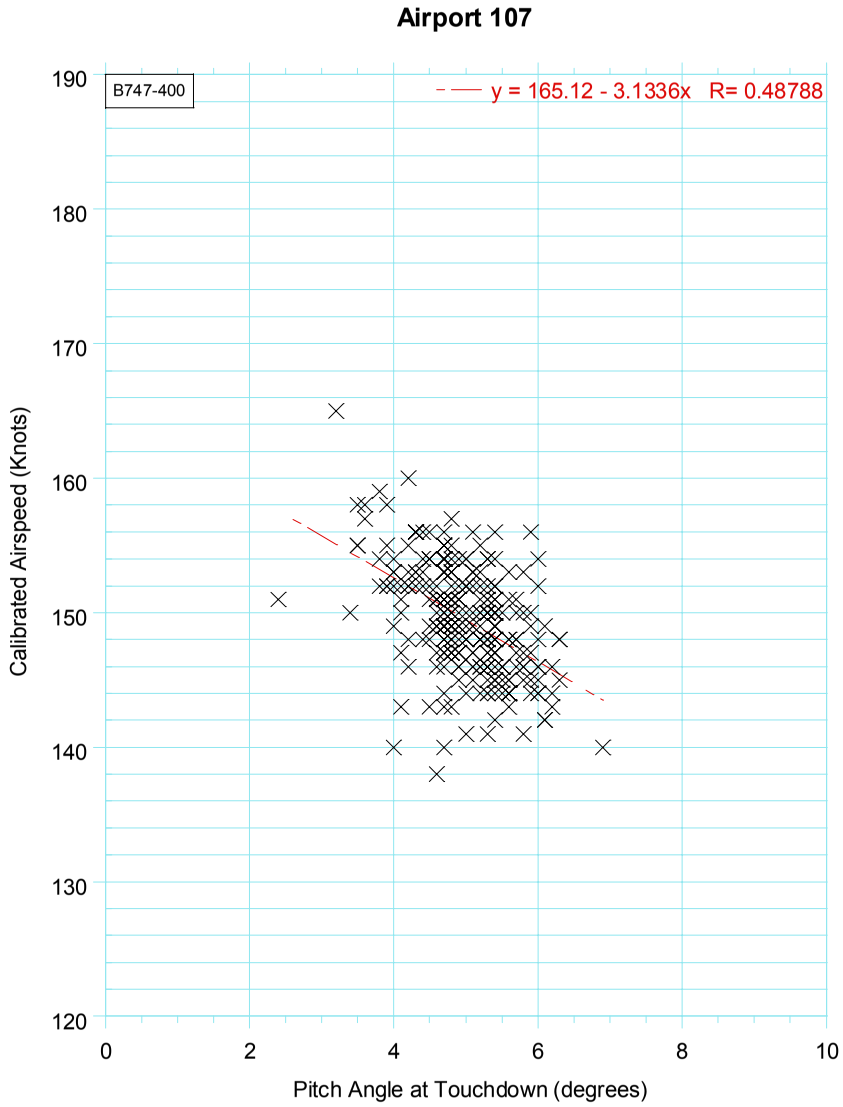

FIGURE C-4. CALIBRATED AIRSPEED VS PITCH ANGLE AT TOUCHDOWN, AIRPORT 107 ELEVATION < 500 FEET

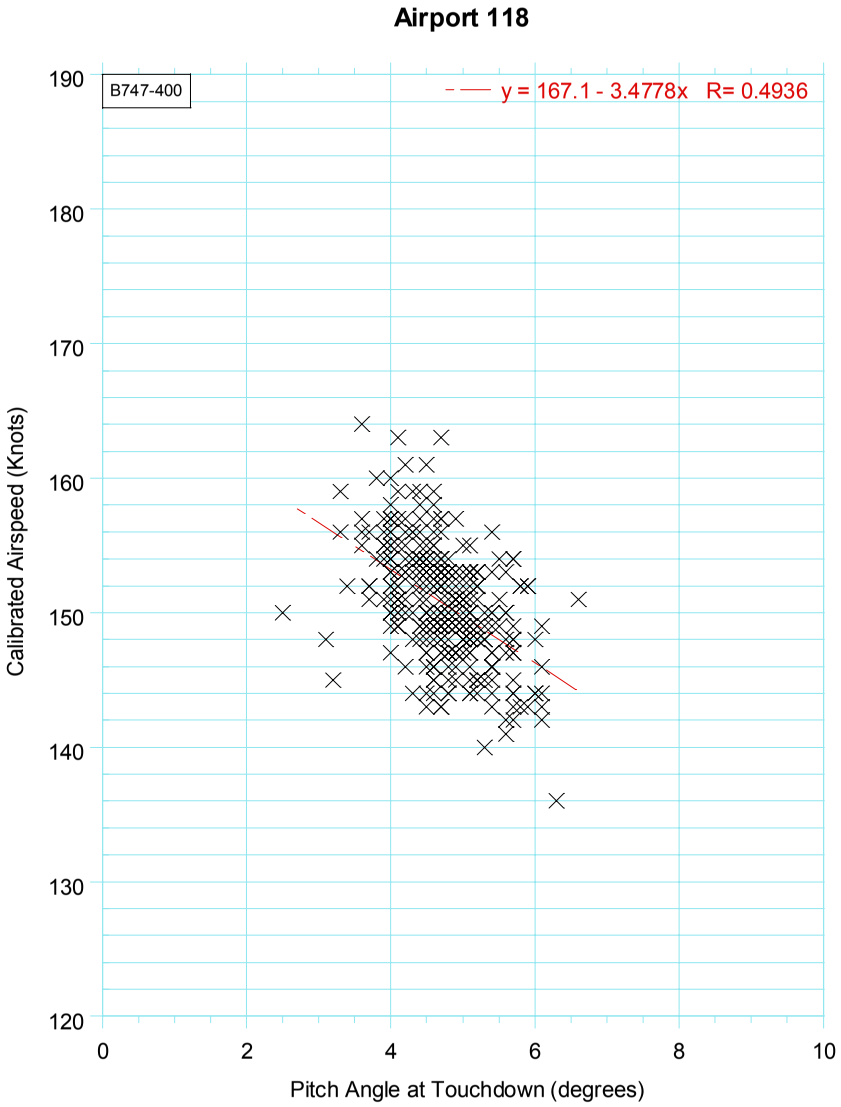

FIGURE C-5. CALIBRATED AIRSPEED VS PITCH ANGLE AT TOUCHDOWN, AIRPORT 118 ELEVATION < 500 FEET

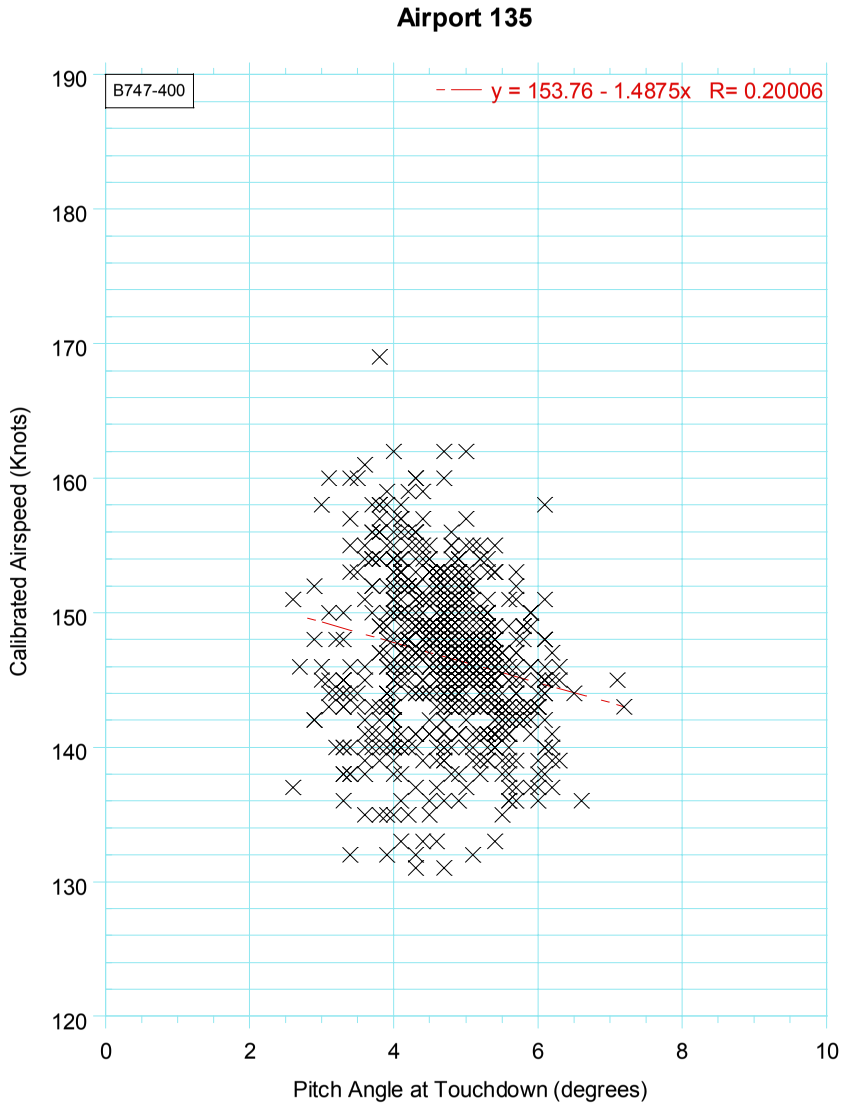

FIGURE C-6. CALIBRATED AIRSPEED VS PITCH ANGLE AT TOUCHDOWN, AIRPORT 135 ELEVATION < 500 FEET

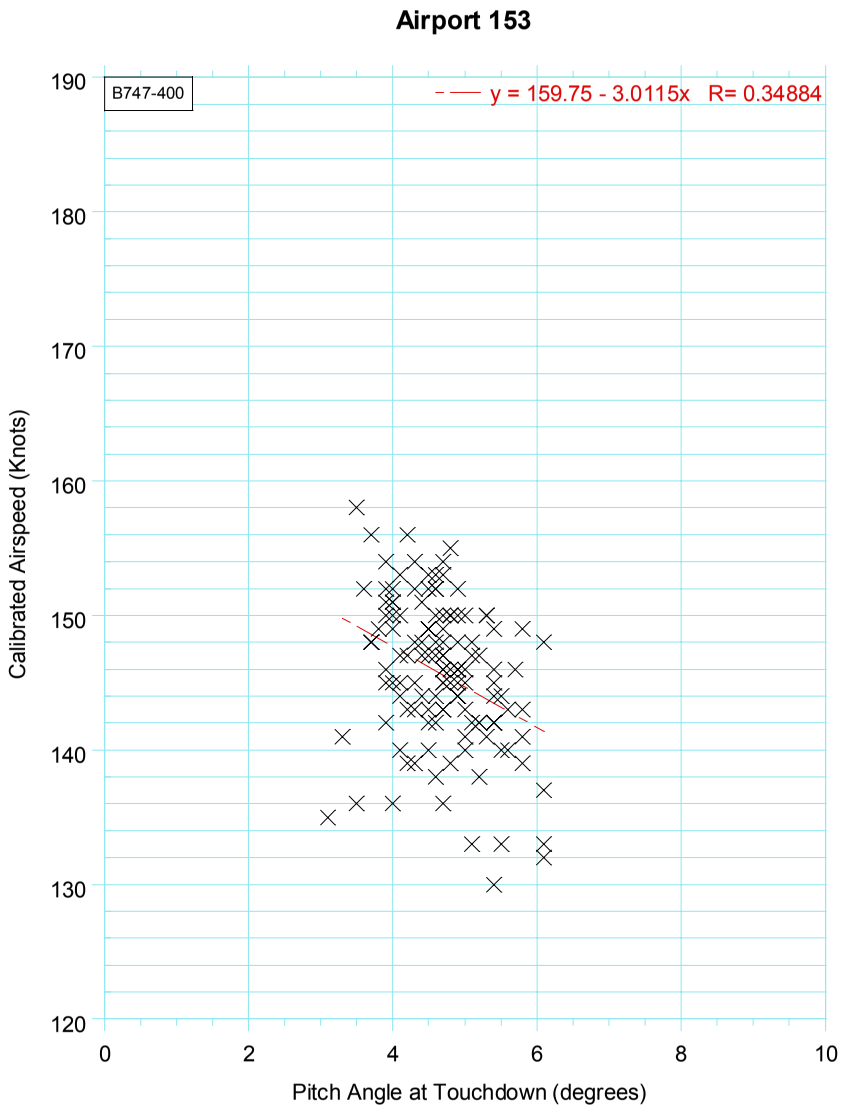

FIGURE C-7. CALIBRATED AIRSPEED VS PITCH ANGLE AT TOUCHDOWN, AIRPORT 153 ELEVATION < 500 FEET

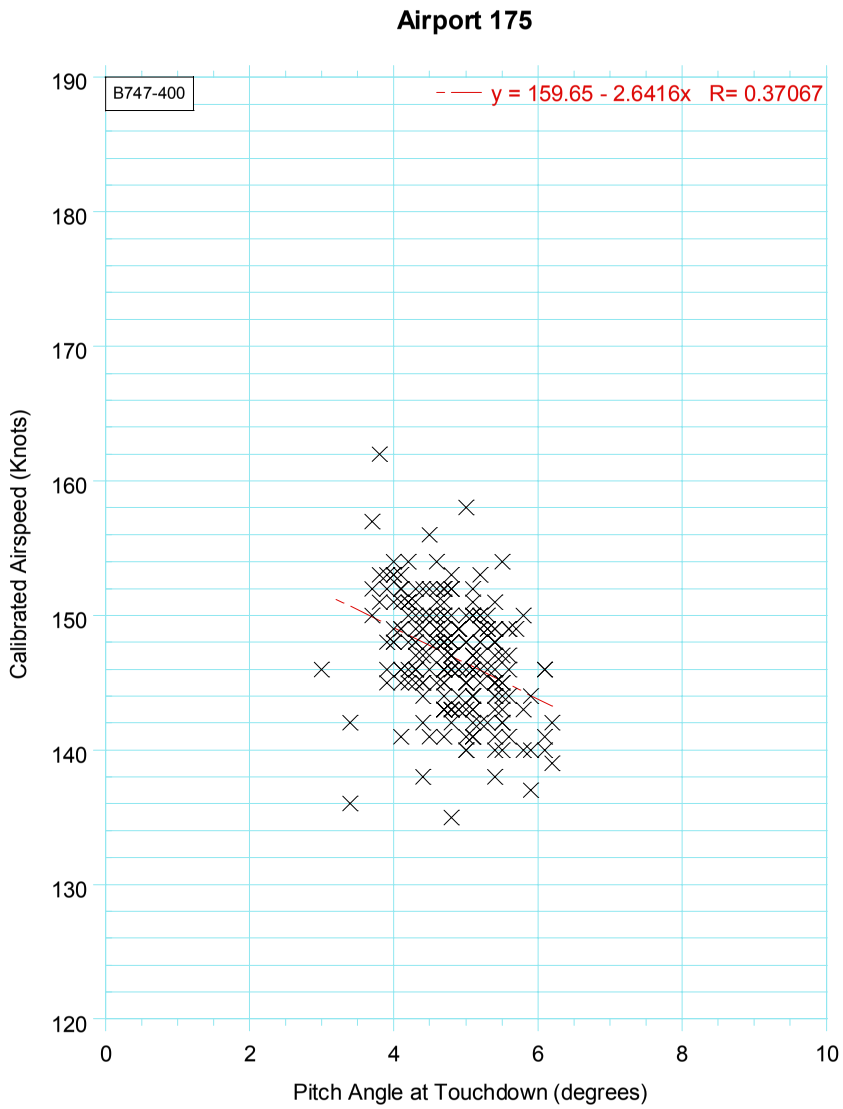

FIGURE C-8. CALIBRATED AIRSPEED VS PITCH ANGLE AT TOUCHDOWN, AIRPORT 175 ELEVATION < 500 FEET

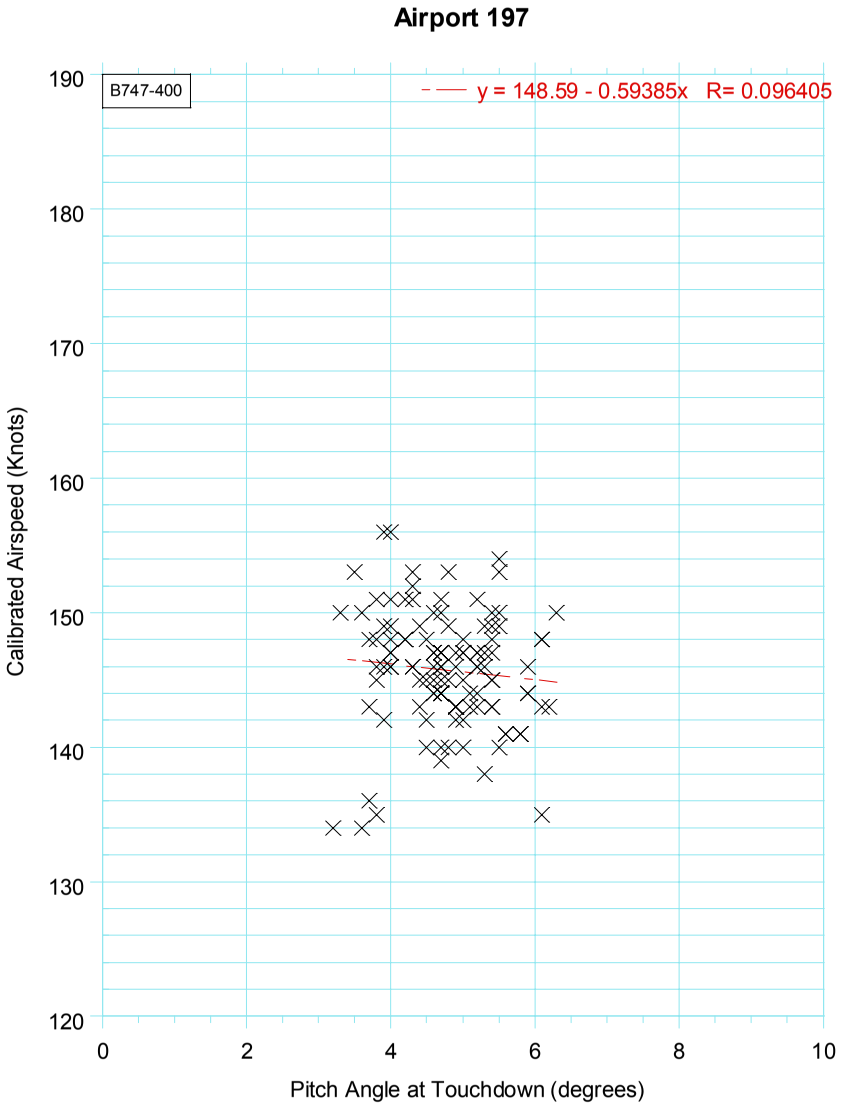

FIGURE C-9. CALIBRATED AIRSPEED VS PITCH ANGLE AT TOUCHDOWN, AIRPORT 197 ELEVATION < 500 FEET

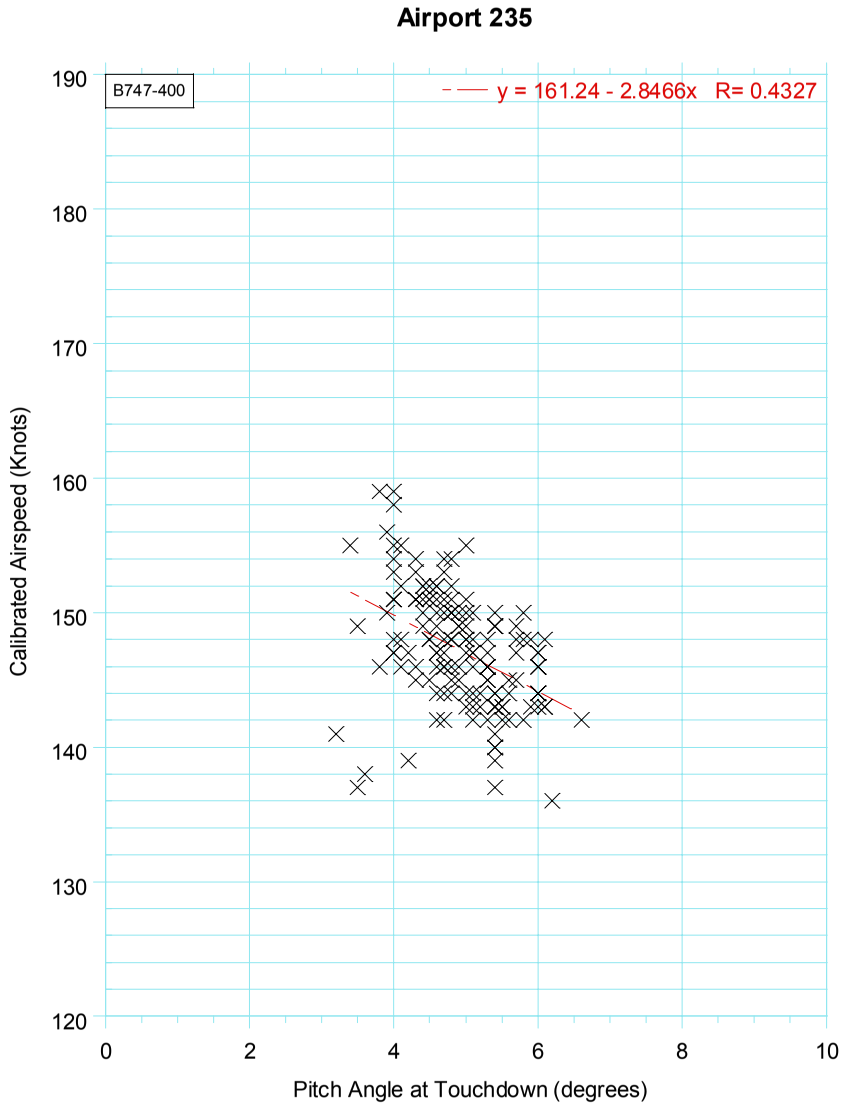

FIGURE C-10. CALIBRATED AIRSPEED VS PITCH ANGLE AT TOUCHDOWN, AIRPORT 235 ELEVATION < 500 FEET

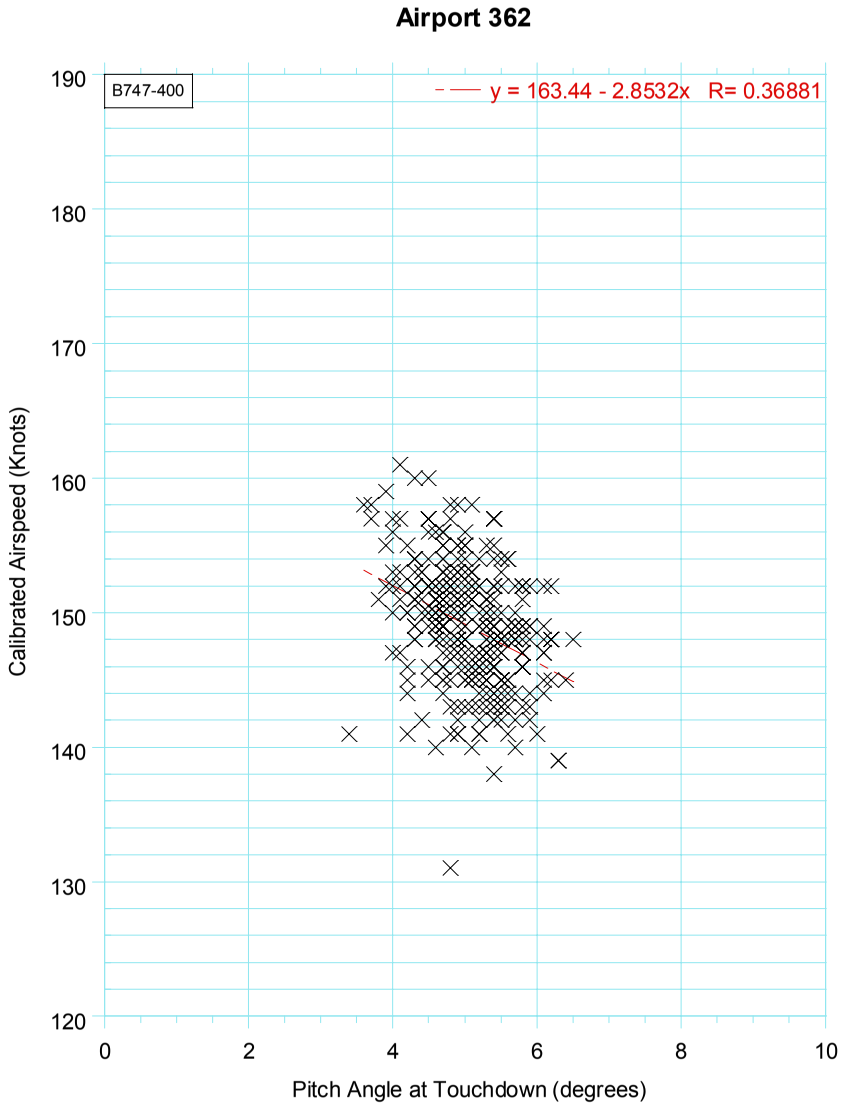

FIGURE C-11. CALIBRATED AIRSPEED VS PITCH ANGLE AT TOUCHDOWN, AIRPORT 362 ELEVATION < 500 FEET

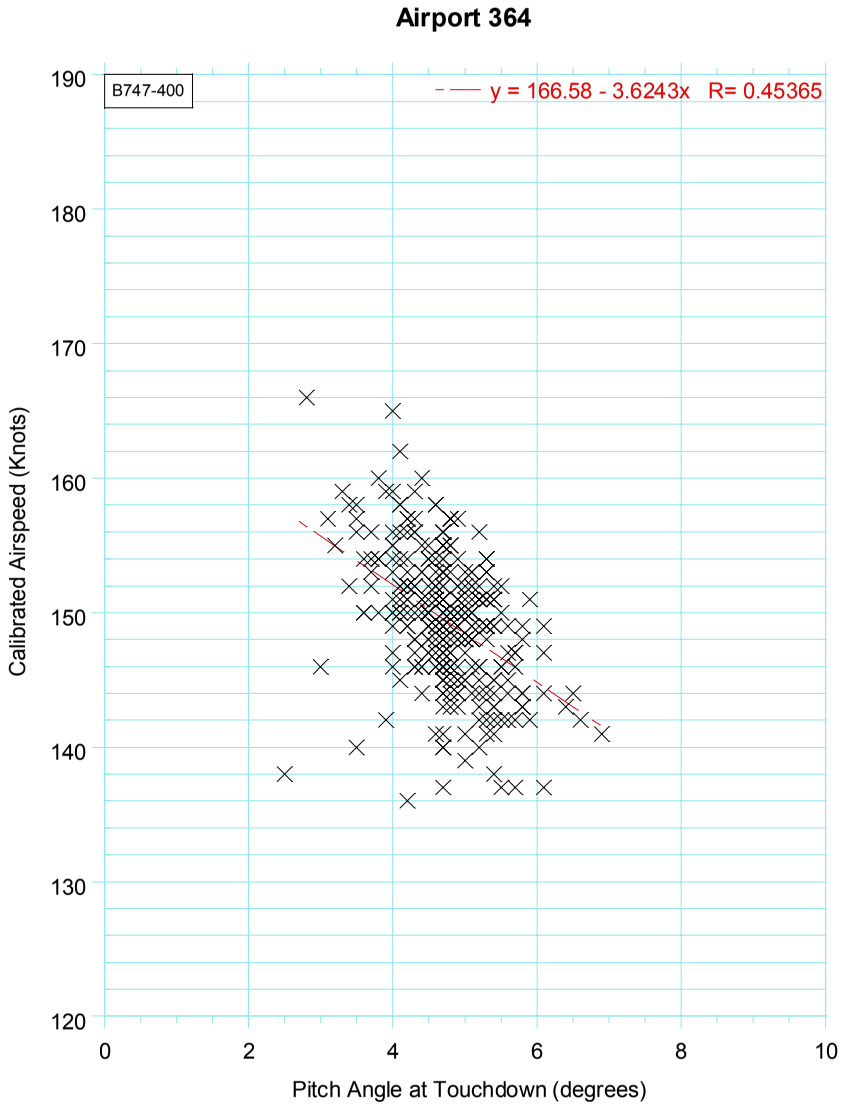

FIGURE C-12. CALIBRATED AIRSPEED VS PITCH ANGLE AT TOUCHDOWN, AIRPORT 364 ELEVATION < 500 FEET

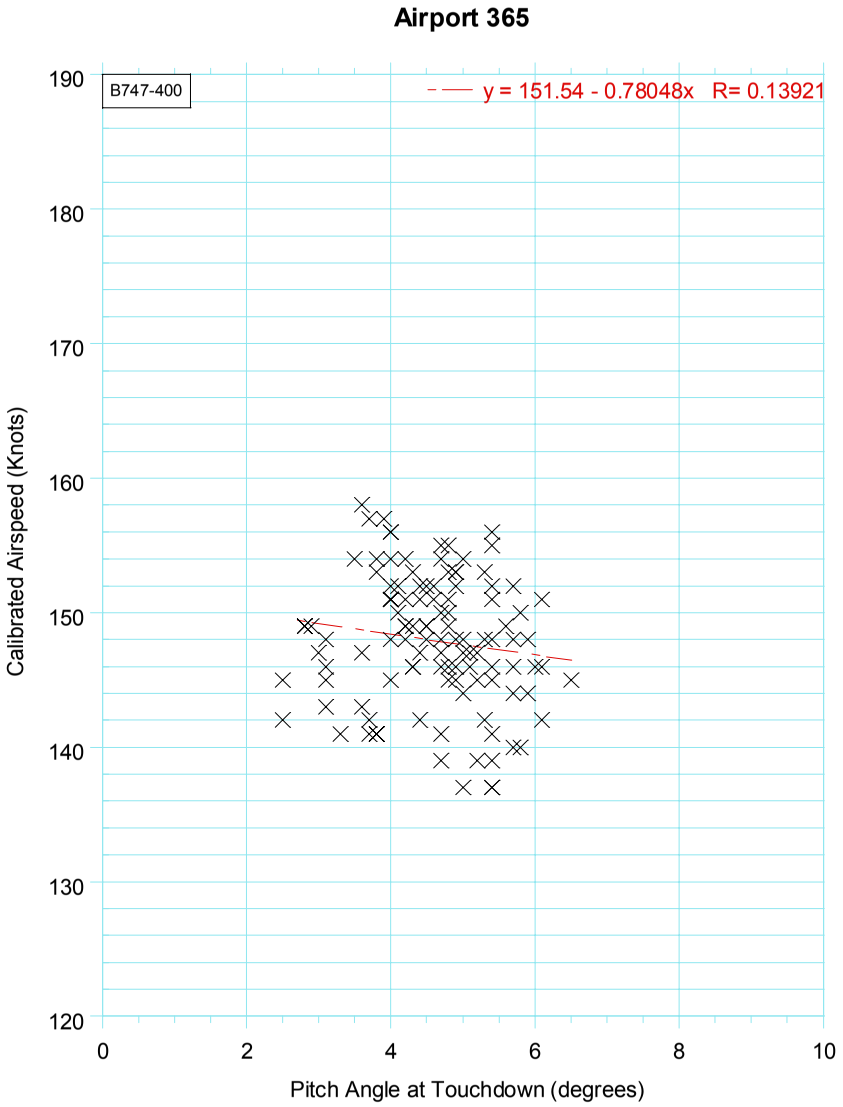

FIGURE C-13. CALIBRATED AIRSPEED VS PITCH ANGLE AT TOUCHDOWN, AIRPORT 365 ELEVATION < 500 FEET

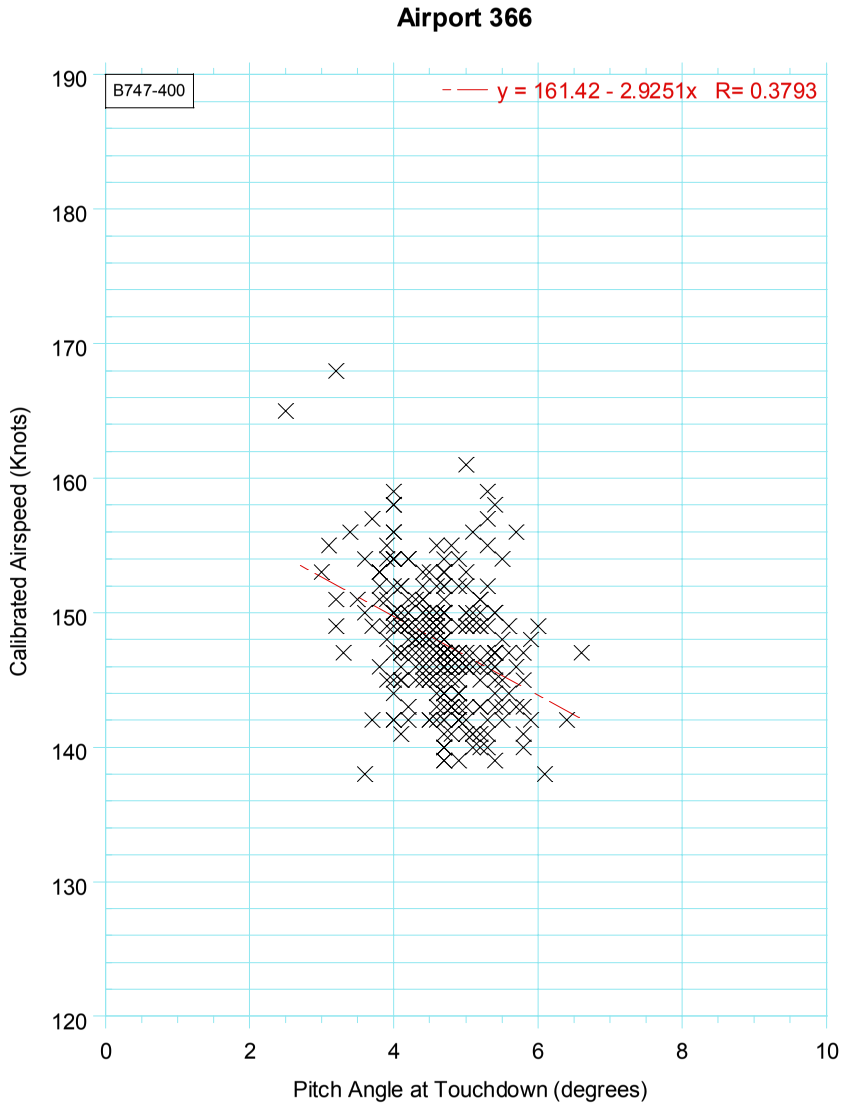

FIGURE C-14. CALIBRATED AIRSPEED VS PITCH ANGLE AT TOUCHDOWN, AIRPORT 366 ELEVATION < 500 FEET

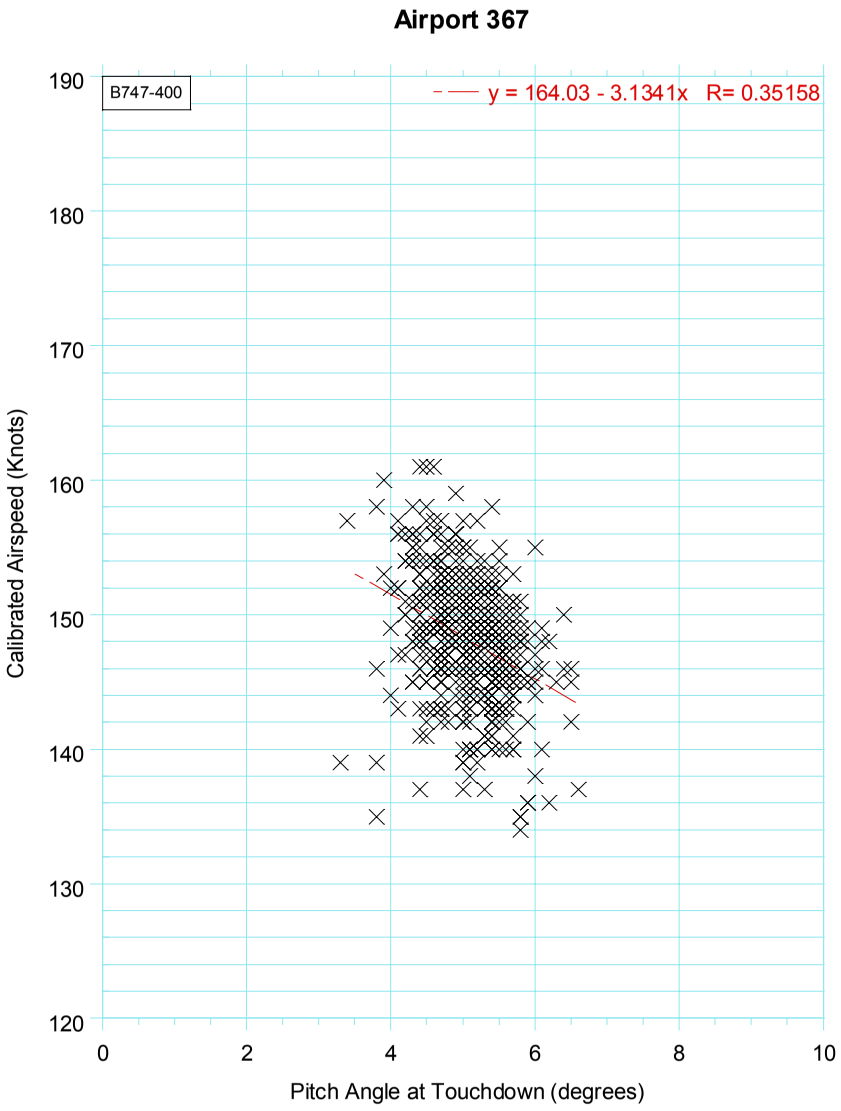

FIGURE C-15. CALIBRATED AIRSPEED VS PITCH ANGLE AT TOUCHDOWN, AIRPORT 367 ELEVATION < 500 FEET

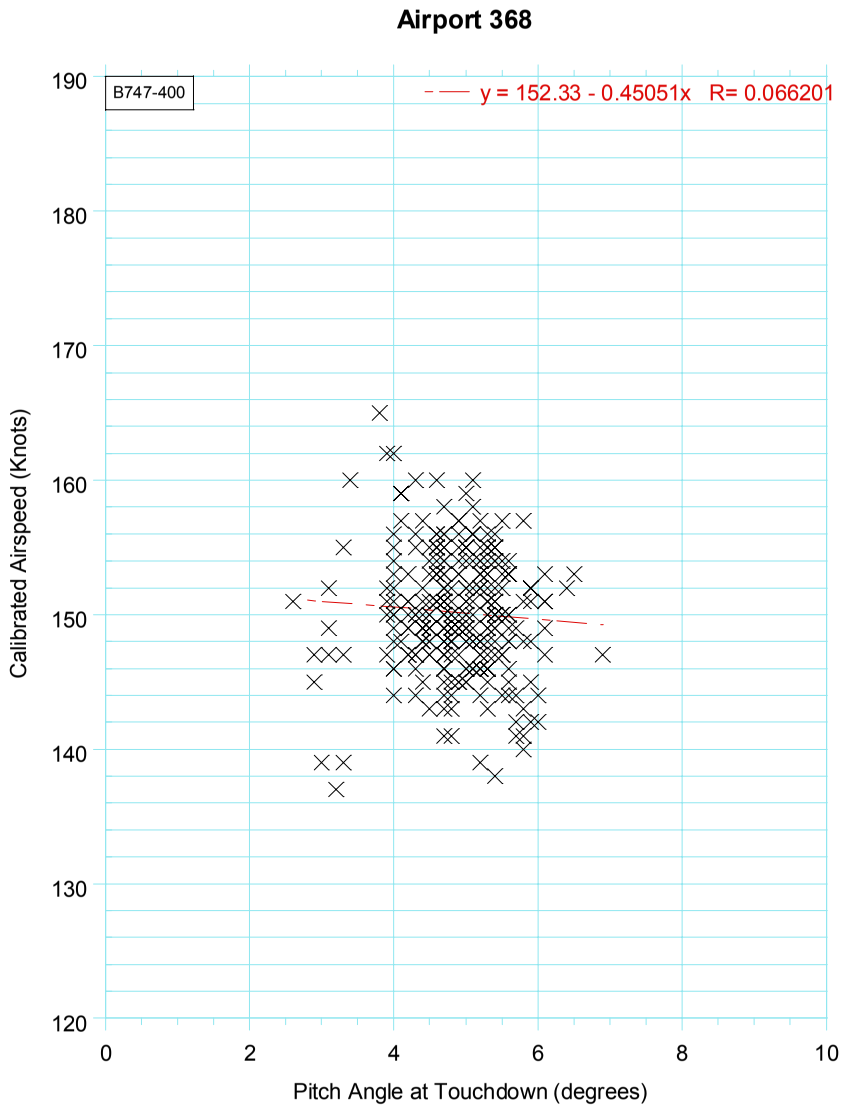

FIGURE C-16. CALIBRATED AIRSPEED VS PITCH ANGLE AT TOUCHDOWN, AIRPORT 368 ELEVATION < 500 FEET

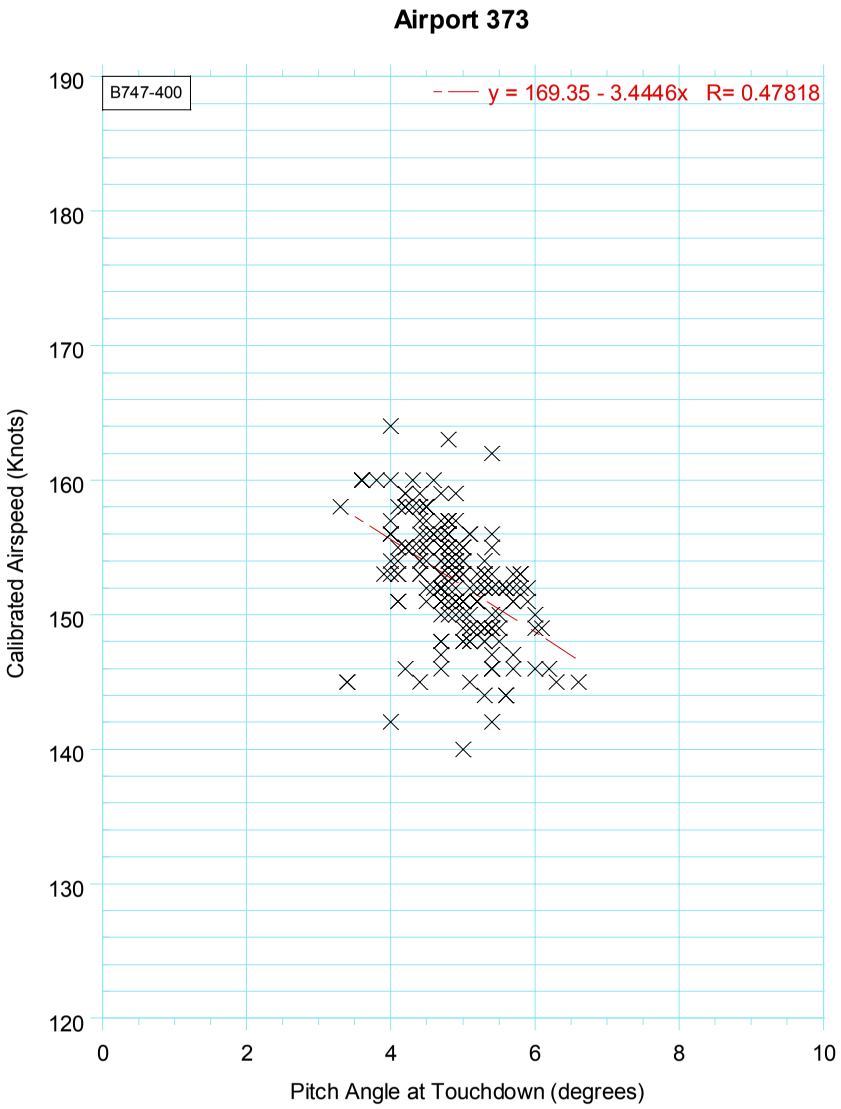

FIGURE C-17. CALIBRATED AIRSPEED VS PITCH ANGLE AT TOUCHDOWN, AIRPORT 373 ELEVATION < 500 FEET

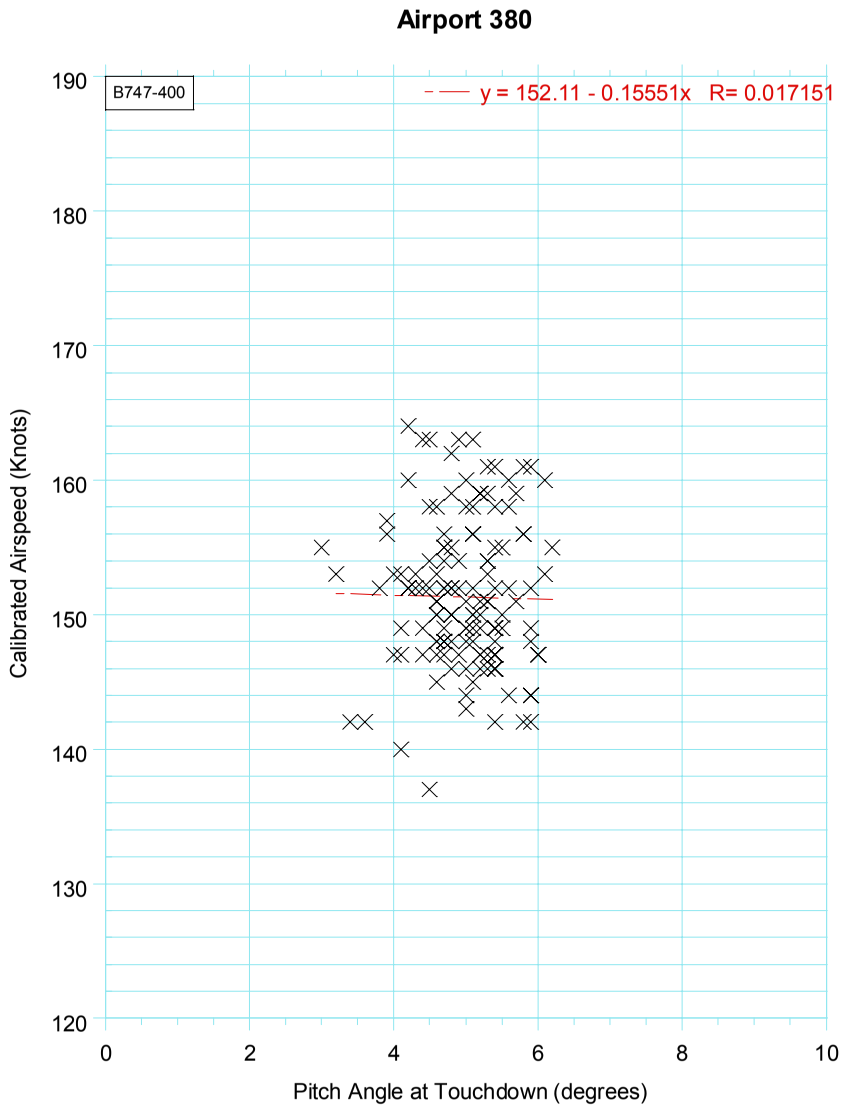

FIGURE C-18. CALIBRATED AIRSPEED VS PITCH ANGLE AT TOUCHDOWN, AIRPORT 380 ELEVATION < 500 FEET

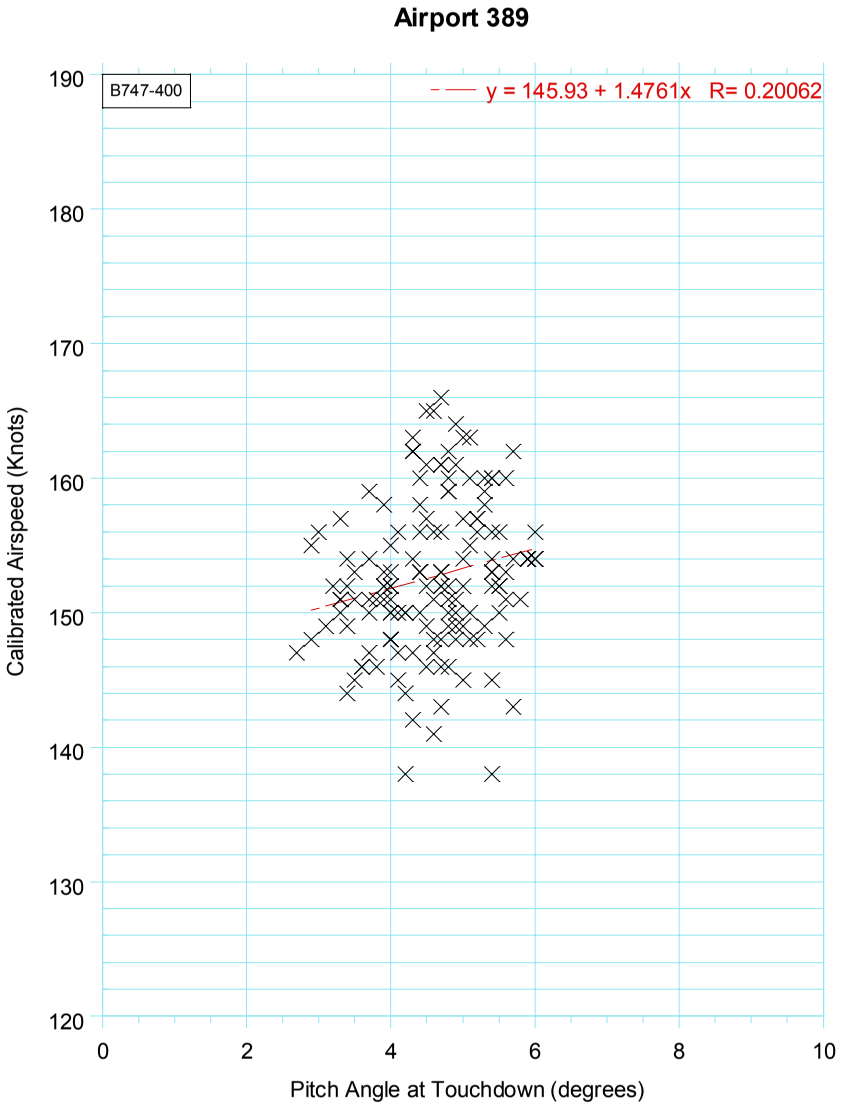

FIGURE C-19. CALIBRATED AIRSPEED VS PITCH ANGLE AT TOUCHDOWN, AIRPORT 389 ELEVATION < 500 FEET

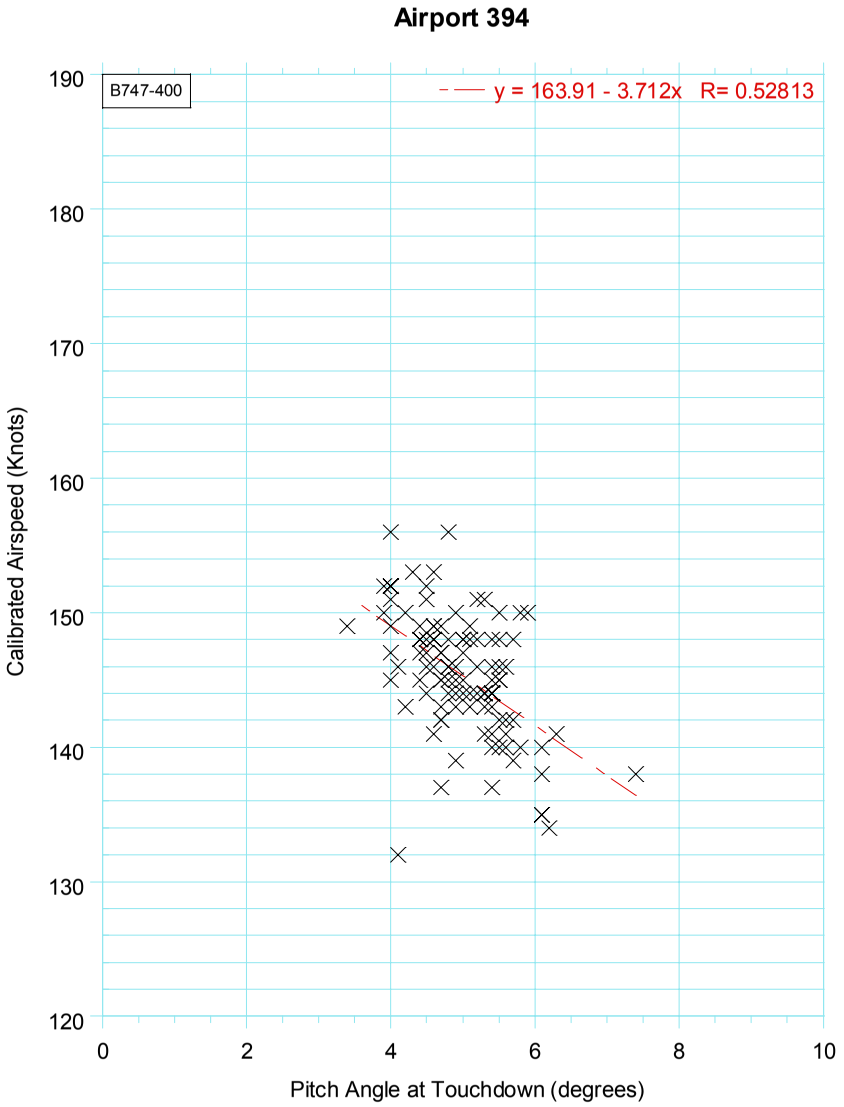

FIGURE C-20. CALIBRATED AIRSPEED VS PITCH ANGLE AT TOUCHDOWN, AIRPORT 394 ELEVATION < 500 FEET

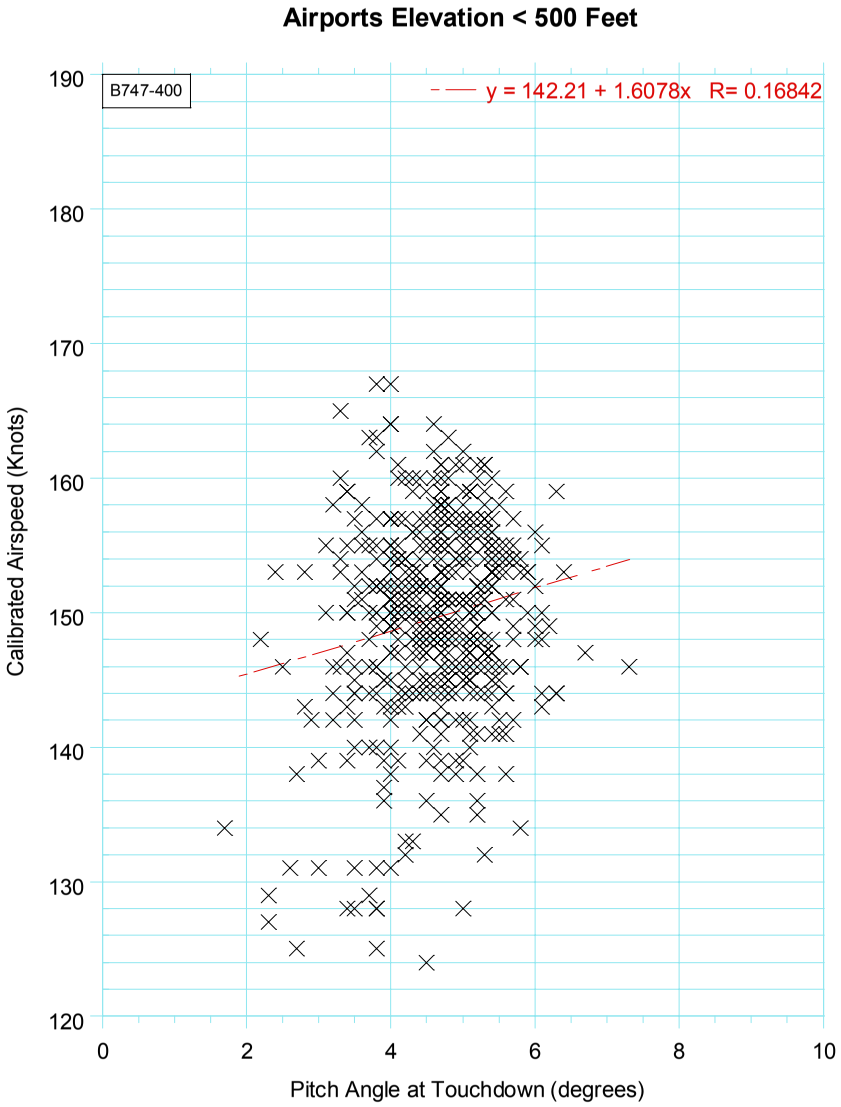

FIGURE C-21. CALIBRATED AIRSPEED VS PITCH ANGLE AT TOUCHDOWN, AIRPORTS ELEVATION < 500 FEET

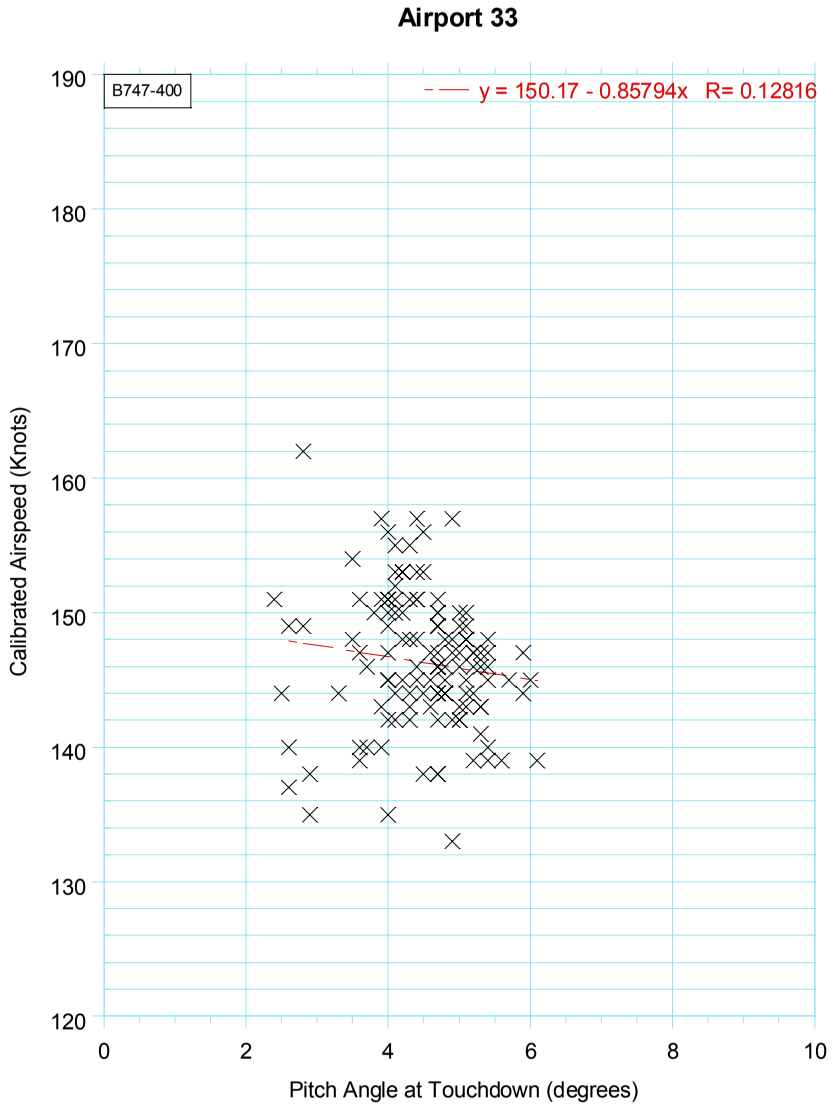

FIGURE C-22. CALIBRATED AIRSPEED VS PITCH ANGLE AT TOUCHDOWN, AIRPORT 33 ELEVATION 500-1000 FEET

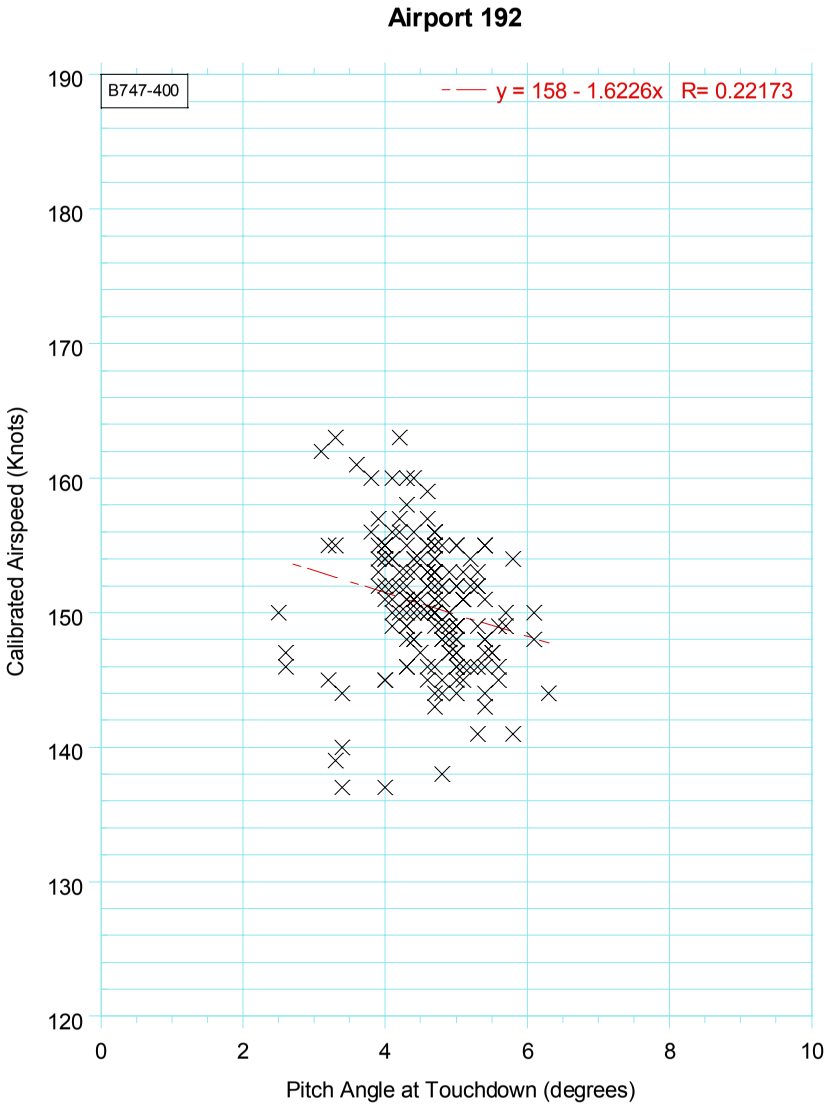

FIGURE C-23. CALIBRATED AIRSPEED VS PITCH ANGLE AT TOUCHDOWN, AIRPORT 192 ELEVATION 500-1000 FEET

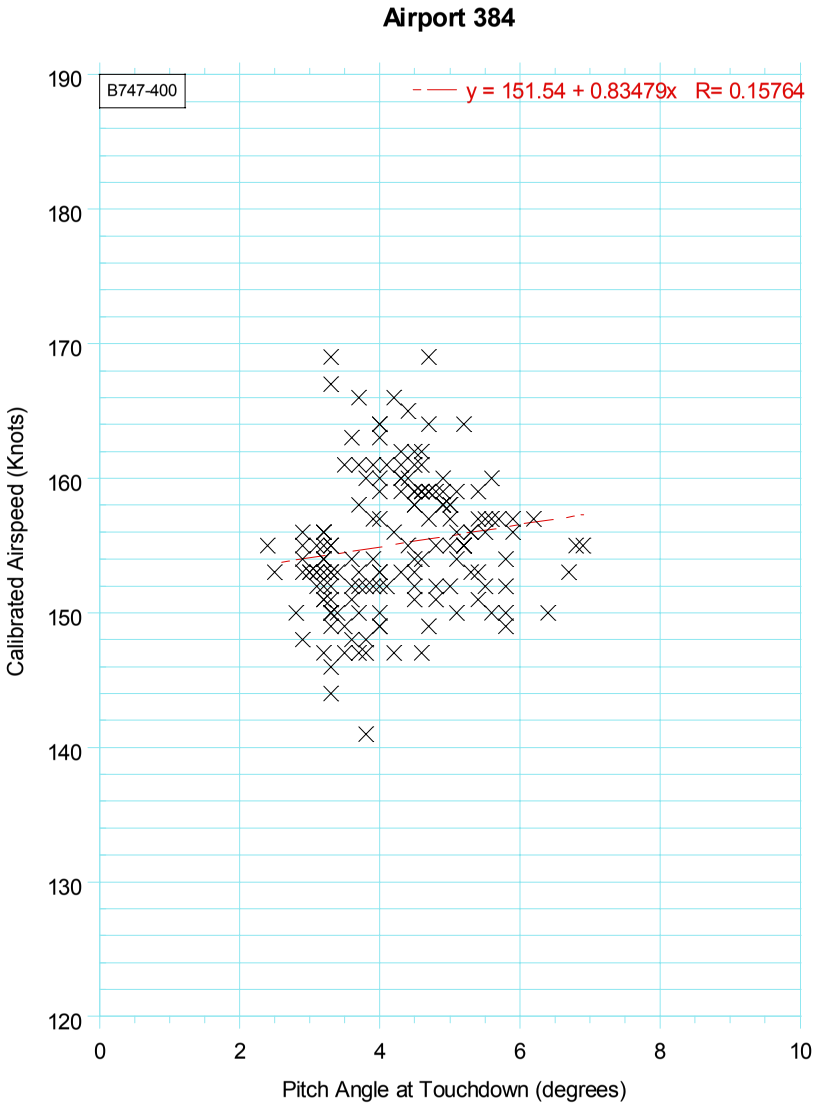

FIGURE C-24. CALIBRATED AIRSPEED VS PITCH ANGLE AT TOUCHDOWN, AIRPORT 384 ELEVATION 500-1000 FEET

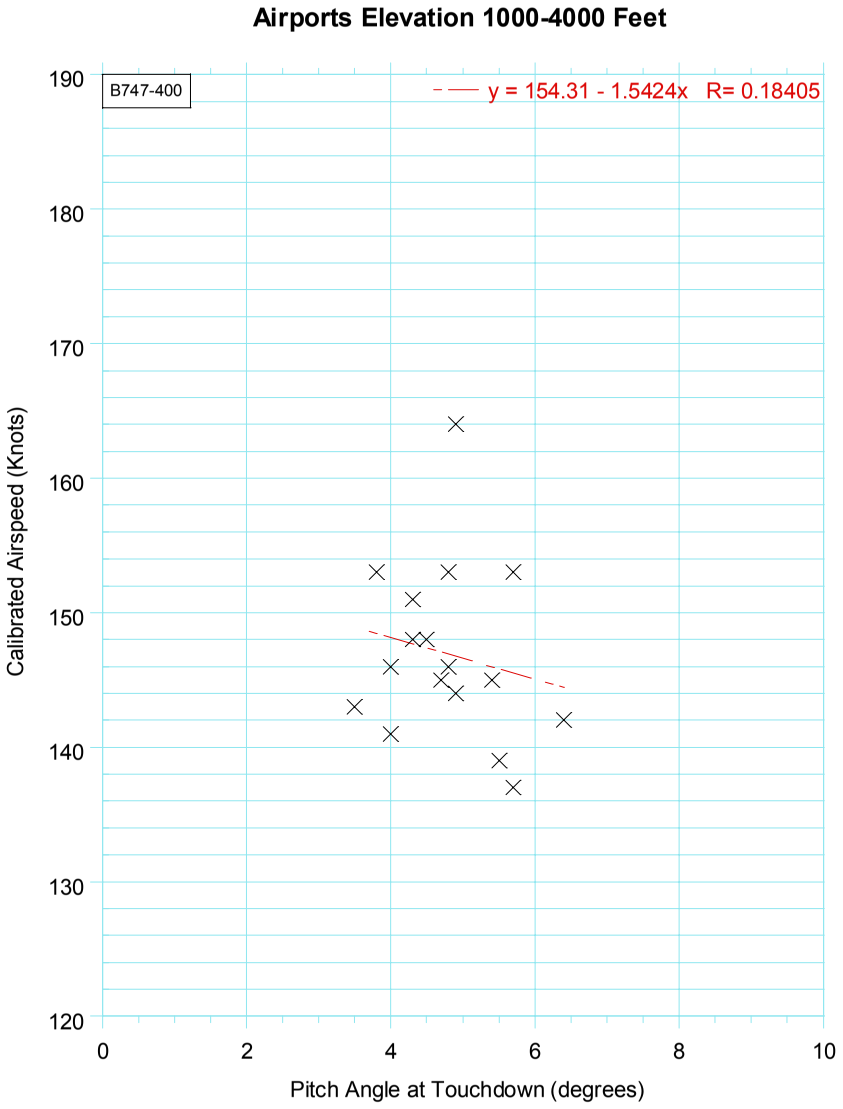

FIGURE C-25. CALIBRATED AIRSPEED VS PITCH ANGLE AT TOUCHDOWN, AIRPORTS ELEVATION 1000-4000 FEET

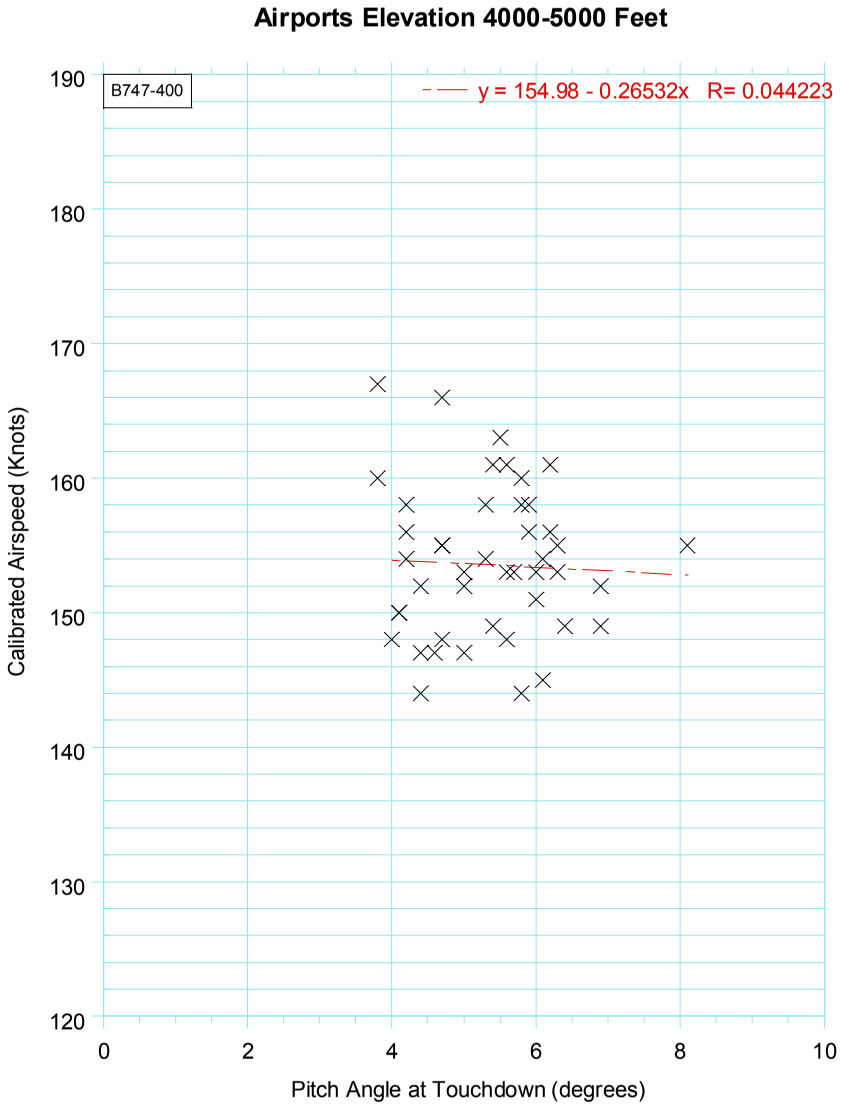

FIGURE C-26. CALIBRATED AIRSPEED VS PITCH ANGLE AT TOUCHDOWN, AIRPORTS ELEVATION 4000-5000 FEET

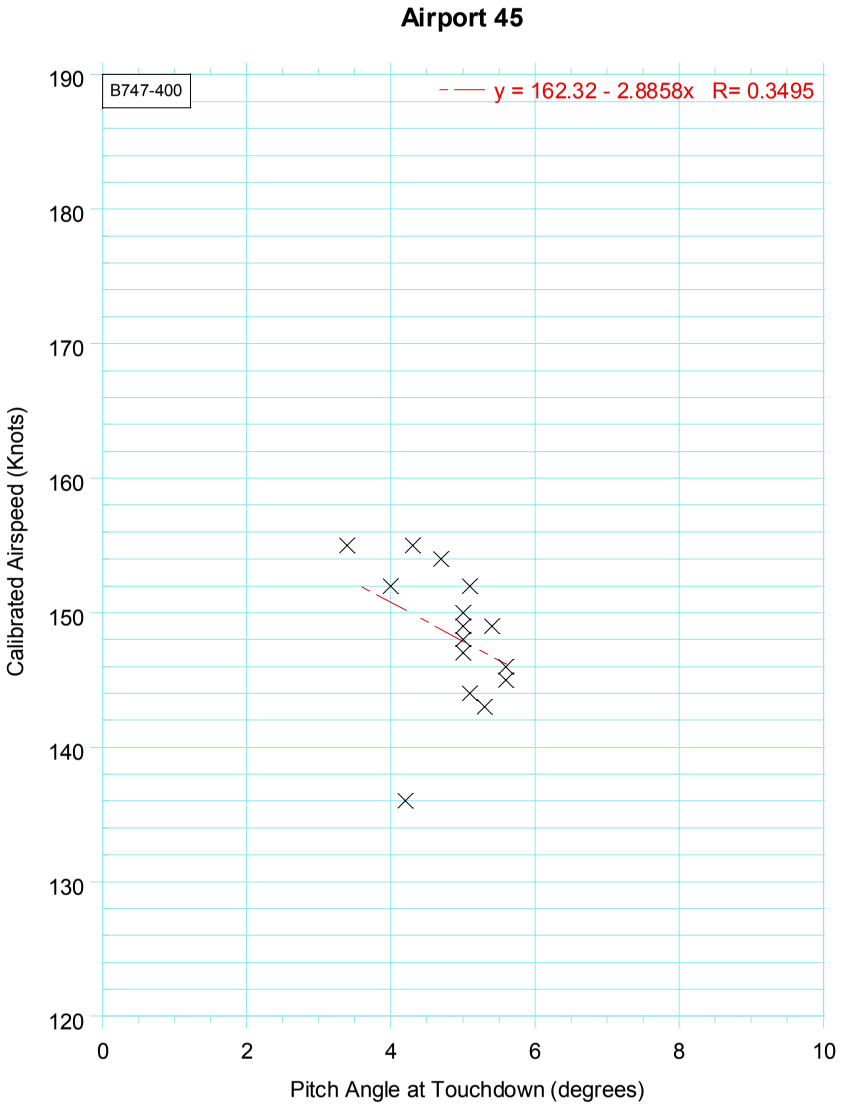

FIGURE C-27. CALIBRATED AIRSPEED VS PITCH ANGLE AT TOUCHDOWN, AIRPORT 45 ELEVATION > 5000 FEET

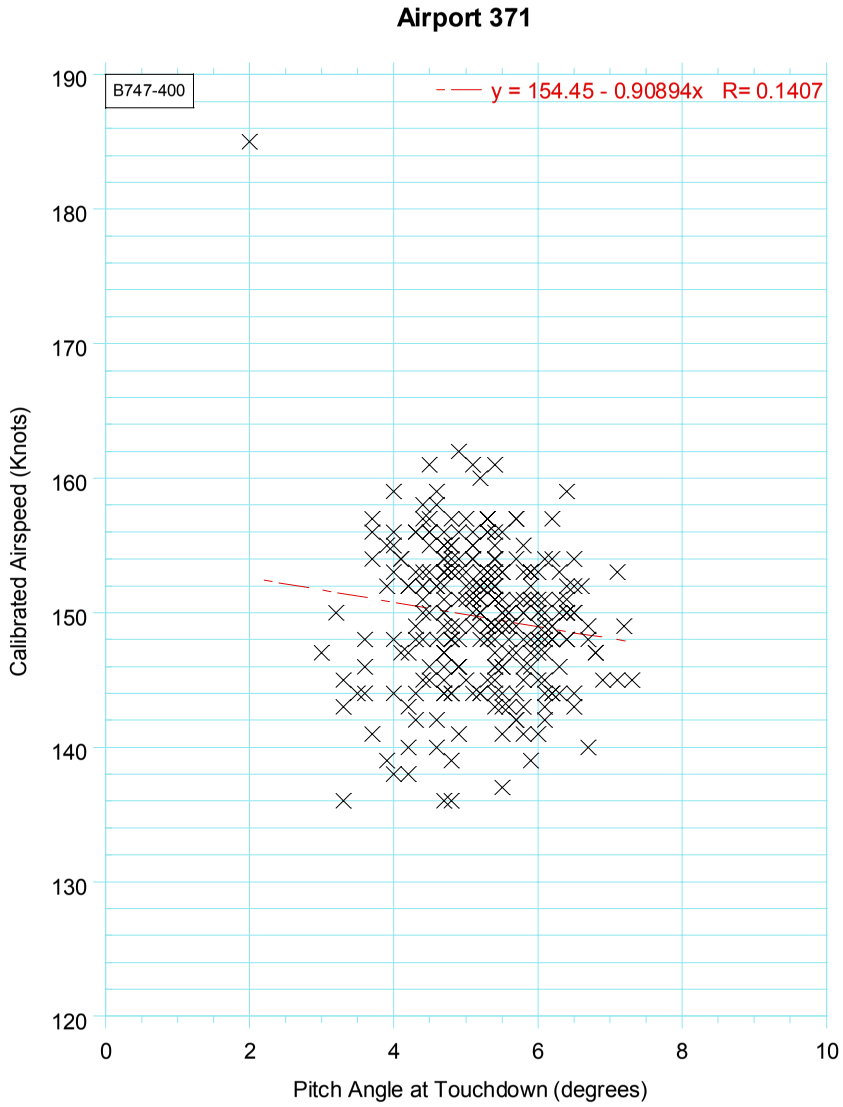

FIGURE C-28. CALIBRATED AIRSPEED VS PITCH ANGLE AT TOUCHDOWN, AIRPORT 371 ELEVATION > 5000 FEET

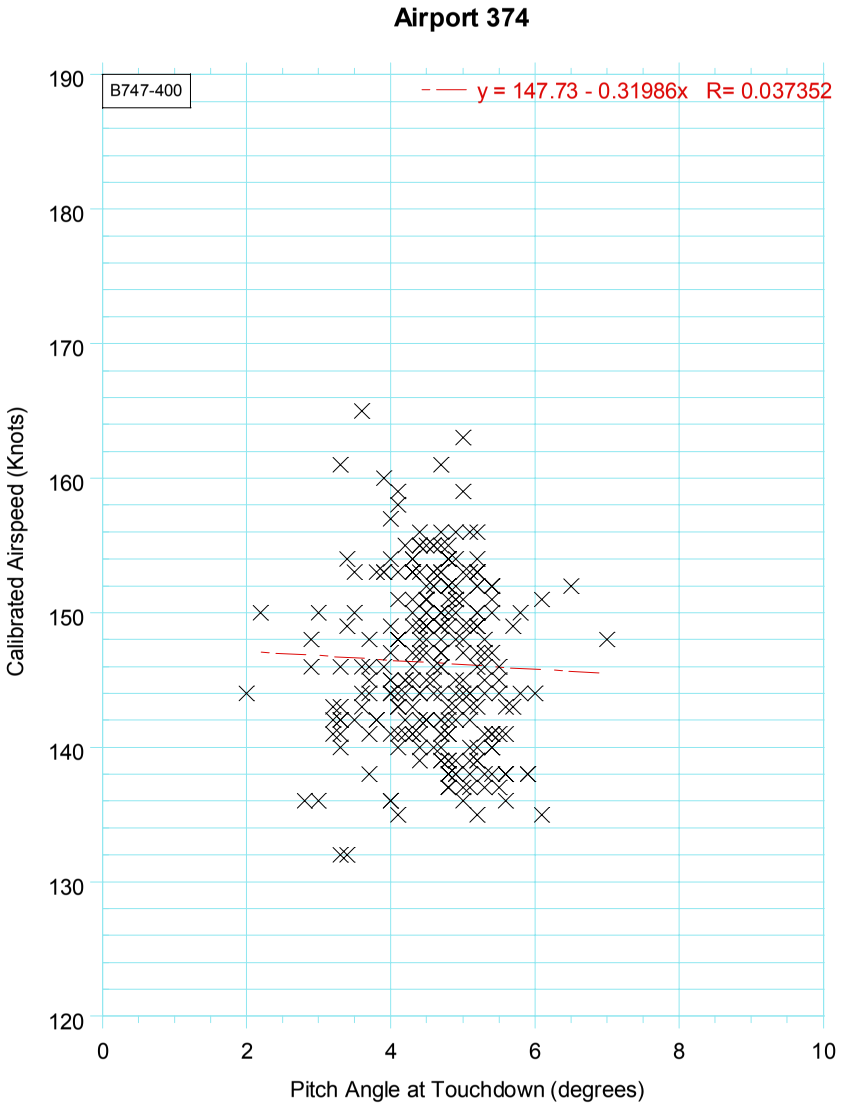

FIGURE C-29. CALIBRATED AIRSPEED VS PITCH ANGLE AT TOUCHDOWN, AIRPORT 374 ELEVATION > 5000 FEET

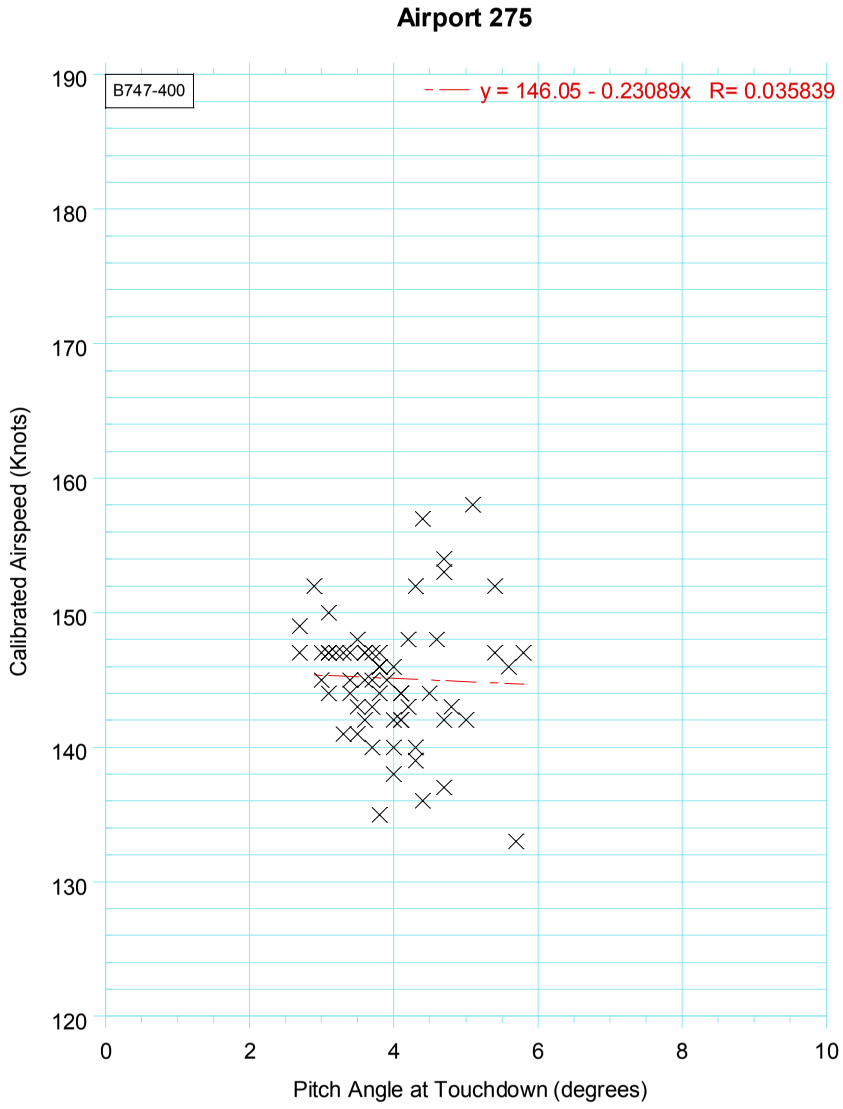

FIGURE C-30. CALIBRATED AIRSPEED VS PITCH ANGLE AT TOUCHDOWN, AIRPORT 275 ELEVATION > 5000 FEET

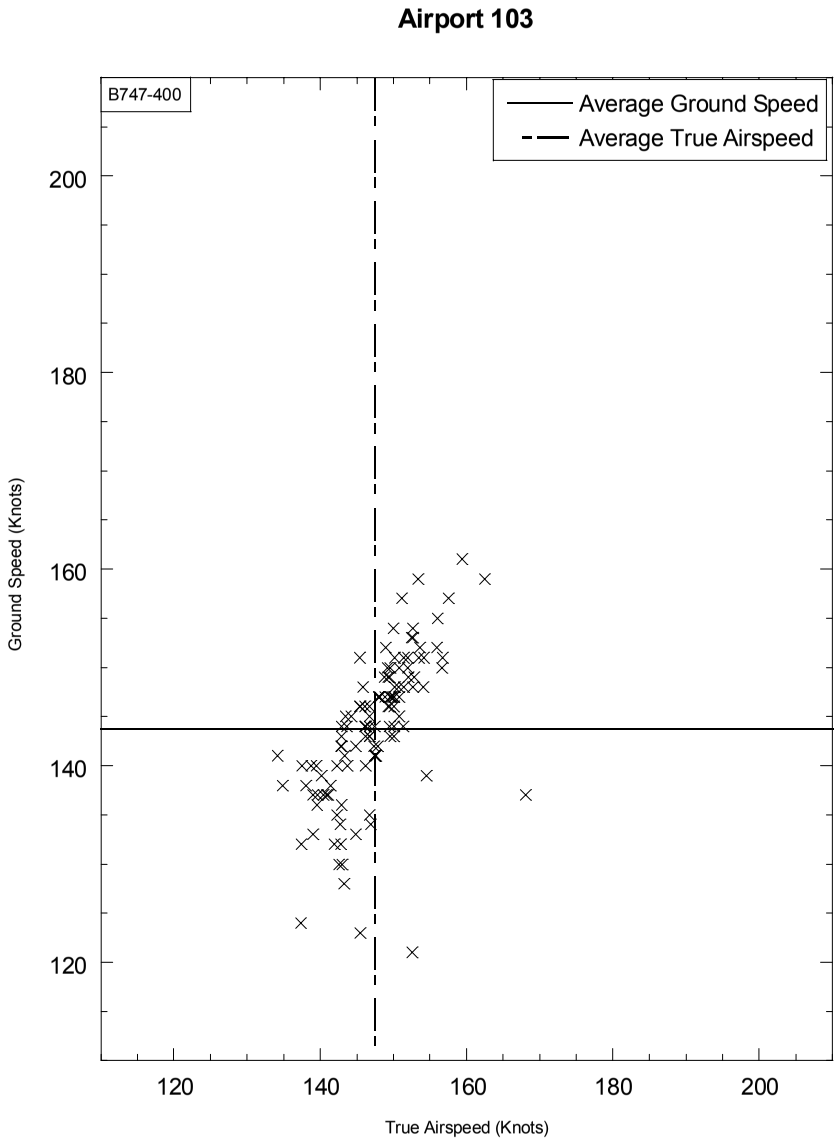

FIGURE C-31. GROUND SPEED VS TRUE AIRSPEED AT TOUCHDOWN, AIRPORT 103 ELEVATION < 500 FEET

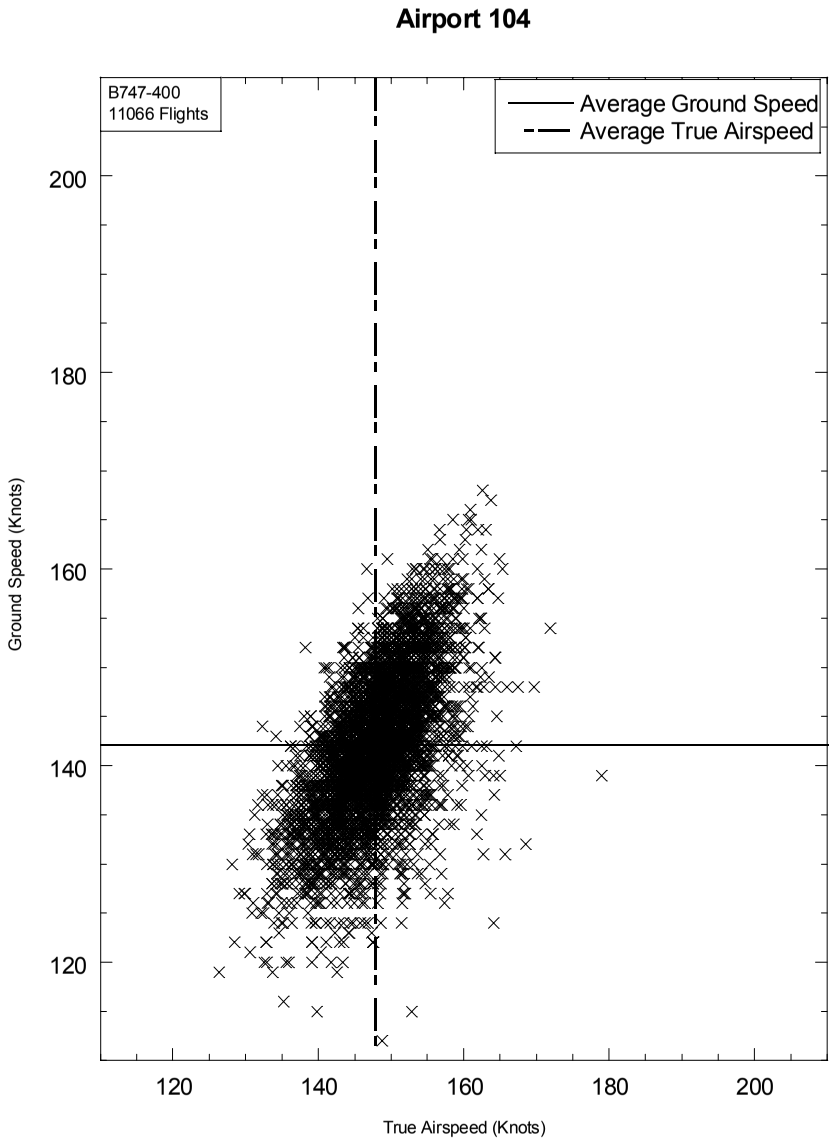

FIGURE C-32. GROUND SPEED VS TRUE AIRSPEED AT TOUCHDOWN, AIRPORT 104 ELEVATION < 500 FEET

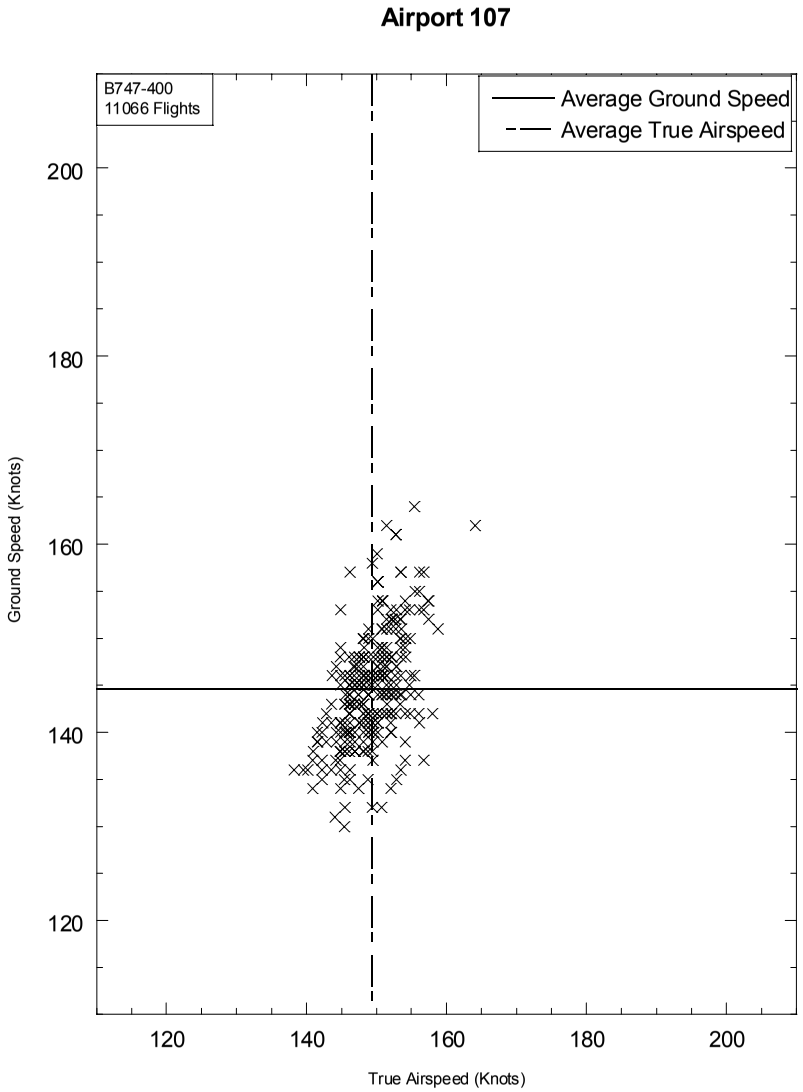

FIGURE C-33. GROUND SPEED VS TRUE AIRSPEED AT TOUCHDOWN, AIRPORT 107 ELEVATION < 500 FEET

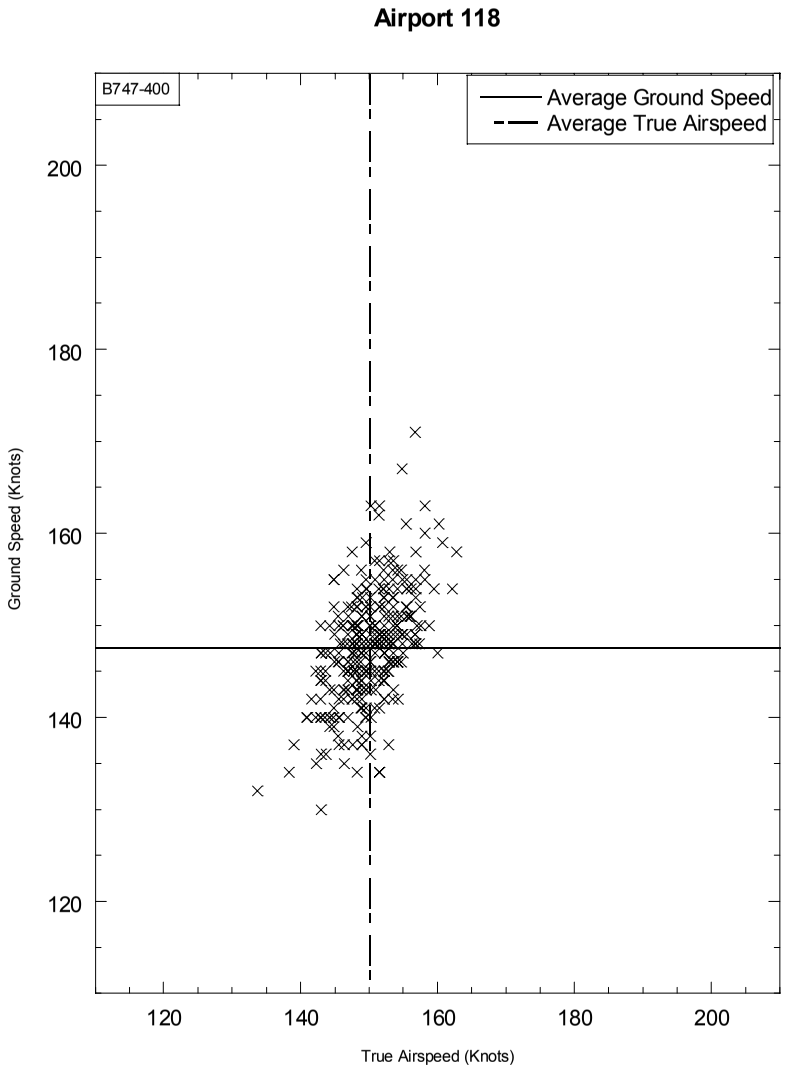

FIGURE C-34. GROUND SPEED VS TRUE AIRSPEED AT TOUCHDOWN, AIRPORT 118 ELEVATION < 500 FEET

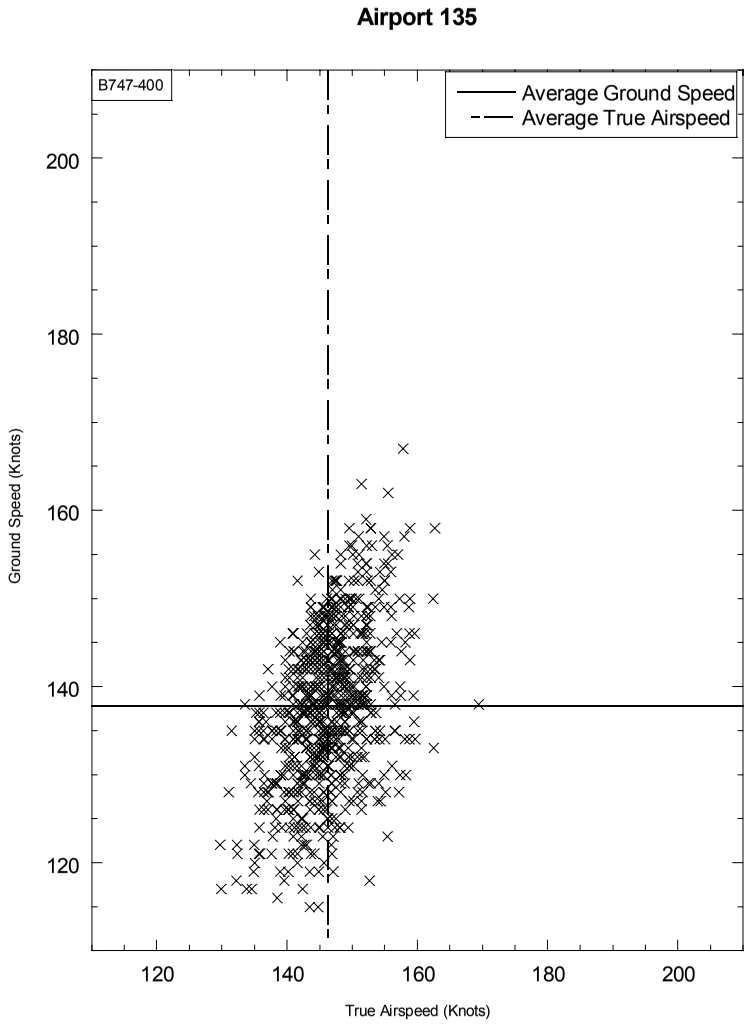

FIGURE C-35. GROUND SPEED VS TRUE AIRSPEED AT TOUCHDOWN, AIRPORT 135 ELEVATION < 500 FEET

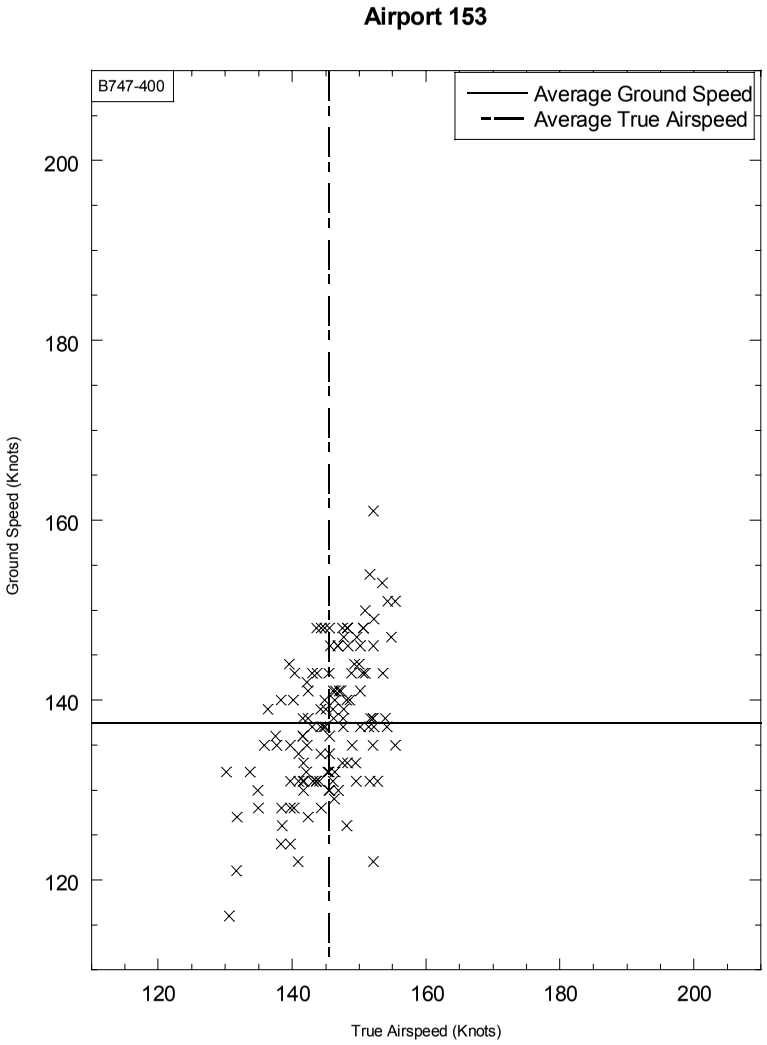

FIGURE C-36. GROUND SPEED VS TRUE AIRSPEED AT TOUCHDOWN, AIRPORT 153 ELEVATION < 500 FEET

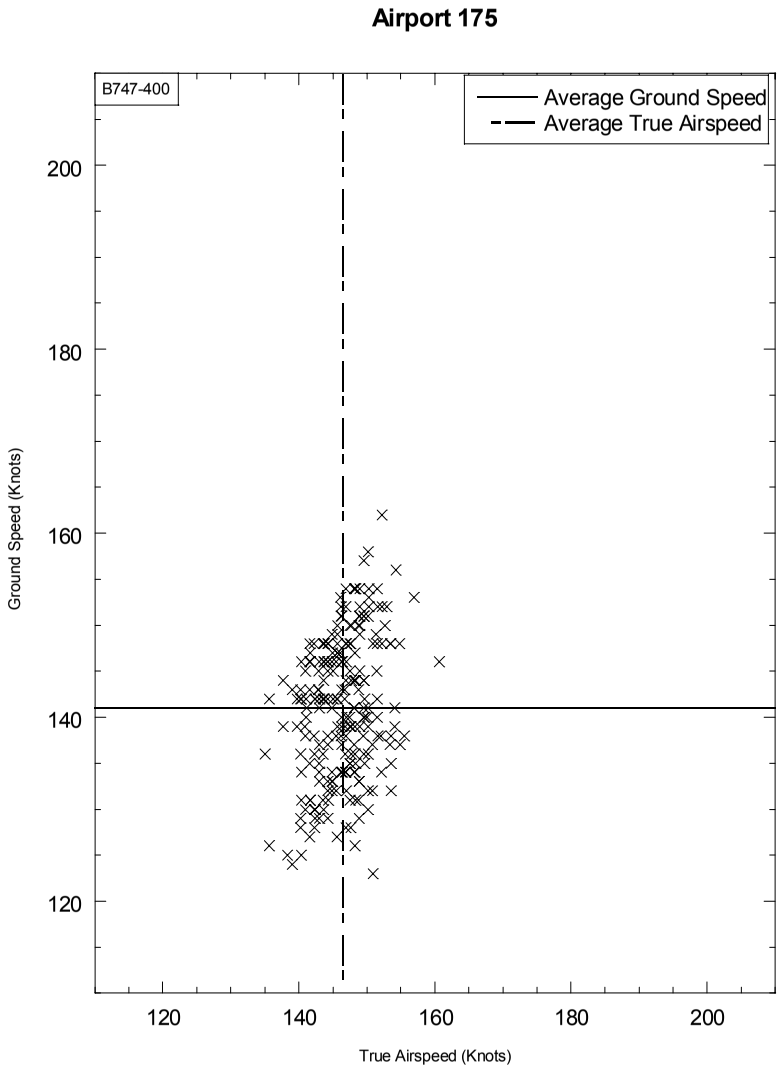

FIGURE C-37. GROUND SPEED VS TRUE AIRSPEED AT TOUCHDOWN, AIRPORT 175 ELEVATION < 500 FEET

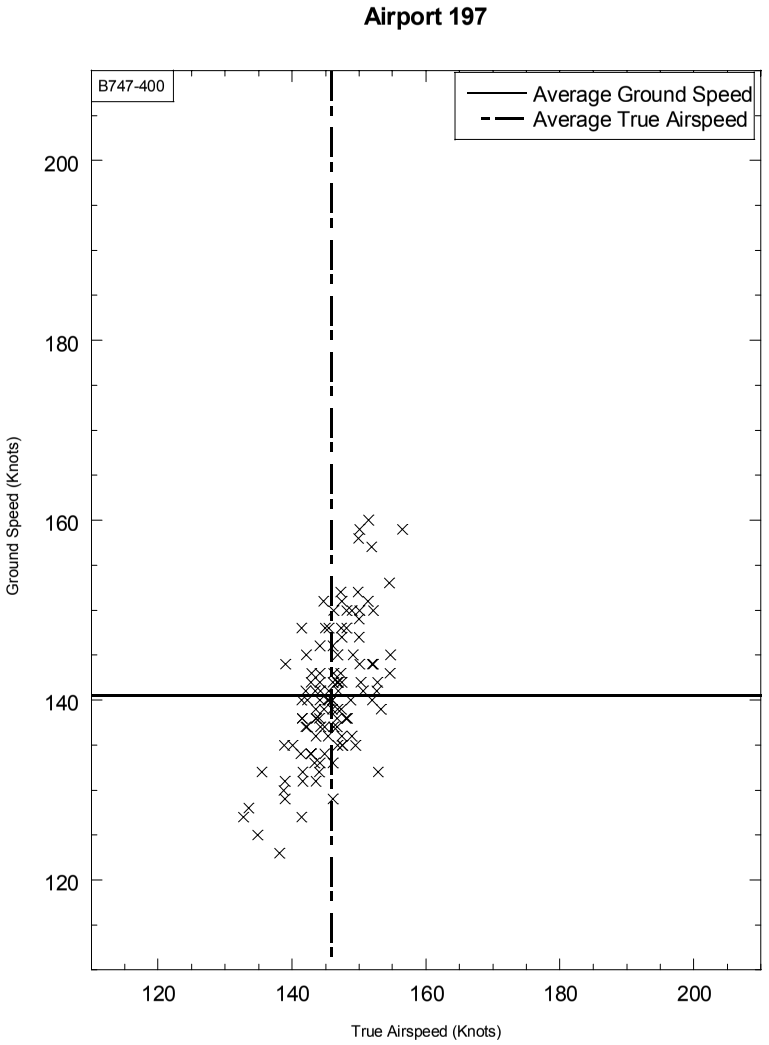

FIGURE C-38. GROUND SPEED VS TRUE AIRSPEED AT TOUCHDOWN, AIRPORT 197 ELEVATION < 500 FEET

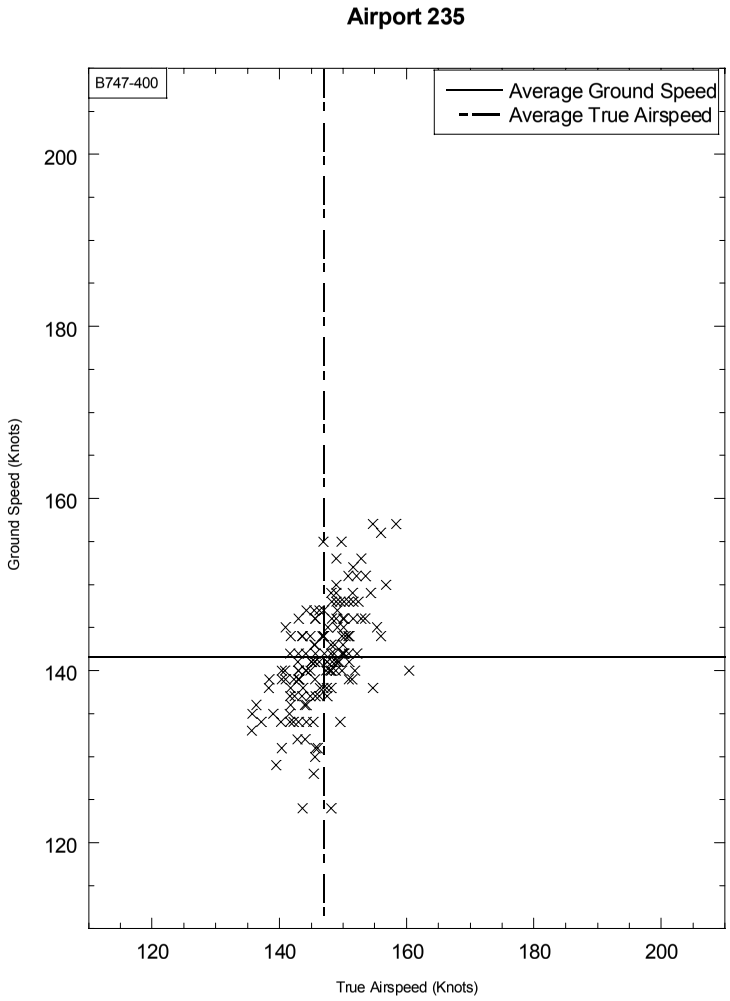

FIGURE C-39. GROUND SPEED VS TRUE AIRSPEED AT TOUCHDOWN, AIRPORT 235 ELEVATION < 500 FEET

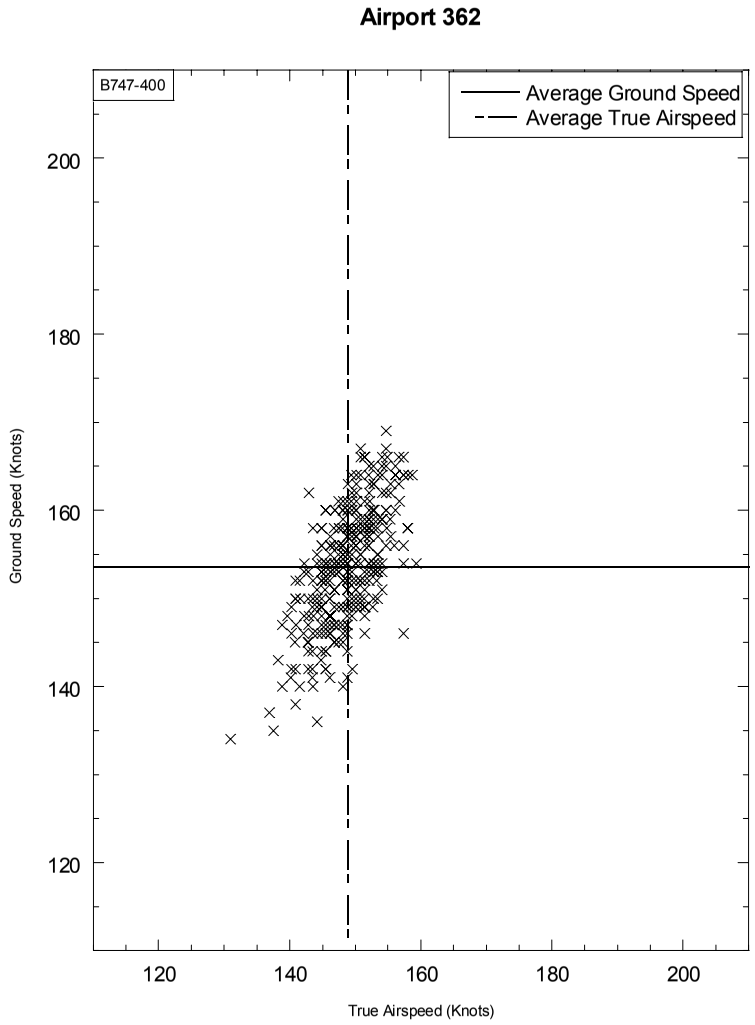

FIGURE C-40. GROUND SPEED VS TRUE AIRSPEED AT TOUCHDOWN, AIRPORT 362 ELEVATION < 500 FEET

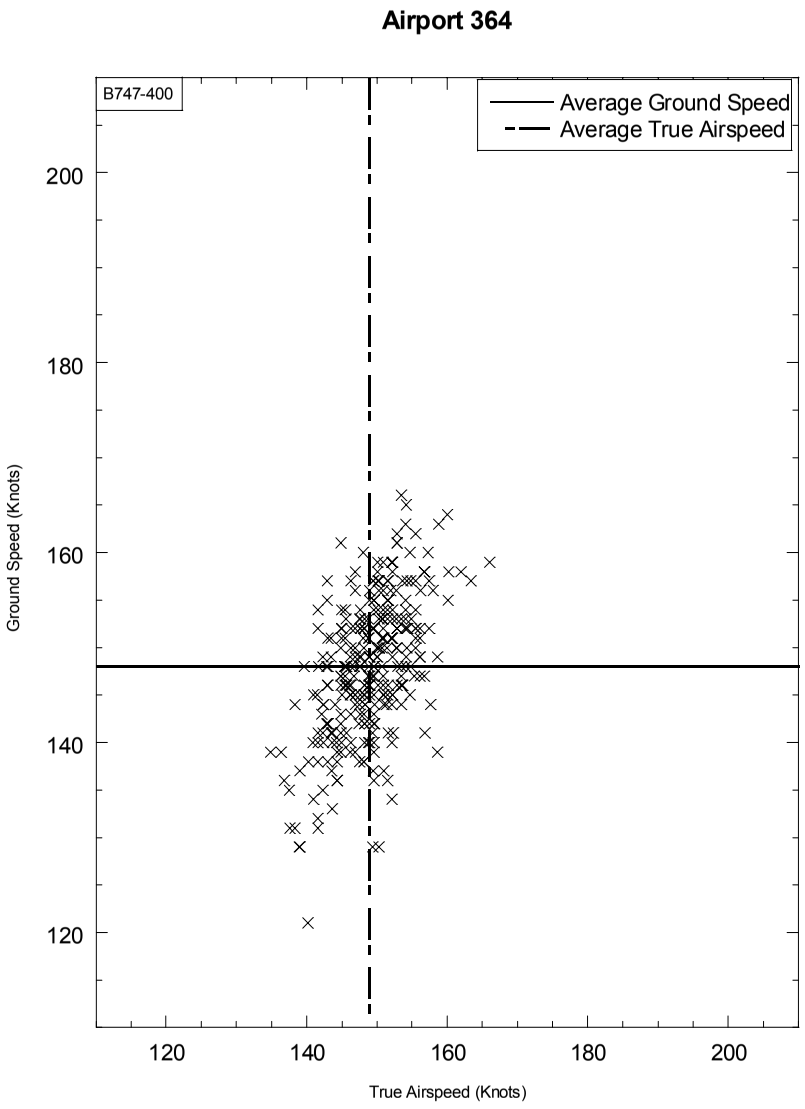

FIGURE C-41. GROUND SPEED VS TRUE AIRSPEED AT TOUCHDOWN, AIRPORT 364 ELEVATION < 500 FEET

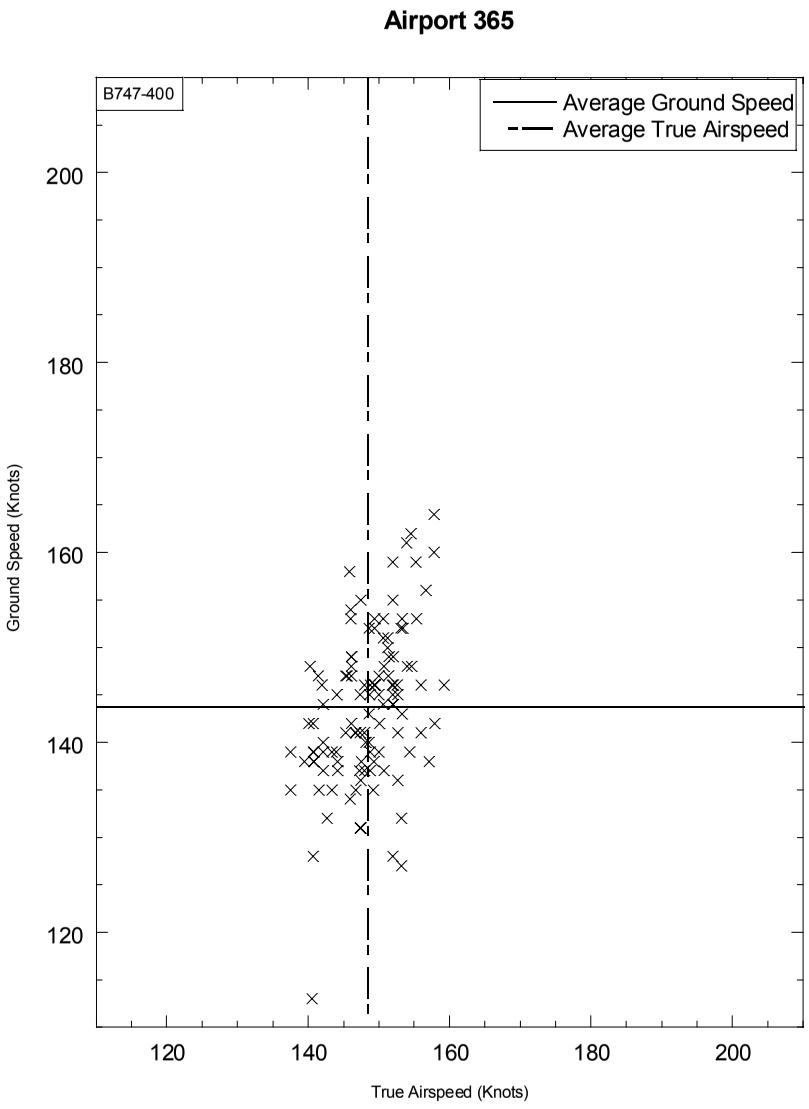

FIGURE C-42. GROUND SPEED VS TRUE AIRSPEED AT TOUCHDOWN, AIRPORT 365 ELEVATION < 500 FEET

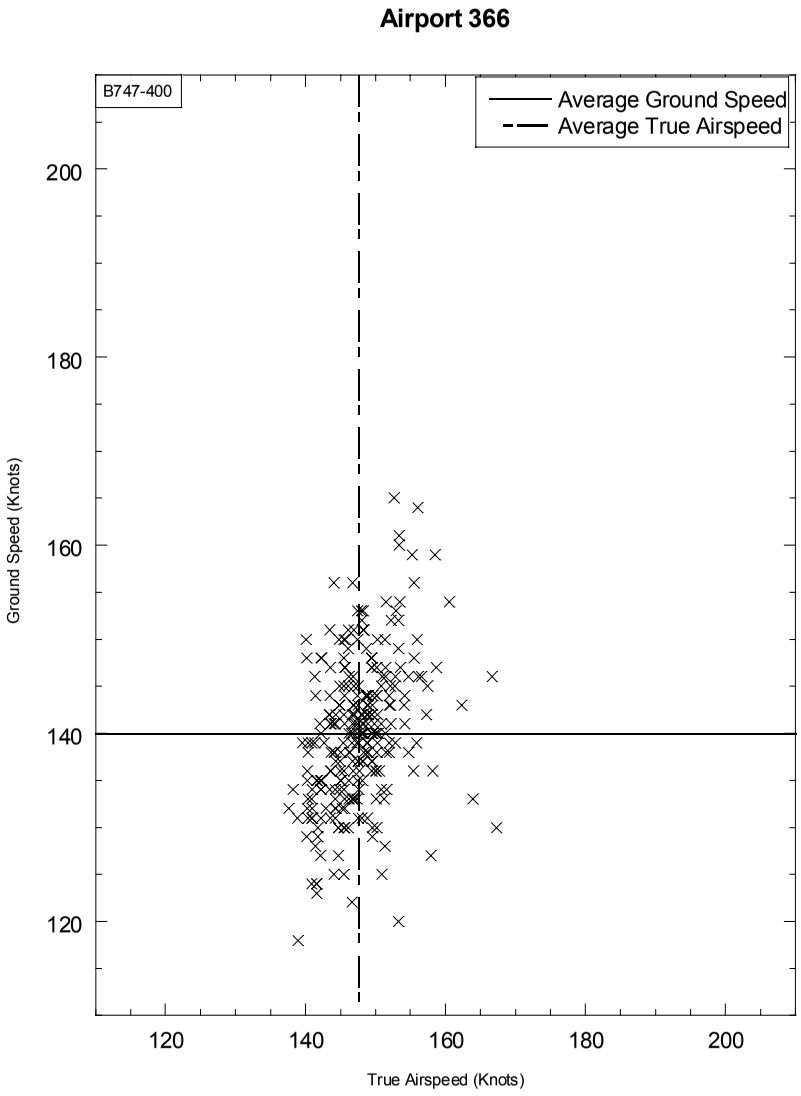

FIGURE C-43. GROUND SPEED VS TRUE AIRSPEED AT TOUCHDOWN, AIRPORT 366 ELEVATION < 500 FEET

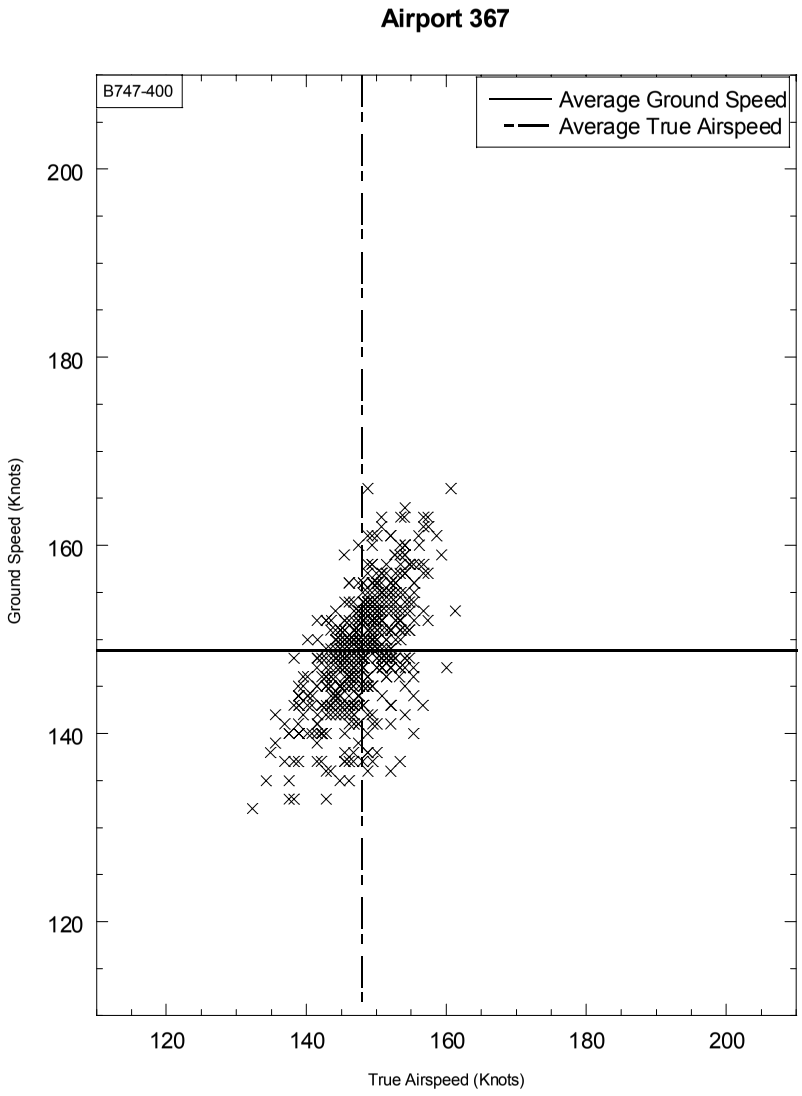

FIGURE C-44. GROUND SPEED VS TRUE AIRSPEED AT TOUCHDOWN, AIRPORT 367 ELEVATION < 500 FEET

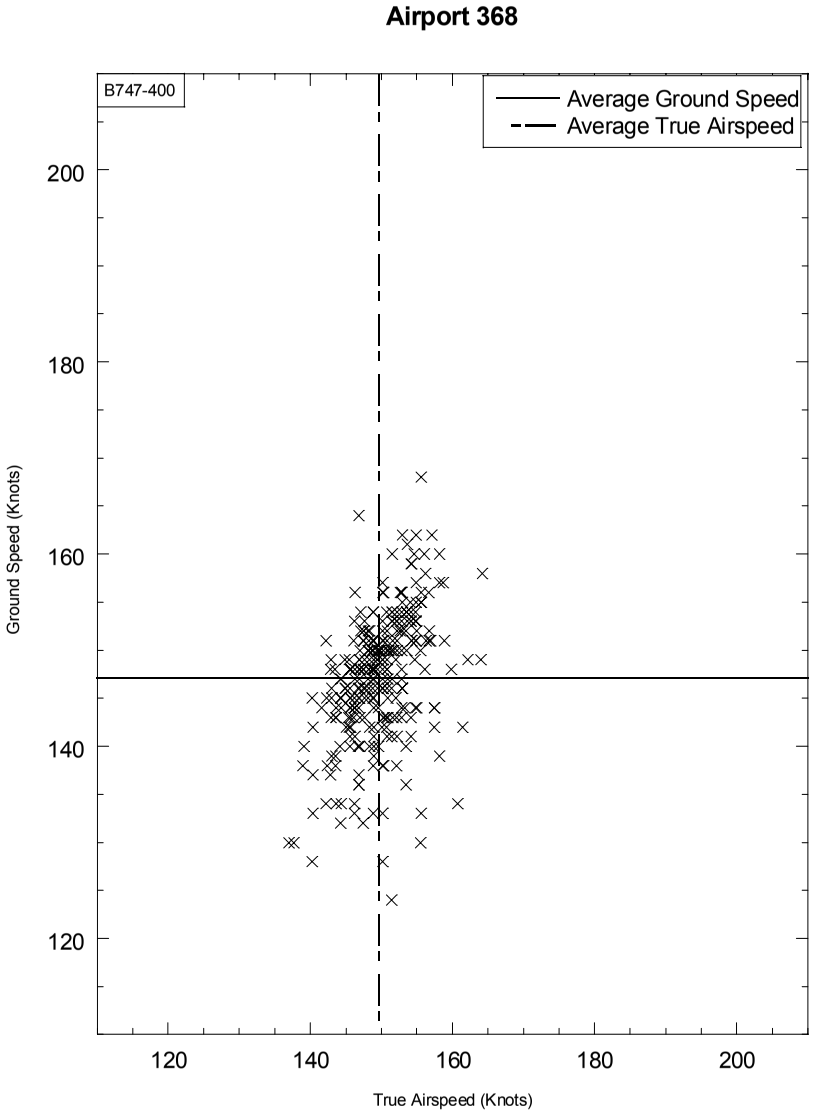

FIGURE C-45. GROUND SPEED VS TRUE AIRSPEED AT TOUCHDOWN, AIRPORT 368 ELEVATION < 500 FEET

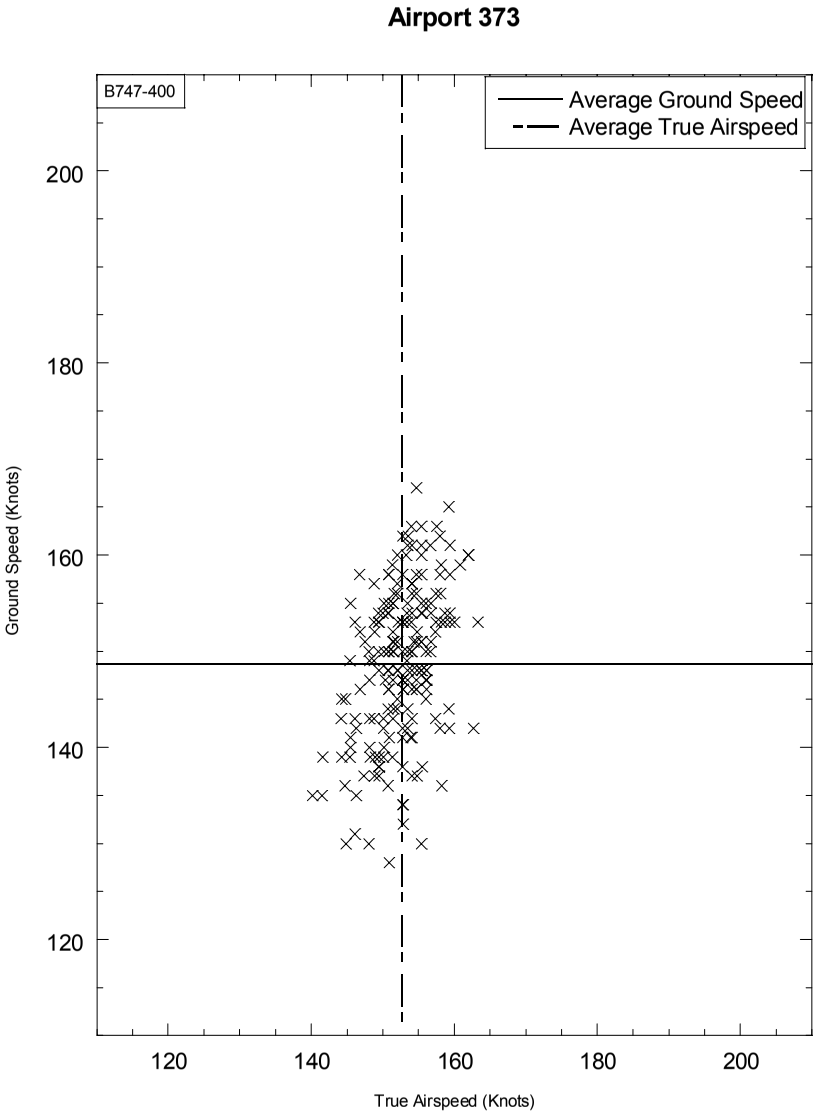

FIGURE C-46. GROUND SPEED VS TRUE AIRSPEED AT TOUCHDOWN, AIRPORT 373 ELEVATION < 500 FEET

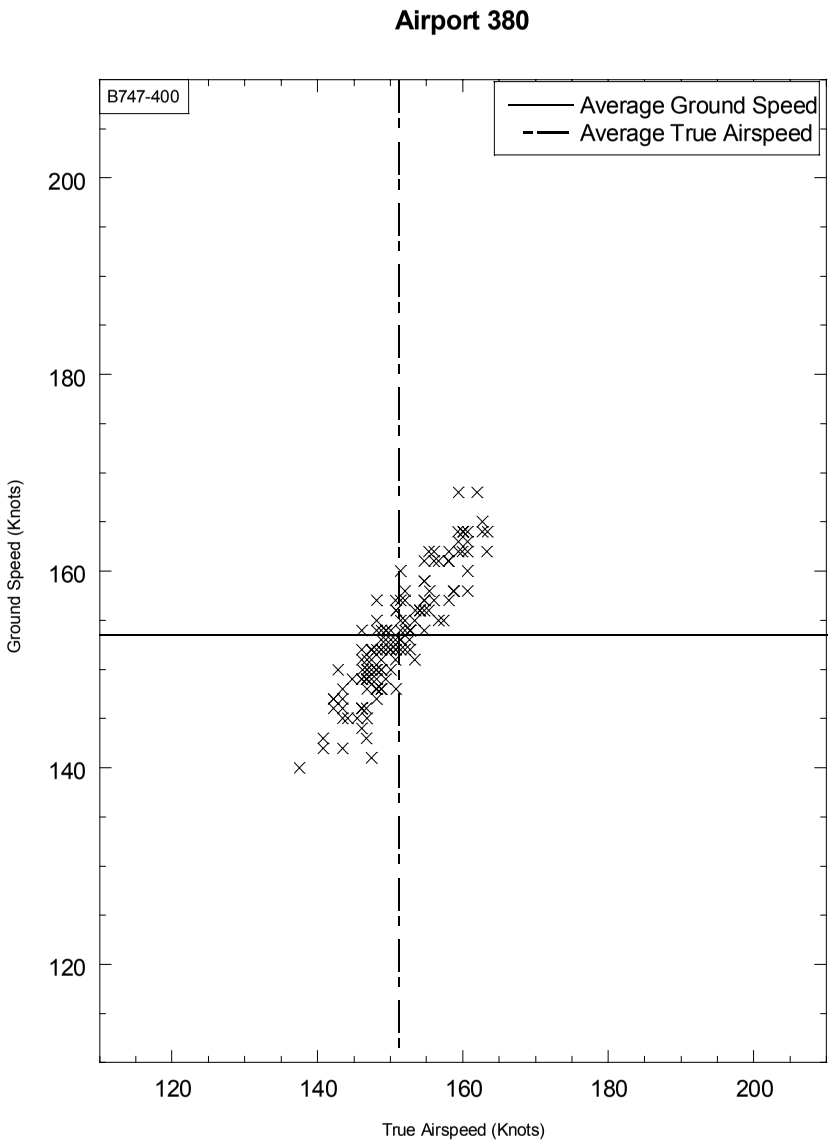

FIGURE C-47. GROUND SPEED VS TRUE AIRSPEED AT TOUCHDOWN, AIRPORT 380 ELEVATION < 500 FEET

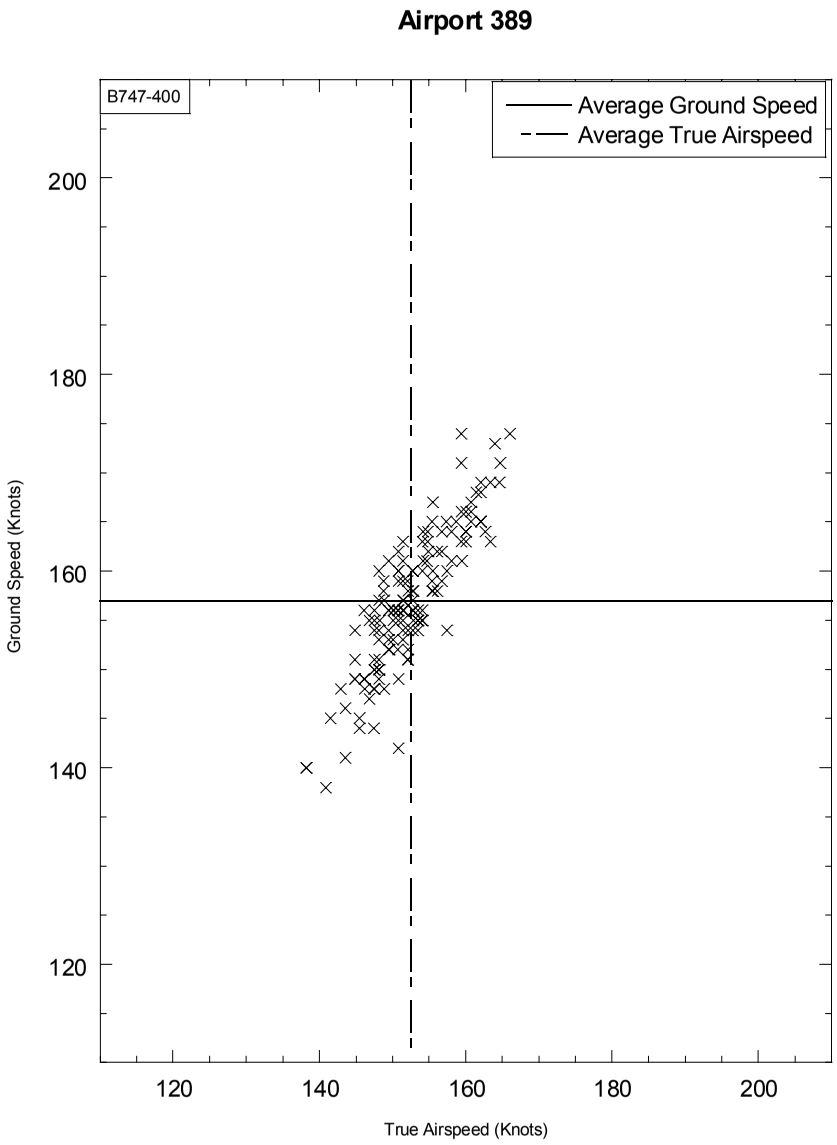

FIGURE C-48. GROUND SPEED VS TRUE AIRSPEED AT TOUCHDOWN, AIRPORT 389 ELEVATION < 500 FEET

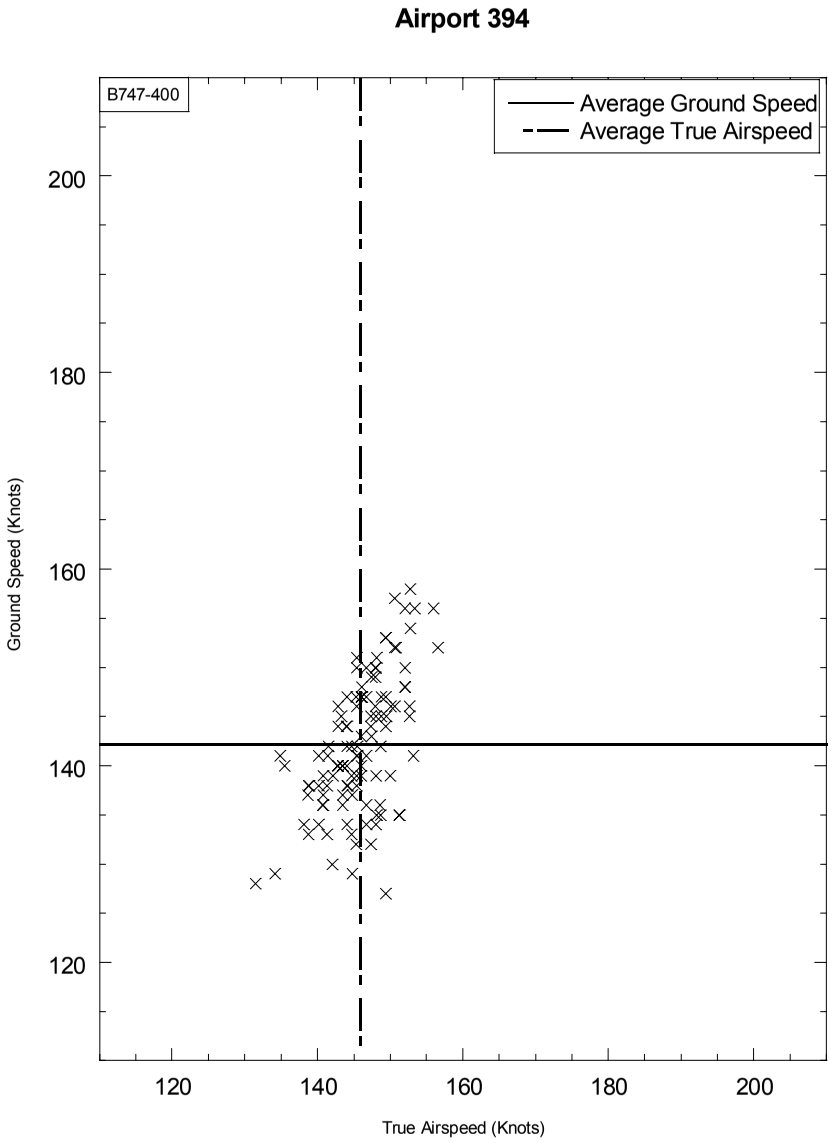

FIGURE C-49. GROUND SPEED VS TRUE AIRSPEED AT TOUCHDOWN, AIRPORT 394 ELEVATION < 500 FEET

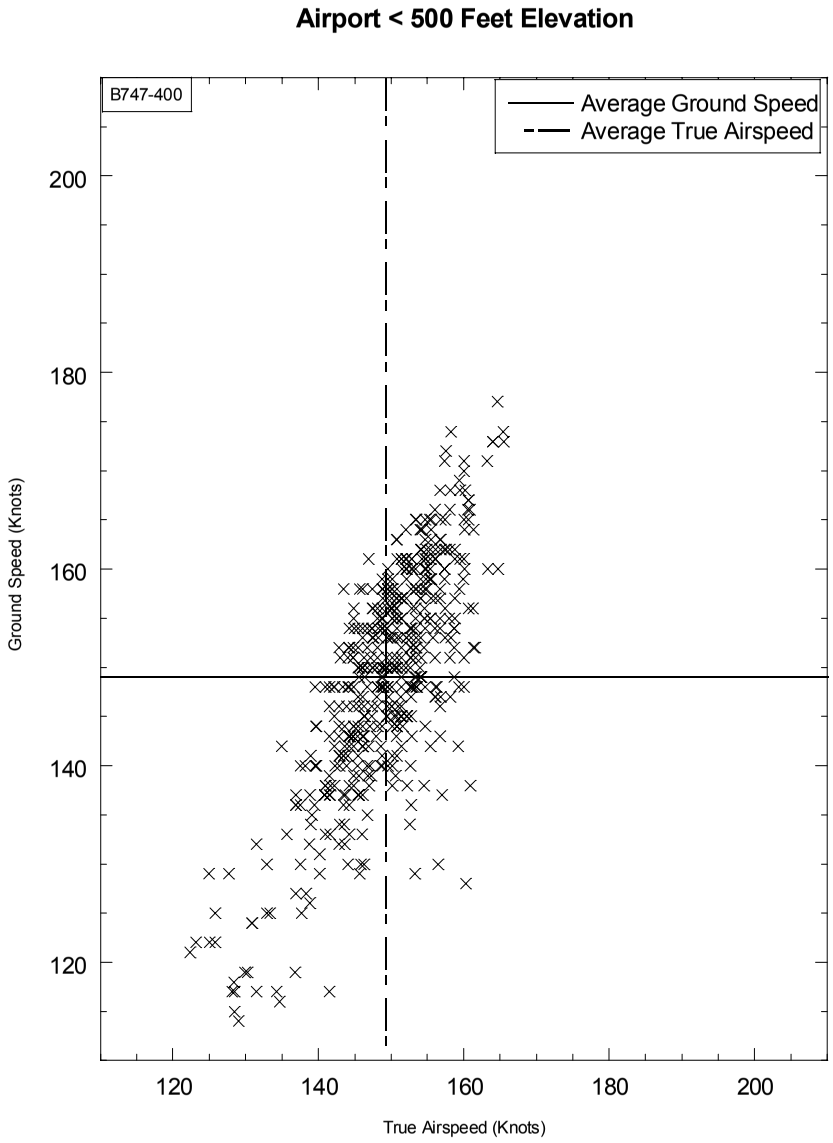

FIGURE C-50. GROUND SPEED VS TRUE AIRSPEED AT TOUCHDOWN, AIRPORTS ELEVATION < 500 FEET

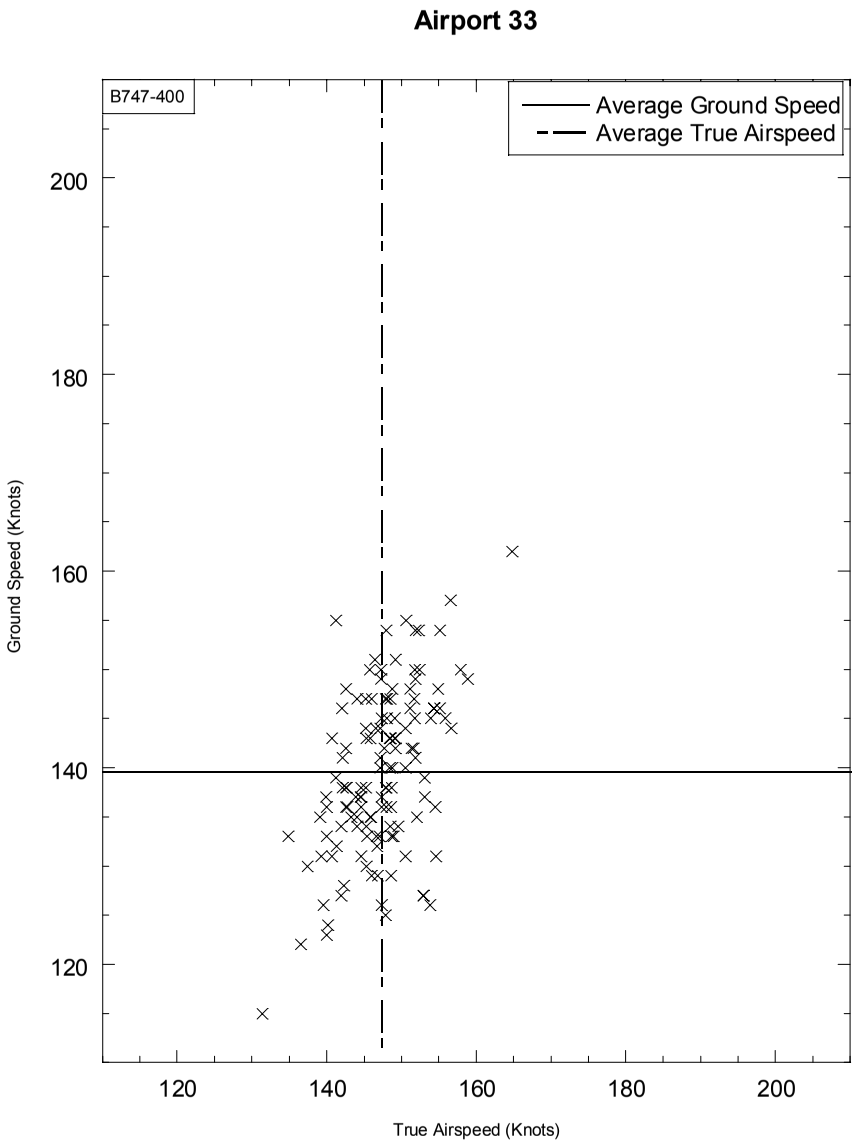

FIGURE C-51. GROUND SPEED VS TRUE AIRSPEED AT TOUCHDOWN, AIRPORT 33 ELEVATION 500-1000 FEET

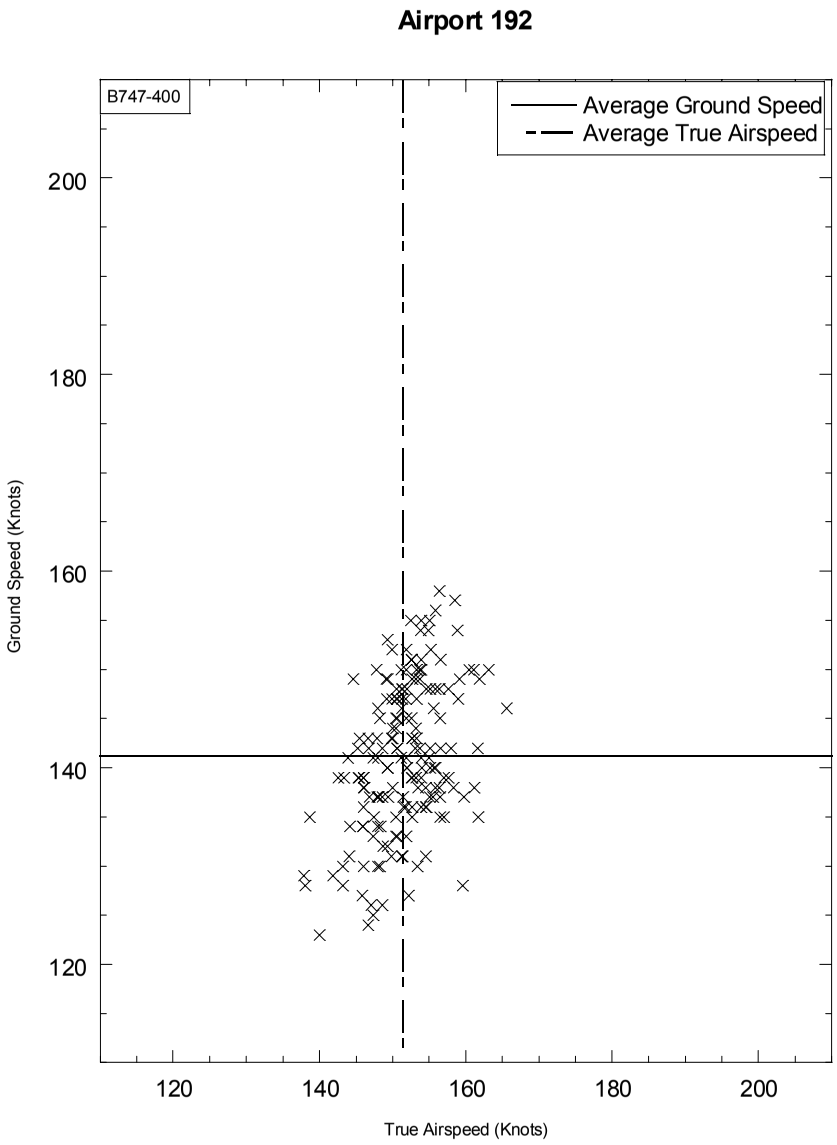

FIGURE C-52. GROUND SPEED VS TRUE AIRSPEED AT TOUCHDOWN, AIRPORT 192 ELEVATION 500-1000 FEET

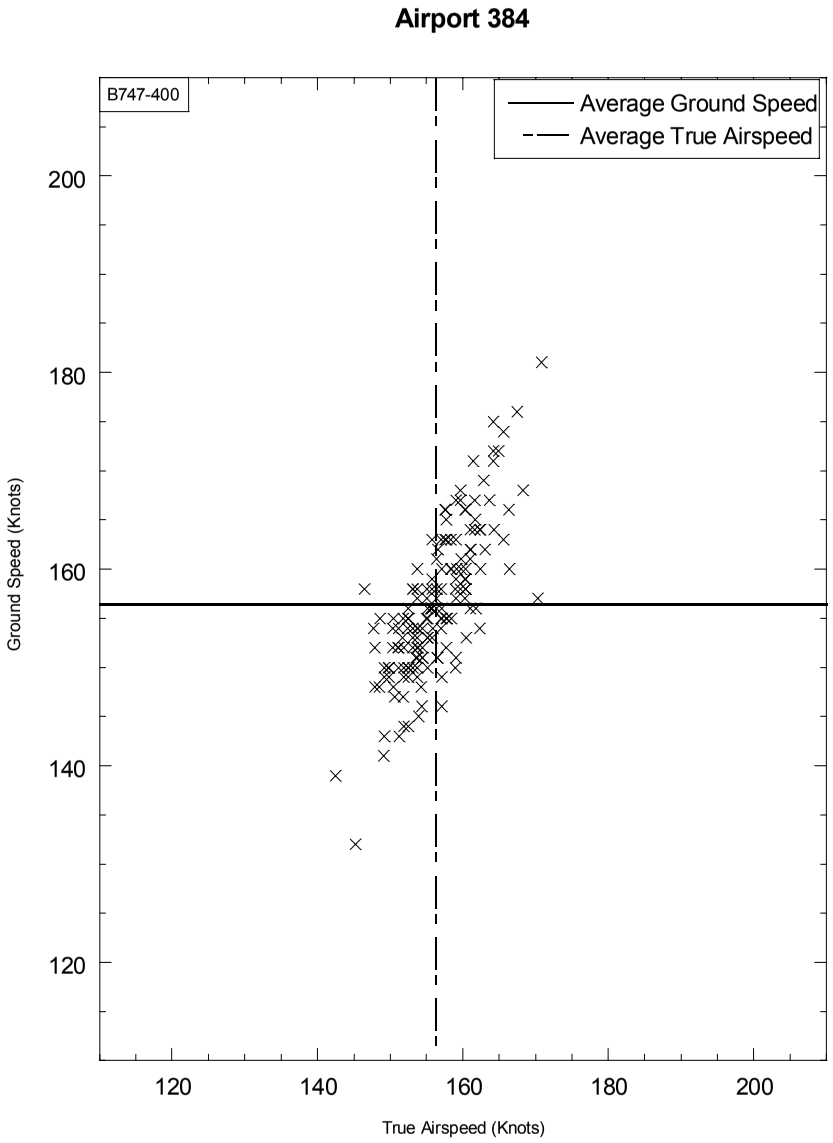

FIGURE C-53. GROUND SPEED VS TRUE AIRSPEED AT TOUCHDOWN, AIRPORT 384 ELEVATION 500-1000 FEET

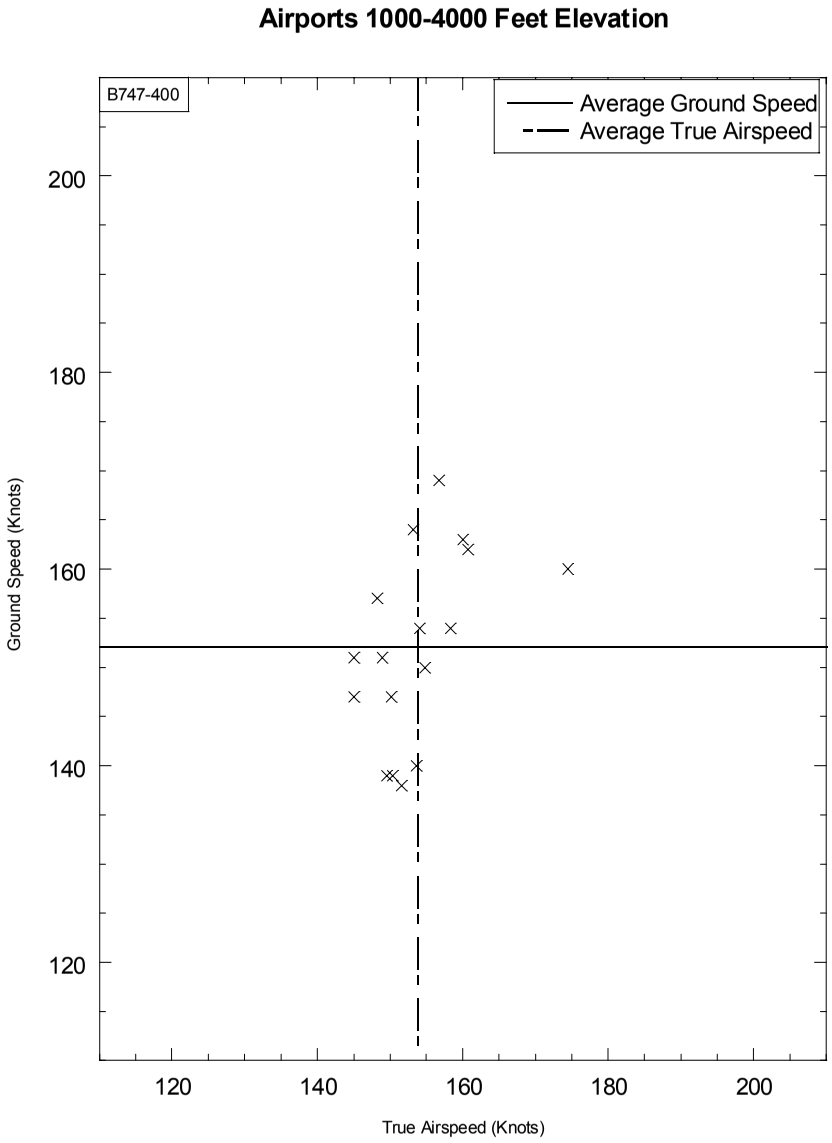

FIGURE C-54. GROUND SPEED VS TRUE AIRSPEED AT TOUCHDOWN, AIRPORTS ELEVATION 1000-4000 FEET

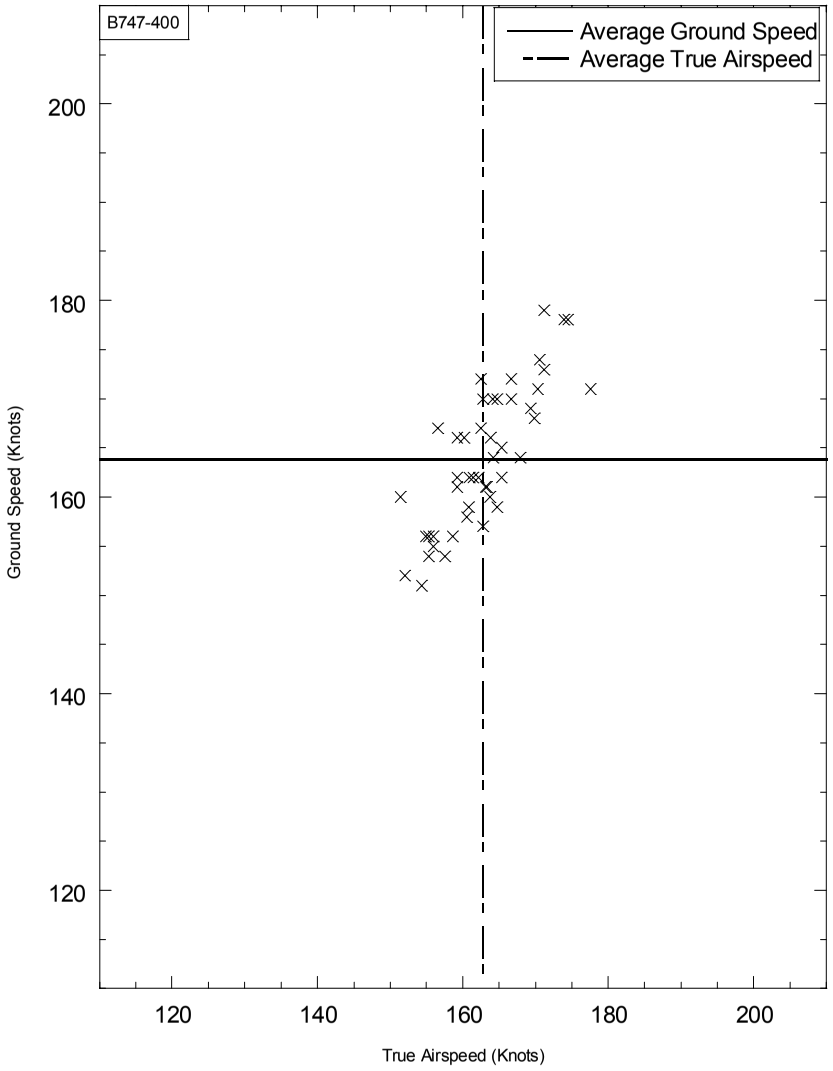

FIGURE C-55. GROUND SPEED VS TRUE AIRSPEED AT TOUCHDOWN, AIRPORTS ELEVATION 4000-5000 FEET

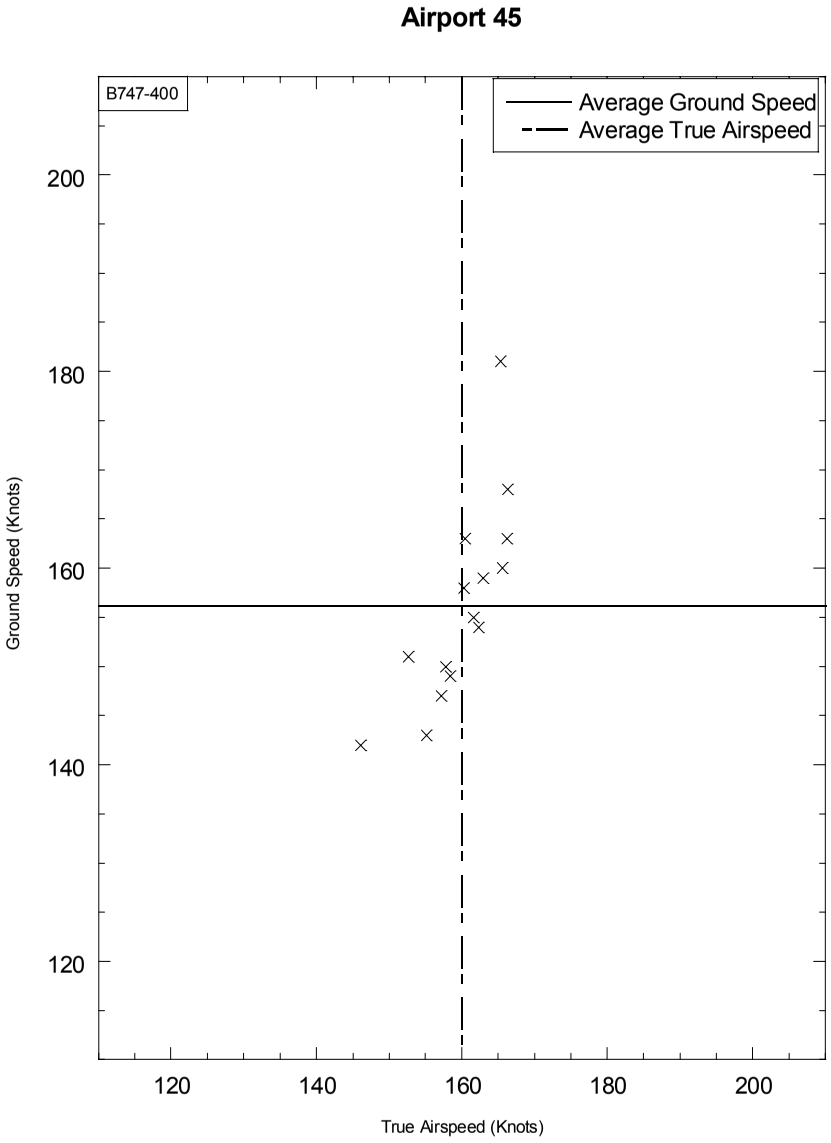

FIGURE C-56. GROUND SPEED VS TRUE AIRSPEED AT TOUCHDOWN, AIRPORT 45 ELEVATION > 5000 FEET

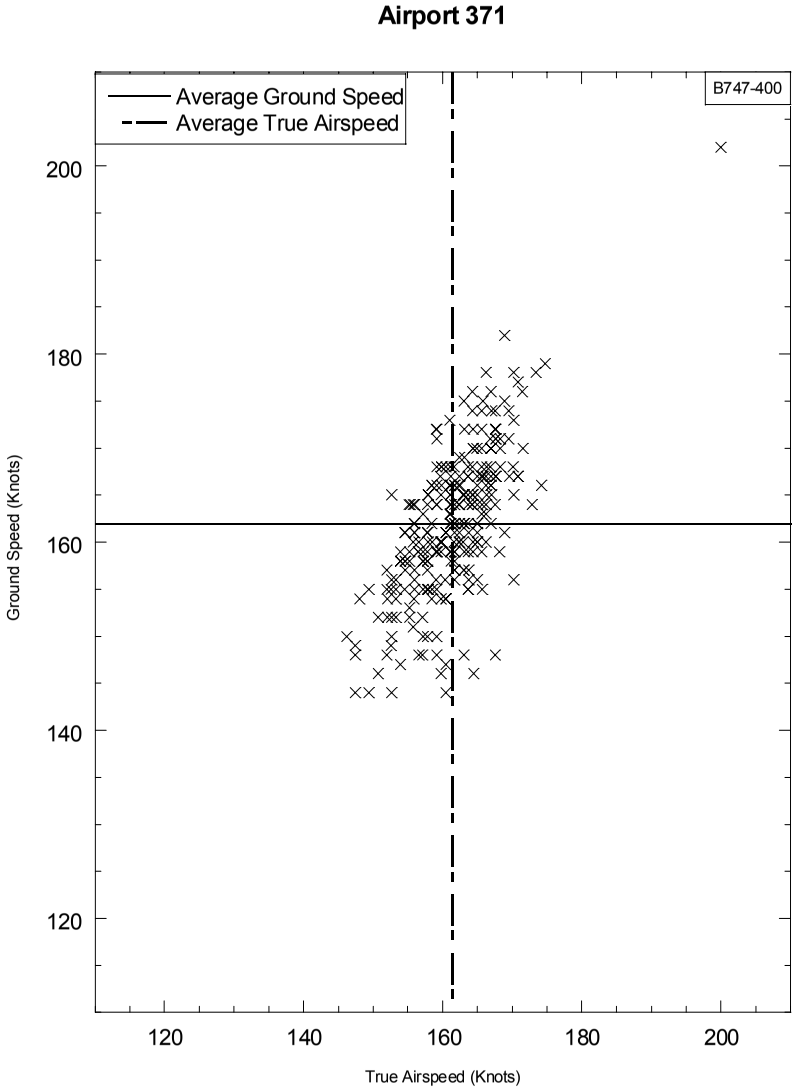

FIGURE C-57. GROUND SPEED VS TRUE AIRSPEED AT TOUCHDOWN, AIRPORT 371 ELEVATION >5000 FEET

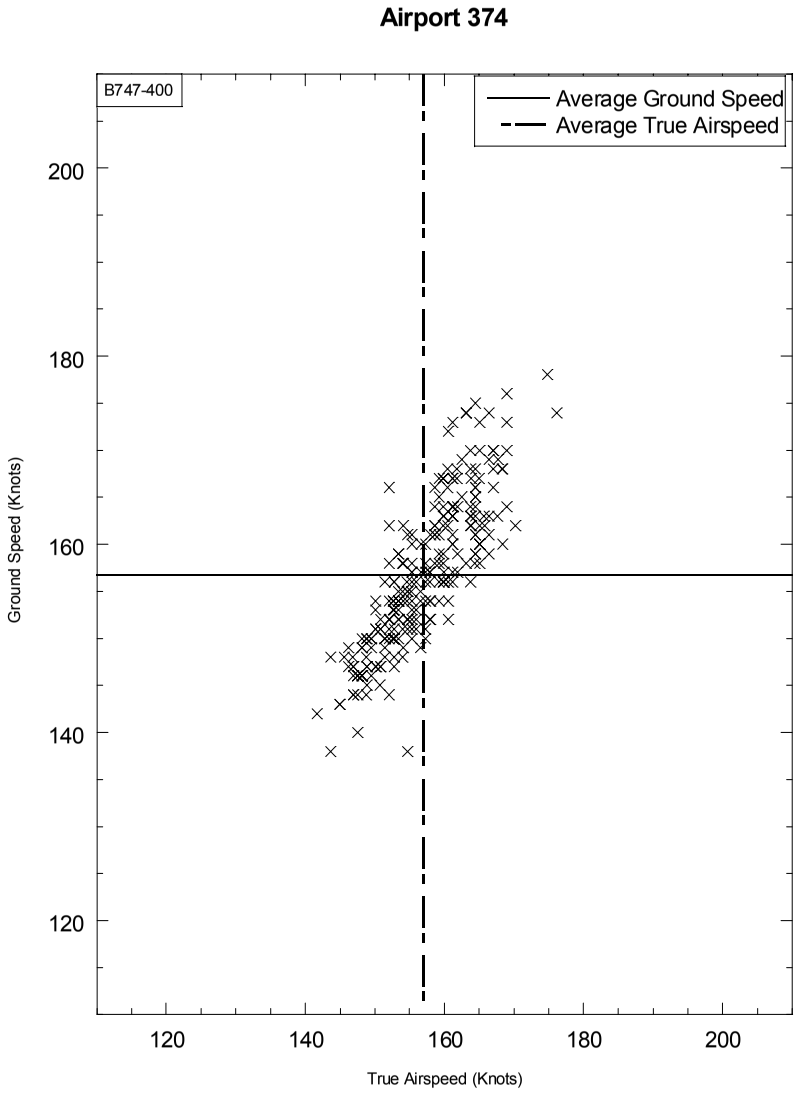

FIGURE C-58. GROUND SPEED VS TRUE AIRSPEED AT TOUCHDOWN, AIRPORT 374 ELEVATION > 5000 FEET

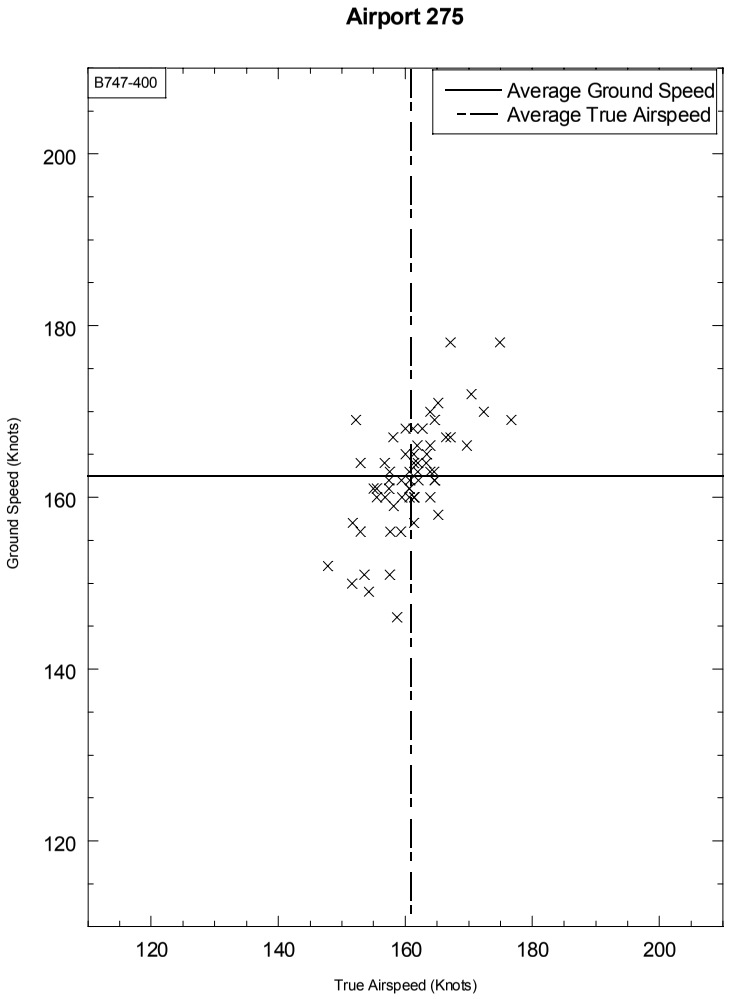

FIGURE C-59. GROUND SPEED VS TRUE AIRSPEED AT TOUCHDOWN, AIRPORT 275 ELEVATION > 5000 FEET

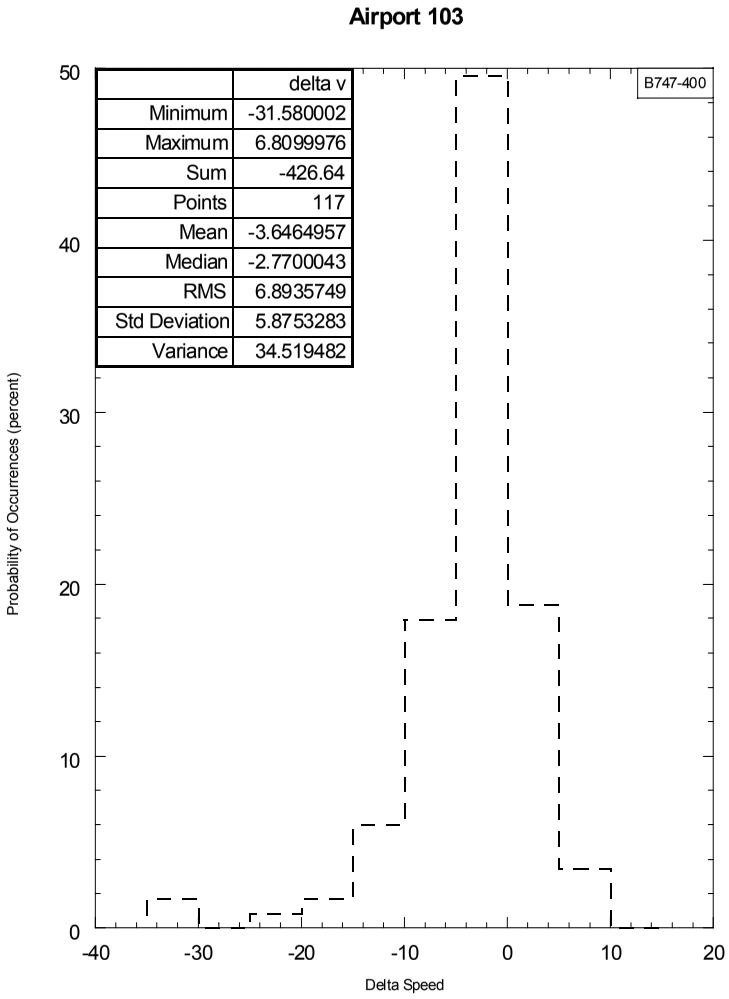

FIGURE C-60. DELTA V (GROUND SPEED-TRUE AIRSPEED) AT TOUCHDOWN, AIRPORT 103 ELEVATION < 500 FEET

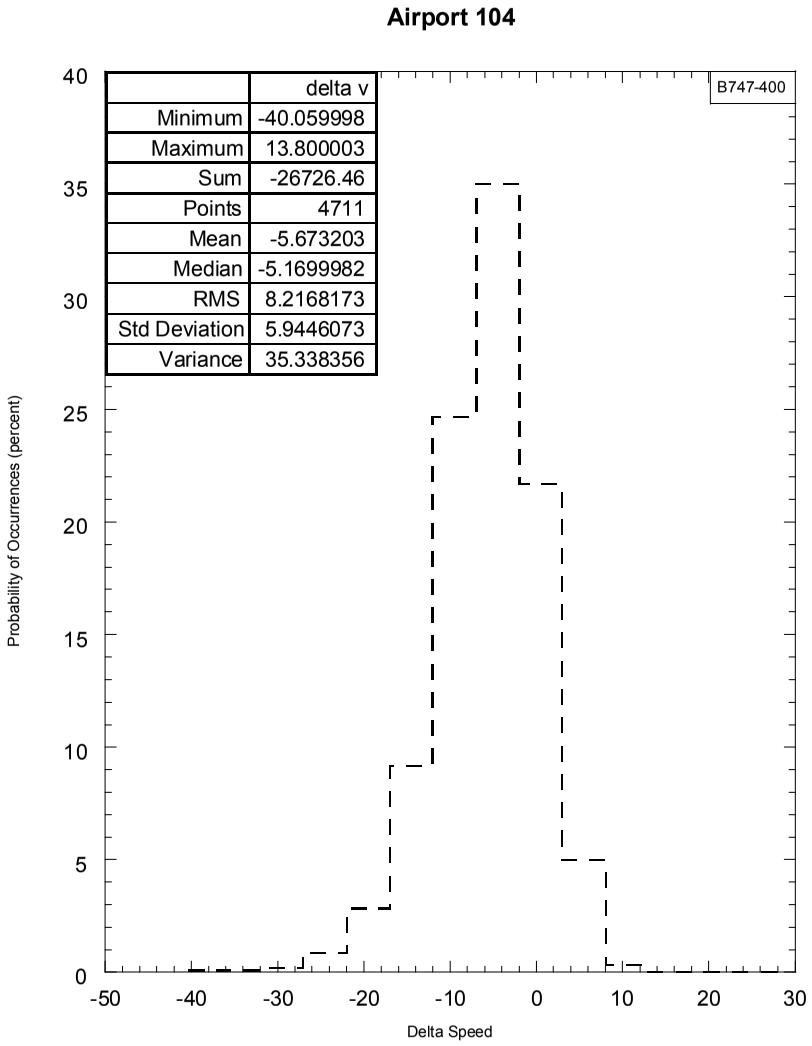

FIGURE C-61. DELTA V (GROUND SPEED-TRUE AIRSPEED) AT TOUCHDOWN, AIRPORT 104 ELEVATION < 500 FEET

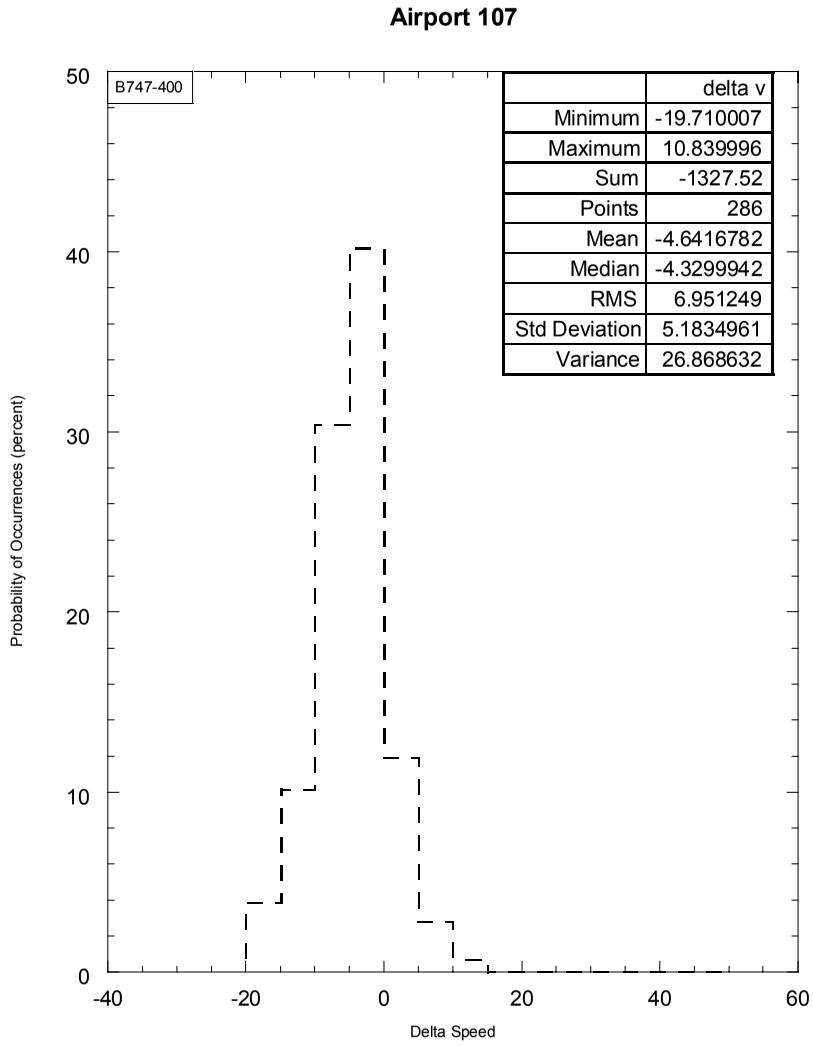

FIGURE C-62. DELTA V (GROUND SPEED-TRUE AIRSPEED) AT TOUCHDOWN, AIRPORT 107 ELEVATION < 500 FEET

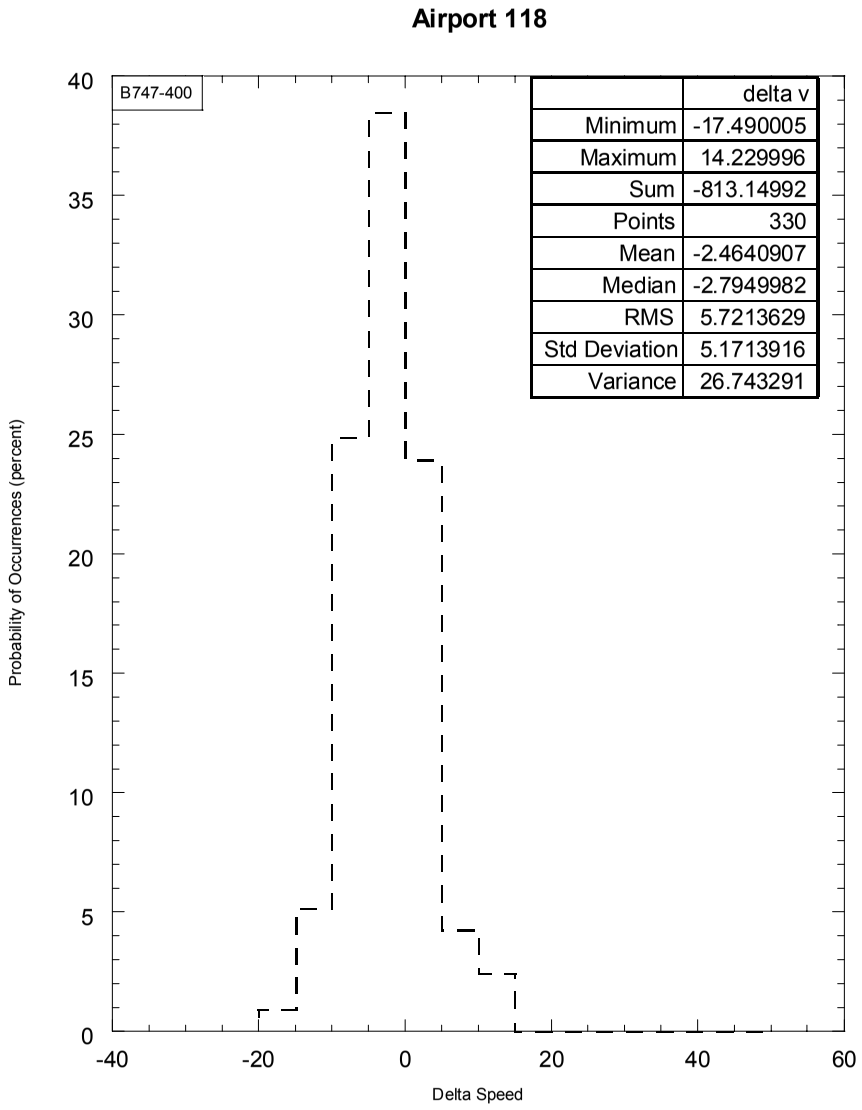

FIGURE C-63. DELTA V (GROUND SPEED-TRUE AIRSPEED) AT TOUCHDOWN, AIRPORT 118 ELEVATION < 500 FEET

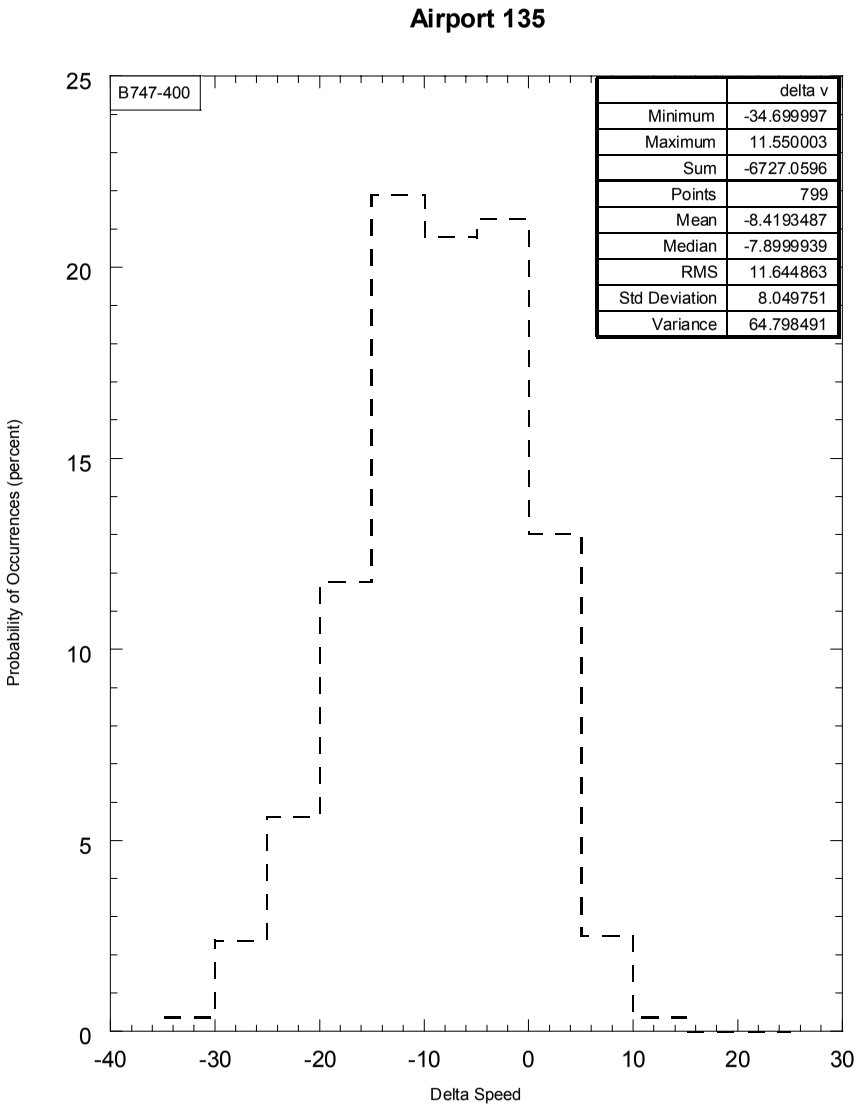

FIGURE C-64. DELTA V (GROUND SPEED-TRUE AIRSPEED) AT TOUCHDOWN, AIRPORT 135 ELEVATION < 500 FEET

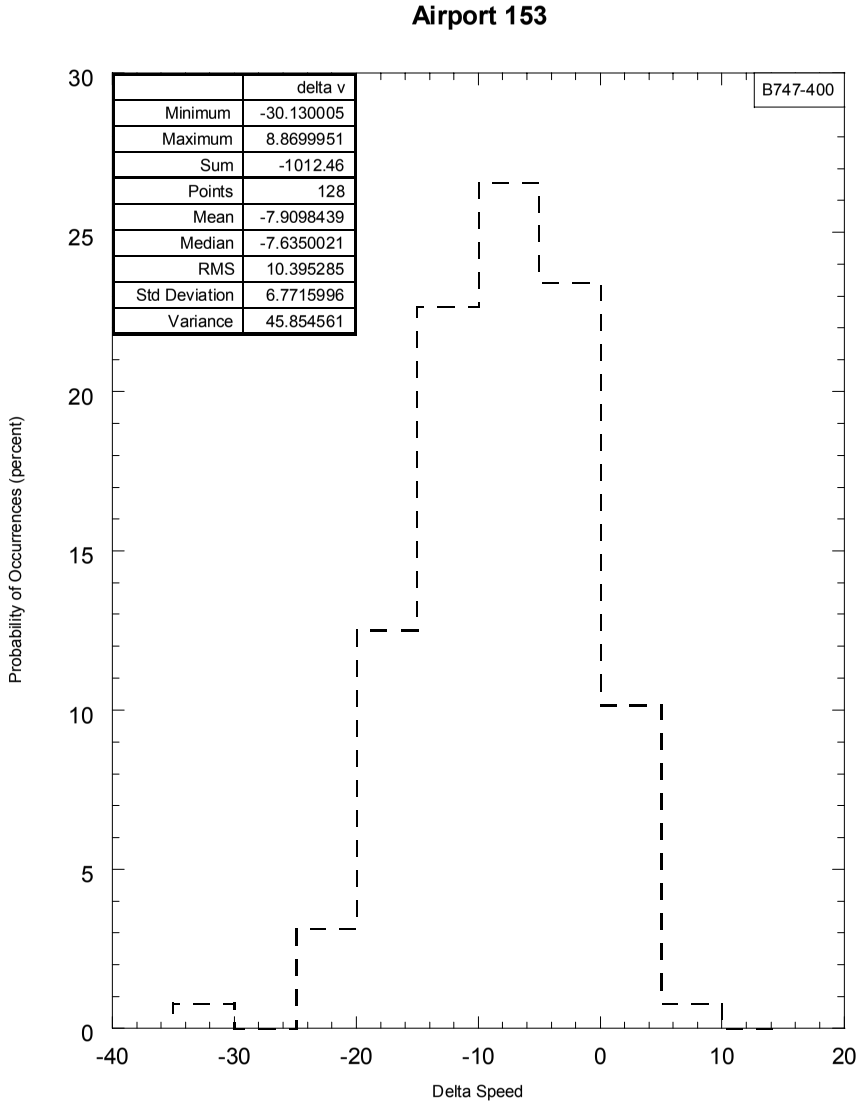

FIGURE C-65. DELTA V (GROUND SPEED-TRUE AIRSPEED) AT TOUCHDOWN, AIRPORT 153 ELEVATION < 500 FEET

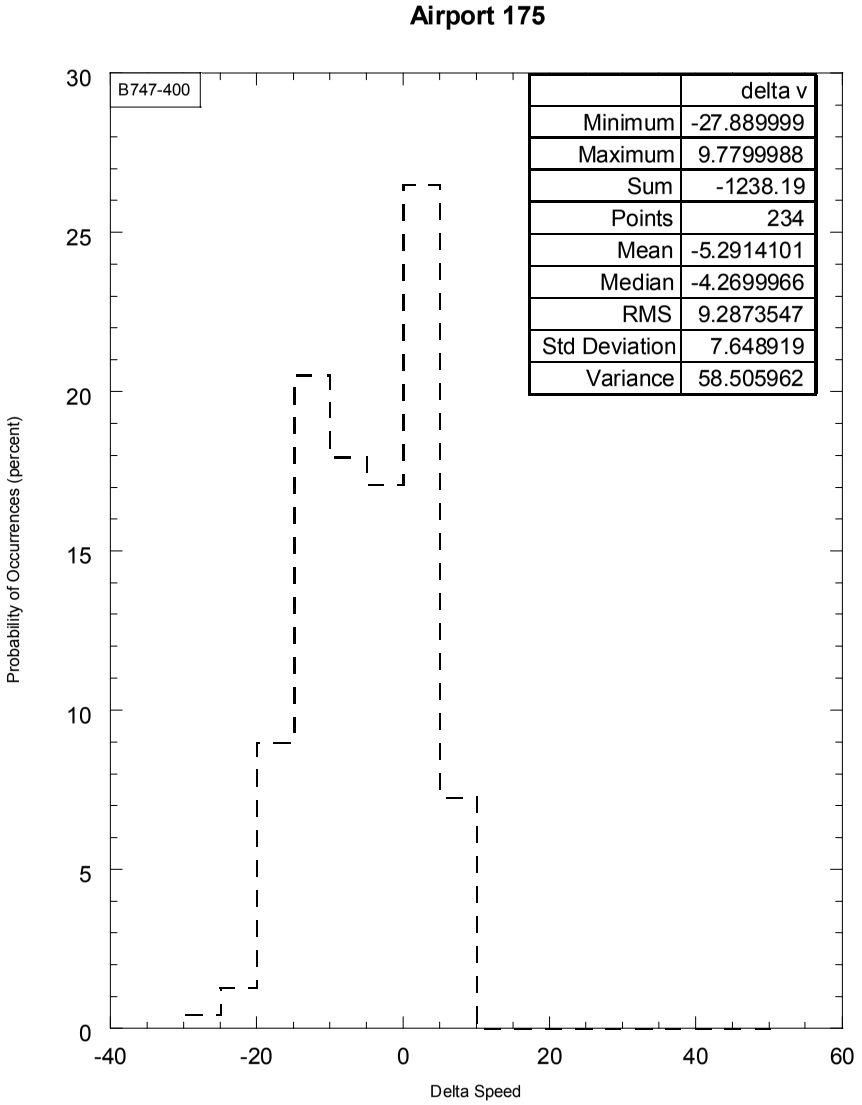

FIGURE C-66. DELTA V (GROUND SPEED-TRUE AIRSPEED) AT TOUCHDOWN, AIRPORT 175 ELEVATION < 500 FEET

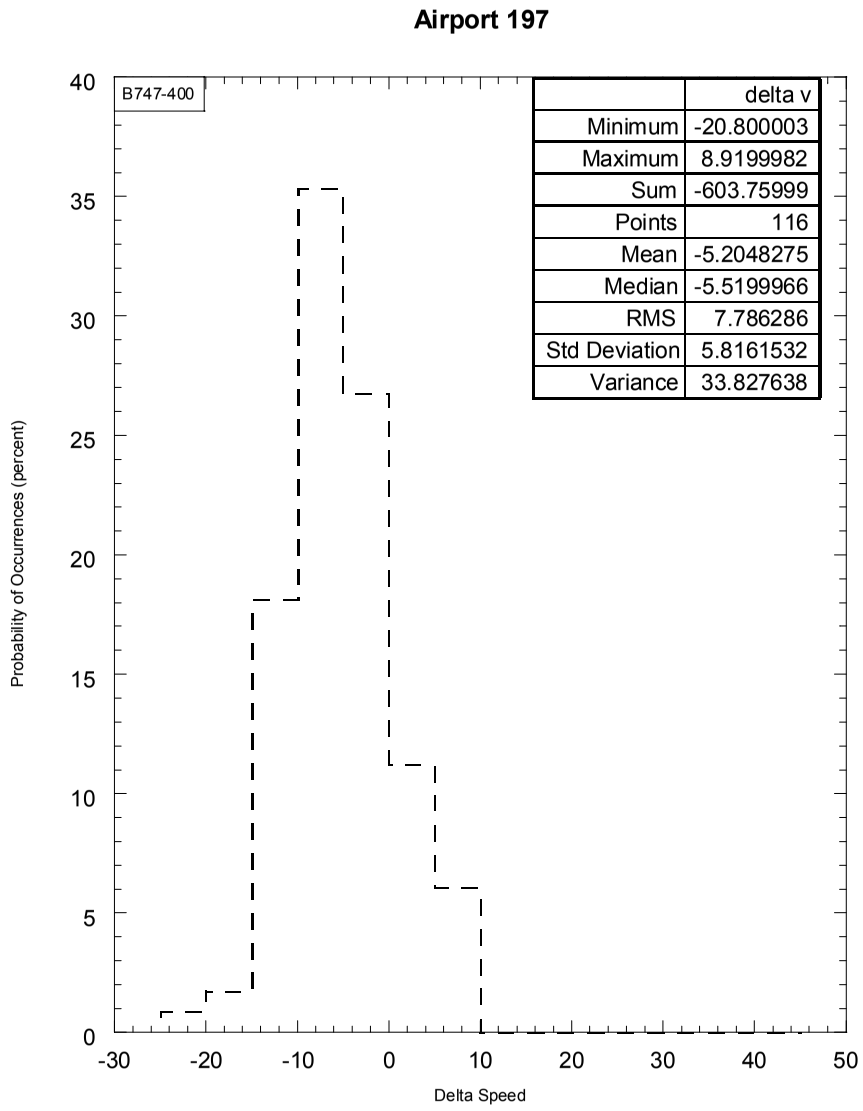

FIGURE C-67. DELTA V (GROUND SPEED-TRUE AIRSPEED) AT TOUCHDOWN, AIRPORT 197 ELEVATION < 500 FEET

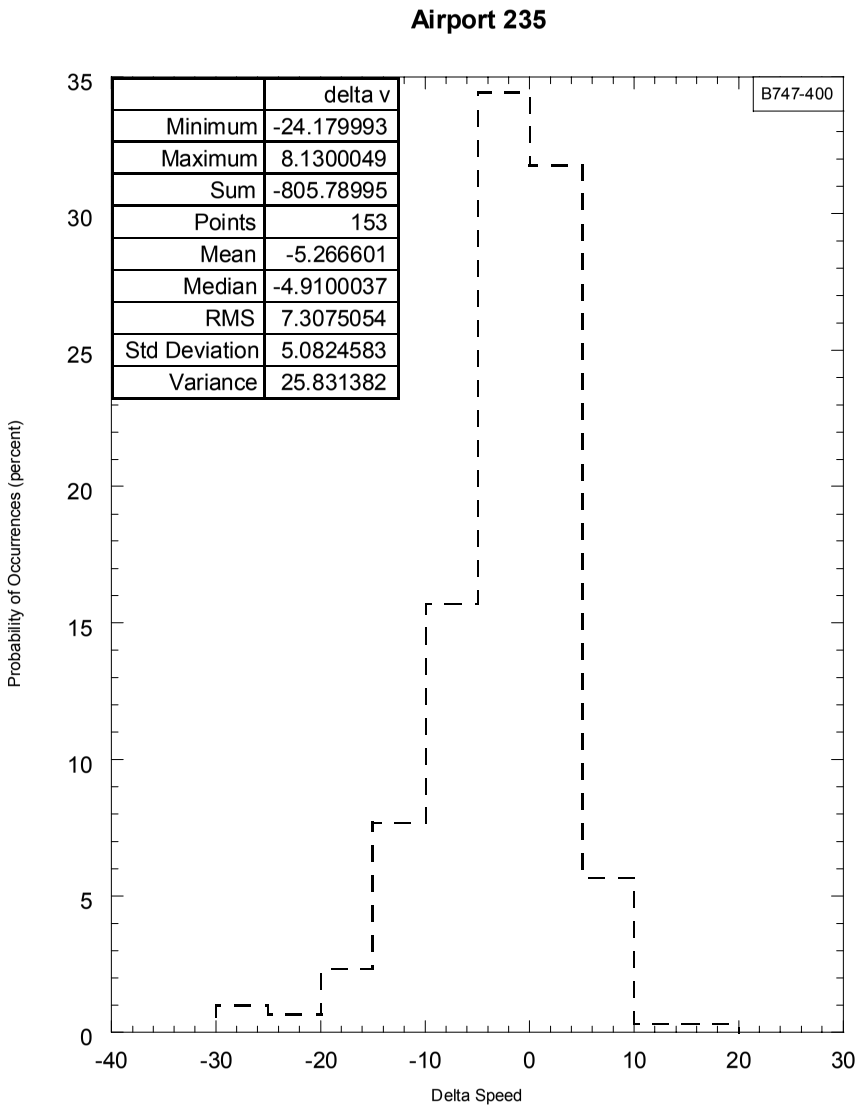

FIGURE C-68. DELTA V (GROUND SPEED-TRUE AIRSPEED) AT TOUCHDOWN, AIRPORT 235 ELEVATION < 500 FEET

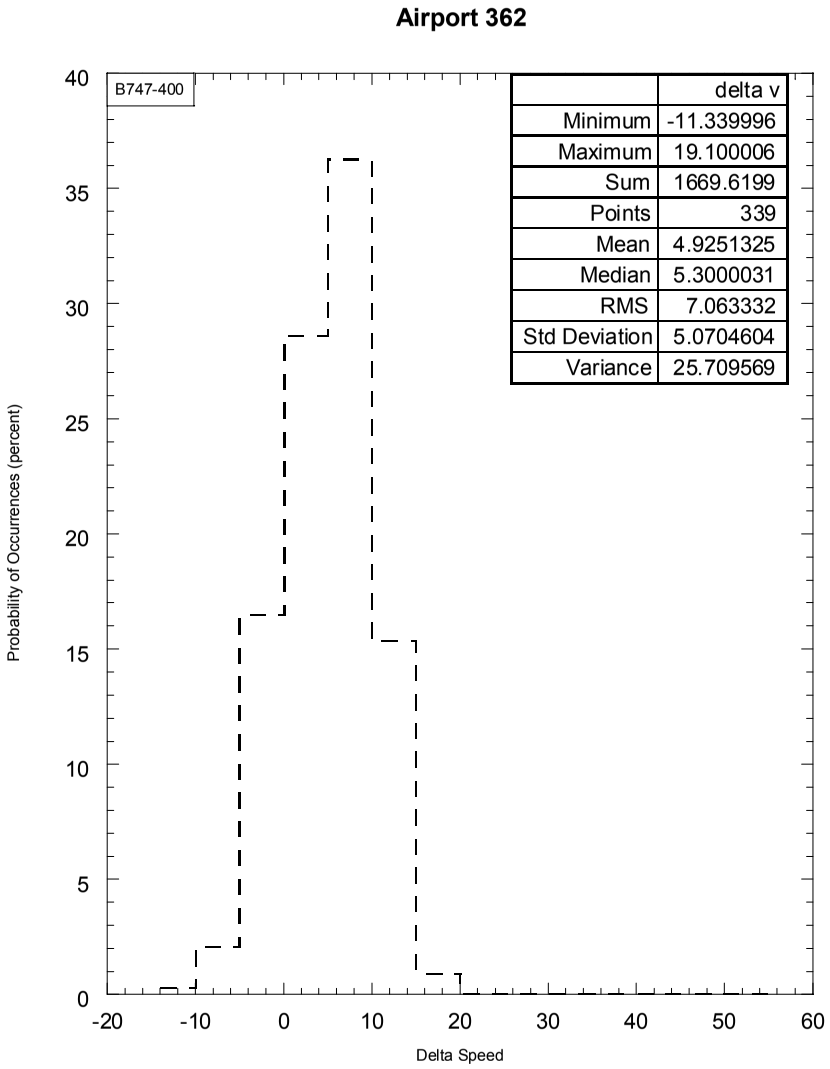

FIGURE C-69. DELTA V (GROUND SPEED-TRUE AIRSPEED) AT TOUCHDOWN, AIRPORT 362 ELEVATION < 500 FEET

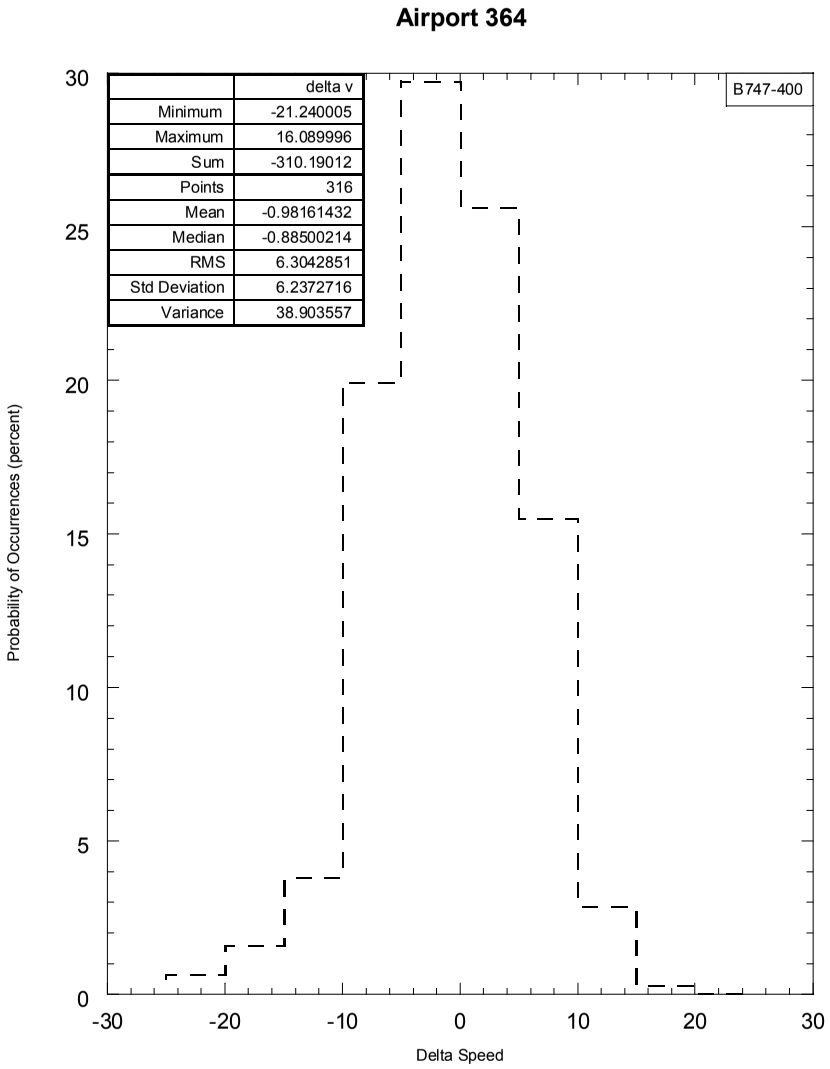

FIGURE C-70. DELTA V (GROUND SPEED-TRUE AIRSPEED) AT TOUCHDOWN, AIRPORT 364 ELEVATION < 500 FEET

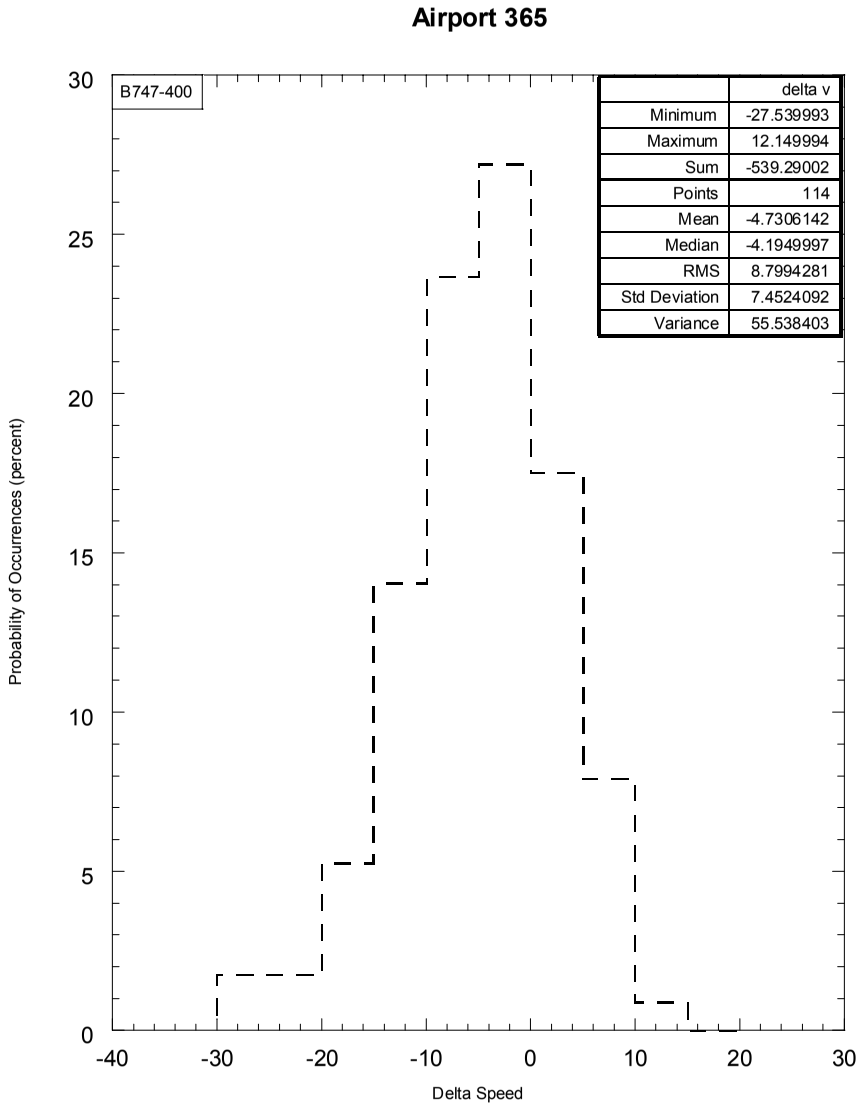

FIGURE C-71. DELTA V (GROUND SPEED-TRUE AIRSPEED) AT TOUCHDOWN, AIRPORT 365 ELEVATION < 500 FEET

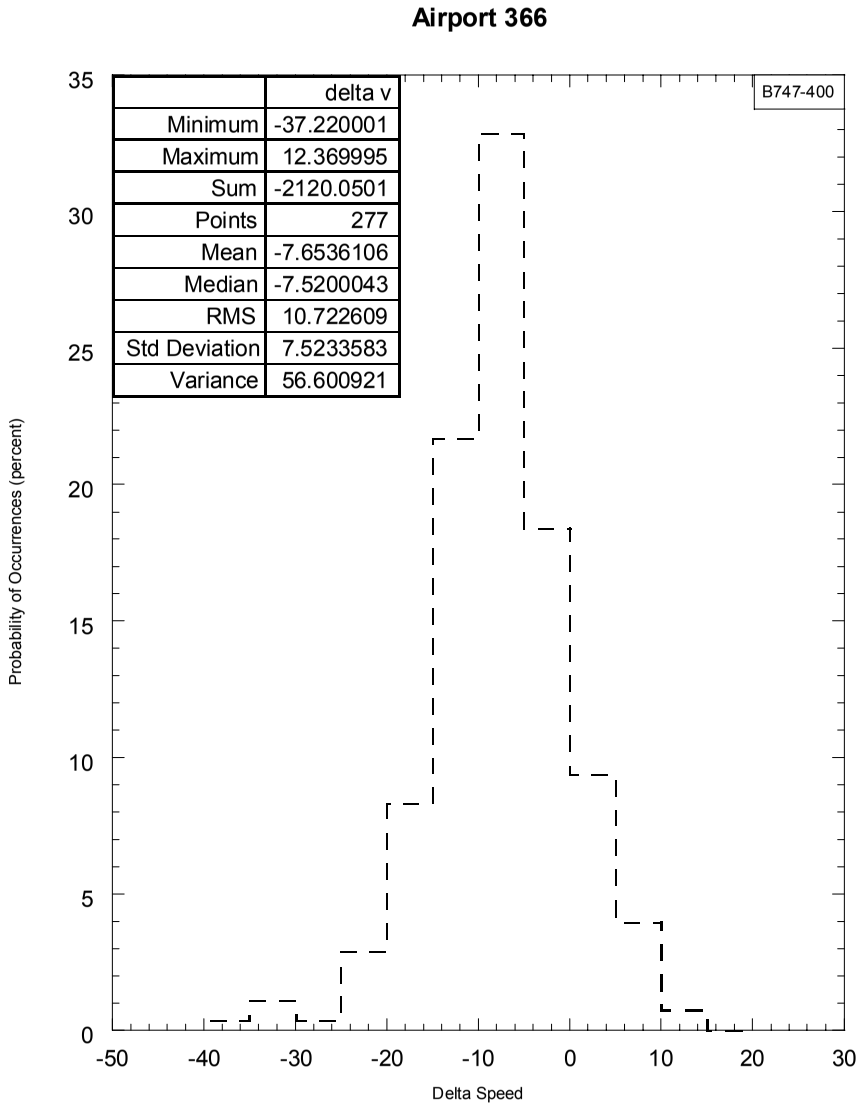

FIGURE C-72. DELTA V (GROUND SPEED-TRUE AIRSPEED) AT TOUCHDOWN, AIRPORT 366 ELEVATION < 500 FEET

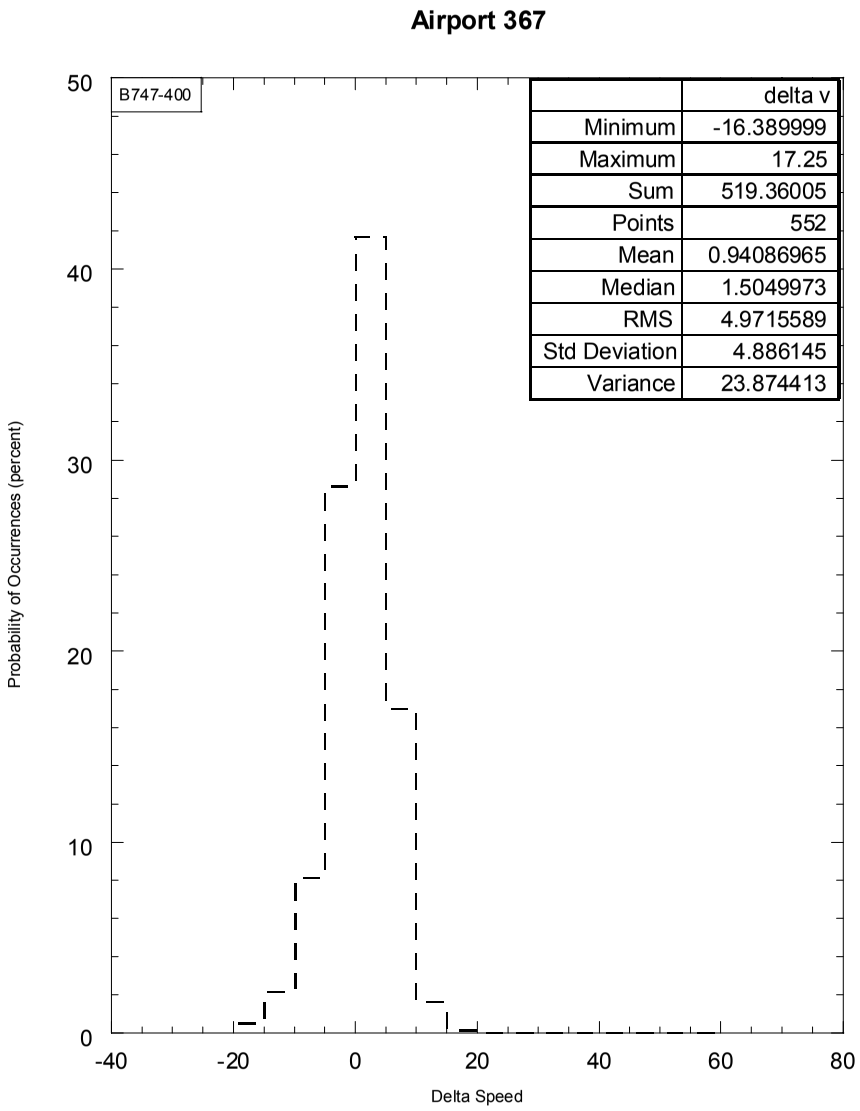

FIGURE C-73. DELTA V (GROUND SPEED-TRUE AIRSPEED) AT TOUCHDOWN, AIRPORT 367 ELEVATION < 500 FEET

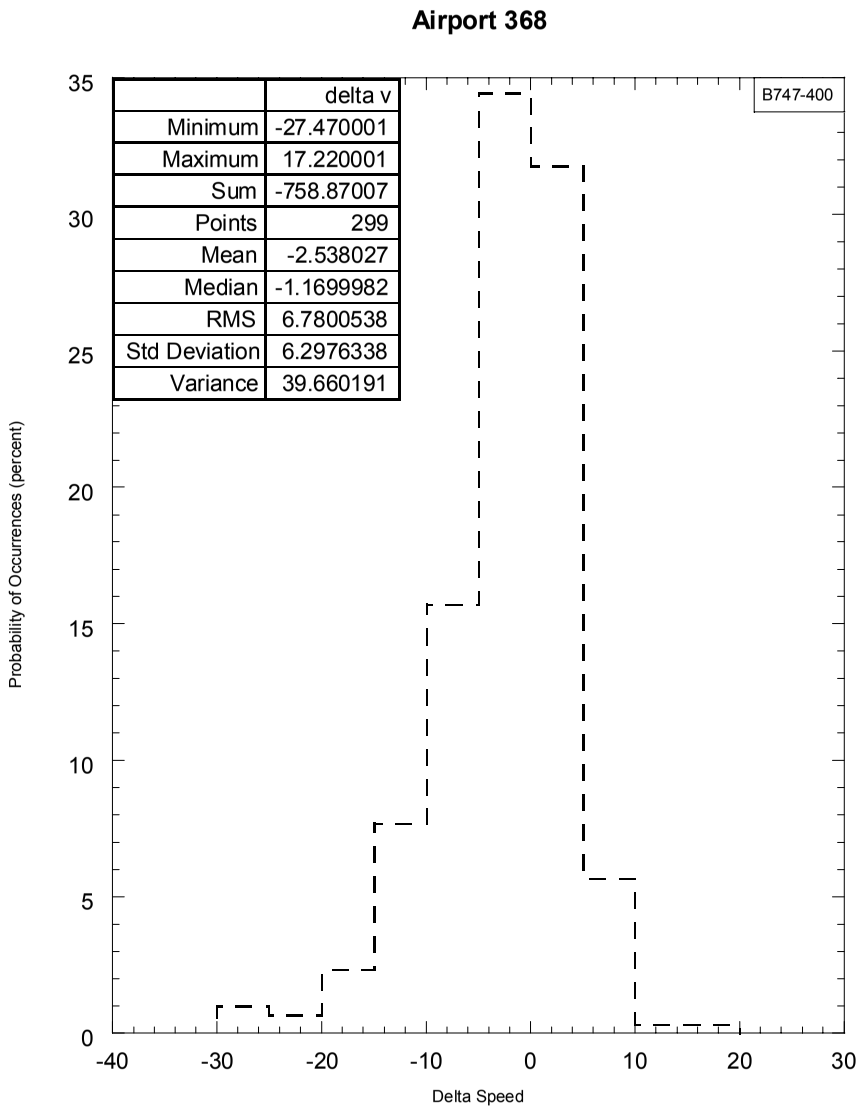

FIGURE C-74. DELTA V (GROUND SPEED-TRUE AIRSPEED) AT TOUCHDOWN, AIRPORT 368 ELEVATION < 500 FEET

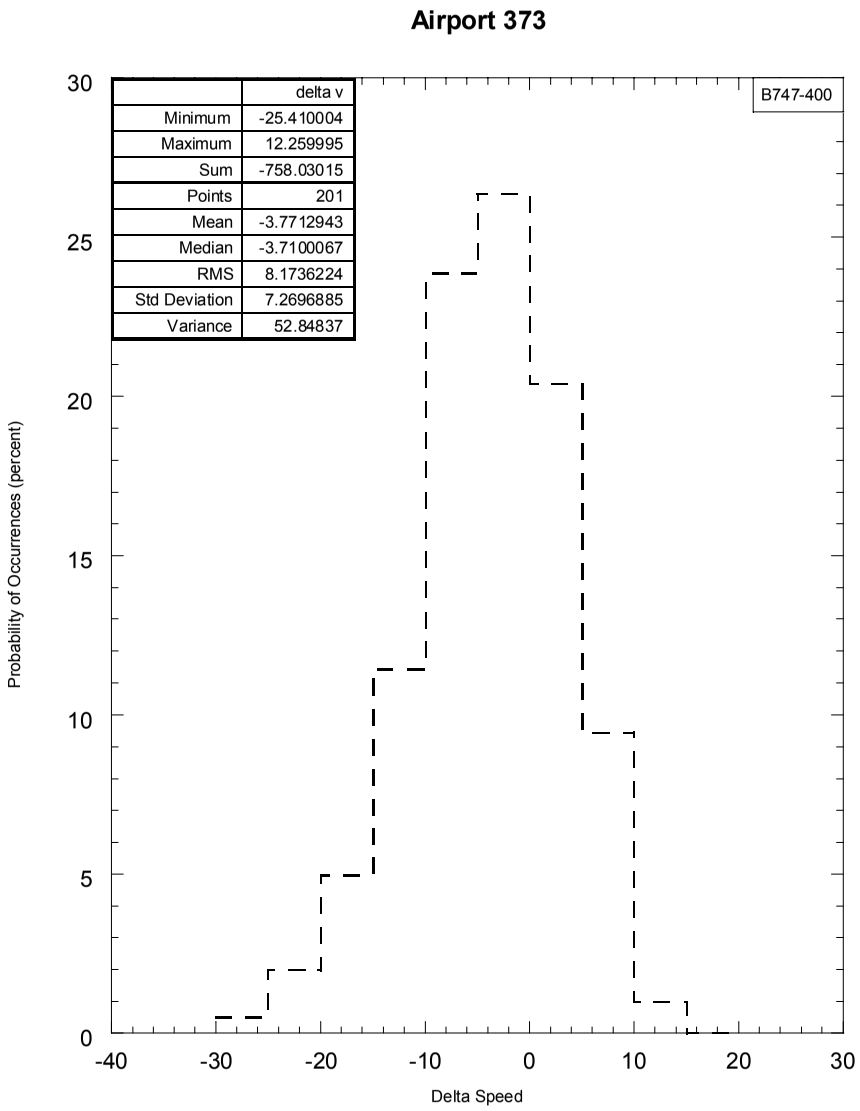

FIGURE C-75 DELTA V (GROUND SPEED-TRUE AIRSPEED) AT TOUCHDOWN, AIRPORT 373 ELEVATION < 500 FEET

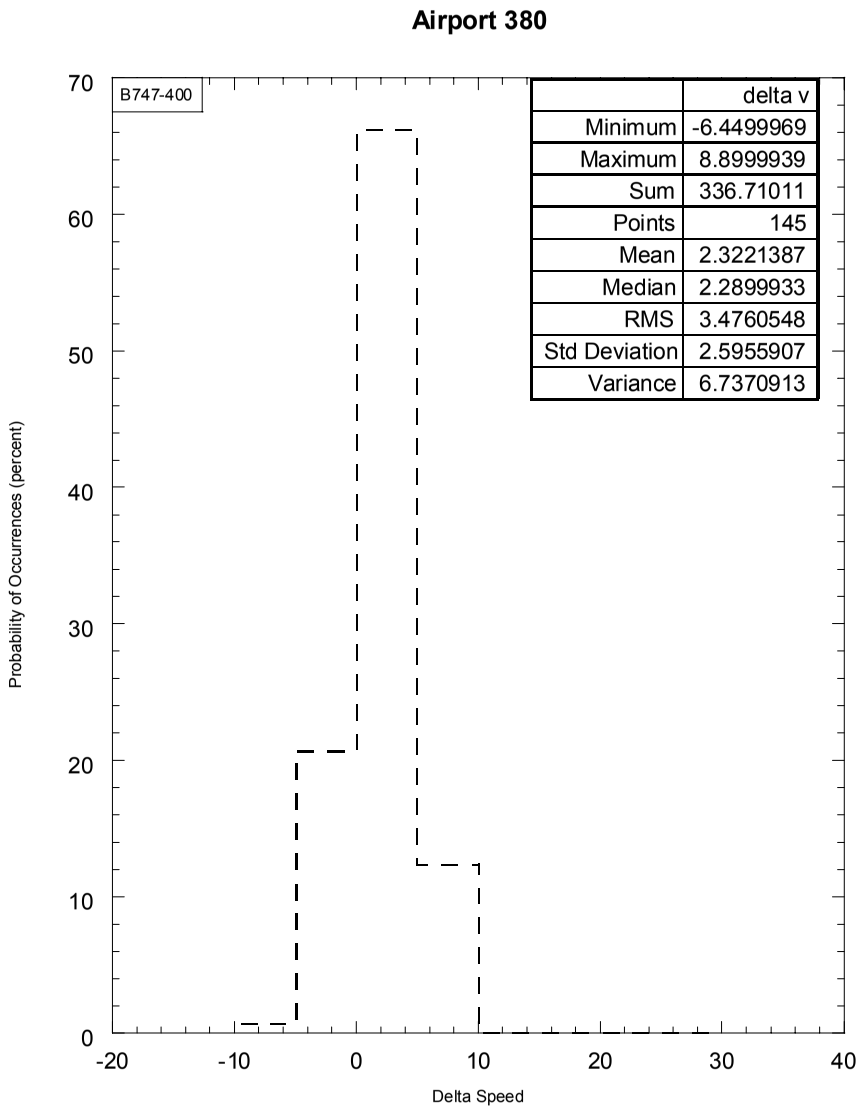

FIGURE C-76. DELTA V (GROUND SPEED-TRUE AIRSPEED) AT TOUCHDOWN, AIRPORT 380 ELEVATION < 500 FEET

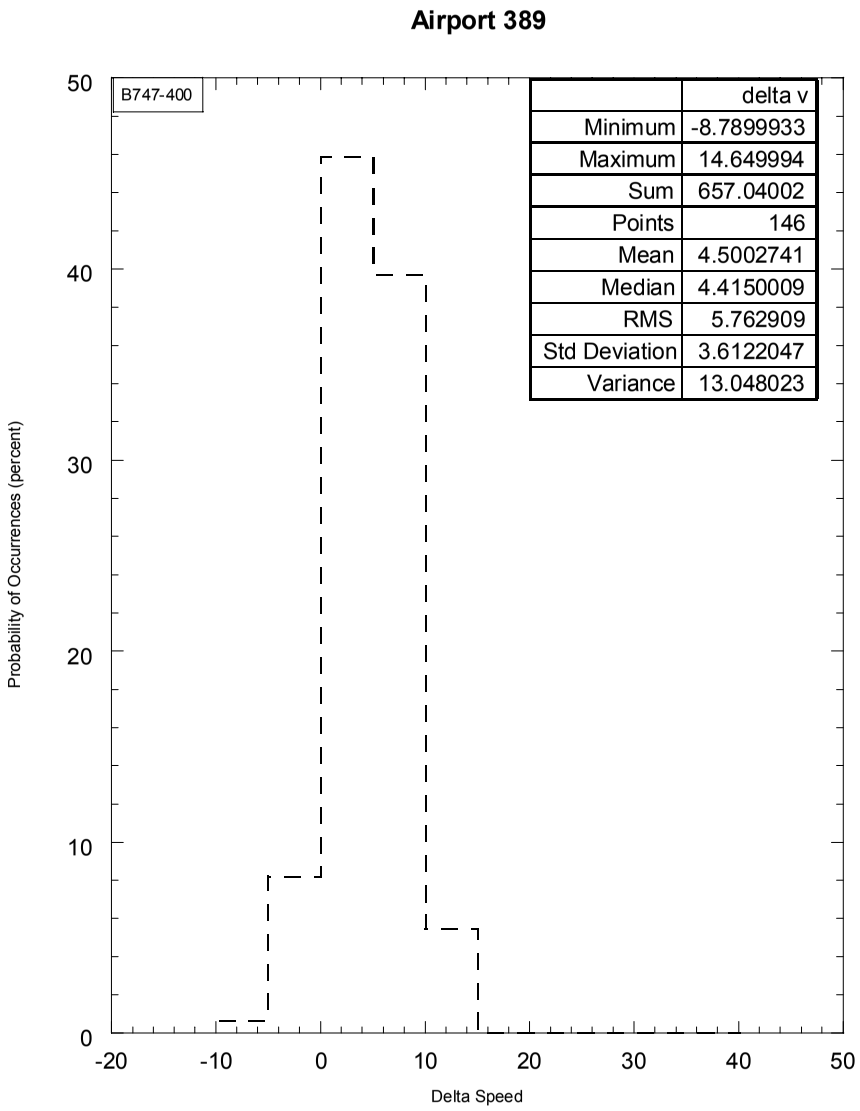

FIGURE C-77 DELTA V (GROUND SPEED-TRUE AIRSPEED) AT TOUCHDOWN, AIRPORT 389 ELEVATION < 500 FEET

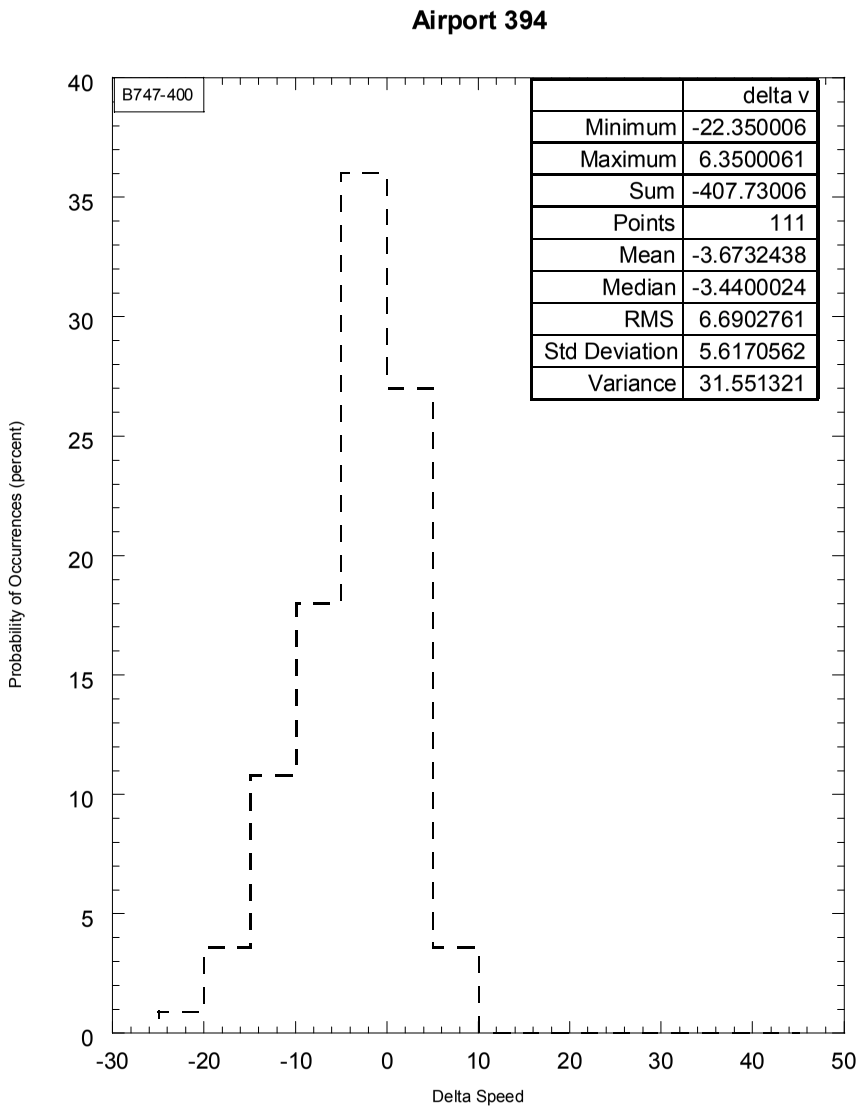

FIGURE C-78. DELTA V (GROUND SPEED-TRUE AIRSPEED) AT TOUCHDOWN, AIRPORT 394 ELEVATION < 500 FEET

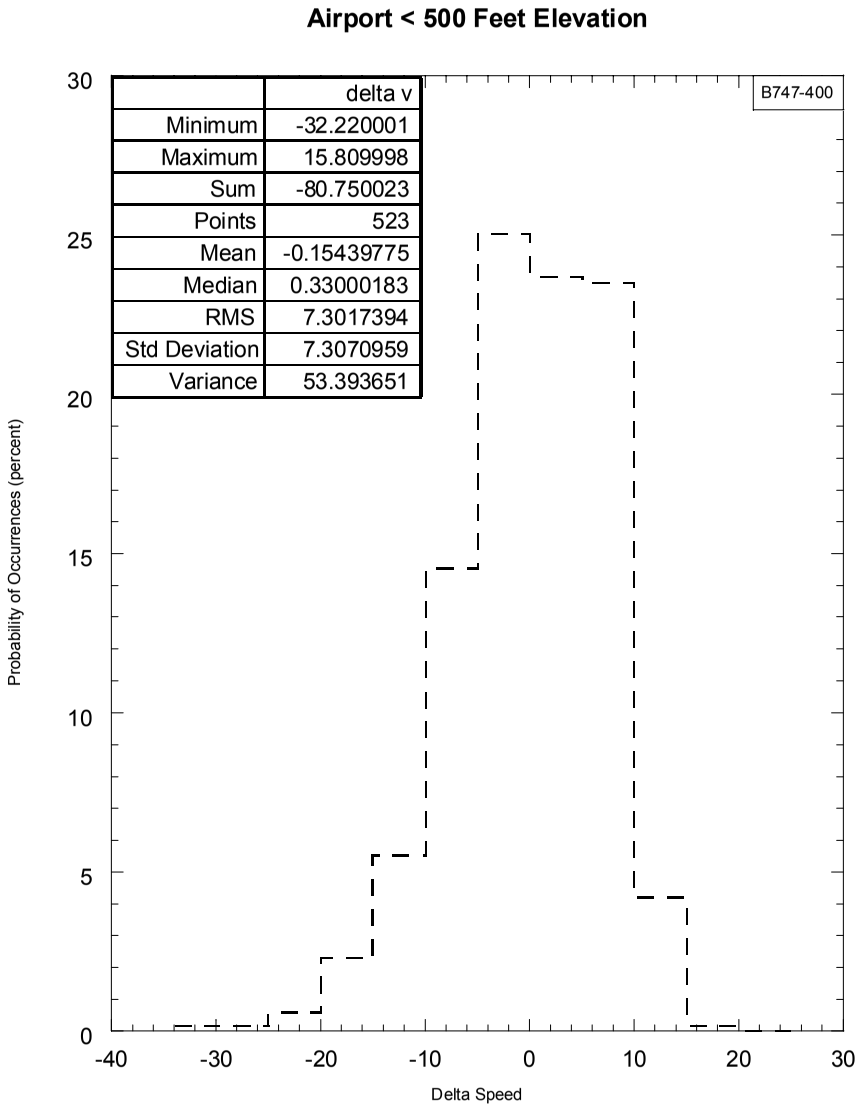

FIGURE C-79 DELTA V (GROUND SPEED-TRUE AIRSPEED) AT TOUCHDOWN, AIRPORTS ELEVATION < 500 FEET

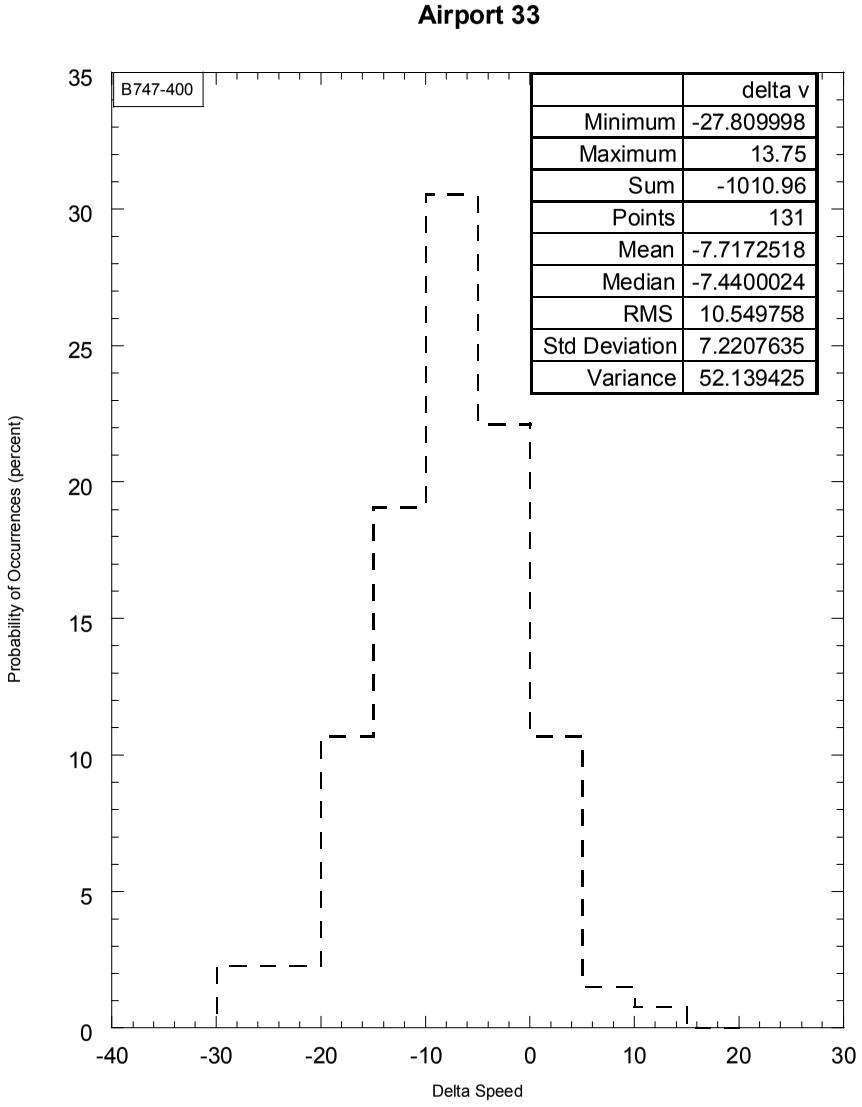

FIGURE C-80. DELTA V (GROUND SPEED-TRUE AIRSPEED) AT TOUCHDOWN, AIRPORT 33 ELEVATION 500-1000 FEET

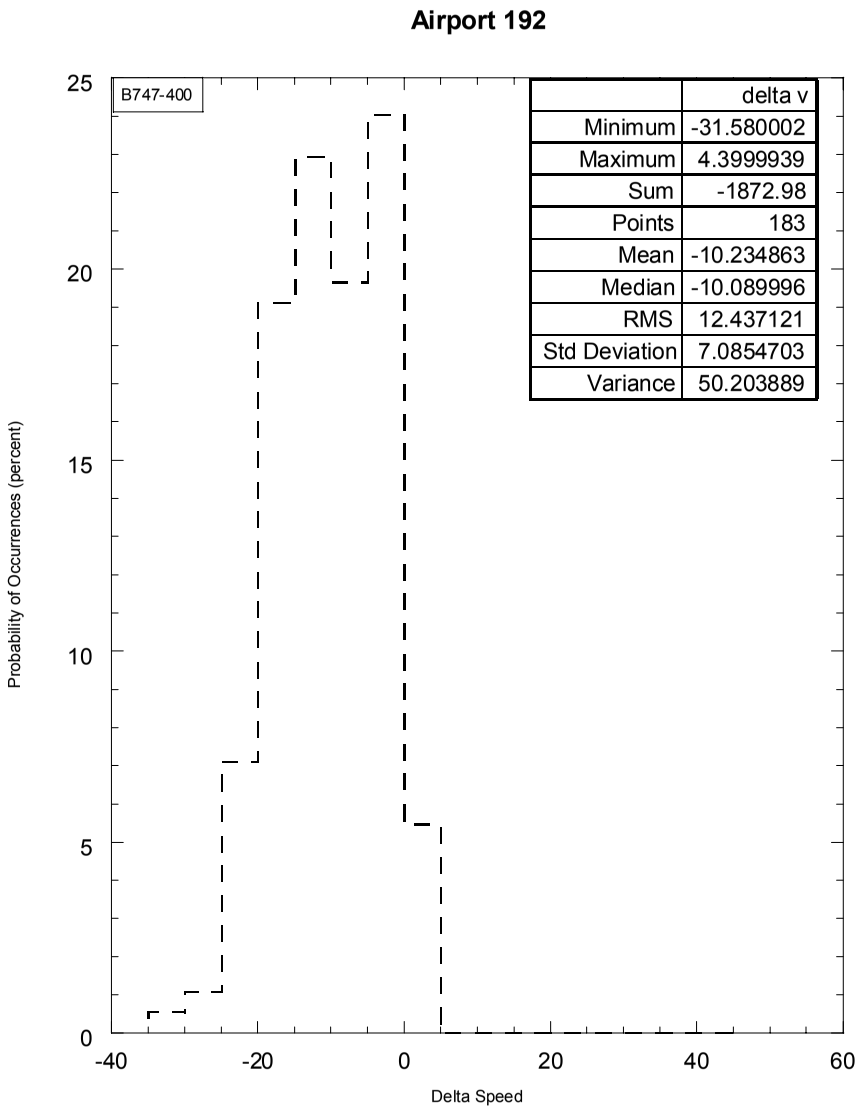

FIGURE C-81 DELTA V (GROUND SPEED-TRUE AIRSPEED) AT TOUCHDOWN, AIRPORT 192 ELEVATION 500-1000 FEET

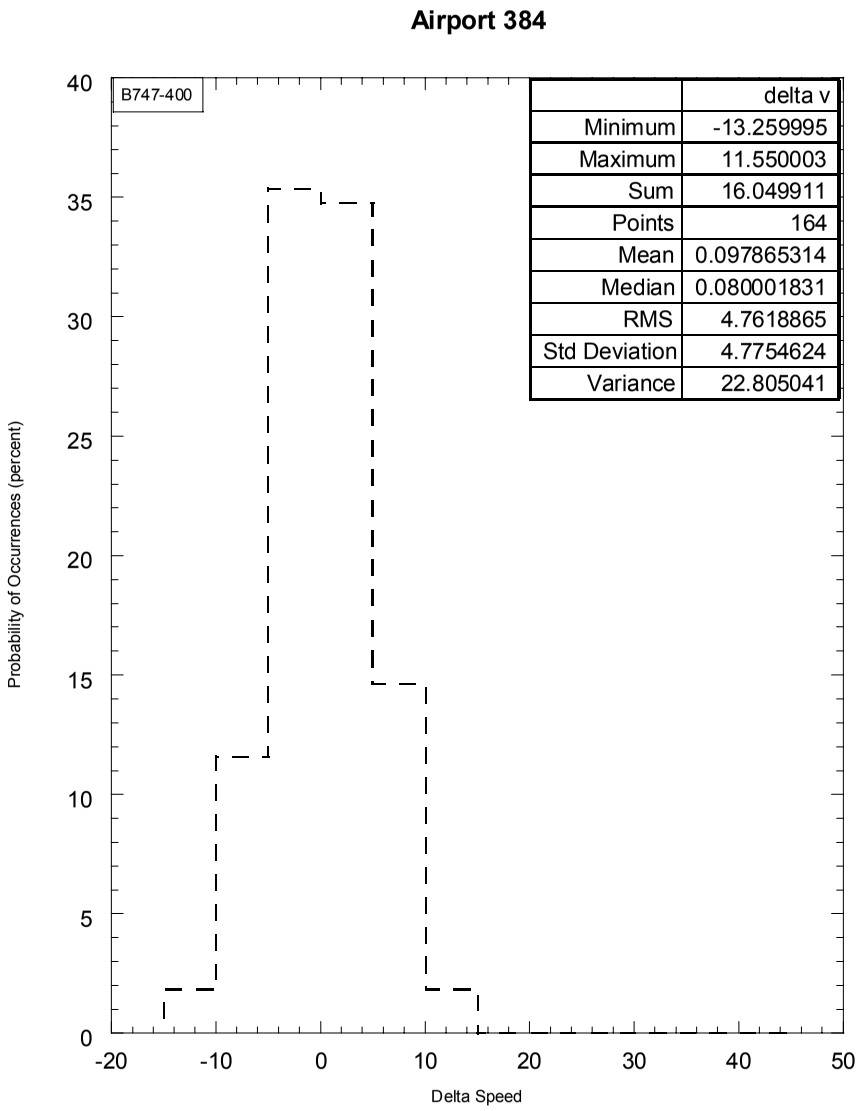

FIGURE C-82. DELTA V (GROUND SPEED-TRUE AIRSPEED) AT TOUCHDOWN, AIRPORT 384 ELEVATION 500-1000 FEET

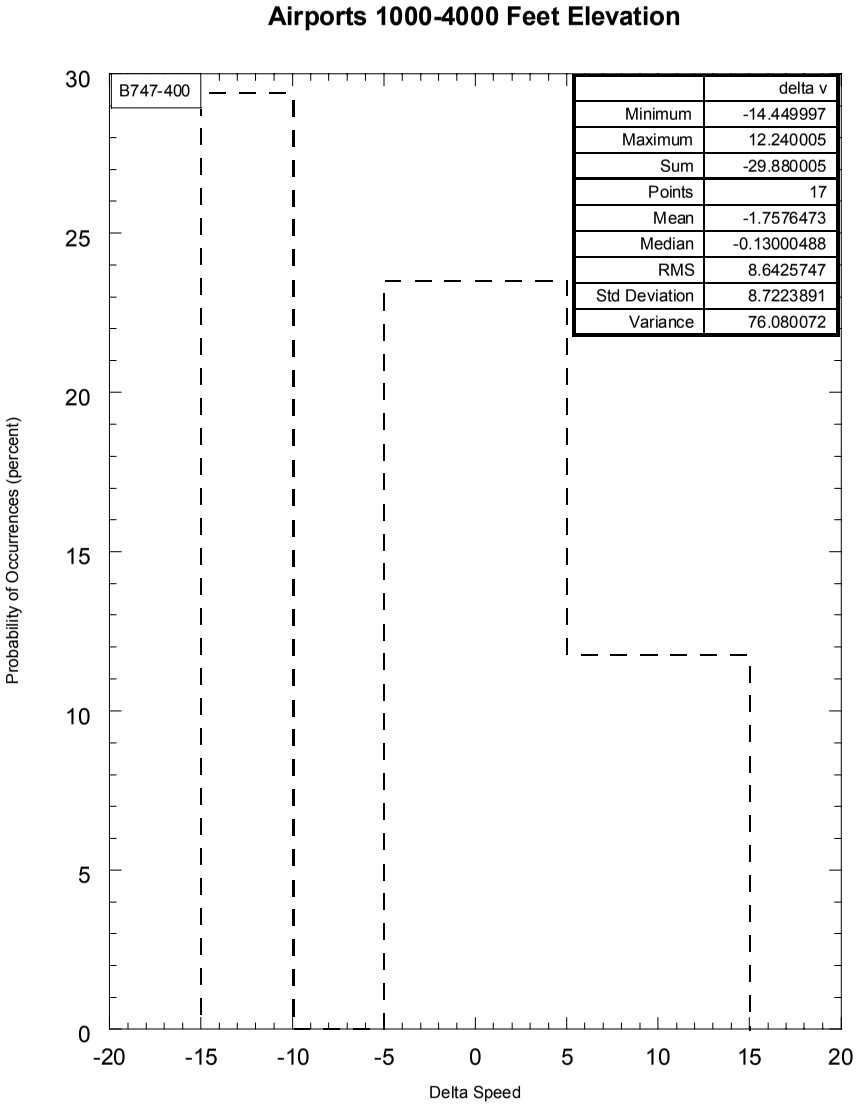

FIGURE C-83 DELTA V (GROUND SPEED-TRUE AIRSPEED) AT TOUCHDOWN, AIRPORTS ELEVATION 1000-4000 FEET

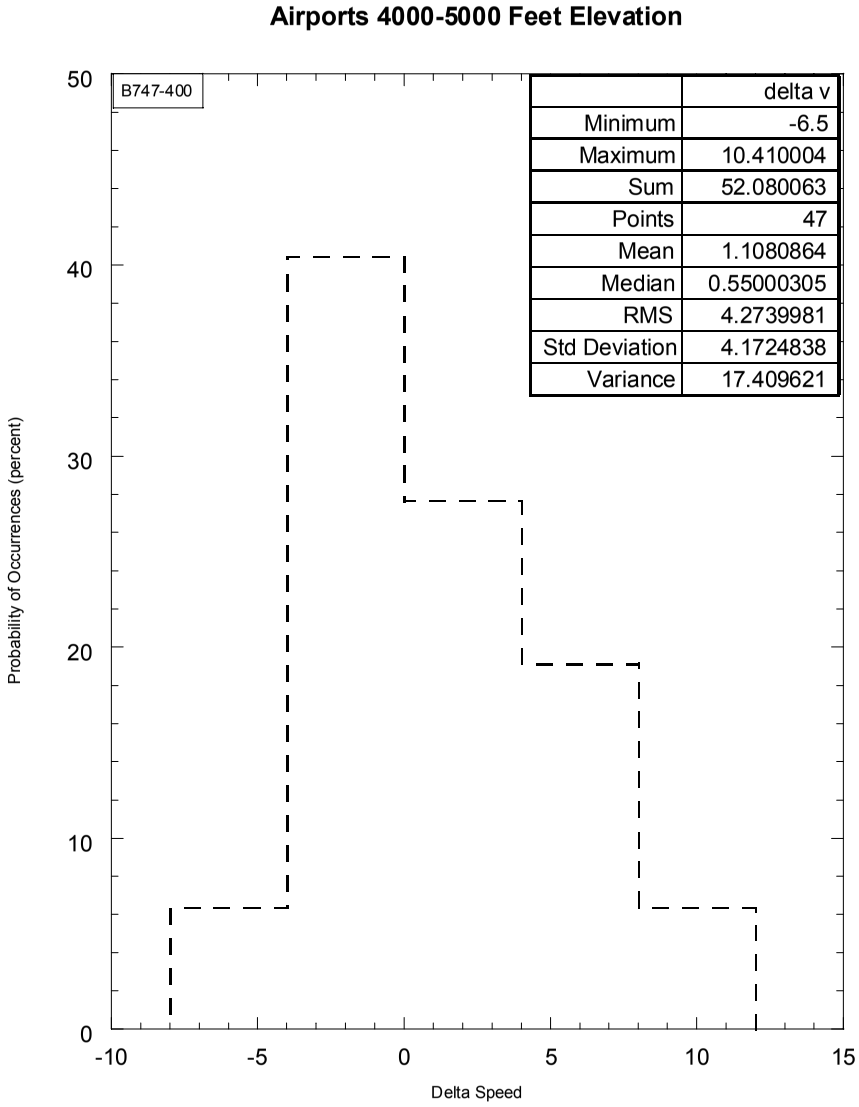

FIGURE C-84. DELTA V (GROUND SPEED-TRUE AIRSPEED) AT TOUCHDOWN, AIRPORTS ELEVATION 4000-5000 FEET

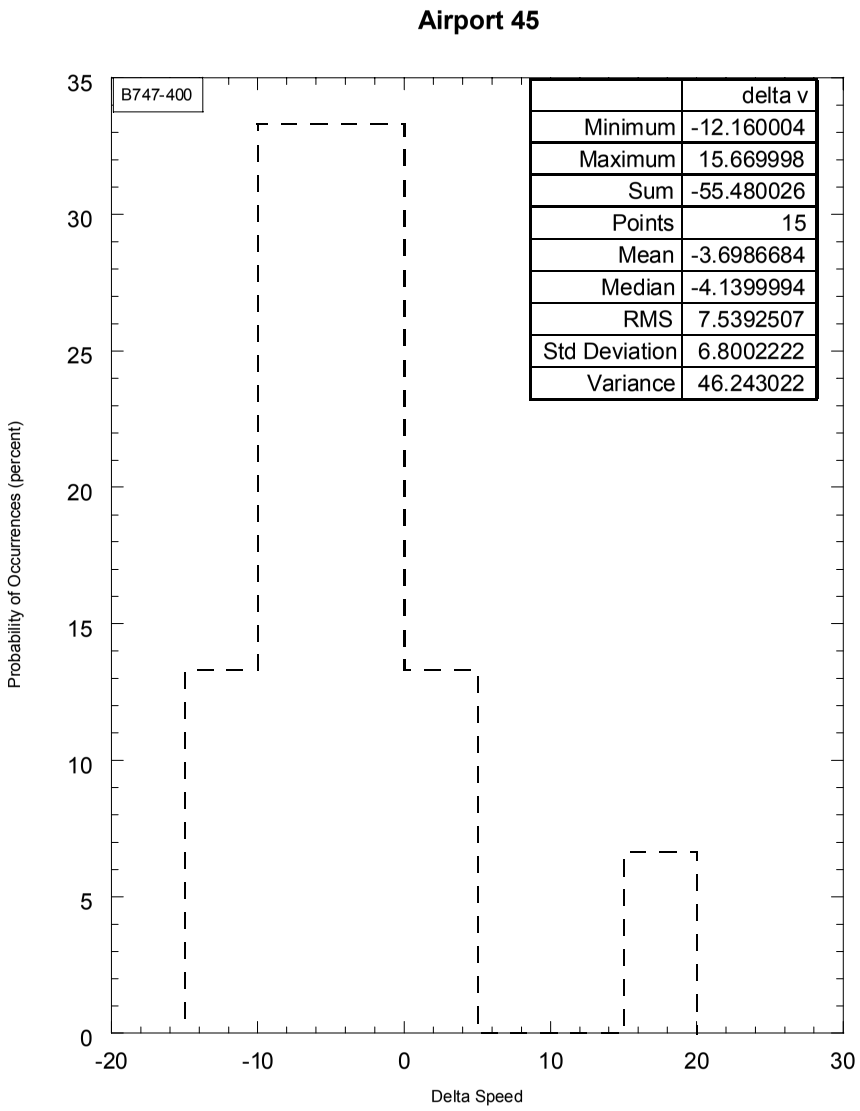

FIGURE C-85 DELTA V (GROUND SPEED-TRUE AIRSPEED) AT TOUCHDOWN, AIRPORT 45 ELEVATION > 5000 FEET

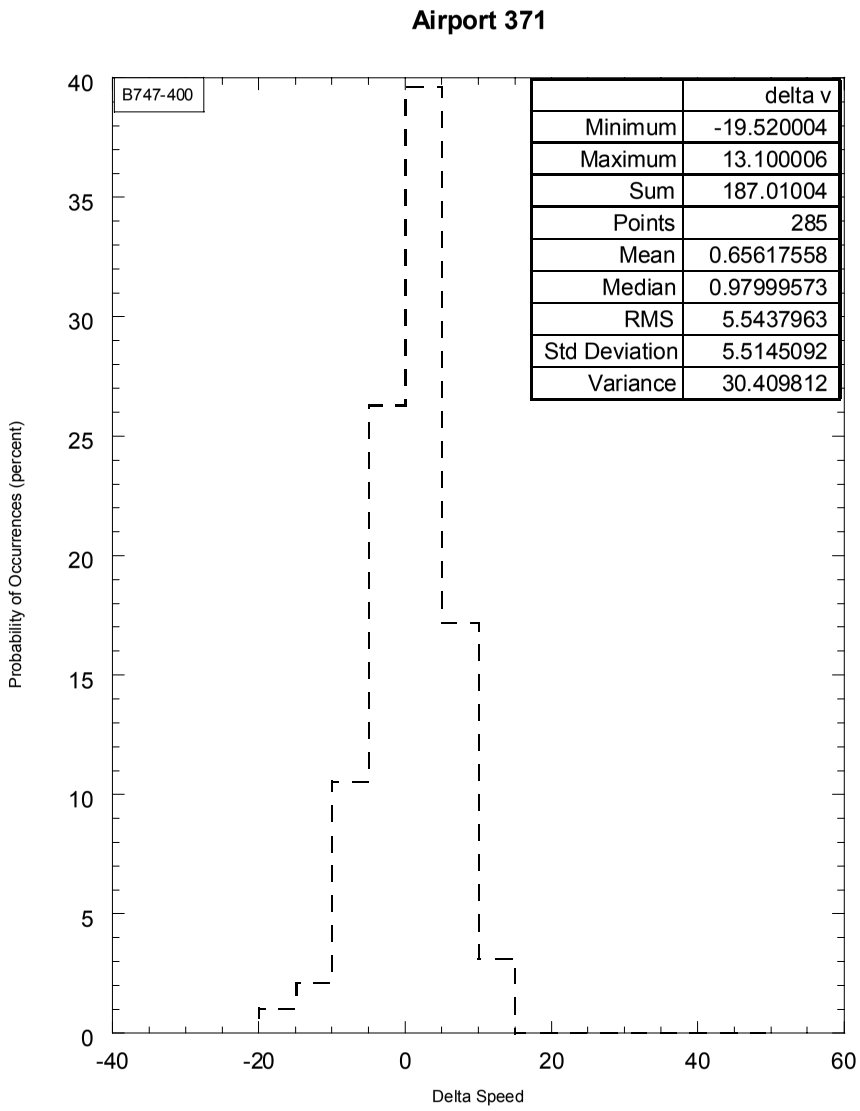

FIGURE C-86. DELTA V (GROUND SPEED-TRUE AIRSPEED) AT TOUCHDOWN, AIRPORT 371 ELEVATION > 5000 FEET

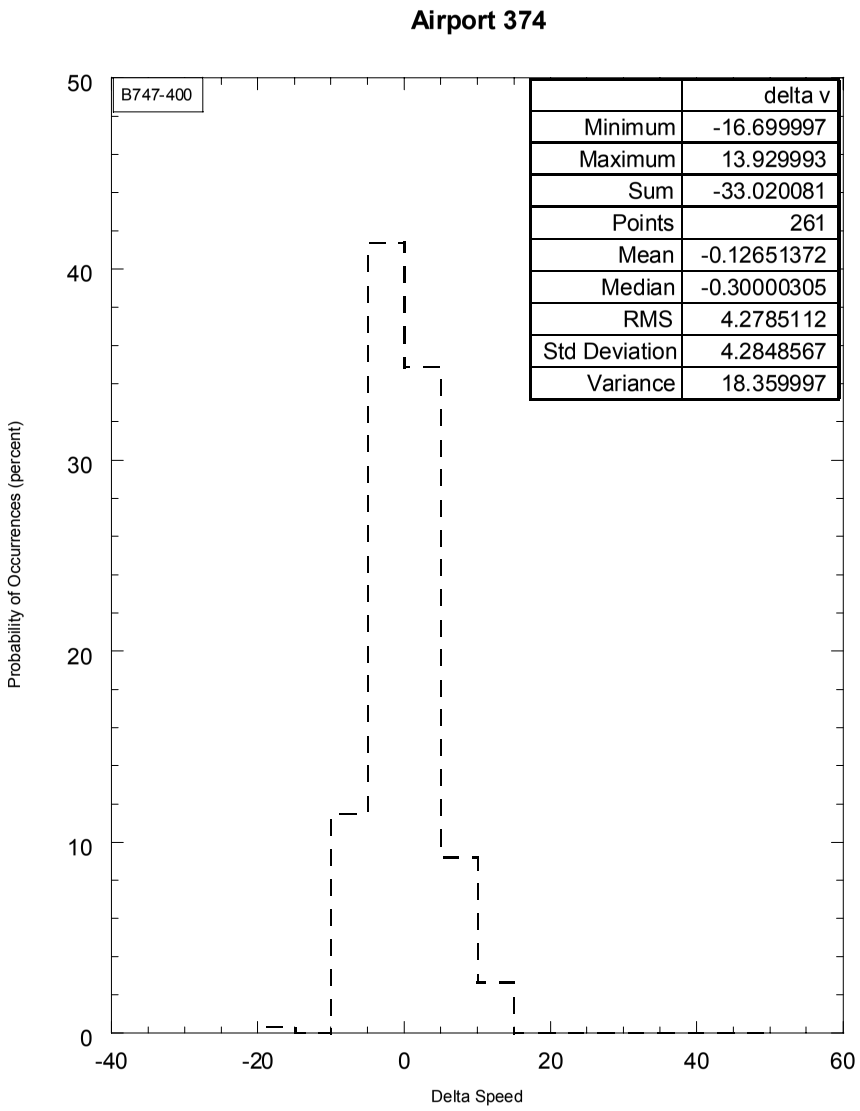

FIGURE C-87. DELTA V (GROUND SPEED-TRUE AIRSPEED) AT TOUCHDOWN, AIRPORT 374 ELEVATION > 5000 FEET

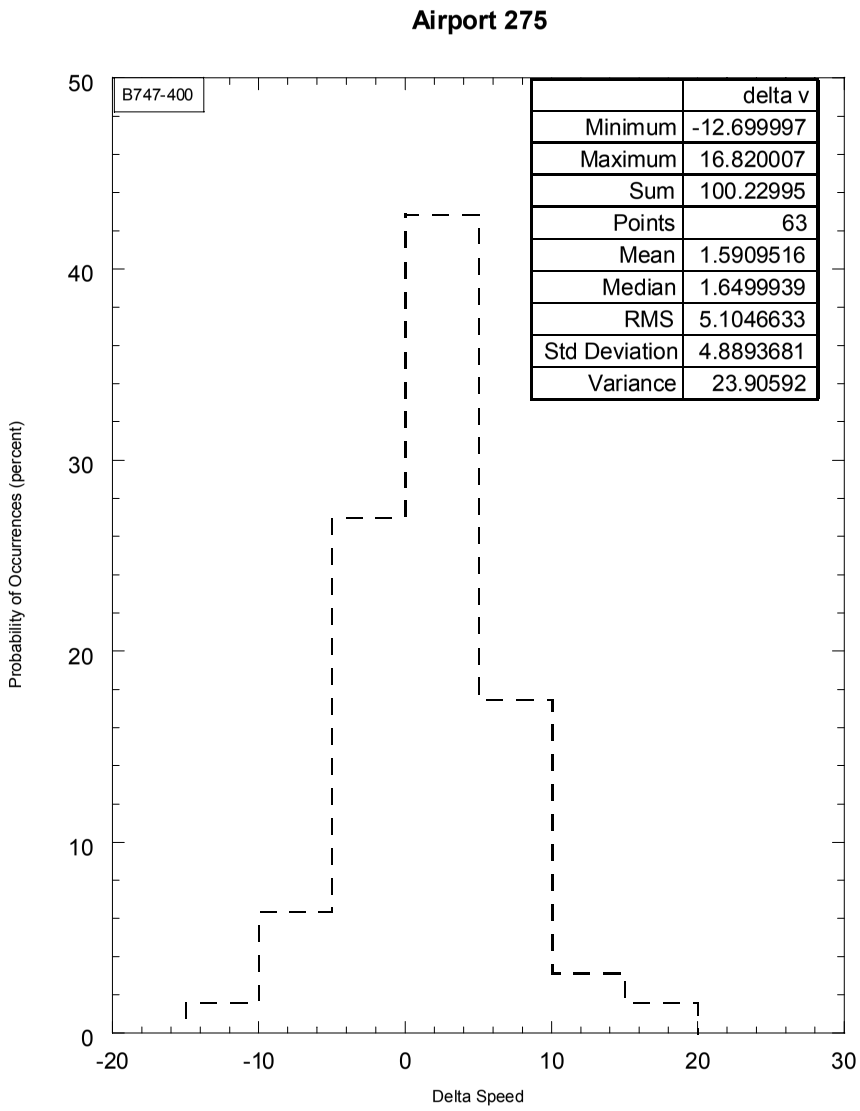

FIGURE C-88. DELTA V (GROUND SPEED-TRUE AIRSPEED) AT TOUCHDOWN, AIRPORT 275 ELEVATION > 5000 FEET

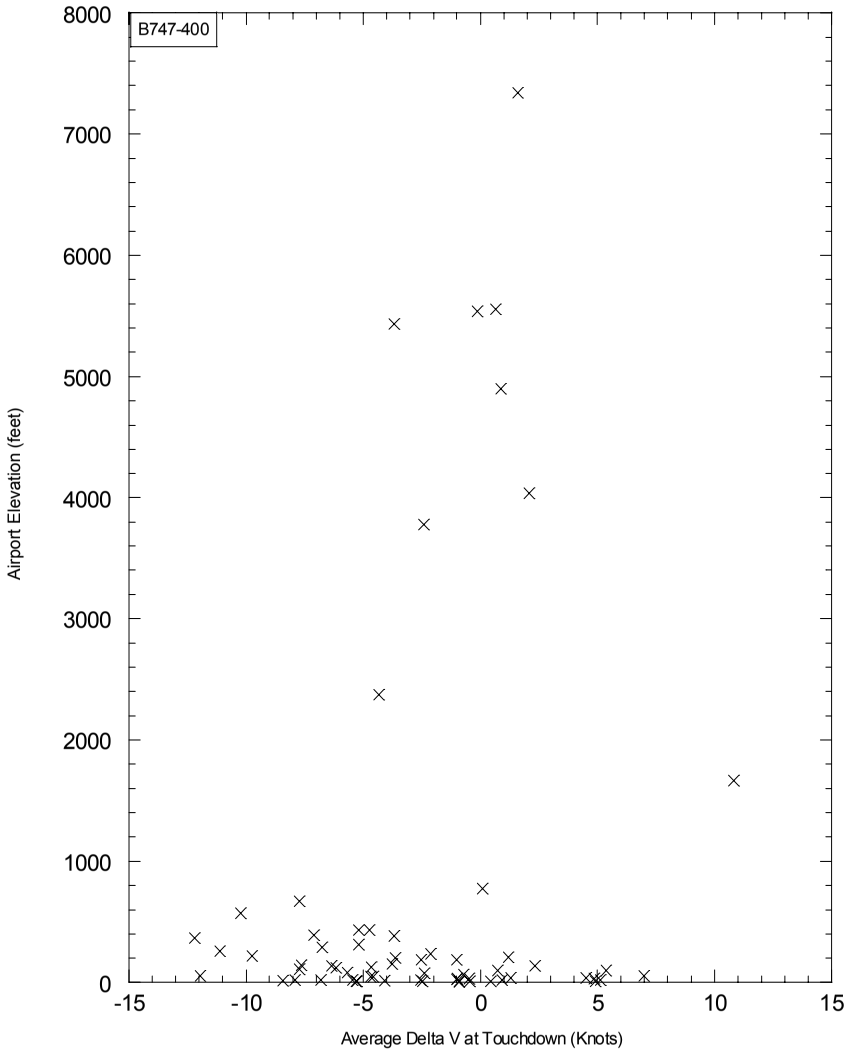

FIGURE C-89. AIRPORT ELEVATION VS AVERAGE DELTA V AT TOUCHDOWN

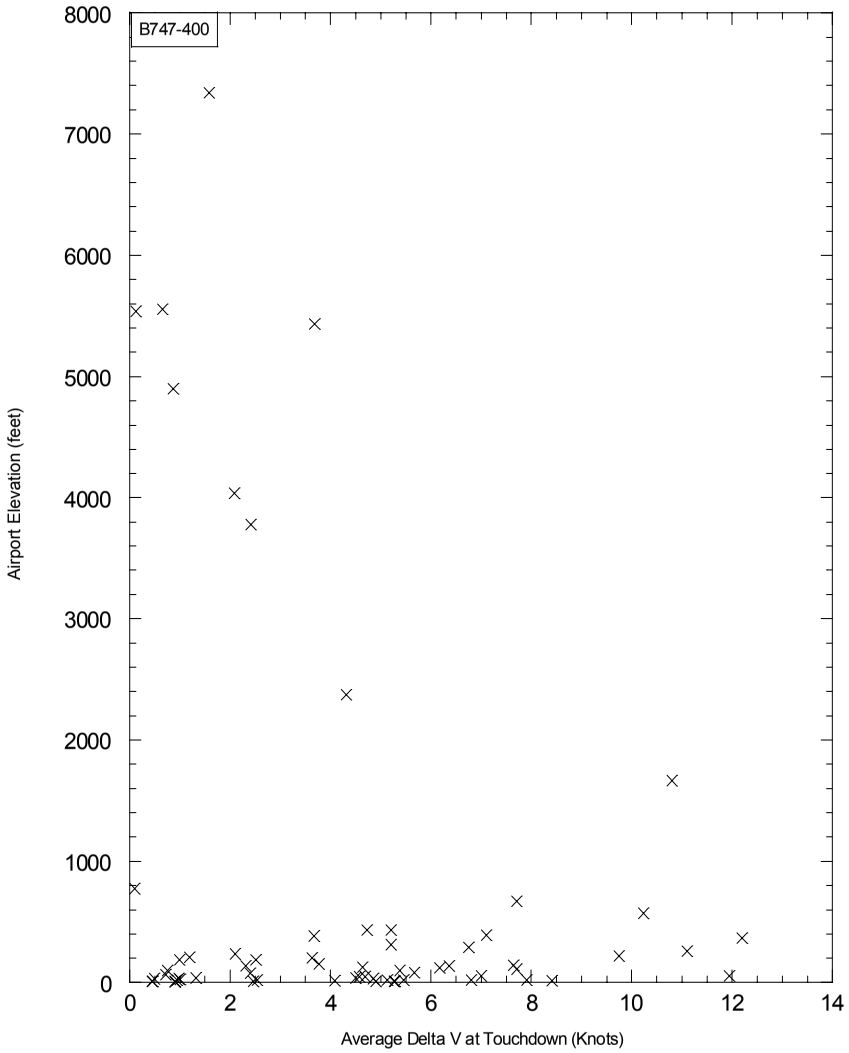

FIGURE C-90. AIRPORT ELEVATION VS ABSOLUTE VALUE OF AVERAGE DELTA V AT TOUCHDOWN

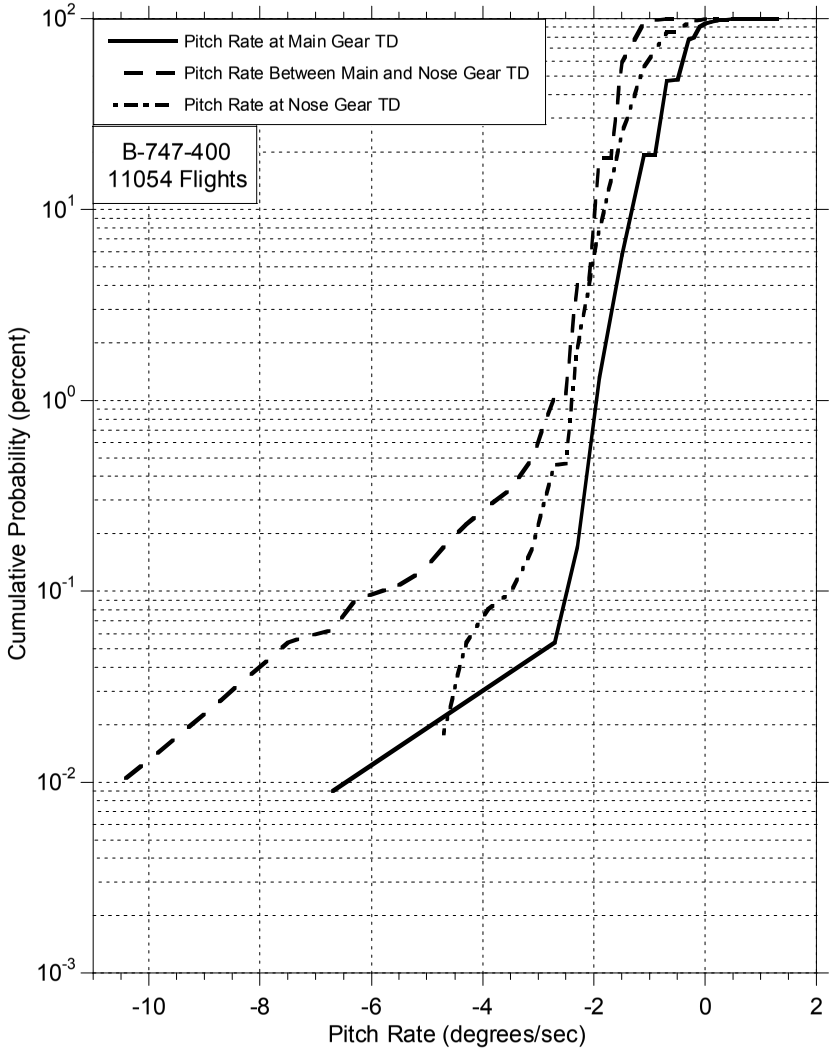

FIGURE C-91. CUMULATIVE PROBABILITY OF PITCH RATE AT GEAR TOUCHDOWN

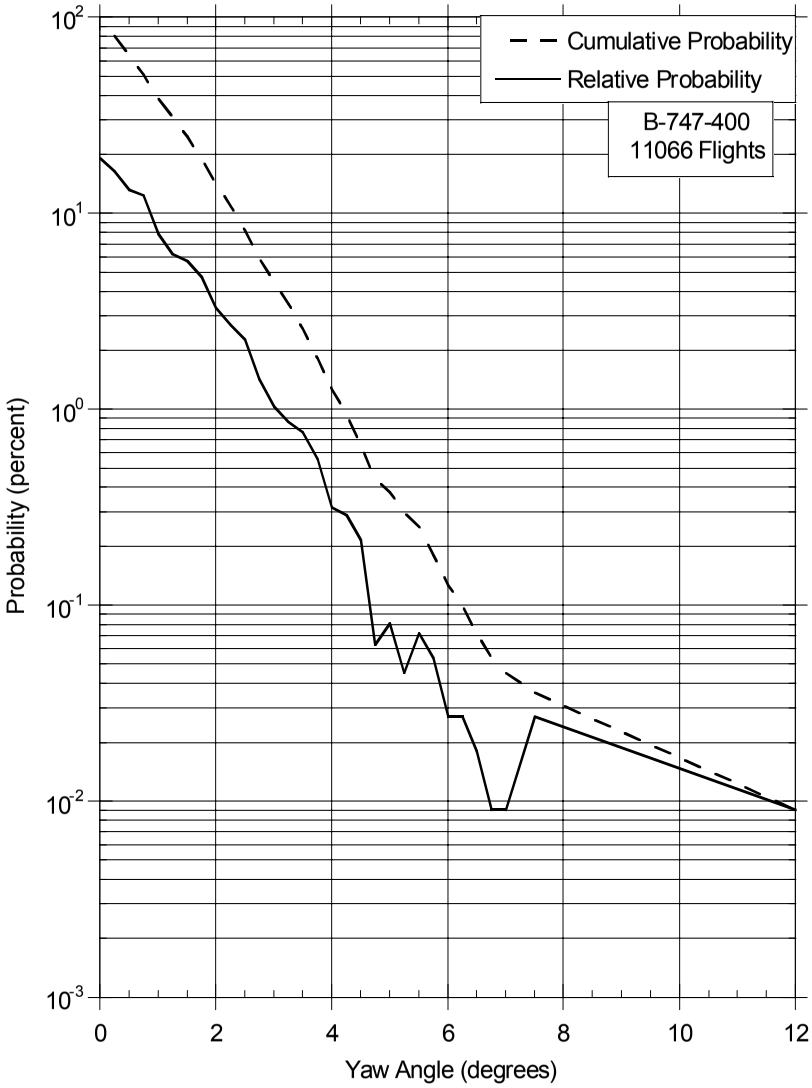

FIGURE C-92. PROBABILITY DISTRIBUTIONS OF MAXIMUM YAW ANGLE AT TOUCHDOWN

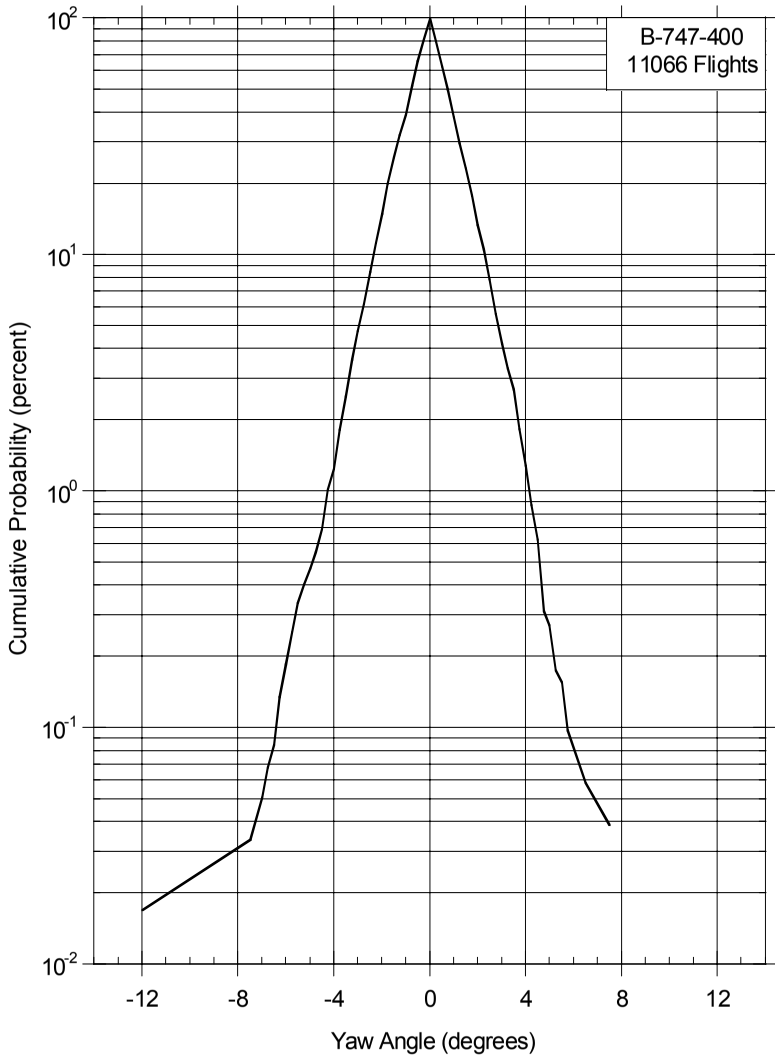

FIGURE C-93. CUMULATIVE PROBABILITY OF YAW ANGLE AT TOUCHDOWN

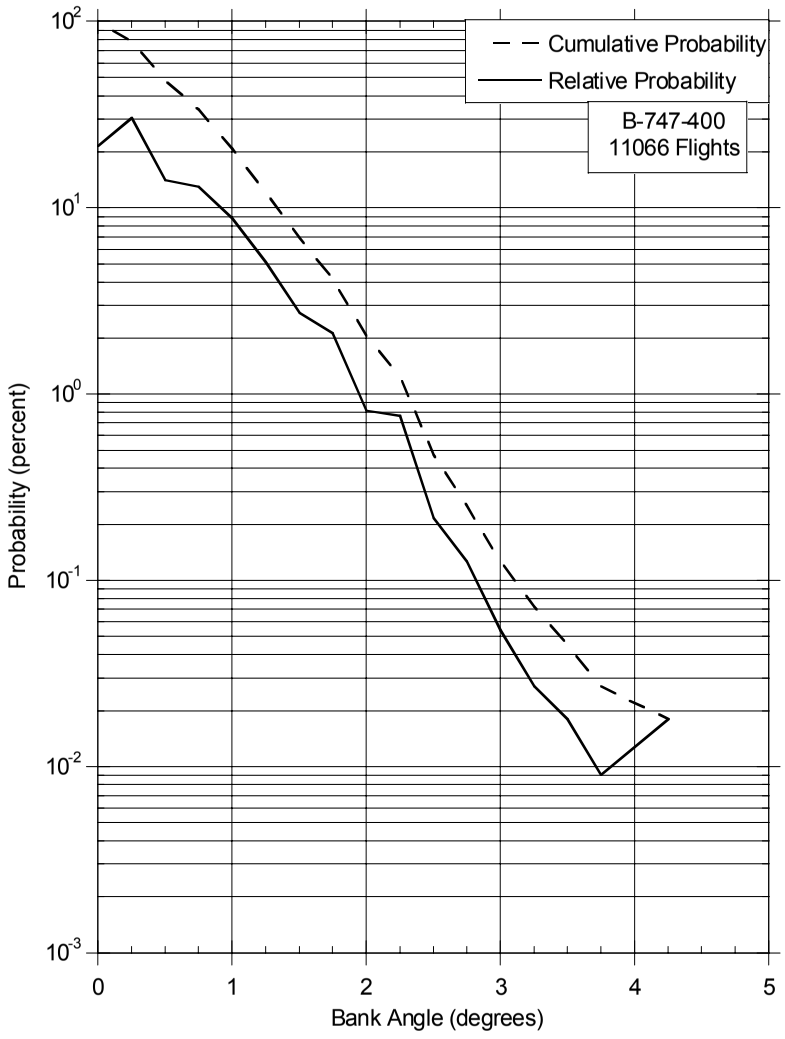

FIGURE C-94. PROBABILITY DISTRIBUTIONS OF MAXIMUM BANK ANGLE AT TOUCHDOWN

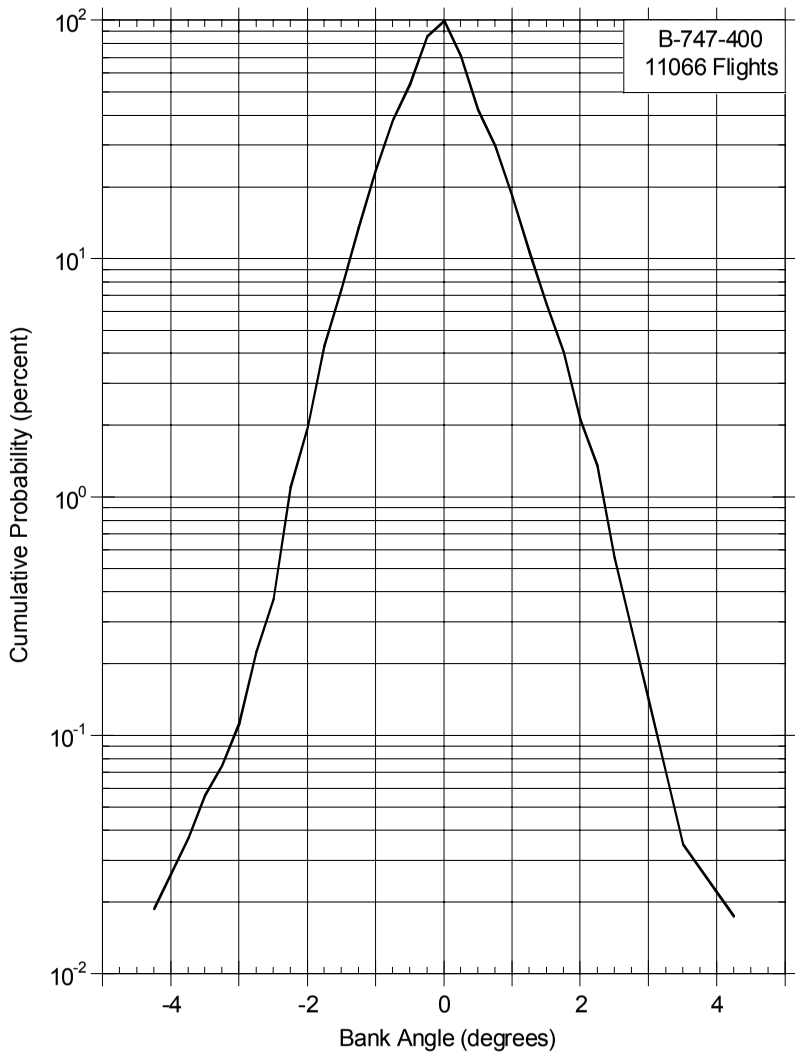

FIGURE C-95. CUMULATIVE PROBABILITY OF BANK ANGLE AT TOUCHDOWN

APPENDIX D—DESCENT RATE STATISTICS

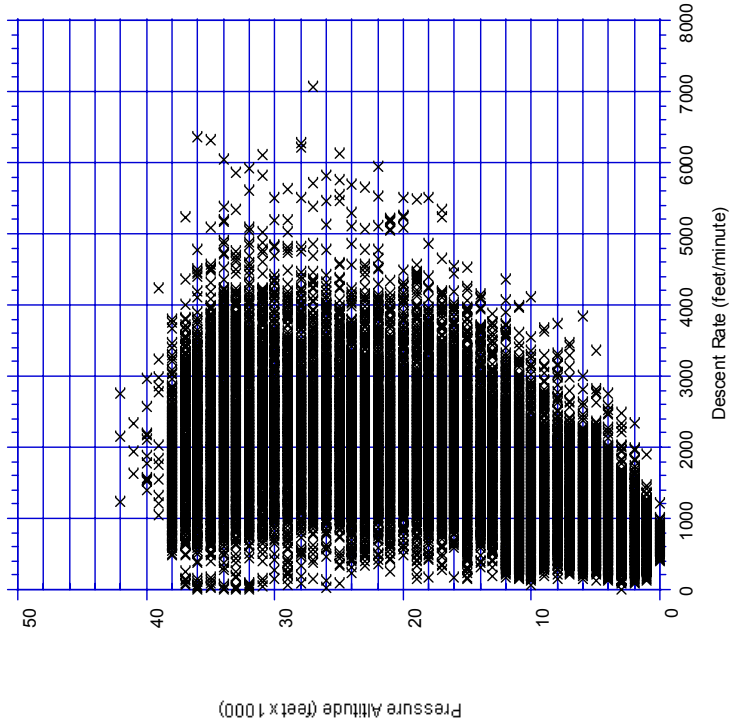

FIGURE D-2. DESCENT RATE AT PRESSURE ALTITUDE FOR CAPACITY-UNLIMITED AIRPORTS WITH HOLD TIMES

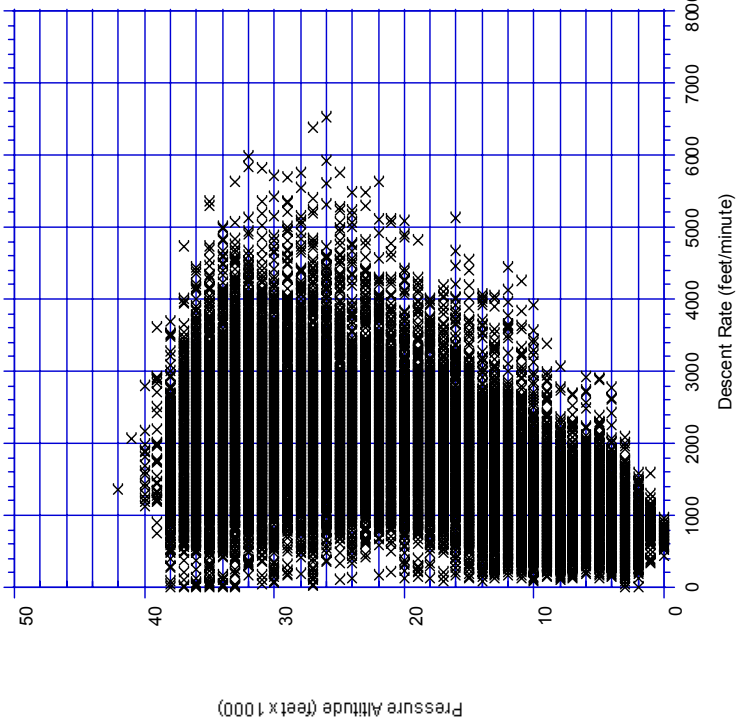

FIGURE D-1. DESCENT RATE AT PRESSURE ALTITUDE FOR CAPACITY-LIMITED AIRPORTS WITH HOLD TIMES

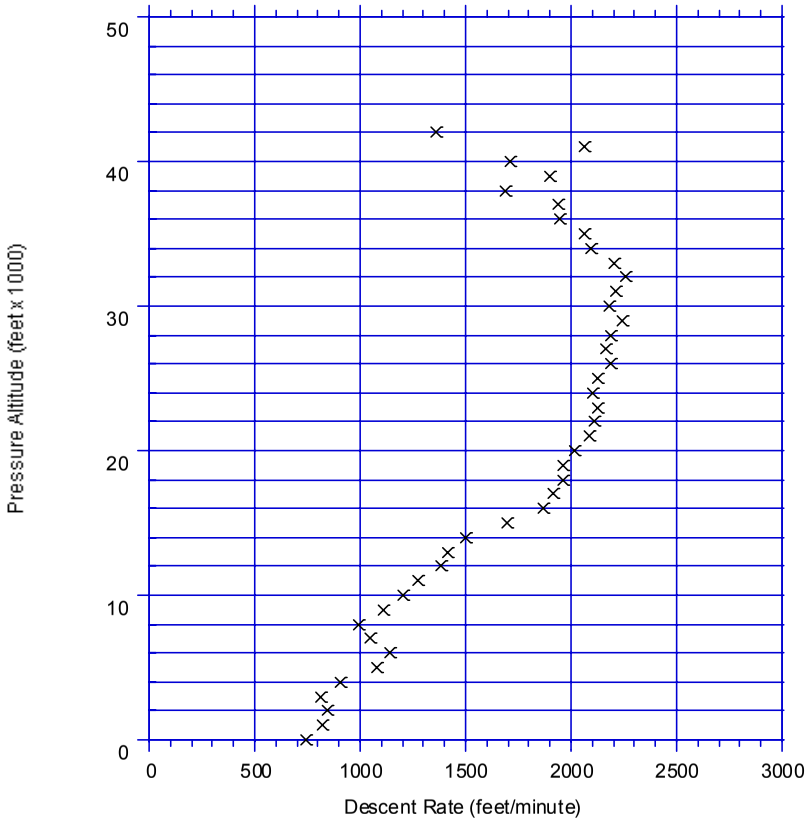

FIGURE D-3. MEAN DESCENT RATE AT PRESSURE ALTITUDE FOR CAPACITY-LIMITED AIRPORTS WITH HOLD TIMES

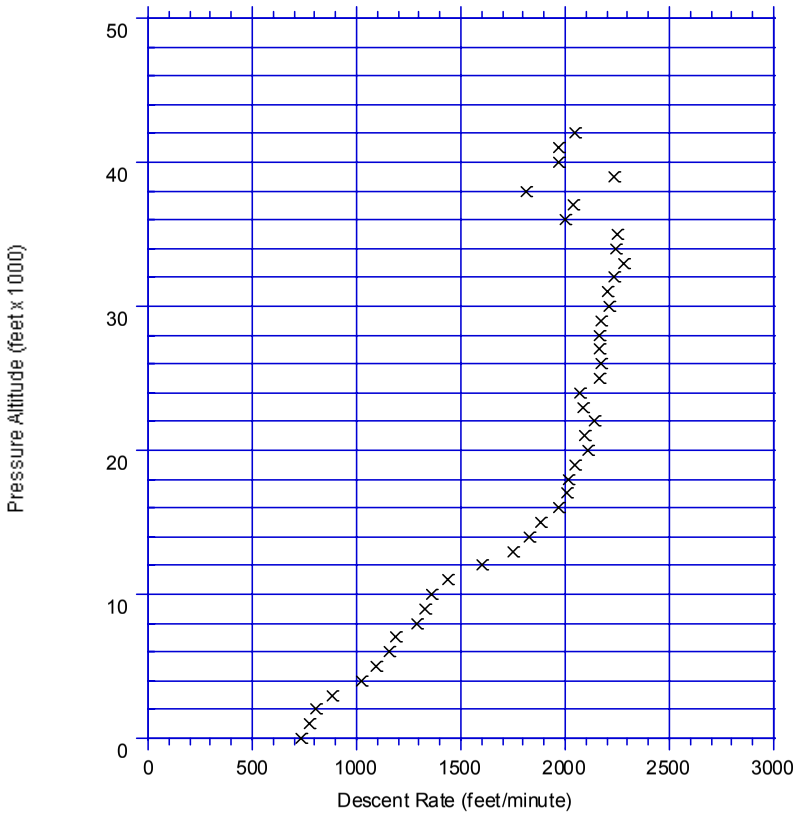

FIGURE D-4. MEAN DESCENT RATE AT PRESSURE ALTITUDE FOR CAPACITY-UNLIMITED AIRPORTS WITH HOLD TIMES

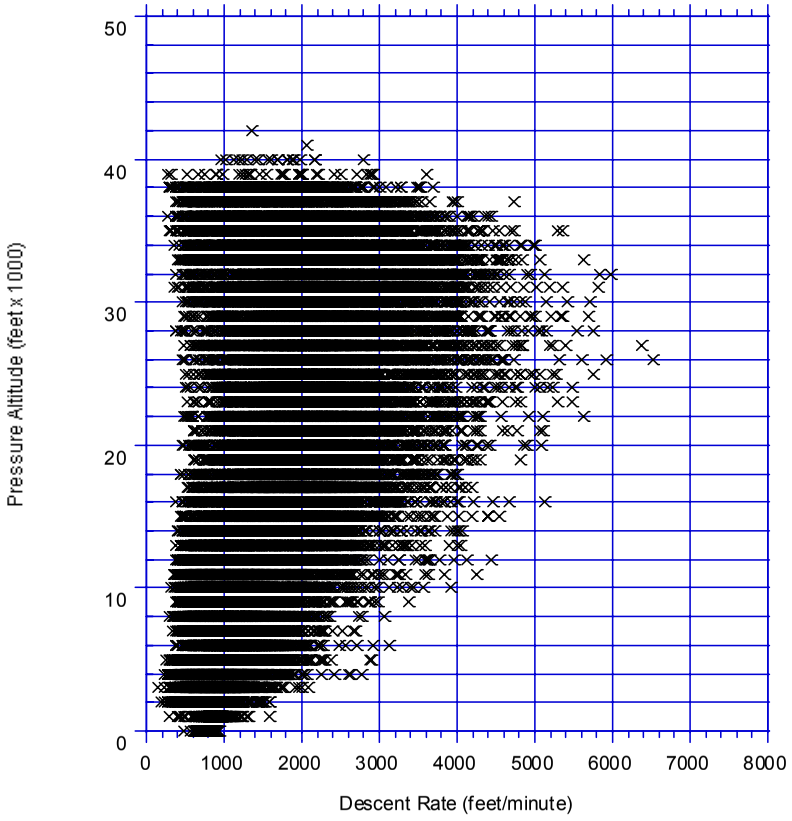

FIGURE D-5. DESCENT RATE AT PRESSURE ALTITUDE FOR CAPACITY-LIMITED AIRPORTS WITH HOLD TIMES REMOVED

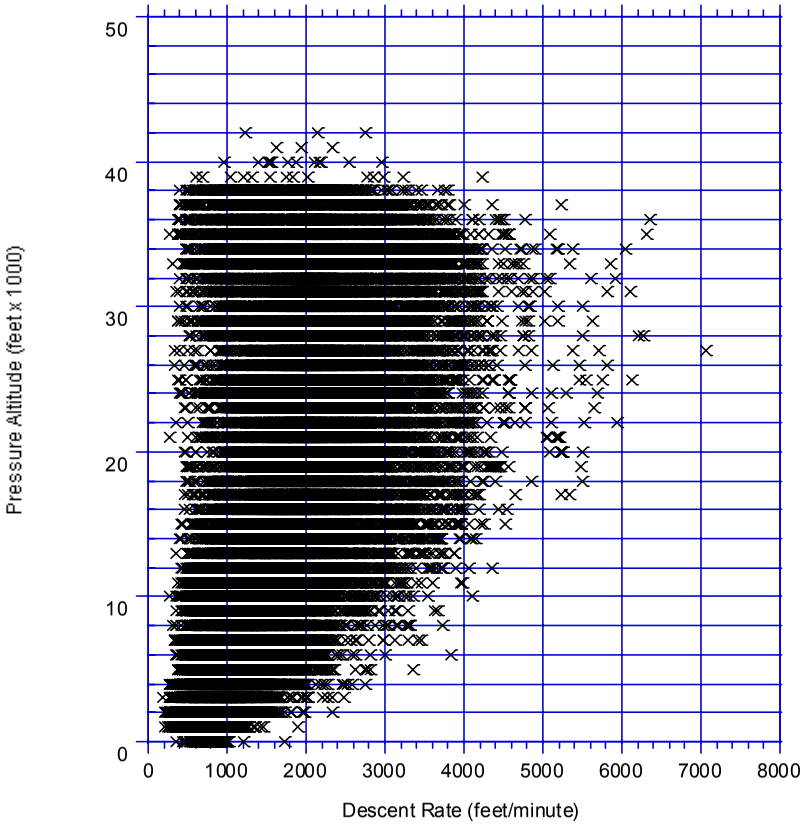

FIGURE D-6. DESCENT RATE AT PRESSURE ALTITUDE FOR CAPACITY-UNLIMITED AIRPORTS WITH HOLD TIMES REMOVED

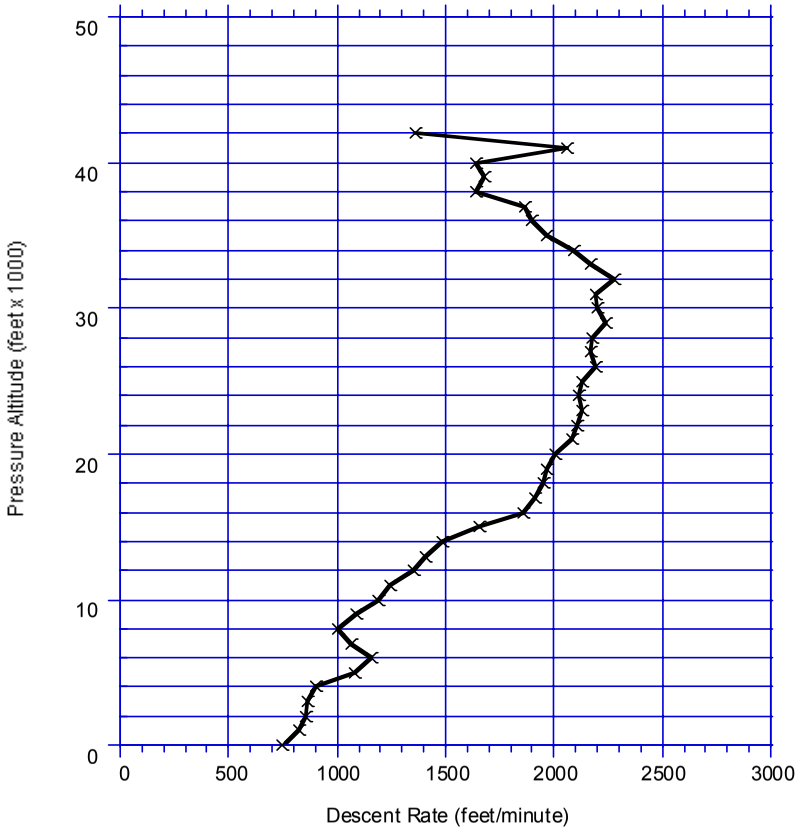

FIGURE D-7. MEAN DESCENT RATE AT PRESSURE ALTITUDE FOR CAPACITY-LIMITED AIRPORTS WITH HOLD TIMES REMOVED

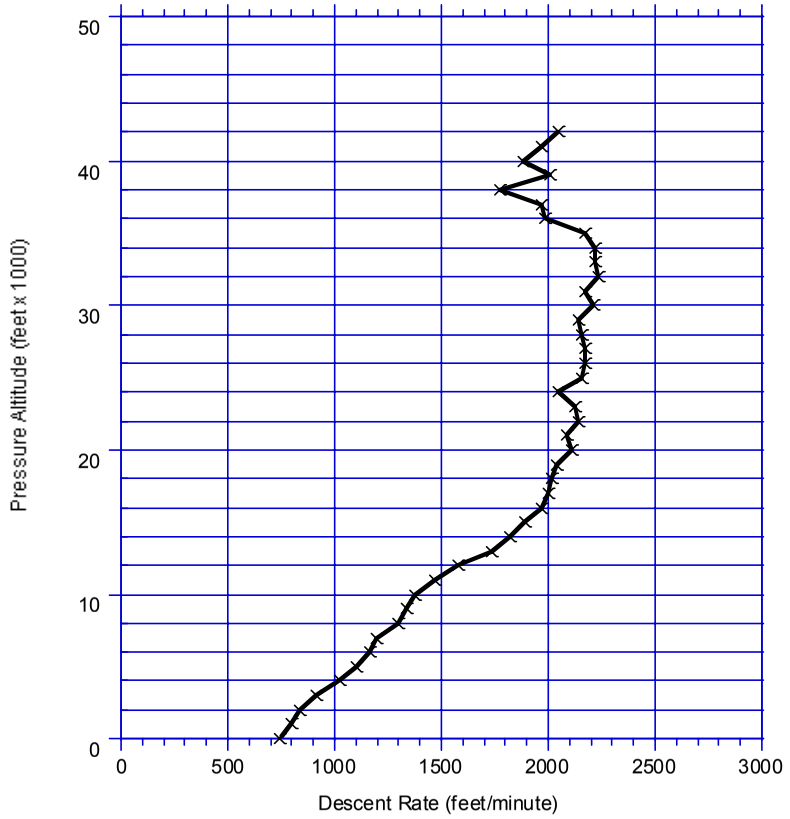

FIGURE D-8. MEAN DESCENT RATE AT PRESSURE ALTITUDE FOR CAPACITY-UNLIMITED AIRPORTS WITH HOLD TIMES REMOVED

Flight Sequence Number	Maximum Descent Rate	Pressure Altitude
2838	6520	26,000
2838	6372	27,000
3212	5989	32,000
1030	5916	26,000
2971	5820	31,000
2793	5760	25,000
2838	5748	28,000
3033	5706	30,000
2971	5695	29,000

FIGURE D-9. MAXIMUM DESCENT RATE FOR CAPACITY-LIMITED FLIGHTS

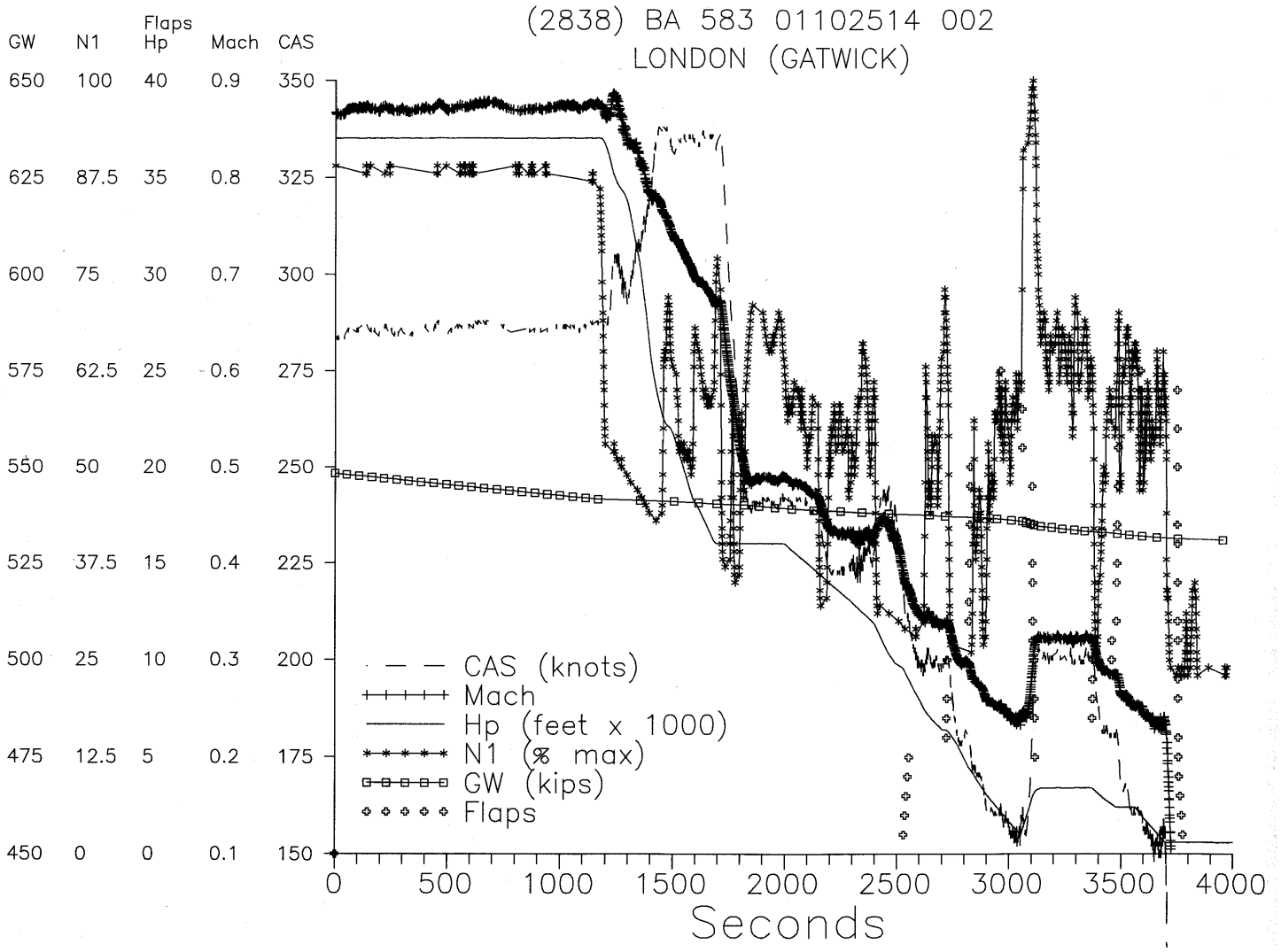

FIGURE D-10. ACTUAL DESCENT PROFILES BEGINNING BEFORE DESCENT PHASE FOR CAPACITY-LIMITED FLIGHT (FLIGHT SEQUENCE NUMBER 2838)

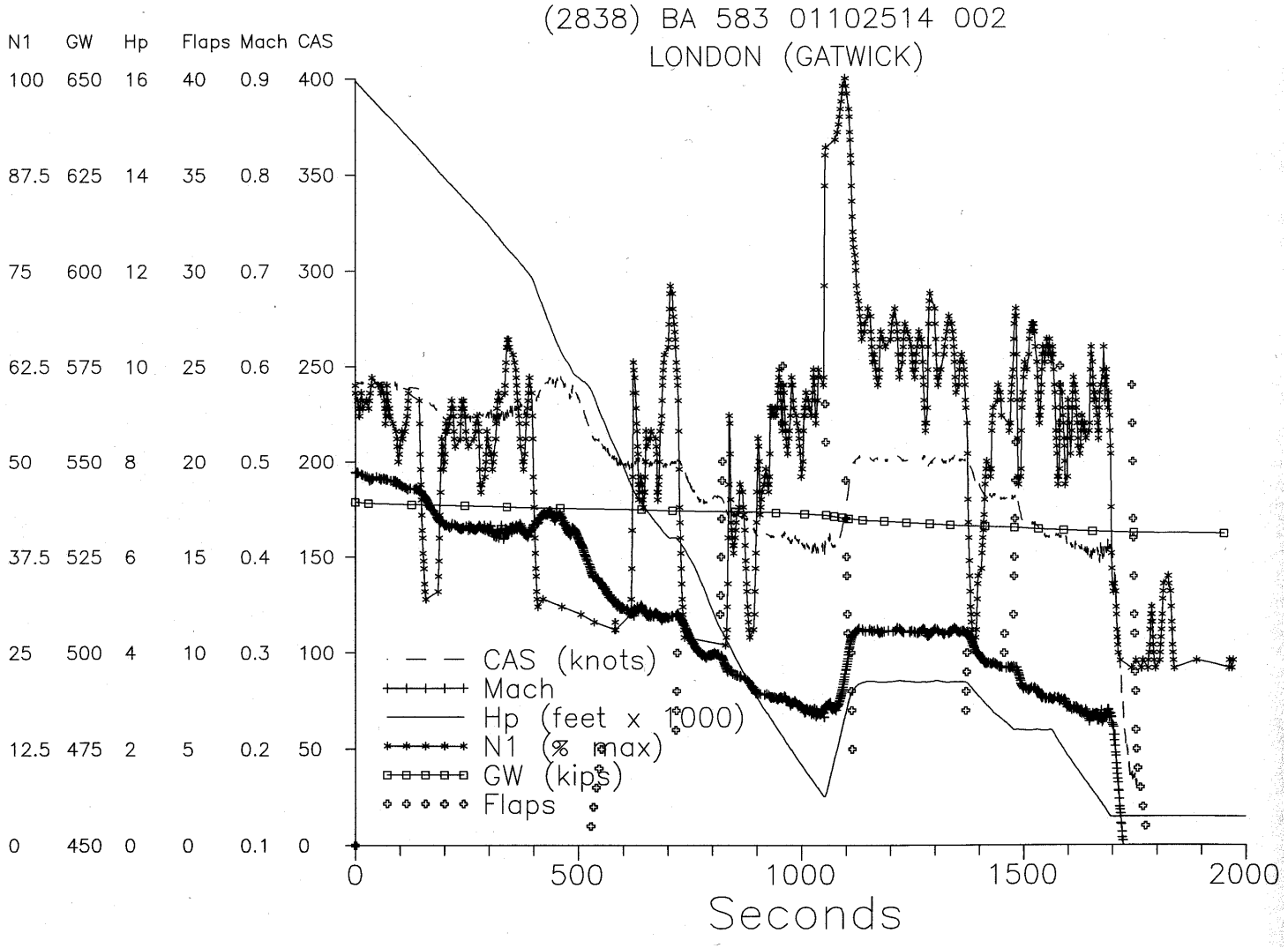

FIGURE D-11. ACTUAL DESCENT PROFILES BELOW 15K FEET FOR CAPACITY-LIMITED FLIGHT (FLIGHT SEQUENCE NUMBER 2838)

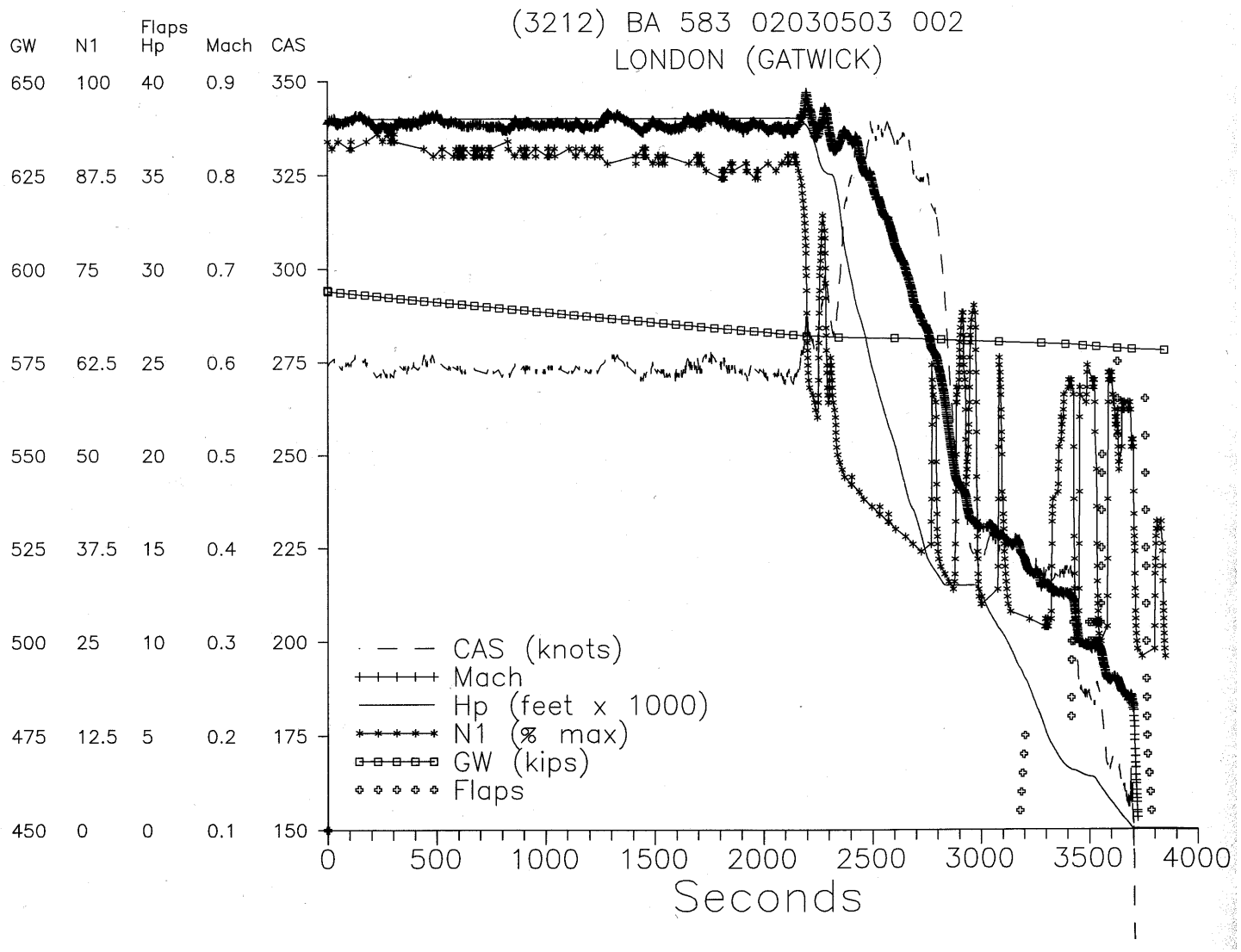

FIGURE D-12. ACTUAL DESCENT PROFILES BEGINNING BEFORE DESCENT PHASE FOR CAPACITY-LIMITED FLIGHT (FLIGHT SEQUENCE NUMBER 3212)

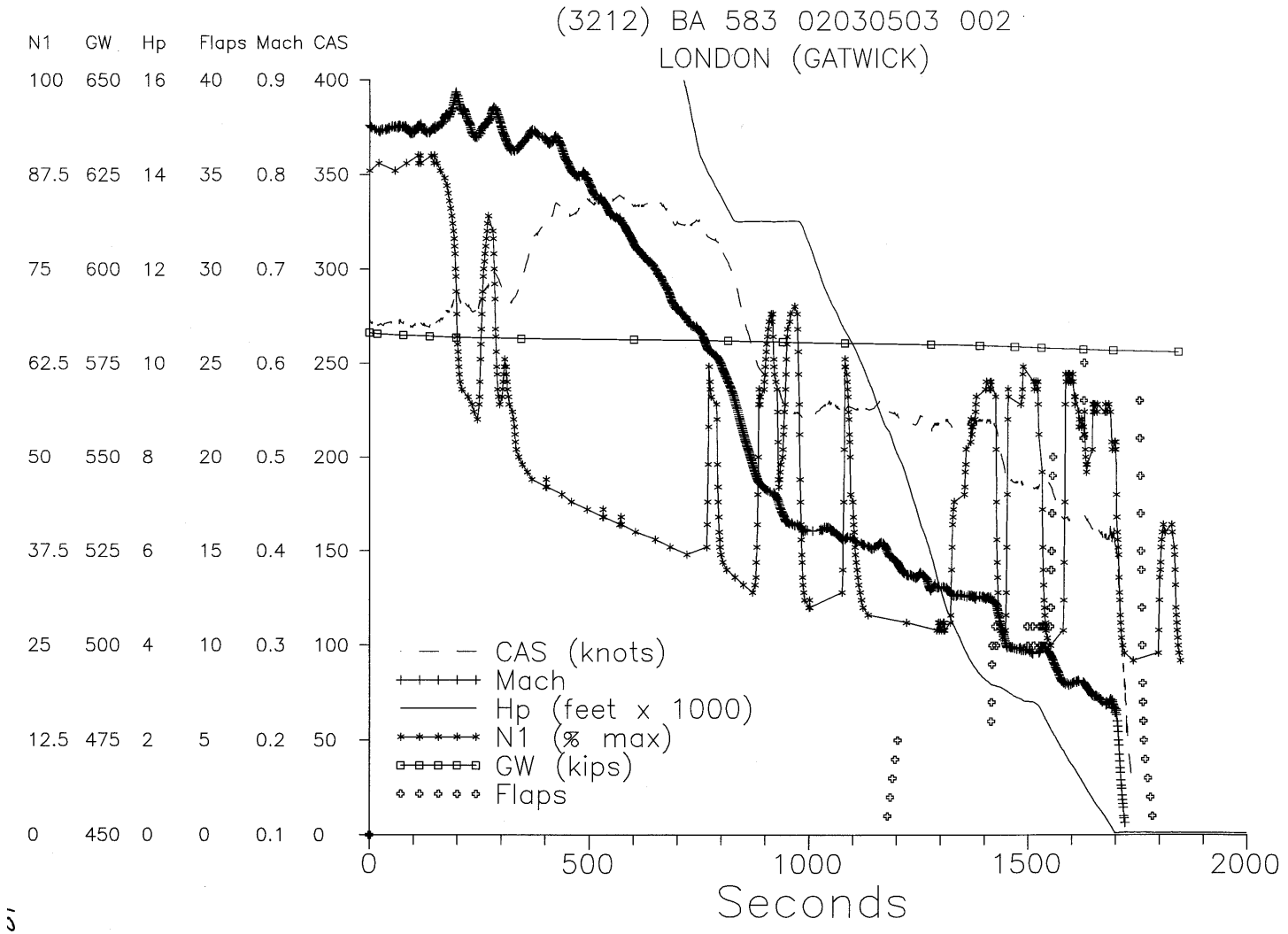

FIGURE D-13. ACTUAL DESCENT PROFILES BELOW 15K FEET FOR CAPACITY-LIMITED FLIGHT (FLIGHT SEQUENCE NUMBER 3212)

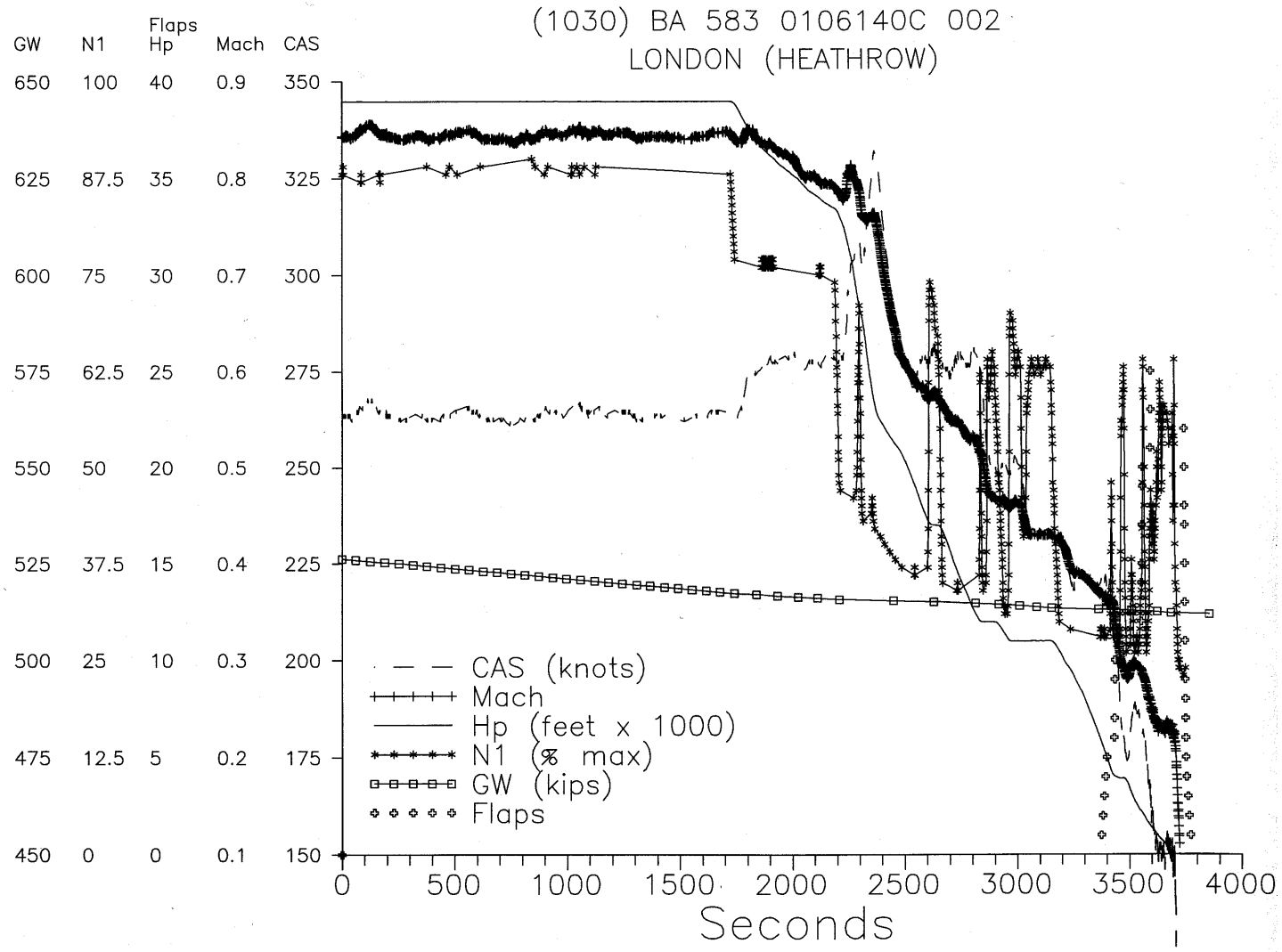

FIGURE D-14. ACTUAL DESCENT PROFILES BEGINNING BEFORE DESCENT PHASE FOR CAPACITY-LIMITED FLIGHT (FLIGHT SEQUENCE NUMBER 1030)

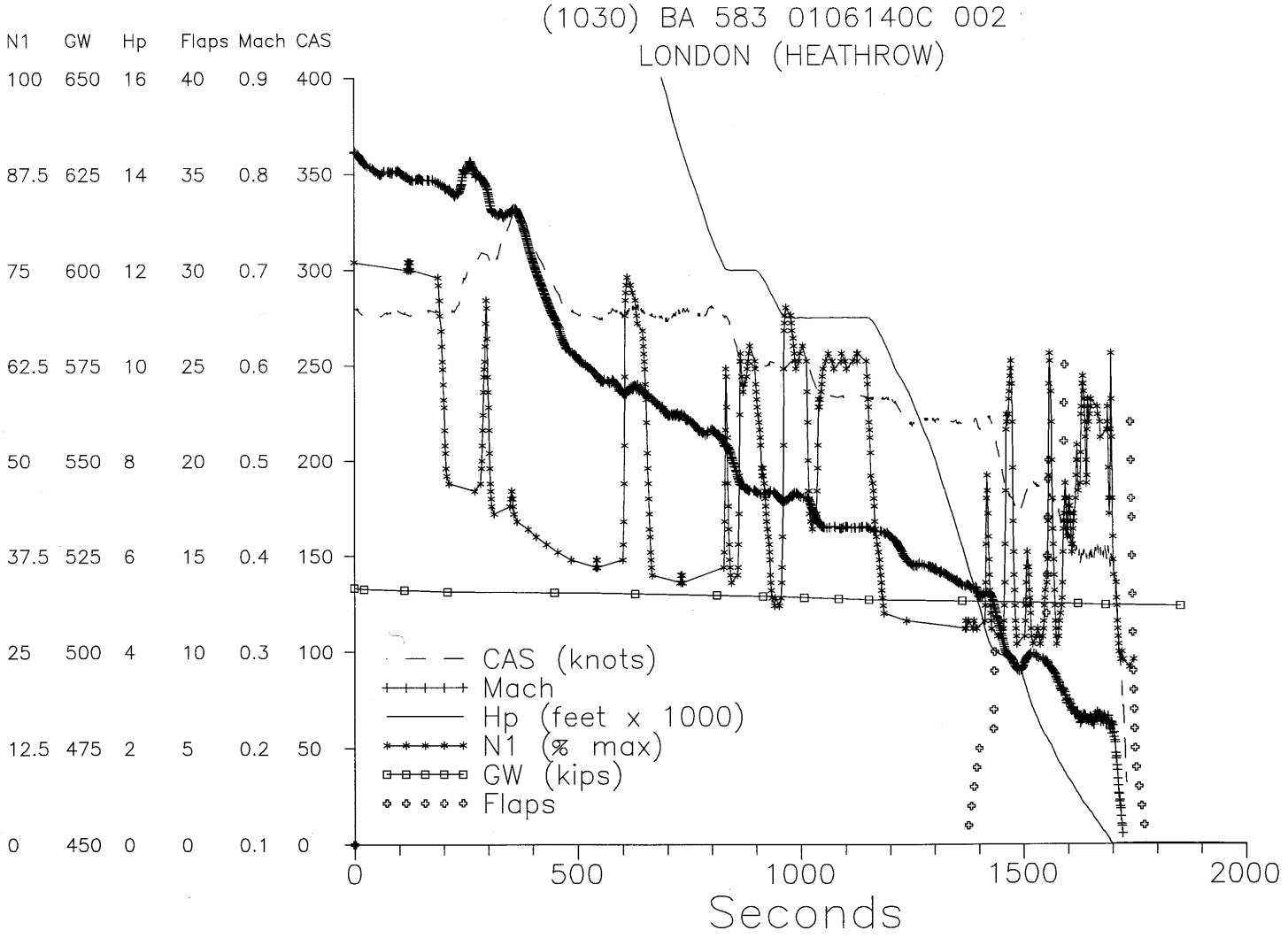

FIGURE D-15. ACTUAL DESCENT PROFILES BELOW 15K FEET FOR CAPACITY-LIMITED FLIGHT (FLIGHT SEQUENCE NUMBER 1030)

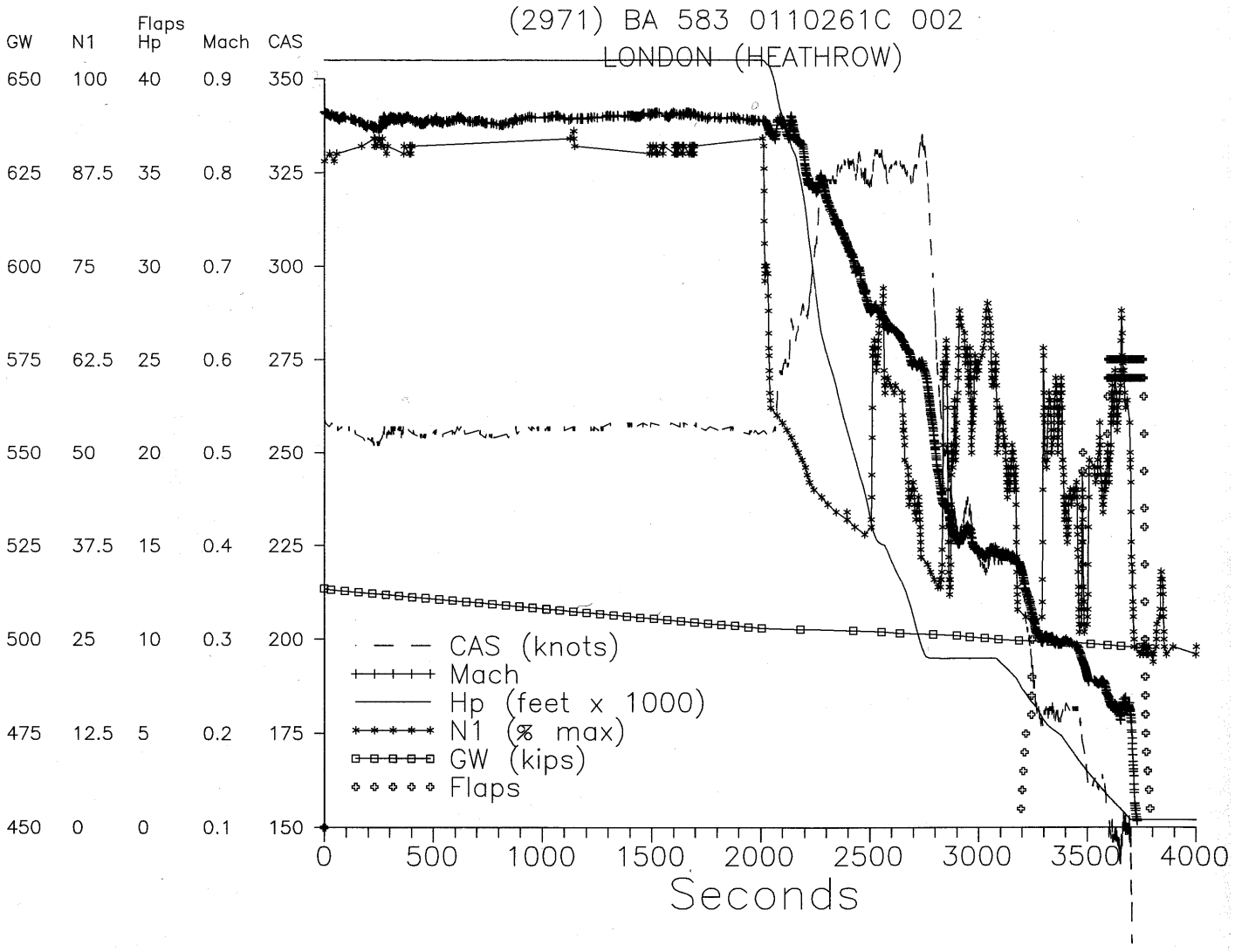

FIGURE D-16. ACTUAL DESCENT PROFILES BEGINNING BEFORE DESCENT PHASE FOR CAPACITY-LIMITED FLIGHT (FLIGHT SEQUENCE NUMBER 2971)

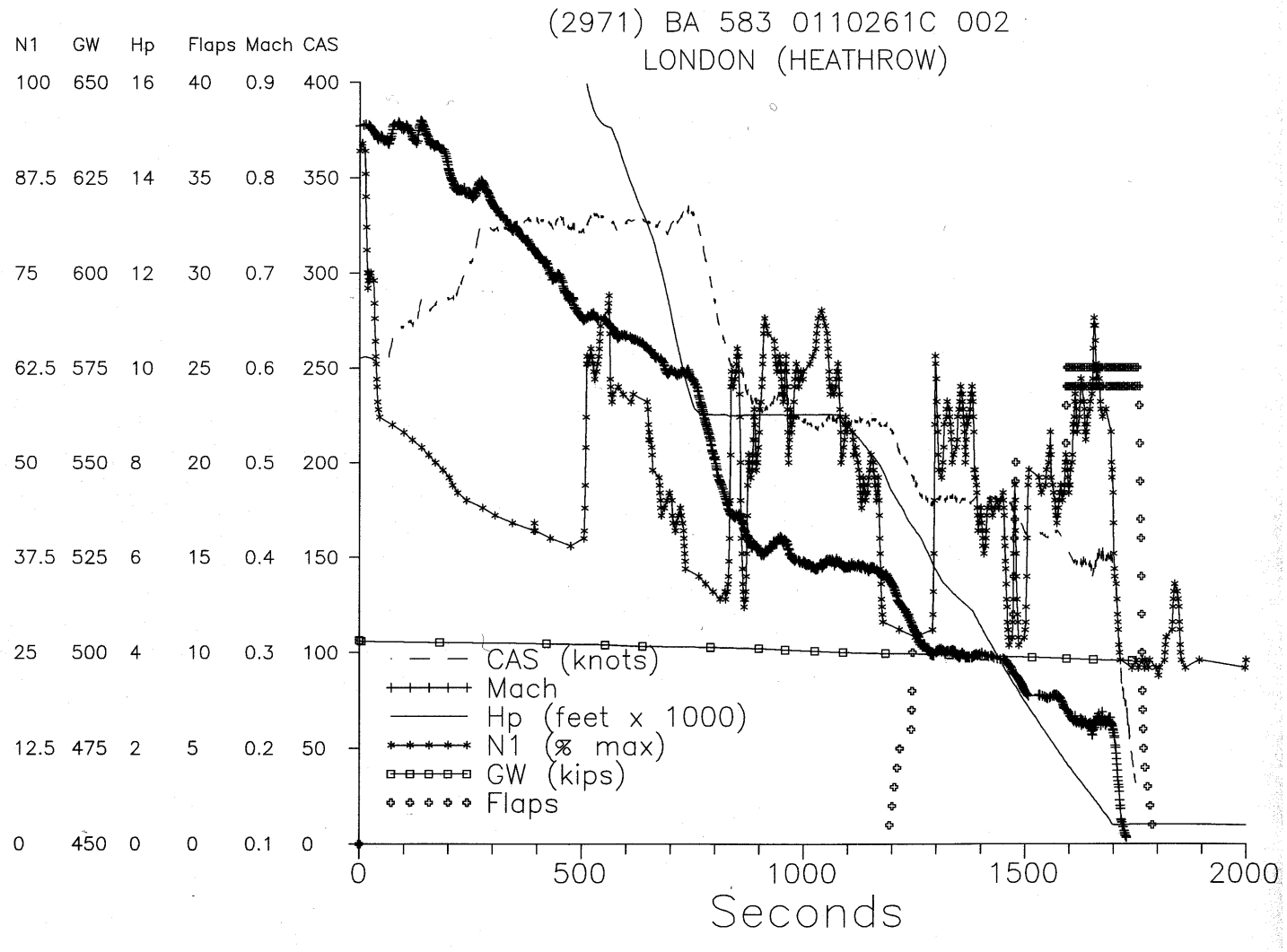

FIGURE D-17. ACTUAL DESCENT PROFILES BELOW 15K FEET FOR CAPACITY-LIMITED FLIGHT (FLIGHT SEQUENCE NUMBER 2971)

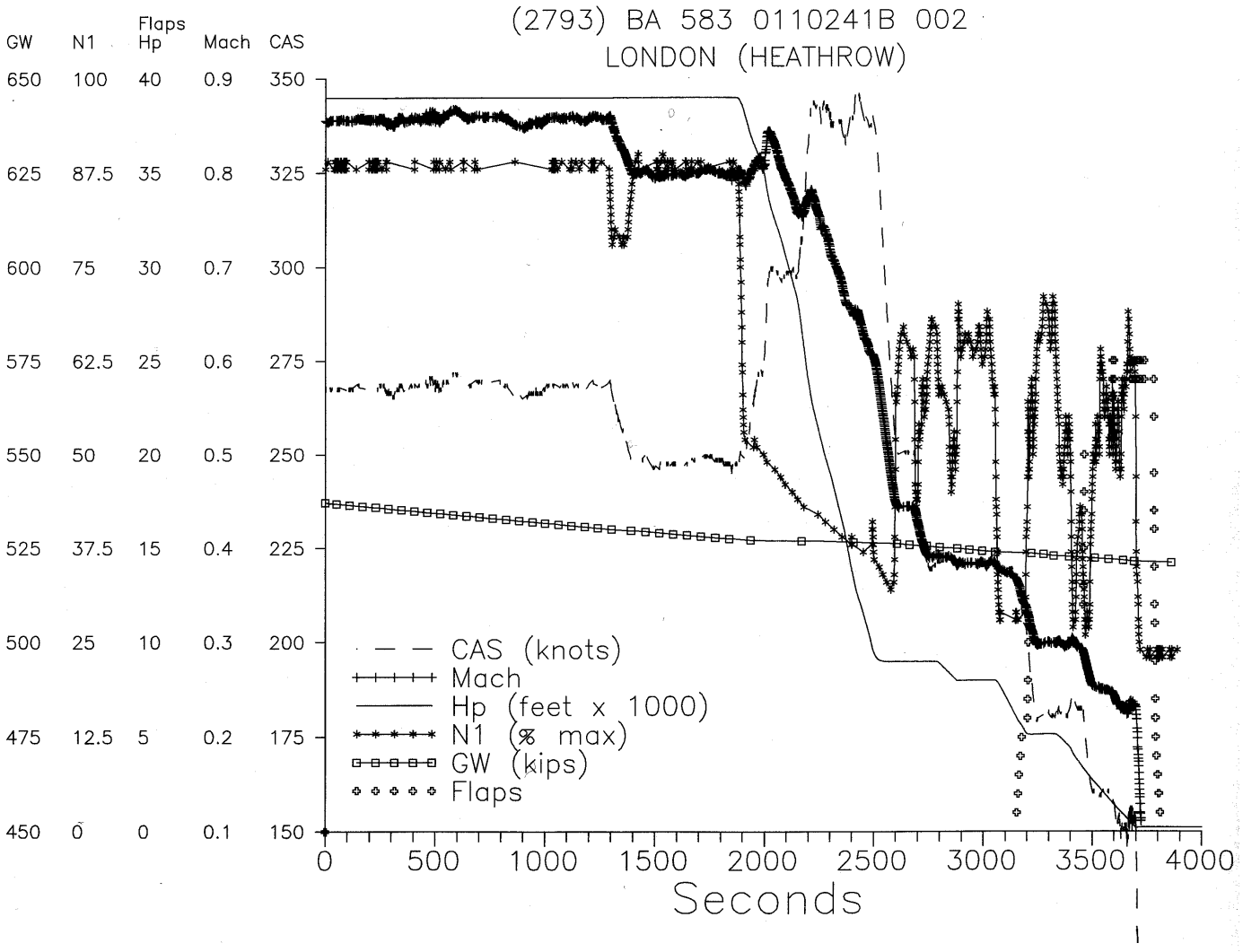

FIGURE D-18. ACTUAL DESCENT PROFILES BEGINNING BEFORE DESCENT PHASE FOR CAPACITY-LIMITED FLIGHT (FLIGHT SEQUENCE NUMBER 2793)

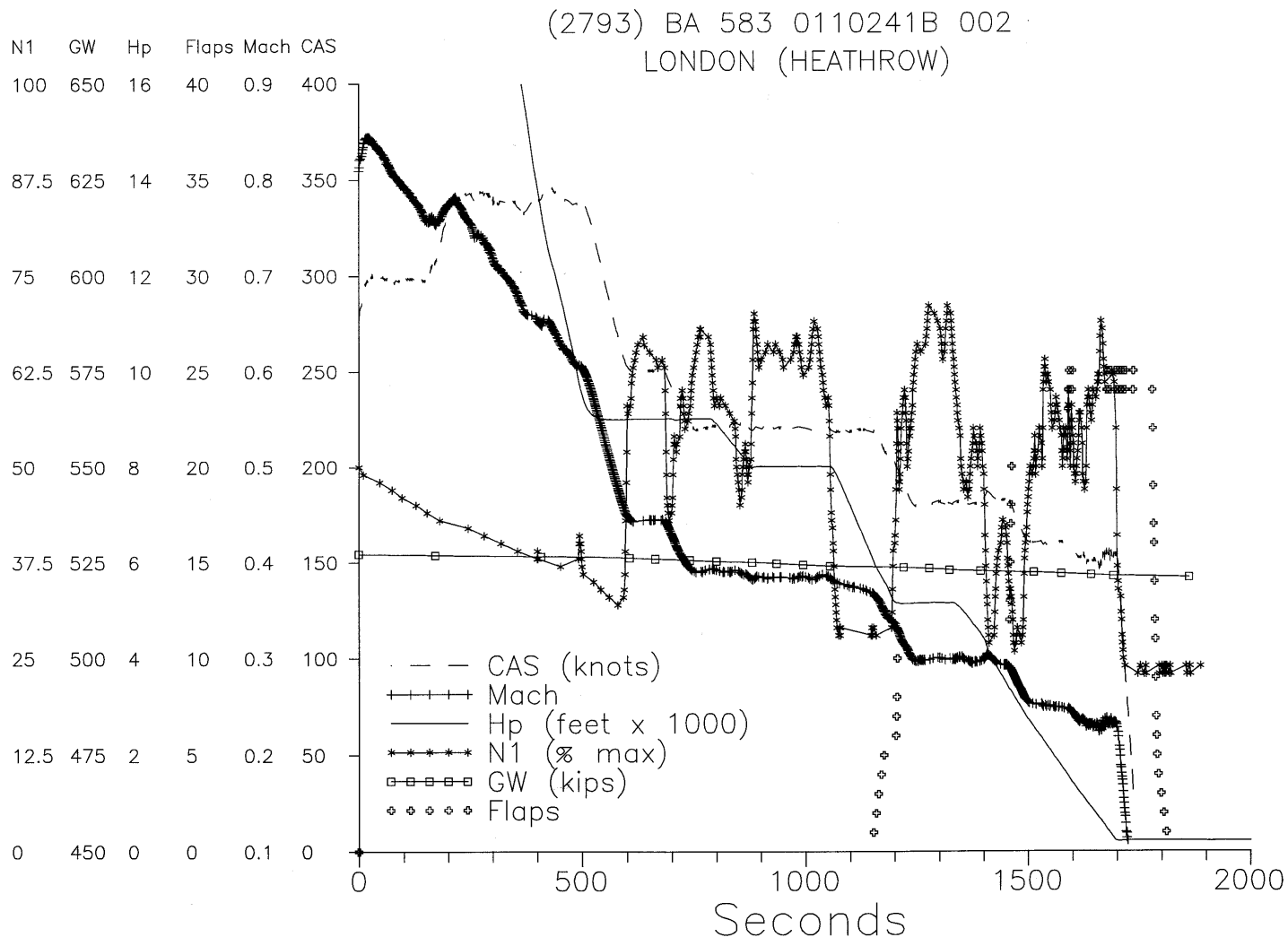

FIGURE D-19. ACTUAL DESCENT PROFILES BELOW 15K FEET FOR CAPACITY-LIMITED FLIGHT (FLIGHT SEQUENCE NUMBER 2793)

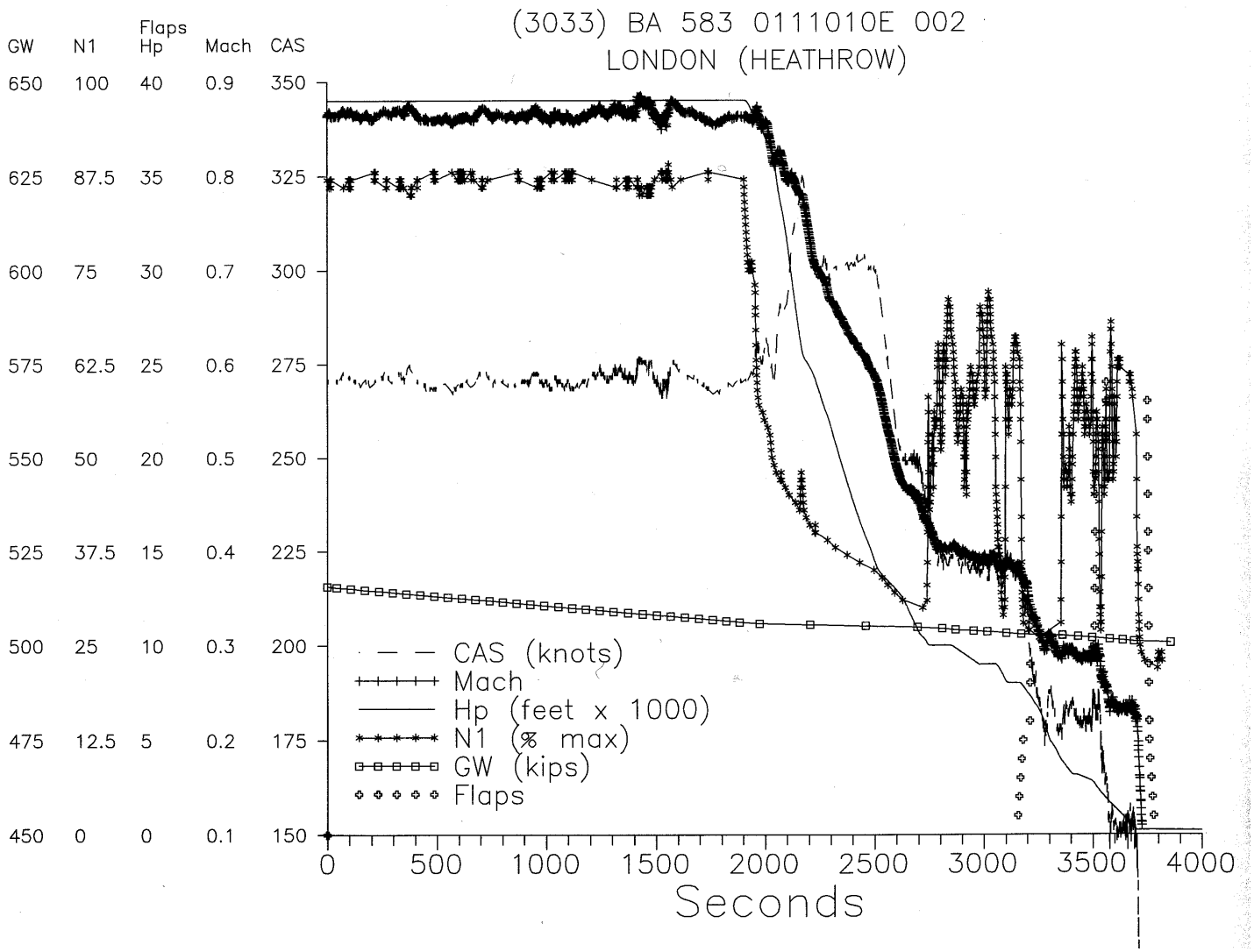

FIGURE D-20. ACTUAL DESCENT PROFILES BGINNING BEFORE DESCENT PHASE FOR CAPACITY-LIMITED FLIGHT (FLIGHT SEQUENCE NUMBER 3033)

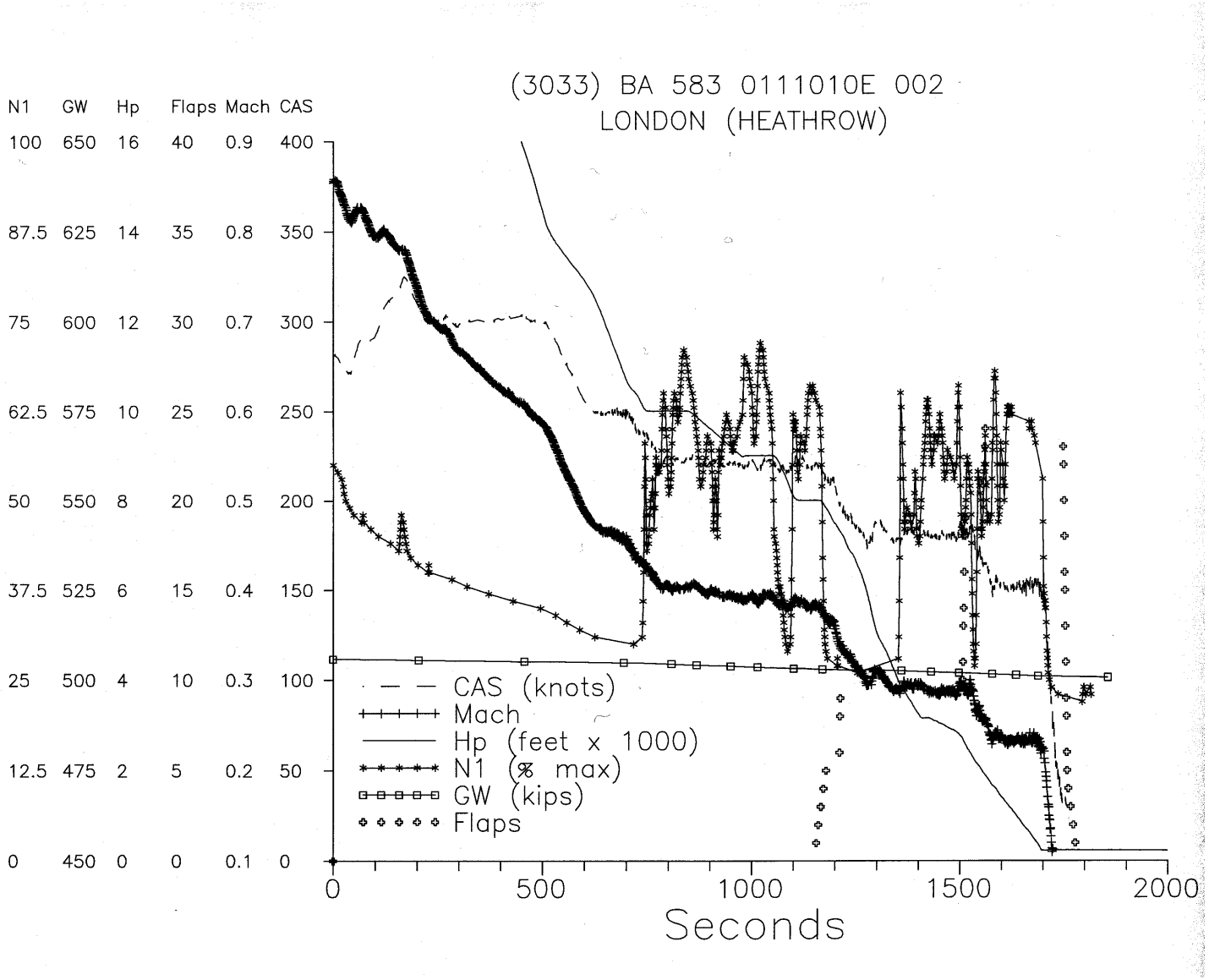

FIGURE D-21. ACTUAL DESCENT PROFILES BELOW 15K FEET FOR CAPACITY-LIMITED FLIGHT (FLIGHT SEQUENCE NUMBER 3033)

Flight Sequence Number	Maximum Descent Rate	Pressure Altitude
1038	7067	27,000
3574	6347	36,000
3574	6324	35,000
1038	6273	28,000
2267	6207	28,000
1038	6120	25,000
3574	6102	31,000
3574	6036	34,000
3034	5940	22,000
3574	5910	32,000
3574	5856	33,000
2360	5808	31,000
1038	5808	26,000
2021	5748	25,000
2267	5700	27,000

FIGURE D-22. MAXIMUM DESCENT RATE FOR NON-CAPACITY-LIMITED AIRPORTS

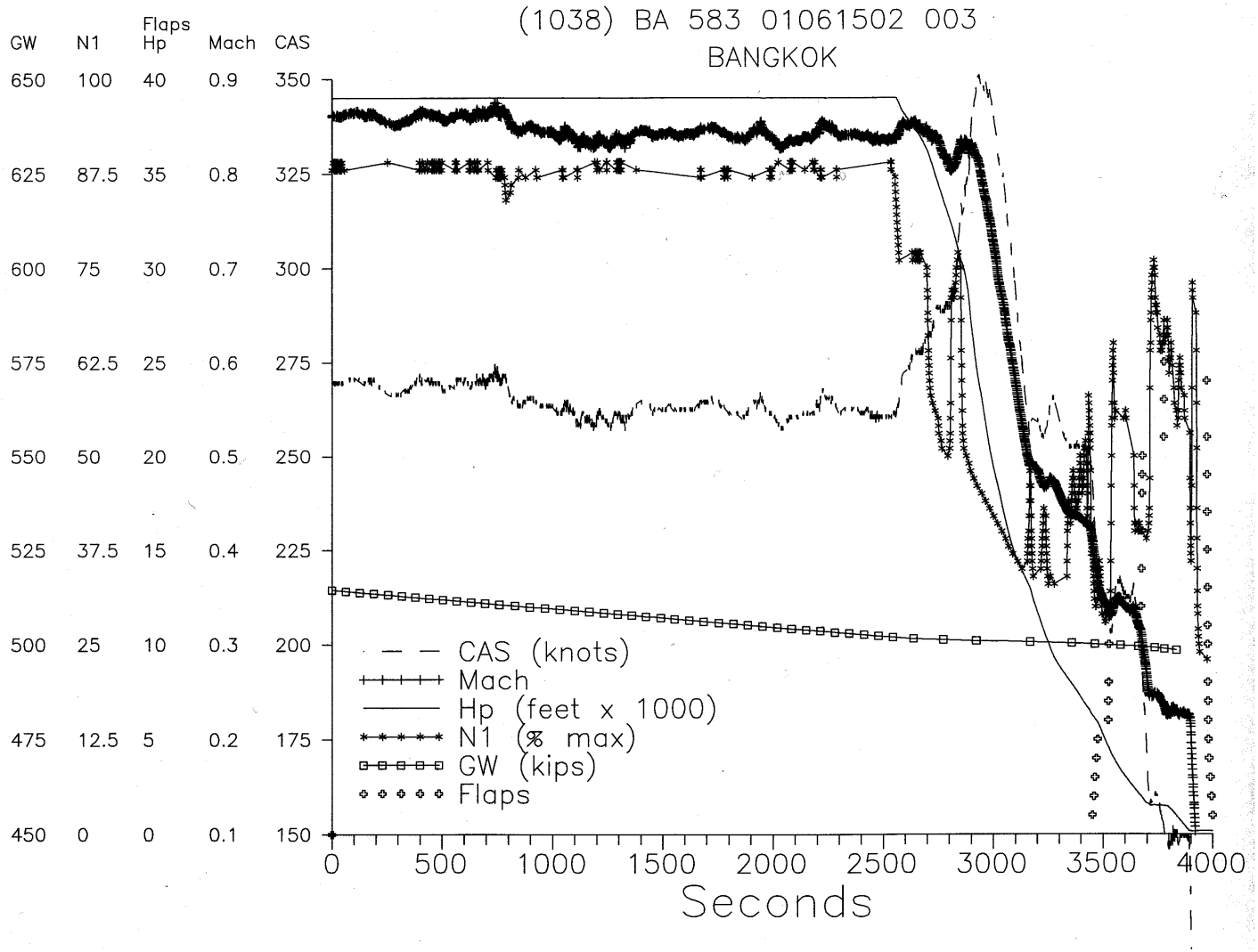

FIGURE D-23. ACTUAL DESCENT PROFILES BEGINNING BEFORE DESCENT PHASE FOR NON-CAPACITY-LIMITED FLIGHT (FLIGHT SEQUENCE NUMBER 1038)

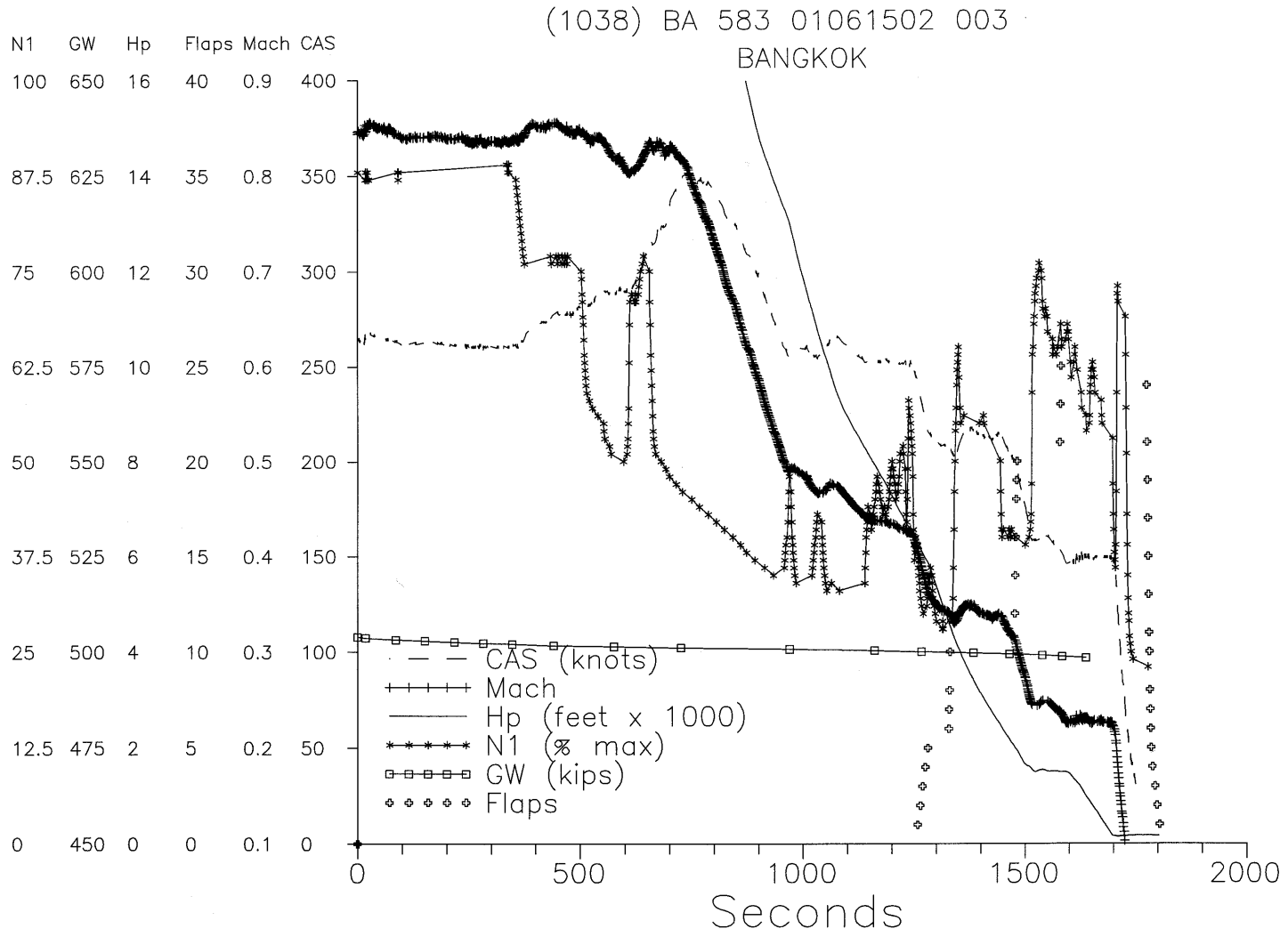

FIGURE D-24. ACTUAL DESCENT PROFILES BELOW 15K FEET FOR NON-CAPACITY-LIMITED FLIGHT (FLIGHT SEQUENCE NUMBER 1038)

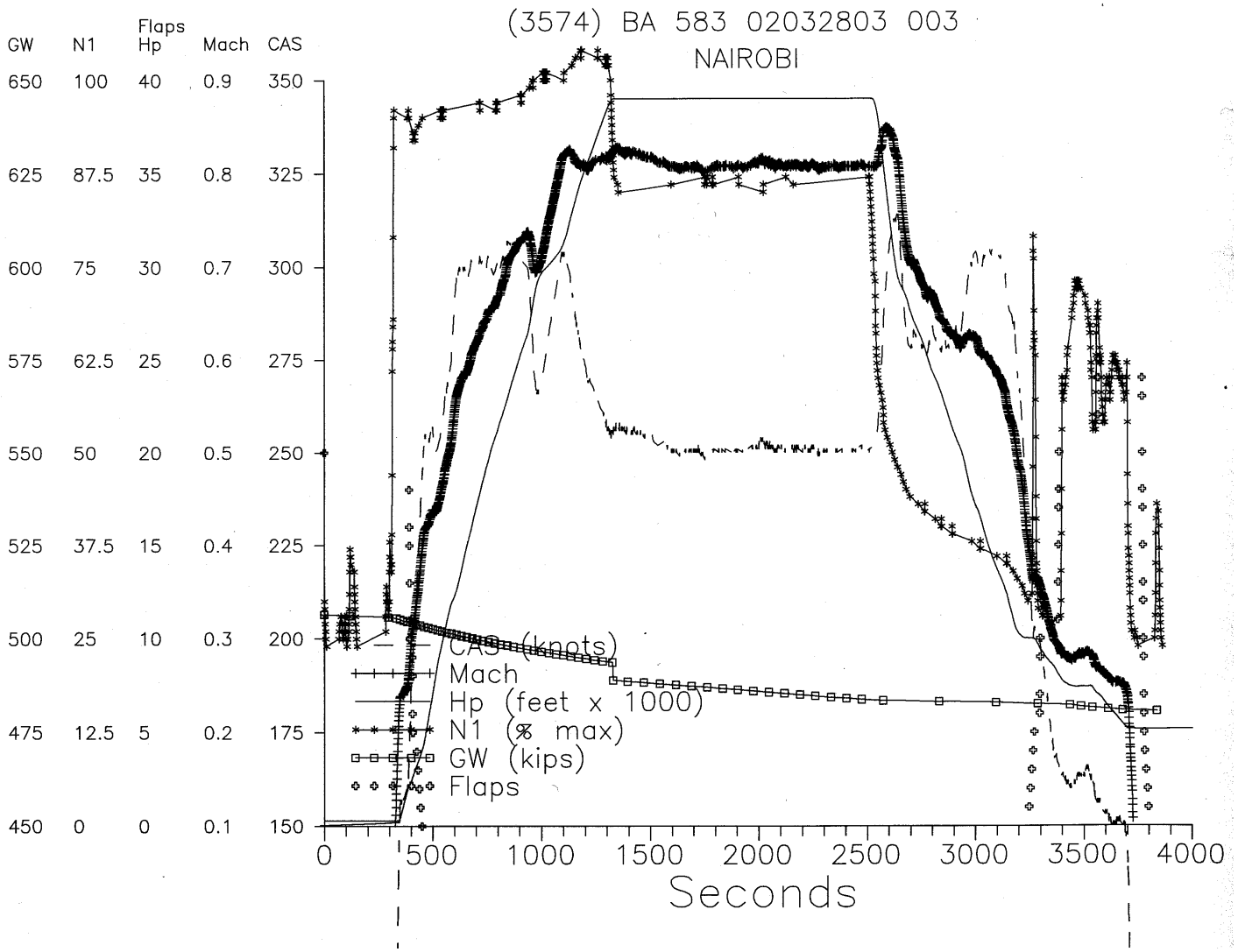

FIGURE D-25. ACTUAL DESCENT PROFILES BEGINNING BEFORE DESCENT PHASE FOR NON-CAPACITY-LIMITED FLIGHT (FLIGHT SEQUENCE NUMBER 3574)

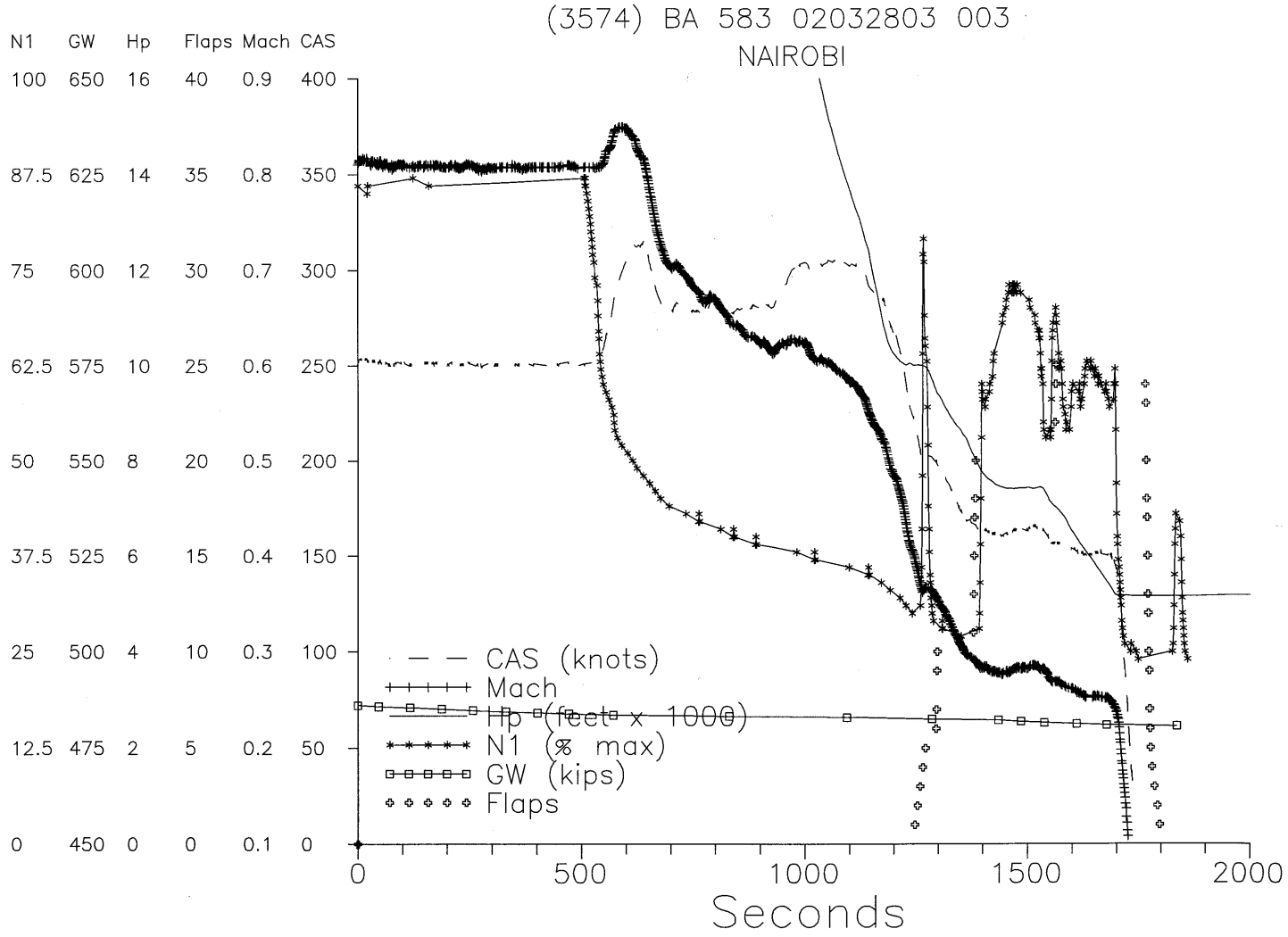

FIGURE D-26. ACTUAL DESCENT PROFILES BELOW 15K FEET FOR NON-CAPACITY-LIMITED FLIGHT (FLIGHT SEQUENCE NUMBER 3574)

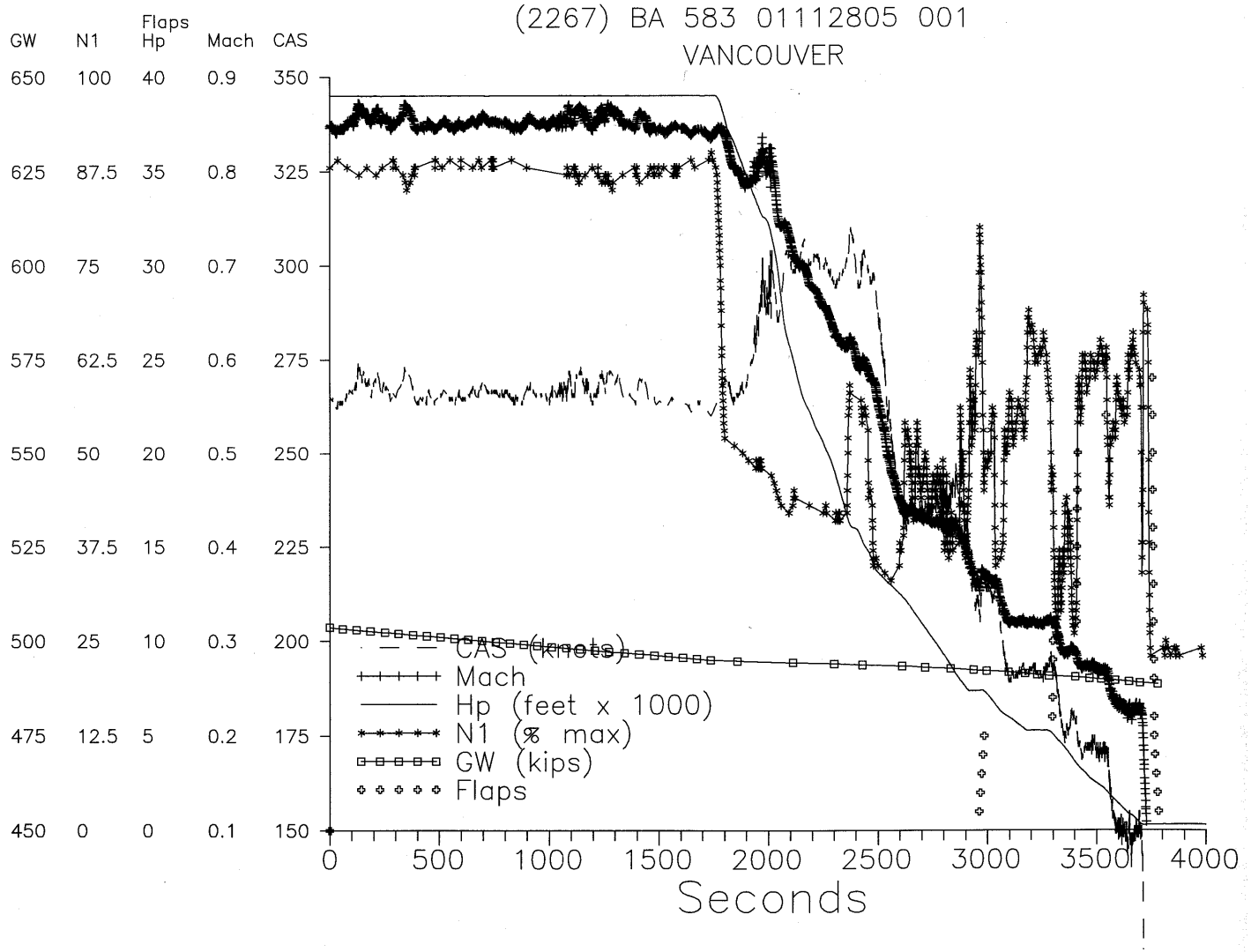

FIGURE D-27. ACTUAL DESCENT PROFILES BEGINNING BEFORE DESCENT PHASE FOR NON-CAPACITY-LIMITED FLIGHT (FLIGHT SEQUENCE NUMBER 2267)

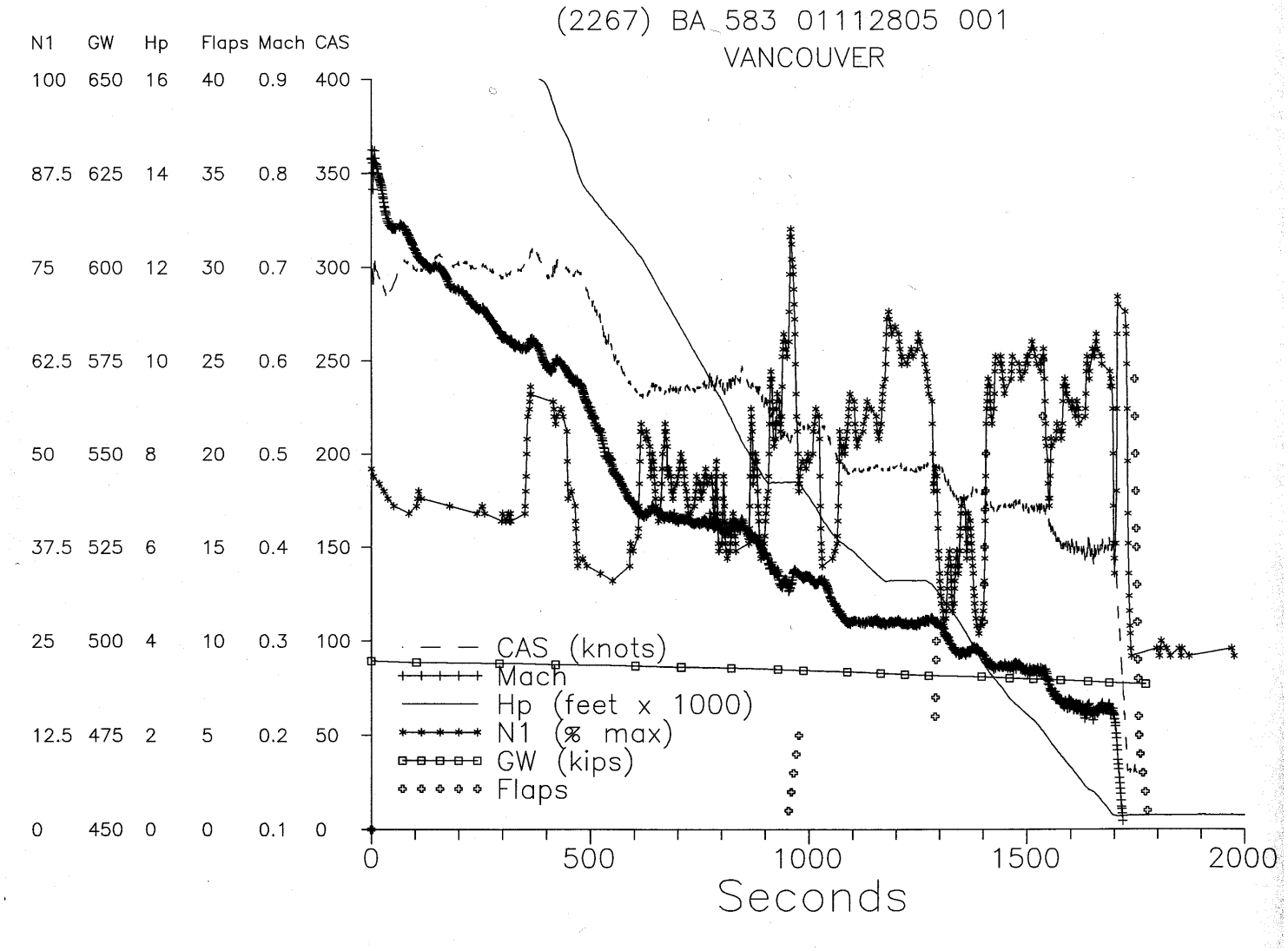

FIGURE D-28. ACTUAL DESCENT PROFILES BELOW 15K FEET FOR NON-CAPACITY-LIMITED FLIGHT (FLIGHT SEQUENCE NUMBER 2267)

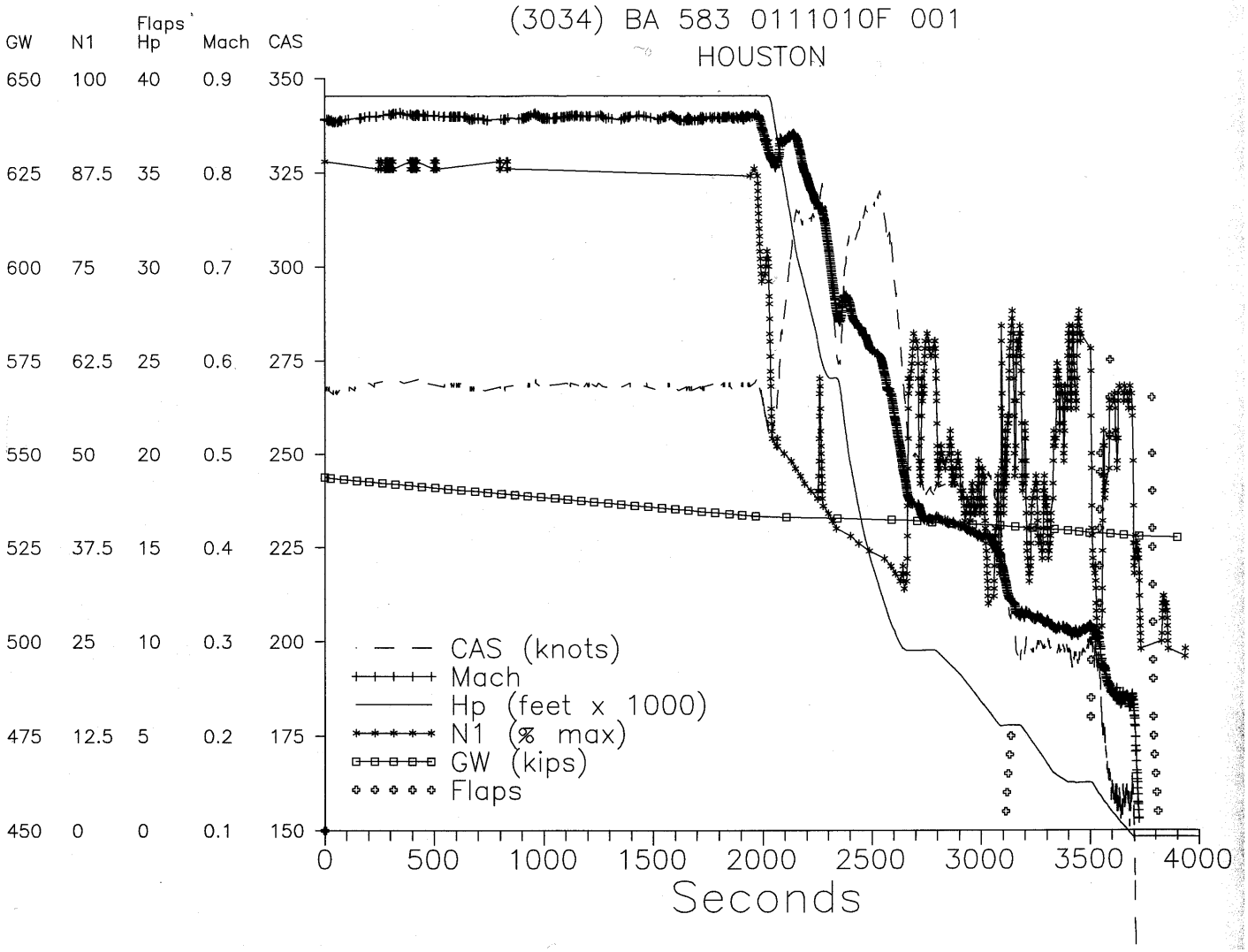

FIGURE D-29. ACTUAL DESCENT PROFILES BEGINNING BEFORE DESCENT PHASE FOR NON-CAPACITY-LIMITED FLIGHT (FLIGHT SEQUENCE NUMBER 3034)

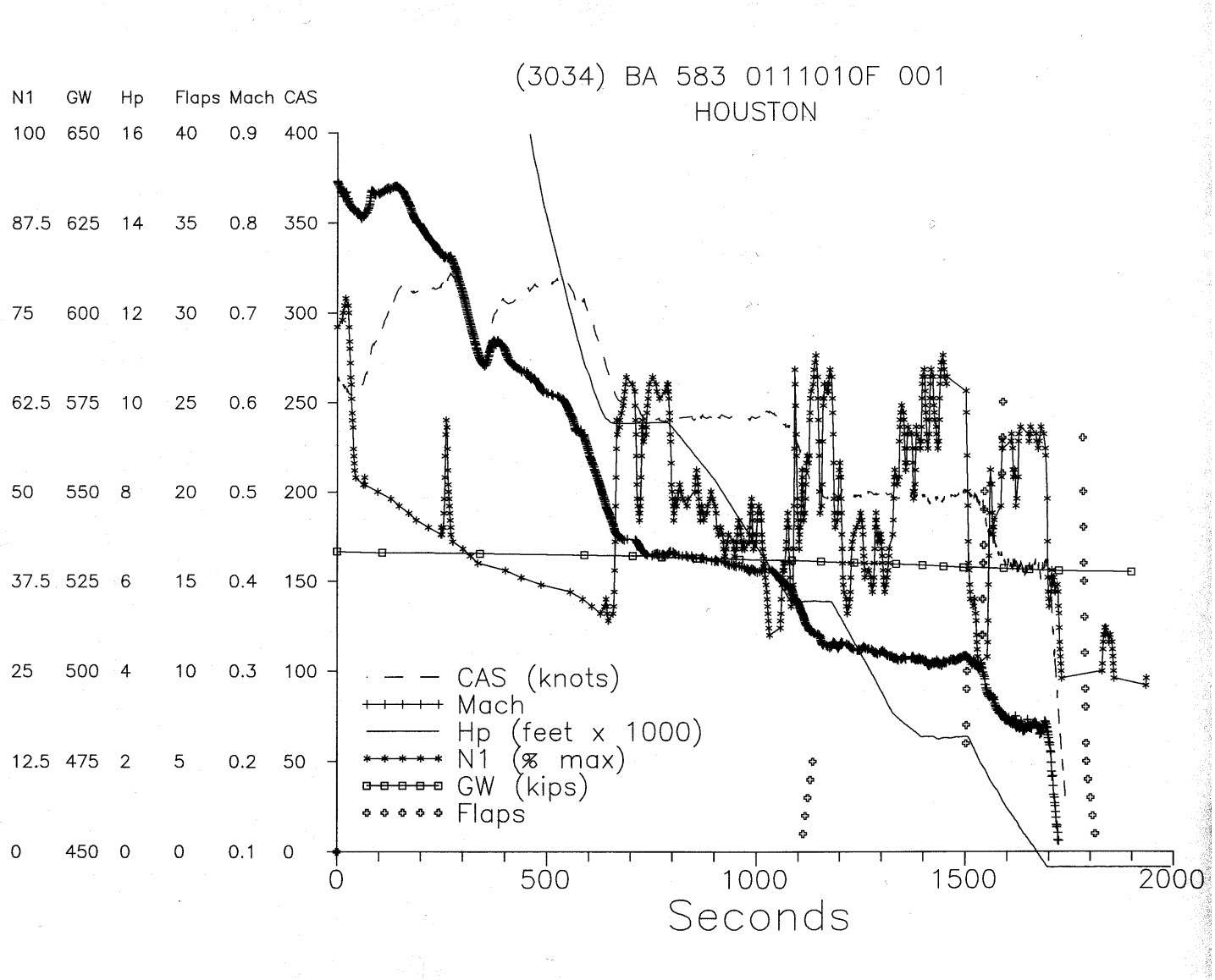

FIGURE D-30. ACTUAL DESCENT PROFILES BELOW 15K FEET FOR NON-CAPACITY-LIMITED FLIGHT (FLIGHT SEQUENCE NUMBER 3034)

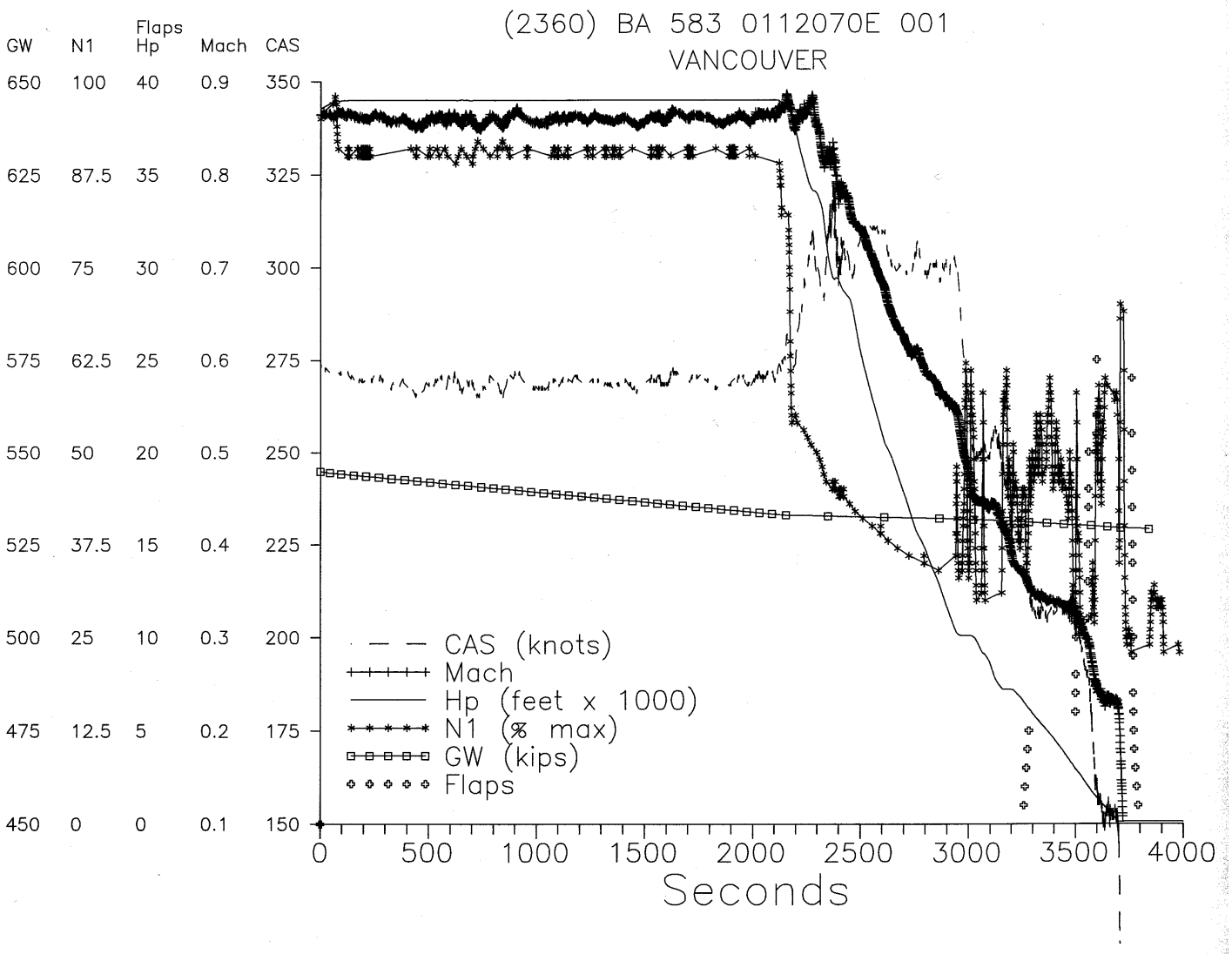

FIGURE D-31. ACTUAL DESCENT PROFILES BEGINNING BEFORE DESCENT PHASE FOR NON-CAPACITY-LIMITED FLIGHT (FLIGHT SEQUENCE NUMBER 2360)

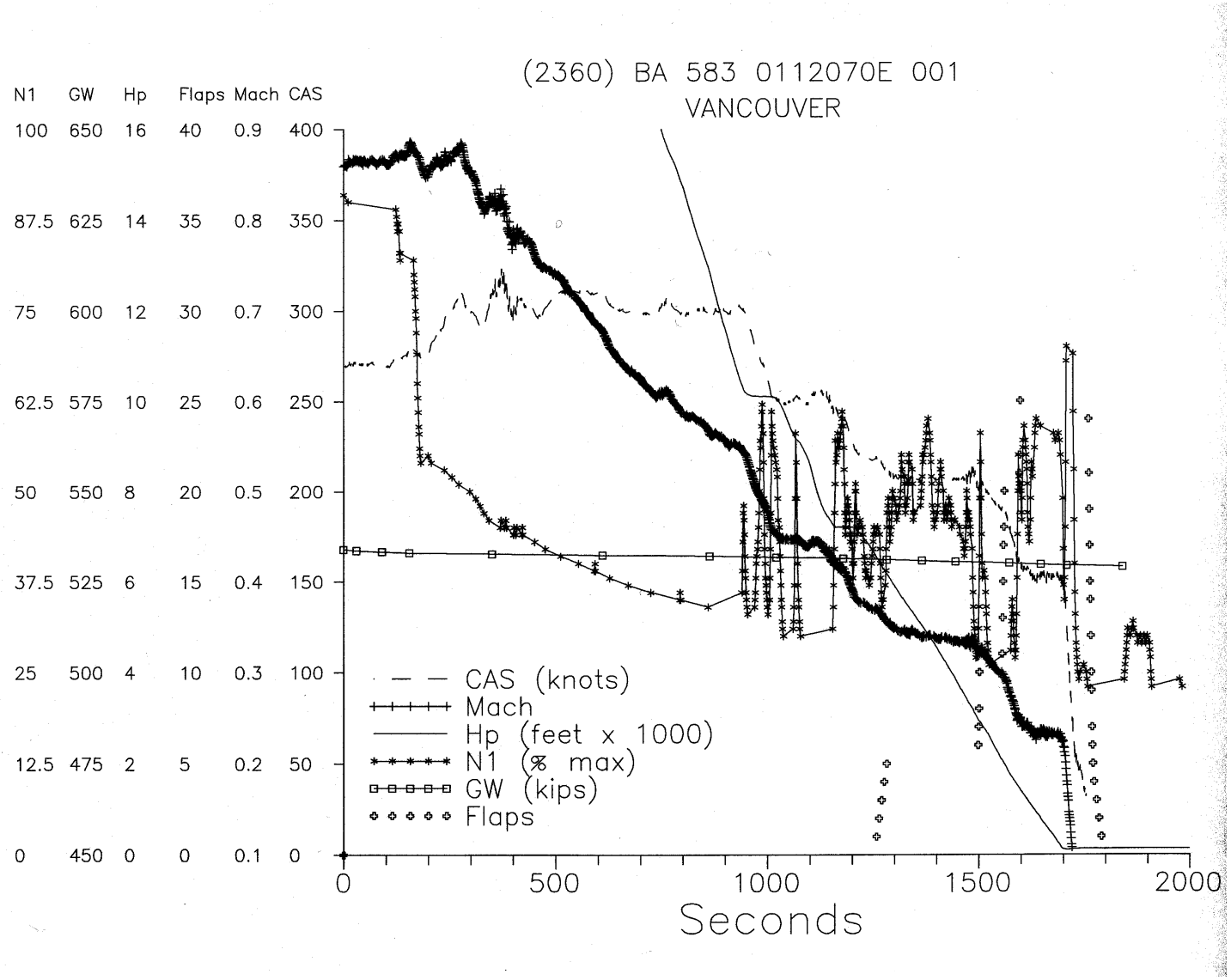

FIGURE D-32. ACTUAL DESCENT PROFILES BELOW 15K FEET FOR NON-CAPACITY-LIMITED FLIGHT (FLIGHT SEQUENCE NUMBER 2360)

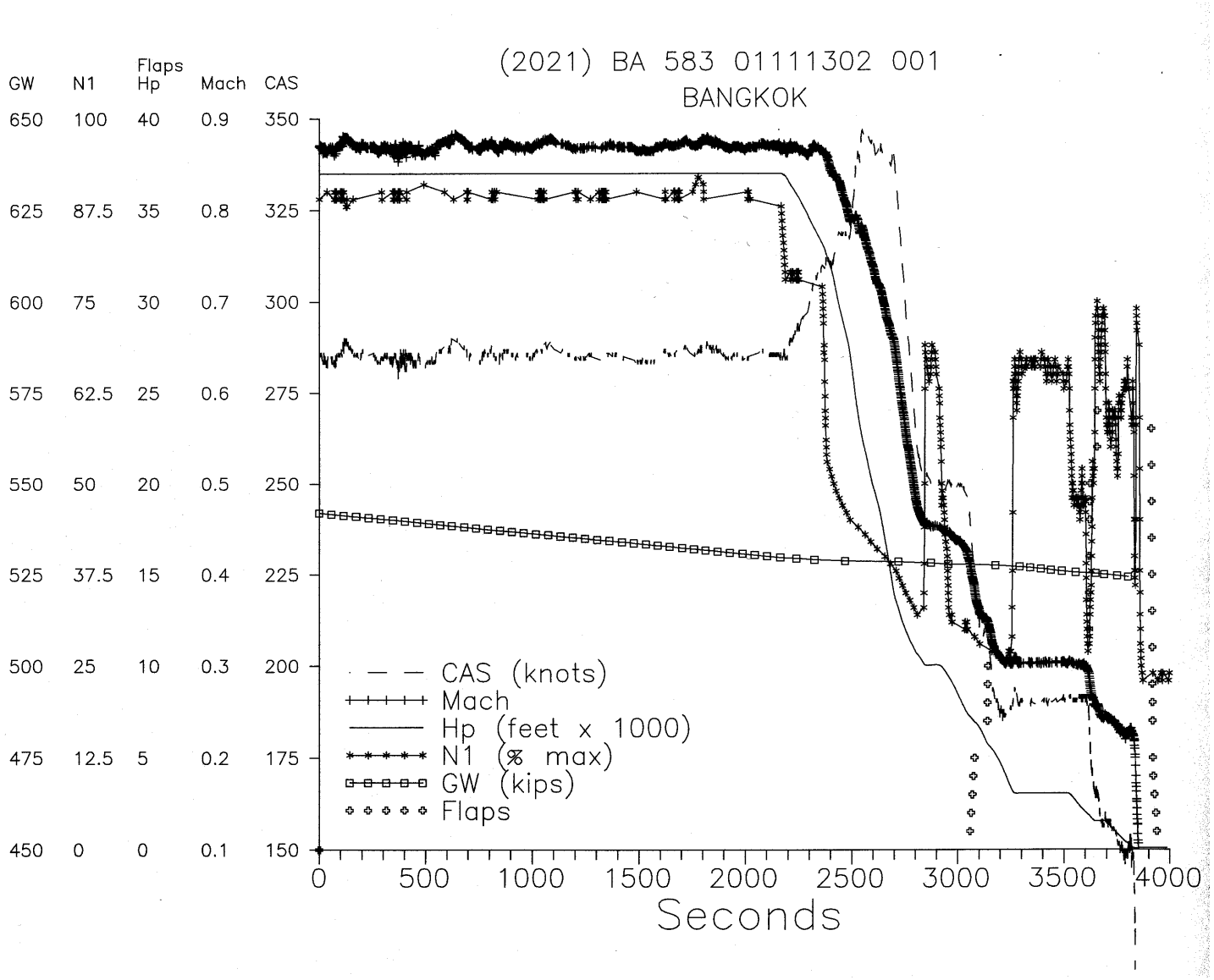

FIGURE D-33. ACTUAL DESCENT PROFILES BEGINNING BEFORE DESCENT PHASE FOR NON-CAPACITY-LIMITED FLIGHT (FLIGHT SEQUENCE NUMBER 2021)

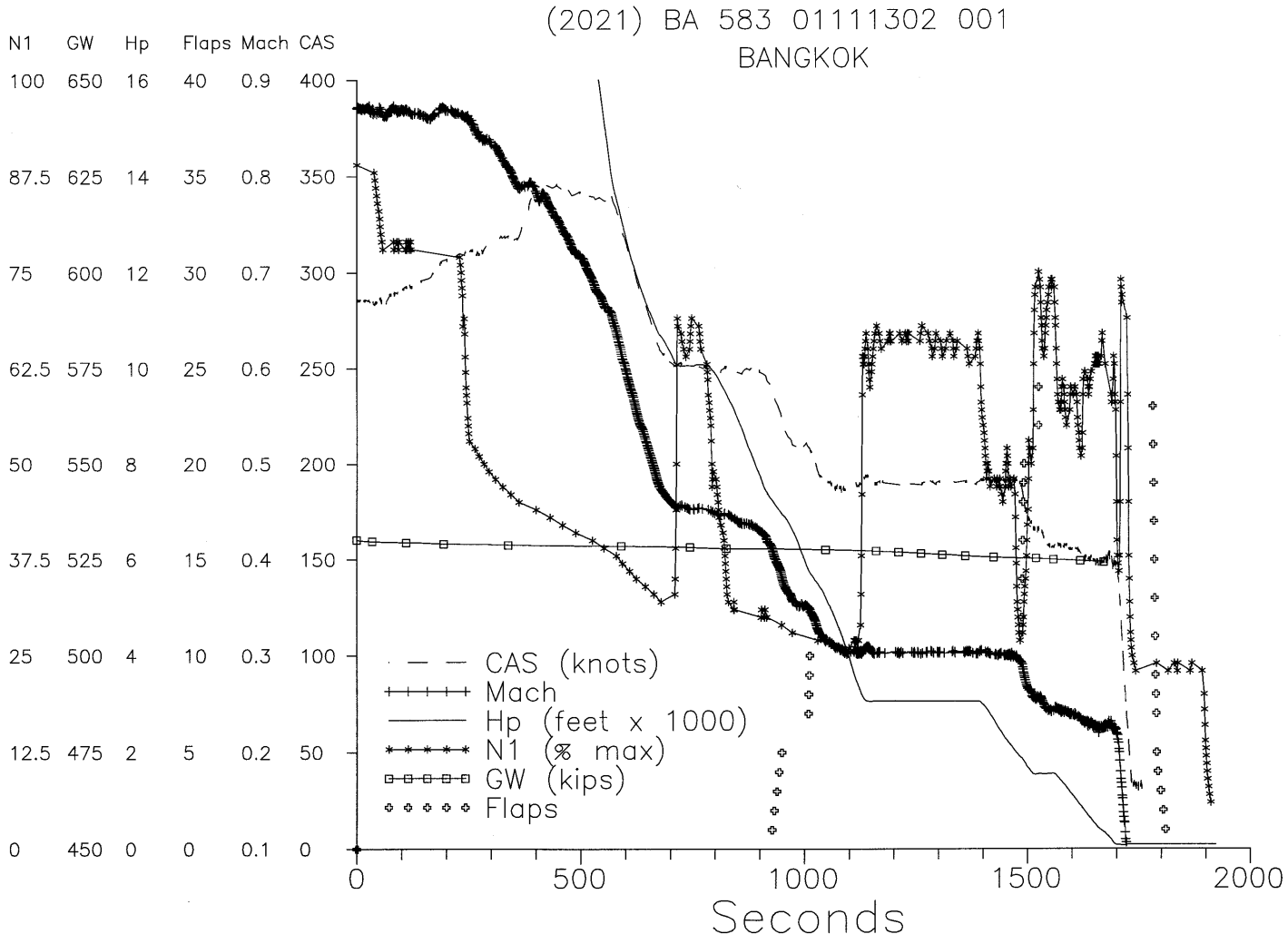

FIGURE D-34. ACTUAL DESCENT PROFILES BELOW 15K FEET FOR NON-CAPACITY-LIMITED FLIGHT (FLIGHT SEQUENCE NUMBER 2021)

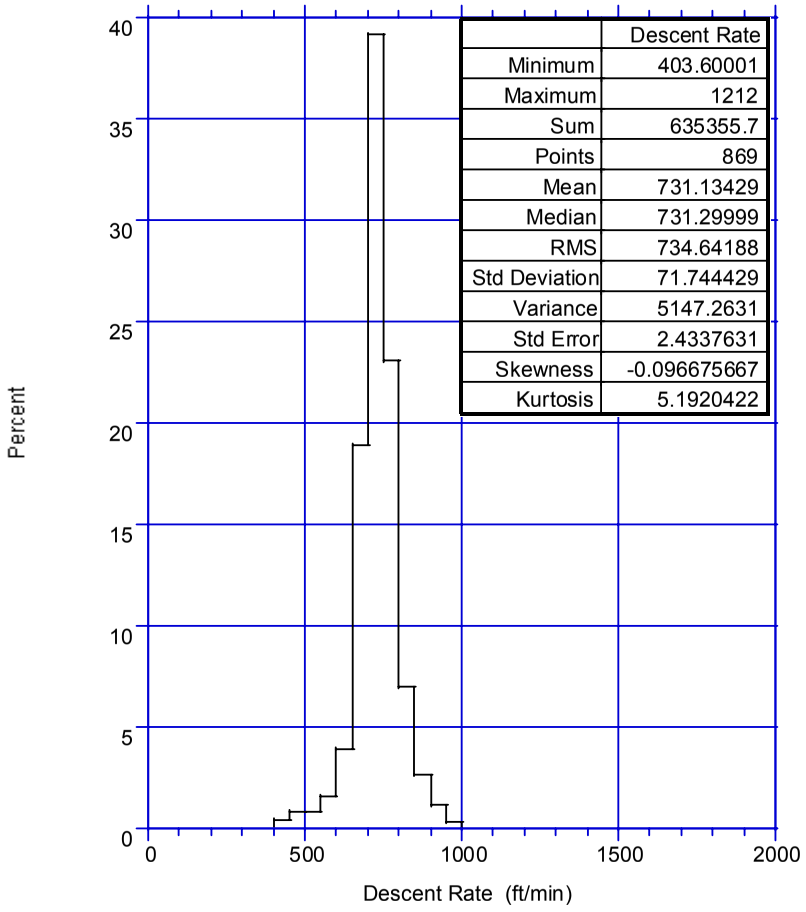

FIGURE D-35. PROBABILITY OF DESCENT RATE FOR DESCENTS BETWEEN 0-1000 FEET, NON-CAPACITY-LIMITED AIRPORTS

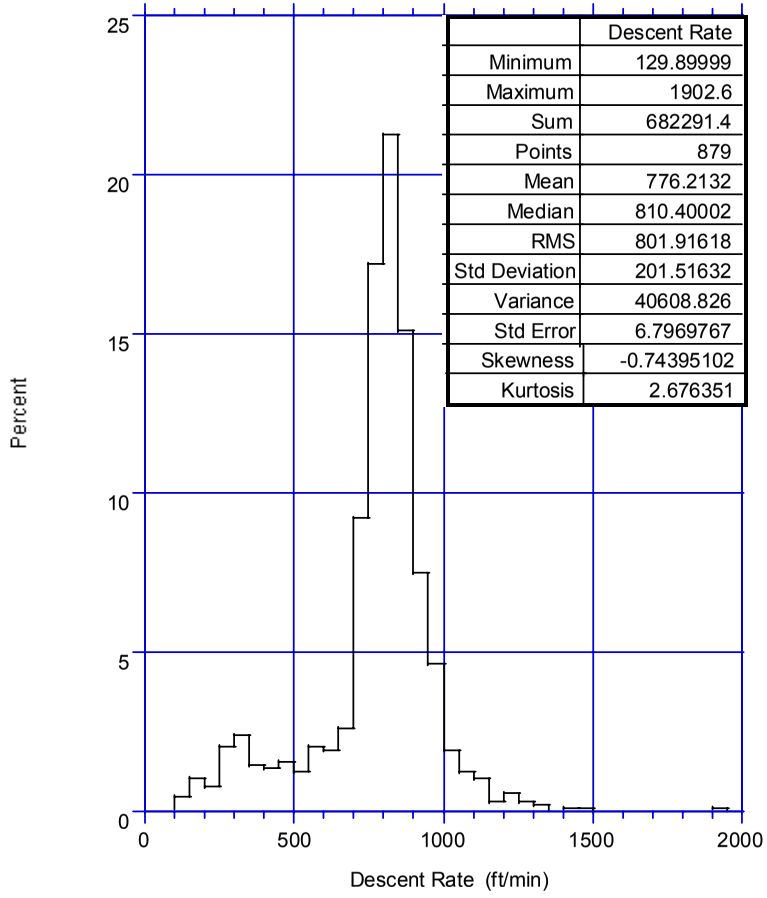

FIGURE D-36. PROBABILITY OF DESCENT RATE FOR DESCENTS BETWEEN 1000-2000 FEET, NON-CAPACITY-LIMITED AIRPORTS

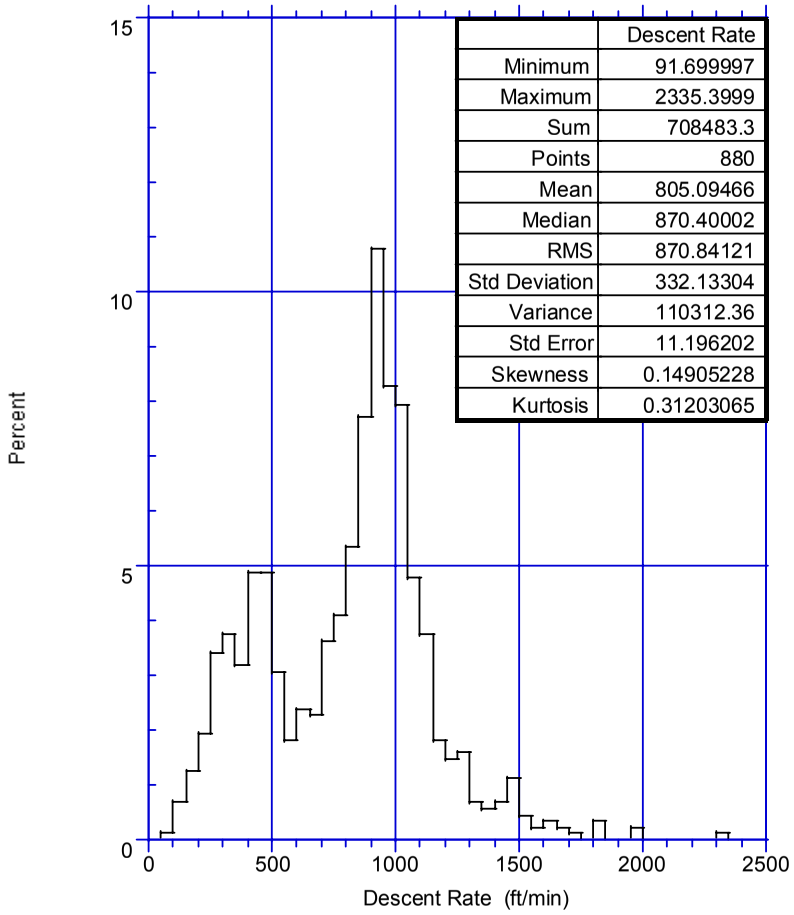

FIGURE D-37. PROBABILITY OF DESCENT RATE FOR DESCENTS BETWEEN 2000-3000 FEET, NON-CAPACITY-LIMITED AIRPORTS

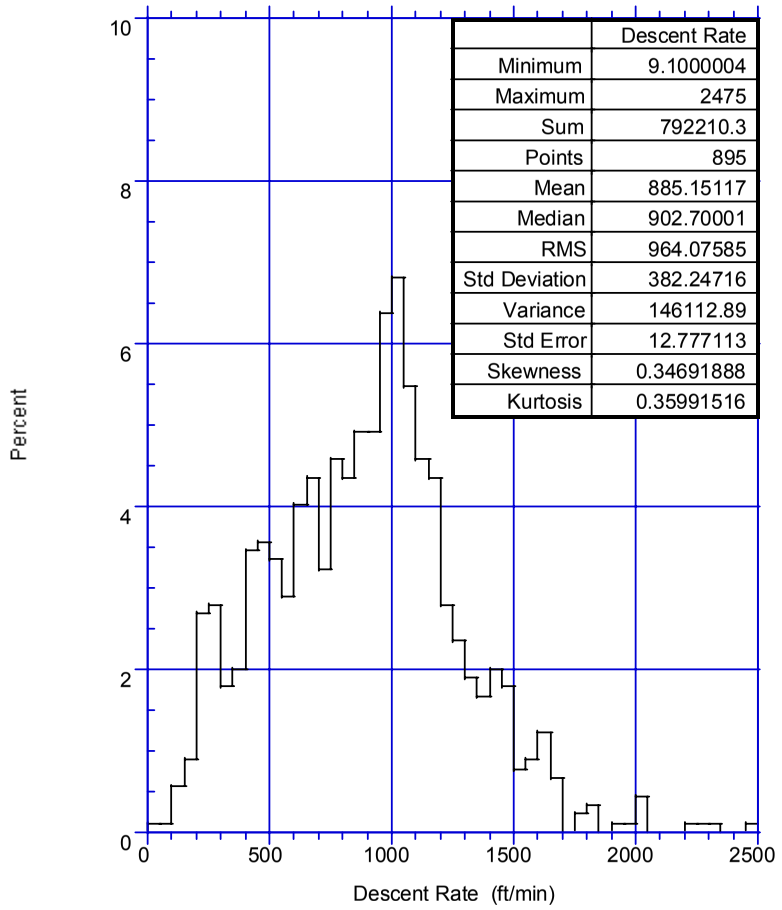

FIGURE D-38. PROBABILITY OF DESCENT RATE FOR DESCENTS BETWEEN 3000-4000 FEET, NON-CAPACITY-LIMITED AIRPORTS

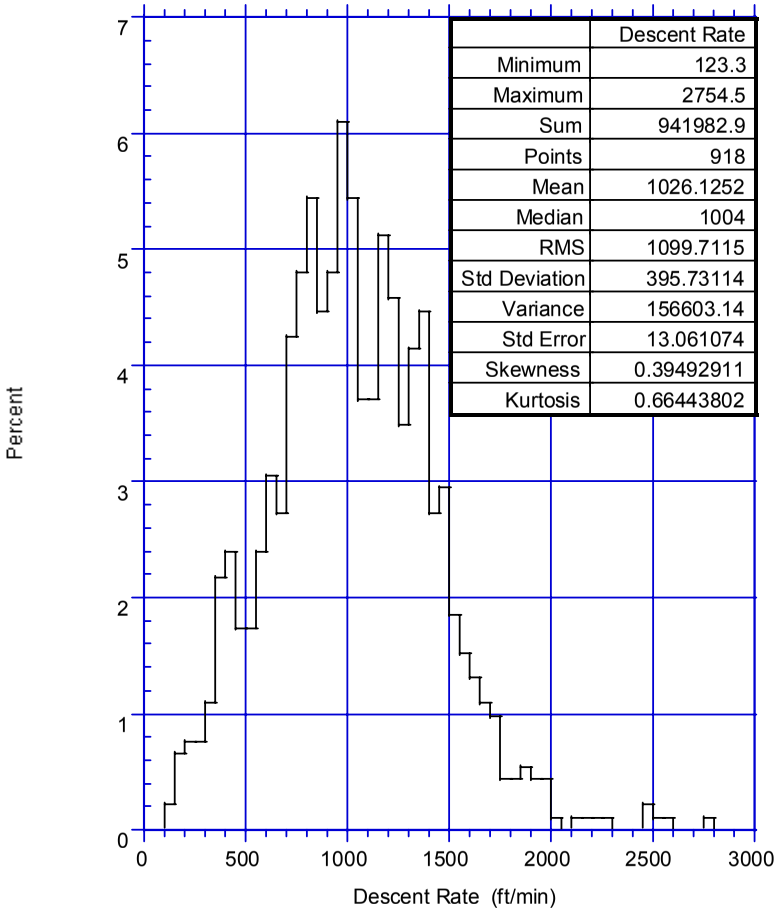

FIGURE D-39. PROBABILITY OF DESCENT RATE FOR DESCENTS BETWEEN 4000-5000 FEET, NON-CAPACITY-LIMITED AIRPORTS

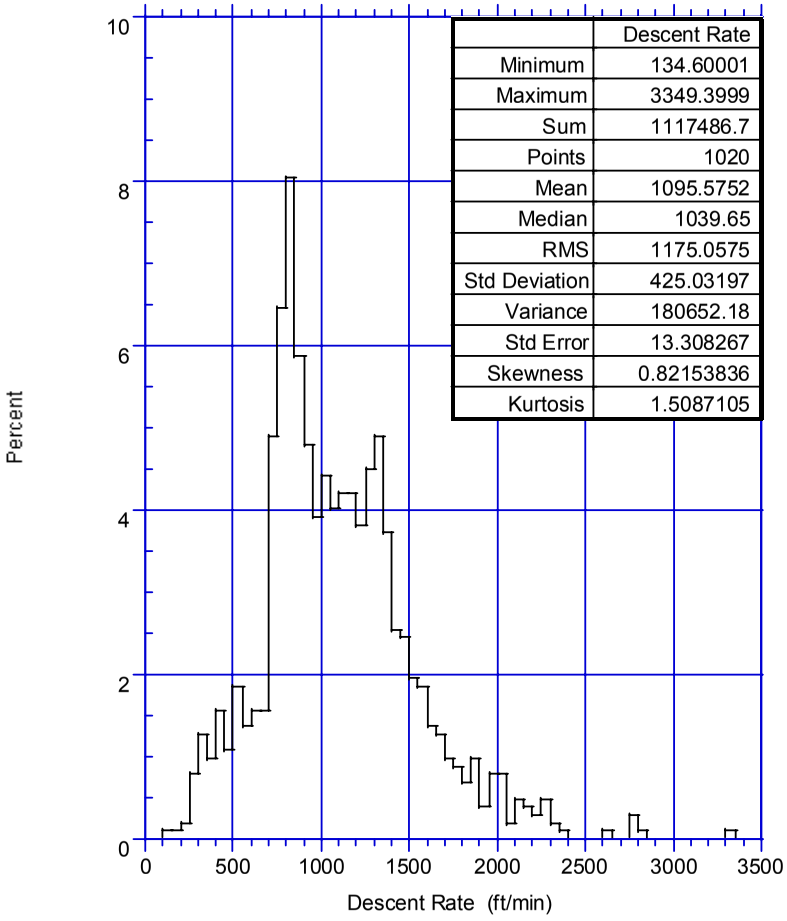

FIGURE D-40. PROBABILITY OF DESCENT RATE FOR DESCENTS BETWEEN 5000-6000 FEET, NON-CAPACITY-LIMITED AIRPORTS

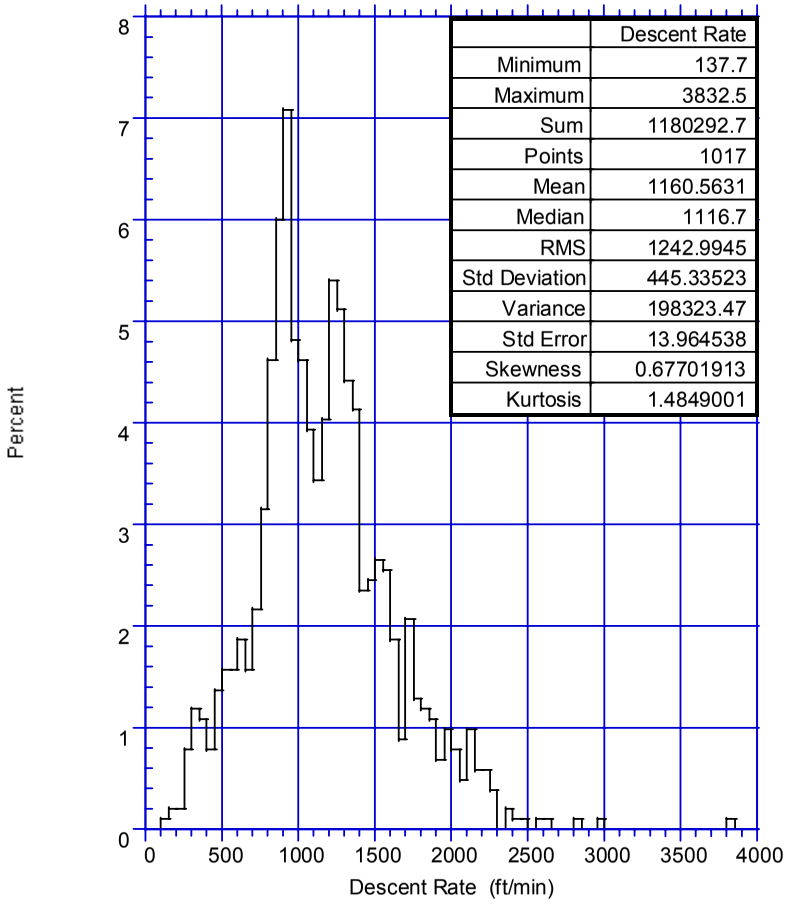

FIGURE D-41. PROBABILITY OF DESCENT RATE FOR DESCENTS BETWEEN 6000-7000 FEET, NON-CAPACITY-LIMITED AIRPORTS

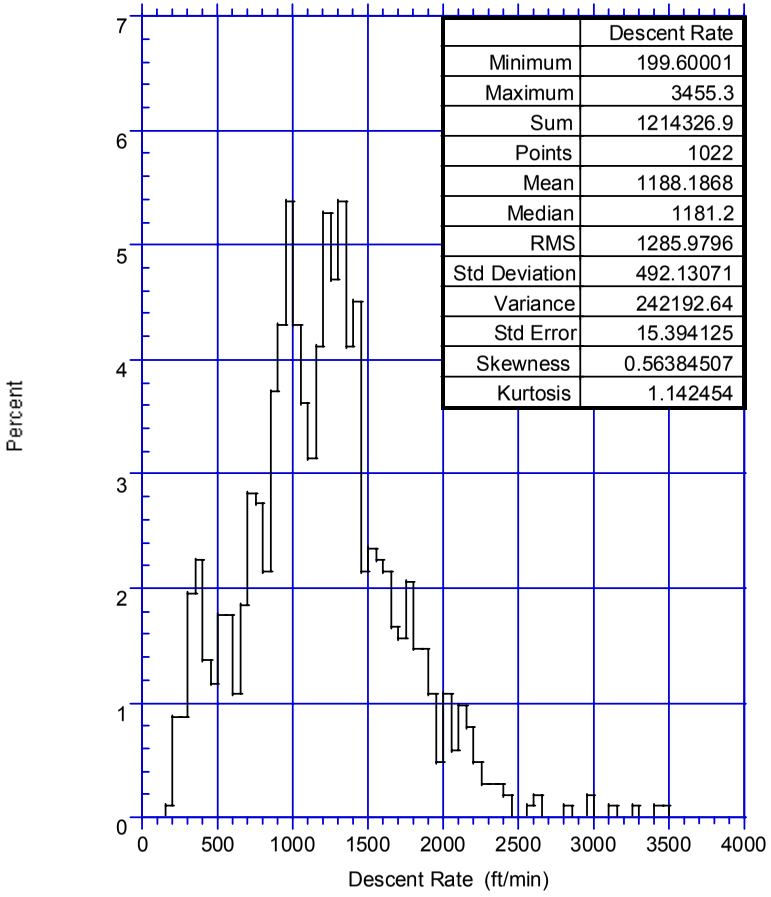

FIGURE D-42. PROBABILITY OF DESCENT RATE FOR DESCENTS BETWEEN 7000-8000 FEET, NON-CAPACITY-LIMITED AIRPORTS

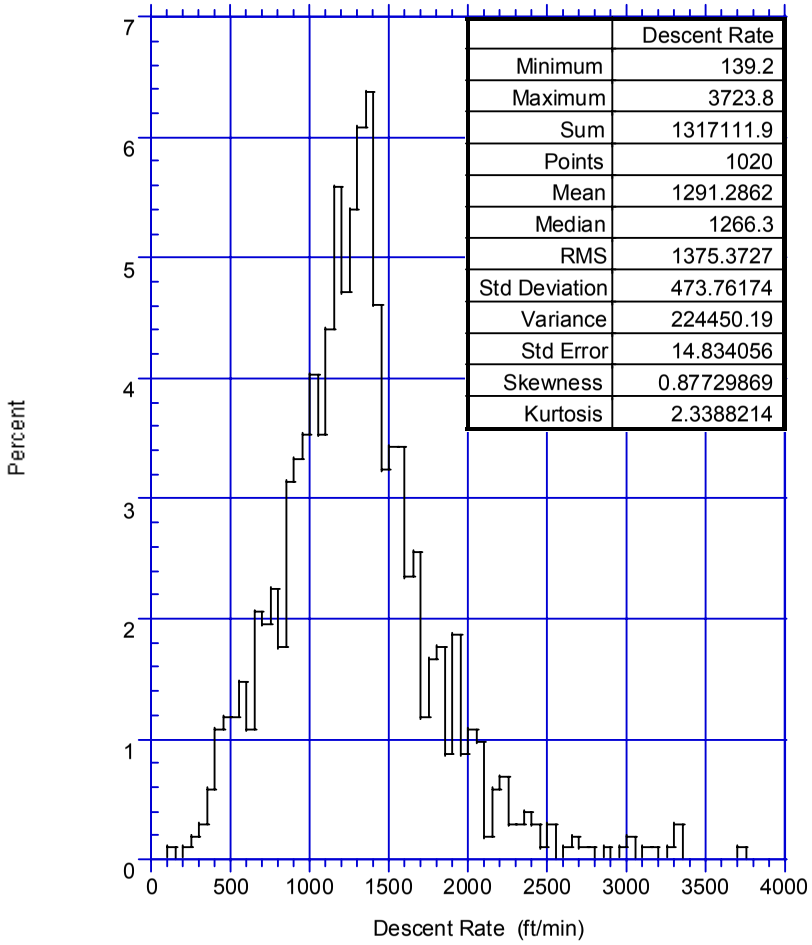

FIGURE D-43. PROBABILITY OF DESCENT RATE FOR DESCENTS BETWEEN 8000-9000 FEET, NON-CAPACITY-LIMITED AIRPORTS

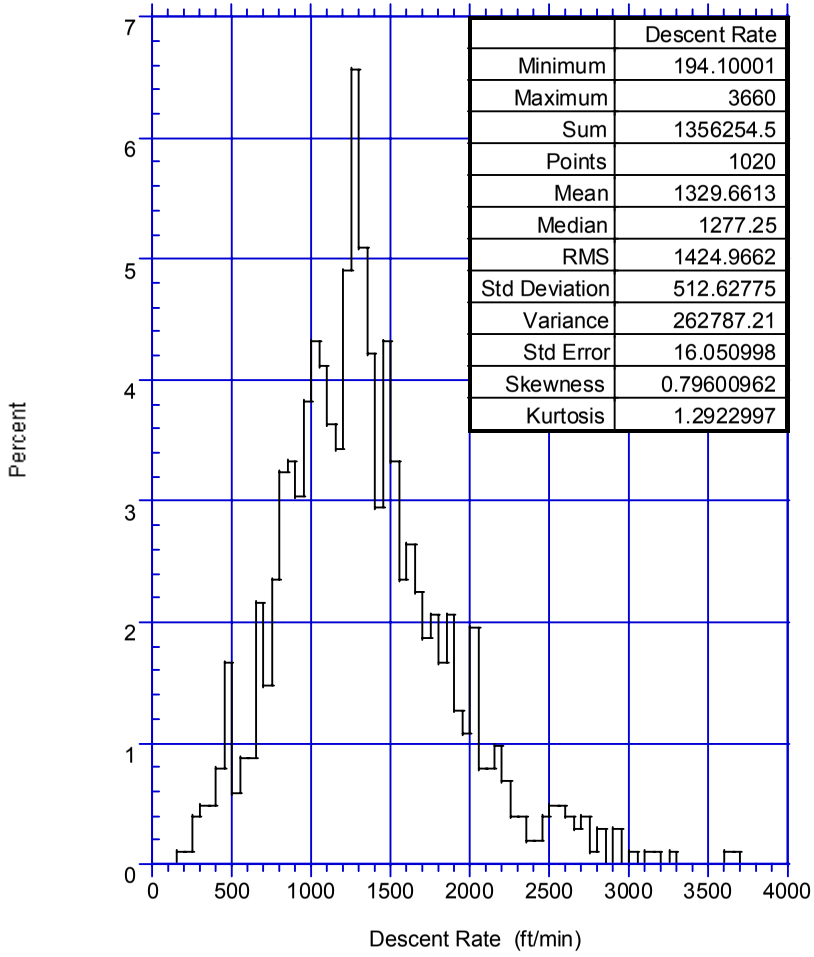

FIGURE D-44. PROBABILITY OF DESCENT RATE FOR DESCENTS BETWEEN 9,000-10,000 FEET, NON-CAPACITY-LIMITED AIRPORTS

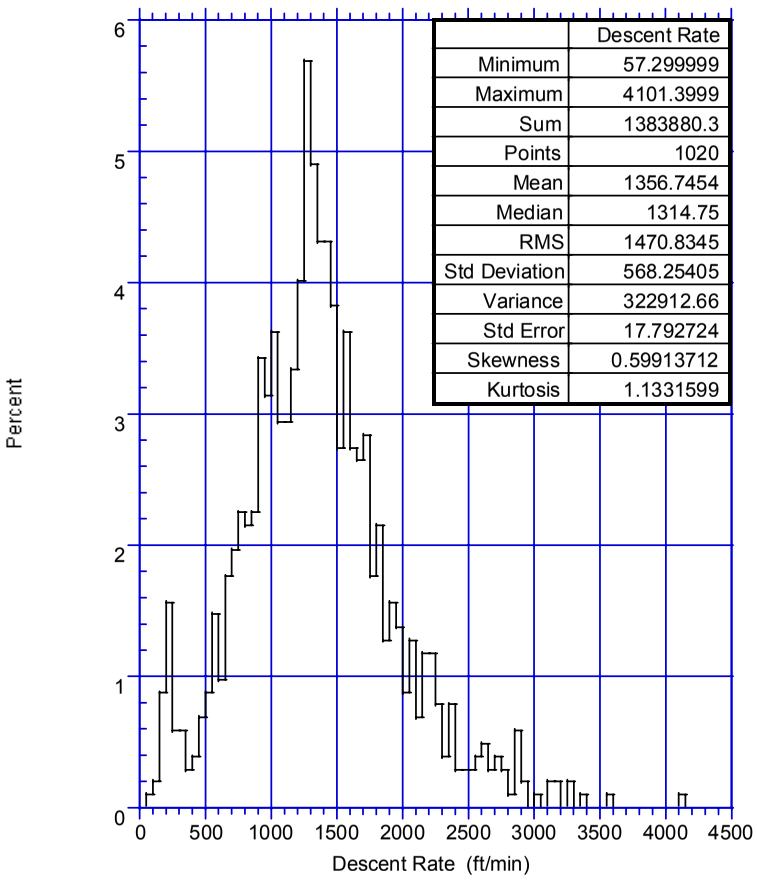

FIGURE D-45. PROBABILITY OF DESCENT RATE FOR DESCENTS BETWEEN 10,000-11,000 FEET, NON-CAPACITY-LIMITED AIRPORTS

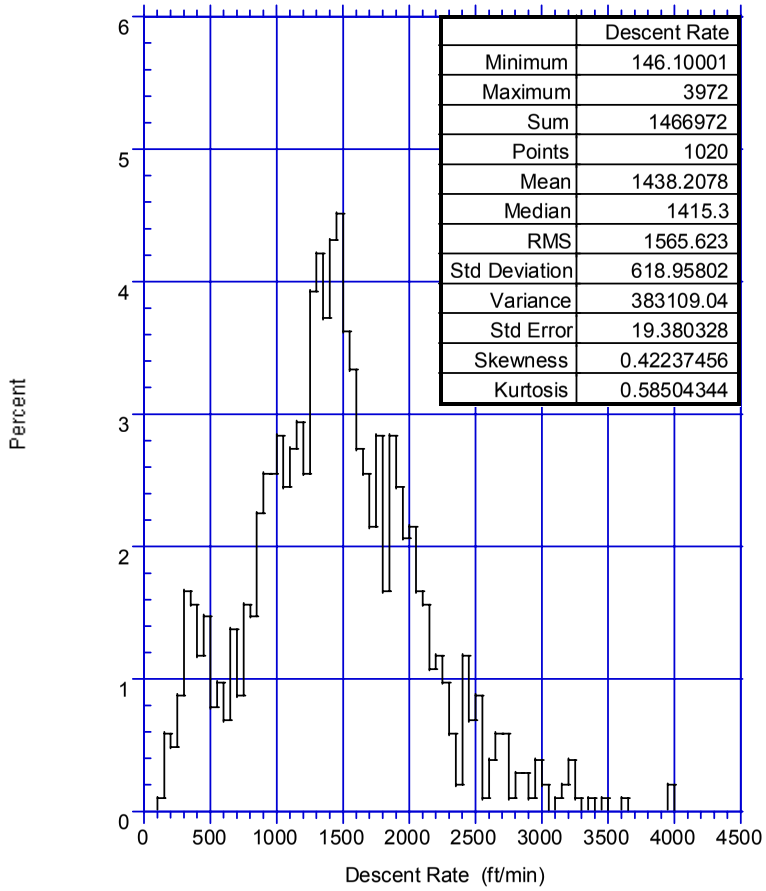

FIGURE D-46. PROBABILITY OF DESCENT RATE FOR DESCENTS BETWEEN 11,000-12,000 FEET, NON-CAPACITY-LIMITED AIRPORTS

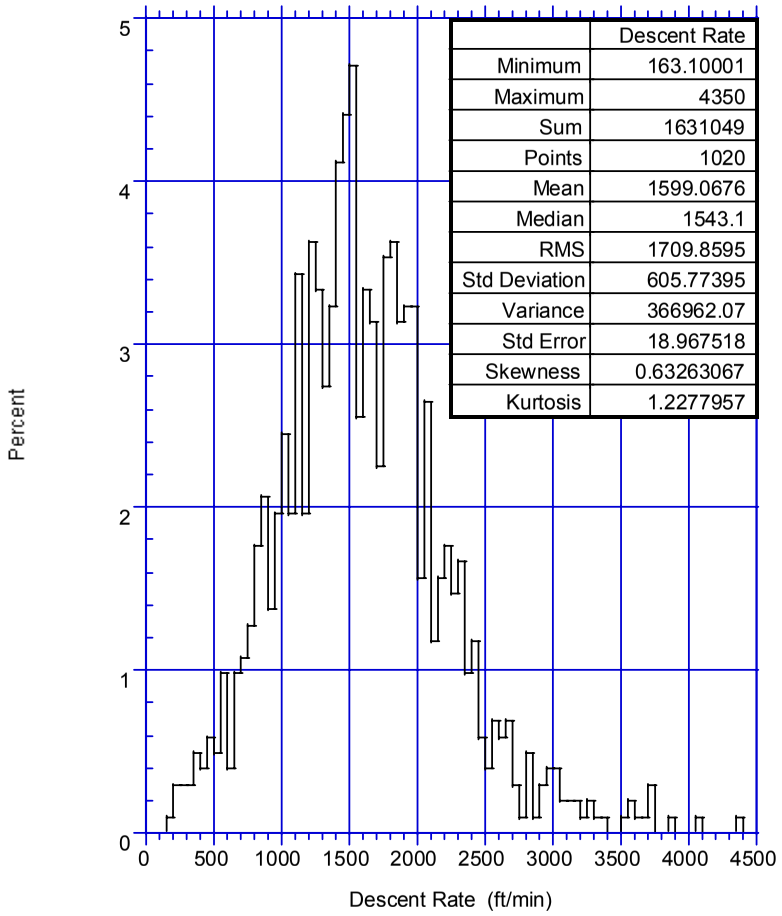

FIGURE D-47. PROBABILITY OF DESCENT RATE FOR DESCENTS BETWEEN 12,000-13,000 FEET, NON-CAPACITY-LIMITED AIRPORTS

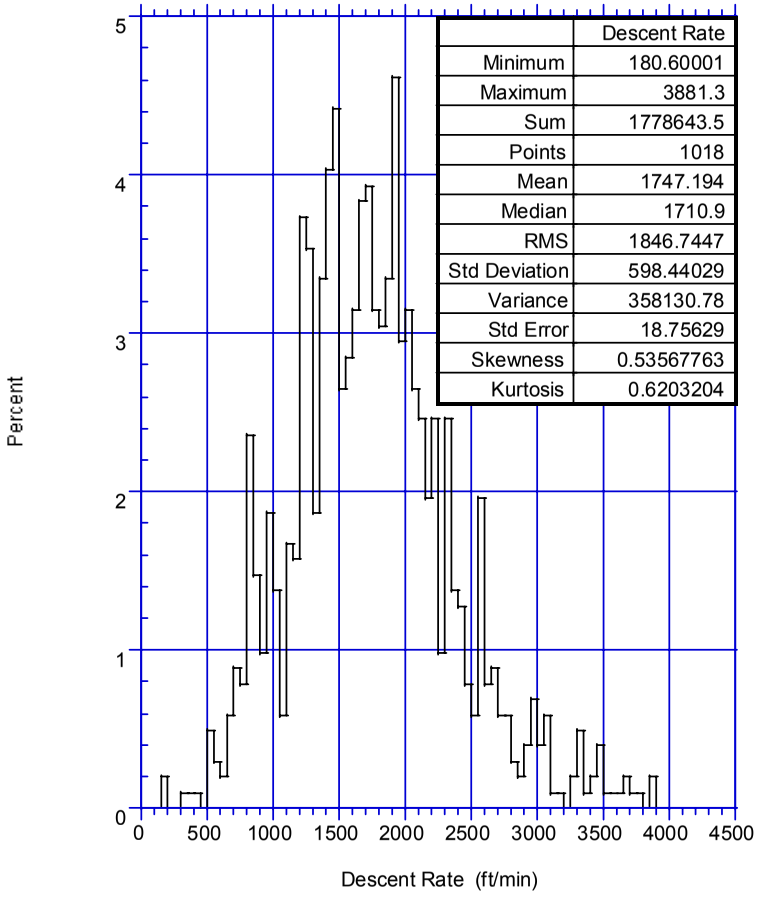

FIGURE D-48. PROBABILITY OF DESCENT RATE FOR DESCENTS BETWEEN 13,000-14,000 FEET, NON-CAPACITY-LIMITED AIRPORTS

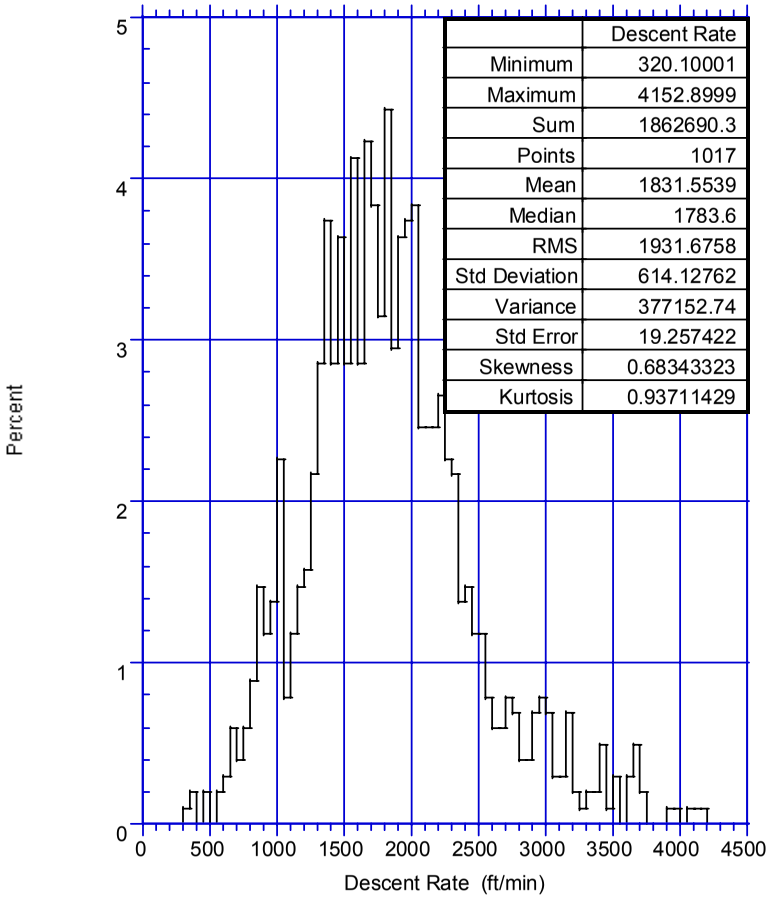

FIGURE D-49. PROBABILITY OF DESCENT RATE FOR DESCENTS BETWEEN 14,000-15,000 FEET, NON-CAPACITY-LIMITED AIRPORTS

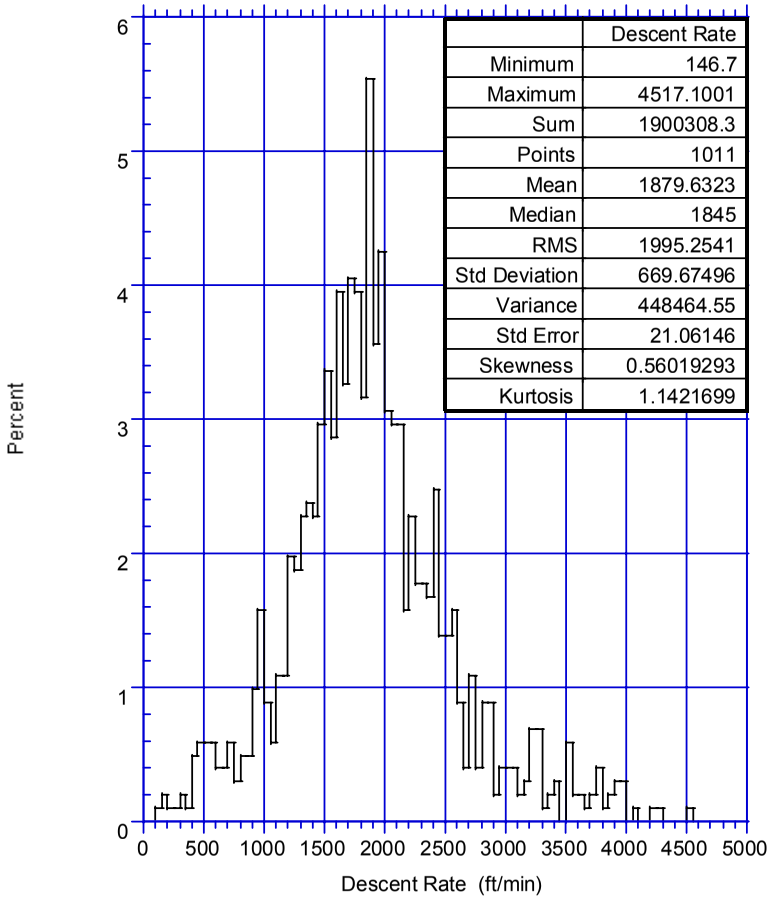

FIGURE D-50. PROBABILITY OF DESCENT RATE FOR DESCENTS BETWEEN 15,000-16,000 FEET, NON-CAPACITY-LIMITED AIRPORTS

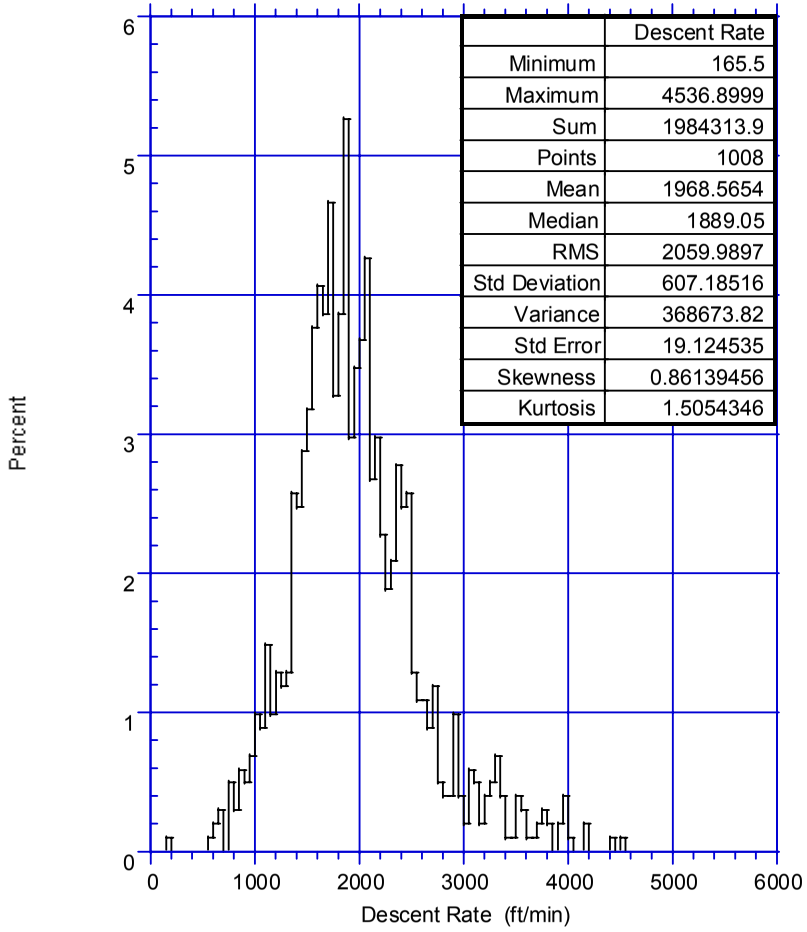

FIGURE D-51. PROBABILITY OF DESCENT RATE FOR DESCENTS BETWEEN 16,000-17,000 FEET, NON-CAPACITY-LIMITED AIRPORTS

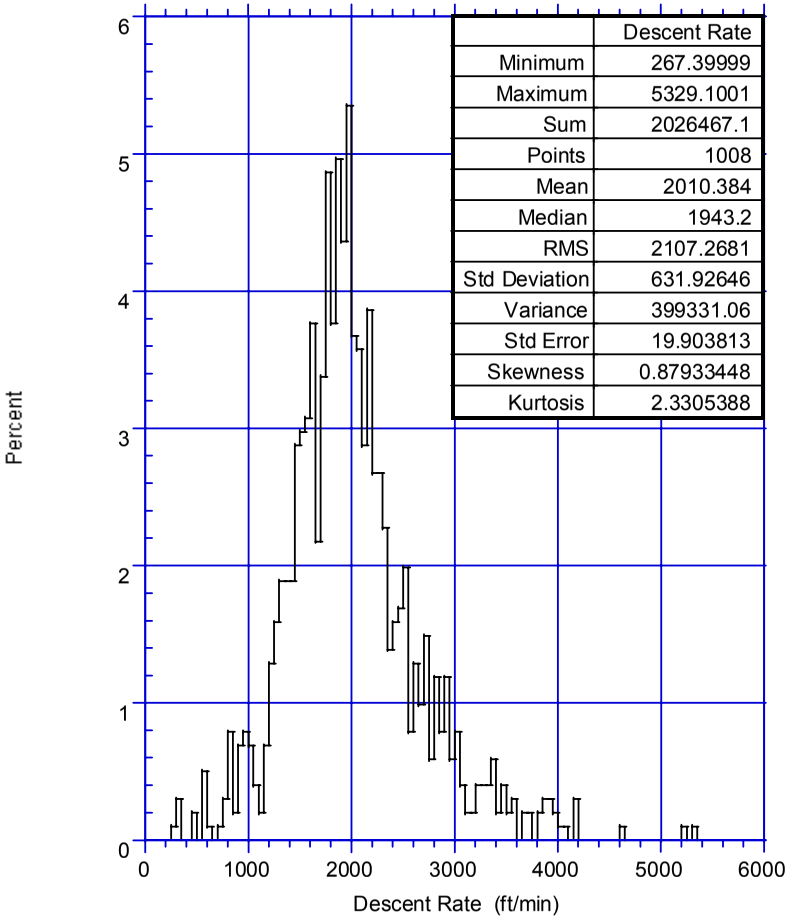

FIGURE D-52. PROBABILITY OF DESCENT RATE FOR DESCENTS BETWEEN 17,000-18,000 FEET, NON-CAPACITY-LIMITED AIRPORTS

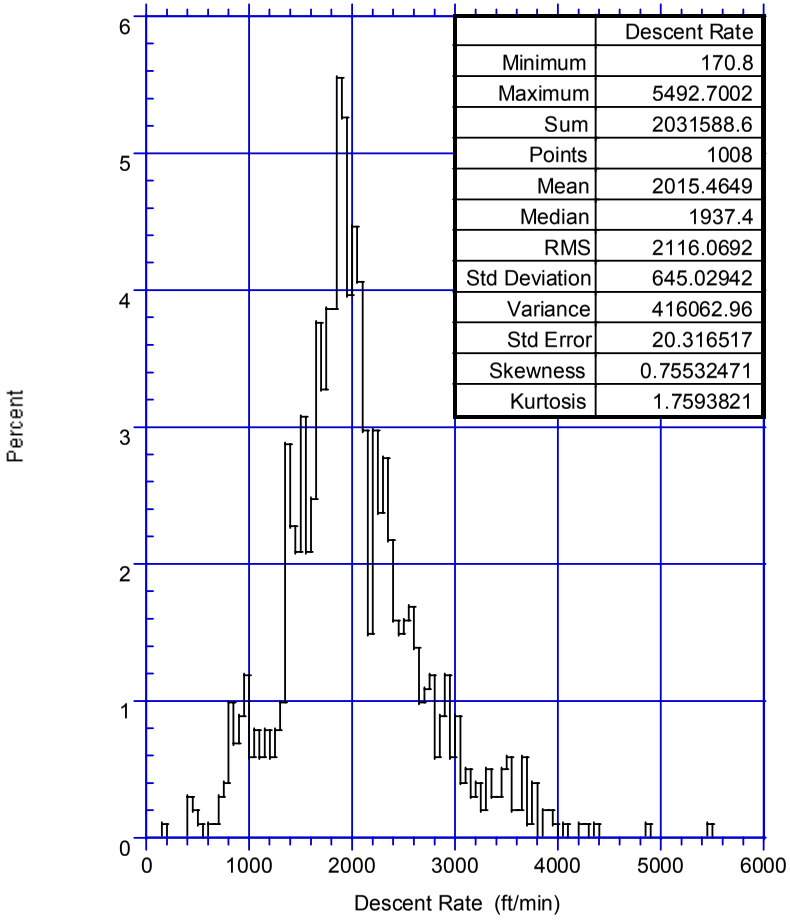

FIGURE D-53. PROBABILITY OF DESCENT RATE FOR DESCENTS BETWEEN 18,000-19,000 FEET, NON-CAPACITY-LIMITED AIRPORTS

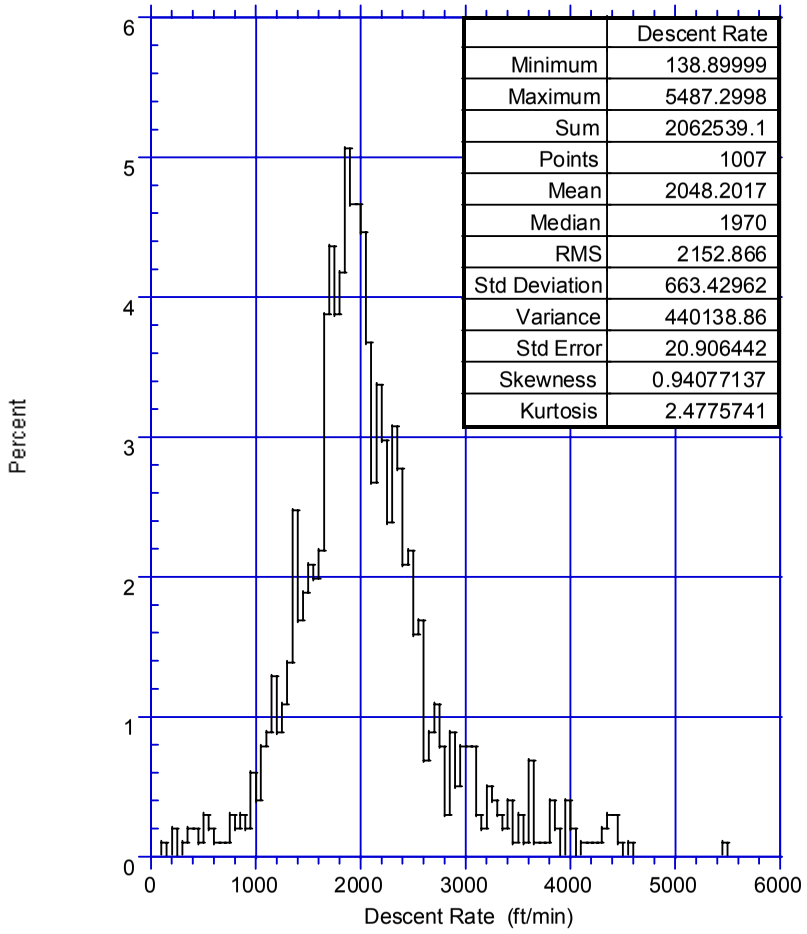

FIGURE D-54. PROBABILITY OF DESCENT RATE FOR DESCENTS BETWEEN 19,000-20,000 FEET, NON-CAPACITY-LIMITED AIRPORTS

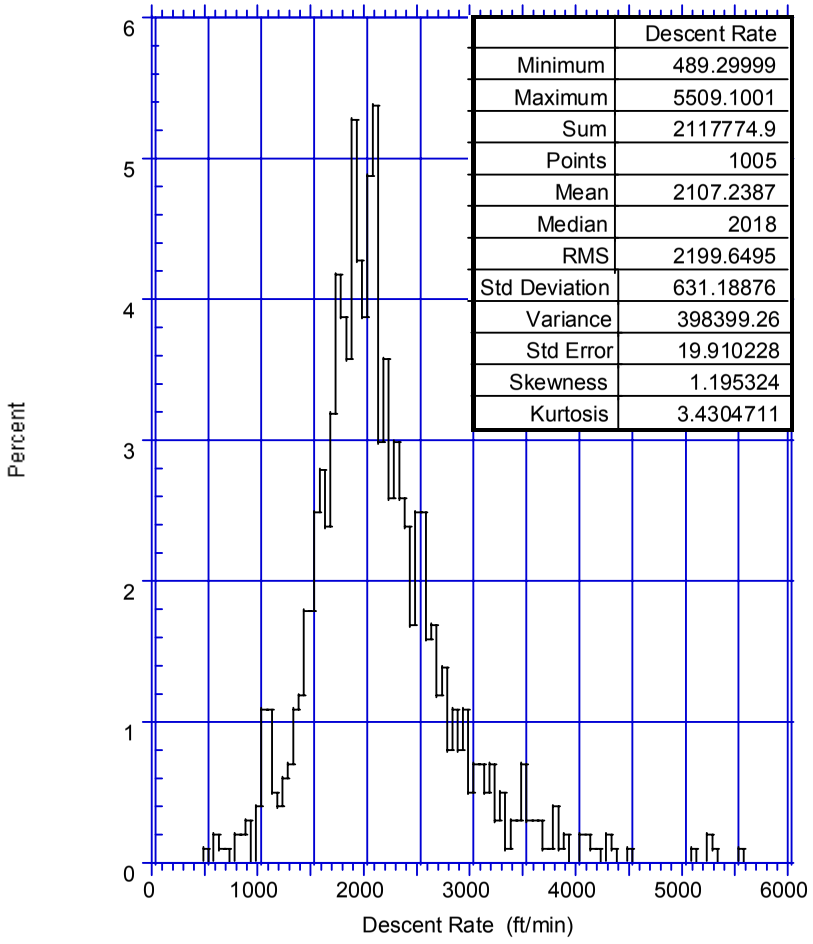

FIGURE D-55. PROBABILITY OF DESCENT RATE FOR DESCENTS BETWEEN 20,000-21,000 FEET, NON-CAPACITY-LIMITED AIRPORTS

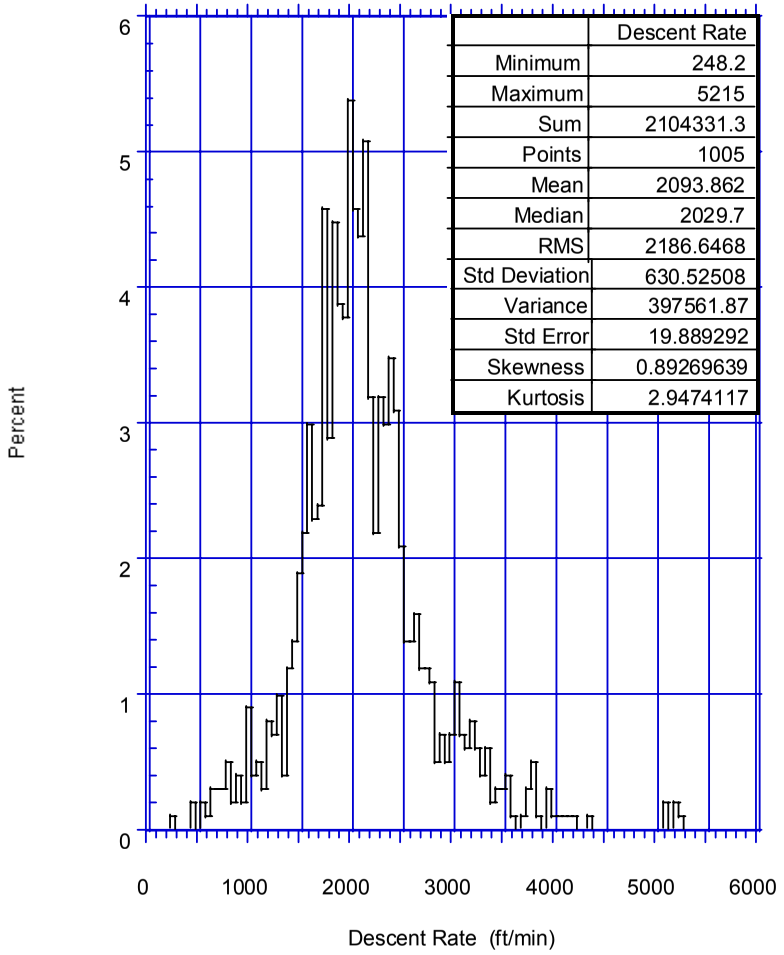

FIGURE D-56. PROBABILITY OF DESCENT RATE FOR DESCENTS BETWEEN 21,000-22,000 FEET, NON-CAPACITY-LIMITED AIRPORTS

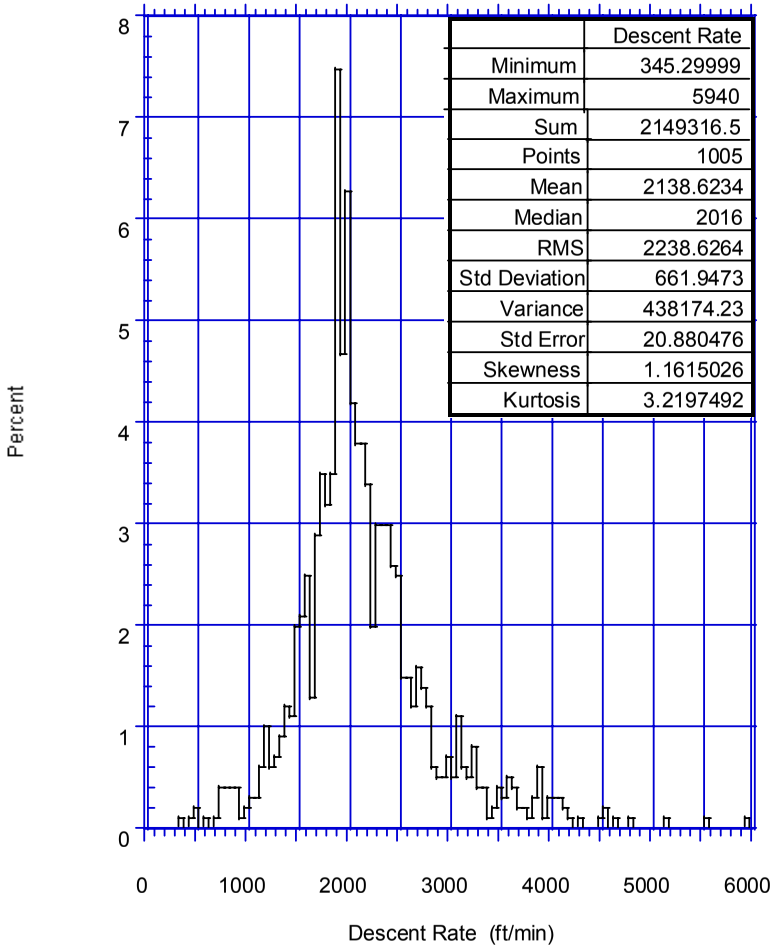

FIGURE D-57. PROBABILITY OF DESCENT RATE FOR DESCENTS BETWEEN 22,000-23,000 FEET, NON-CAPACITY-LIMITED AIRPORTS

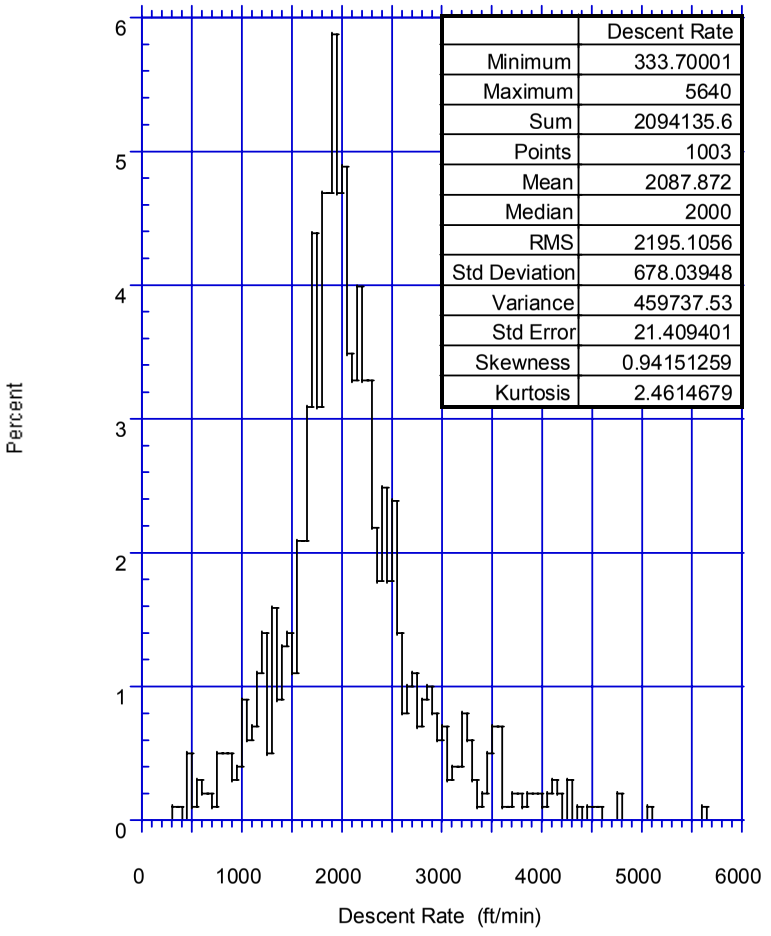

FIGURE D-58. PROBABILITY OF DESCENT RATE FOR DESCENTS BETWEEN 23,000-24,000 FEET, NON-CAPACITY-LIMITED AIRPORTS

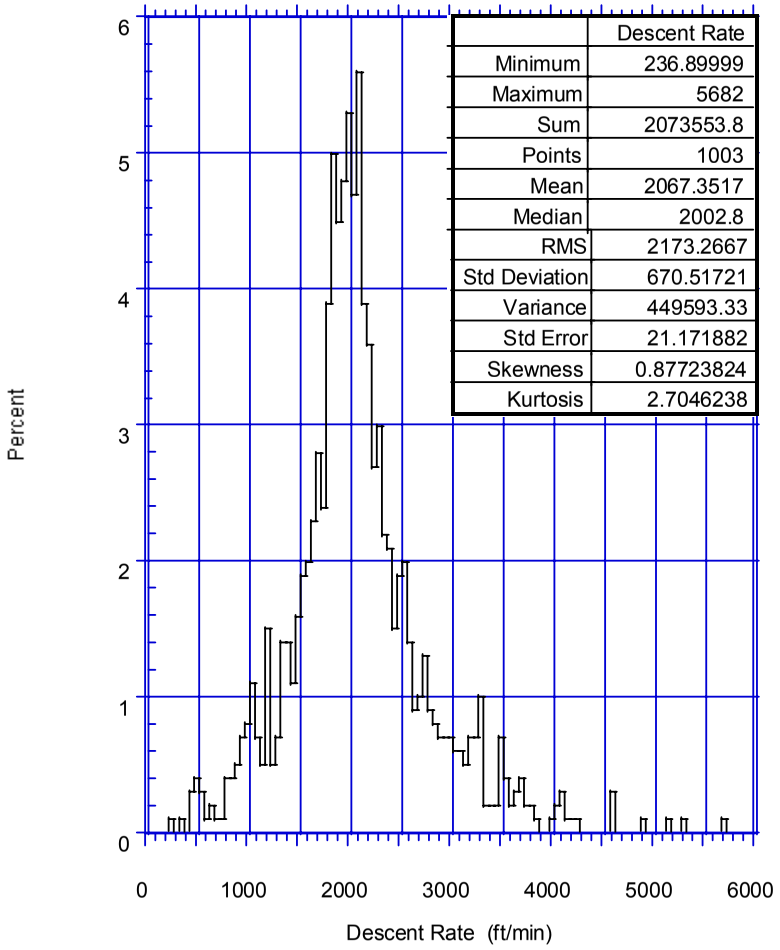

FIGURE D-59. PROBABILITY OF DESCENT RATE FOR DESCENTS BETWEEN 24,000-25,000 FEET, NON-CAPACITY-LIMITED AIRPORTS

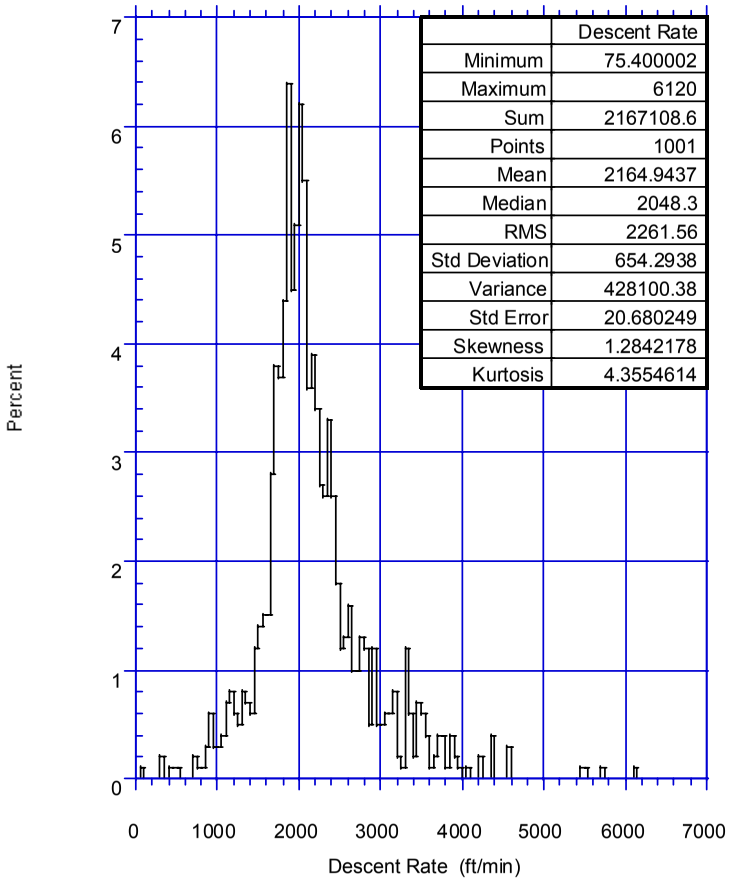

FIGURE D-60. PROBABILITY OF DESCENT RATE FOR DESCENTS BETWEEN 25,000-26,000 FEET, NON-CAPACITY-LIMITED AIRPORTS

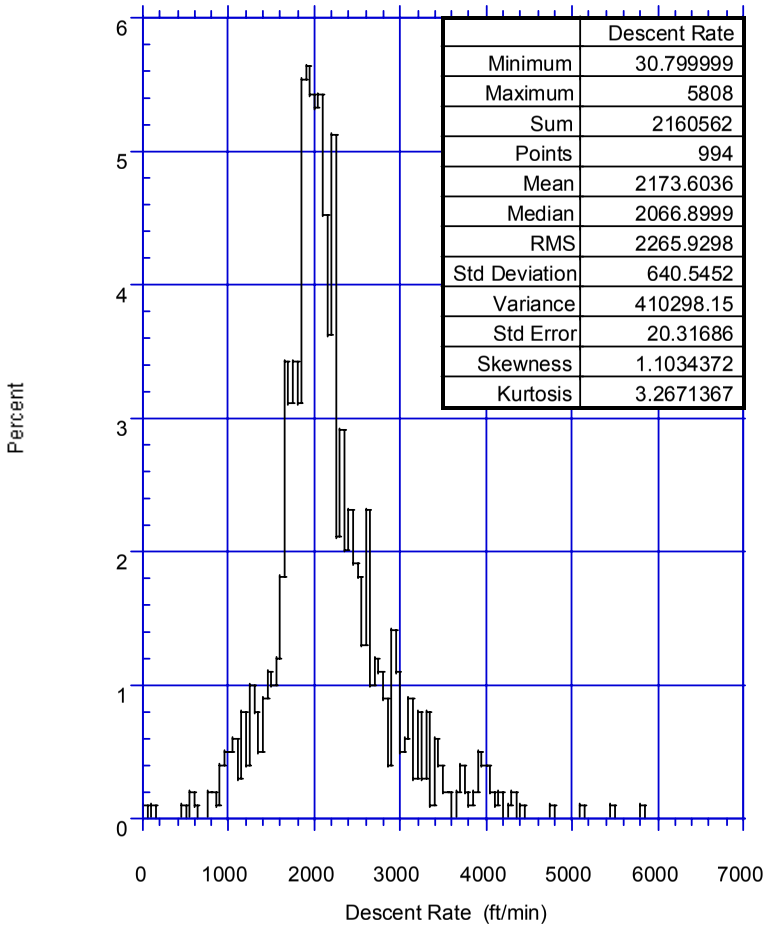

FIGURE D-61. PROBABILITY OF DESCENT RATE FOR DESCENTS BETWEEN 26,000-27,000 FEET, NON-CAPACITY-LIMITED AIRPORTS

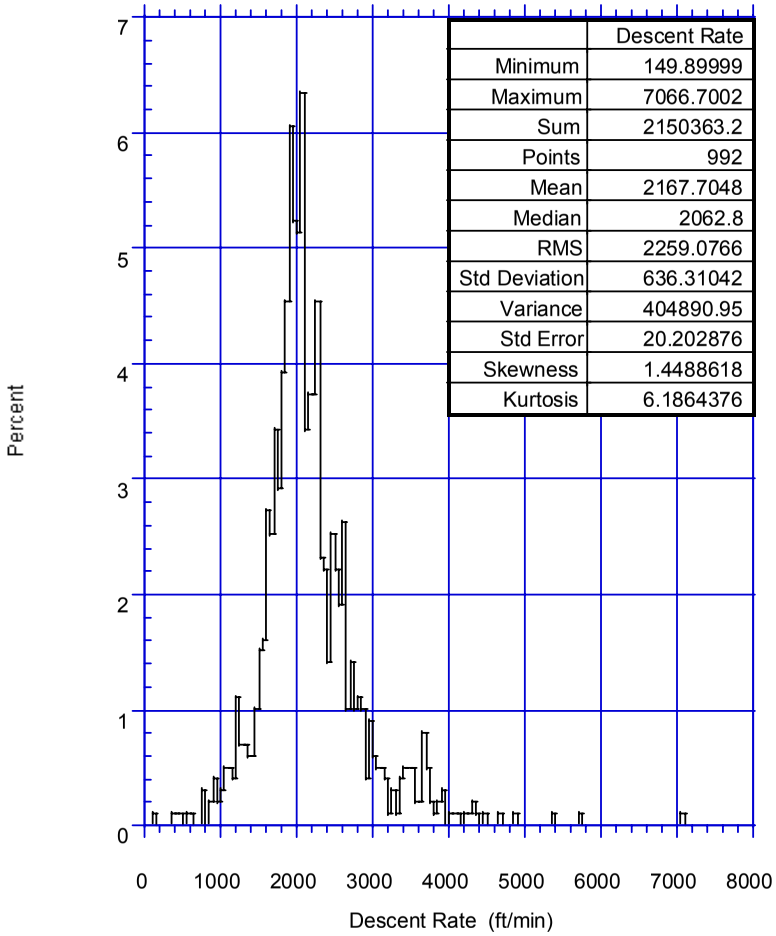

FIGURE D-62. PROBABILITY OF DESCENT RATE FOR DESCENTS BETWEEN 27,000-28,000 FEET, NON-CAPACITY-LIMITED AIRPORTS

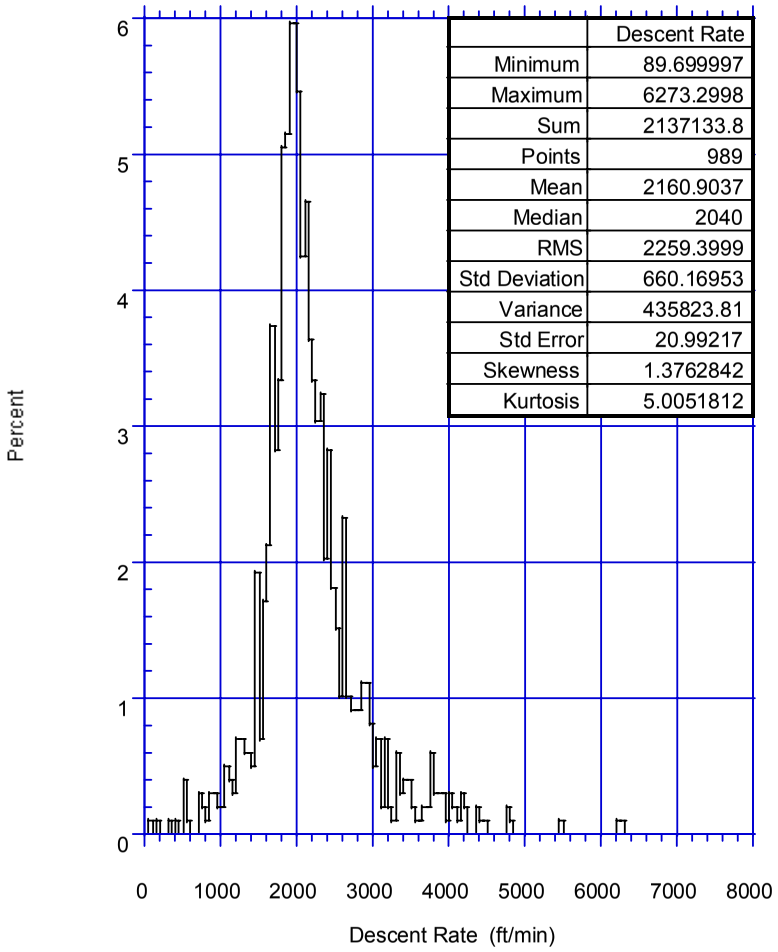

FIGURE D-63. PROBABILITY OF DESCENT RATE FOR DESCENTS BETWEEN 28,000-29,000 FEET, NON-CAPACITY-LIMITED AIRPORTS

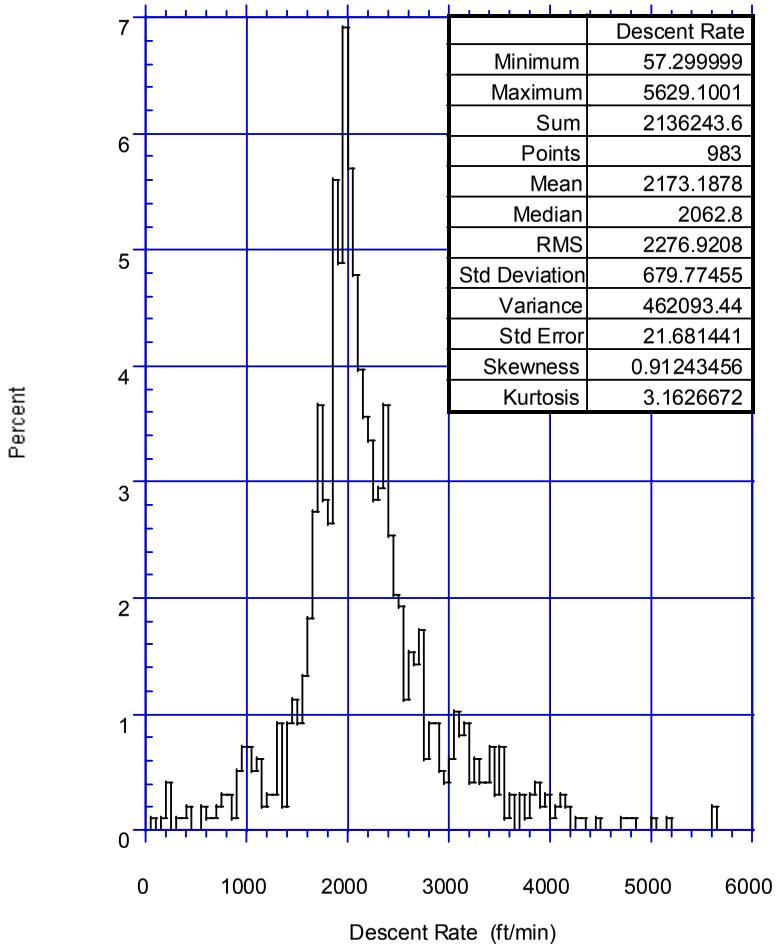

FIGURE D-64. PROBABILITY OF DESCENT RATE FOR DESCENTS BETWEEN 29,000-30,000 FEET, NON-CAPACITY-LIMITED AIRPORTS

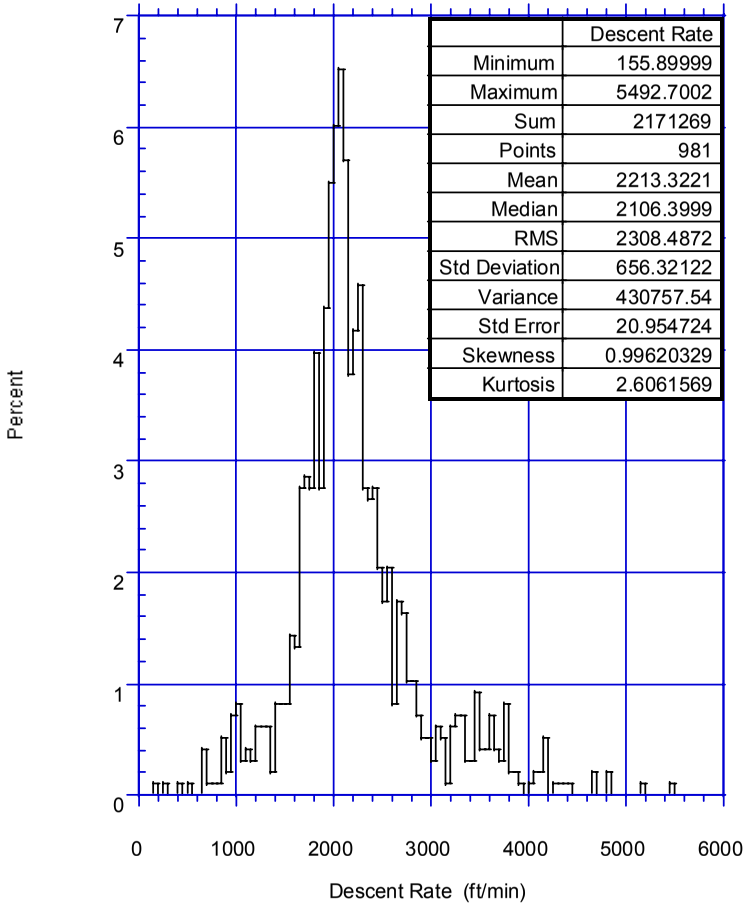

FIGURE D-65. PROBABILITY OF DESCENT RATE FOR DESCENTS BETWEEN 30,000-31,000 FEET, NON-CAPACITY-LIMITED AIRPORTS

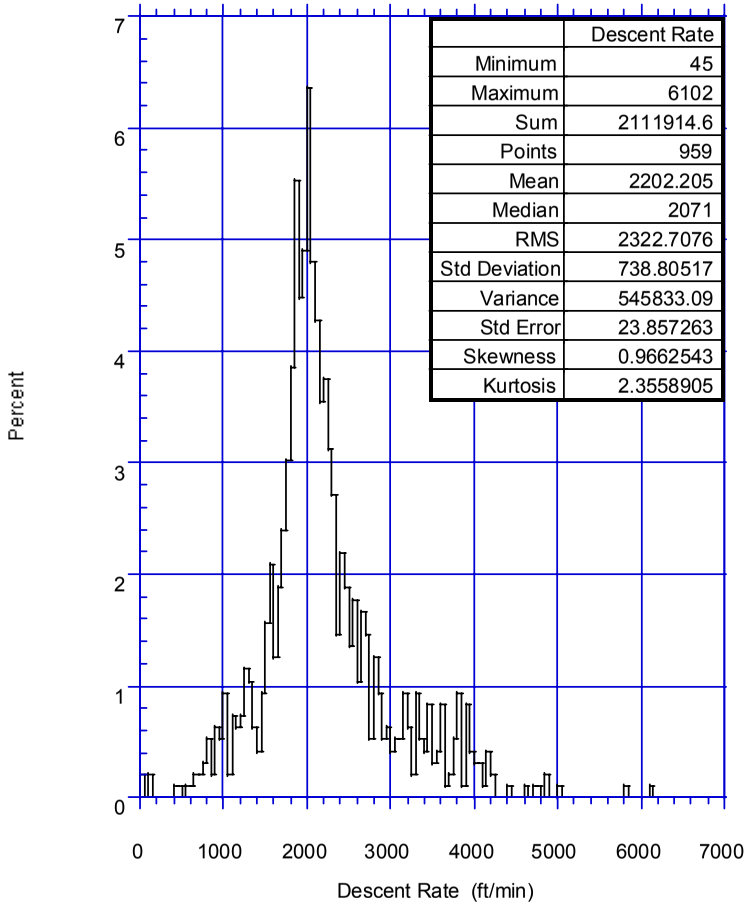

FIGURE D-66. PROBABILITY OF DESCENT RATE FOR DESCENTS BETWEEN 31,000-32,000 FEET, NON-CAPACITY-LIMITED AIRPORTS

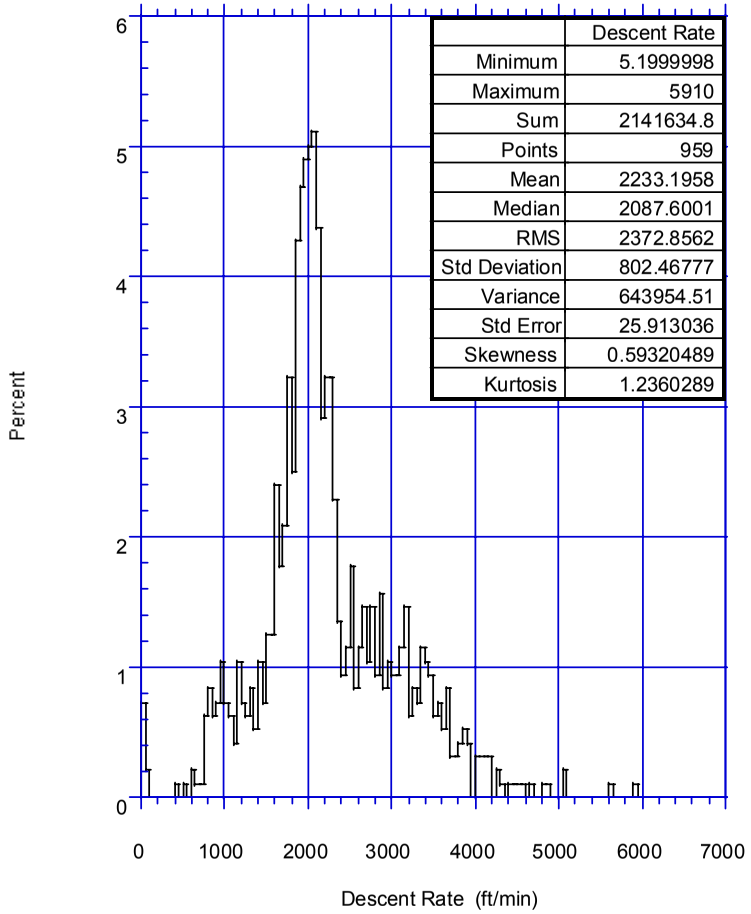

FIGURE D-67. PROBABILITY OF DESCENT RATE FOR DESCENTS BETWEEN 32,000-33,000 FEET, NON-CAPACITY-LIMITED AIRPORTS

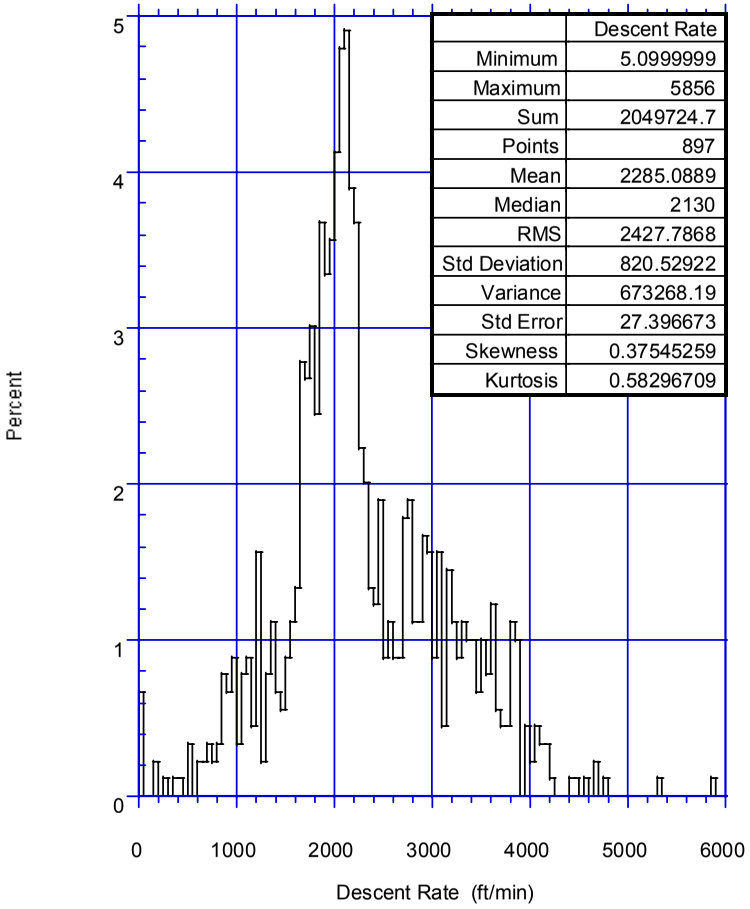

FIGURE D-68. PROBABILITY OF DESCENT RATE FOR DESCENTS BETWEEN 33,000-34,000 FEET, NON-CAPACITY-LIMITED AIRPORTS

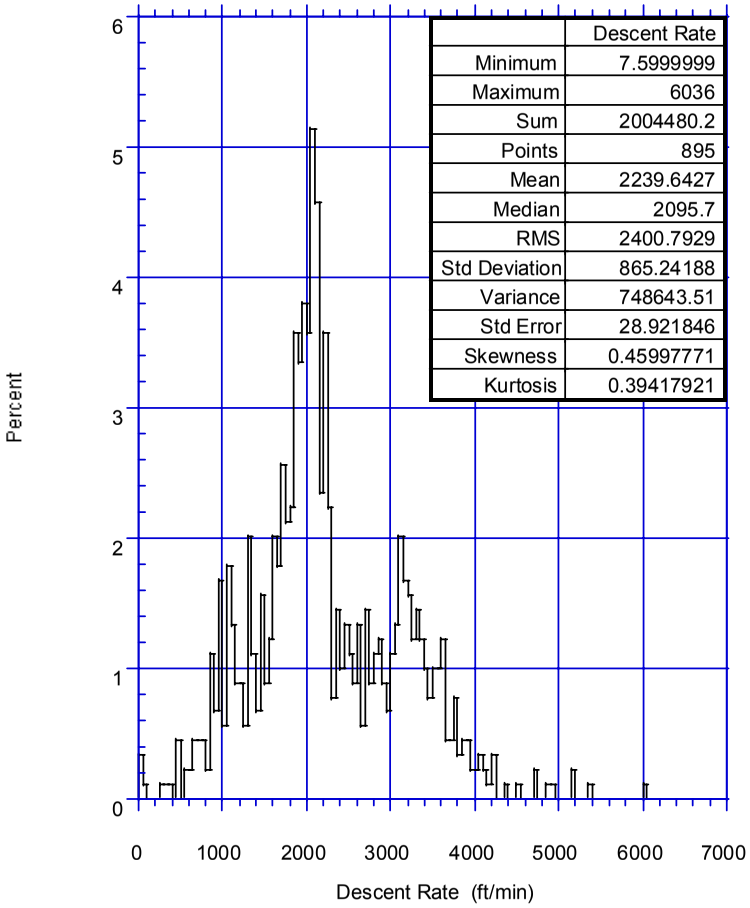

FIGURE D-69. PROBABILITY OF DESCENT RATE FOR DESCENTS BETWEEN 34,000-35,000 FEET, NON-CAPACITY-LIMITED AIRPORTS

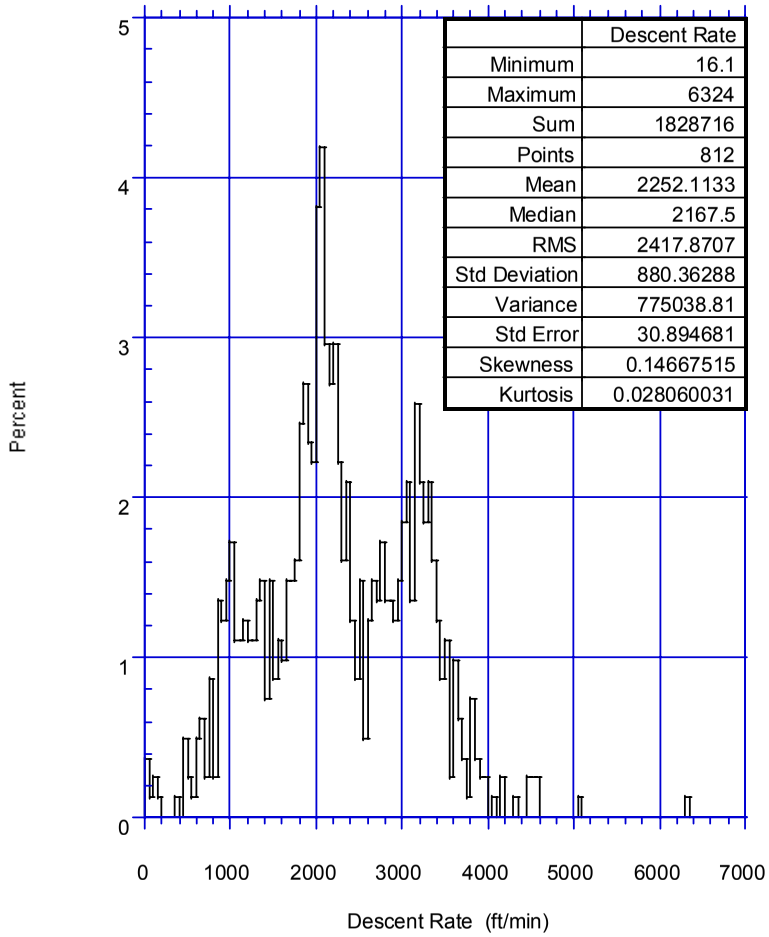

FIGURE D-70. PROBABILITY OF DESCENT RATE FOR DESCENTS BETWEEN 35,000-36,000 FEET, NON-CAPACITY-LIMITED AIRPORTS

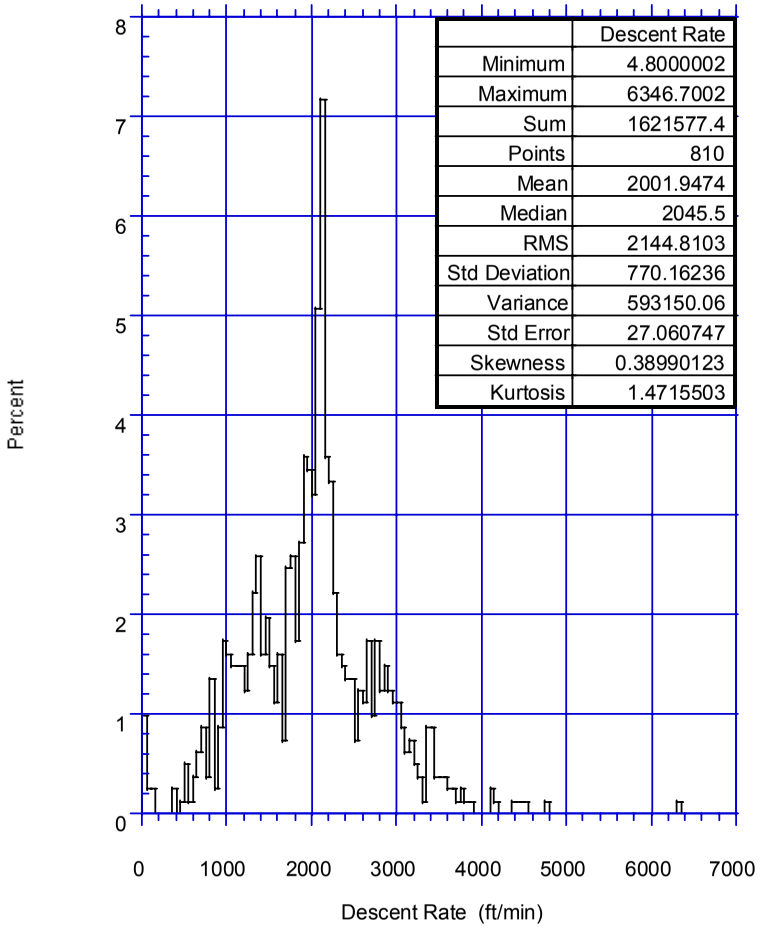

FIGURE D-71. PROBABILITY OF DESCENT RATE FOR DESCENTS BETWEEN 36,000-37,000 FEET, NON-CAPACITY-LIMITED AIRPORTS

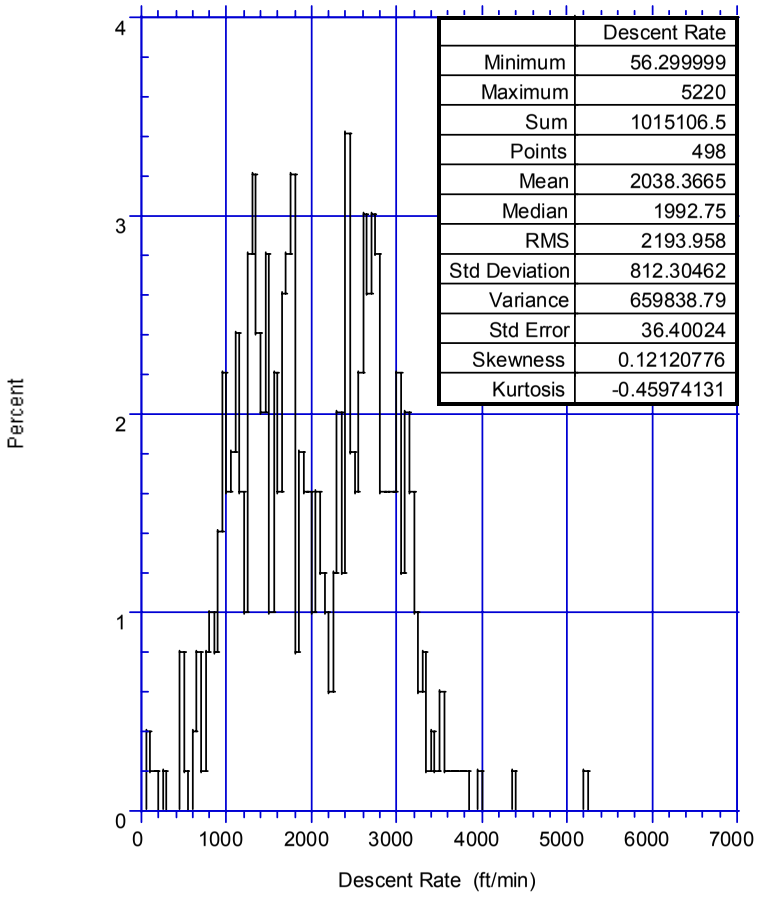

FIGURE D-72. PROBABILITY OF DESCENT RATE FOR DESCENTS BETWEEN 37,000-38,000 FEET, NON-CAPACITY-LIMITED AIRPORTS

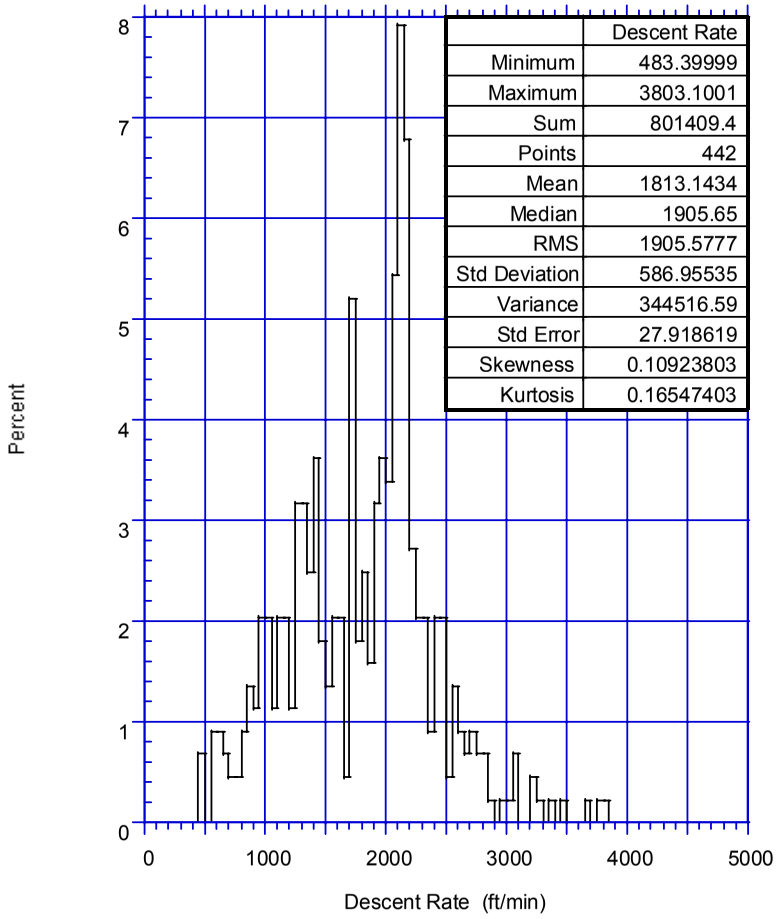

FIGURE D-73. PROBABILITY OF DESCENT RATE FOR DESCENTS BETWEEN 38,000-39,000 FEET, NON-CAPACITY-LIMITED AIRPORTS

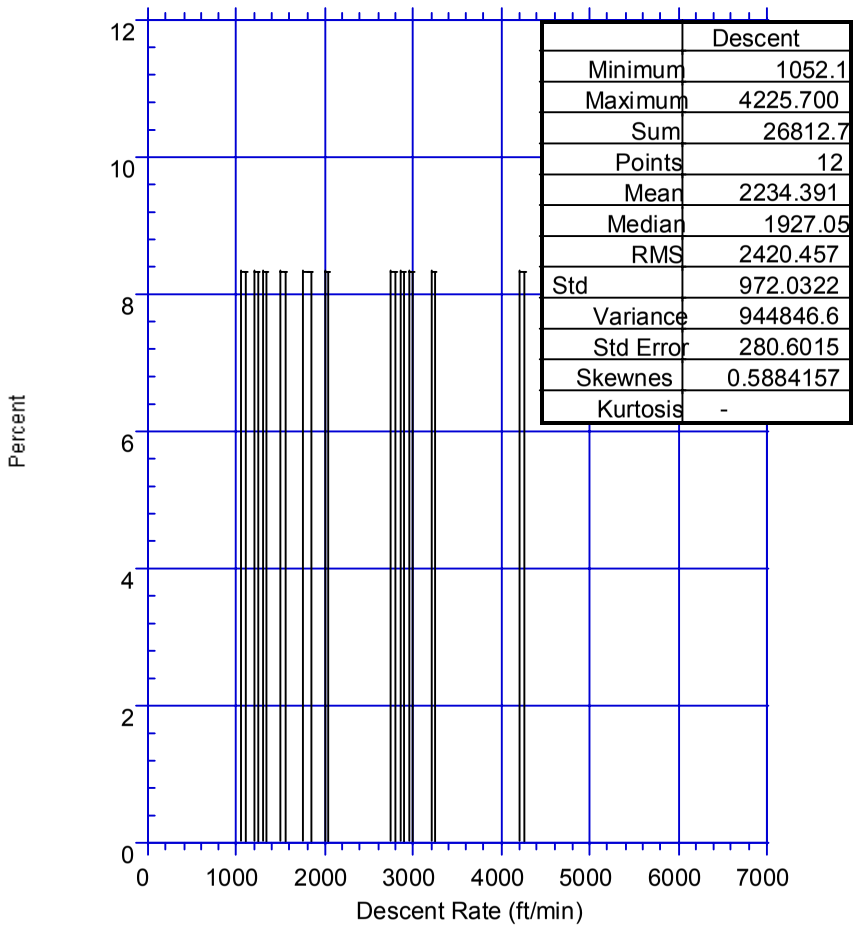

FIGURE D-74. PROBABILITY OF DESCENT RATE FOR DESCENTS BETWEEN 39,000-40,000 FEET, NON-CAPACITY-LIMITED AIRPORTS

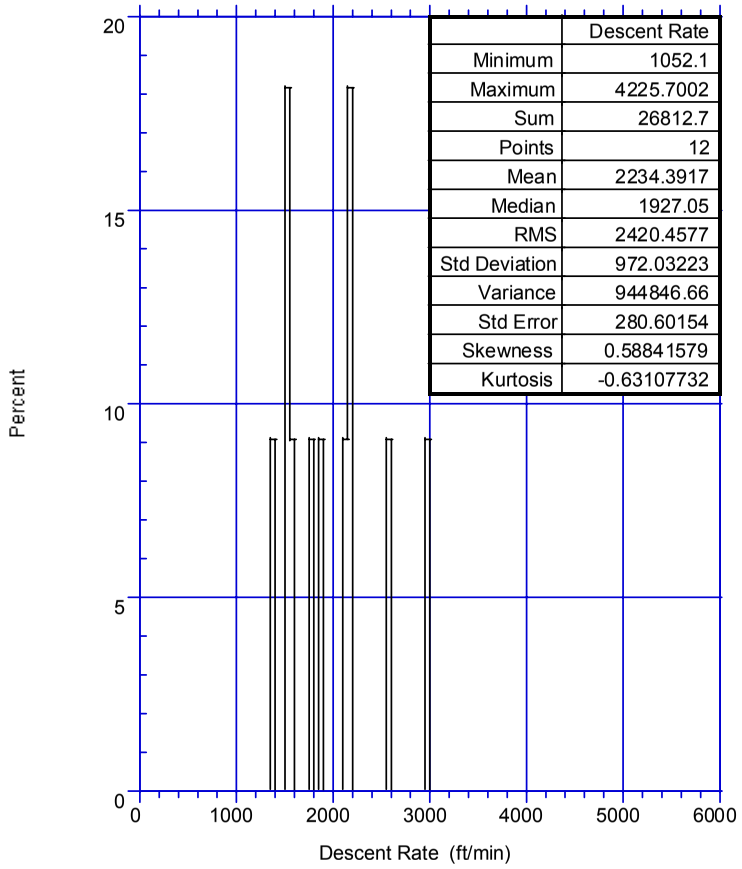

FIGURE D-75. PROBABILITY OF DESCENT RATE FOR DESCENTS BETWEEN 40,000-41,000 FEET, NON-CAPACITY-LIMITED AIRPORTS

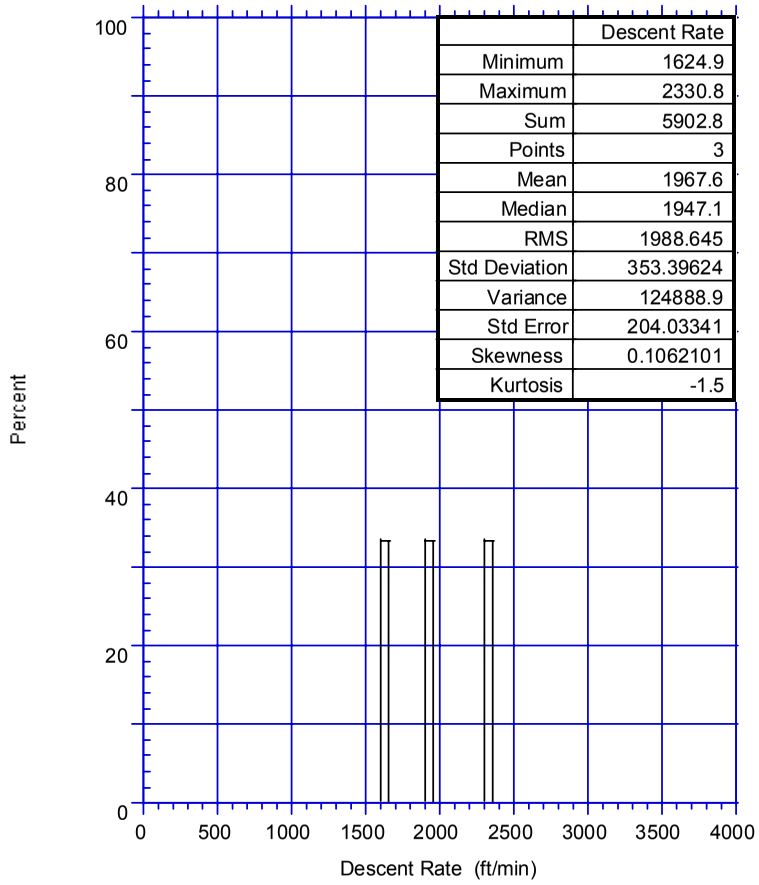

FIGURE D-76. PROBABILITY OF DESCENT RATE FOR DESCENTS BETWEEN 41,000-42,000 FEET, NON-CAPACITY-LIMITED AIRPORTS

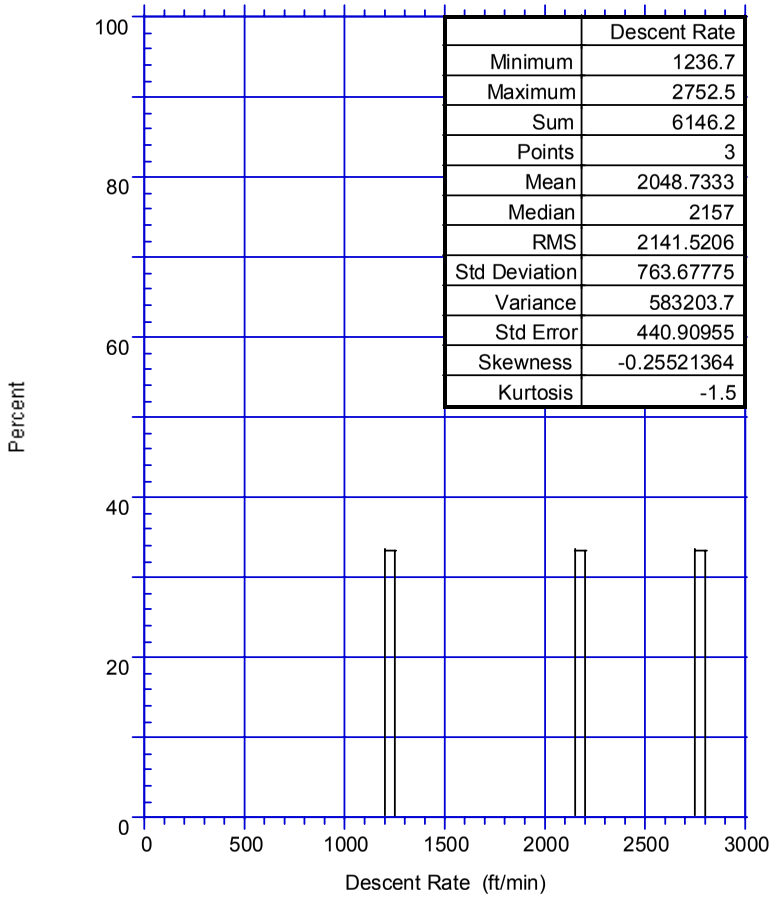

FIGURE D-77. PROBABILITY OF DESCENT RATE FOR DESCENTS BETWEEN 42,000-43,000 FEET, NON-CAPACITY-LIMITED AIRPORTS

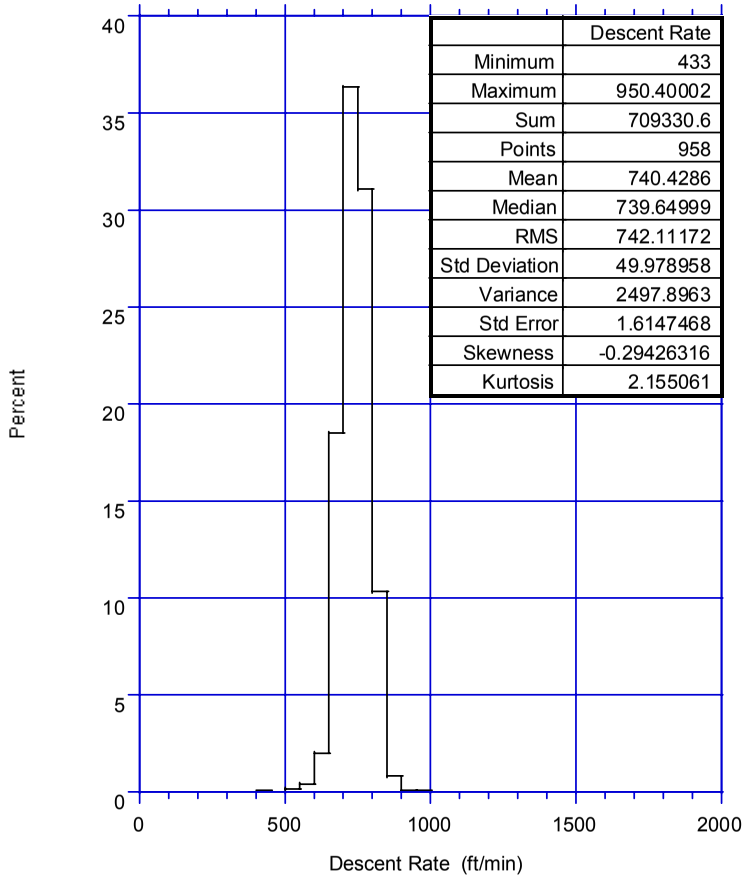

FIGURE D-78. PROBABILITY OF DESCENT RATE FOR DESCENTS BETWEEN 0-1000 FEET, CAPACITY-LIMITED AIRPORTS

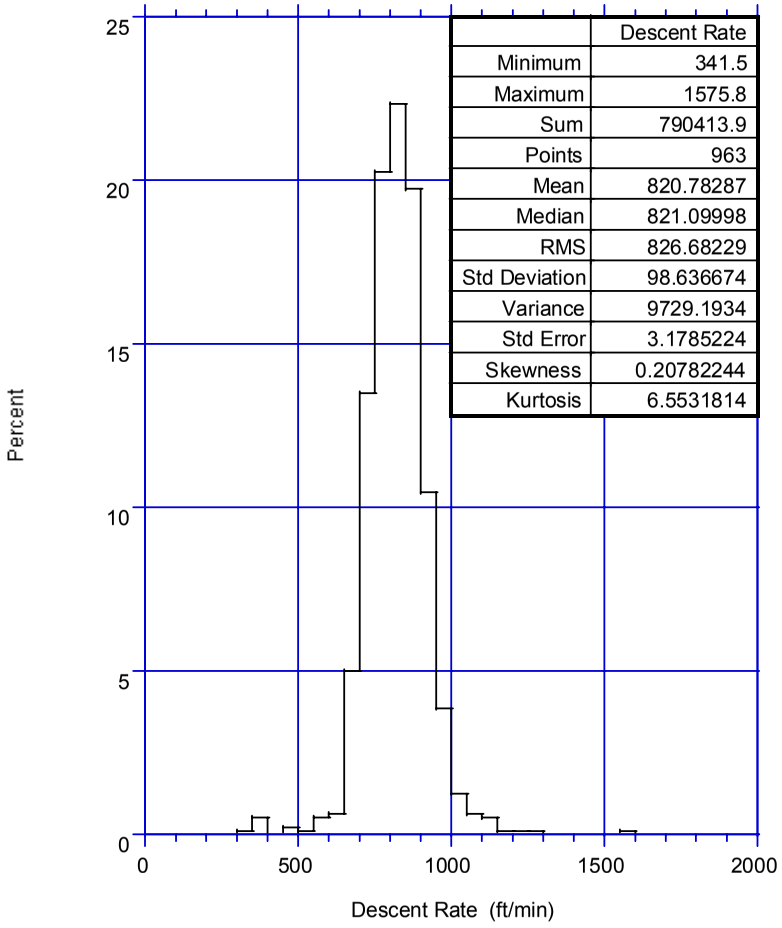

FIGURE D-79. PROBABILITY OF DESCENT RATE FOR DESCENTS BETWEEN 1000-2000 FEET, CAPACITY-LIMITED AIRPORTS

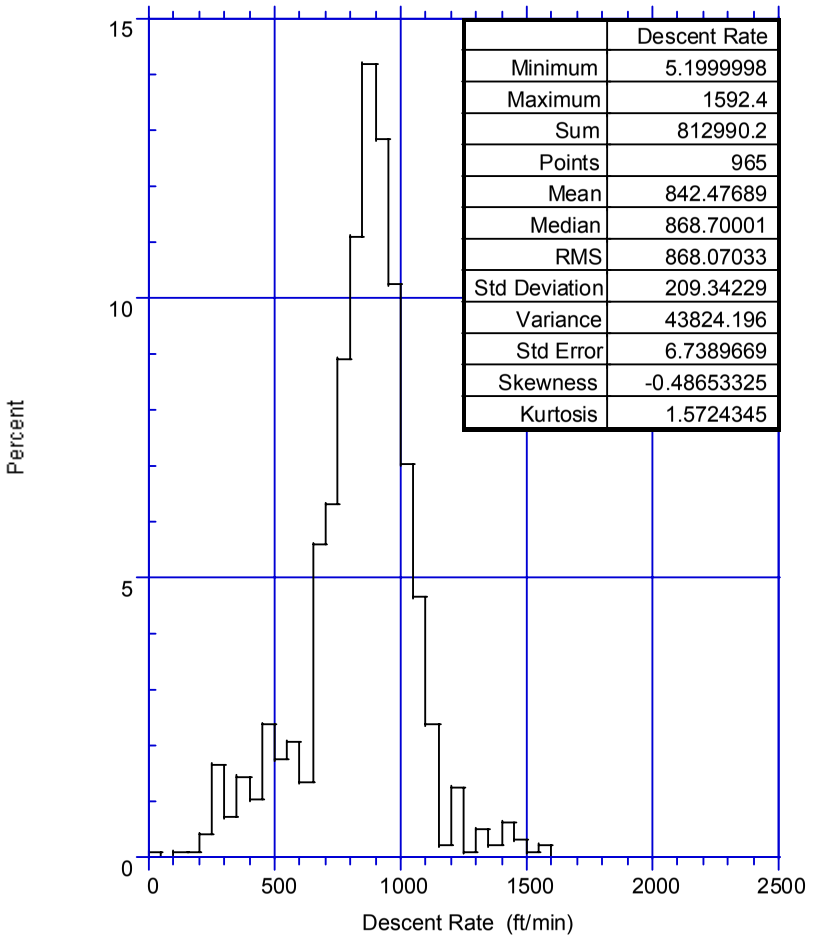

FIGURE D-80. PROBABILITY OF DESCENT RATE FOR DESCENTS BETWEEN 2000-3000 FEET, CAPACITY-LIMITED AIRPORTS

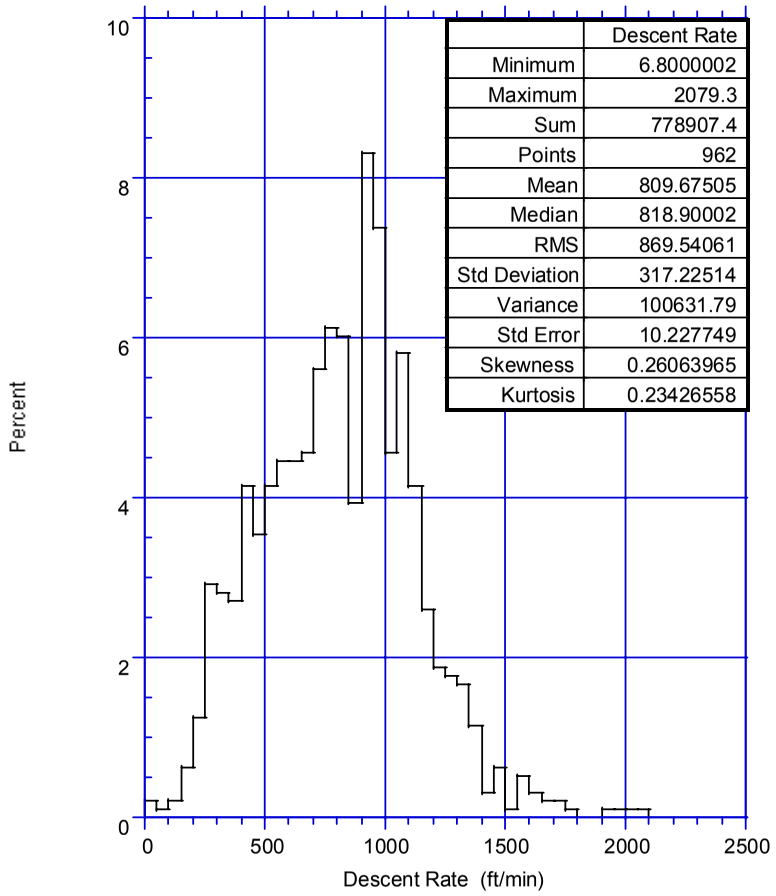

FIGURE D-81. PROBABILITY OF DESCENT RATE FOR DESCENTS BETWEEN 3000-4000 FEET, CAPACITY-LIMITED AIRPORTS

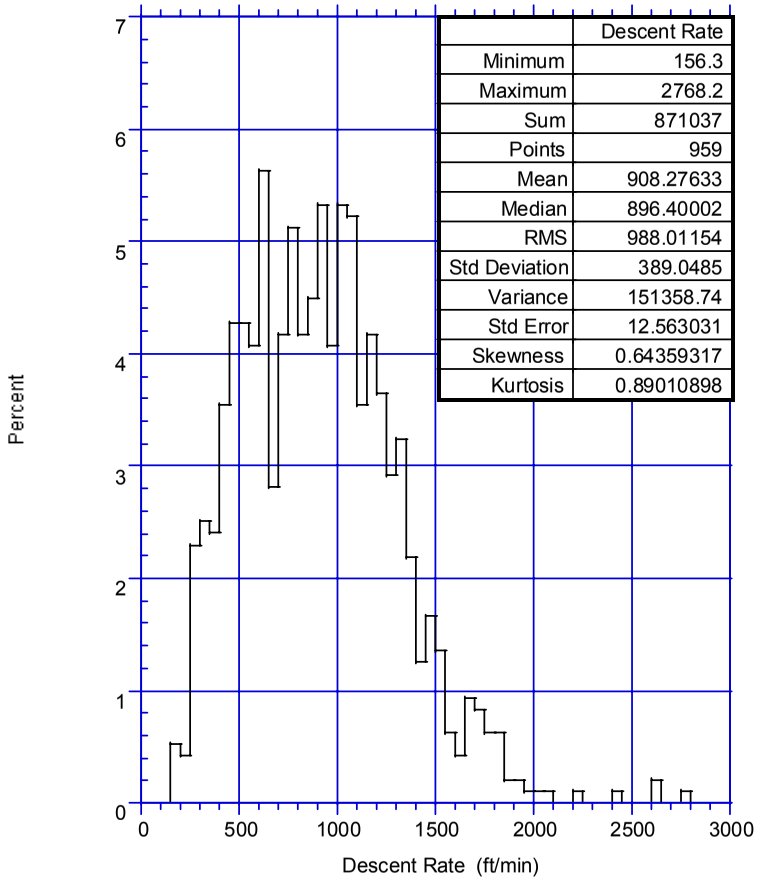

FIGURE D-82. PROBABILITY OF DESCENT RATE FOR DESCENTS BETWEEN 4000-5000 FEET, CAPACITY-LIMITED AIRPORTS

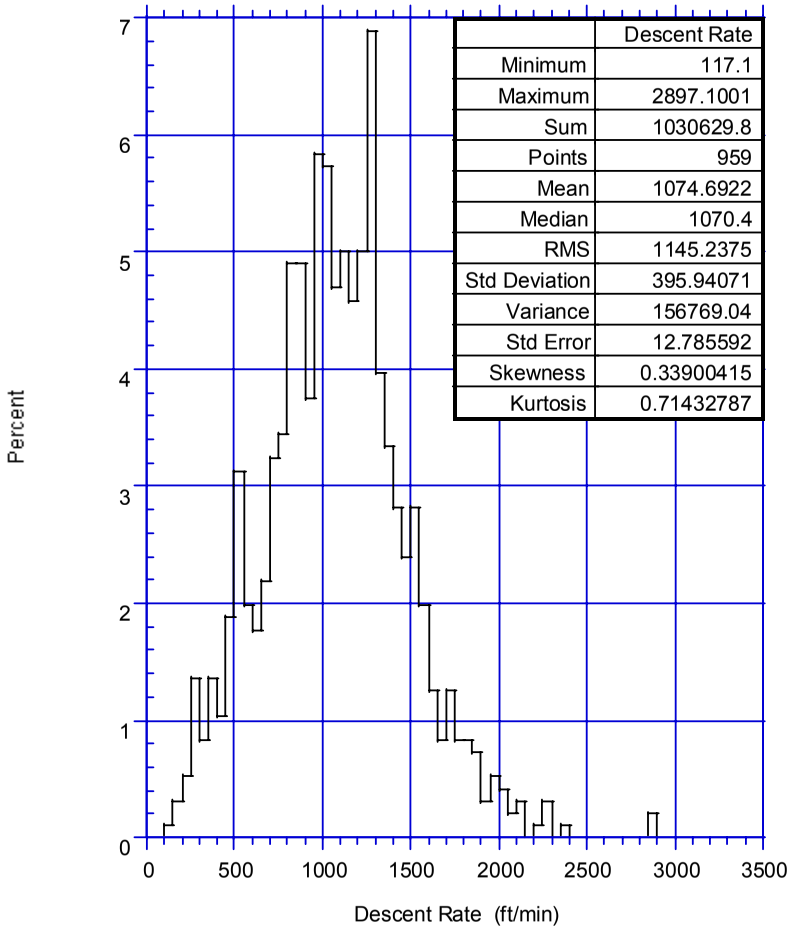

FIGURE D-83. PROBABILITY OF DESCENT RATE FOR DESCENTS BETWEEN 5000-6000 FEET, CAPACITY-LIMITED AIRPORTS

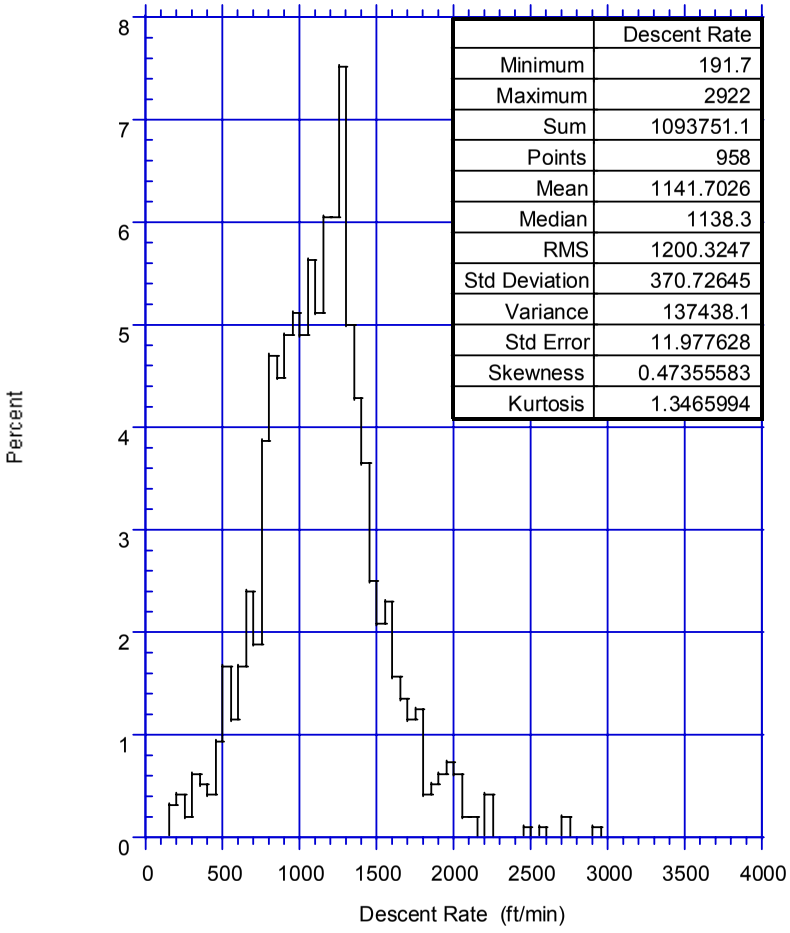

FIGURE D-84. PROBABILITY OF DESCENT RATE FOR DESCENTS BETWEEN 6000-7000 FEET, CAPACITY-LIMITED AIRPORTS

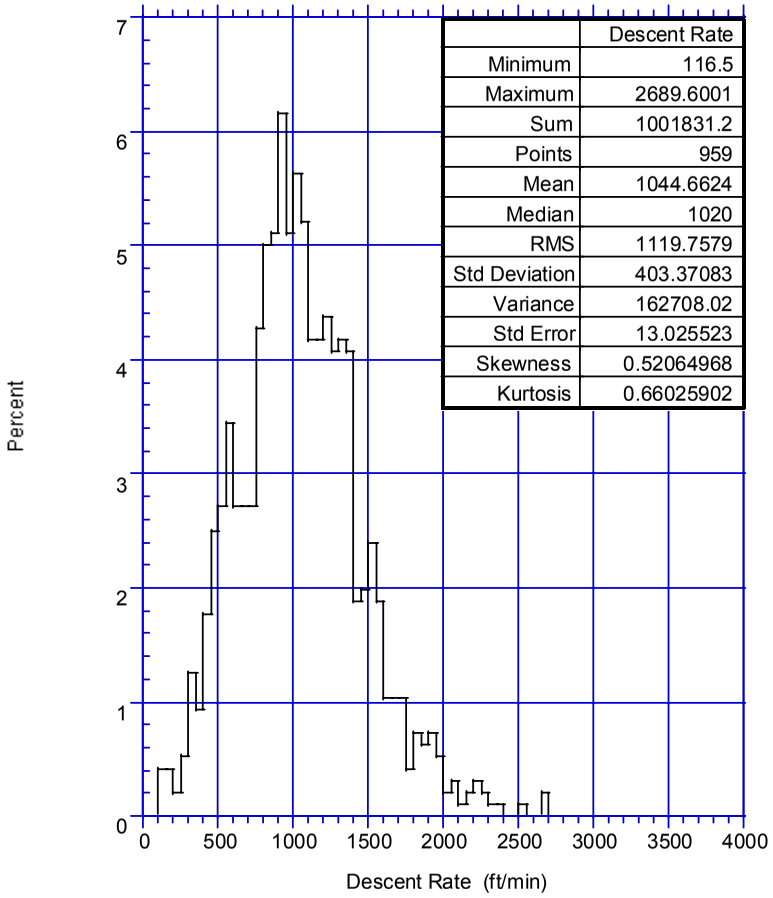

FIGURE D-85. PROBABILITY OF DESCENT RATE FOR DESCENTS BETWEEN 7000-8000 FEET, CAPACITY-LIMITED AIRPORTS

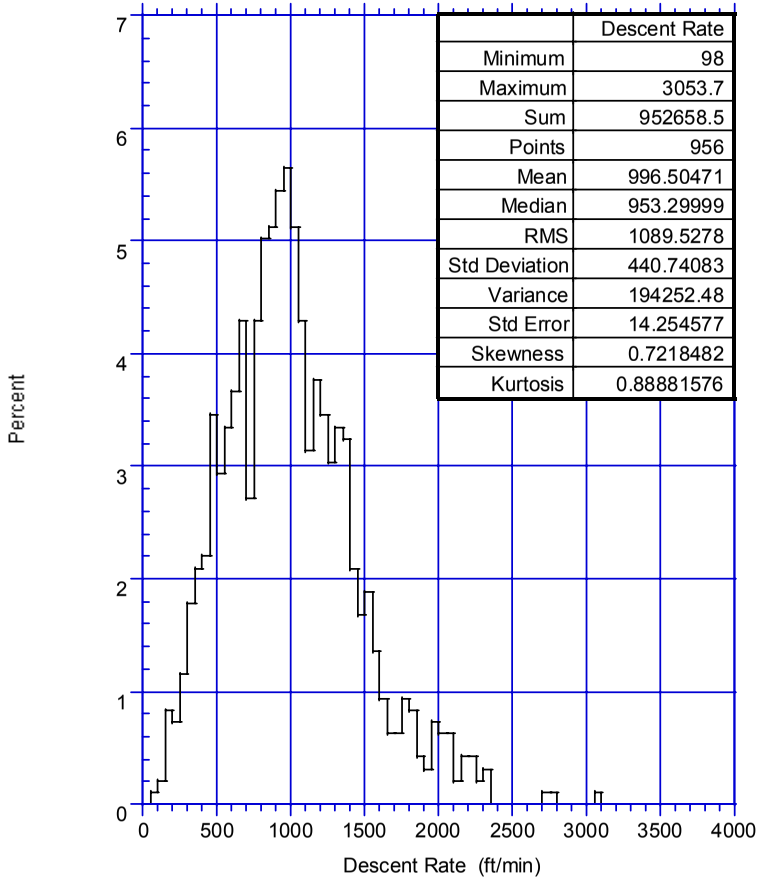

FIGURE D-86. PROBABILITY OF DESCENT RATE FOR DESCENTS BETWEEN 8000-9000 FEET, CAPACITY-LIMITED AIRPORTS

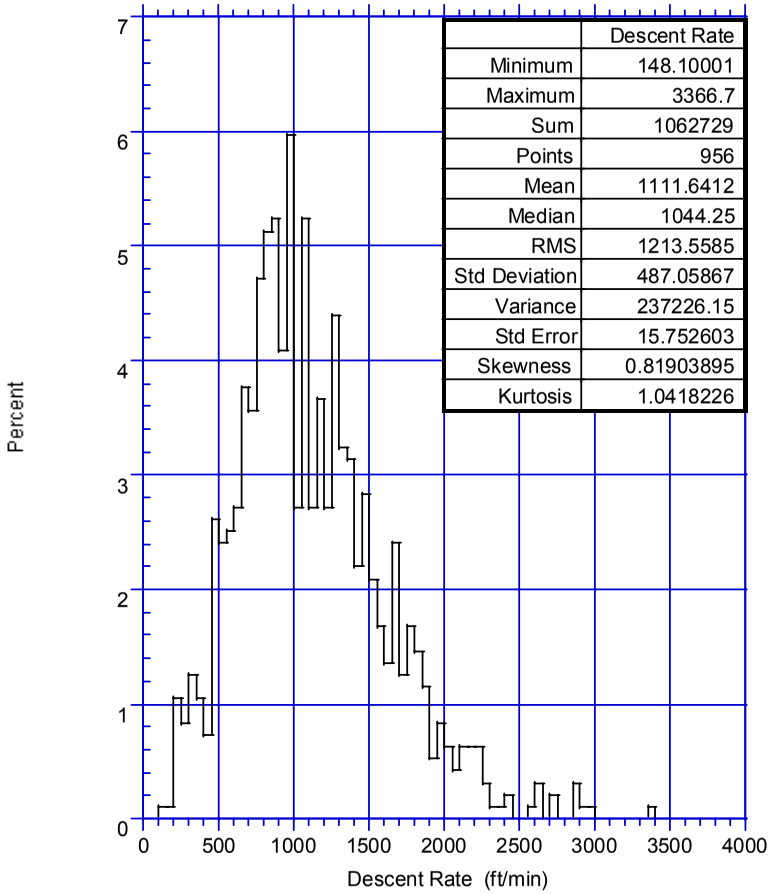

FIGURE D-87. PROBABILITY OF DESCENT RATE FOR DESCENTS BETWEEN 9,000-10,000 FEET, CAPACITY-LIMITED AIRPORTS

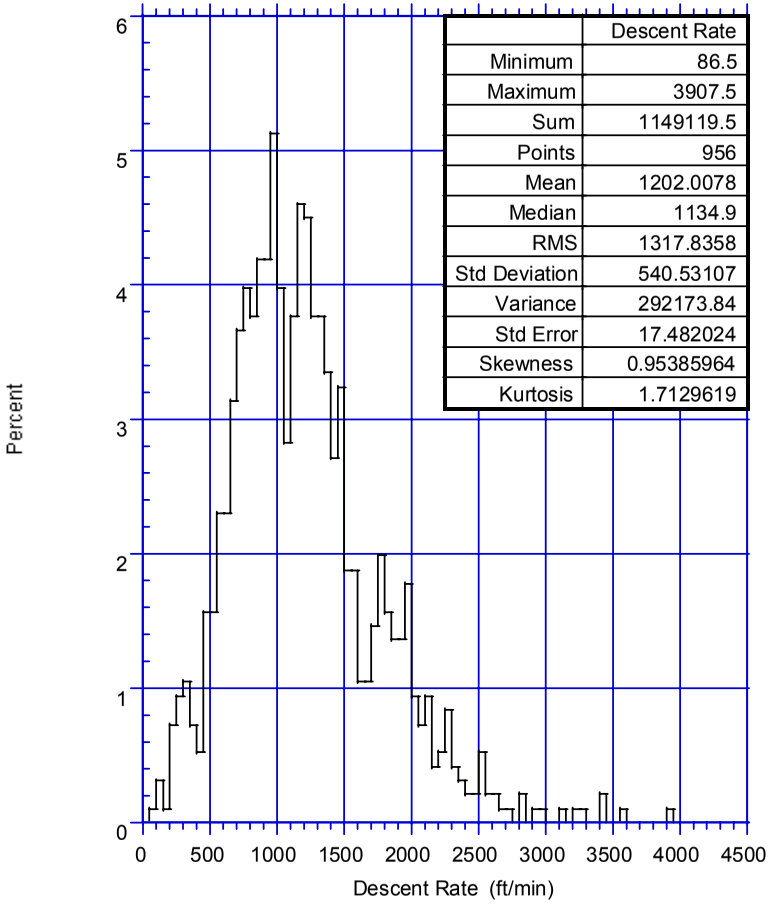

FIGURE D-88. PROBABILITY OF DESCENT RATE FOR DESCENTS BETWEEN 10,000-11,000 FEET, CAPACITY-LIMITED AIRPORTS

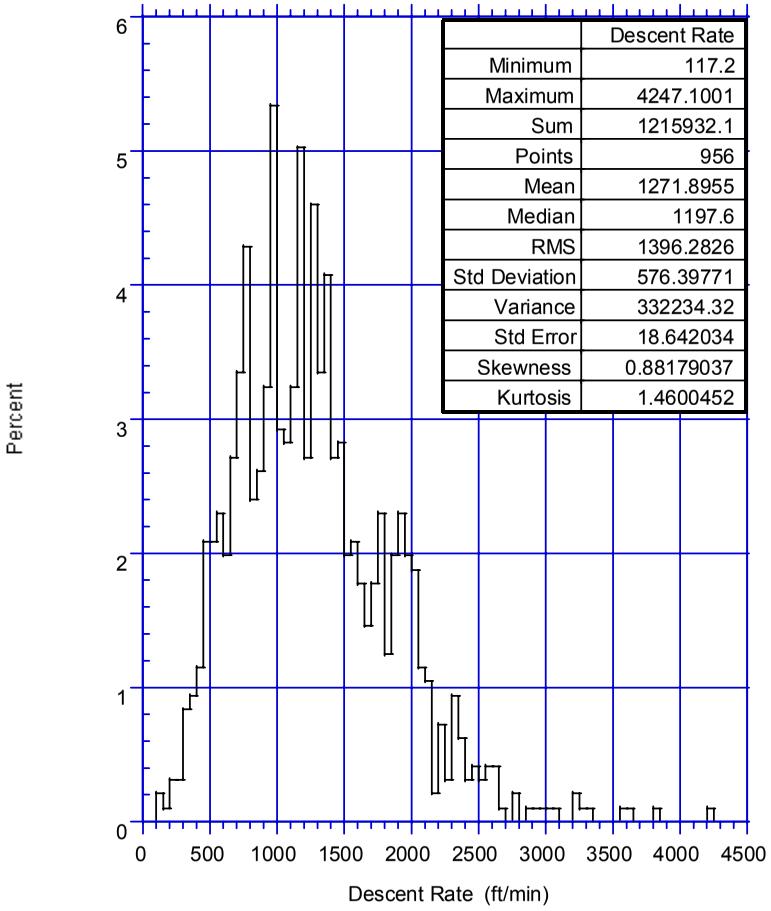

FIGURE D-89. PROBABILITY OF DESCENT RATE FOR DESCENTS BETWEEN 11,000-12,000 FEET, CAPACITY-LIMITED AIRPORTS

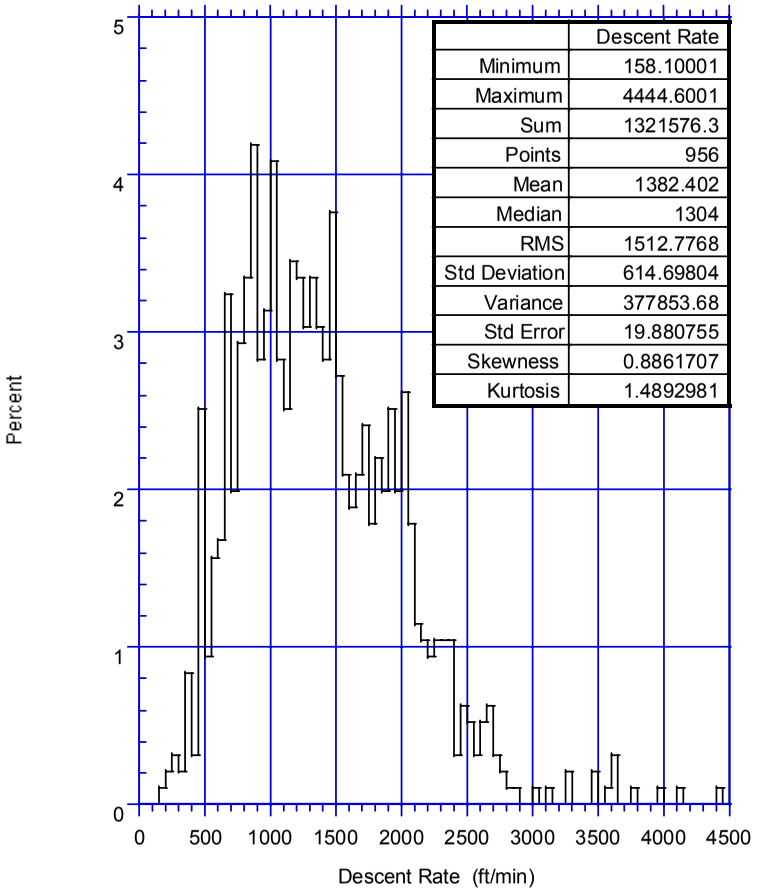

FIGURE D-90. PROBABILITY OF DESCENT RATE FOR DESCENTS BETWEEN 12,000-13,000 FEET, CAPACITY-LIMITED AIRPORTS

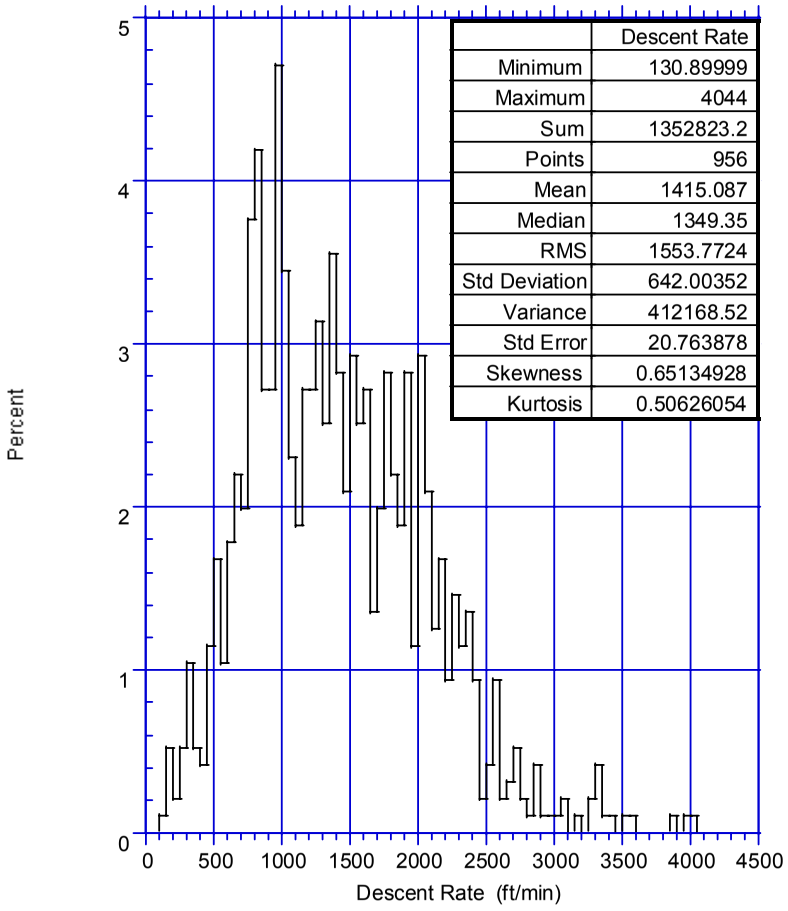

FIGURE D-91. PROBABILITY OF DESCENT RATE FOR DESCENTS BETWEEN 13,000-14,000 FEET, CAPACITY-LIMITED AIRPORTS

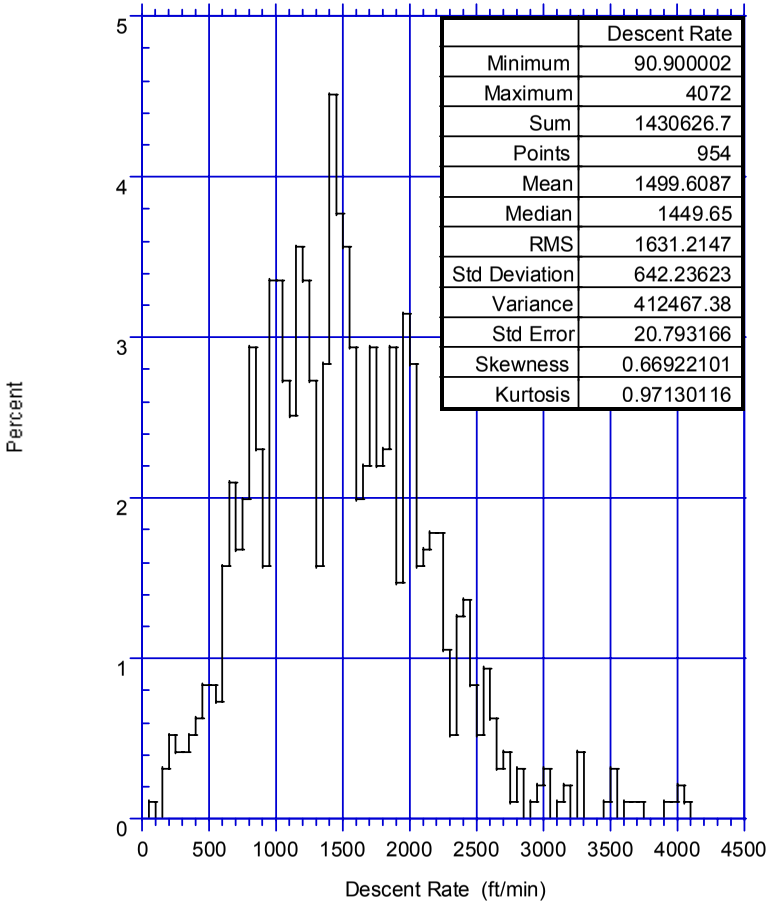

FIGURE D-92. PROBABILITY OF DESCENT RATE FOR DESCENTS BETWEEN 14,000-15,000 FEET, CAPACITY-LIMITED AIRPORTS

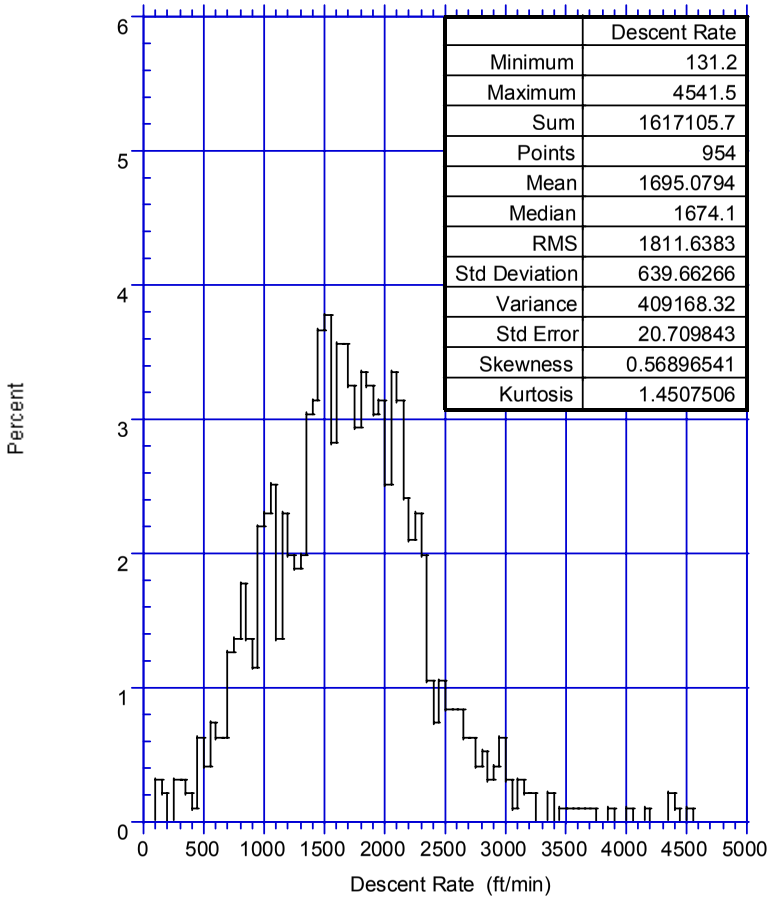

FIGURE D-93. PROBABILITY OF DESCENT RATE FOR DESCENTS BETWEEN 15,000-16,000 FEET, CAPACITY-LIMITED AIRPORTS

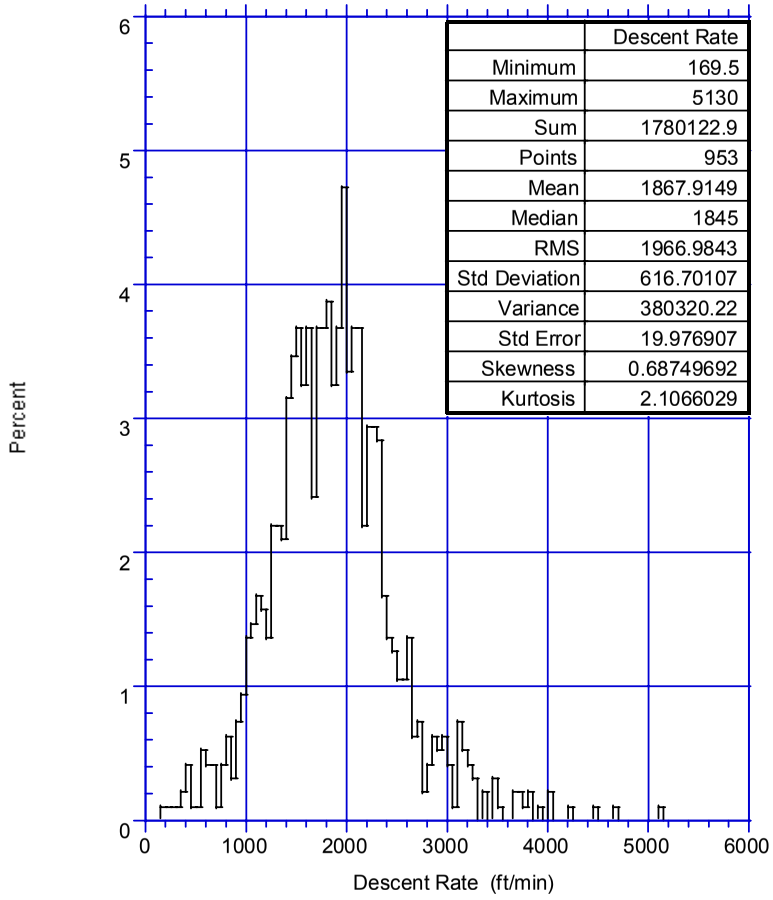

FIGURE D-94. PROBABILITY OF DESCENT RATE FOR DESCENTS BETWEEN 16,000-17,000 FEET, CAPACITY-LIMITED AIRPORTS

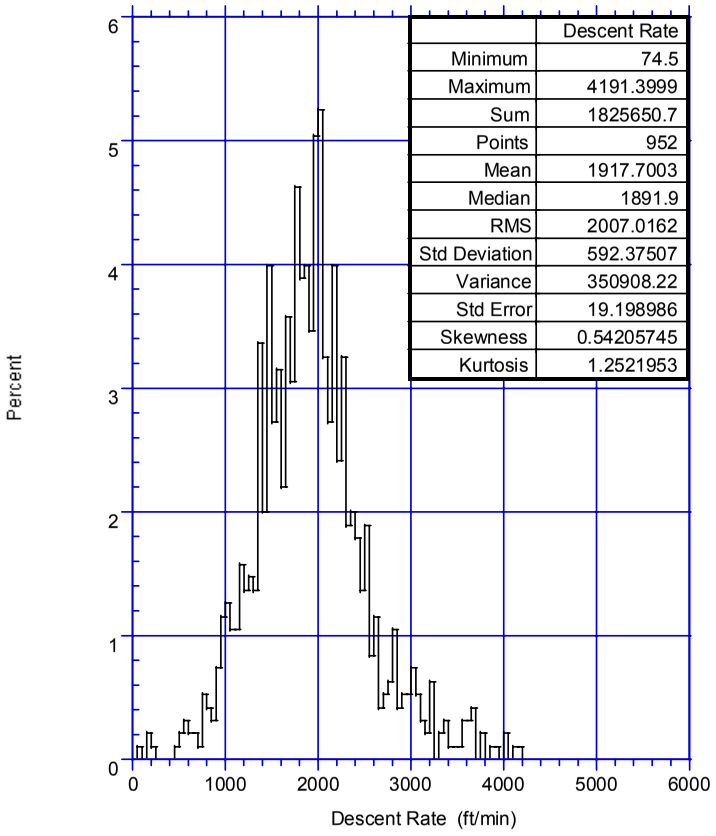

FIGURE D-95. PROBABILITY OF DESCENT RATE FOR DESCENTS BETWEEN 17,000-18,000 FEET, CAPACITY-LIMITED AIRPORTS

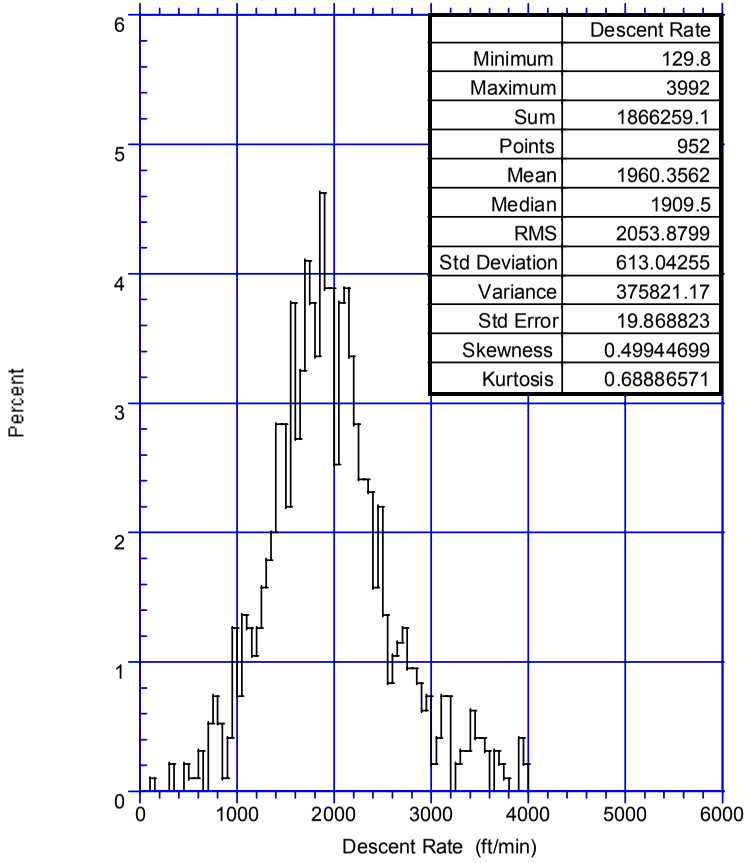

FIGURE D-96. PROBABILITY OF DESCENT RATE FOR DESCENTS BETWEEN 18,000-19,000 FEET, CAPACITY-LIMITED AIRPORTS

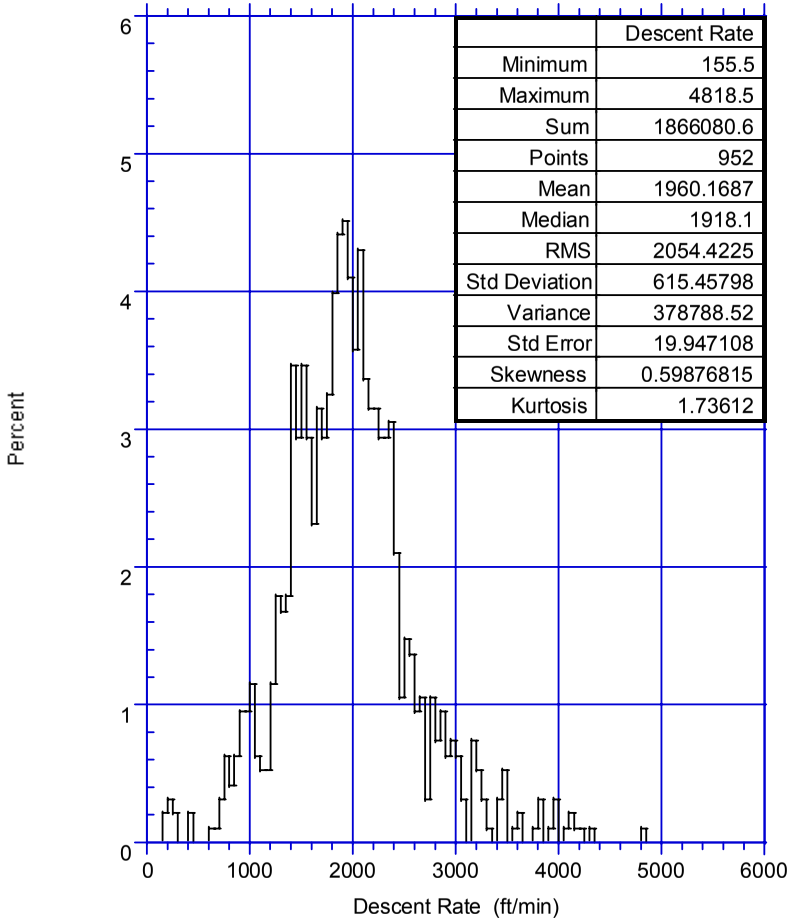

FIGURE D-97. PROBABILITY OF DESCENT RATE FOR DESCENTS BETWEEN 19,000-20,000 FEET, CAPACITY-LIMITED AIRPORTS

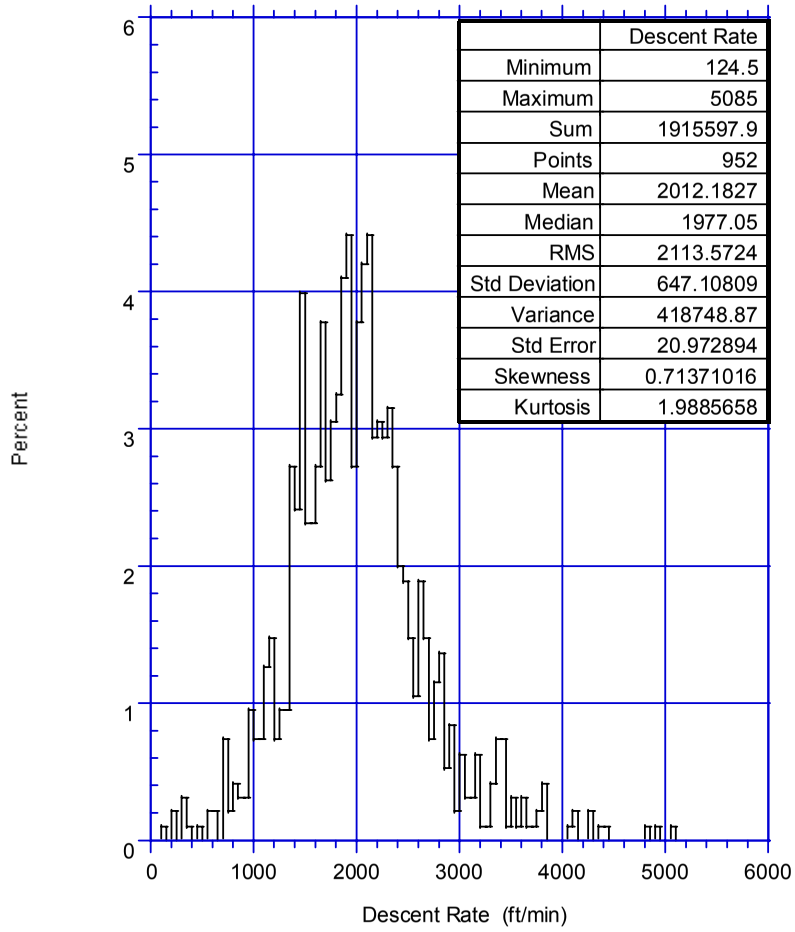

FIGURE D-98. PROBABILITY OF DESCENT RATE FOR DESCENTS BETWEEN 20,000-21,000 FEET, CAPACITY-LIMITED AIRPORTS

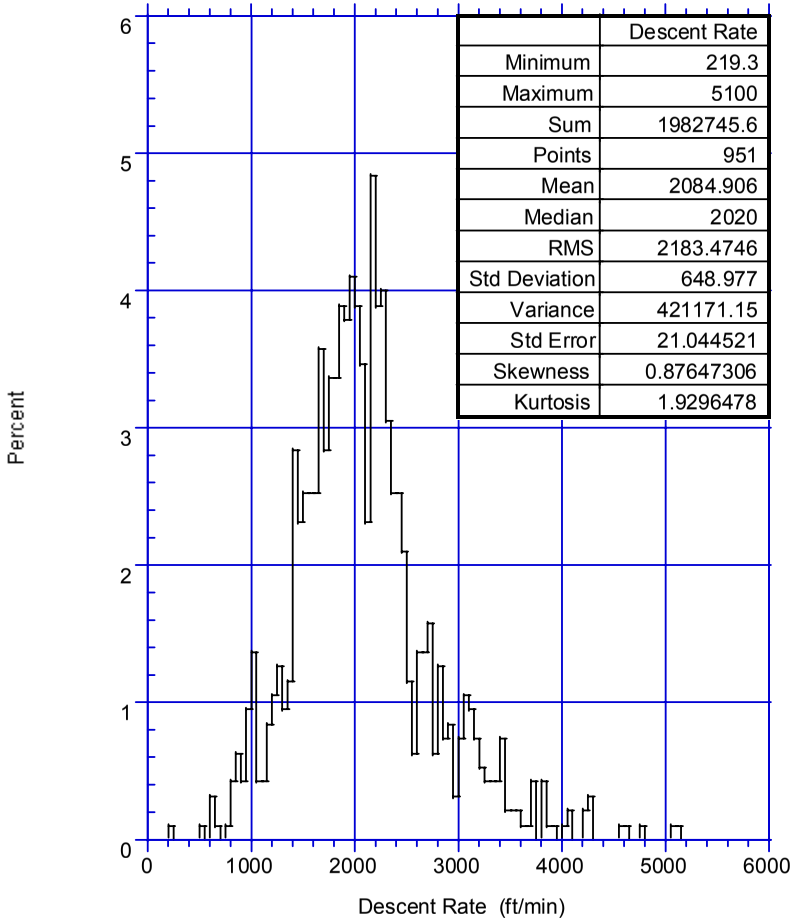

FIGURE D-99. PROBABILITY OF DESCENT RATE FOR DESCENTS BETWEEN 21,000-22,000 FEET, CAPACITY-LIMITED AIRPORTS

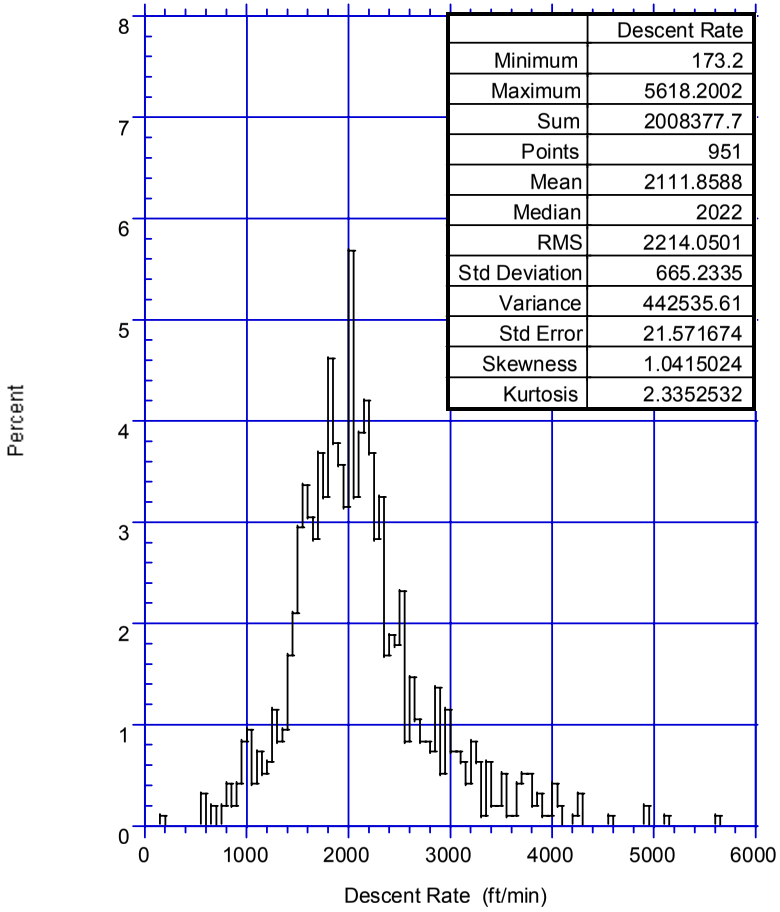

FIGURE D-100. PROBABILITY OF DESCENT RATE FOR DESCENTS BETWEEN 22,000-23,000 FEET, CAPACITY-LIMITED AIRPORTS

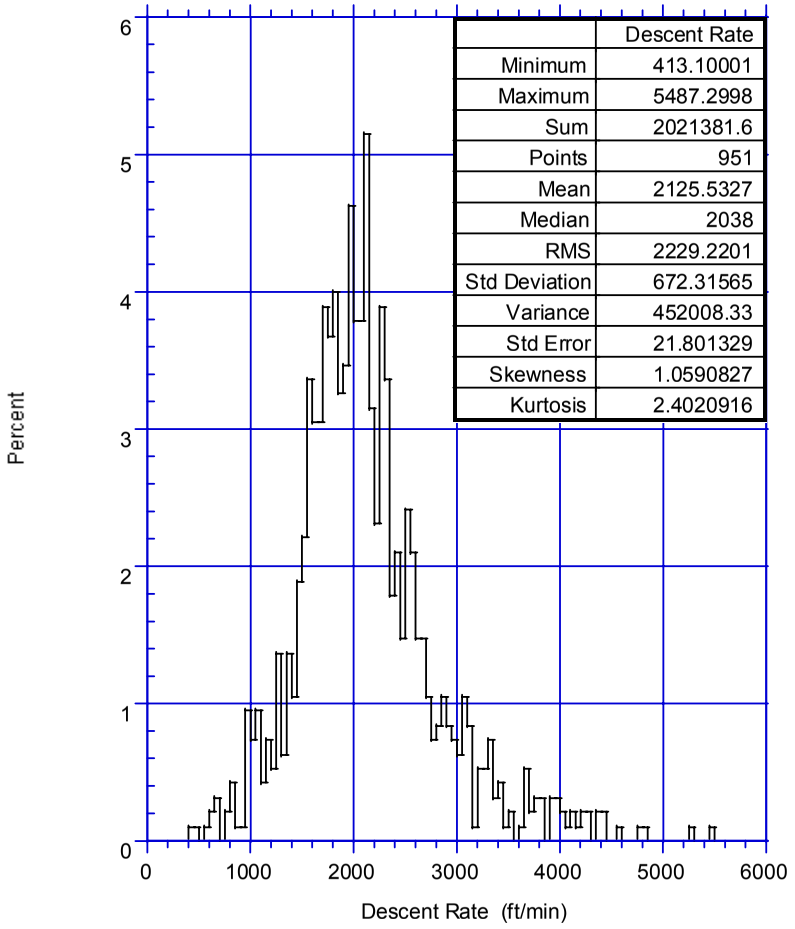

FIGURE D-101. PROBABILITY OF DESCENT RATE FOR DESCENTS BETWEEN 23,000-24,000 FEET, CAPACITY-LIMITED AIRPORTS

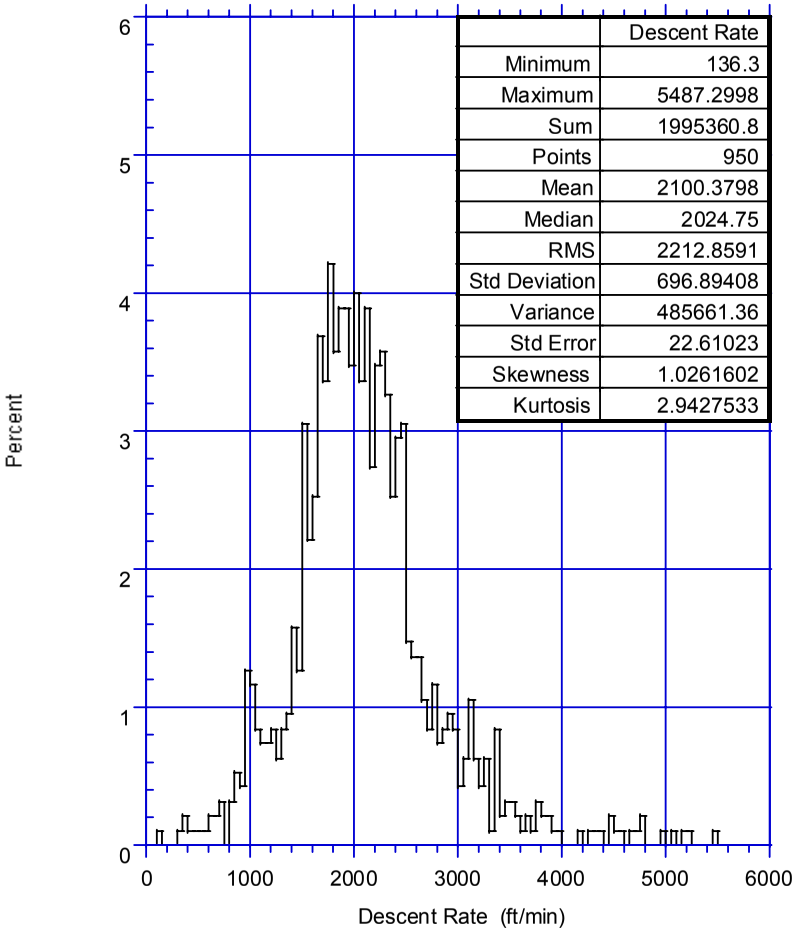

FIGURE D-102. PROBABILITY OF DESCENT RATE FOR DESCENTS BETWEEN 24,000-25,000 FEET, CAPACITY-LIMITED AIRPORTS

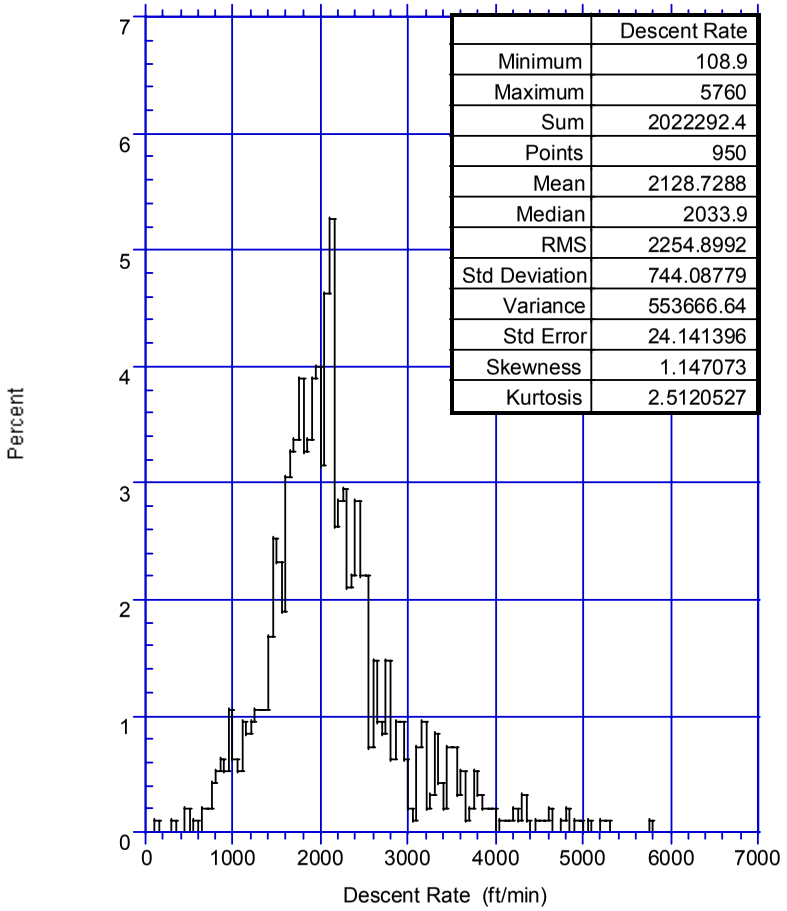

FIGURE D-103. PROBABILITY OF DESCENT RATE FOR DESCENTS BETWEEN 25,000-26,000 FEET, CAPACITY-LIMITED AIRPORTS

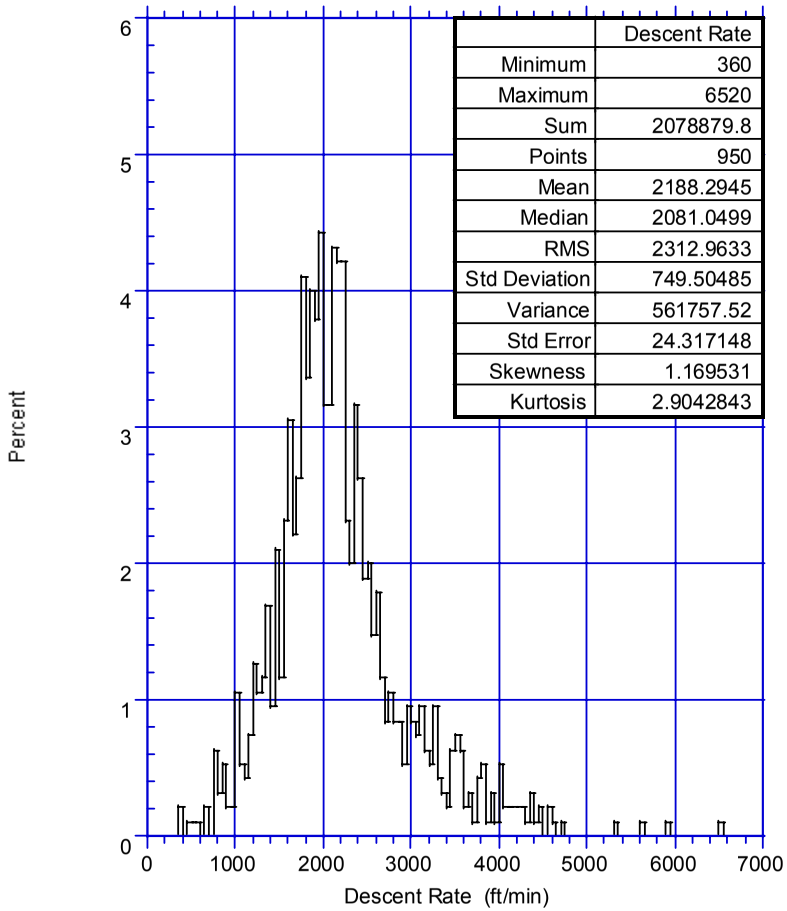

FIGURE D-104. PROBABILITY OF DESCENT RATE FOR DESCENTS BETWEEN 26,000-27,000 FEET, CAPACITY-LIMITED AIRPORTS

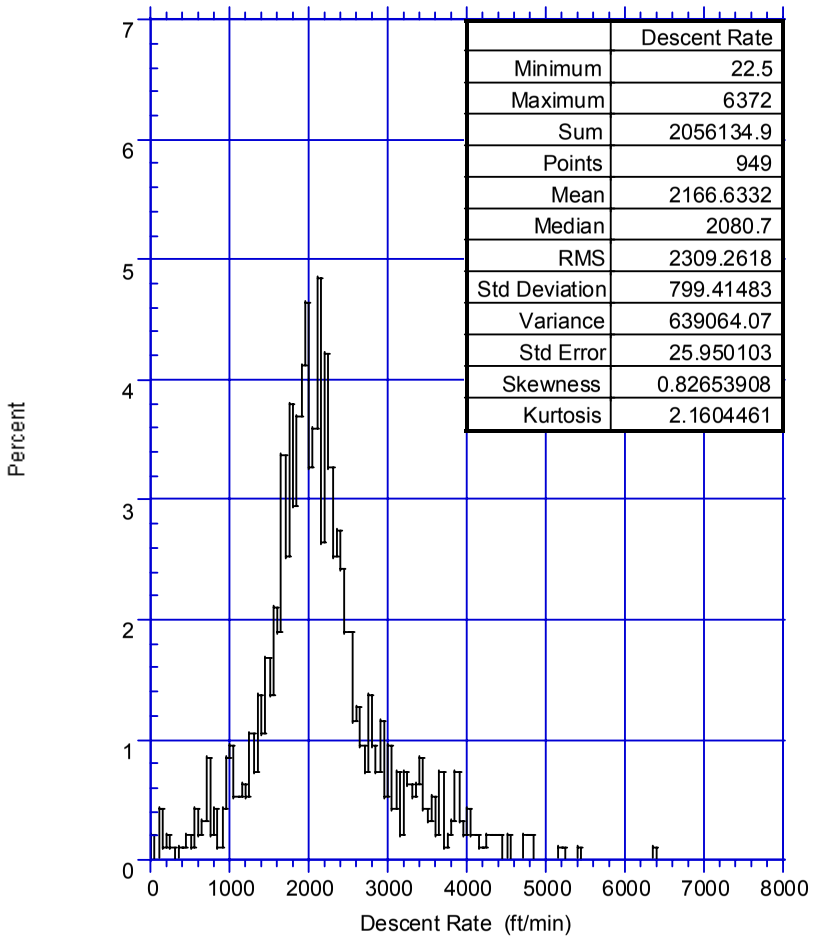

	Descent Rate
Minimum	22.5
Maximum	6372
Sum	2056134.9
Points	949
Mean	2166.6332
Median	2080.7
RMS	2309.2618
Std Deviation	799.41483
Variance	639064.07
Std Error	25.950103
Skewness	0.82653908
Kurtosis	2.1604461

FIGURE D-105. PROBABILITY OF DESCENT RATE FOR DESCENTS BETWEEN 27,000-28,000 FEET, CAPACITY-LIMITED AIRPORTS

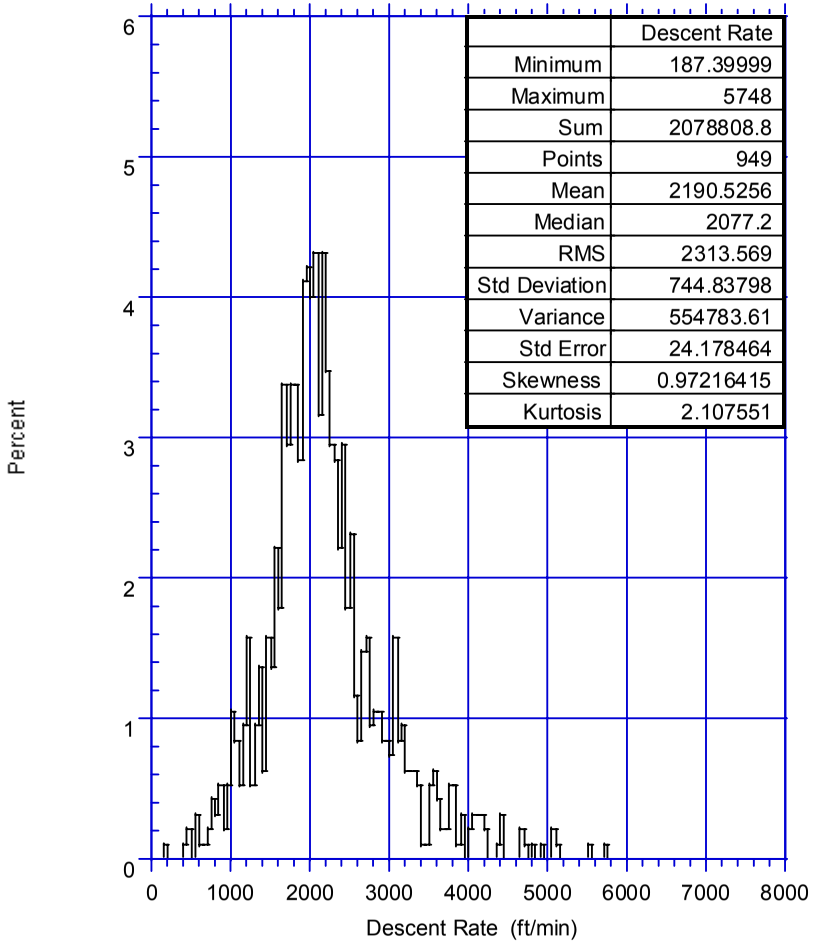

	Descent Rate
Minimum	187.39999
Maximum	5748
Sum	2078808.8
Points	949
Mean	2190.5256
Median	2077.2
RMS	2313.569
Std Deviation	744.83798
Variance	554783.61
Std Error	24.178464
Skewness	0.97216415
Kurtosis	2.107551

FIGURE D-106. PROBABILITY OF DESCENT RATE FOR DESCENTS BETWEEN 28,000-29,000 FEET, CAPACITY-LIMITED AIRPORTS

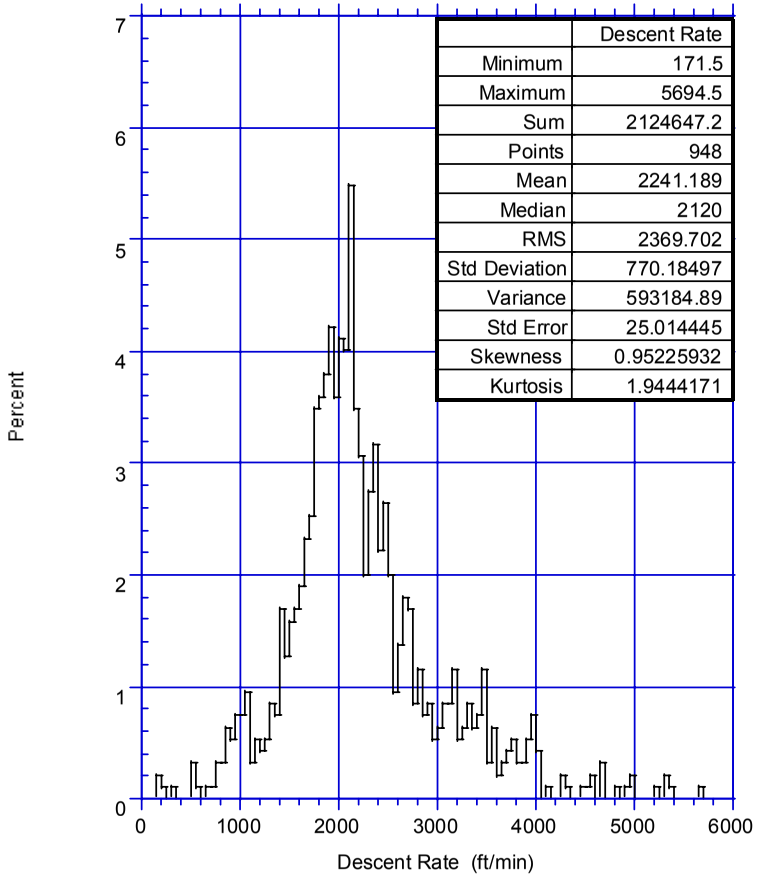

FIGURE D-107. PROBABILITY OF DESCENT RATE FOR DESCENTS BETWEEN 29,000-30,000 FEET, CAPACITY-LIMITED AIRPORTS

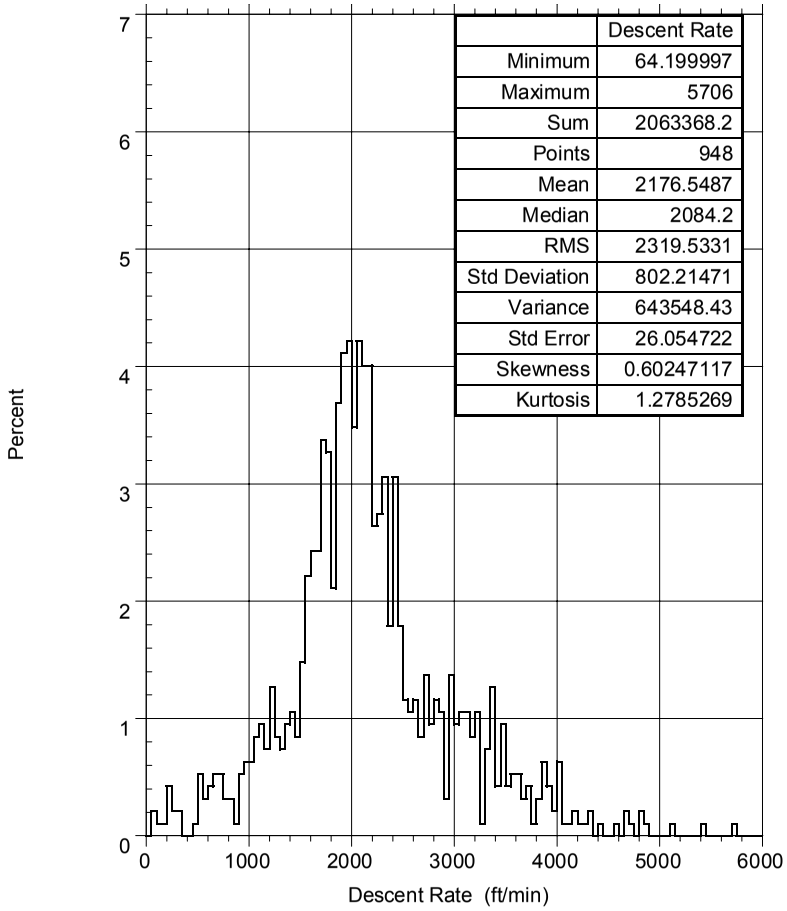

FIGURE D-108. PROBABILITY OF DESCENT RATE FOR DESCENTS BETWEEN 30,000-31,000 FEET, CAPACITY-LIMITED AIRPORTS

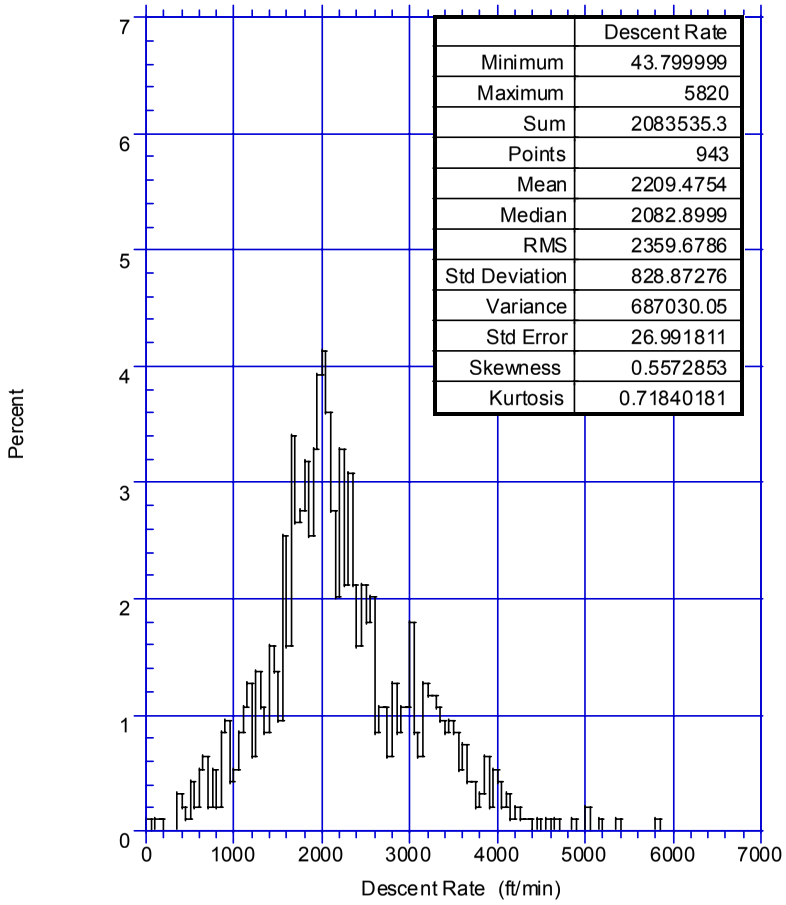

	Descent Rate
Minimum	43.799999
Maximum	5820
Sum	2083535.3
Points	943
Mean	2209.4754
Median	2082.8999
RMS	2359.6786
Std Deviation	828.87276
Variance	687030.05
Std Error	26.991811
Skewness	0.5572853
Kurtosis	0.71840181

FIGURE D-109. PROBABILITY OF DESCENT RATE FOR DESCENTS BETWEEN 31,000-32,000 FEET, CAPACITY-LIMITED AIRPORTS

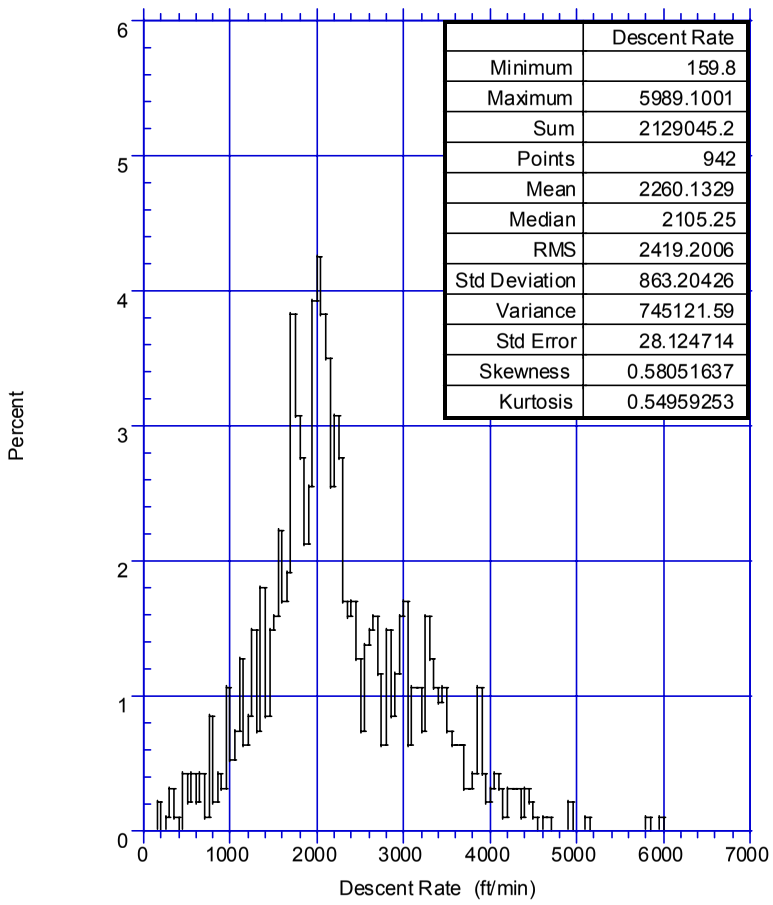

	Descent Rate
Minimum	159.8
Maximum	5989.1001
Sum	2129045.2
Points	942
Mean	2260.1329
Median	2105.25
RMS	2419.2006
Std Deviation	863.20426
Variance	745121.59
Std Error	28.124714
Skewness	0.58051637
Kurtosis	0.54959253

FIGURE D-110. PROBABILITY OF DESCENT RATE FOR DESCENTS BETWEEN 32,000-33,000 FEET, CAPACITY-LIMITED AIRPORTS

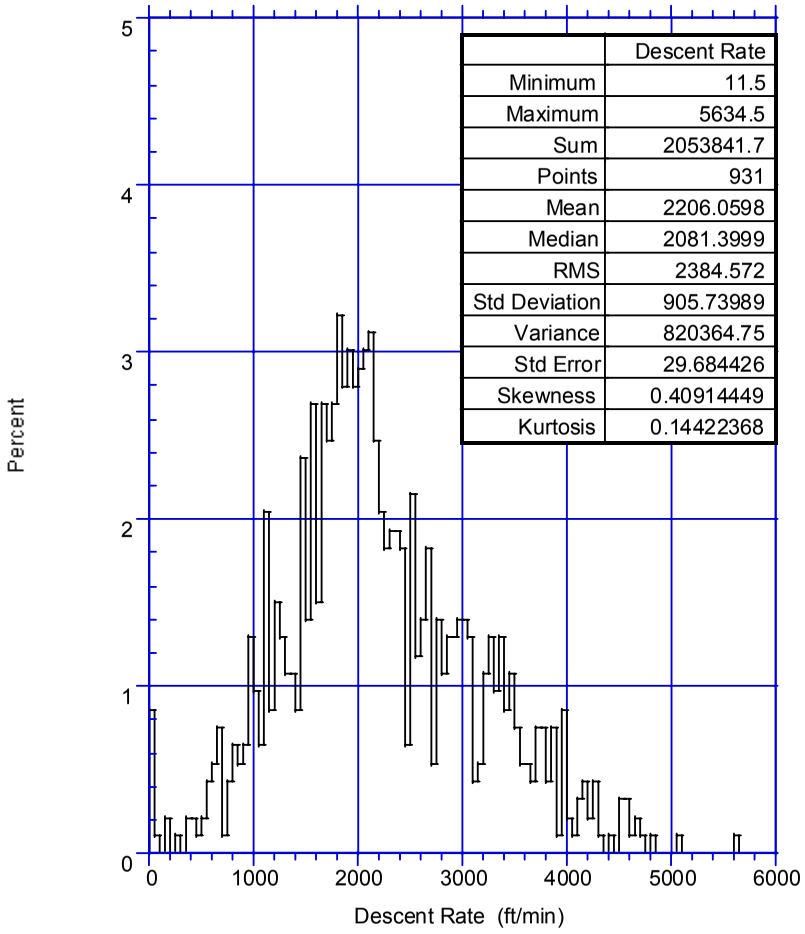

FIGURE D-111. PROBABILITY OF DESCENT RATE FOR DESCENTS BETWEEN 33,000-34,000 FEET, CAPACITY-LIMITED AIRPORTS

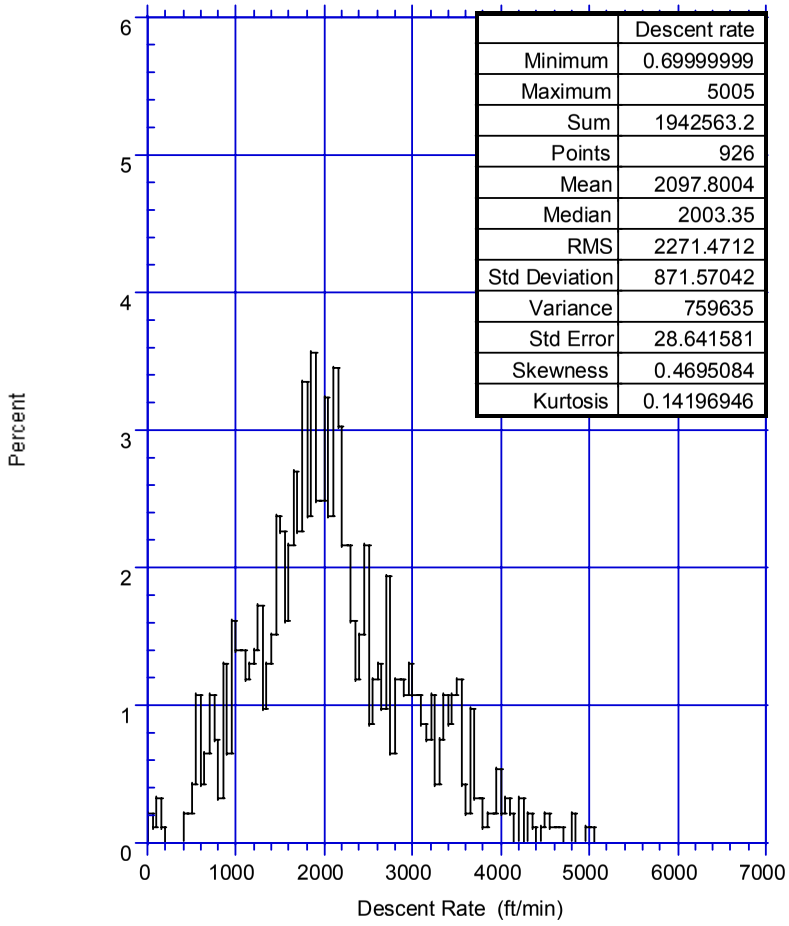

FIGURE D-112. PROBABILITY OF DESCENT RATE FOR DESCENTS BETWEEN 34,000-35,000 FEET, CAPACITY-LIMITED AIRPORTS

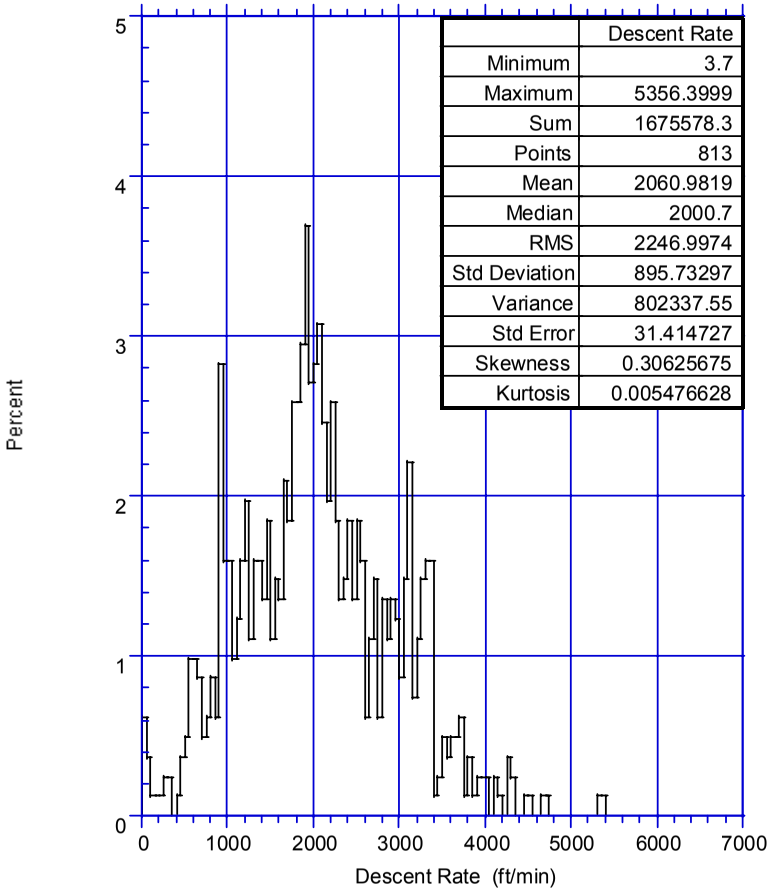

FIGURE D-113. PROBABILITY OF DESCENT RATE FOR DESCENTS BETWEEN 35,000-36,000 FEET, CAPACITY-LIMITED AIRPORTS

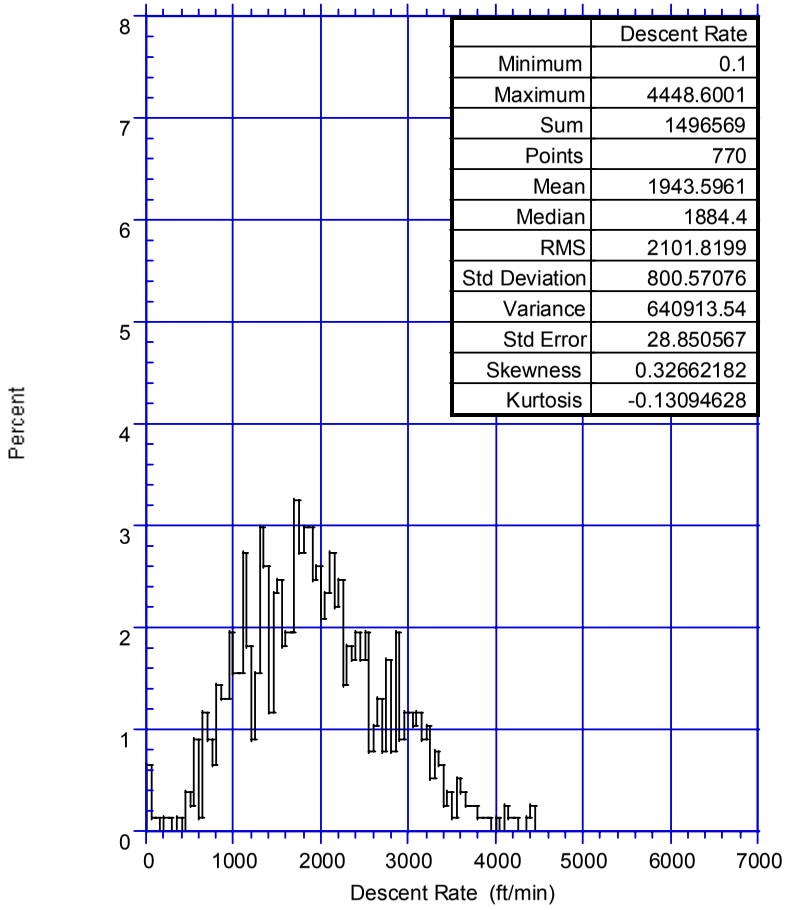

FIGURE D-114. PROBABILITY OF DESCENT RATE FOR DESCENTS BETWEEN 36,000-37,000 FEET, CAPACITY-LIMITED AIRPORTS

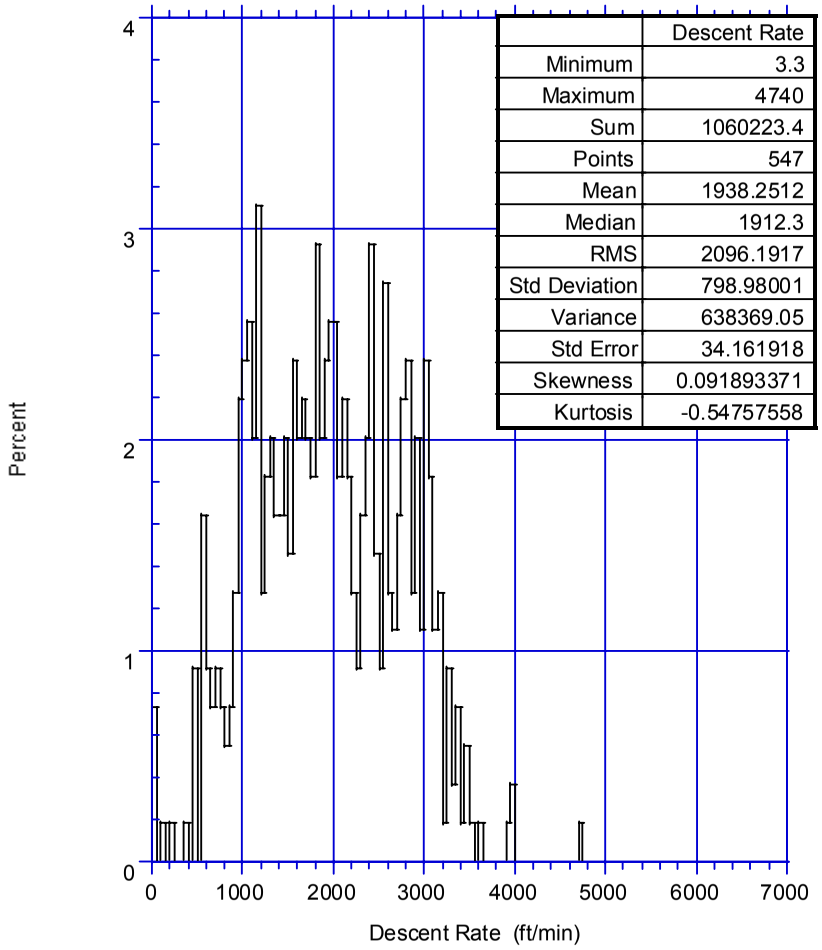

FIGURE D-115. PROBABILITY OF DESCENT RATE FOR DESCENTS BETWEEN 37,000-38,000 FEET, CAPACITY-LIMITED AIRPORTS

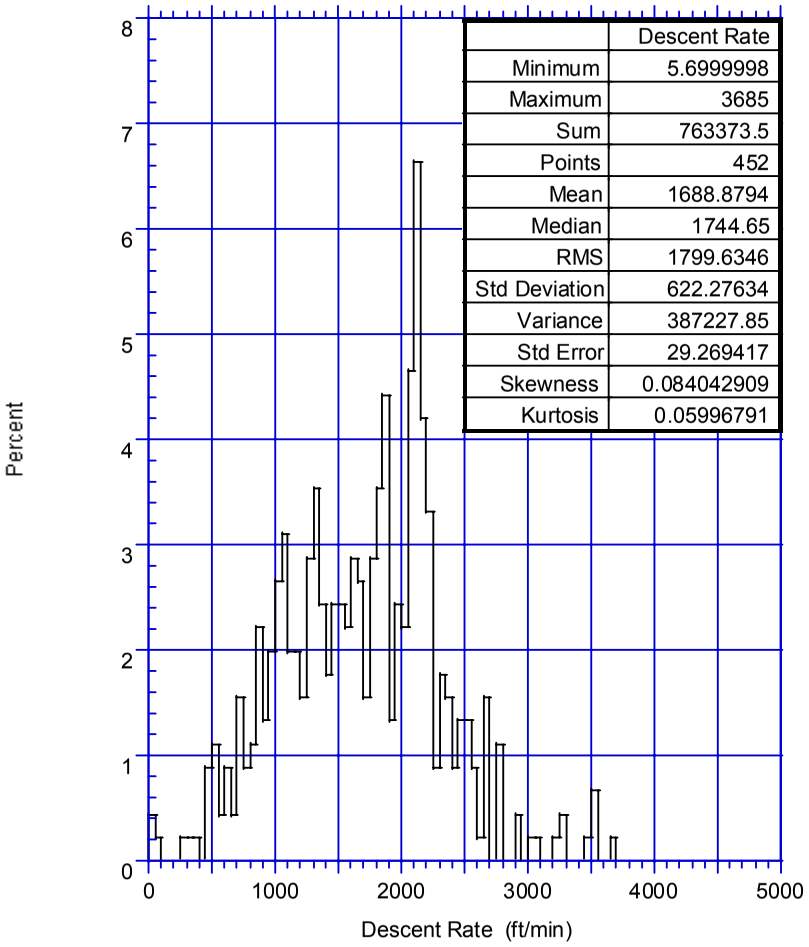

FIGURE D-116. PROBABILITY OF DESCENT RATE FOR DESCENTS BETWEEN 38,000-39,000 FEET, CAPACITY-LIMITED AIRPORTS

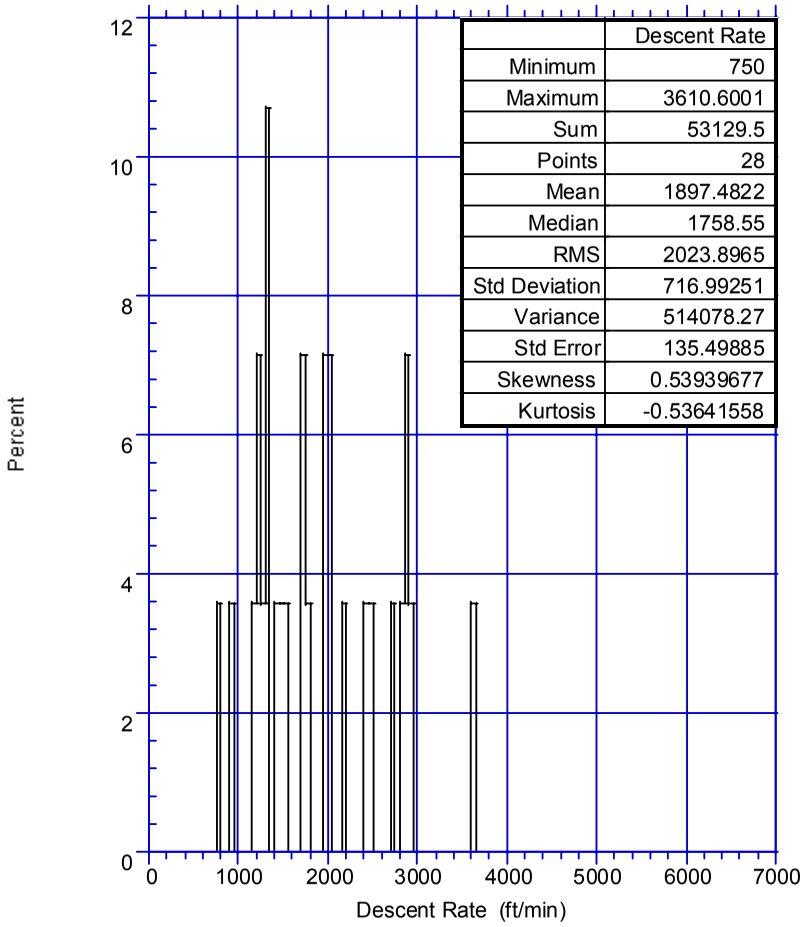

FIGURE D-117. PROBABILITY OF DESCENT RATE FOR DESCENTS BETWEEN 39,000-40,000 FEET, CAPACITY-LIMITED AIRPORTS

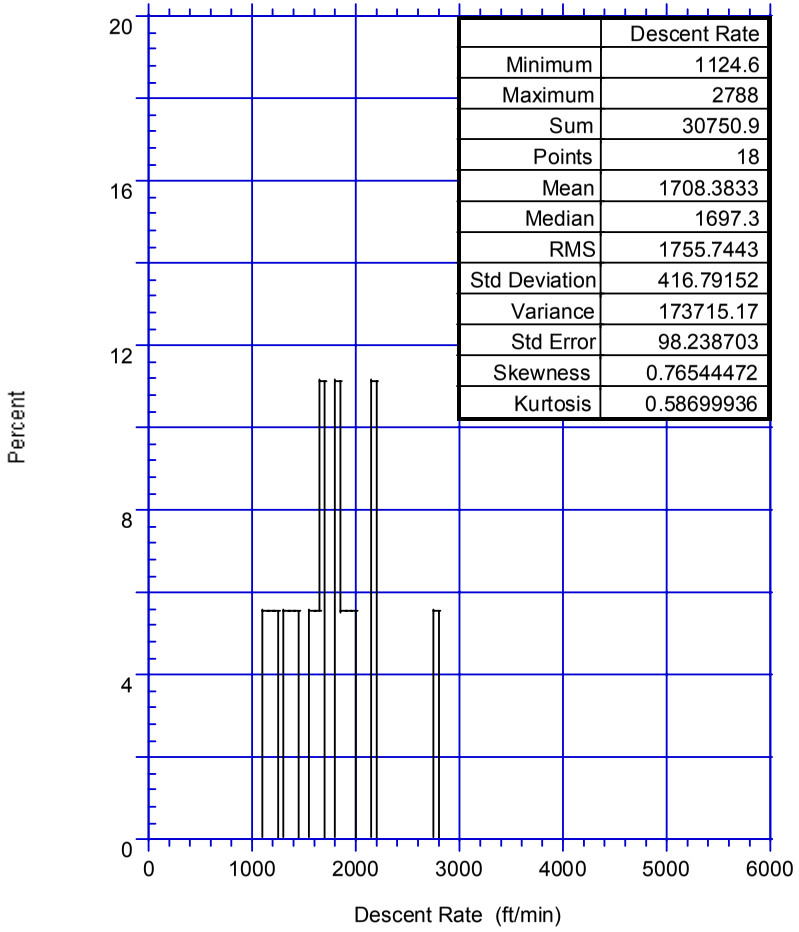

FIGURE D-118. PROBABILITY OF DESCENT RATE FOR DESCENTS BETWEEN 40,000-41,000 FEET, CAPACITY-LIMITED AIRPORTS

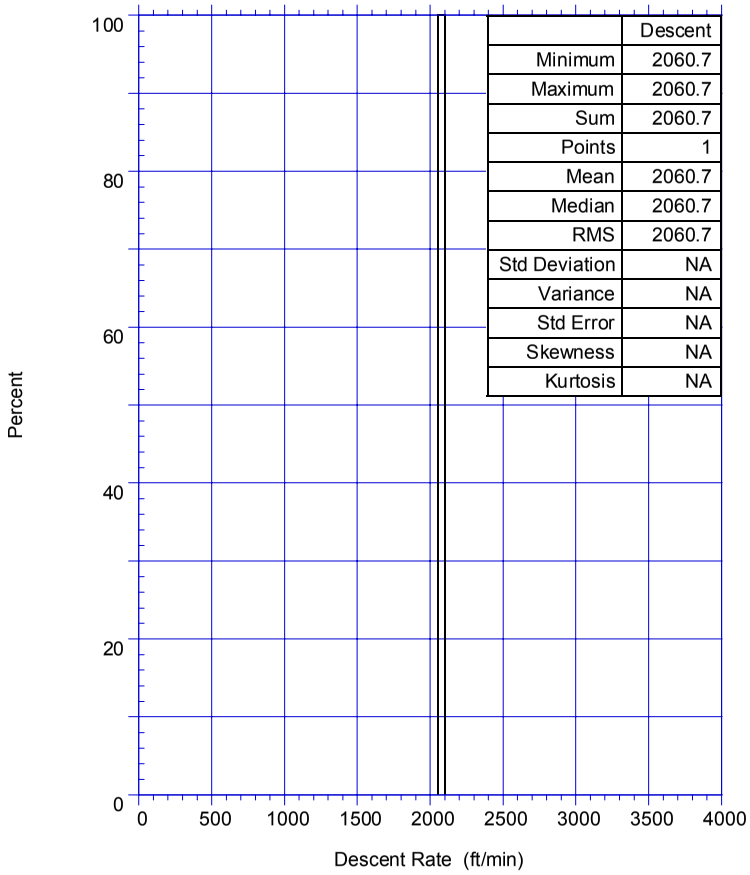

FIGURE D-119. PROBABILITY OF DESCENT RATE FOR DESCENTS BETWEEN 41,000-42,000 FEET, CAPACITY-LIMITED AIRPORTS

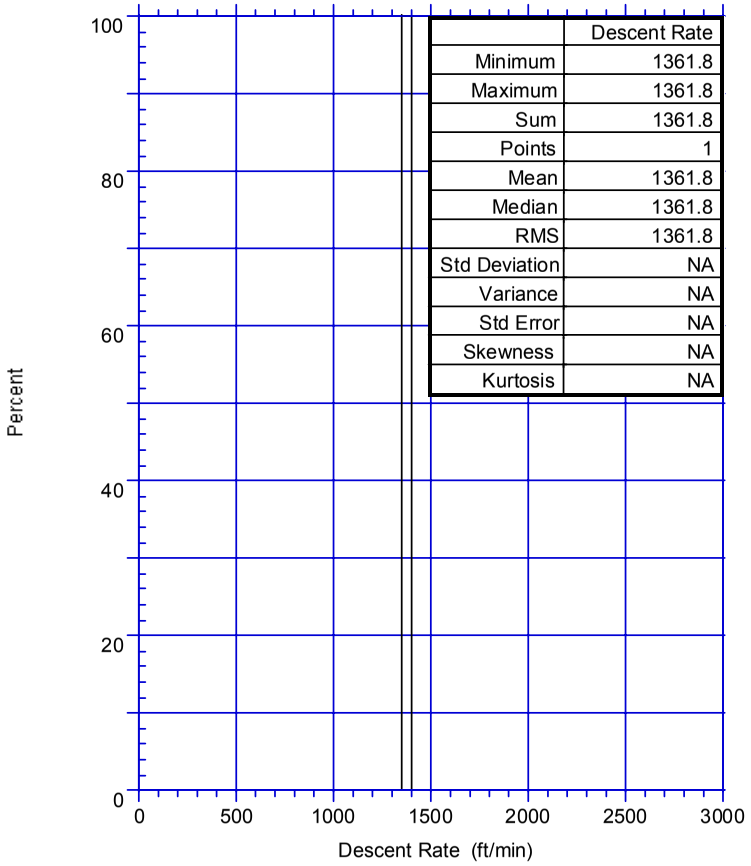

FIGURE D-120. PROBABILITY OF DESCENT RATE FOR DESCENTS BETWEEN 42,000-43,000 FEET, CAPACITY-LIMITED AIRPORTS

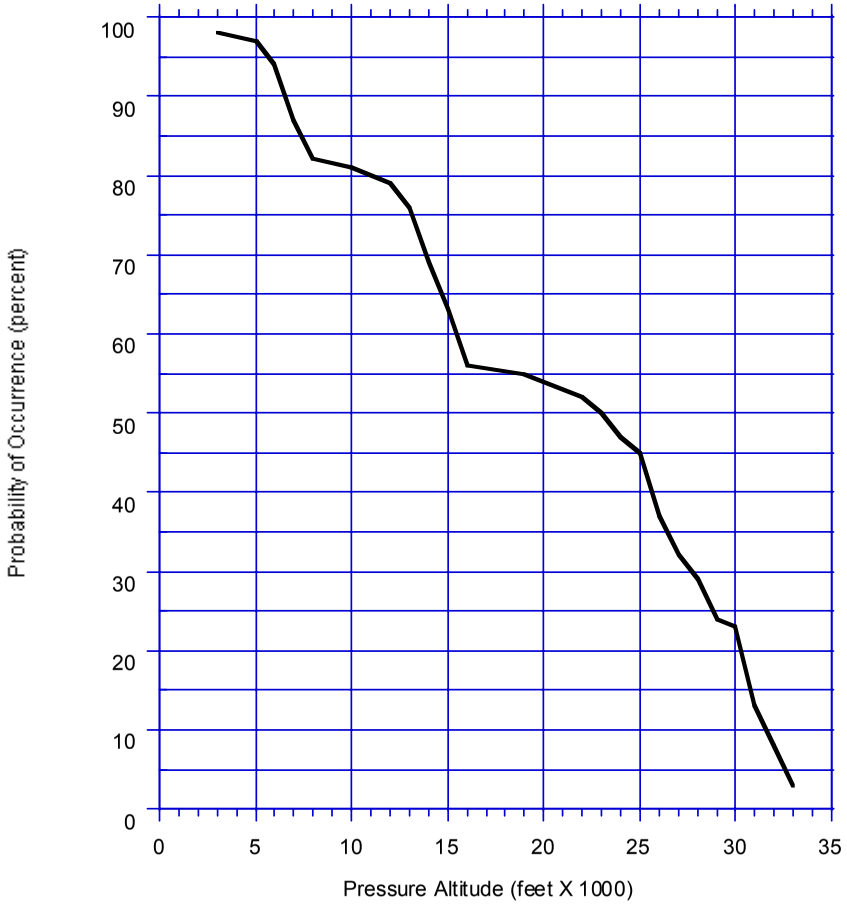

FIGURE D-121. PROBABILITY OF OCCURRENCE OF INITIAL CRUISE ALTITUDE FOR FLIGHTS LESS THAN 300 NAUTICAL MILES (61 FLIGHTS)

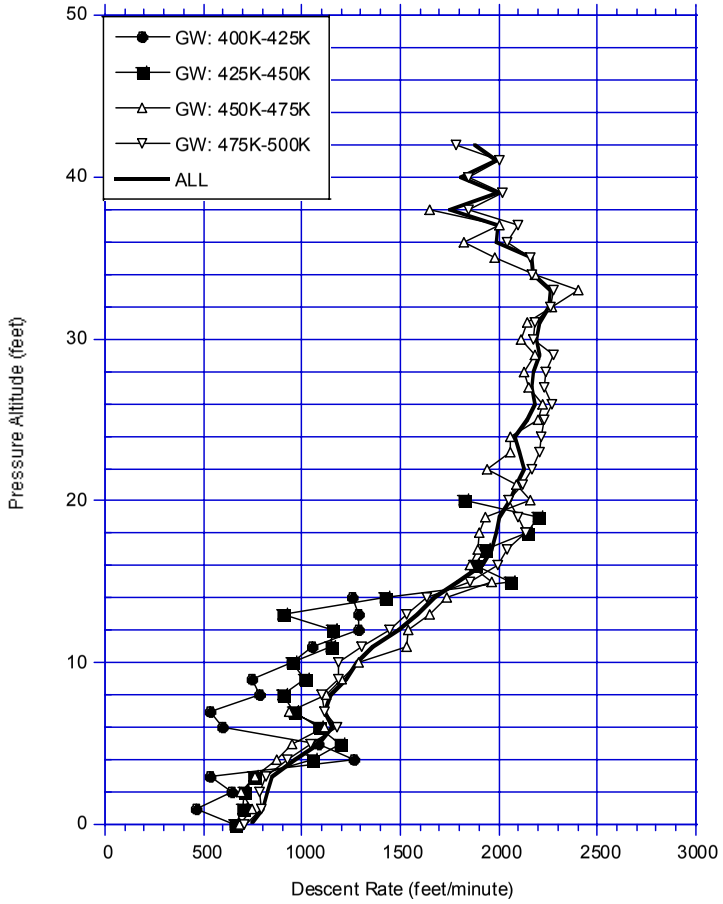

FIGURE D-122. MEAN DESCENT RATES AT PRESSURE ALTITUDE BY GROSS WEIGHT BANDS, 400-500K

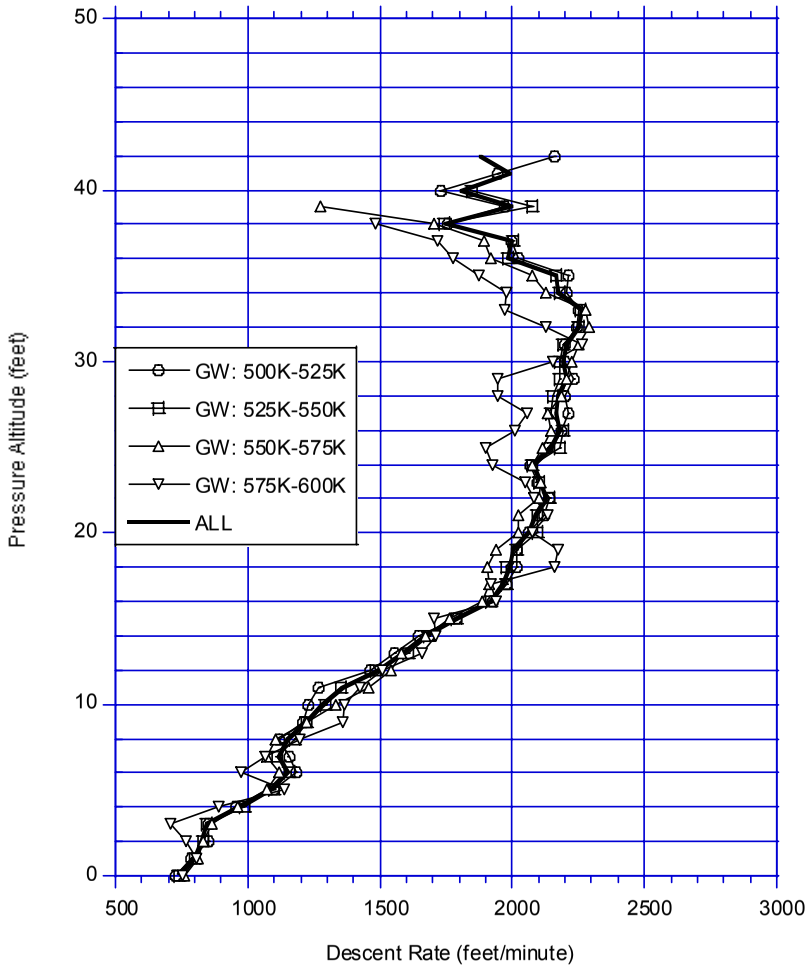

FIGURE D-123. MEAN DESCENT RATES AT PRESSURE ALTITUDE BY GROSS WEIGHT BANDS, 500-600K

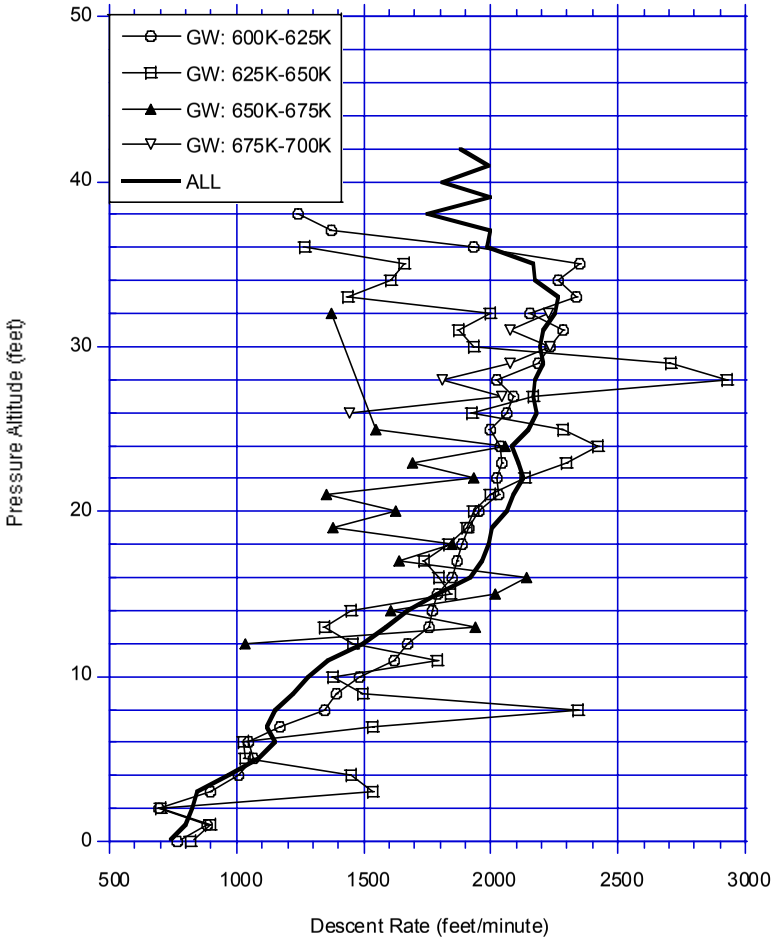

FIGURE D-124. MEAN DESCENT RATES AT PRESSURE ALTITUDE BY GROSS WEIGHT BANDS, 600-700K

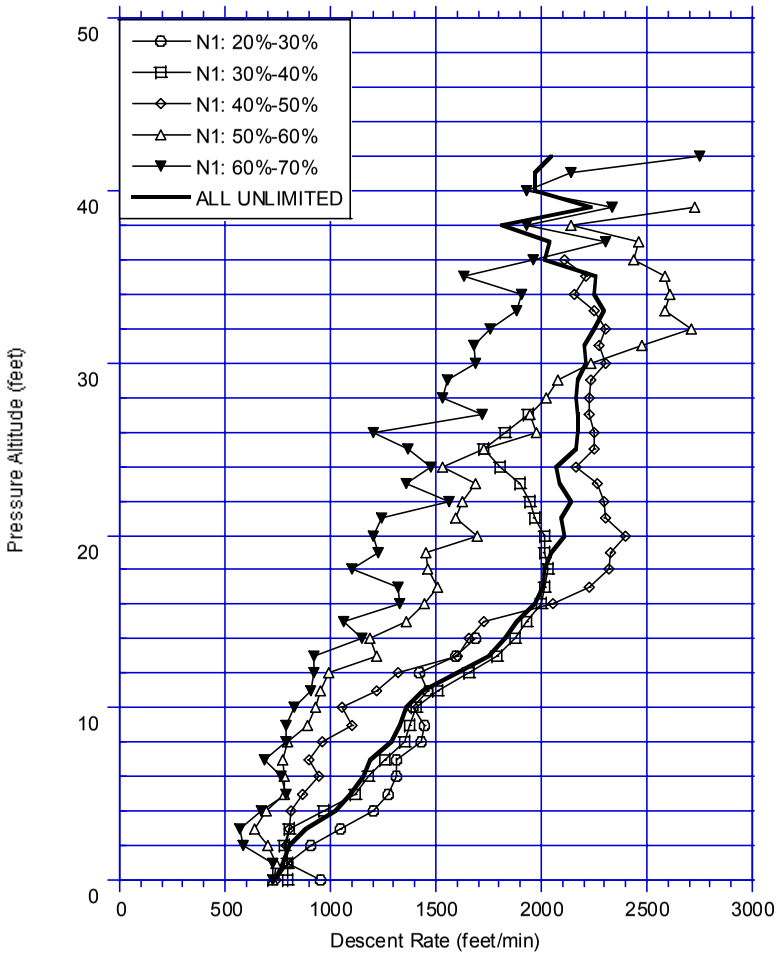

FIGURE D-125. MEAN DESCENT RATE INTO CAPACITY-UNLIMITED AIRPORTS AT PRESSURE ALTITUDE BY N1 RANGE (20%-70%)

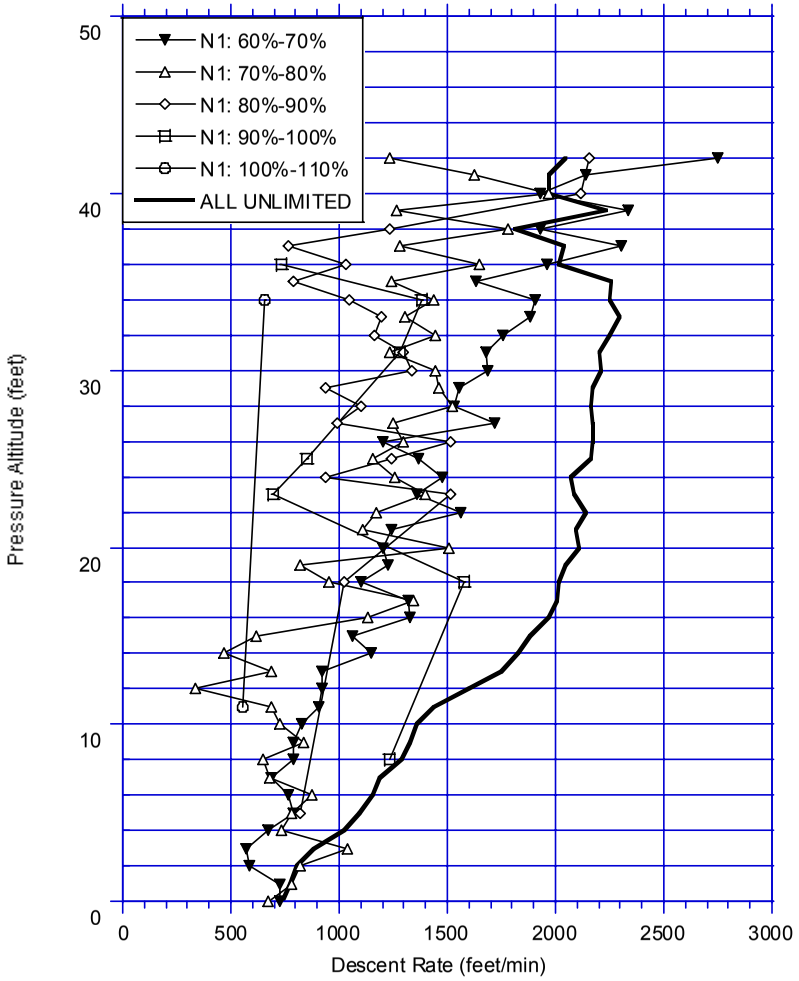

FIGURE D-126. MEAN DESCENT RATE INTO CAPACITY-UNLIMITED AIRPORTS AT PRESSURE ALTITUDE BY N1 RANGE (60%-110%)

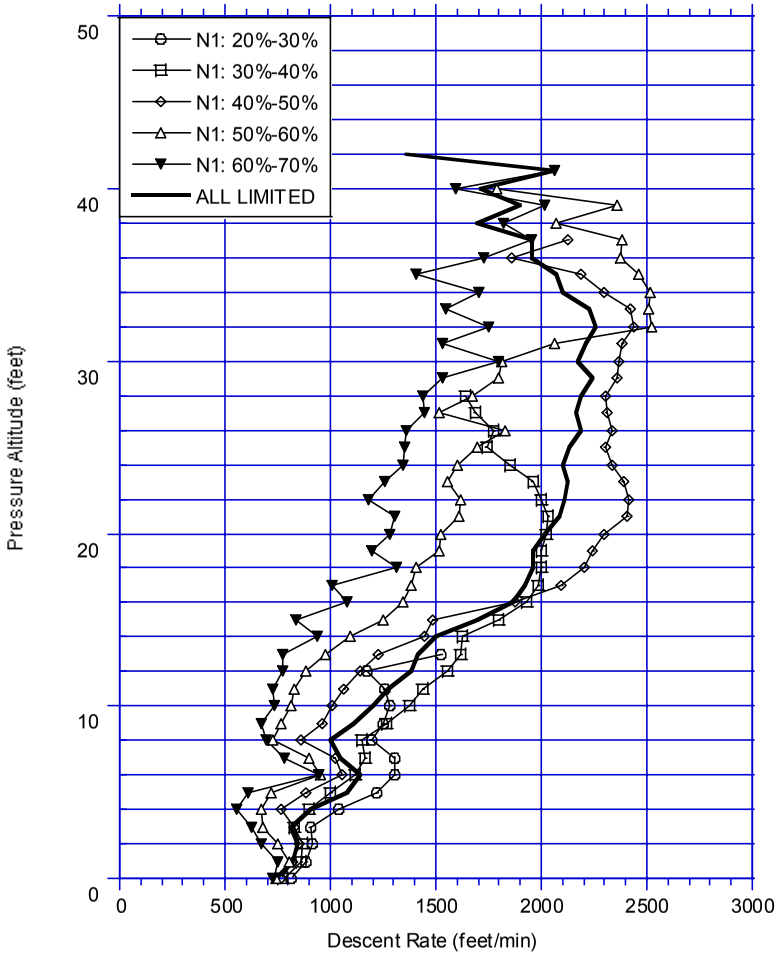

FIGURE D-127. MEAN DESCENT RATE INTO CAPACITY-LIMITED AIRPORTS AT PRESSURE ALTITUDE BY N1 RANGE (20%-70%)

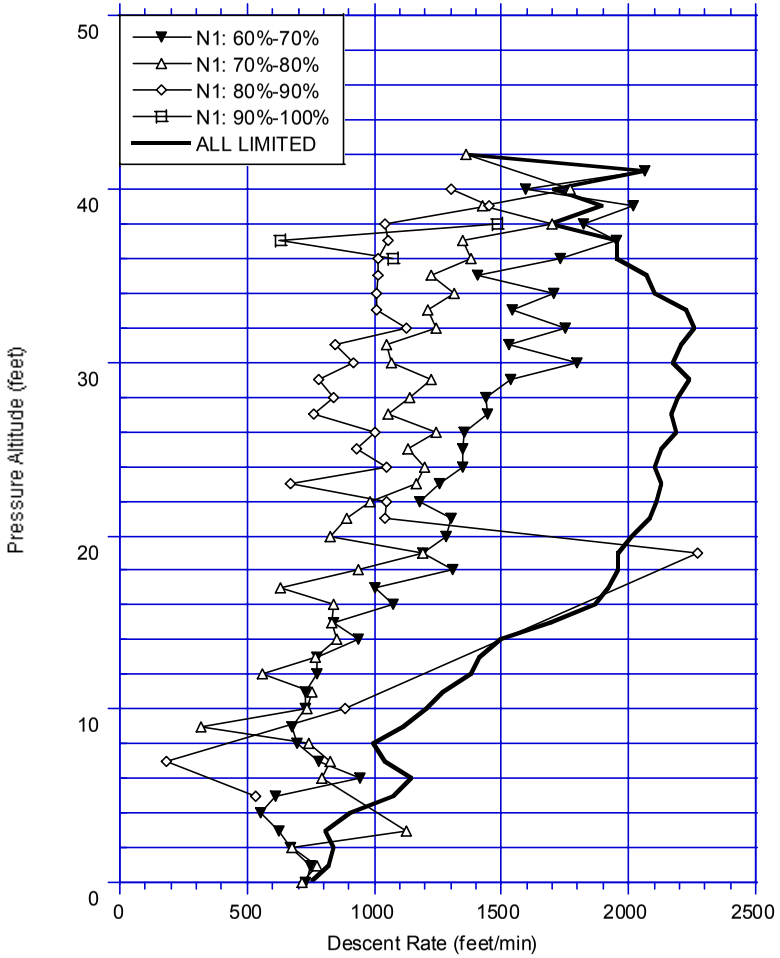

FIGURE D-128. MEAN DESCENT RATE INTO CAPACITY-LIMITED AIRPORTS AT PRESSURE ALTITUDE BY N1 RANGE (60%-110%)

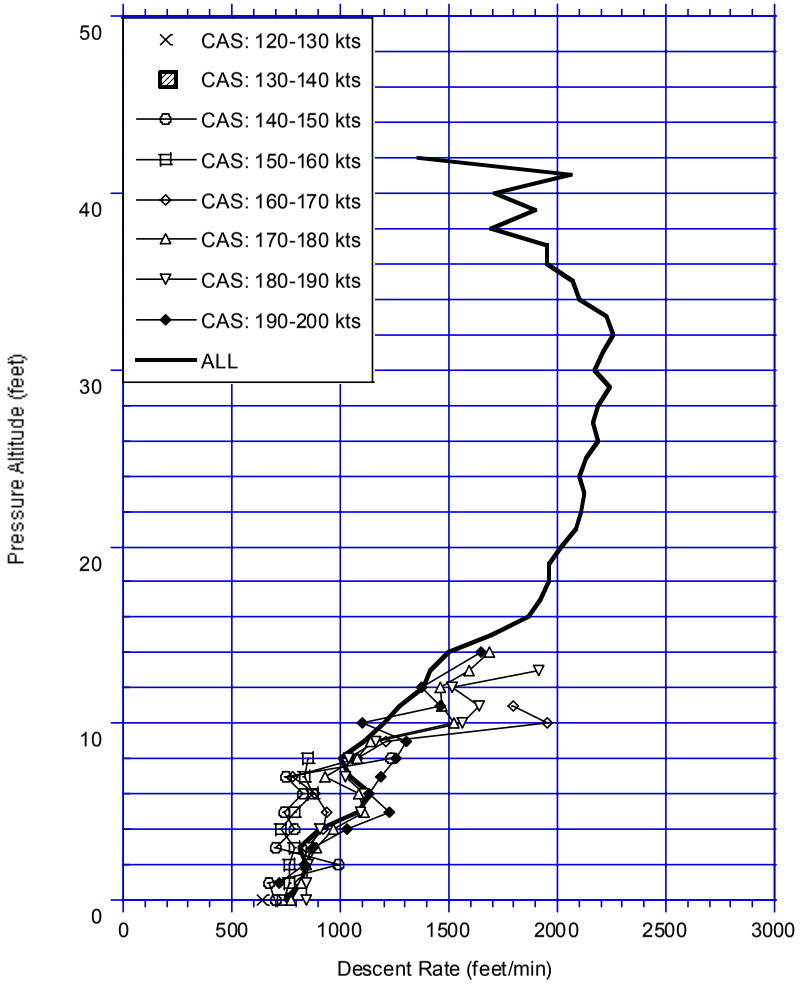

FIGURE D-129. MEAN DESCENT RATE AT PRESSURE ALTITUDE BY CAS RANGE (120-200 KTS)

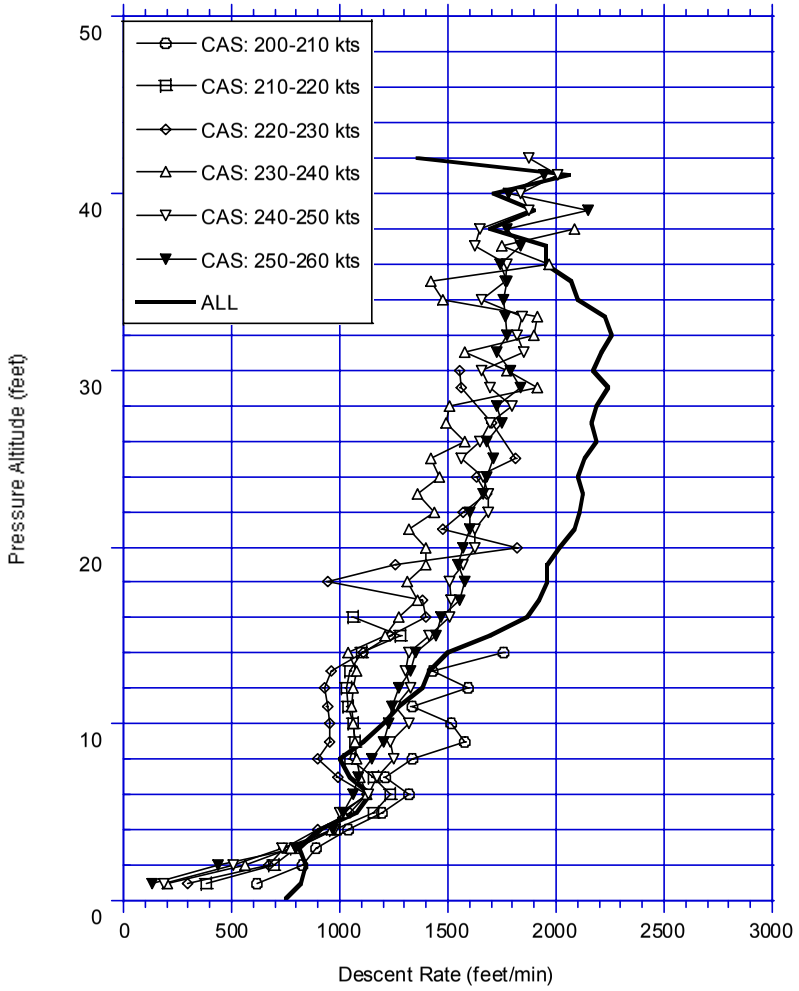

FIGURE D-130. MEAN DESCENT RATE AT PRESSURE ALTITUDE BY CAS RANGE (200-260 KTS)

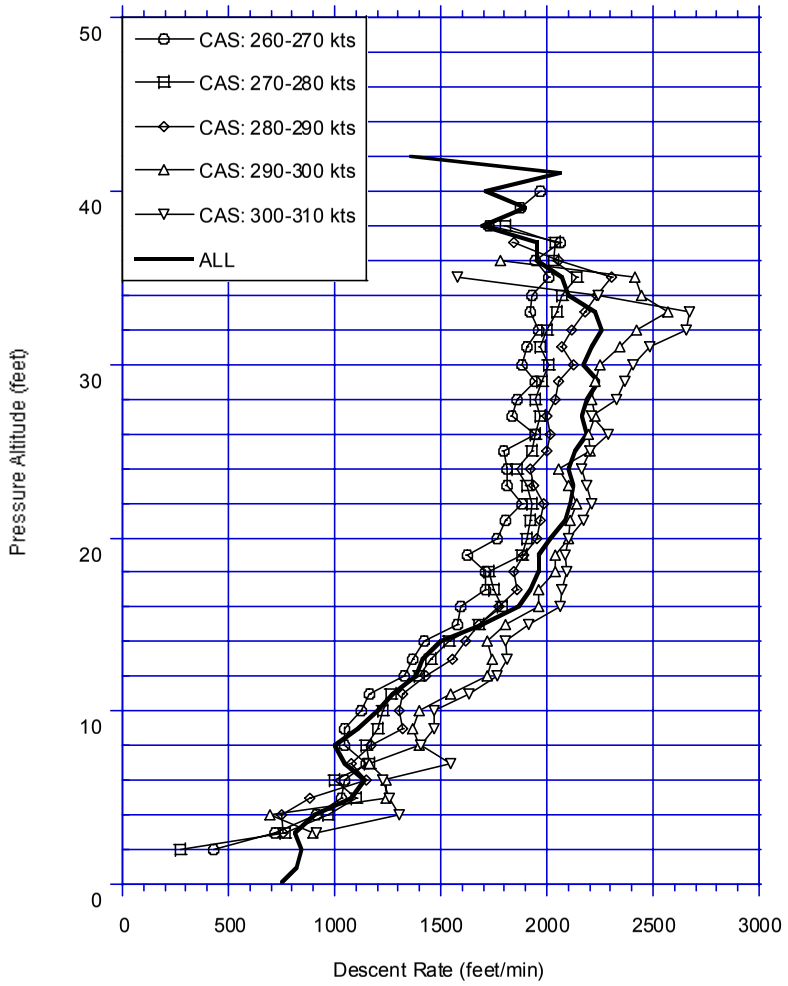

FIGURE D-131. MEAN DESCENT RATE AT PRESSURE ALTITUDE BY CAS RANGE (260-310 KTS)

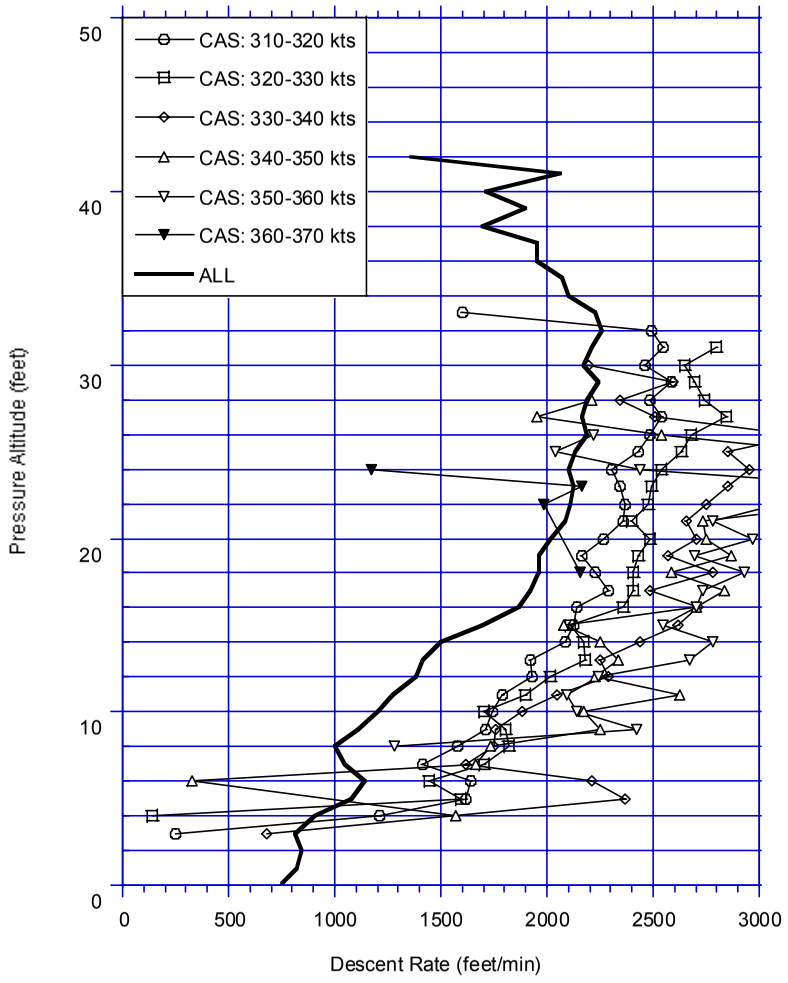

FIGURE D-132. MEAN DESCENT RATE AT PRESSURE ALTITUDE BY CAS RANGE (310-370 KTS)

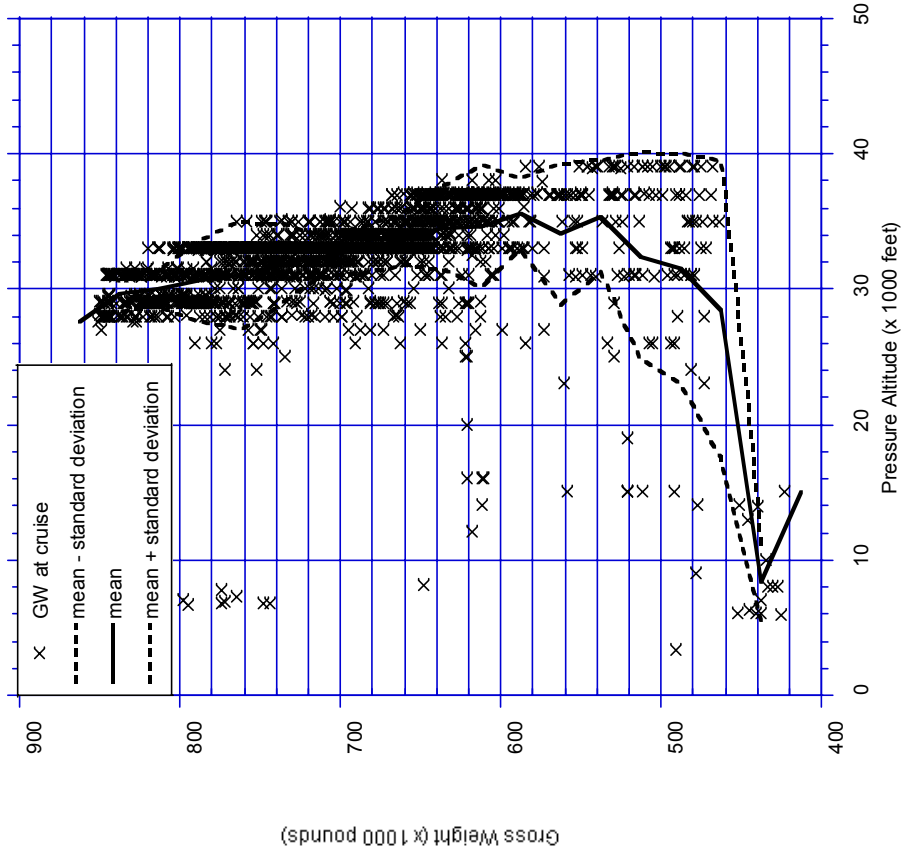

FIGURE D-133. GROSS WEIGHT AND PRESSURE ALTITUDE AT START OF FIRST CRUISE